BOEING

299 pp.

NASA CR 114315
Boeing Report D6-24850

AVAILABLE TO THE PUBLIC

STATIC TESTS OF A 0.7 SCALE AUGMENTOR WING FLAP FOR THE MODIFIED C-8A AIRPLANE - TEST RESULTS AND ANALYSIS

By

D. L. Harkonen, C. F. Wintermeyer,
and F. L. Wright

May 1971

Prepared under Contract No. NAS2-6025 by
THE BOEING COMPANY
Commercial Airplane Division
Renton, Washington

for

NATIONAL AERONAUTICS AND SPACE ADMINISTRATION
Ames Research Center

THE BOEING COMPANY

COMMERCIAL AIRPLANE DIVISION

RENTON, WASHINGTON

NASA CR 114315

DOCUMENT NO D6-24850

TITLE: STATIC TESTS OF A 0.7 SCALE AUGMENTOR WING FLAP FOR THE MODIFIED C-8A AIRPLANE - TEST RESULTS AND ANALYSIS

MODEL Modified C-8A

ISSUE NO. 4 TO: ______ (DATE)

Contract NAS2-6025

NOT REPRODUCIBLE

Prepared by	D.L. Harkonen	5/4/71
Prepared by	C. F. Wintermeyer	5/4/71
PREPARED BY	F. L. Wright	5/3/71
SUPERVISED BY	B. Neal	5/5/71
APPROVED BY	G. E. Tagge	5/5/71
APPROVED BY	H. Skavdahl	5-5-71
Approved by	R. H. Ashleman	5-5-71
		(DATE)

The report was prepared under Contract No. NAS2-6005

by THE BOEING COMPANY, Seattle, Washington for

Ames Research Center.

LIST OF ACTIVE PAGES

SECTION	PAGE NUMBER	REV SYM	ADDED PAGES						SECTION	PAGE NUMBER	REV SYM	ADDED PAGES					
			PAGE NUMBER	REV SYM	PAGE NUMBER	REV SYM	PAGE NUMBER	REV SYM				PAGE NUMBER	REV SYM	PAGE NUMBER	REV SYM	PAGE NUMBER	REV SYM
	1									51							
	2									52							
	3									53							
	4									54							
	5									55							
	6									56							
	7									57							
	8									58							
	9									59							
	10									60							
	11									61							
	12									62							
	13									63							
	14									64							
	15									65							
	16									66							
	17									67							
	18									68							
	19									69							
	20									70							
	21									71							
	22									72							
	23									73							
	24									74							
	25									75							
	26									76							
	27									77							
	28									78							
	29									79							
	30									80							
	31									81							
	32									82							
	33									83							
	34									84							
	35									85							
	36									86							
	37									87							
	38									88							
	39									89							
	40									90							
	41									91							
	42									92							
	43									93							
	44									94							
	45									95							
	46									96							
	47									97							
	48									98							
	49									99							
	50									100							

AD 1546 B

NASA CR-114,315
NAS2-6025

LIST OF ACTIVE PAGES

SECTION	PAGE NUMBER	REV SYM	ADDED PAGES						SECTION	PAGE NUMBER	REV SYM	ADDED PAGES					
			PAGE NUMBER	REV SYM	PAGE NUMBER	REV SYM	PAGE NUMBER	REV SYM				PAGE NUMBER	REV SYM	PAGE NUMBER	REV SYM	PAGE NUMBER	REV SYM
	101									151							
	102									152							
	103									153							
	104									154							
	105									155							
	106									156							
	107									157							
	108									158							
	109									159							
	110									160							
	111									161							
	112									162							
	113									163							
	114									164							
	115									165							
	116									166							
	117									167							
	118									168							
	119									169							
	120									170							
	121									171							
	122									172							
	123									173							
	124									174							
	125									175							
	126									176							
	127									177							
	128									178							
	129									179							
	130									180							
	131									181							
	132									182							
	133									183							
	134									184							
	135									185							
	136									186							
	137									187							
	138									188							
	139									189							
	140									190							
	141									191							
	142									192							
	143									193							
	144									194							
	145									195							
	146									196							
	147									197							
	148									198							
	149									199							
	150									200							

AD 1348 B

LIST OF ACTIVE PAGES

SECTION	PAGE NUMBER	REV SYM	ADDED PAGES					
			PAGE NUMBER	REV SYM	PAGE NUMBER	REV SYM	PAGE NUMBER	REV SYM
	201							
	202							
	203							
	204							
	205							
	206							
	207							
	208							
	209							
	210							
	211							
	212							
	213							
	214							
	215							
	216							
	217							
	218							
	219							
	220							
	221							
	222							
	223							
	224							
	225							
	226							
	227							
	228							
	229							
	230							
	231							
	232							
	233							
	234							
	235							
	236							
	237							
	238							
	239							
	240							
	241							
	242							
	243							
	244							
	245							
	246							
	247							
	248							
	249							
	250							

SECTION	PAGE NUMBER	REV SYM	ADDED PAGES					
			PAGE NUMBER	REV SYM	PAGE NUMBER	REV SYM	PAGE NUMBER	REV SYM
	251							
	252							
	253							
	254							
	255							
	256							
	257							
	258							
	259							
	260							
	261							
	262							
	263							
	264							
	265							
	266							
	267							
	268							
	269							
	270							
	271							
	272							
	273							
	274							
	275							
	276							
	277							
	278							
	279							
	280							
	281							
	282							
	283							
	284							
	285							
	286							
	287							
	288							
	289							
	290							
	291							
	292							
	293							
	294							

AD 1545B

REVISIONS			
REV SYM	DESCRIPTION	DATE	APPROVAL

AD 1546 C

CONTENTS

ABSTRACT

A static test investigation has been made of an augmentor-wing flap system for the Modified C-8A jet STOL research airplane. Tests were conducted using a 0.7 scale model which had a span of 95 inches, a flap chord of 30 inches, and a full span double slot nozzle. The sensitivity of augmentor performance to geometrical variables and the noise characteristics of the augmentor-wing measured at flap angles from 6° to 75°. Flap surface static pressures and total pressures within the augmentor were also measured. The augmentor performance was found to be sensitive to the flap coanda surface position and flow blockage within the augmentor. Nozzle total pressure ratio was also an important parameter. The optimum flap pivot point for the aircraft was determined. The augmentation ratios with this pivot point location were near the maximum measured for flap angles from 30° to 65°. The maximum augmentation ratio, based on isentropic thrust at the duct entrance, was 1.27 at 30° flap angle. The corresponding augmentation ratio based on actual nozzle performance was 1.39. As the augmentor passage was blocked off by a moveable segment of the flap, ("lift-dump"), the thrust of the augmentor decreased until slightly negative thrust occurred with the passage completely blocked.

LIST OF FIGURES

LIST OF FIGURES (CONT'D)

LIST OF FIGURES (CONT'D)

LIST OF FIGURES (CONT'D)

LIST OF FIGURES (CONT'D)

AD 1546 D

LIST OF FIGURES (CONT'D)

LIST OF FIGURES (CONT'D)

AD 1546 D

LIST OF FIGURES (CONT'D)

LIST OF FIGURES (CONT'D)

AD 1546D

16

LIST OF FIGURES (CONT'D)

LIST OF FIGURES (CONT'D)

LIST OF FIGURES (CONT'D)

LIST OF FIGURES (CONT'D)

INTRODUCTION AND SUMMARY

The augmentor wing concept for achieving very high wing lift coefficients has been under study for several years by NASA and The DeHavilland Aircraft of Canada, Limited (References 1-3). A program has been undertaken by the United States and Canadian Governments to procure an Augmentor Wing Jet STOL Research Aircraft by modifying a C-8A "Buffalo" aircraft (see Figure 1). The Boeing Company is under contract to NASA to modify the airframe including the augmentor flap system and The DeHavilland Aircraft of Canada, Limited is under contract to the Department of Industry, Trade, and Commerce of Canada to provide the nacelle/propulsion system package for the aircraft. This test investigation was conducted as part of the aircraft modification program.

A static test program has been completed on an augmentor-wing flap system for this airplane. A sketch of the major elements of the augmentor flap system is shown below

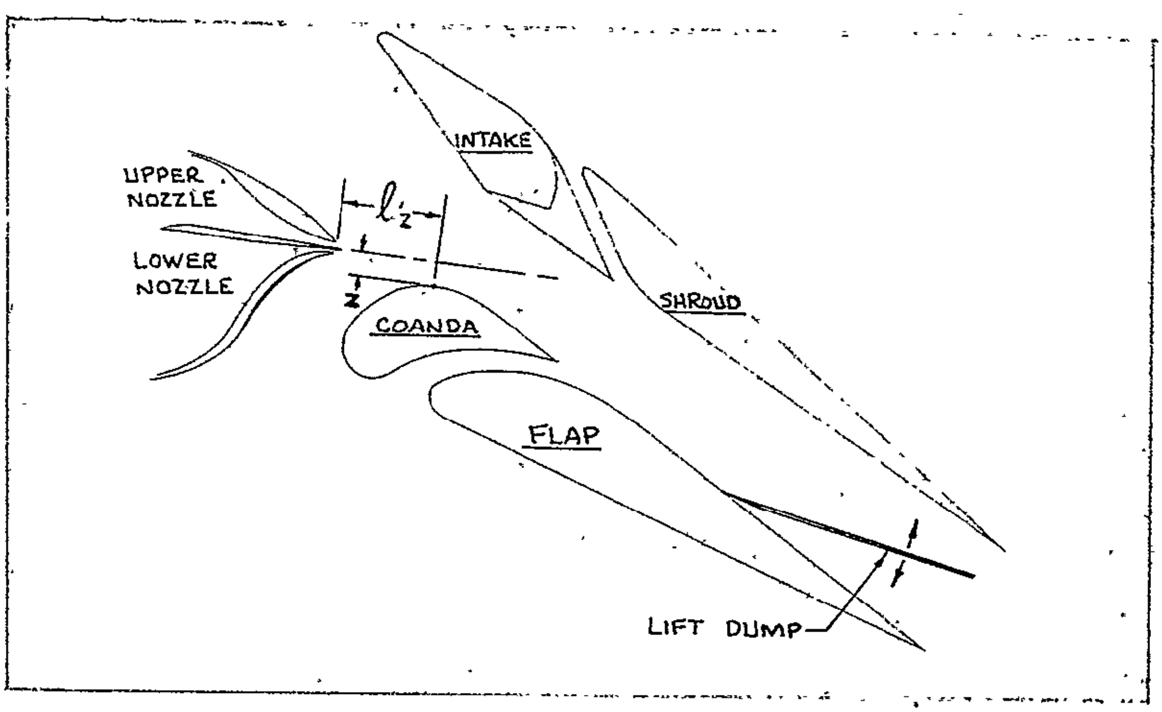

Augmentor-Wing Flap System Elements

The objectives of the test program were to determine the following:

1. The thrust augmentation characteristics of the augmentor flap at large scale.
2. The sensitivity of augmentor performance to small changes in geometry such as might be caused by deflection under flight load conditions.
3. Augmentor choke effectiveness as a means of thrust spoiling. This is used on the airplane as a means of lateral control and lift dumping.
4. An understanding of the flow mechanism within the augmentor by means of surface pressure and rake total pressure measurements.
5. Nozzle flow angularity (turning vane effectiveness), discharge coefficient, velocity coefficient along with momentum distribution characteristics of the augmentor.
6. Augmentor noise characteristics.
7. Hinge-moment verification for design assumptions used for augmentor choke control surface.

Based on the test facility maximum continuous airflow capacity and the trade-off between model flap chord length and span section length, a 0.7 scale model of a complete duct-nozzle augmentor flap system was constructed and tested. The model simulated one half of one side of the airplane augmentor flap system. The model had a span of 95 inches and a flap chord of 30 inches. The model could be used to simulate either the wing panel inboard or outboard of the

nacelle by rerouting the air supply system and changing the duct area distributions by means of duct liners.

The following geometric variations were investigated during the test — augmentor throat spacing, intake door opening, lift dump angle, diffuser exit angle and Coanda flap positions relative to the slot nozzle exit at several flap deflection angles. In addition to testing these geometric variables for thrust performance, model acoustic levels, augmentor static pressures and exit momentum data were recorded.

Augmentor performance in this report is presented in terms of the ratio of measured resultant thrust to the isentropic thrust at the augmentor nozzle entrance. Augmentation ratio can also be expressed as the ratio of measured resultant thrust to the measured nozzle thrust. The Figure below presents the maximum levels of augmentation produced by the model for both definitions.

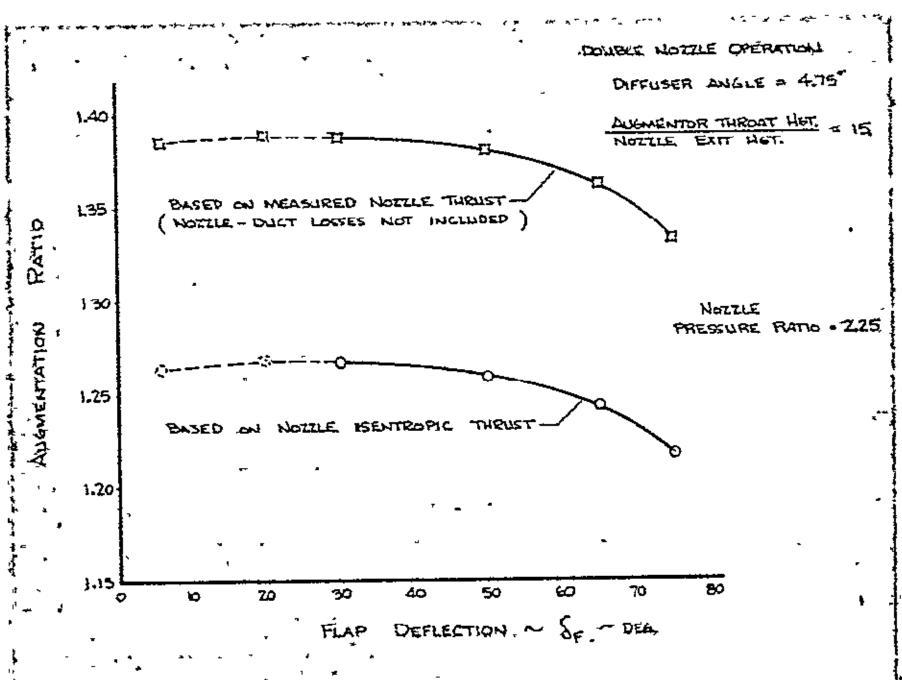

Maximum Measured Augmentation Ratio

Test results indicated the highest static thrust augmentation was obtained with the diffuser angle set between 4° and 5° using an augmentor throat to nozzle height ratio (ℓ_T/h_N) between 15 and 17. The static test results showed that the augmentor was fairly insensitive to movements in the Coanda flap ℓ_Z direction but small changes in the Z direction could greatly affect performance. Thrust augmentation was determined for a large range Coanda flap positions (ℓ_Z & Z). A typical performance contour plot is shown below. The sensitivity to variations in the Coanda flap position relative to the nozzle exit at $\delta_F = 30^\circ$ is similar to other flap angles tested.

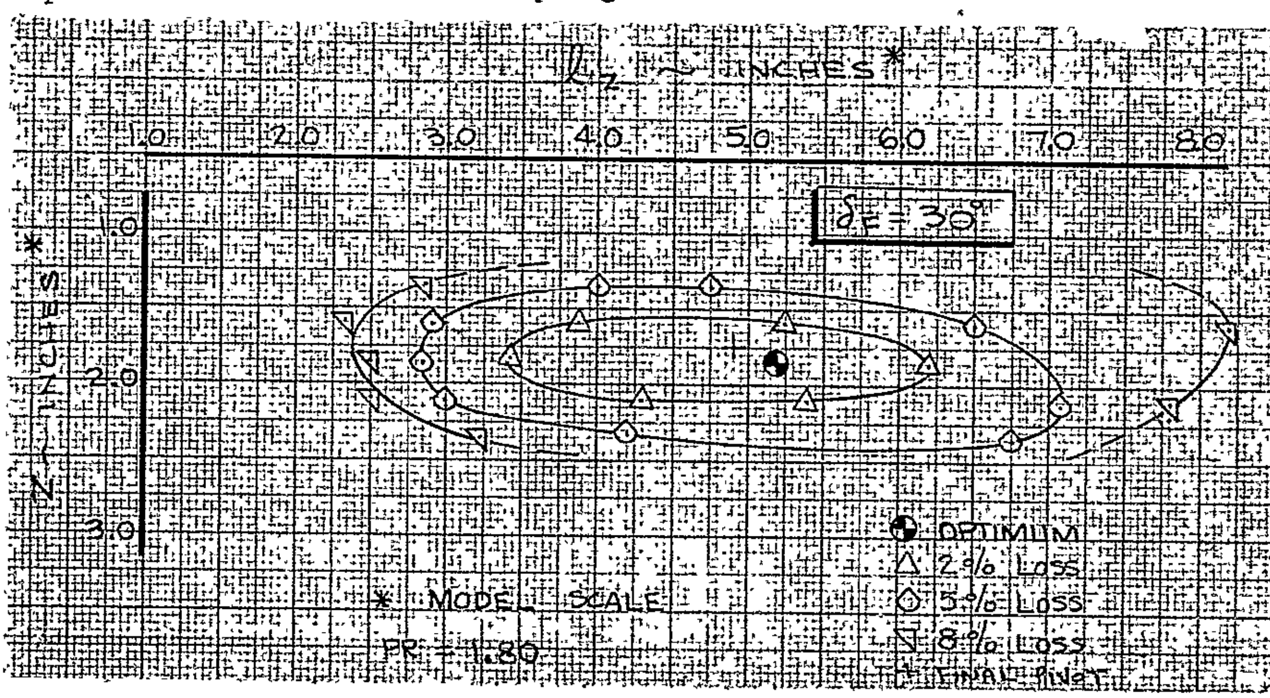

Augmentor-Flap Performance Contour Map at 30° Flap Angle

The test also showed that small local obstructions in the throat of the augmentor produced significant losses in augmentation, while large variations in the intake door opening produced little effect on performance. The "lift dump" tests showed that the augmentor thrust could be smoothly spoiled from maximum augmentation to slightly negative thrust values.

Flap static pressure data was used to determine airplane flap loads and hinge moments and also as an aid in understanding the augmentor flow characteristics. Total pressure surveys were taken at the augmentor exit to detect flow separation along the flap span and to evaluate the capability for determining airplane augmentor static performance.

The augmentor was tested with both nozzles operating (double nozzle) and with the nozzles operating individually (singe nozzle). A single flap pivot point for the airplane augmentor flap was selected which was a compromise between single nozzle (engine out) and double nozzle (two engine) operation. The Figure below compares estimated airplane augmentor static performance versus flap deflection angle for the airplane flap pivot point selected. The maximum performance obtained, assuming infinite variation of the pivot point is also shown. It is of interest to note that performance near the optimum obtained by the model can be achieved for the flap deflection angles of major interest (30° to 65°) by using a simple fixed pivot position in the airplane design.

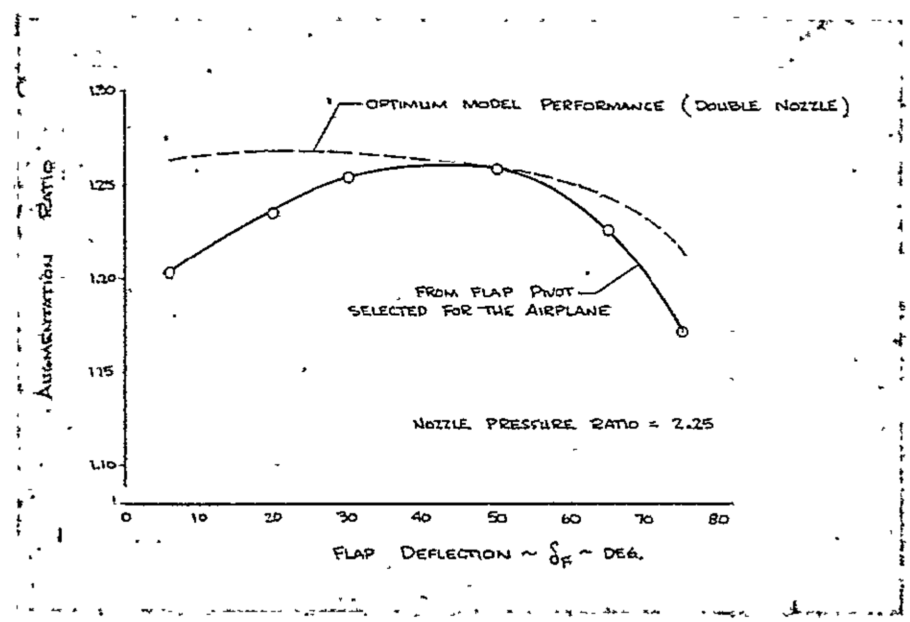

Estimated Static Airplane Performance
With Design Refinements from 0.7 Scale
Test Results

In addition to the conclusions discussed above, the following were also observed:

- o The 0.7 scale model developed approximately 4% higher thrust augmentation than the Ames Phase IV test model (Reference 3).

- o Maximum nozzle velocity coefficient attained was 0.9[illegible], at a pressure ratio of [illegible].5.

- o The model upper nozzle turning vanes overturned the flow 3.5°.

- o The augmentor performance was not sensitive to upper and lower nozzles operating at moderately unequal pressure ratios.

- o The passage between the intake door and the upper nozzle external surface should be convergent or parallel to provide vibration-free operation.

Acoustic measurements were recorded during the static test of the jet-augmentor flap system. The object of these recordings was to determine the basic noise characteristics and verify predicted noise levels of the augmentor system. The noise at the optimum performance configuration was a broad-band distribution of energy between [illegible] and [illegible] cps. Small movements from the optimum position of the flap system relative to the axis of the slot nozzle caused descrete tones to be generated. The maximum perceived noise levels were observed to occur about 40° from the flap system centerline and were within 1 to 3.5 PNdb of estimates made prior to the test. At lower pressure ratios, the noise level of the 30° flap configuration is consistently higher than the levels for the higher flap angles.

Based on this test program, and the above conclusions, the following design features were incorporated in the Modified C-5A Airplane design:

AD 1546D

1. Flap diffuser angle was established at 4.75°

2. Flap pivot point was located to obtain the best compromise between engine out (single nozzle) at 30° flap angle and two engine (double nozzle) at 30° and 65° flap angle augmentor performance.

3. Upper nozzle turning vane exit angle was adjusted to eliminate flow over-turning and minimize double nozzle cross flow losses.

4. The flap internal support brackets and intake door arm were designed to eliminate obstructions in the augmentor throat.

5. Intake door angle at the "flaps up" position was adjusted to eliminate possible vibration.

The estimated airplane augmentor performance based on static test data is approximately 3% higher than that produced by the full airplane model with similar flap geometry tested in the Ames 40' x 80' wind tunnel. Since the airplane performance is based on this wind tunnel data the static test has indicated with a high degree of confidence that the augmentor flap system will perform satisfactorily and will not significantly contribute to the aircraft noise levels on the Modified C-8A airplane.

SYMBOLS

AF	Axial force per unit span, lb/in
A_J	Jet exit area, in^2
A_{LN}, ALN	Average measured lower nozzle exit area, in^2
AR	Static augmentation ratio, $\frac{T}{M_{M_{UN}} \cdot V_{I_{UN}} + M_{M_{LN}} \cdot V_{I_{LN}}}$ see Appendix.
ARC_1	Calculated augmentation ratio at the lower span flap exit rake, see Appendix.
ARC_2	Calculate augmentation ratio at the upper span flap exit rake, see Appendix.
A_{UN}, AUN	Average measured upper nozzle exit area, in^2
C	Chord of individual flap element, in
C_A, CA	Sectional axial force coefficient, AF/qc
C_{DLN}, CDLN	Lower nozzle discharge coefficient, $\frac{M_{M_{LN}}}{M_{I_{LN}}}$, see Appendix.
C_{DUN}, CDUN	Upper nozzle discharge coefficient, $\frac{M_{M_{UN}}}{M_{I_{UN}}}$, see Appendix.
C_{J_I}	Augmentor isentropic jet thrust coefficient, $\frac{T_I}{q\ S_{REF}}$
$C_{M_{LE}}$, CPM	Sectional pitching moment coefficient about leading edge, M/qc^2
C_N, CN	Sectional normal force coefficient, N_F/qc
C_P	Static pressure coefficient, $\frac{P_s - P_o}{q}$
C.P.	Center of pressure/chord

AD 1546D

SYMBOLS (Cont'd)

CHOKE	Choke deflection angle, degree
D	Drag force, lb
FLAP	Flap deflection angle, degrees
HM	Section hinge moment, in-lb/in
h_N	Sum of the upper and lower nozzle exit gaps, in
L	Lift force, lb
ℓ_e, LE	Average distance between the trailing edges of the augmentor flaps, in.
ℓ_i, LI	Average distance from the intake door to the nearest point on the upper nozzle external surface, in
ℓ_T, LT	Distance measured from the most point of the flat portion of the Coanda flap and the perpendicular to the flat portion of the Coanda flap to the intake door, in
ℓ_T/h_N	Ratio of augmentor throat height to total nozzle exit gap
ℓ'_Z, LZ	Distance from the nozzle exit measured parallel to the geometric nozzle centerline to the point on the Coanda flap nearest the geometric nozzle centerline, in.
M_J	Jet mass flow rate, lb/sec
M	Pitching moment per unit span, in-lb/in
N_F	Normal force per unit span, lb/in
$N_H/\sqrt{T_1}$	Engine power setting parameter, rpm/ $^{\circ}K$
NOZFLO	Indicator for mode of nozzle operation

NOZFLO	Mode of Nozzle Operation
0	Double Nozzle
1	Upper Nozzle
2	Lower Nozzle

SYMBOLS (Cont'd)

NOZ-PR	Nominal nozzle pressure ratio, P_T/P_A
P_A, P_{AMB}	Ambient pressure, psia
PR	Nozzle pressure ratio, P_T/P_A
P_{TDA}	Equivalent average duct entrance pressure based on weighted nozzle flow rates, psia
P_{TID}	Inner duct entrance pressure, psia
P_{TOD}	Outer duct entrance pressure, psia
P_{TLN}	Lower nozzle average exit pressure, psia
P_{TUN}	Upper nozzle average exit pressure, psia
Q, q	Dynamic pressure, psi, psf
S	Side force, lb
S_{REF}	Wing reference area, ft^2
T	Resultant thrust, lb
TP	Test point
VJ	Jet exit velocity, ft/sec
X	Axial distance from leading edge to the flap pivot, in
X/C	Non-dimensional distance from leading edge along flap element chord
Z	Distance measured perpendicularly from the nozzle geometric centerline to the nearest point on the Coanda flap, in
Z_P	Normal distance from leading edge to the flap pivot, in

SYMBOLS (Cont'd)

α_W	Wing angle of attack, degrees
β, BETA	Resultant side thrust angle, degrees
δ_F, DELF	Flap deflection angle, degrees
δ_{CHOKE}	Choke deflection angle, degrees
ϕ	Angle of flap element chord relative to wing chord plane, degrees
ρ	Air density, Slugs/cu.ft.
θ	Resultant vertical thrust angle, degrees
θ_e	Flap diffuser angle, degrees
θ_i	Intake door angle, degrees

AD 1546 D

Test Configuration. The primary nozzle for the augmentor (ejector) flap system model was built as a scaled version of that planned for the airplane (Fig 2) with a lower and upper slot nozzle, separated by a thin splitter, and fed by a double duct (inner and outer) system as shown in Figure 6. The airplane outboard duct-nozzle system called for a tapered inner duct and a tapered outer duct whereas with the inboard system only the inner duct would be tapered as shown in Figure 4. The model was built with a constant area outer duct integral with a tapered inner duct. Figures 4 and 7 illustrate how the model was converted from the outboard simulation by removing the tapered liner from the outer duct and inserting a constant area liner. The crescent shaped constant area liner was required to preserve proper outer duct Mach number simulation for the inboard tests. For inboard double nozzle tests both the upper nozzle air and the lower nozzle air were supplied through the outer duct. The air that did not escape from the upper nozzle was dumped into a plenum from which it was fed to the lower nozzle. For the upper nozzle only tests, the air that would have normally been spplied to the lower nozzles was passed back across the balance and dumped overboard. The "dump" flow approximated the outboard upper nozzle flow that is normally supplied through the inboard outer duct. The liner was required to reduce the outer duct area in order to simulate the airplane outer duct Mach number distribution for the inboard tests.

Nozzle exit area adjustment on the model was provided by using removable nozzle lips and shims to set any desired exit gap (±12% from nominal) as shown in Figure 6.

The nozzles and splitter were connected by a row (upper and lower) of turning vanes that were designed to reduce turning losses and to provide a minimum of crossflow between upper and lower streams for both inboard and outboard systems. The turning vanes for both nozzles were spaced 1.4 inch apart and their chord lengths were 1.61 inch (model scale) and 1.26 inch (model scale) for the upper and lower nozzle, respectively (Figures 7 and 8). The model was built with one set of turning vanes for the lower nozzle and two sets of turning vanes for the upper nozzle (inboard and outboard simulation). Air was supplied to the inner duct (lower nozzle) through a 1-1/2D turning elbow and a cascade turning vane section as shown in Figure 9. Figures 10 and 11 show how the outer duct (upper nozzle) was supplied with air from a plenum during the outboard simulation tests and through a duct and a drilled plate (choke plate) during the inboard simulation. The drilled plate was designed to back pressure the upstream ducting and reduce the flow distortion at the total pressure rake at the entrance of the outer duct.

The tapered inner duct used in the test model represented only one half of the duct system on one side of the airplane so the inboard end of tapered inner duct necessarily presented a blunt surface at the entrance of the outer duct flow. To minimize flow disturbances in the model outer duct flow, an axisymmetric nose fairing was fitted to the large end of the tapered inner duct as shown in Figures 7 and 8.

All of the augmentor flap elements except the Coanda flap were fabricated in one 95" long constant spanwise section (Figures 12 and 13). The Coanda flap was built in three span section lengths with a break at both flap bracket stations. The model flap structure for all elements was basically

made up of ribs wrapped with .090 in. aluminum skin which resulted in very stiff flap sections. The intake flap was built with a fixed aft section and a movable forward section (±30° from its flat position), as shown below.

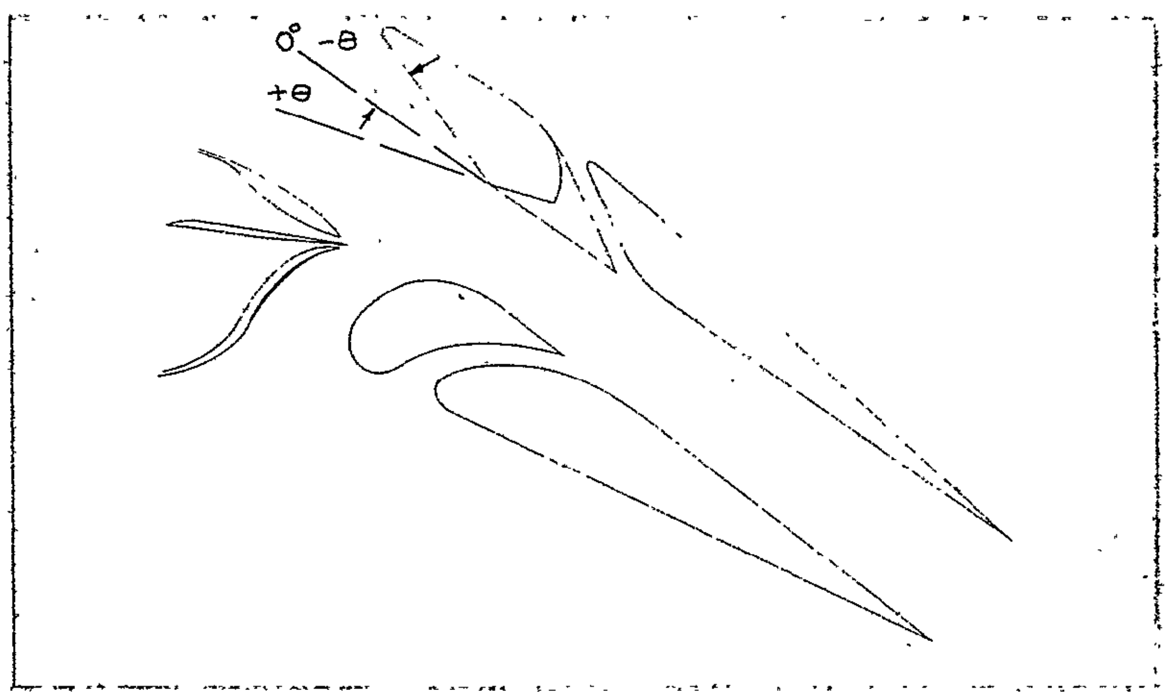

INTAKE DOOR ANGLE VARIATION

The leading edges of both flap elements of the upper flap section (intake and shroud) were fitted with bellmouth entries (Figure) and were installed during all "flaps on" runs except two runs near the end of the test. The elliptical shaped bellmouths were used to preclude any possibility of flow separation during the static tests.

For most of the "flaps on" tests the upper and lower flap sections of the augmentor were held in their relative positions by adjustable turnbuckle links located at the two flap bracket stations (1/4 span in from each end) as shown in Figure 14. These links provided quite a large range of flap throat (ℓ_T), flap exit (ℓ_e), and diffuser included angle (θ_e) adjustment. During the inboard simulation tests, the turnbuckle links were replaced with a pylon strut support as shown in Figure 15. This strut which was representative of that designed for the airplane and remained on the model for the remainder of the test.

The aerodynamic loads on the augmentor flaps were carried entirely by the two main flap support brackets located at 1/4 span positions (Figure 16). These flap support brackets also were designed with rotation and translation adjustment which allowed variations in ℓ_T and S.

Figure 16 also illustrates how the vertically mounted 95" span model was bounded by end plates that were large enough to provide flow guidance during all flap position variations.

The sketch shows that the airplane lift dump or augmentor choke system was represented on the model by a full span hinged plate connected to the lower aft flap (Figures 17 and 18). The model lift dump was tested on the outboard simulation only. It was adjustable in rotation such that the flap exit opening could be varied from ℓ_e = 0 (lift dump fully closed) to ℓ_e = 6.16 in (lift dump fully open.)

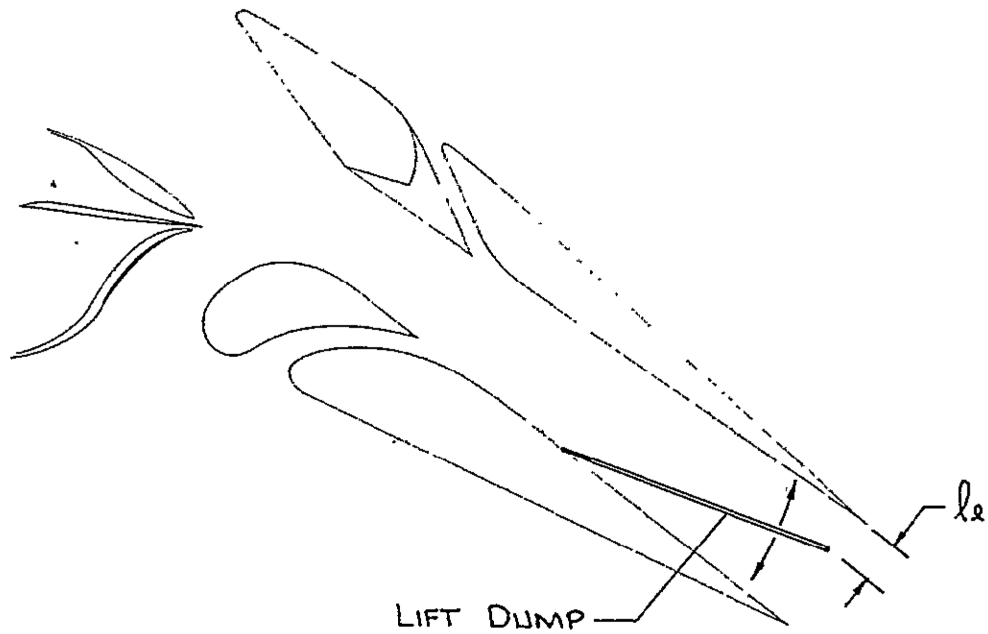

LIFT DUMP AS SIMULATED ON THE MODEL

In an attempt to make a direct performance comparison with the Ames wind tunnel, half-scale model (Reference [illegible]), 1 -inch long flap extensions (upper and lower) were installed and tested on our model with the flaps set at $\delta_f = 50°$; see Figure 19.

During the inboard simulation tests, a complete simulation of the airplane augmentor system was tested. In addition to the pylon struts, which replaced the turnbuckle linkage, Figures 20 and 21 show the simulated main support brackets, two intake door arms (bent and straight), and two small "bumps" on the Coanda surface which were fabricated and tested. The "bumps" on the Coanda flap represented protrusions on the airplane Coanda flap that were designed to cover cutouts in Coanda surface.

<u>Instrumentation</u>. Two total pressure probes at the outer duct entrance were used to sense the upper nozzle entrance pressure during the outboard simulation tests (Figure 7). The pressure ratio, measured here, was defined as

the "charging station" for the isentropic conditions used in the performance calculations. For the inboard simulation, a 12-probe rake at the other end of the outer duct was used for this purpose. The total pressure "charging station" selected for the lower nozzle was located upstream of the inner duct cascade turning vanes and consisted of an eight-probe total pressure rake. The selection of the "charging station" locations was based on consideration of airplane total pressure rake installation ease, airplane-model augmentor performance level correlation and ease of pressure measurement in areas of potentially lowest flow distortion.

During the "flaps off" tests, 12 single total pressure probes were installed in the exits of both upper and lower nozzles (Figure 22) evenly spaced across the span of the model. These probes were used to examine the nozzle exit spanwise pressure distribution.

Single P_T probes were also installed inside both ducts spaced at approximately 1/3 model span positions (Figure 7).

Both the inner and outer ducts were instrumented with 10 static pressure taps evenly distributed spanwise along the ducts and positioned in the forward part of the duct away from the nozzles (Figure 6).

A total of 176 static pressure taps were installed on the augmentor flaps. The static taps were distributed among three chord rows and two span rows as shown in Figures 23, 24, 25, and 26. The center chord row had a larger concentration of static taps than the upper and lower chord rows. The internal surfaces of the intake flap and the Coanda flap each were instrumented with a span row of static taps evenly spaced between the end plates at approximately

4 inch intervals. The full span hinged plate that represented the airplane "lift dump" was instrumented with 13 evenly spaced static taps at the model center chord on the "flow side" surface. The static taps on the flaps and on the lift dump were used to provide data for the flap loads and hinge moment analysis.

Figures 27 and 28 show the two manually adjustable total pressure rakes that were installed during the flap exit pressure surveys. Each rake consisted of 20 evenly spaced total pressure probes and were fitted to a sliding track to allow for setting the rakes at any model span position.

In order to examine the position of the nozzle jet sheet near the throat of the augmentor, a 12-probe total pressure rake was fitted to the model as shown in Figure 29 and tested at several model span positions. The probes were spaced 0.13 in. apart and during the tests involving this rake (termed the Coanda rake throughout this report), one probe was selected as a reference probe and positioned at the nozzle geometric centerline.

<u>Facility</u>. The 95-inch span augmentor flap model and platform type 6 component force balance with its support stand were set up at the Boeing north end nozzle test complex (Figure 30). The facility possessed the capability for independently measuring the two metered airflow supplies with a continuous air flow capacity of 10 lb/sec per line. The test control building housed a test control panel and a punch paper tape data system. The test data, recorded on punched paper tape, was reduced by the Boeing Mechanical Laboratories computer program #480.01 and processed by the Boeing SDS 92 computer.

Due to the height of the installed model and force balance and the requirements for measuring model noise data, the assembly was set up just outside the nozzle test complex building. In order to minimize the effects of inclement weather on the model, a canvas awning was installed over the installation. The vertically mounted test model was oriented such that the augmentor flaps directed the mixed flow away from the test complex building where acoustic microphones were set up at a 50-foot radius from the model (Figure 31).

Acoustic measurements were recorded at 10° intervals from the flap system centerline. The acoustic data is discussed in a following section of this report. The measured noise levels were not significantly affected by the buildings, equipment, ground cover, or air supply line noise.

The primary nozzle airflow rates were measured with Hersel type venturi flow meters. Prior to the test, the flow meters were calibrated against a standard nozzle which is the established flow measurement standard within the Boeing propulsion and wind tunnel laboratories. The calibrations resulted in making slight adjustments to the standard published ASME venturi flow coefficients and were incorporated in the computer program airflow calculation subroutine.

The static calibrations of the platform-type force balance demonstrated repeatability of $\pm$.25% of the model maximum thrust values. The force balance was fitted with a weather-tight covering and was kept at a constant temperature above ambient with electric heating elements.

All pressure transducers used during the test were installed in a temperature controlled oven to assure maximum pressure measurement accuracy.

Test Plan. Before the model was installed on the 6-component force balance, a check calibration of the balance was conducted. A complete calibration of the balance was not necessary, as this had been performed previously at the Boeing wind tunnel complex. The check calibration conducted at the test site consisted of loading all pertinent balance components from zero to the maximum expected load in increments. The loads were applied to the balance using a hydraulic actuator in series with a standard calibration load cell which was calibrated with calibrated weights that are traceable to the National Bureau of Standards. The bellows-flexure air supply lines (Figure [illegible]) that bridge the balance were pressurized in increments and any significant interactions that resulted were incorporated in the data reduction program. The interactions recorded on the lift and drag balance components at maximum supply line pressure were less than 0.1% of the maximum thrust produced by the model.

The model nozzle (outboard configuration), wing section, plenum, ducting and support frame were installed on the platform balance as an assembled unit and leveled with shims to set the nozzle exit in a vertical line (Figure 30).

The first configuration tested was the outboard nozzle with the flaps off as shown in Figure 33. During an attempt to operate the model under heated air conditions, an explosion occurred in the upper nozzle supply duct damaging the model severely. A thorough investigation of the incident resulted in the general conclusion that reignition of a residual volume of fuel-air mixture in the nozzle supply ducting occurred. The model was removed from the test site and sent to the shop for repair. After prompt repair and

reassembly of the nozzle, inspection of the hardware revealed evidence of some warpage in the repaired nozzle. This warpage can be described as a bow in the nozzle exit, as much as 0.3 inch across the span of the model. Correction of the warpage was not possible, and the model was then set up at the test site and prepared for testing using ambient temperature air only.

The test was divided into two major phases: the outboard simulation and the inboard simulation. For both simulations the nozzle was tested with the augmentor flaps on and flaps off. With the flaps off, nozzle performance (velocity coefficient and discharge coefficient) were determined for all three modes of nozzle operation: both nozzles (double), upper nozzle only, and lower nozzle only flowing. In order to determine the nozzle exit span-wise pressure distribution, twelve single total pressure probes were installed in an even distribution across the nozzle span in the exits of both upper and lower nozzles (Figure 22). During the outboard nozzle tests, some attempts were made to measure nozzle exit side flow angles locally behind the nozzle turning vanes by using a yaw probe.

When the augmentor flaps were initially set up for the outboard nozzle simulation, a large range of Coanda ℓ'_Z and Z movements were calibrated against a grid pointer system designed into the adjustable main flap support brackets. During the optimization tests this provided a quicker method for changing the flap settings than using measurements made at the Coanda flap each time.

The relative positions of the upper and lower flap assemblies were set with a specially made tool that provided for a constant fore and aft setting used

throughout the test and allowed for setting a wide range of throat spacings. The flap diffuser angle (θ_e) was set with another tool preset to the desired angle. Due to manufacturing tolerances in the long span model flap sections, some variation in the flap exit width (ℓ_e) across the span existed with the diffuser angle set equal at the two flap bracket stations ($\pm$.2"). An average ℓ_e was determined from several measurements taken along the span.

Surveys of the augmentor flap exit were conducted for several configurations during both outboard and inboard simulation tests (Figures 27 and 28). This was done by measuring flap exit total pressure using two 20-probe rakes connected to a bracket that was adjustable spanwise. Being a manually adjustable rake, a thorough survey of the augmentor exit was very time consuming so this data was only recorded at nozzle pressure ratios equal to 1.8 and 2.25 (estimated approach and takeoff power settings for the Modified C-8A).

After completion of the outboard simulation tests, the upper nozzle lip and associated turning vanes were replaced with another upper nozzle lip with turning vanes designed to turn the flow entering from the other end of the outer duct. At the same time, the tapered liner in the outer duct was removed and replaced with the constant section liner. This configuration, with the upper nozzle flow and lower nozzle flow entering from opposite ends of the model, represented the inboard simulation.

In order to provide "on line" calculations of model augmentation ratio, a manual calculation technique was used. This required the test facility operator to set the model conditions at prescribed pressure ratios, thus establishing the nozzle's thrust level. The augmentor performance could then be closely determined from the force balance outputs printed out on the raw

data tapes. The hand calculated values were usually within 1% of the computer calculated levels and provided an immediate evaluation of the relative performance levels of the various test configurations.

It was originally planned that during the inboard simulation tests (double and upper nozzle modes) the lower nozzle flow would be measured with a flow nozzle that was installed in the air plenum tank. The lower nozzle flow rates measured with this method were not repeatable and were quite different in absolute level from lower nozzle flow rates calculated during the outboard tests. There was insufficient time available to investigate and remedy this problem, but it is believed that the erratic flow measurements were caused by high flow distortion near the flow nozzle entrance in the plenum. It was therefore decided to set the lower nozzle flow rate for the inboard simulation (double and upper nozzle modes) equal to the lower nozzle flow rates established during the outboard tests, since the lower nozzle was not effectively altered during the configuration changeover. For all inboard tests, the upper nozzle flow rate was determined by subtracting the lower nozzle flow (from outboard data) or the "dump flow" from the total flow.

Most of the double nozzle ℓ'_Z - Z optimization tests along with the lift dump tests were conducted with the outboard simulation configuration. Some double nozzle Z optimization tests and all of the single nozzle Z optimization tests were conducted with the inboard simulation configuration. Table I on the next page summarizes the major configurations that were tested. Detail model definition and test data is contained in Reference 4 and computer tabulated data is contained in Reference 12.

TABLE I

SIMULATION	NOZZLE OPERATION MODE	OPTIMIZATION: Z	OPTIMIZATION: [illegible]/Z	NOZZLE RAKE SURVEY	FLAP EXIT SURVEY	ACOUSTIC DATA	LOADS DATA	LIFT DUMP TESTS	[illegible] S1, h/hN ▷1	S_L VARIATION	[illegible] FLAP GEOMETRY
OUTBOARD	DOUBLE	δf=30° 122-[illegible] 55 374-427 65° 279-[illegible] 75° [illegible]	δf=55° 152-22[illegible] 60° 374-427 65° 217-[illegible] 75° [illegible]	δf=30° 373-[illegible] δf=65° [illegible] 378	δf=30° 226-306 65° 349-[illegible]	▷1	δf=75°, 65°, 55°, 35°, 20°, 6° [illegible]-475	δf=30° 473-[illegible] δf=65° 507-[illegible]	δf=30° 74-151 256-247	δf=30° 248-[illegible] δf=65° 363-[illegible]	—
	UPPER	— ▷2	—	δf=30° 379-397 δf=65° 349-378	—	—	δf=75°, 65°, 50°, 35°, 20°, 6° 450-475	δf=30° 470-505 δf=65° 507-5[illegible]	—	—	—
	LOWER	—	—	δf=30° 379-387 δf=65° [illegible]-378	—	—	δf=75°, 65°, 50°, 35°, 20°, 6° 450-475	δf=30° 416-506 δf=65° 507-5[illegible]	—	—	—
INBOARD	DOUBLE	δf=30° 6[illegible]-627 δf=65° 6[illegible]-627 ▷3	—	[illegible] 6[illegible]-650 δf=30° [illegible] δf=65° [illegible]	δf=30° 657-[illegible] δf=65° [illegible]	FLAPS OFF 627	δf=30°, 65°, 6° 729-740	—	—	—	[illegible]
	UPPER	δf=30° 762-771 δf=65° 772-781	—	[illegible]	δf=30° 6[illegible] δf=65° [illegible]	—	—	—	—	—	—
	LOWER	δf=30° [illegible] δf=65° 683-[illegible]	—	[illegible] 610-[illegible] δf=30° 6[illegible] δf=65° [illegible]	δf=30° [illegible] δf=65° 5[illegible]	—	—	—	—	—	—

▷1 FLAPS OFF [illegible] δf=30° [illegible], 155, [illegible], 373, 476 δf=50° 271, 464, 411, 412, 218 δf=65° [illegible] δf=75° 455, 457

▷2 h/[illegible] OPTIMIZATION – SINGLE NOZZLE RUNS [δf=30° 267-270 δf=65° 341-344]

▷3 NOT A COMPLETE OPTIMIZATION – 650-657

Nozzle Performance

Velocity Coefficient. The nozzle performance characteristics, with the flaps off, were determined for both inboard and outboard simulations for the three nozzle operation modes (double, upper, and lower). Nozzle velocity coefficients and discharge coefficients for both simulations and all operation modes are presented on Figures 34 through 39. Peak velocity coefficient C_V for both inboard and outboard simulations is approximately 0.92 for double nozzle operation and is slightly lower for single nozzle operation. The small thrust losses under single nozzle operation were attributed to base drag effects at the exit of the non-operating nozzle. Several runs were conducted with the upper and lower nozzles operating at different pressure ratios. The plot on Figure 40 indicates that the double nozzle performance for equal and unequal pressure ratios is essentially the same. A comparison of the inboard and outboard nozzle performance levels shows agreement within one percent as shown on Figures 34 through 39.

Nozzle velocity coefficient, the nozzle efficiency parameter, reflects thrust losses compared to a fully expanded nozzle passing the same mass flow. The isentropic velocity used in the thrust calculation for the fully expanded nozzle is a function of the total pressure ratio measured at the station selected to assess or "charge" system thrust losses. It follows that the absolute performance levels of any thrust system are directly dependent on the "charging station" selected for the performance calculations. Figure 41 shows four levels of C_V calculated for four different stations in the model for the outboard simulation under double nozzle operation. It is essential that when comparing absolute performance levels between different models that definition of the specific "charging station" location is known.

Also shown on Figure 41 is the nozzle performance level measured during the Ames Phase I wind tunnel model test (Reference 2). The charging station used for the Ames wind tunnel model performance calculations can be best compared with the Boeing "duct average" charging station. A performance comparison between the two models shows that the Boeing nozzle is from 2% to 3% higher than the Ames wind tunnel nozzle performance. Using a semi-emperical method (Reference 5), which correlates peak nozzle velocity coefficient with a function of the hydraulic diameter at the nozzle throat, peak nozzle velocity coefficient for the Boeing 0.7 scale model slot nozzle was 0.93 as shown on Figure 41. This value was compared with the level based on the nozzle exit total pressure. The peak velocity coefficient calculated from the semi-emperical method is within 0.5% of the Boeing measured value.

Discharge Coefficient. Examination of the nozzle discharge coefficient (C_D) data for both inboard and outboard simulations shows a consistent difference between the lower and upper nozzle absolute levels as shown on Figures 34 through 37. These C_D level differences can be attributed to the difference in the lower and upper nozzle "charging stations" and the inability to accurately measure the exit area of the nozzle of this type. The C_D values under single nozzle operation for the outboard simulation were approximately 2% higher than the levels measured during double nozzle operation. This was believed to be due to deflection of the thin splitter (area change) during single nozzle testing with a slot nozzle of this type, since a 2% change in exit area can result from only a .003" deflection of the splitter at the nozzle throat. The slopes of the C_D curves consistently show a decrease in discharge coefficient with increasing pressure ratio. This is opposite the characteristic of a nozzle with vena contracta effects. The explanation for this phenomenon, at

least for the unchoked conditions, is based on the discharge coefficient in this case being applied to a duct-nozzle system. The ability of the slot nozzles to flow fully is controlled somewhat by the turning effectiveness as the flow enters the nozzles from the supply ducts. As the duct Mach number increases, the ability of the nozzle near the supply duct to flow effectively decreases. However, examination of the nozzle exit spanwise total pressure distribution data does not indicate this effect with increasing pressure ratio, but this data should not be considered conclusive due to the limited number of nozzle span positions examined.

Nozzle Exit Pressure Distribution. Nozzle exit spanwise total pressure distribution data for both inboard and outboard simulations and for both upper and lower nozzles are presented on Figures 42 and 43 . For the most part, the data shows that the nozzle exit spanwise pressure distribution is quite constant except for the nozzle areas near the duct entrance.

Nozzle Supply Duct Mach Number and Pressure Losses. The nozzle supply duct Mach number was measured at several positions in both the inner and outer ducts for both simulations. Plots showing the measured duct Mach number compared to the airplane design values (which included aileron airflow) for both simulations are shown in Figures 44 through 46. A Mach number plot for the inner duct inboard simulation is not enclosed as this configuration was the same as that simulated for the outboard. The measured values from the model test show close agreement with the design values. Figure 47 shows the magnitude of the system total pressure losses for both the upper nozzle (outer duct) and the lower nozzle (inner duct) as a function of pressure ratio.

NOZZLE FLOW ANGLES

Resultant vertical and side thrust angles were computed from the model lift, negative drag and side forces. The directions "vertical" and "side" refer to the orientation of the system as installed on the airplane. Plots of both nozzle vertical (Figures 48 through 55) and side thrust (Figures 56 through 63) angles versus nozzle pressure ratio for both inboard and outboard simulations are shown.

Vertical Flow Angles. If the nozzle thrust were acting along the nozzle splitter centerline which was set at 8° relative to the wing chord plane the vertical thrust angle would be 8°, as shown below.

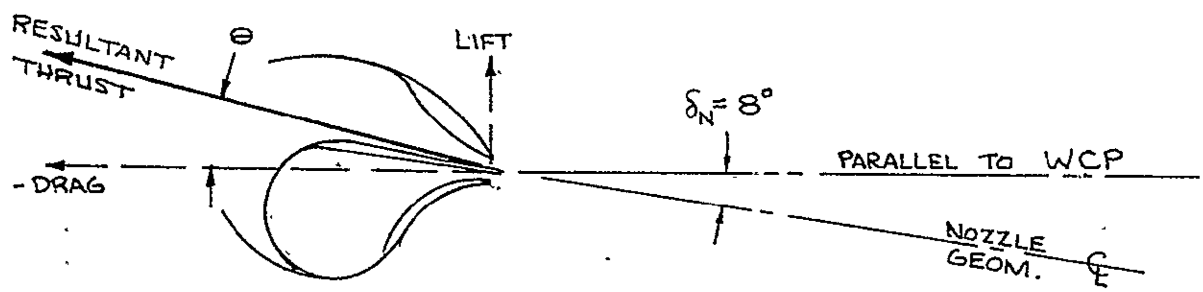

NOZZLE CENTERLINE GEOMETRY

Figures 48 and 49 summarize the variation of vertical thrust angle with pressure ratio. Under upper nozzle operation, the vertical thrust angle θ varied generally from 10° to 13.5° for both inboard and outboard simulations. θ varied from 6.5° to 9.5° for the double nozzle configuration. The vertical thrust angles produced by the lower nozzle demonstrated poor repeatability comparing the data from the inboard and outboard configurations shown on Figures 48 and ~~49~~ 50. For the inboard simulation, θ varied from 2° to 3° (Figure ~~49~~ 50) but varied from 5° to 8° for the outboard configuration (Figure 48). The data does consistently show that during single nozzle operation, the

flow bends in the direction of the non-operating nozzle (see sketch below) and with both streams flowing (double nozzle operation), the combined flow follows the splitter center line within $\pm 1°$. ~~as shown below~~.

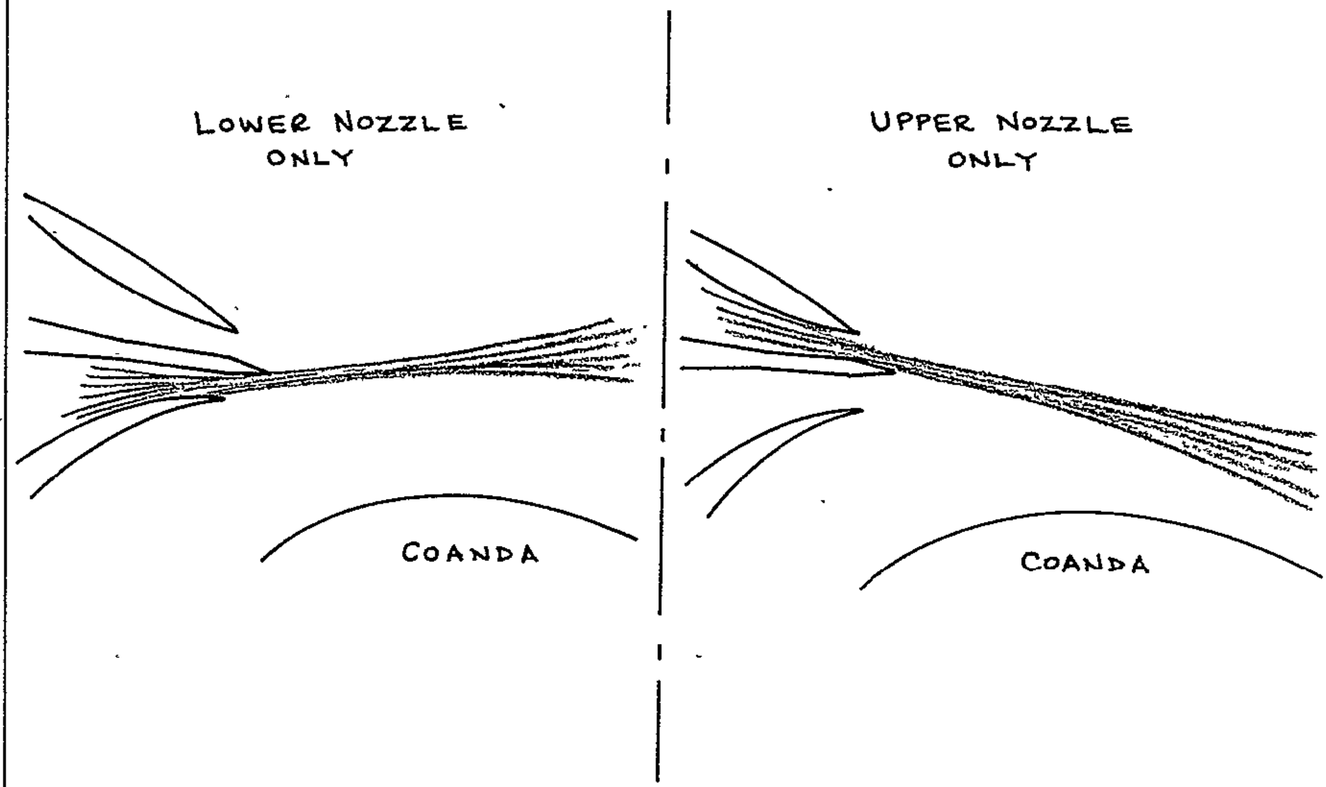

Jet Deflection - Single Nozzle Operation

The effects of these nozzle flow angle characteristics on augmentor performance are discussed in the section on Augmentor Performance.

<u>Side Flow Angles</u>. Figures 56 and 57 summarize the resultant side thrust angle data and provides an indication of the effectiveness of the nozzle turning vanes.

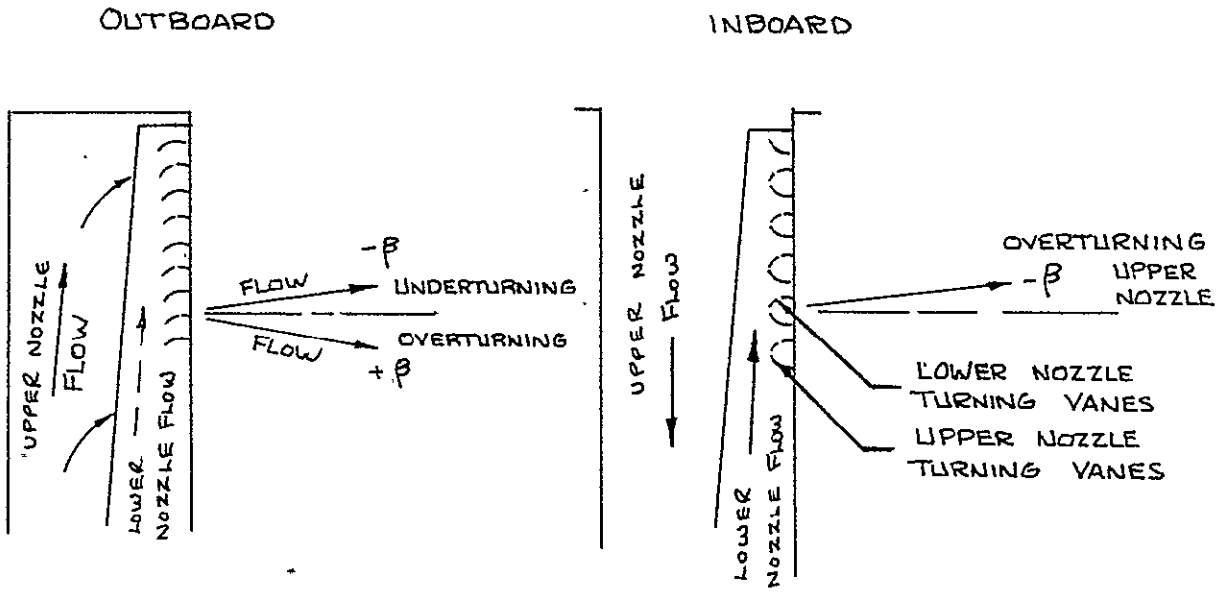

JET EXIT FLOW ANGLES

Under all modes of nozzle operation with the outboard simulation, the side thrust angles were positive (overturning) or close to zero. Overturning for the upper nozzle was approximately twice that of the lower nozzle and varied from 4° to 1.5° depending on the pressure ratio. Both nozzles operating together resulted in producing flow with very little overturning (Figure 56).

With the inboard simulation the lower nozzle and turning vanes, which were not changed, repeated approximately the same amounts of overturning as with the outboard simulation (Figures 56 and 57). The upper and double nozzle operation modes resulted in negative side thrust angles varying from -2° to -3° (Figure 57). The sketches above show the flow directions for both inboard and outboard simulation.

It appears that with the inboard simulation, the upper nozzle is dominant in influencing the double nozzle flow angles. The negative sign on the side thrust angles indicates overturning again with the upper nozzle system as occurred with the outboard simulation (Figure 57). The effects of flow overturning and the resulting cross flow on augmentor performance are discussed in the section on inboard augmentor performance.

Coanda Rake Survey. Several runs were conducted on the inboard simulation with the Coanda rake installed with the flaps off. Coanda rake pressure data was recorded at seven model span positions for all three modes of nozzle operation. Plots of the location of the peak pressure in the Z direction plotted relative to the geometric nozzle centerline at nozzle pressure ratios of 1.88 and 2.27 are enclosed on Figure 64. The data shows the deviations in the local flow direction across the span of the model. The flow from the lower nozzle operating alone is directed away from the Coanda flap and the flow from the upper nozzle operating alone bends toward the Coanda which agrees in trend with the nozzle vertical thrust data. The location of the peak pressure at $\ell_{1,Z}$ distance from the nozzle exit shows considerable deviation from the measured nozzle ℄ . It therefore must be concluded that these flow deviations are caused by local irregularities in the thin nozzle splitter. Plots of the Coanda rake total pressure profiles recorded at the seven span positions for the double nozzle configurations are enclosed on Figures 65 ~~and~~ thru 67.

Augmentor Performance - Outboard Simulation

Proper positioning of the four-element augmentor flaps with respect to the primary nozzle exit will greatly augment the nozzle thrust by proper mixing and diffusion of the primary and induced air systems. Thrust augmentation is also sensitive to the ratio of augmentor throat width (ℓ_T) to the primary nozzle exit height (h_N) and the augmentor flap diffuser angle (θ_e). Maximum thrust for an augmentor (ejector) with a fixed length will be attained when the induced flow is maximum and the mixing process progresses through the entire diffuser length without flow separation. Data from tests of an augmentor with similar flap geometry indicated that maximum augmentation for this model would be attained with the Coanda flap set relative to the nozzle exit at ℓ'_Z = 5.18" and Z = 1.85" with a flap deflection angle of 30°.

Effect of θ_e and ℓ_T/h_N. With the flap deflection angle δ_F set at 30°, the Coanda flap position set at nominal (ℓ'_Z = 5.18", Z = 1.85") and under double nozzle operation, variations in the basic augmentor variables were tested for augmentation performance. As the test progressed it was evident that these values of ℓ'_Z and Z were close to optimum for δ_F = 30°. Quite a large range of flap diffuser angles θ_e and ratios of augmentor throat height (ℓ_T) to nozzle exit height (h_N) were investigated. Figure 68 shows that a flap diffuser angle of θ_e of 4° produced the highest augmentation with a rather sharp drop in performance at θ_e = 3°. With the flap diffuser angle held at 4°, augmentor performance is essentially constant for throat to nozzle height ratios ℓ_T/h_N varying from 15 to 17 with a small thrust drop at ℓ_T/h_N = 13 as illustrated in Figure 69.

Effect of Intake Door Angle (θ_i) Position. Plots, showing the effect of varying the intake door angle θ_i on performance for $\delta_F = 30°$ and $65°$, are shown in Figures 70 and 71. Although the effects on performance are slight through the range of θ_i tested, peak augmentation was obtained at $\theta_i = -10°$ for both flap angles tested.

Coanda Flap Position (ℓ'_Z-Z) Optimization. Coanda position optimizations for both ℓ'_Z movements parallel to nozzle centerline and Z (movements perpendicular to the nozzle centerline) were conducted with the outboard simulation at $\delta_F = 30°, 50°, 65°$, and $75°$. Plots of augmentation ratio versus Coanda flap position at nozzle pressure ratios equal to 1.8 and 2.25 are enclosed on Figures 72 through 89. More complete optimizations were conducted at $\delta_F = 30°$ and $65°$ as these flap deflections were the airplane takeoff and approach flap settings, respectively. Summary plots of the ℓ'_Z-Z optimizations for all four flap deflections showing the peak performance position and % loss contours are enclosed on Figures 90 and 91. The data shows that augmentor performance is not sensitive to moderate movements in the ℓ'_Z direction but performance can be effected severely for relatively small movements in the Z direction. For some ℓ'_Z positions at the higher flap deflections $\delta_F = 65°$ and $75°$, performance decreases rapidly as the Z position is increased beyond a certain point (i.e. the Coanda surface is moved down relative to the nozzle) as shown on Figures 84 and 87. This is due to loss of nozzle jet flow attachment on the Coanda and main flap elements being more sensitive at the larger flow turning angles.

Several runs were conducted during the outboard simulation with the flap deflection angle at 30° and ℓ'_Z = 5.18 and Z = 1.85. Figure 92 shows the augmentation ratio versus nozzle pressure ratio for all of these runs and is an indication of the long term repeatability of the test facility. This data not only reflects the repeatability of the force balance and nozzle flow measurements but the ability to repeat the flap settings relative to the nozzle exit.

<u>Comparison with Theoretical Augementor Performance</u> . The bar chart below shows that the augmentor is very sensitive to inlet recovery loss. With augmentor flap skin friction, a 1-1/2% inlet recovery loss and a nozzle velocity coefficient of 0.92 included, the calculated performance shows excellent agreement with the measured value.

Reference 10 describes an analytical method of predicting ejector performance. This program was used to compute the performance for the 0.7 scale augmentor-flap model tested here. Augmentation ratio was calculated showing the effects of the various system losses and are presented below.

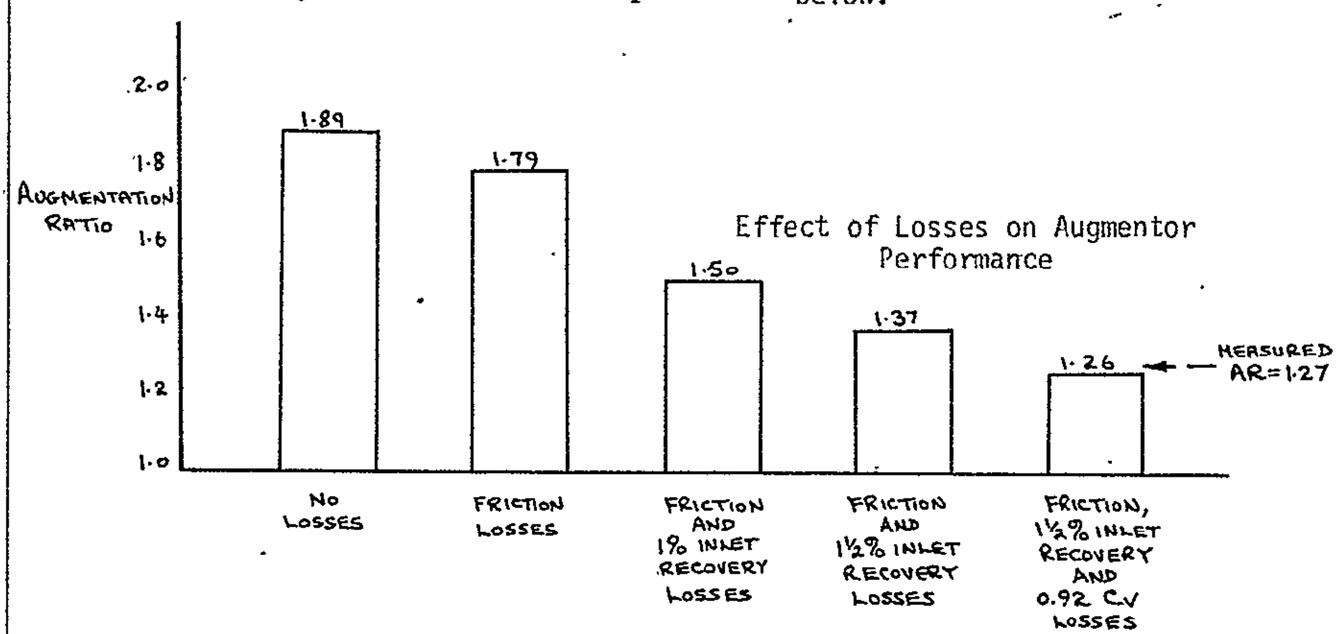

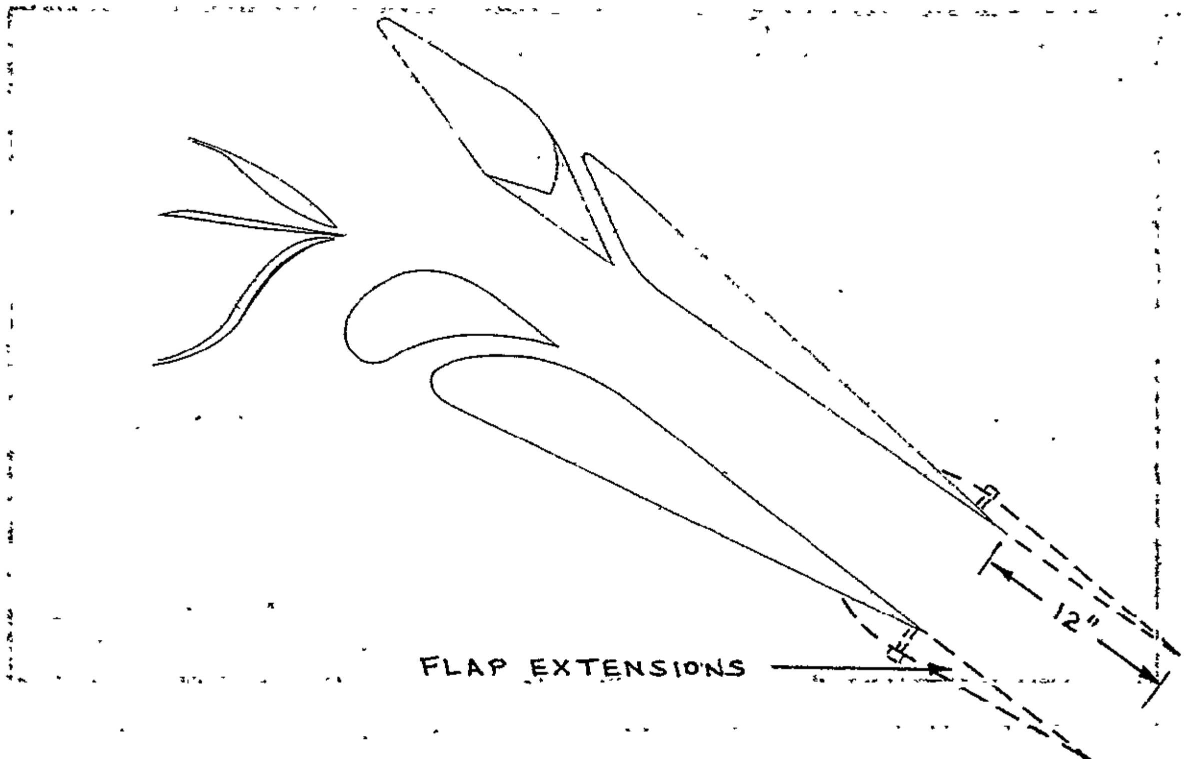

FLAP EXTENSIONS TESTED TO DUPLICATE AMES
PHASE IV TEST (Reference 2)

<u>Effect of Augmentor Flap Extensions</u>. In an attempt to obtain data for direct comparison with the Ames Phase IV wind tunnel test full span augmentor model (Reference 2), the augmentor flap was extended 12" as shown above and tested with a throat to nozzle height ratio of 12.4. With the flap deflection angle δ_F set at 50° and the ℓ_{1Z} position set at 4.46", a Z optimization was conducted. An increase of 0.03 in augmentation ratio was realized at a Z = 1.40" with the 12" flap extension. A plot of augmentation ratio versus Z for this configuration is enclosed on Figure 91. The peak augmentation values compare very closely with the Ames model static performance levels when the nozzle performance differences are accounted for. With the 12" flap extensions installed on the 0.7 scale model, a peak augmentation ratio of 1.28 was attained, whereas the Ames Phase IV model produced an augmentation ratio of 1.22.

Figure 41 shows a 3% difference in nozzle performance between the two models indicating that the augmentor pumping capabilities of the two are approximately the same.

Lift Dump Performance. The lift dump (augmentor choke) tests were conducted only with the outboard simulation at δ_F = 30° and 65°. Plots of augmentor performance for all nozzle operation modes with the lift dump installed are enclosed on Figures 94 and 95. Augmentation drops smoothly as the flap exit opening ℓ_e is reduced until finally a slight negative thrust is produced with the lift dump closing off the augmentor exit completely (ℓ_e = 0).

Single Nozzle Operation. Although ℓ'_Z-Z optimizations were not conducted for single nozzle operation with the outboard simulation, single nozzle performance was measured at δ_F = 30° and 65° (at optimum ℓ'_Z and Z from double nozzle tests). Plots showing the single nozzle performance versus nozzle pressure ratio are enclosed on Figures 96 and 97. Augmentation produced by the upper nozzle operating was somewhat higher than the double nozzle performance as was expected, but the lower nozzle augmentation was down significantly from the double nozzle performance. Both single nozzle performance levels should have been significantly higher than the double nozzle levels due to the geometric increase in both the throat to nozzle height ratio ℓ_T/h_N (area ratio) and augmentor length to nozzle height ratio (mixing length). Examination of the vertical thrust angle data (Figure 48) shows the large differences in nozzle jet direction between the three nozzle operation modes. The lower nozzle configuration in particular, directs the nozzle jet away from the Coanda flap as shown on the next page which results in poor lower nozzle augmentation without adjustments in the Z position. However, single nozzle "Z" optimizations were conducted.

with the inboard simulation and the performance levels attained are discussed in the section on inboard augmentor performance.

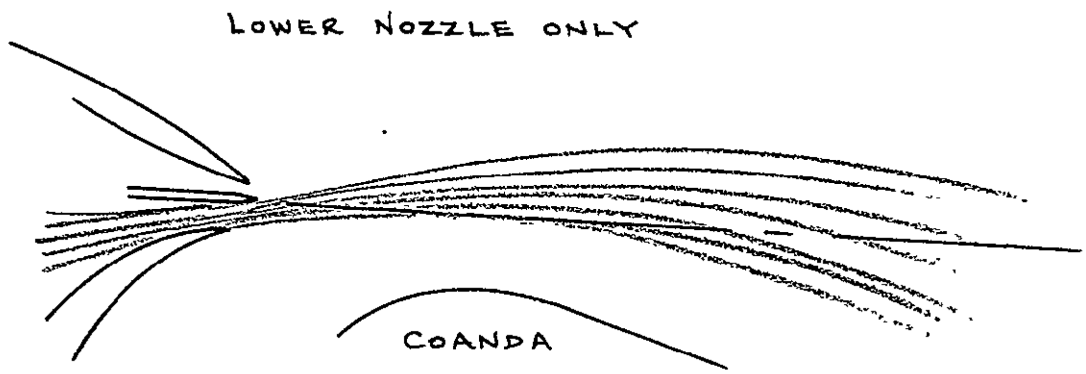

SINGLE NOZZLE OPERATION

Augmentation with Nozzles Operating at Unequal Pressure Ratios. A few double nozzle runs were conducted at $\delta_F = 30°$ and $65°$ with the lower nozzle operating at higher pressure ratio than the upper nozzle as will occur on the Modified C-8A aircraft. Figure 98 shows the performance levels compared to mean levels representing several runs from equal pressure ratio conditions. At $\delta_F = 30°$ the data shows a small drop in performance at the lower pressure ratios although the levels are very close to being within the scatter band of data from the numerous runs at equal pressure ratios. At $\delta_F = 65°$ the data scatter from the two unequal pressure ratio runs makes any comparison inconclusive.

Effect of Sealing End Plate Gaps. Due to an imperfection in the alignment of the model flaps and end plates, a small gap between the Coanda flap and the

AD 1546D

upper end plate existed, particularly at the higher flap deflections. Also, a 3/8 inch wide cutout existed in the Coanda flap leading edge at the two main flap support bracket statinns to allow for rotation of the flap assembly, Fig.14. Runs were conducted at each of the flap deflections δ_F = 30° and 50° with the upper end plate gap sealed and the Coanda flap cutouts filled in and faired smooth. Plots comparing the performance differences between the sealed and unsealed configurations at both flap deflections tested are enclosed on Figure 99. At δ_F - 30°, the end plate gap sealing and Coanda cut out fairing resulted in an apparent one point gain in augmentation, although the data is within the scatter band of data from all of the unsealed runs. No difference in performance was measured at δ_F = 50°.

Coanda Rake Total Pressure Data. During the outboard simulation tests, Coanda rake pressure data was recorded at 3 span positions at δ_F = 30° and 2 span positions at δ_F = 65°. The Z positions of the peak pressures recorded are plotted at each span position are shown on Figure 100. The data does indicate, for the center portion of the model, that center of the nozzle jet is not directed along geometric nozzle centerline but is bent towards the Coanda flap for both flap angles under double nozzle operation.

Flap Exit Surveys. During the outboard simulation tests, augmentor flap exit total pressure data was recorded at 5 inch intervals across the model span at δ_F = 30° and 65° under double nozzle operation. Figures 101 and 102 show the calculated flap exit augmentation at each span position for δ_F = 30° and 65° respectively. Although the average calculated flap exit augmentation (1.26 at δ_F = 30°, 1.29 at δ_F = 65°) agrees reasonably well with the augmentation measured with the balance (1.24 at δ_F = 30°, 1.25 at δ_F = 65°), the flap exit

survey data shows large variations in thrust across the model span. For each span location of low thrust a corresponding area of high thrust exists at adjacent span positions indicating that even though the thrust is low locally the augmentor develops good overall performance by momentum re-distribution.

The total pressure distribution between the flap and shroud trailing edges is illustrated in Figure 103. This illustration indicates that the flow is well attached to the lower flap, surface but is separated on the shroud in places.

Augmentor Flow Distribution. Using flap static pressure data and total measured augmentor thrust measured with both upper and lower nozzles operating at a pressure ratio of 2.25, an analysis was made to determine the approximate individual flow rates passing through the four augmentor flap inlets. The flow rate calculated for each passage was based on the measured differential pressure at the surface static tap and its adjacent geometric area. The following flow rates were calculated for the individual augmentor inlet passages:

BLC slot	7.86 lb/sec
Quaternary Slot	7.7 lb/sec
Tertiary Passage	30.8 lb/sec
Secondary Passage	37.1 lb/sec
TOTAL INDUCED FLOW	83.46 lb/sec
Plus Primary Flow	19.43 lb/sec
TOTAL AUGMENTOR FLOW	102.89 lb/sec

Based on the measured resultant augmentor thrust, the total augmentor airflow was calculated to be 93.8 lb/sec and compares reasonably well with the sum of the individual flow rates.

Coanda Flap Position (Z) Optimization (Double Nozzle). With the inboard simulation Z position optimizations were conducted for all three nozzle operation modes. The ℓ_{n} positions were selected as the optimum as determined from the outboard tests for each particular flap deflection. With double nozzle operation complete Z optimizations were conducted at $\delta_F = 30°$ and $65°$ and a partial optimization was done at $\delta_F = 6°$. Figures 104, 105 and 106 show the variation in double nozzle augmentor performance versus Z position. A complete optimization was not conducted at $\delta_F = 6°$ due to Z movement constraints on the model.

Inboard Performance Levels. The augmentation levels produced by the double nozzle inboard simulation are consistently lower (2 to 4 points) than the levels measured during the outboard simulation tests (compare Figure 104 with 74 and Figure 105 with 84). Examination of the resultant side thrust data from the flaps off tests reveals that the flow is being overturned for both upper and lower nozzle for both inboard and outboard simulations. The result is that with the inboard simulation some crossflow of the two nozzle streams exists in the mixing zones of the augmentor (ejector) and is a possible explanation for the inboard performance loss. This explanation is somewhat inconclusive after comparing the single nozzle augmentation levels between the inboard and outboard simulations. The upper and lower nozzle Z optimization plots for the inboard simulation ($\delta_F = 30°$ and $65°$) are presented on Figures 107, 108, 109 and 110 respectively. Comparison of this data with the single nozzle performance (outboard) presented in Figures 96 and 97 reveals that the lower nozzle

(inboard and outboard) performance shows good agreement but the upper nozzle (outboard simulation) augmentation is approximately four points higher than measured during the inboard tests at a comparative Z position for $\delta_F = 30^\circ$. The reason for this is not clear as this performance difference did not occur at $\delta_F = 65^\circ$ (Figures 97 and 103). During all inboard simulation tests (double nozzle), the upper nozzle operated at a higher pressure ratio than the lower nozzle due to the model ducting arrangement. This might account for some of the augmentation loss with the inboard simulation. The effect on performance with the upper nozzle operating at a higher pressure than the lower nozzle was not investigated. As a result of the upper nozzle turning vanes consistently over-turning the flow, the exit turning vane angle for the airplane design was reduced from 1[illegible]° to 14½°.

<u>Vibration Effects of Intake Door Position at Flaps Up ($\delta_F = 6^\circ$).</u> During performance runs, with the flaps up ($\delta_F = 6^\circ$) and the intake door angle (θ_i) set at -20°, the model emitted a strong low frequency sound with attendant vibration.

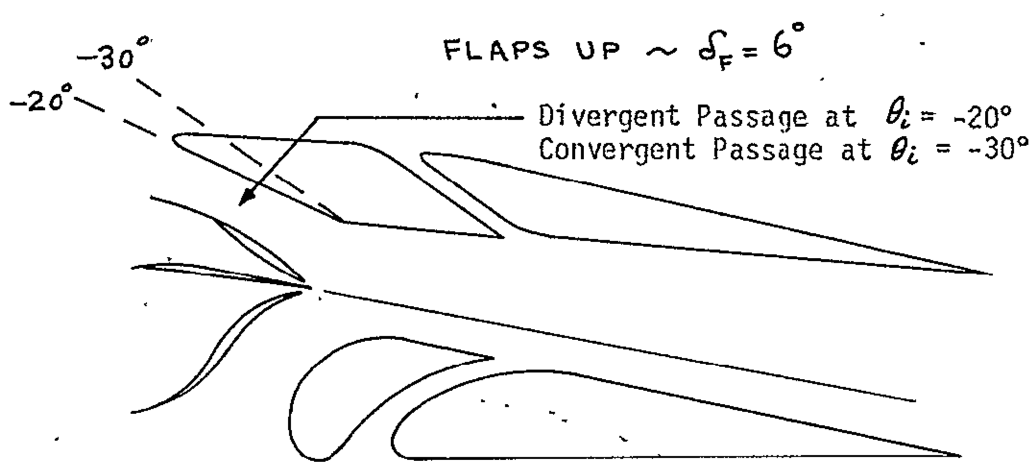

INTAKE DOOR GEOMETRY

Examination of the passage between the intake door and the upper nozzle external contour indicated the existance of a slightly divergent passage (see sketch on previous page). Based on the presumption that this might cause flow instability and result in low frequency vibration, the intake was opened in increments to a maximum attainable opening of -30°. The low frequency noise and vibration were completely eliminated only when the intake was opened fully to -30°. Inspection of the model revealed that with the intake door at 30°, the intake passage was slightly convergent, supporting the conclusion that the vibration was caused by the divergent passage. To minimize the possibility of this vibration occurring on the airplane and resulting in potential structural fatigue, the intake door angle for the airplane was opened up from -26° to -30° at the flaps up position.

Effects of Simulated Airplane Flap Support Bracketry. While the inboard simulation tests were being conducted, designs of the airplane augmentor flap support bracketry were finalized. In order to determine the effects the airplane flap support hardware might have on the model augmentor performance, scaled simulations of the airplane flap brackets were fabricated and installed on the model in a series of configurations. The adjustable turn-buckle links, connecting the upper and lower augmentor flap elements, were removed and replaced with pylon type support struts (Figure 15). Performance tests were conducted with the pylon struts installed at δ_F = 6°, 30° and 65°. No difference in augmentation was realized at δ_F = 6°, but at the higher turning angles (flap deflections), δ_F = 30° and 65°, significant gains in performance were attained. Plots of augmentation versus nozzle pressure ratio for δ_F = 6°, 30° and 65° are presented on Figures 111, 112 and 113 respectively. The increase in augmentation at δ_F = 30° and 65° is believed mainly due to the

AD 1546D

REV SYM

removal of the turnbuckle links from the throat of the augmentor being replaced with the pylon struts located further back in the diffuser section, as shown in the sketch below. The pylon struts were also much "cleaner" aerodynamically than the adjustable links, and are much less likely to cause separation within the augmentor.

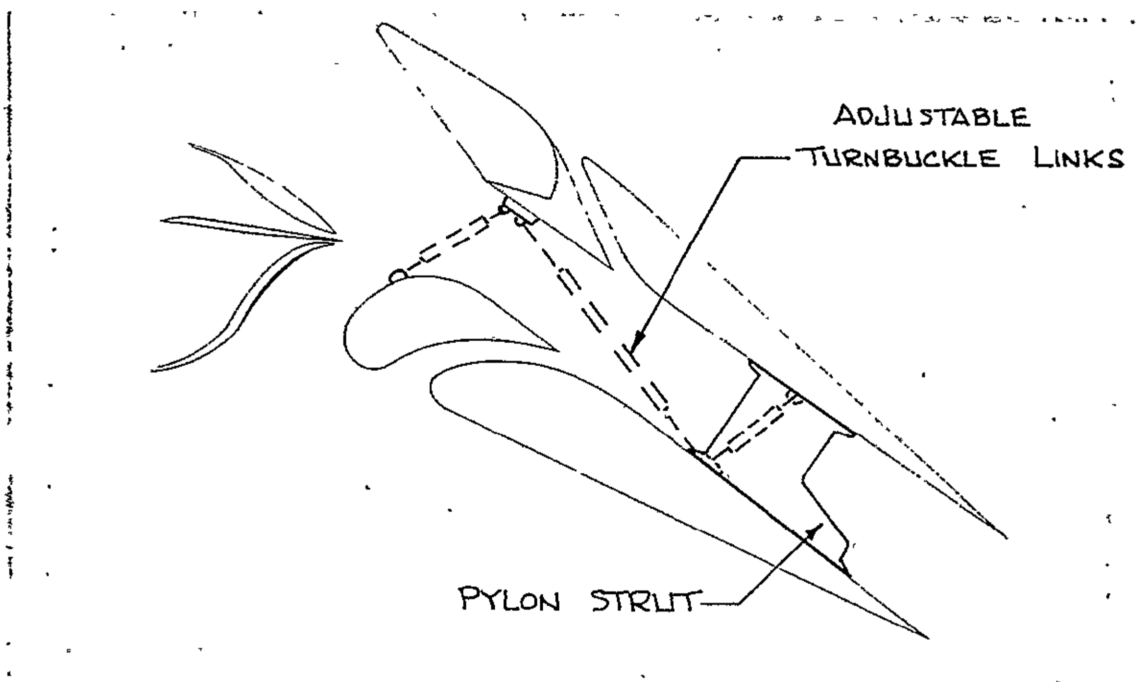

COMPARISON OF TURNBUCKLES AND PYLON STRUTS

With the pylon struts installed, the remainder of the flap bracketry simulating the current airplane design was added to the model. This included an 0.8 inch wide spanwise plug fitted in the exits of both nozzles at both flap bracket stations which represented the area blockage that

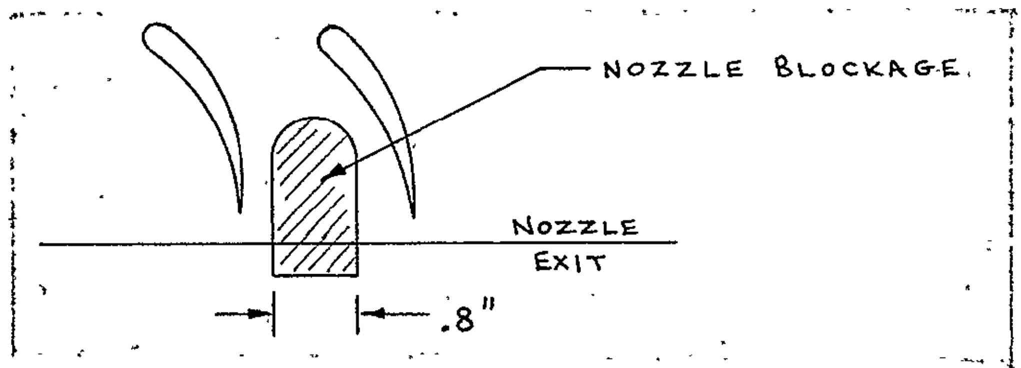

NOZZLE BLOCKAGE GEOMETRY

would result from structural supports in the airplane nozzle design as shown in the sketch above. Nozzle only performance was measured with the nozzle blockage installed. No loss in velocity coefficient was measured (Figure 37).

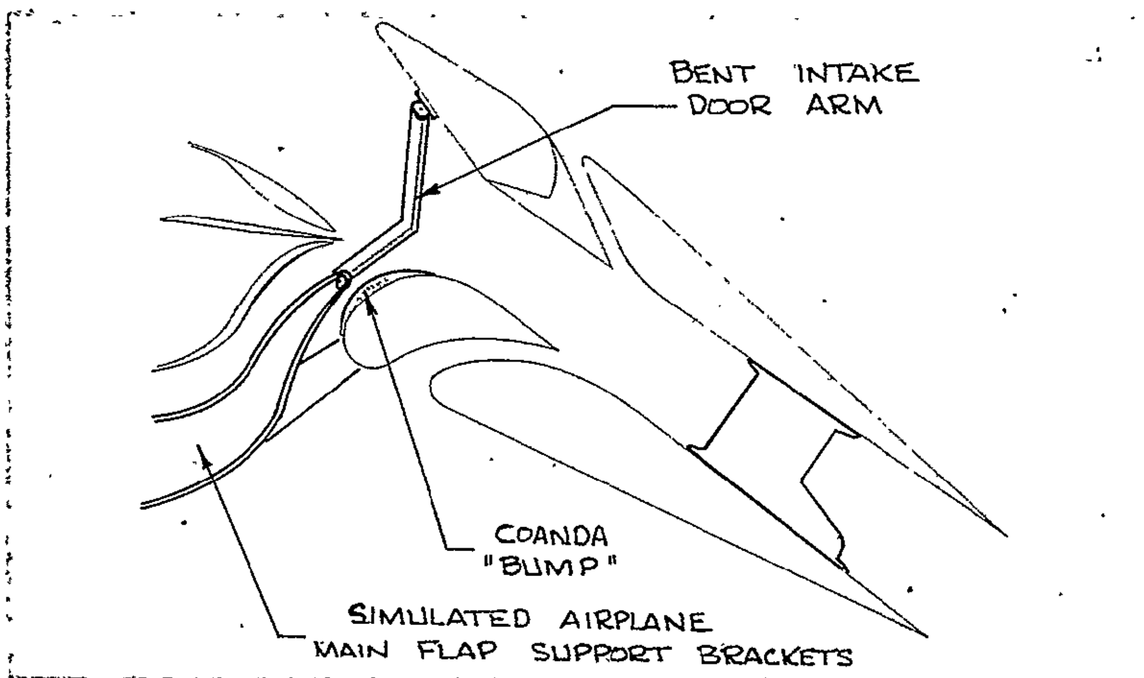

BENT INTAKE DOOR ARM CONFIGURATION

The airplane configuration also included a bent intake door arm and local protrusions ("Coanda bumps") on the upper surface of the Coanda flap at the flap bracket stations that were designed to cover cutouts in the flap necessary for actuator linkage as shown in the above sketch and in Figure 20.

The complete airplane simulation was then tested at δ_F = 0°, 30° and 65°. No difference in performance was measured at δ_F = 30°, a small loss was realized

AD 1546D

at $\delta_F = 6^\circ$ (flaps up) but a significant performance drop was recorded at $\delta_F = 65^\circ$. (Refer to Figures 114, 115, and 116). Due to the motion of the intake arm as the flaps are rotated, the "elbow" of the bent arm moved near the throat of the augmentor at $\delta_F = 65^\circ$. Based on the assumption that this caused the significant reduction in augmentation at $\delta_F = 65^\circ$, the configuration was tested again except with the bent intake door arm removed. Figure 117 shows that the performance is back to the level measured with only pylon struts installed. With the flap deflection still at 65° a straight intake door arm was installed on the model and tested, as shown in the sketch below.

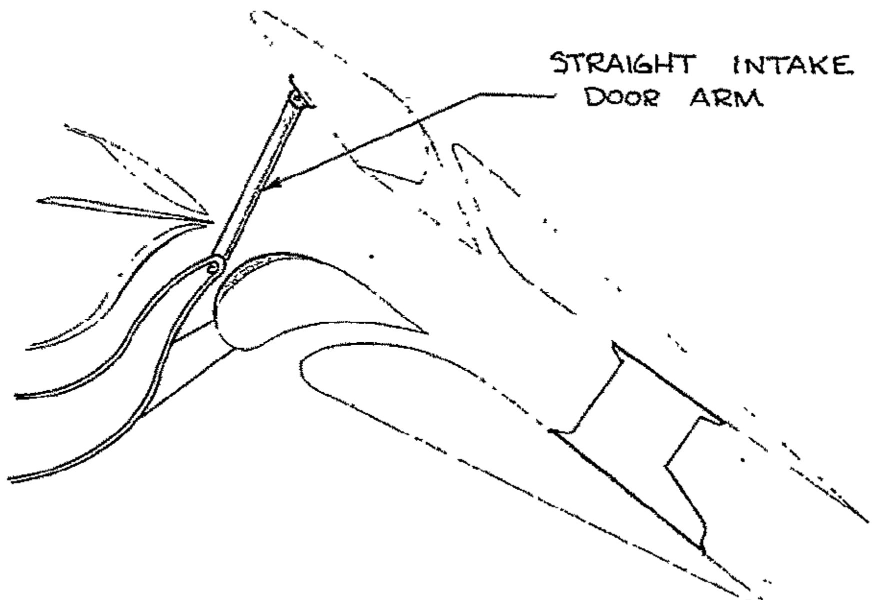

STRAIGHT INTAKE DOOR ARM CONFIGURATION

No loss in augmentation was measured with the straight arm installed as shown in Figure 118, supporting the assumption that the augmentor throat must be "clean" across the entire span of the augmentor for maximum performance. As a result of these data, the straight intake door arm was incorporated in the airplane design.

Effect of Blocking Off Quaternary Slot. In order to determine the effect of the quaternary slot on static augmentation, the slot was taped shut and performance measured at $\delta_F = 30°$. Figure 119 shows that with the slot area blocked and without compensating for the area reduction by adjustments in the other intake passages, a two point loss in augmentation resulted.

Effect of Closing Intake at Flaps Up ($\delta_F = 6°$). It was also of interest to measure the augmentor performance with the intake door fully closed ($\theta_i = 0$) in the event of this occurrance in flight with flaps up ($\delta_F = 6°$). Figure 120 shows the drastic reduction in static augmentation that resulted (augmentation ratio = 0.75). This thrust level, which is even below the flaps off performance ($C_V = .92$), is reasonable to expect with the severe base drag forces occurring in the augmentor with the intake door closed.

Effect of Upper Flap Intake Bellmouths. The entire test was conducted with the intake bellmouths installed on the leading edges of the intake flap and shroud to eliminate the possibility of flow separation during static conditions (Figure 3). Two runs were conducted with the bellmouth entries removed with the flap deflection set at 30°. Figure 121 shows essentially that no change in performance resulted from the bellmouths removed.

Coanda Rake Total Pressure Data. Peak pressure values from the Coanda rake surveys plotted versus model span recorded at $\delta_F = 30°$ and 65° for all nozzle operation modes are presented on Figures 122, 123, and 124 The warpage in the slot nozzles and splitters results in a variation in the Z location of the peak pressure near the augmentor throat of $\pm.25$ inch across the span of the model. The flow is directed away from the Coanda flap with the lower nozzle

flowing and bends toward the Coanda flap with the upper nozzle flowing. For double nozzle operation a pressure ratio of 2.25 (airplane takeoff), the average (arithmetic) peak Z position of the nozzle flow across the model span was 1.66 inch at $\delta_F = 30°$ compared to the geometric Z of 1.35 inch and 1.55 inch at $\delta_F = 65°$ (Z geom. = 1.40 inch). This indicates that the augmentor bends the nozzle flow towards the Coanda surface.

<u>Augmentor Flap Exit Surveys</u>. More thorough pressure surveys of the augmentor exit were conducted during the inboard simulation than during the outboard simulation. Flap exit pressure data was recorded at 2 inch span intervals for $\delta_F = 30°$ and 65° at all three modes of nozzle operation. Presented in Figure 125 is the calculated flap augmentation ratio plotted versus model span for the inboard simulation with the flap deflection angle at 30° and both nozzles operating. The data shows considerable thrust variation across the model span as occurred with the outboard flap exit surveys (Figures 101 and 102), but the average of the calculated augmentation values (1.0[illegible]) is considerably lower than that measured with the force balance (1.2[illegible]). This poor correlation of the calculated and measured augmentation is most likely due to moisture accumulation in the flap exit pressure probes which would cause erroneous pressure measurements. Based on this data, it appears doubtful that accurate airplane augmentor performance can be determined by this method in inclement weather conditions.

<u>Augmentation Ratio at $\delta_F = 20°$, 50° and 75°</u>. Double nozzle augmentation versus nozzle pressure ratio plots for $\delta_F = 20°$, 50° and 75° are presented on Figures 126, 127, 128 and 129. The inboard simulation performance levels are lower than those measured with the outboard simulation at these flap deflections. The reason is believed to be due to the crossflow in the augmentor mixing zones.

<u>Coanda Flap Pivot Point Selection.</u> The single nozzle Z optimizations were conducted in order to provide data in consideration of "engine out" performance in selecting the airplane flap pivot point position in relation to the nozzle. Figure 130 presents augmentation ratio versus Z position for all three modes of nozzle operation at δ_F = 30° and 65°. Maximum performance is developed at a different Z position for each nozzle operation mode. In order to maintain high augmentation during single nozzle operation (engine out) slight loss in performance for the double nozzle condition (two engines) was accepted. A "best compromise" in performance between double nozzle and single nozzle Z position was selected from this summary plot. The target Z positions were selected as Z = 1.75" model scale at δ_F = 30° and 1.30" model scale at δ_F = 65°. Because some of the configurations were not tested with the pylon strut support struts installed, all levels on Figure 130 are corrected for the pylon strut installation where necessary. Figure 131 shows the path of $\ell_{'Z}$ and Z as a function of flap deflection that resulted from the final airplane pivot point selection. Data from the complete $\ell_{'Z}$-Z optimizations conducted during the outboard simulation (Figures 90 and 91) showed the performance effects of being off optimum $\ell_{'Z}$ and Z. A 2% loss boundary is shown on both ℓ'_Z and Z variations versus flap deflection.

<u>Estimated Airplane Augmentor Performance.</u> Figure 132 shows the difference between the airplane augmentor performance (a fixed pivot point) and the optimum augmentor performance (varying pivot point). It can be seen that the airplane pivot point was selected to give optimum performance at a flap deflection of 50°, this giving the best compromise between the 30° (takeoff) and the 65° (approach) design points, and between the single and double nozzle operation performance levels.

Augmentor Flap Static Pressure Data

Introduction. Augmentor flap section pressure data from the 0.7 scale augmentor wing flap static test have been plotted and integrated to give section normal force coefficient, axial force coefficient, pitching moment coefficient about the leading edge of each element, and center of pressure, for the intake, shroud, Coanda, flap segment and choke. Section flap hinge moments were obtained by applying the section loadings of each element to the full scale Modified C-8A flap geometry. Static augmentor flap and choke hinge moments were determined for one flap segment of the full scale Modified C-8A. An equivalent dynamic pressure for the static test was derived and a comparison of element section loadings between the static test and the NASA-Ames Phase IV test was made.

Plotted Flap Static Pressure Data. The augmentor flap static pressure data have been plotted in the form of pressure coefficient (C_p) versus the non-dimensional position of the tap along the chord (X/C). A dynamic pressure of 1.0 psi has been used for C_p. Figures 133 through 137 identify the pertinent geometry, pressure tap locations, pressure data quality and interpolation and extrapolation instructions for the center chord flap elements. The five elements are the intake, shroud, Coanda, flap and augmentor choke. Figures 138 through 167 present sample plotted data for the outboard flap simulation, dual and upper nozzle operation, flaps 30° with a choke deflection of 19°, for a range of nozzle pressure ratios from 1.1 to 2.5.

Integrated Flap Static Pressure Data. The pressure coefficient curves are given in Figures 138 through 167 and the tabulated section coefficients resulting from the integration of this data is contained in Reference 13. In addition, the

pressure coefficients and corresponding X/C values used in the integration are tabulated as well.

Augmentor Flap and Choke Static Hinge Moments

Flap Section Hinge Moments. The Modified C-8A augmentor flap section hinge moments were obtained by applying the element section loadings obtained from integrating the center section pressure data. These section loadings were applied to the full scale augmentor flap geometry. The hinge moment about the Modified C-8A flap pivot was obtained by transferring the loading from the leading edge of each element of the augmentor flap using the following equation. (See Figure 168 for definitions and sign conventions).

$$M_{PIVOT} = \sum_{i=1}^{4} (C_{M_{L.E.}})_i \, q \, (C_i)^2$$

$$+ \sum_{i=1}^{4} (C_{N_i} \cdot q \cdot C_i)(X_i \cos\phi_i + Z_{pi} \sin\phi_i)$$

$$+ \sum_{i=1}^{4} (C_{A_i} \cdot q \cdot C_i)(Z_{pi} \cos\phi_i - X_i \sin\phi_i)$$

where $q = 1$ psi

i	Element
1	Intake
2	Shroud
3	Coanda
4	Flap Segment

$C_{M_{L.E._i}}$, C_{N_i} and C_{A_i} are element section values from the static test; C_i, X_i, Z_{pi} and ϕ_i are full scale Modified C-8A values. Modified C-8A values of C_i,

X_i, Z_{pi} and ϕ_i for flaps 6°, 20°, 30°, 50°, 65° and 75° are given in Table II (page 77). Sample section hinge moments for the integrated pressure data are given in Figure 169.

Flap Static Hinge Moments for One Flap Segment. The hinge moments of one flap segment of the Modified C-8A were based on the center section pressure data from the static test. It was assumed that the center section characteristics were applicable to the entire flap span. Considering the spanwise non-uniformity of the augmentor flap flow, this assumption is not strictly true, but is not greatly in error.

Figure 170 presents the static hinge moments for one flap segment as a function of average nozzle pressure ratio for flaps 6°, 20°, 30°, 50°, 65° and 75°. These hinge moments are for the full scale Modified C-8A flap geometry, double nozzle operation, and with the choke in the faired position. In general, the flap hinge moments increase with an increase in nozzle pressure ratio. The flap hinge moments tend to increase with decreasing flap angle although the flaps 65° data do not fit this trend. Note that at low nozzle pressure ratios, flaps 65° has the largest hinge moments and that the flaps 50° and 75° hinge moments are very small. There is no obvious explanation for this result.

Figures 171 and 172 show the effect of augmentor choke operation on the flap hinge moments for flaps 30° and 65°, respectively. Figure 173 gives the relationship between percentage choke exit closure and choke deflection angle for the static test model. Initially, the flap hinge moments decrease as the choke is deflected from its faired position (0% closure). But as the choke is deflected past the 50% closure position the flap hinge moments increase, until at 100% closure they are about three times the level of the 0% closure position.

It is concluded that the largest flap hinge moments at zero forward speed would occur with the augmentor choke in the 100% closure position at the maximum nozzle pressure ratio.

Choke Hinge Moments for One Flap Segment. The choke hinge moments for one flap segment of the Modified C-8A were also based on the center section pressure data from the static test. Figures 174 and 175 present static choke hinge moments about the choke leading edge as a function of average nozzle pressure ratio for flaps 30° and 65°, respectively. Figures 176 and 177 show choke hinge moments about the 26.2% chord line of the choke which is the pivot point of the full scale choke. These hinge moments are for the full scale Modified C-8A geometry and double nozzle operation.

Examination of the figures show that the choke hinge moments with the choke faired (0% closure) are positive, but become negative for choke closures greater than about 18%. The choke hinge moments are seen to be a direct function of choke closure at a given nozzle pressure ratio. The choke hinge moments at flaps 30° are larger than those at flaps 65°. Also, the hinge moments about the 26.2% chord line are only about one-third of the values for the leading edge.

Derivation of Equivalent Dynamic Pressure for the Static Test. The NASA-Ames wind tunnel force and moment data have been applied to the Modified C-8A by assuming that, essentially, the lift coefficient, drag coefficient and pitching moment coefficient produced at a given value of augmentor isentropic jet thrust coefficient are the same, wind tunnel model and Modified C-8A. Variations in isentropic jet thrust coefficient (C_{J_I}) for the NASA-Ames wind tunnel tests were obtained by varying the isentropic flap thrust while holding

the tunnel dynamic pressure constant; hence, the primary nozzle pressure ratio varied with C_{J_I}.

References 8 and 9 discuss propulsion scaling factors, and jet efflux and intake flow simulation. Reference 9 states that aerodynamic interference effects between the jet efflux and the mainstream flow past the airframe surfaces can be correlated non-dimensionally against a momentum-ratio or effective speed ratio $\left(\sqrt{\rho_o V_o^{\,2}/\rho_J V_J^{\,2}} = V_{eff}\right)$

V_o and V_J are the relevant mainstream and jet velocities, while ρ_o and ρ_J are the corresponding densities. Equally well, a jet momentum coefficient ($C_J \equiv J/q_o S$) can be employed as the primary correlation parameter, where J represents the rate of ejection of momentum, q_o is the mainstream dynamic head and S is a planform area.

Now, C_J is related to the effective speed or velocity ratio by:

$$C_J = \frac{m_J V_J}{q_o \, S_{REF}} = \frac{\rho_J A_J V_J \cdot V_J}{\frac{1}{2} \rho_o V_o^{\,2} \cdot S_{REF}}$$

$$C_J = \frac{2A_J}{S_{REF}} \cdot \frac{1}{\dfrac{\rho_o V_o^{\,2}}{\rho_J V_J^{\,2}}} = \frac{2A_J}{S_{REF}} \cdot \frac{1}{V_{eff}^{\,2}}$$

Since the C_{J_I} of the NASA-Ames Phase IV model and the static test model are assumed to be the same, the preceeding equation implies that if the ratio $2A_J/S_{REF}$ is not the same then the effective velocity ratios will not be equal.

Now

	$\frac{2A_J}{S_{REF}}$
NASA-Ames Phase IV Model	0.00462
0.7 Scale Static Test Model	0.00340

AD 1546 D

REV SYM

73

$$(C_{J_I})_{\text{STATIC TEST}} = (C_{J_I})_{\text{PHASE IV}}$$

$$\frac{(V_{eff})_{\text{STATIC TEST}}}{(V_{eff})_{\text{PHASE IV}}} = \sqrt{\frac{\left(\frac{2A_J}{S_{REF}}\right)_{\text{STATIC TEST}}}{\left(\frac{2A_J}{S_{REF}}\right)_{\text{PHASE IV}}}}$$

$$\frac{(V_{eff})_{\text{STATIC TEST}}}{(V_{eff})_{\text{PHASE IV}}} = \sqrt{\frac{0.0034}{0.00462}} = \sqrt{0.735}$$

$$(V_{eff})_{\text{STATIC TEST}} = (0.858)\ (V_{eff})_{\text{PHASE IV}}$$

For the same nozzle pressure ratio:

$$(\rho_J V_J^2)_{\text{STATIC TEST}} = (\rho_J V_J^2)_{\text{PHASE IV}}$$

Hence:

$$\frac{(V_{eff})_{\text{STATIC TEST}}}{(V_{eff})_{\text{PHASE IV}}} = \sqrt{\frac{(\rho_o V_o^2)_{\text{STATIC TEST}}}{(\rho_o V_o^2)_{\text{PHASE IV}}}}$$

$$= \sqrt{\frac{(q_o)_{\text{STATIC TEST}}}{(q_o)_{\text{PHASE IV}}}}$$

or:

$$\left[(q_o)_{\text{STATIC TEST}}\right]_{\text{EQUIVALENT}} = (q_o)_{\text{PHASE IV}}\ (0.735)$$

$$\left[(q_o)_{\text{STATIC TEST}}\right]_{\text{EQUIVALENT}} = (8\ \text{PSF})(0.735) = 5.9\ \text{PSF}$$

Comparison of Static Test and NASA/Ames Phase IV Section Loadings. Augmentor flap section pressure data from the NASA/Ames Phase IV wind tunnel test have been plotted and integrated. However, flap pressure data were available for only two flap angles, $\delta_F = 50^\circ$ and 75°. It was anticipated that flap pressure data for Flaps 50° and 75°, as well as lower flap angles, would be available from the 0.7 scale static test. It was believed that by using proper scaling and correlation procedures that the Flap 50° and 75° static test pressure data could be "calibrated" using the NASA/Ames Phase IV pressure data. This "calibration" would permit extrapolation of the static test pressure data results for the lower flap angles to forward speed conditions.

The general approach taken was to determine an equivalent dynamic pressure for the static test and show that the slopes of the element (shroud, coanda and flap) section coefficients versus isentropic thrust coefficient (C_{J_I}) curves were the same as those of the NASA/Ames Phase IV test. The intake was not included as it was known that the static intake loads were not directly comparable to the loads at forward speed. C_{J_I} had been shown to be a good correlation parameter for the model loads in the NASA/Ames Phase I and Phase III wind tunnel tests. It was believed that the approach taken is valid since the loading on the augmentor flap is primarily a function of the primary nozzle thrust.

After the equivalent dynamic pressure (5.9 PSF) for the static test is determined, the integrated section pressure data can be converted to aerodynamic coefficient form. The isentropic nozzle thrust (which is a function of nozzle pressure ratio) can also be converted to isentropic thrust coefficient (C_{J_I}) using the equivalent dynamic pressure and scaled wing reference area.

Figure 178 presents C_{J_I} versus average nozzle pressure ratio for the static test model and for the NASA-Ames Phase IV model. C_{J_I} is based on the isentropic thrust equivalent to four flap segments and is for double nozzle operation.

Figures 179 through 190 present a comparison of static test and NASA-Ames Phase IV element section coefficients as a function of isentropic thrust coefficient for flaps 50° and 75°. For flaps 50° there is good agreement between the slopes of the static test and NASA-Ames Phase IV curves. Although the agreement in slopes for flaps 75° is not as good as that for flaps 50°, it is still a fairly reasonable agreement.

TABLE II

TRANSFER CONSTANTS FOR FINDING TOTAL MOMENT ABOUT FLAP PIVOT

Full Scale Modified C-8A Geometry*

δ_F (deg)	Section	X (in)	Z_P (in)	ϕ (deg)	C (in)
6	Intake	11.23	15.96	33	22
	Shroud	-2.94	13.67	10	37.3
	Coanda	4.27	-2.40	-22	13.6
	Flap	-2.08	-2.98	-2.5	36.15
20		7.84	17.4	42	
		-6.23	12.53	24	
		4.72	-1.24	-7	
		-1.28	-3.4	11.9	
30		5.6	17.68	46	
		-8.34	11.23	34	
		4.86	-0.42	2.4	
		-0.66	-3.6	21.9	
50		1.88	17.1	48	
		-11.63	7.78	54	
		4.70	1.27	22.4	
		0.58	-3.87	41.9	
65		-0.35	15.78	53	
		-13.28	4.45	69	
		4.23	2.44	37.4	
		1.57	-3.36	56.9	
75		-1.58	14.66	55	
		-13.82	2.1	79	
		3.73	3.15	47.4	
		2.05	-3.00	66.9	

Acoustic Data

Noise levels were recorded for several configurations simulating operations of the outboard section of the jet-augmentor flap system. Changes in the configuration parameters are listed in Figure 191 as a function of run number. One-third octave band spectra are presented in Figures 192 through 209 for the slot nozzle, 30° flap, 50° flap, 60° flap and 75° flap configurations as a function of pressure ratio and as a function of angle. The maximum perceived noise levels for each configuration as a function of pressure ratio are shown in Figure 210.

Observed in the analysis of the spectra are several constant and variable characteristics. Noise cenetered about the 63 cps one-third octave band is attributed to noise from the microphone system. The spectra exhibit a broad band distribution of energy between 800 and 5000 cps (see Figure 194 and 197). Spurious noise was observed several times throughout the test at the 250-315 cps one-third octave bands. It was determined that this noise came from the microphone and was subsequently eliminated by readjusting the diaphragm of the microphone. The spectra should continue to "fall-off" from 400-500 cps down to the noise floor of approximately 77.5 to 80 db at 50-200 cps. Descrete tones were generated (see Figures 198 and 203) and are considered to be a function of the position parameter Z (Figure 191). These tones are considered to be due to pressure disturbanced propagating through the quaternary slot (the opening between the lower surface of the Coanda and the flap). At several large flap angle configurations there was observed an increase in high frequency energy about the 12,500 cps one-third octave band (See Figures 201, 205 and 208). A narrow band frequency analysis of this high frequency energy is shown in Figure 204. This high frequency

energy is resolved into two components which correspond to the characteristic frequencies of each half of the double slot nozzle. Insufficient information is available to determine why some configurations reinforce the generation of pure tones. The use of the lift dump flap run 476 (Figure 195) caused no observable changes in the characteristics of the spectra.

Peak overall sound pressure levels and peak perceived noise levels were observed to occur approximately at 40° relative to the centerline of the slot nozzle. At a pressure ratio of 2.5, the noise levels of the jet-augmentor 50° flap configuration were approximately 1 PNdB above the estimates made prior to the test. These levels were observed to increase from 1 to 3.5 PNdB as the flap angle varied from the 50° position (see Figure 210). At lower pressure ratios, the noise level of the 30° flap configuration is consistently higher than the levels for the higher flap angles.

CONCLUSIONS

The 0.7 scale full span augmentor flap model which was tested has a very close representation of the system designed for the Modified C-8A airplane, including the nozzle supply ducts, nozzle contours, nozzle turning vanes, duct flow conditions, and augmentor flap geometry. The following summarizes the major conclusions that resulted from this test:

1. The maximum static augmentation ratio produced by the model was 1.39 (based on measured nozzle thrust) and 1.27 (based on nozzle isentropic thrust).

2. The 0.7 scale model developed approximately 4% higher thrust augmentation than the Ames Phase IV test model (Reference 3).

3. Maximum nozzle velocity coefficient attained was 0.92, at a pressure ratio of 2.5.

4. The model upper nozzle turning vanes overturned the flow 3.5° which resulted in changing the design of the airplane turning vanes by this amount.

5. Maximum static thrust augmentation was developed with an augmentor diffuser angle of 4° and an augmentor throat to nozzle height ratio of 15 to 17.

6. Static augmentation was not particularly sensitive to intake door position.

7. The ℓ_z-Z Coanda flap position optimizations demonstrated that model performance was 4 times more sensitive to flap movements in the Z direction than in the ℓ_z direction.

8. The lift dump system smoothly spoiled the augmentor thrust from maximum thrust to slightly negative thrust levels.

9. The augmentor performance was not sensitive to upper and lower nozzles operating at moderately unequal pressure ratios.

10. With an augmentor system exposed inclement weather conditions flap exit momentum surveys is not a reliable method for accurately determining augmentor thrust.

11. The noise levels of the jet-augmentor 50° flap configuration were approximately 1 PNdB above the estimate made prior to the test. The noise levels were observed to increase from 1 to 3.5 PNdB as the flap angle varied from the 50° position.

12. The passage between the intake door and the upper nozzle external surface should be convergent or parallel to provide vibration free operation.

13. The test established that a single flap pivot point could provide satisfactory performance for a large variation of δ_p, and a good compromise between single and double nozzle performance requirements.

14. The augmentor performance is significantly reduced by even small obstructions in the augmentor throat. A straight intake door arm was incorporated in the airplane design to preserve an unobstructed augmentor throat.

15. The addition of simulated airplane flap brackets to the test model did not measurably affect thrust augmentation.

16. Fairly good correlation between the Ames Phase IV (Reference 3) flap section loading and those scaled from the 0.7 scale model using the equivalent velocity method of Reference 8 was obtained.

REFERENCES

1. Whittley, D. C., "The Augmentor-Wing: A New Means of Engine Airframe Integration for STOL Aircraft". Fourth ICAS Conference, 1964.

2. Koenig, D. G., Corsiglia, V. R., Morelli, J. P., "Aerodynamic Characteristics of a Large Scale Model with an Unswept Wing and Augmented Jet Flap", NASA TN D-4610, 1968.

3. Cook, A. M., Aiken, T. N., "Low Speed Aerodynamic Characteristics of a Large Scale STOL Transport Model with an Augmented Jet Flap", NASA TM X-62017 Working Paper #251, 1971.

4. Laurent, J., "Static Tests on a 0.7 Scale Augmentor Wing Flap Suitable for Installation on the Modified C-8A Airplane - Model Description and Test Data", T6-5635, The Boeing Company.

5. Postlewaite, J. E., "Thrust Performance of Suppressor Nozzles" AIAA Journal of Aircraft, Volume 3 No. 66, June 1966.

6. Request for Proposal A-15713 (AC-21), March 6, 1970 NASA-Ames Research Center, Moffett Field, California.

7. Augmentor-Wing Jet Flap STOL Aircraft Application by Modification of an Existing Aircraft - Volume II Technical Proposal, The Boeing Company Commercial Airplane Group, April 1970.

8. Wood, M. N. and Howard, J. B. N., "The Development of Injector Units for Jet-Lift-Engine Simulation on Low Speed Tunnel Models", RAE Tech. Report, 65020, February 1965.

9. Williams, J. and Butler, S. F. J., "Further Developments in Low-Speed Wing-Tunnel Techniques for V/STOL and High-Lift Model Testing", RAE Tech Note No. AERO 2944, January 1964.

10. Yen-Ching Pao, "Parametric Study of Complete Mixing Cylindrical Air Ejector with Exit Diffuser", computer Program TEM-29, D6-8196, February 28, 1962.

11. Ballard, R. E., "Augmentor Wing Flap System Model Acoustic Test", Boeing Company Document D3-8398, 1970.

12. D. L. Harkonen, Static Test of a 0.7 Scale Augmentor Wing Flap for the Modified C-8A Airplane, D6-24934-1TN, The Boeing Company, April 1971, Volumes 1 through 5, Basic Tabulated Data.

13. F. L. Wright, Static Test of a 0.7 Scale Augmentor Wing Flap for the Modified C-8A Airplane, D6-24934-2TN, The Boeing Company, Section Coefficient Tabulated Data.

AD 1546 D

REV SYM

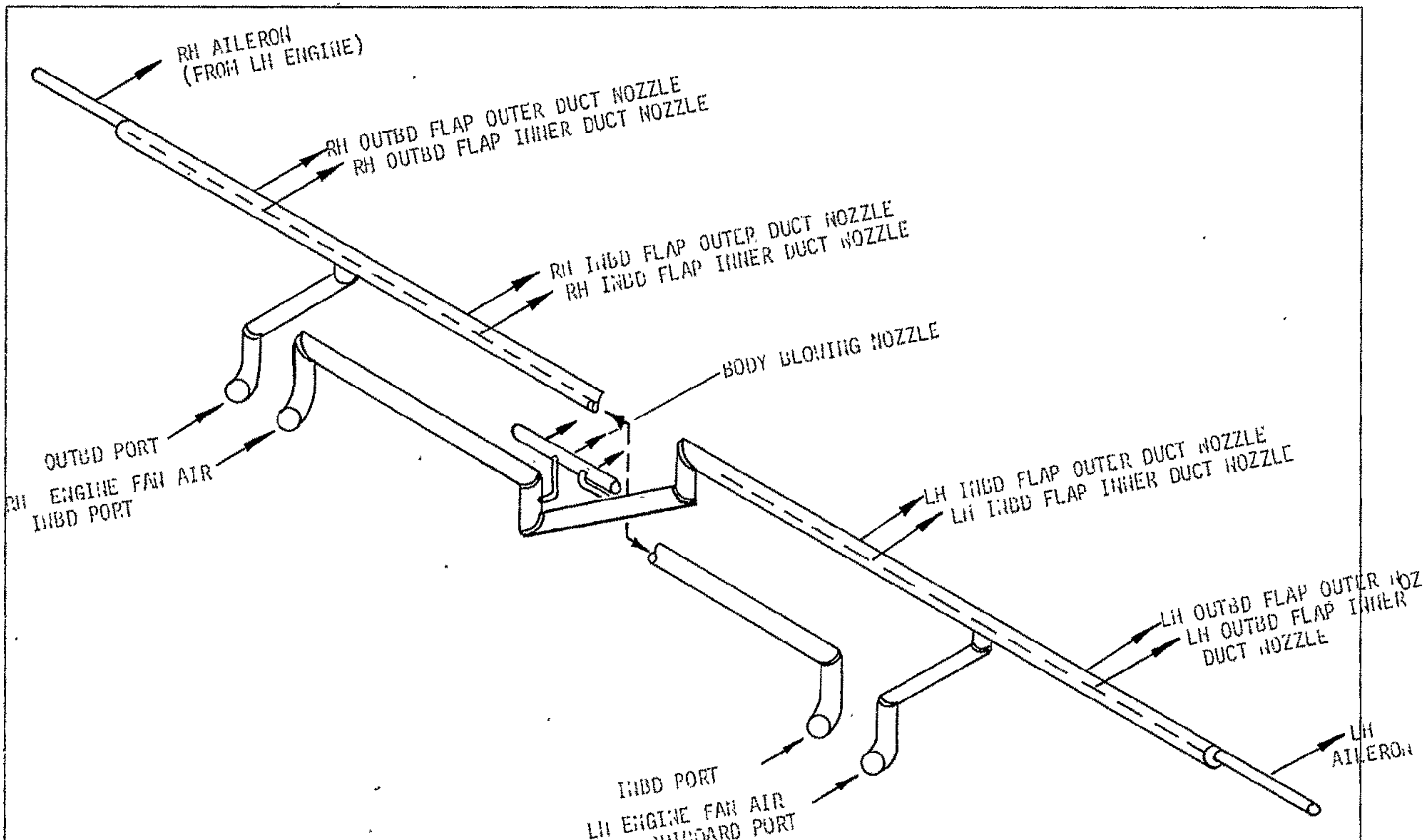

Fig. 2

AUGMENTOR/BLC DUCT SYSTEM SCHEMATIC

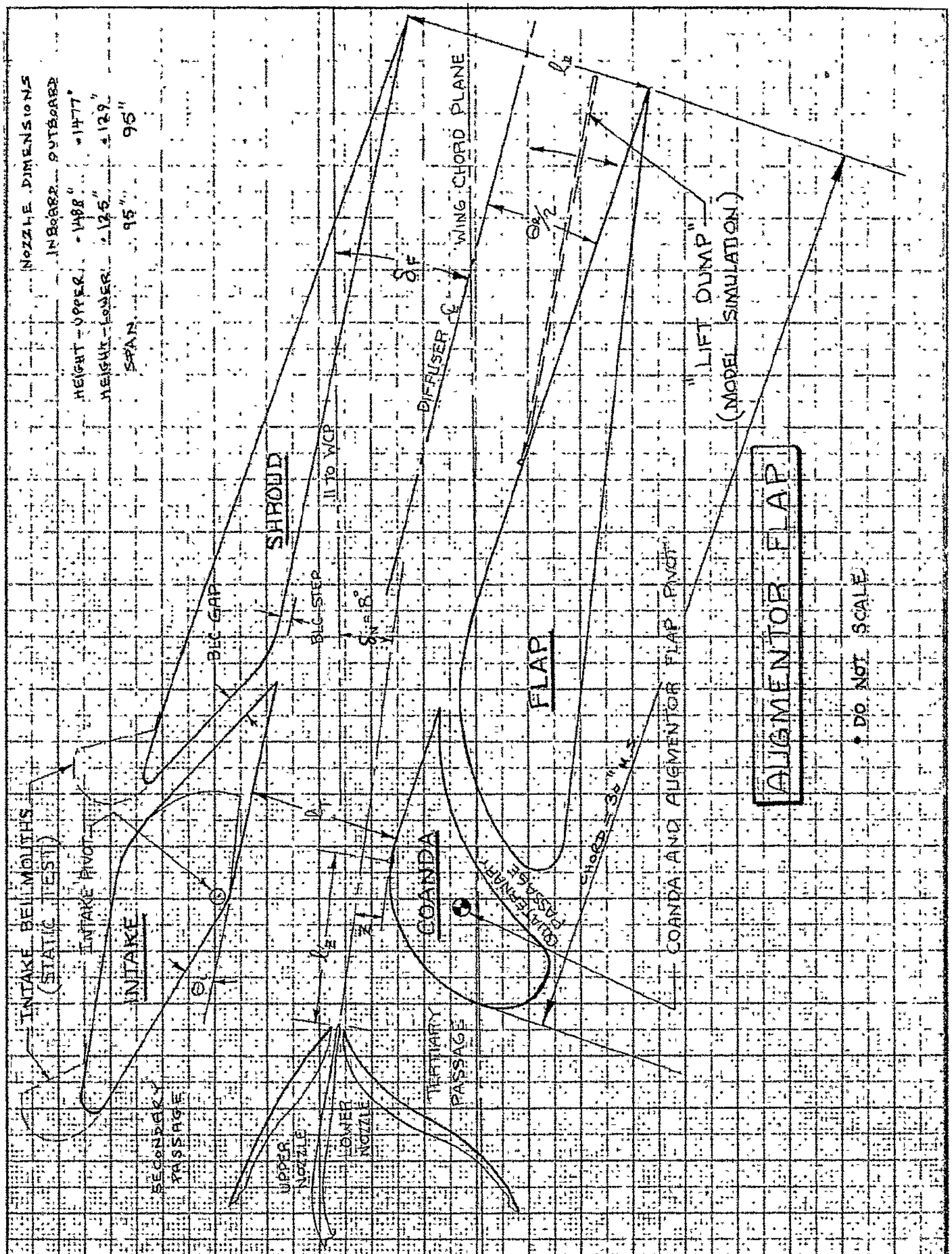

CALC			REVISED	DATE	AUGMENTOR FLAP MODEL NOMENCLATURE	FIG. 3
CHECK						
APR						D6-24850
APR					THE BOEING COMPANY	PAGE 85

5

K+E ALBANENE

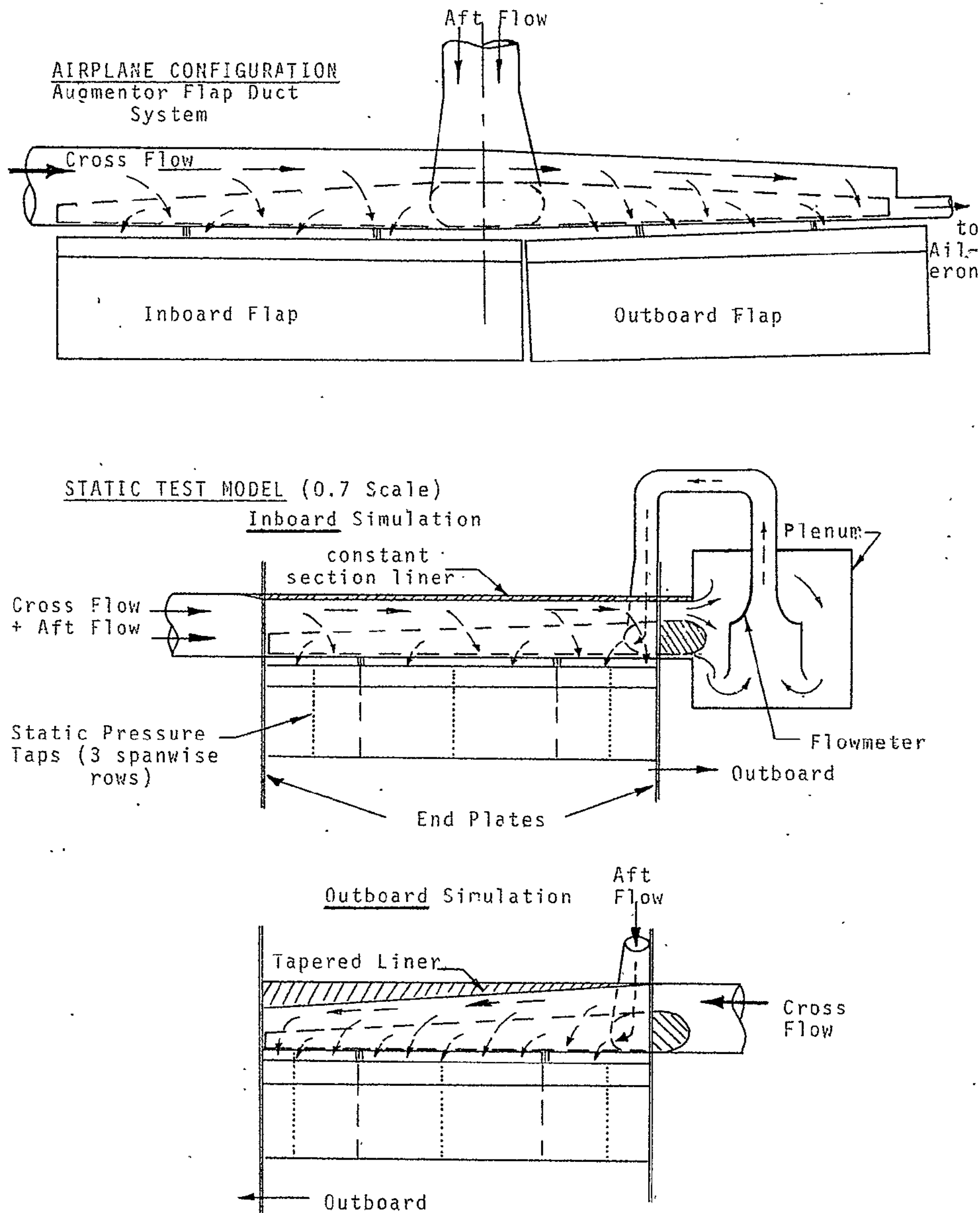

COMPARISON OF AIRPLANE AUGMENTOR FLAP SYSTEM WITH STATIC TEST MODEL SIMULATIONS	FIG. 4
	D6-24850
THE BOEING COMPANY	PAGE 86

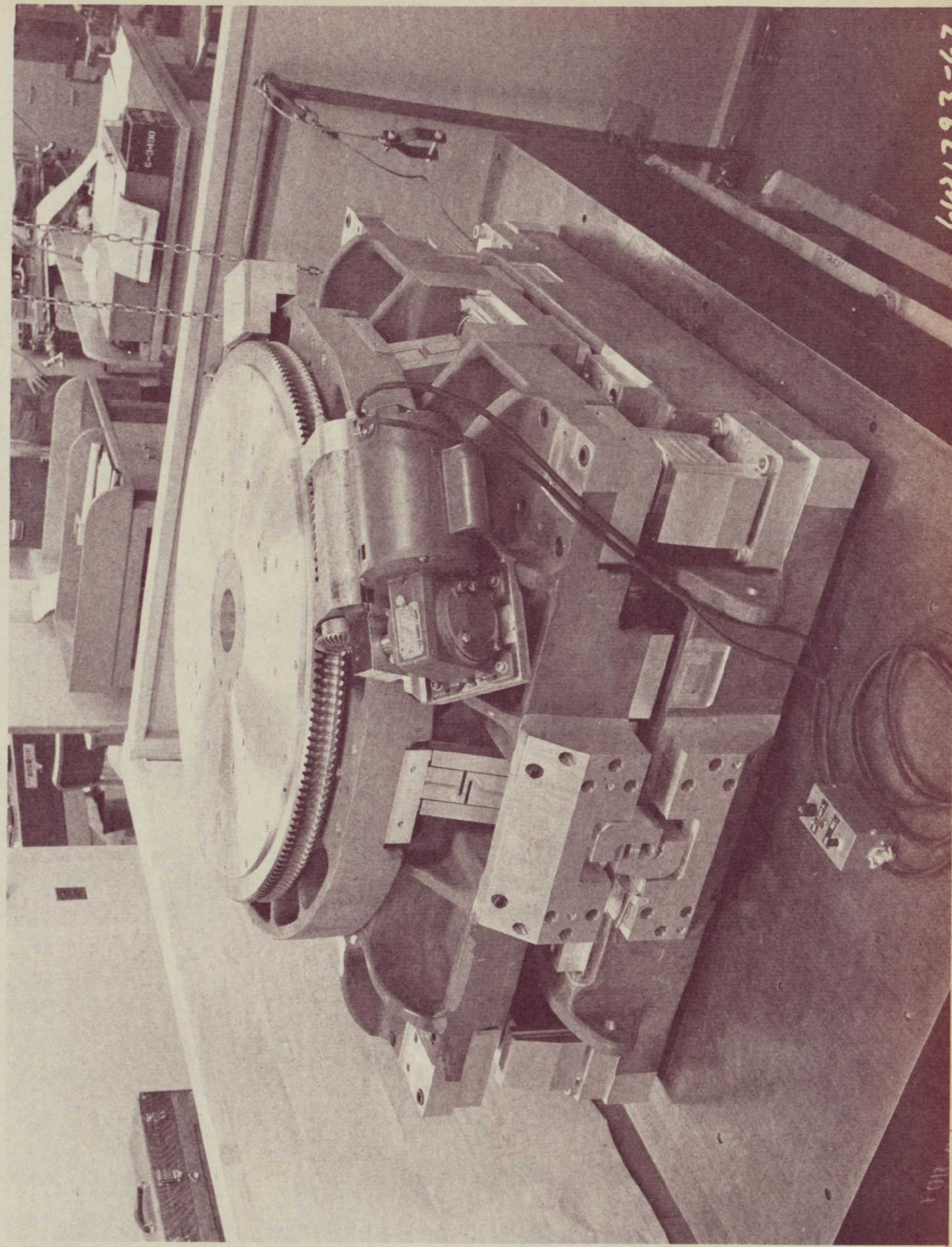

CALC			REVISED	DATE	SIX - COMPONENT FORCE BALANCE	FIG. 5
CHECK						D6-24850
APPD					THE BOEING COMPANY	PAGE 87
APPD						

87

88

AVG. NOZZLE GAPS (IN.)

CONFIG.	UPPER	LOWER
OUTB'D	.148	.125
INB'D	.148	.129

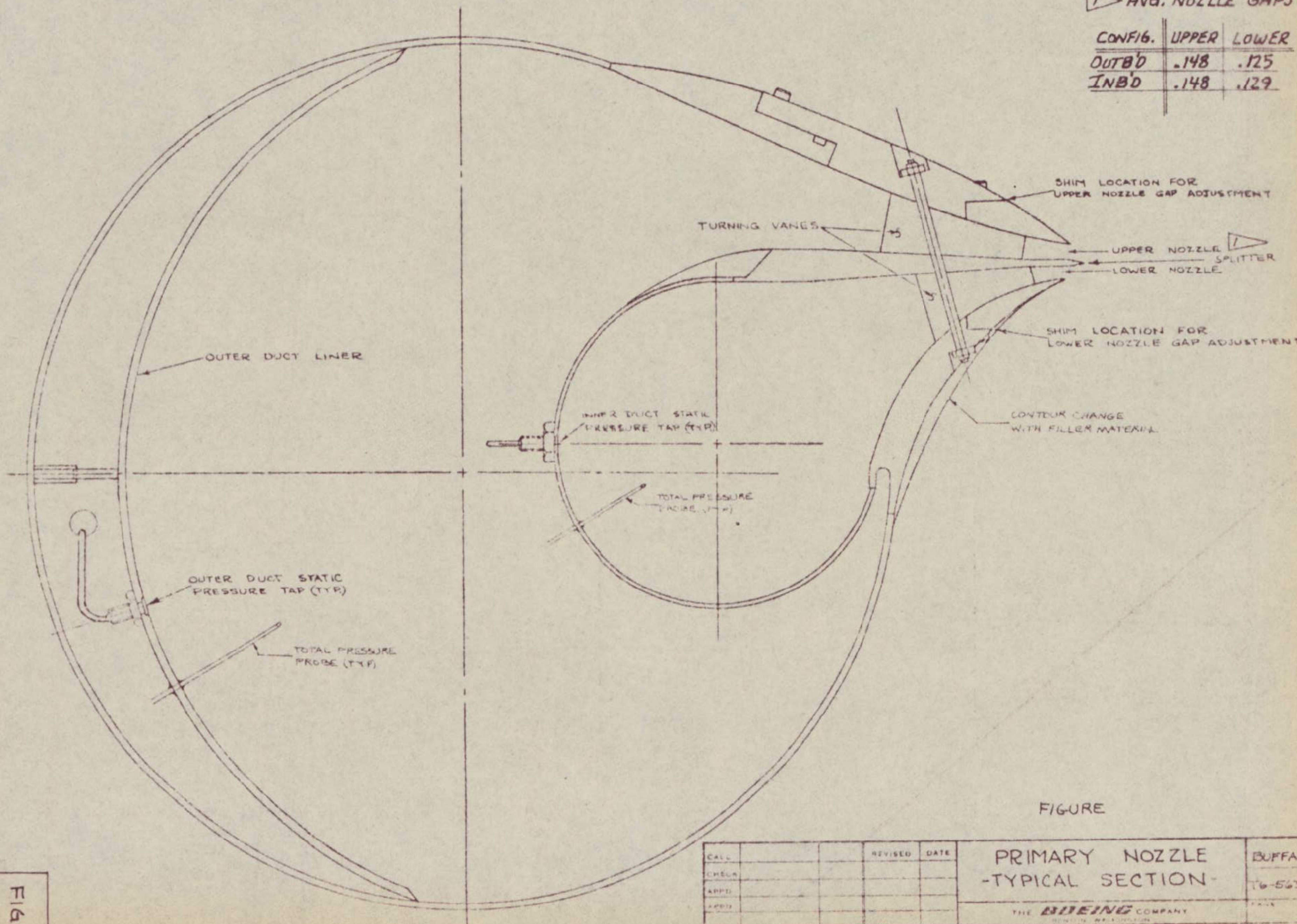

FIGURE

CALC			REVISED	DATE	PRIMARY NOZZLE -TYPICAL SECTION-	BUFFALO
CHECK						T6-5635
APPD					THE BOEING COMPANY	
APPD						

Fig. 6

D6-24850

PAGE 88

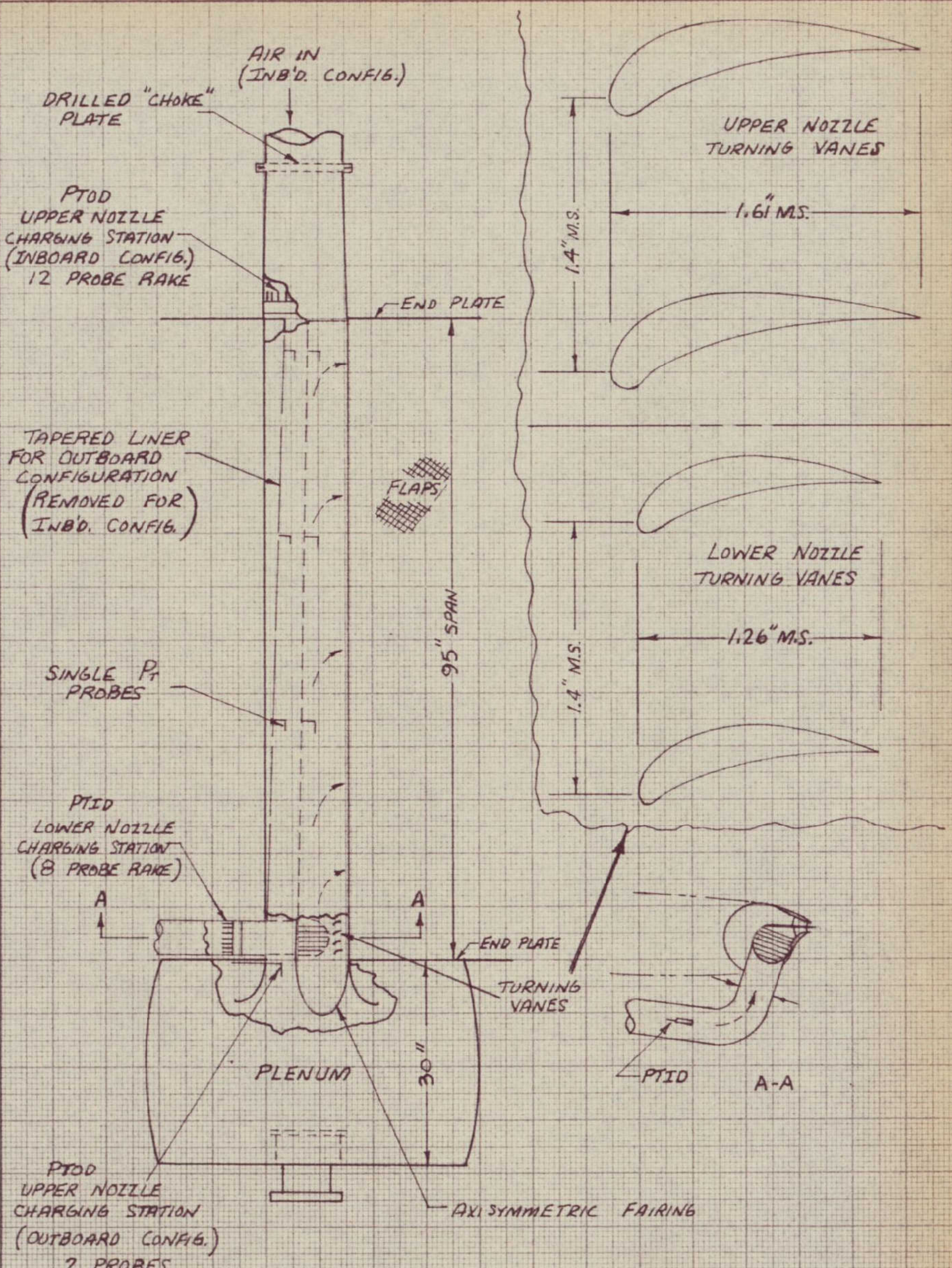

CALC	DLH	3/15/71	REVISED	DATE	0.7 SCALE MODEL AIR SUPPLY DUCT SYSTEM AND NOZZLE TURNING VANES
CHECK					
APR					
APR					THE BOEING COMPANY

FIG. 7

D6-24850

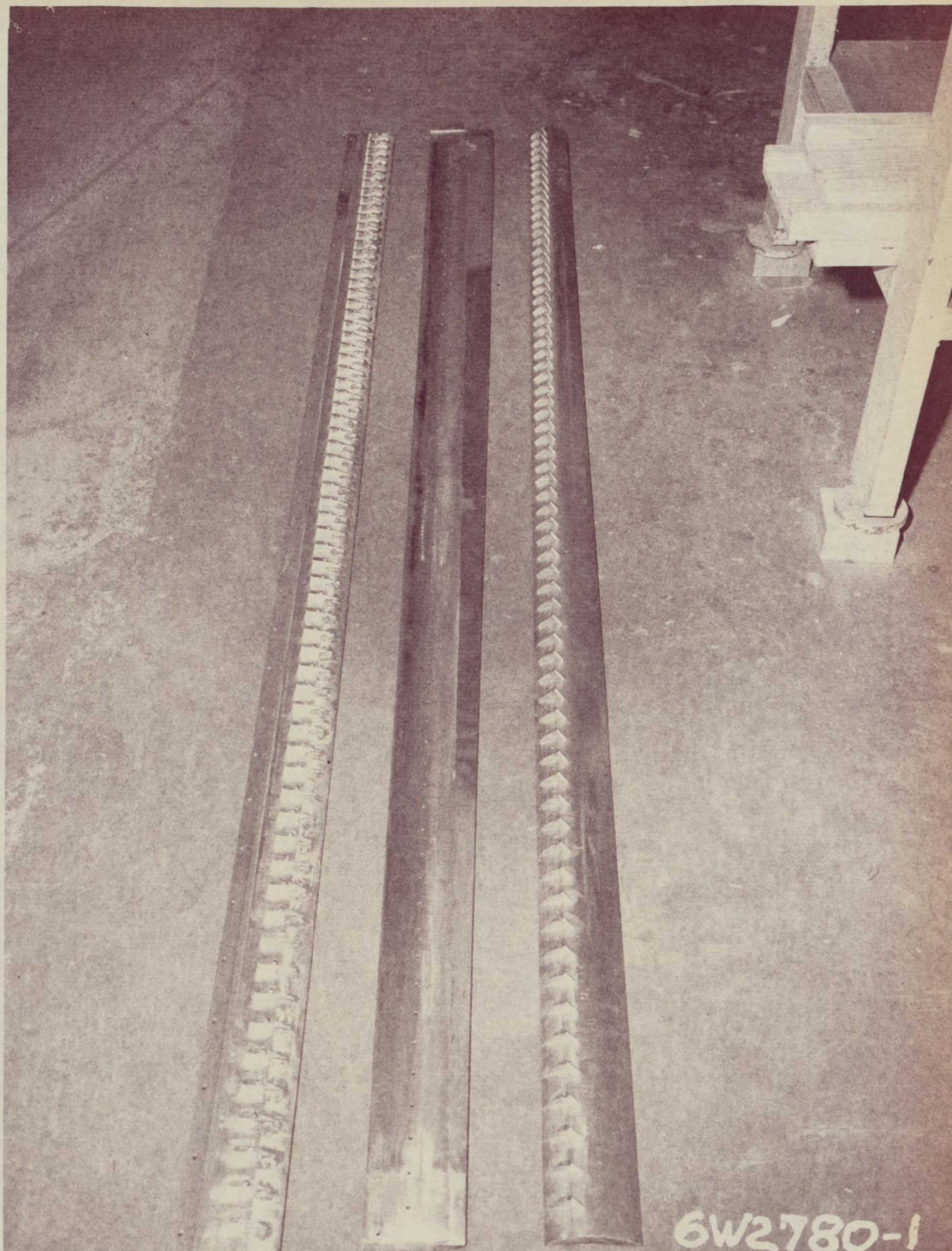

			REVISED	DATE		
CALC					NOZZLE LIPS, TURNING VANES AND FLOW SPLITTER	FIG. 8
CHECK						
APPD						D6-24850
APPD					THE BOEING COMPANY	PAGE 90

90

~~85~~

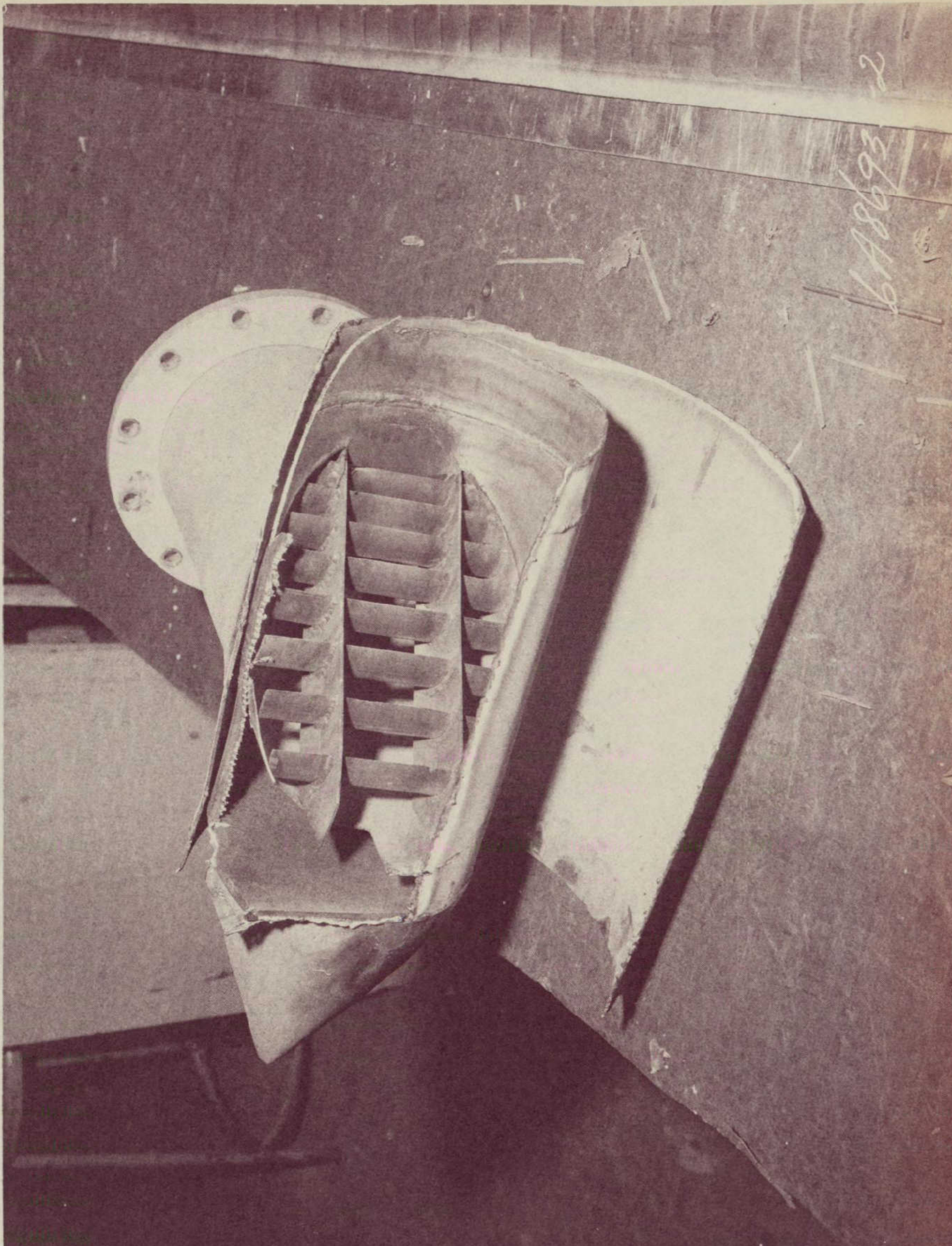

CALC		REVISED	DATE	CASCADE TURNING VANES - LOWER NOZZLE ENTRANCE	FIG. 9
CHECK					D6-24850
APPD					
APPD				THE BOEING COMPANY	PAGE 91

91

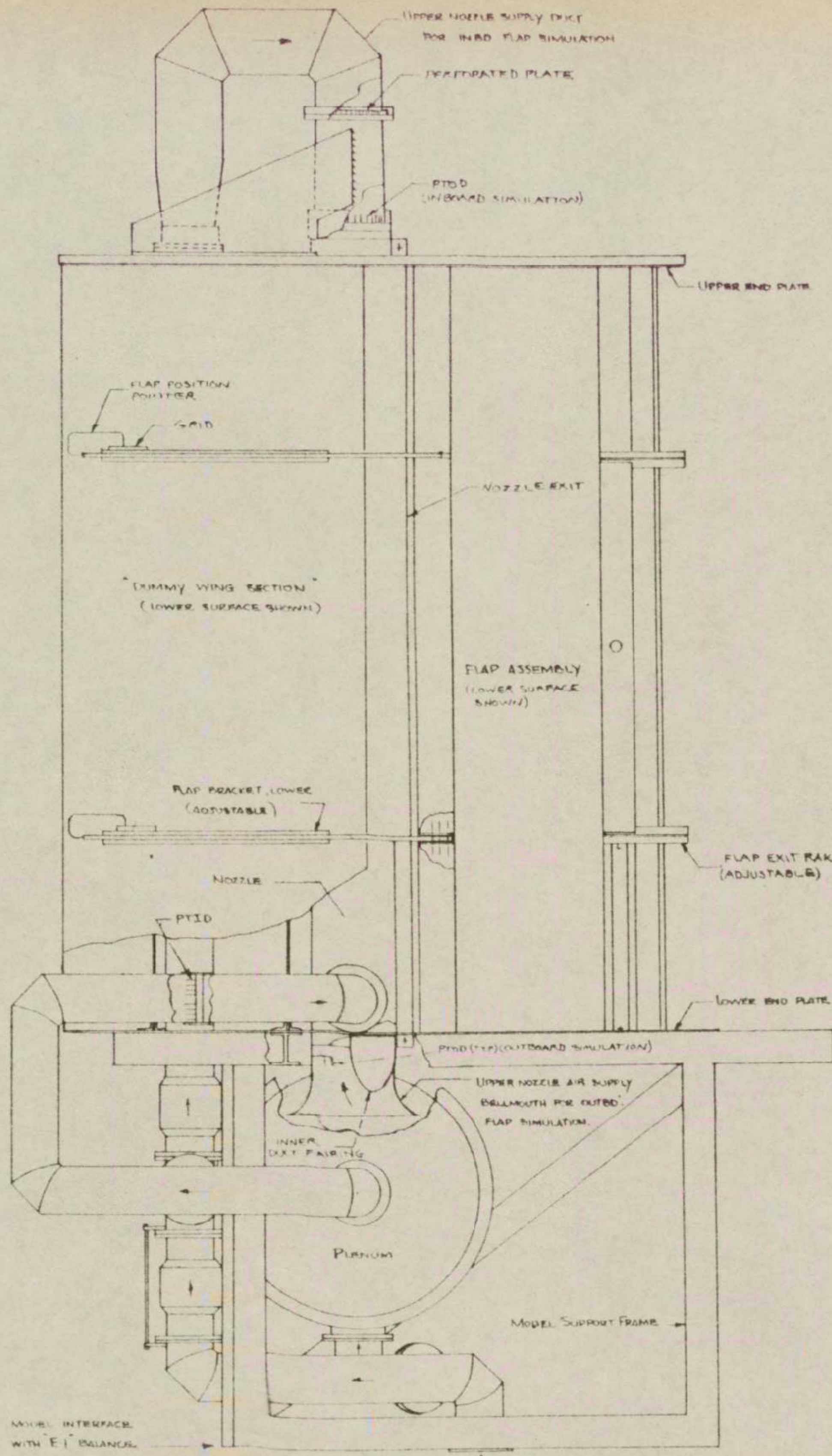

FIGURE 3

CALC			REVISED	DATE	AUGMENTOR FLAP SEGMENT MODEL ASSEMBLY (BALANCE & STAND NOT SHOWN)
CHECK					
APPD	K. Debus				
APPD					THE BOEING COMPANY RENTON, WASHINGTON

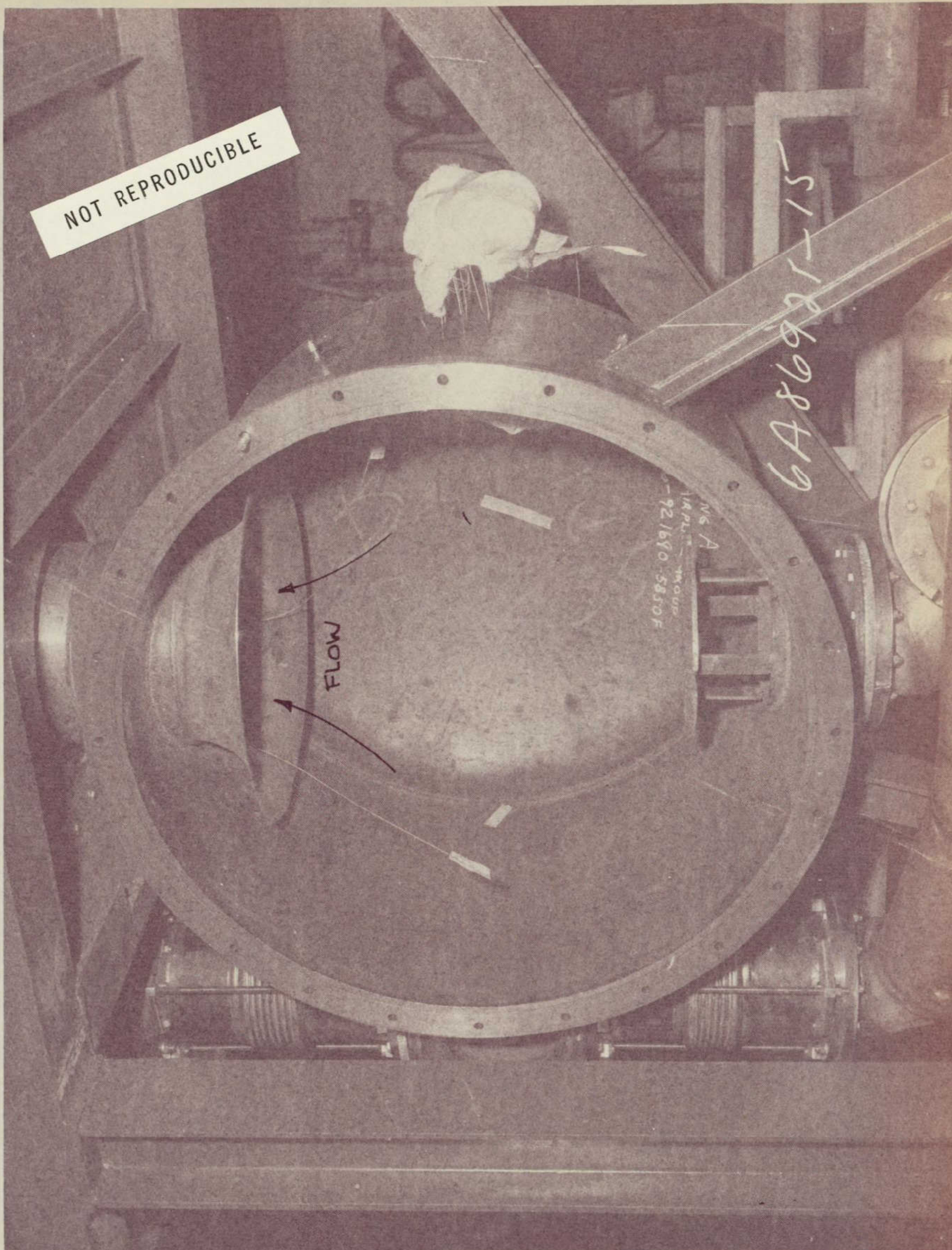

			REVISED	DATE		
CALC					MODEL AIR SUPPLY PLENUM	FIG. 11
CHECK						D6-24850
APPD						
APPD					THE BOEING COMPANY	PAGE 93

93
~~88~~

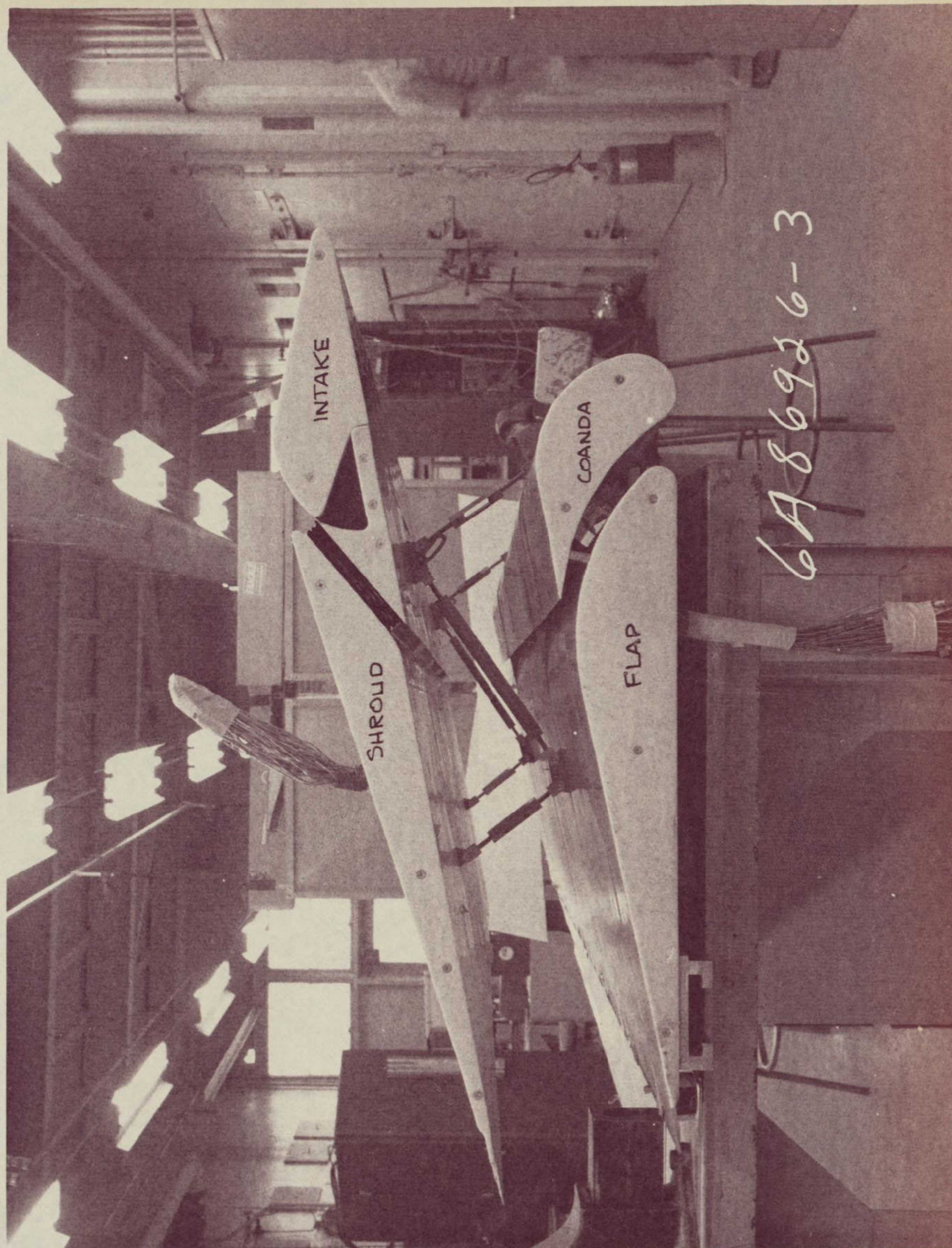

			REVISED	DATE	
CALC					AUGMENTOR FLAP ASSEMBLY
CHECK					
APPD					
APPD					
					THE BOEING COMPANY

FIG. 12

D6-24850

94

AD 973 D-R3

6 7000

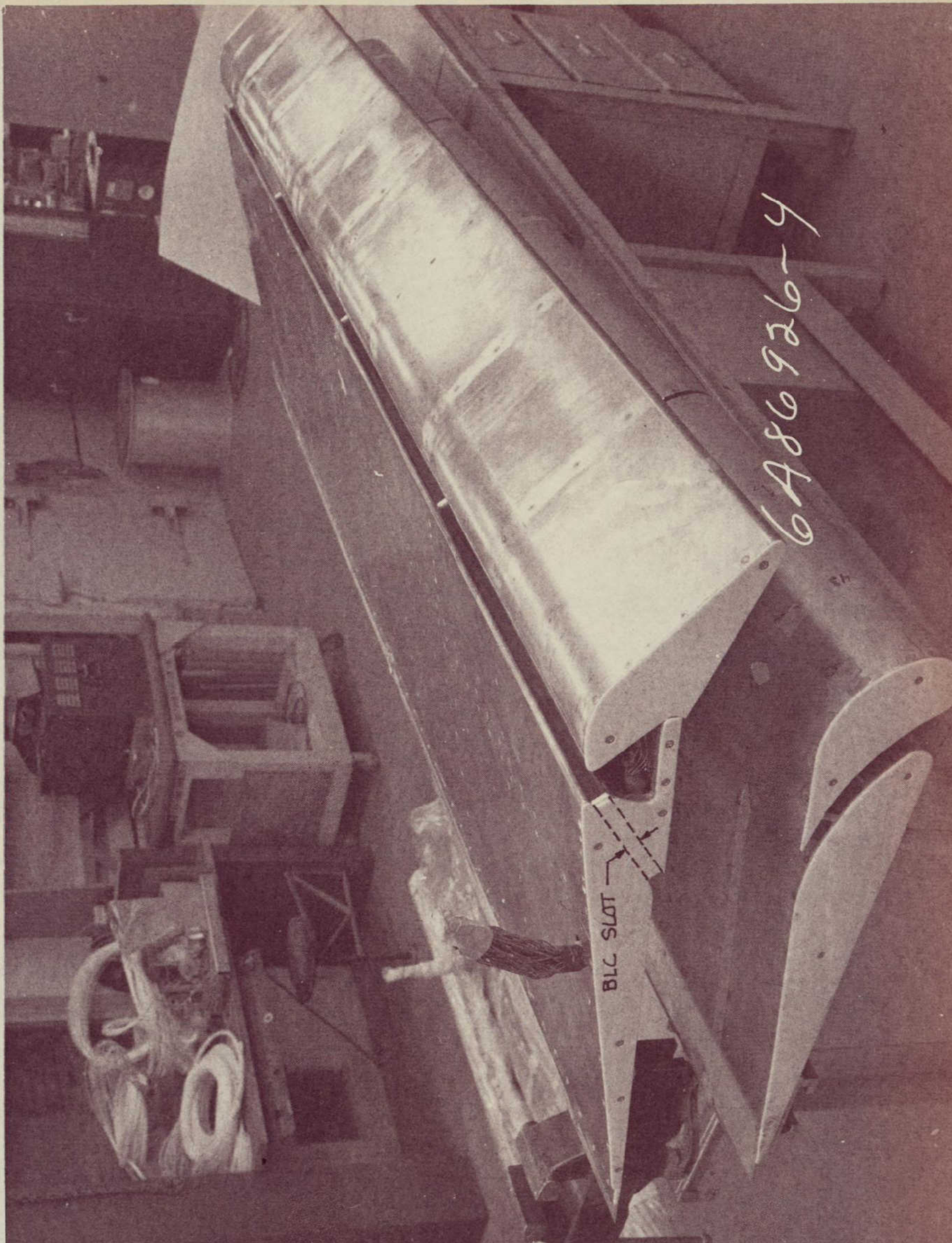

CALC			REVISED	DATE	AUGMENTOR FLAP ASSEMBLY	FIG. 13
CHECK						
APPD						D6-24850
APPD					THE BOEING COMPANY	PAGE 95

95

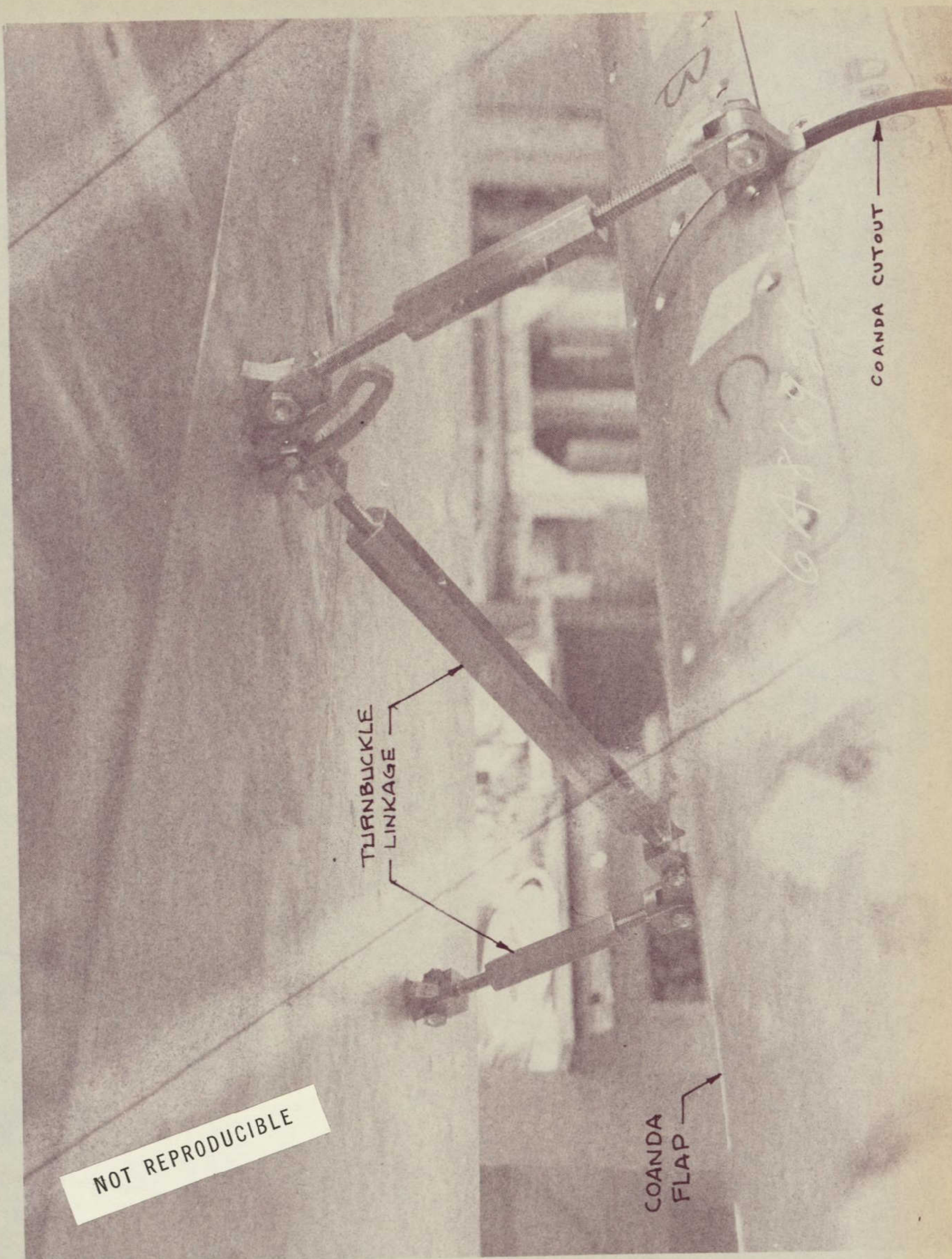

			REVISED	DATE		
CALC					AUGMENTOR FLAP	FIG. 14
CHECK					ADJUSTABLE LINKAGE	D6-24850
APPD						
APPD					THE BOEING COMPANY	PAGE 96

96

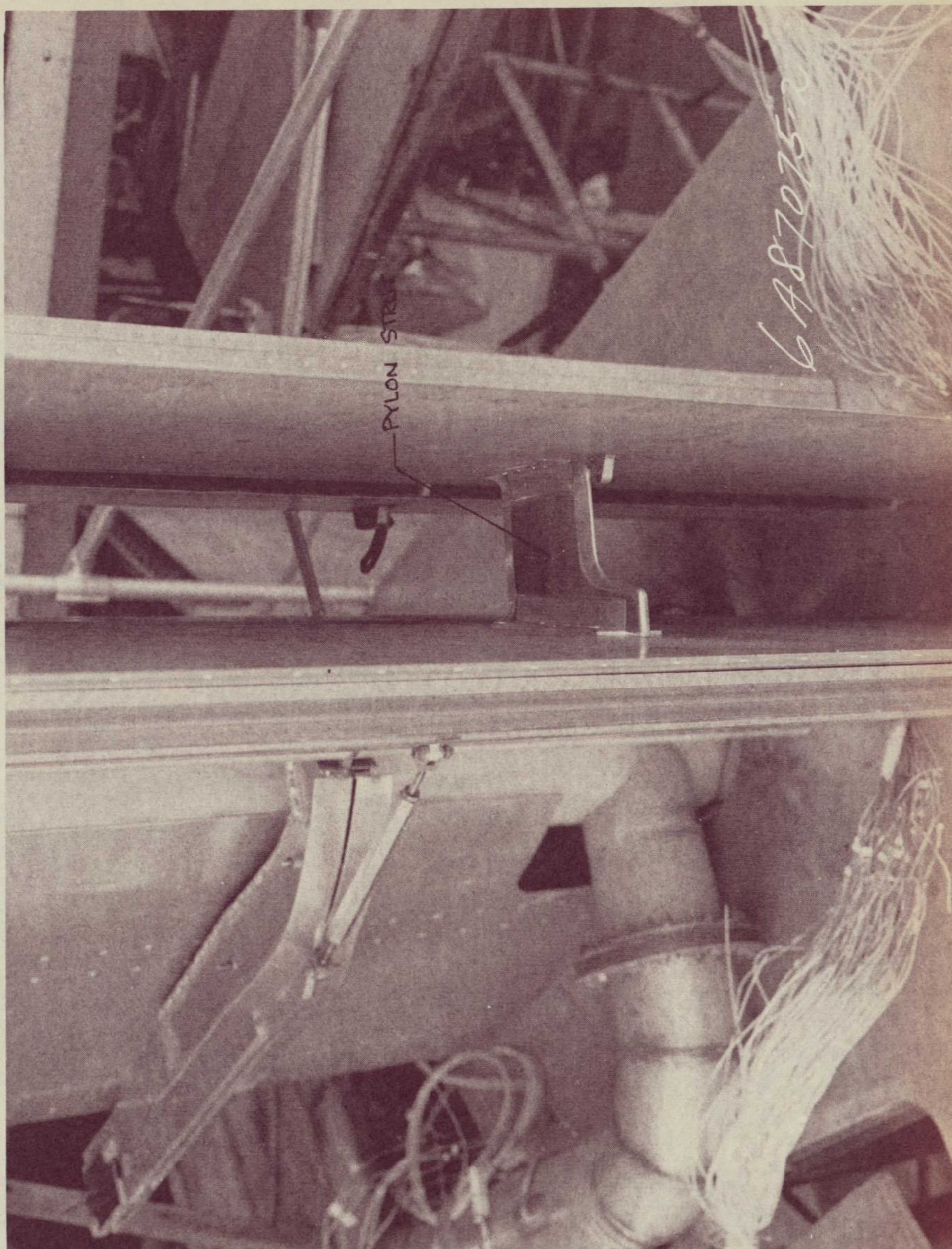

CALC			REVISED	DATE	AUGMENTOR FLAPS WITH SIMULATED AIRPLANE FLAP BRACKETS	FIG. 15
CHECK						D6-24850
APPD						
APPD					THE BOEING COMPANY	PAGE 97

97

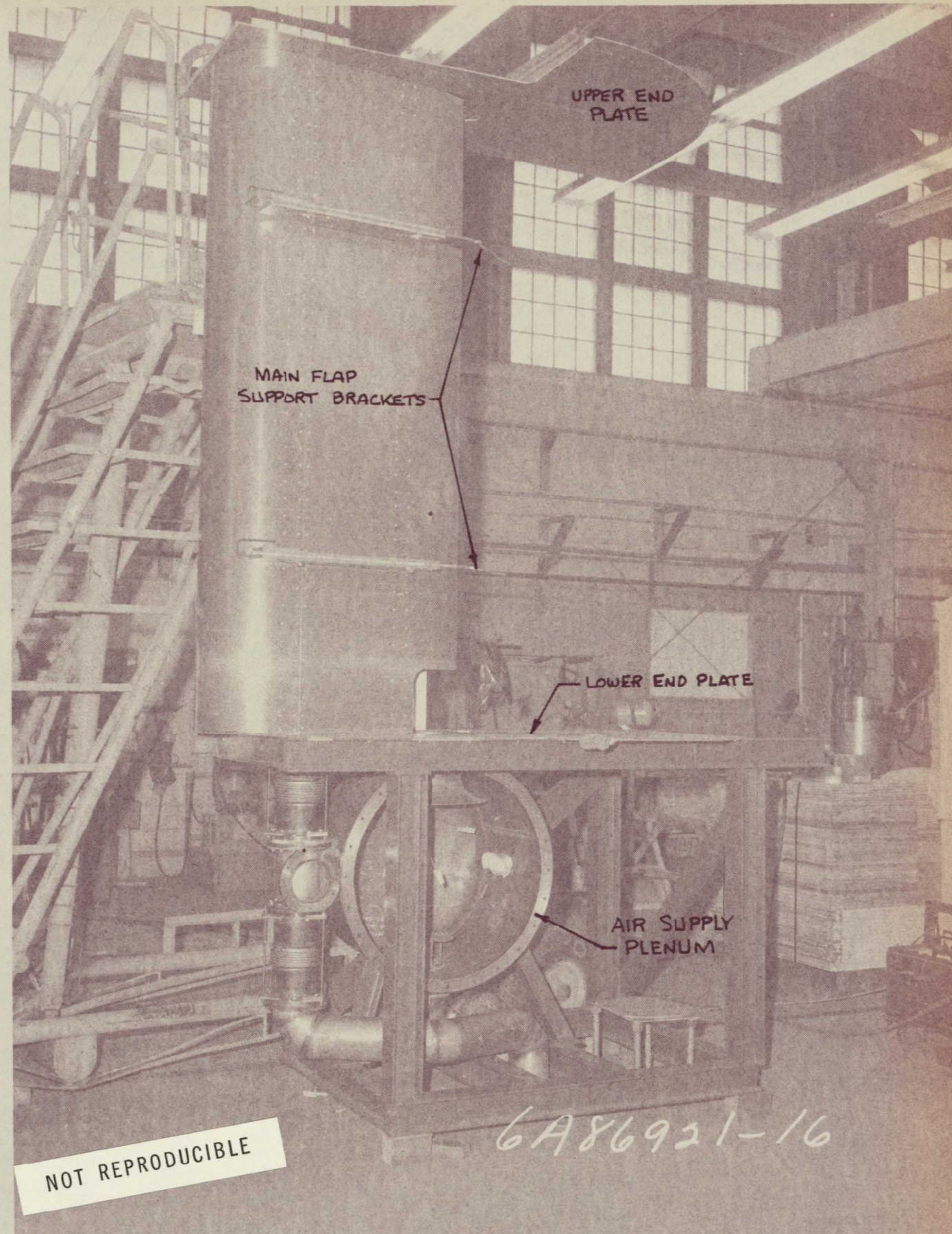

			REVISED	DATE		
CALC					MODEL WING AND SUPPORT STRUCTURE DURING ASSEMBLY	FIG. 16
CHECK						D6-24850
APPD						
APPD					THE BOEING COMPANY	PAGE 98

98

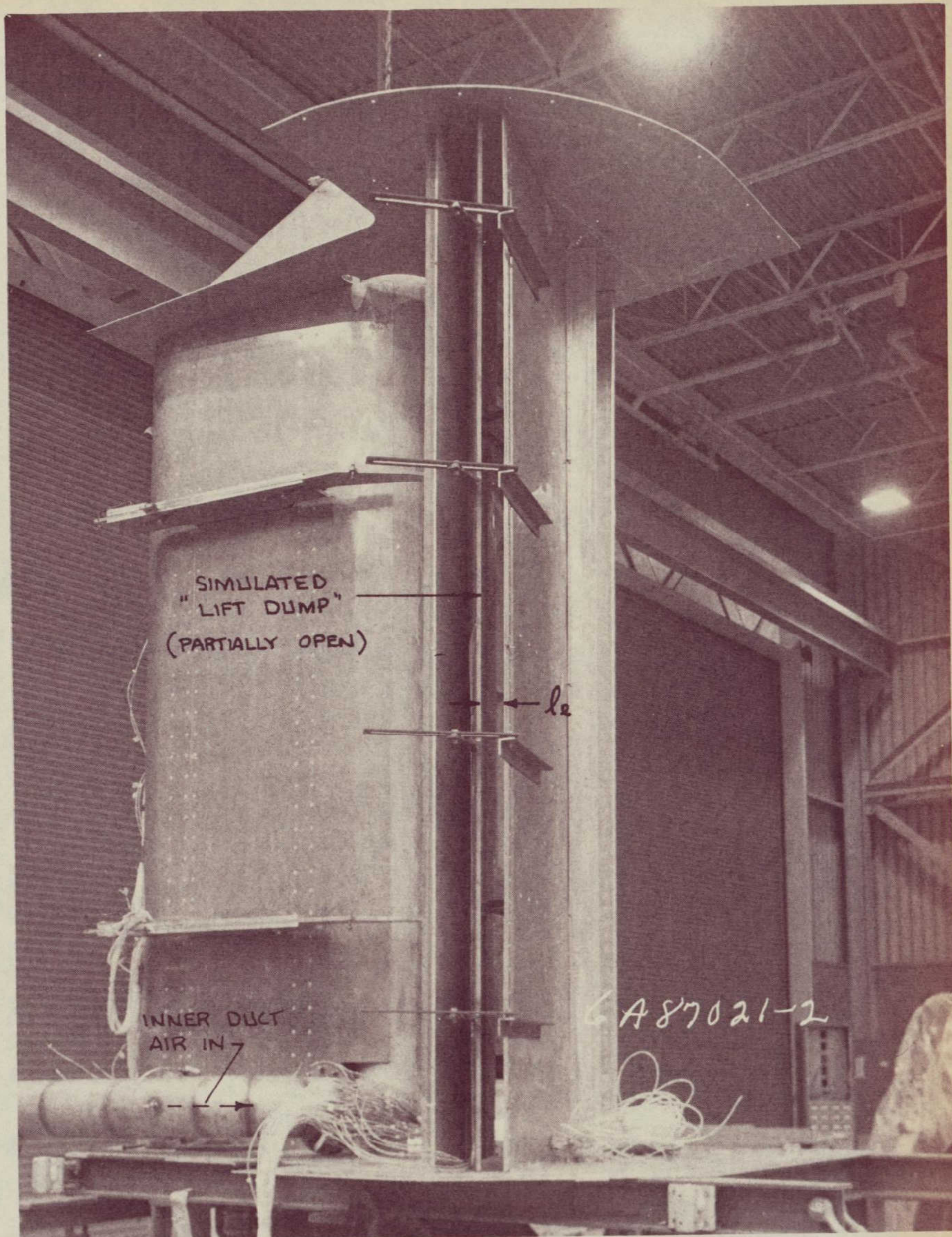

			REVISED	DATE		
CALC					MODEL ASSEMBLY WITH LIFT DUMP INSTALLED	FIG. 17
CHECK						D6-24850
APPD					THE BOEING COMPANY	PAGE 99
APPD						

99

6 7000

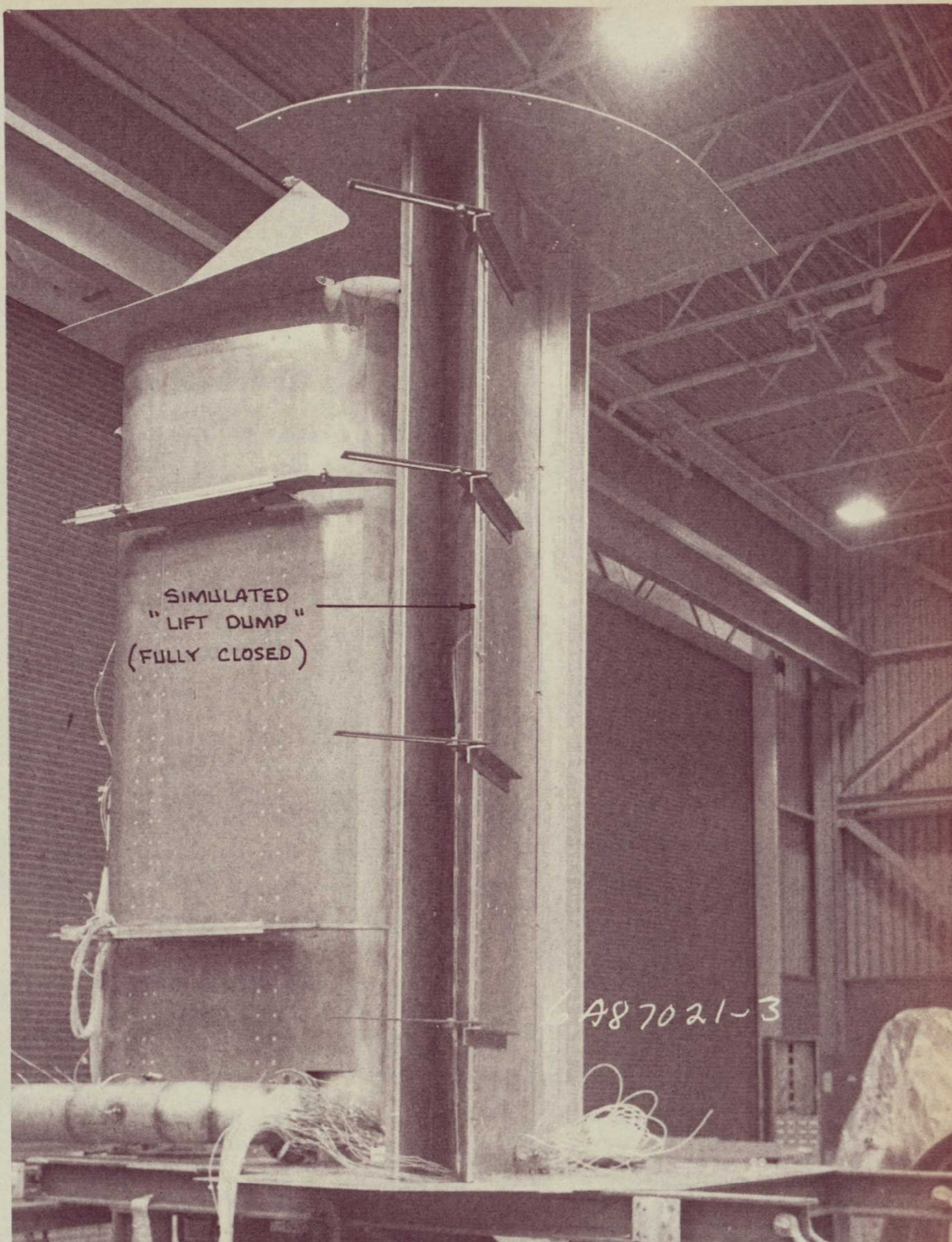

CALC			REVISED	DATE	MODEL ASSEMBLY WITH LIFT DUMP INSTALLED	FIG. 18
CHECK						D6-24850
APPD					THE BOEING COMPANY	PAGE 100
APPD						

100

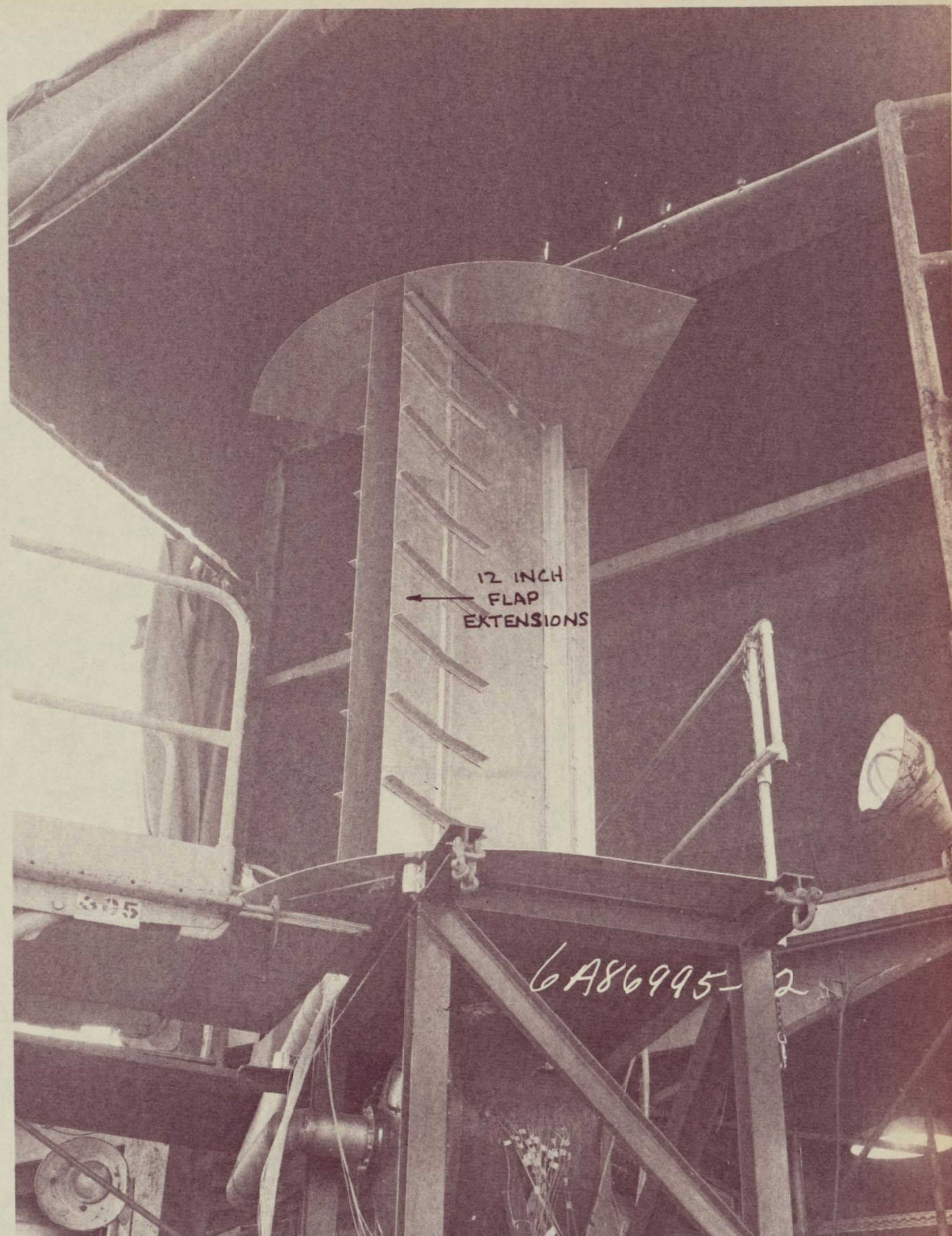

CALC			REVISED	DATE	MODEL ASSEMBLY	FIG. 19
CHECK					WITH 12" FLAP EXTENSIONS	D6-24850
APPD						
APPD					THE BOEING COMPANY	PAGE 101

101

AD 973 D-R3

6 7000

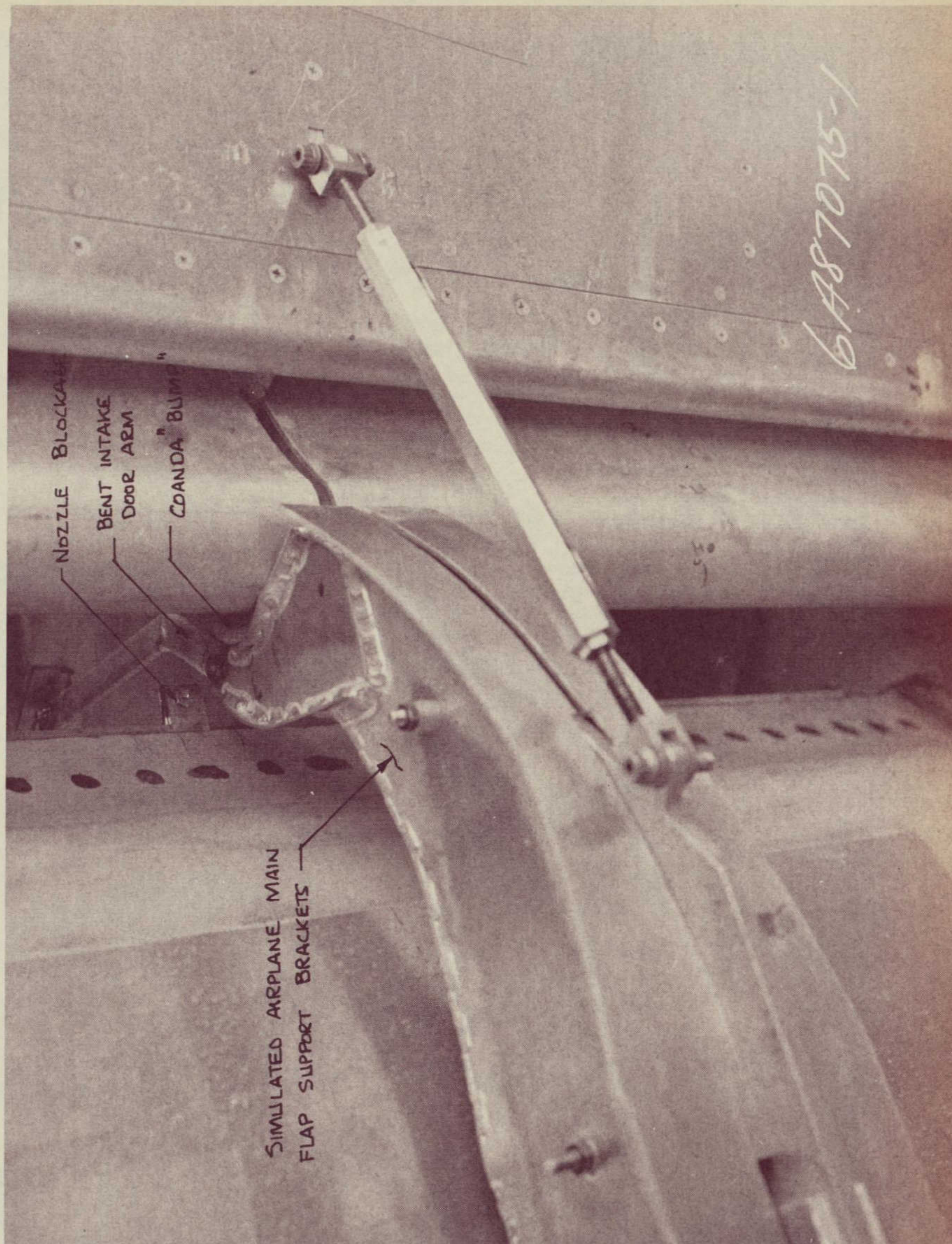

CALC			REVISED	DATE	MODEL WITH SIMULATED AIRPLANE FLAP BRACKETS	FIG. 20
CHECK						D6-24850
APPD					THE BOEING COMPANY	PAGE 102
APPD						

102

97

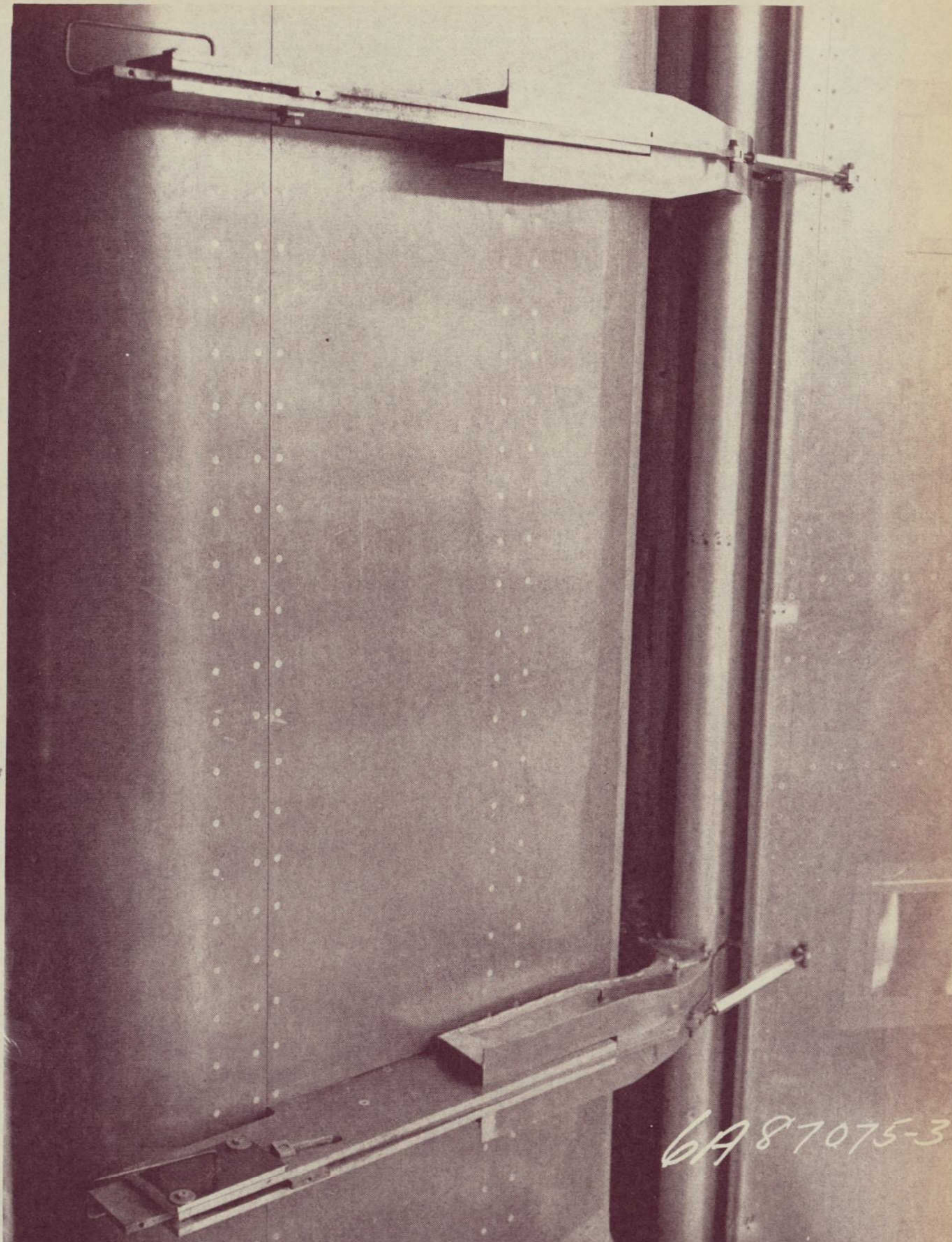

CALC			REVISED	DATE	SIMULATED AIRPLANE MAIN FLAP SUPPORT BRACKETS	FIG. 21
CHECK						D6-24850
APPD					THE BOEING COMPANY	PAGE 103
APPD						

103

~~98~~

CALC			REVISED	DATE	SLOT NOZZLE EXIT	FIG. 22
CHECK					TOTAL PRESSURE PROBES	D6-24850
APPD						
APPD					THE BOEING COMPANY	PAGE 104

104

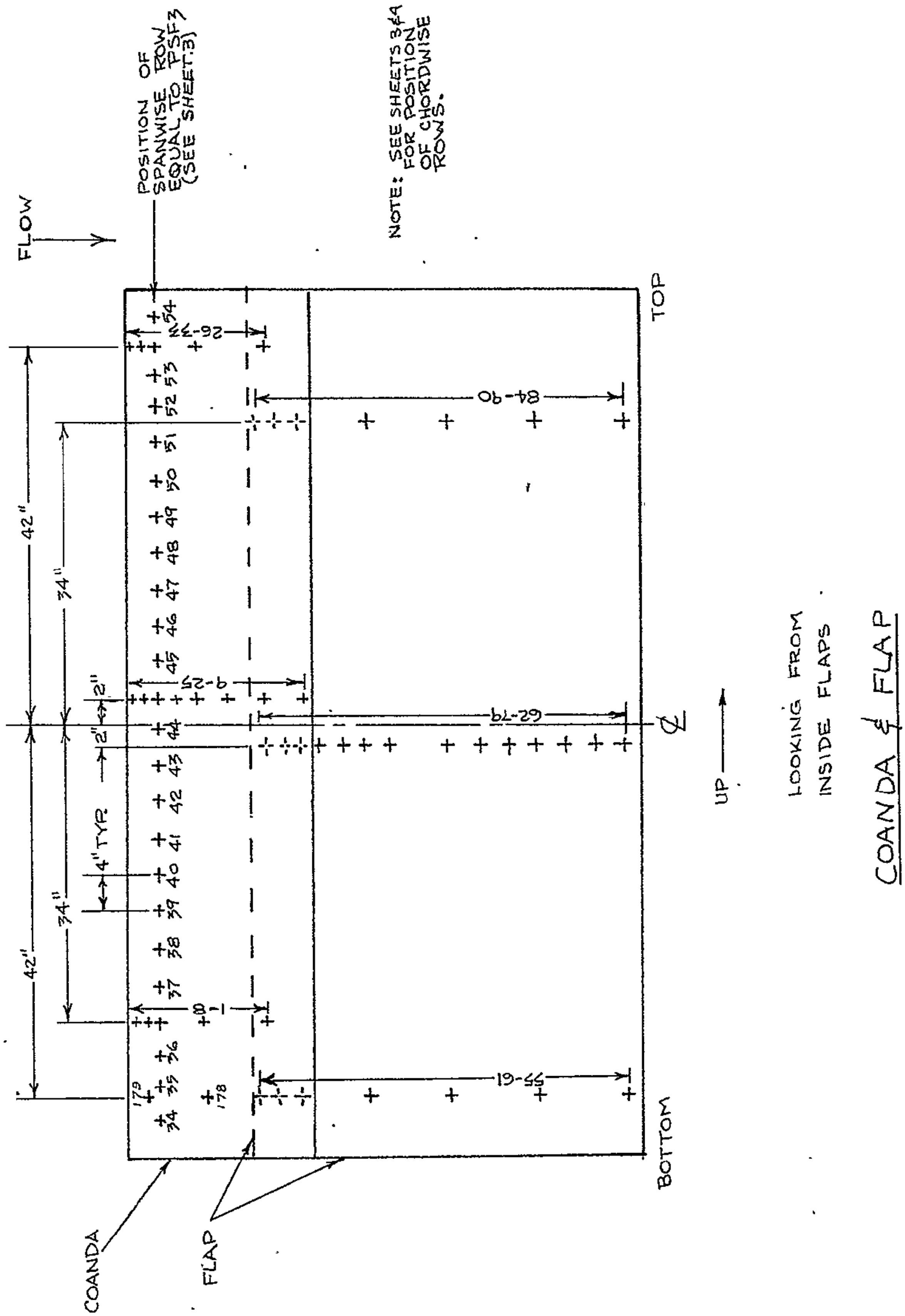

SHEET 1 OF 4

ENGR.	C.R. FULLERTON		REVISED	DATE	FLAP STATIC PRESSURE MEASUREMENT LOCATIONS	FIG. 23
CHECK						D6-24850
APR	K. IKEDA	11/19/73				
APR					THE BOEING COMPANY RENTON, WASHINGTON	PAGE 105

105
~~100~~

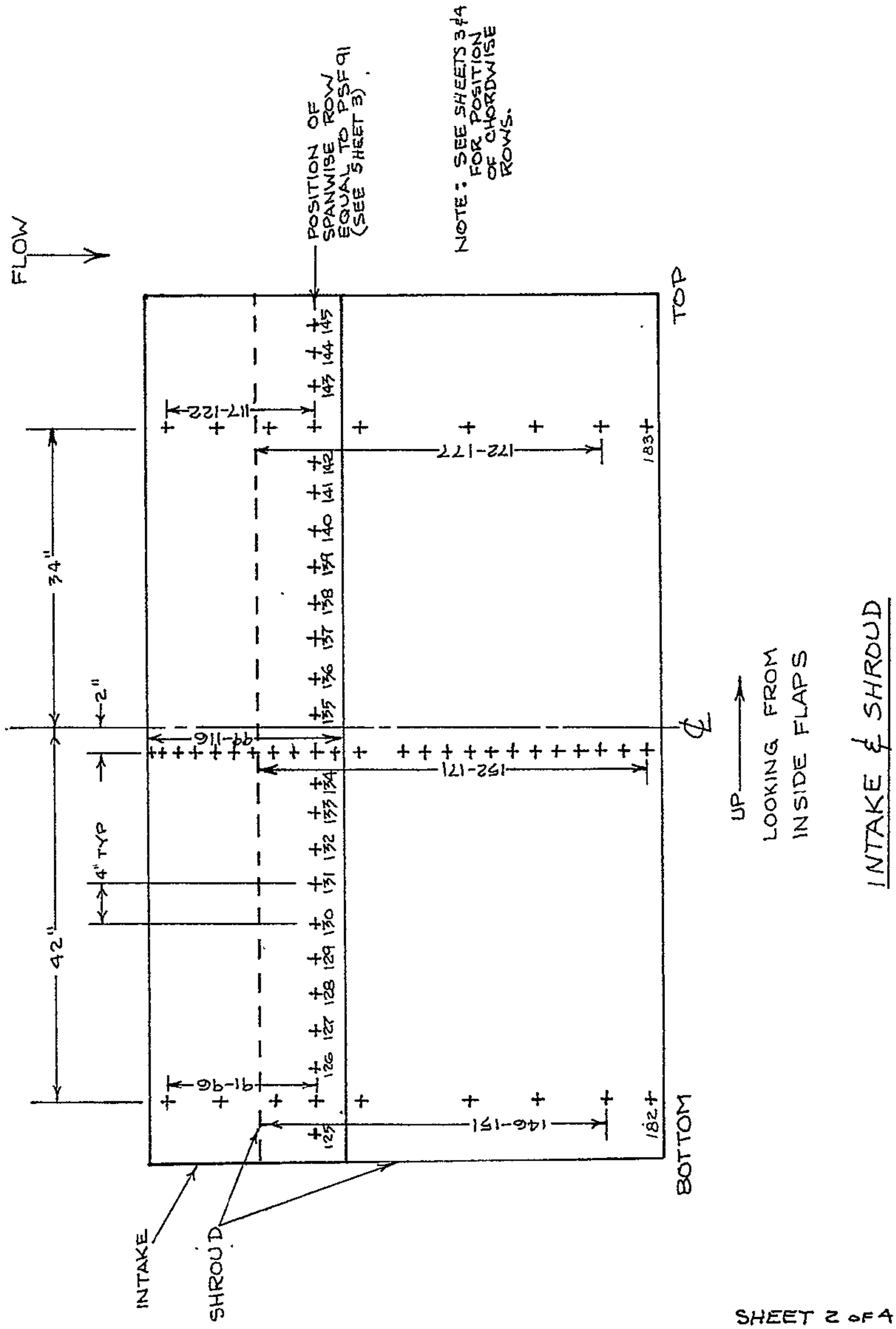

SHEET 2 OF 4

ENGR.	C.E. FULLERTON		REVISED	DATE	FLAP STATIC PRESSURE MEASUREMENT LOCATIONS	FIG. 24
CHECK						D6-24850
APR	K. IKEDA	11/19/70			THE BOEING COMPANY RENTON, WASHINGTON	PAGE 106
APR						

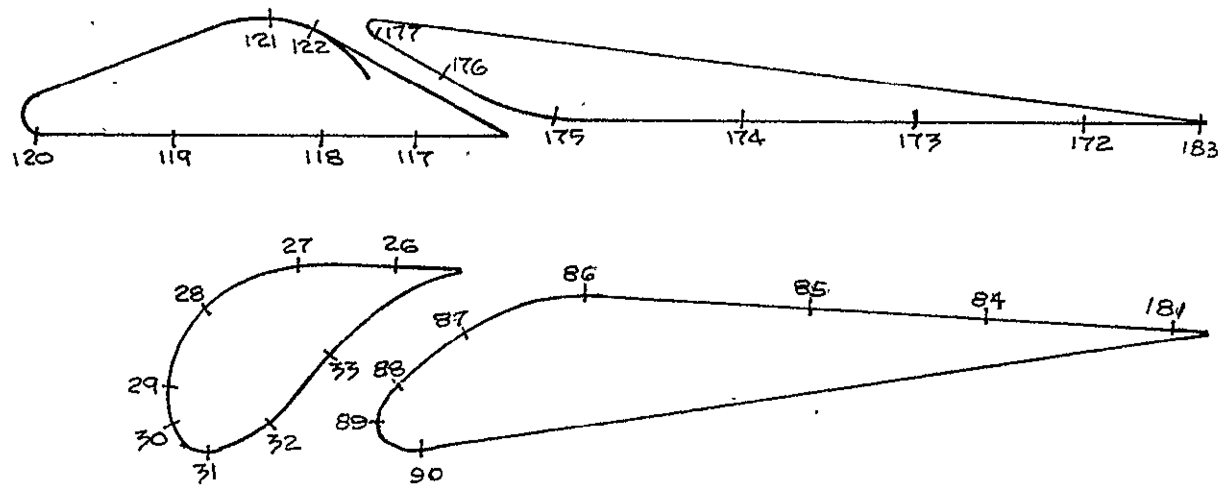

UPPER CHORD

INTAKE & SHROUD

PROBE NO.	DIMENSION * INCHES
91 & 117	2.70
92 & 118	6.20
93 & 119	11.45
94 & 120	14.95
95 & 121	AT TOP AT 0° θi
96 & 122	1.4 FROM 95
182 & 183	.35
146 & 172	3.85
147 & 173	10.15
148 & 174	15.75
149 & 175	20.85
150 & 176	24.15
151 & 177	26.23

* SURFACE DISTANCE FROM TRAILING EDGE

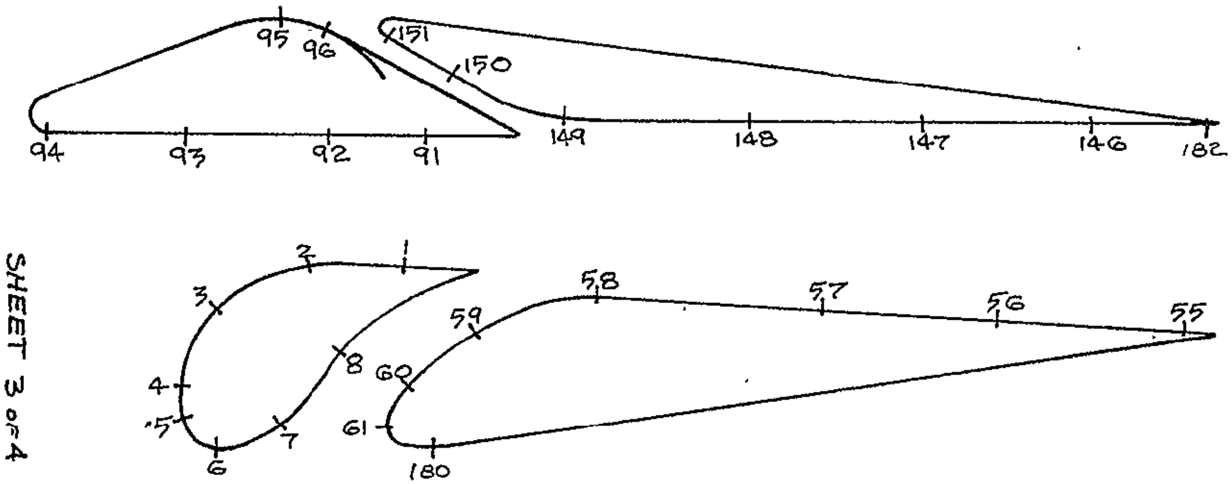

LOWER CHORD

COANDA & FLAP

PROBE NO.	DIMENSION * INCHES
1 & 26	2.30
2 & 27	5.10
3 & 28	7.90
4 & 29	10.70
5 & 30	11.75
6 & 31	13.50
7 & 32	15.20
8 & 33	18.30
55 & 181	.40
56 & 84	7.75
57 & 85	14.75
58 & 86	18.95
59 & 87	23.15
60 & 88	25.60
61 & 89	27.00
180 & 90	28.30

SHEET 3 OF 4

ENGR.	C R. FULLERTON		REVISED	DATE
CHECK				
APR	K. IKEDA	11/19/73		
APR				

FLAP STATIC PRESSURE MEASUREMENT LOCATIONS

FIG. 25

D6-24850

THE BOEING COMPANY
RENTON, WASHINGTON

109
~~102~~

AD 1017-R6

108
~~103~~

CENTER CHORD

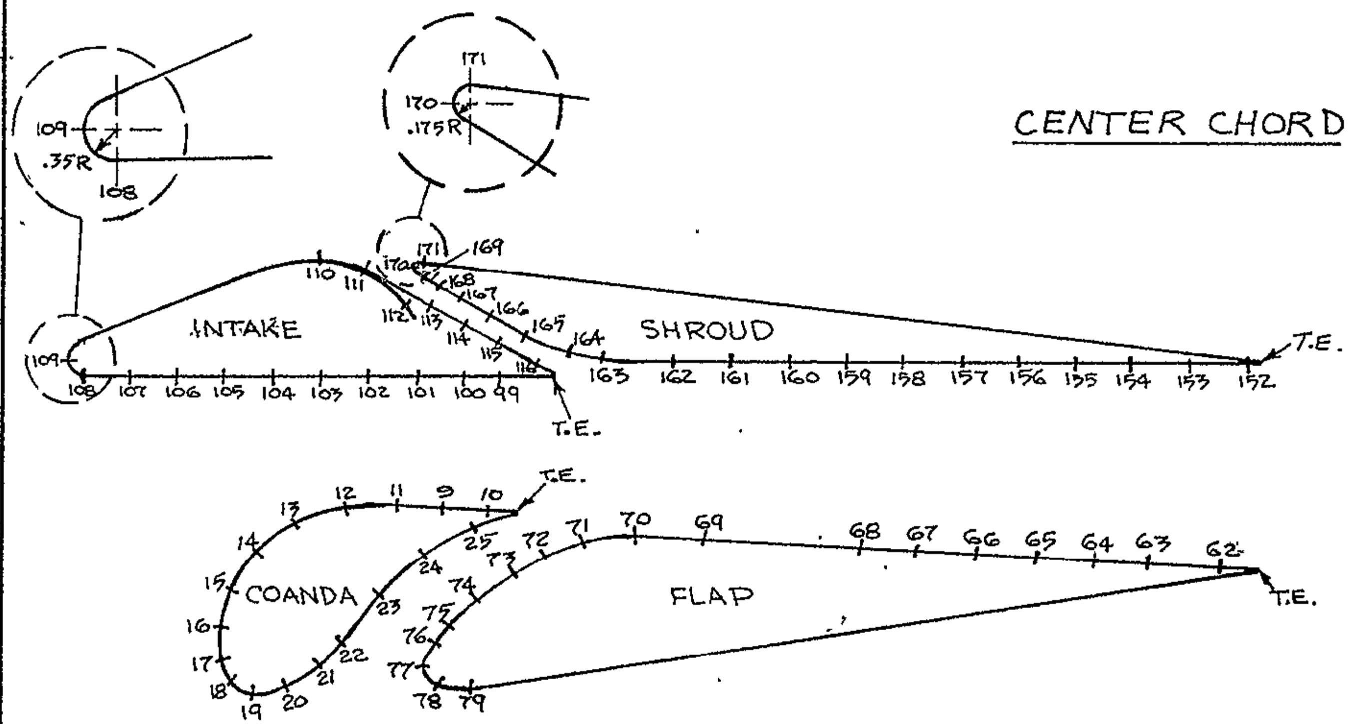

* SURFACE DISTANCE FROM TRAILING EDGE

PROBE NO.	DIMENSION* INCHES
10	.90
9	2.30
11	3.70
12	5.10
13	6.50
14	7.90
15	9.30
16	10.70
17	11.75
18	12.80
19	13.50
20	14.20
21	15.20
22	16.20
23	18.30
24	20.40
25	22.50

COANDA

PROBE NO.	DIMENSION * INCHES
62	.40
63	2.15
64	4.95
65	7.75
66	10.55
67	12.65
68	14.75
69	17.55
70	18.95
71	20.35
72	21.75
73	23.15
74	24.55
75	25.60
76	26.30
77	27.00
78	27.70
79	28.30

FLAP

PROBE NO.	DIMENSION* INCHES
99	.95
100	2.70
101	4.45
102	6.20
103	7.95
104	9.70
105	11.45
106	12.85
107	13.90
108	14.95
109	SEE DETAIL
110	AT TOP AT $\theta_L = 0°$
111	1.4 FROM 110
112	2.8 FROM 110
113	4.55
114	3.15
115	1.75
116	.35

INTAKE

PROBE NO.	DIMENSION * INCHES
152	.35
153	1.75
154	3.85
155	5.95
156	8.05
157	10.15
158	12.25
159	14.35
160	15.75
161	17.15
162	18.55
163	20.85
164	21.35
165	22.75
166	24.15
167	25.20
168	25.70
169	26.23
170	SEE DETAIL
171	SEE DETAIL

SHROUD

SHEET 4 OF 4

ENGR.	C.R. FULLERTON		REVISED	DATE	FLAP STATIC PRESSURE MEASUREMENT LOCATIONS	FIG. 26
CHECK						D6-24850
APR	K. IKEDA	11/19/70			THE BOEING COMPANY RENTON, WASHINGTON	PAGE 108
APR						

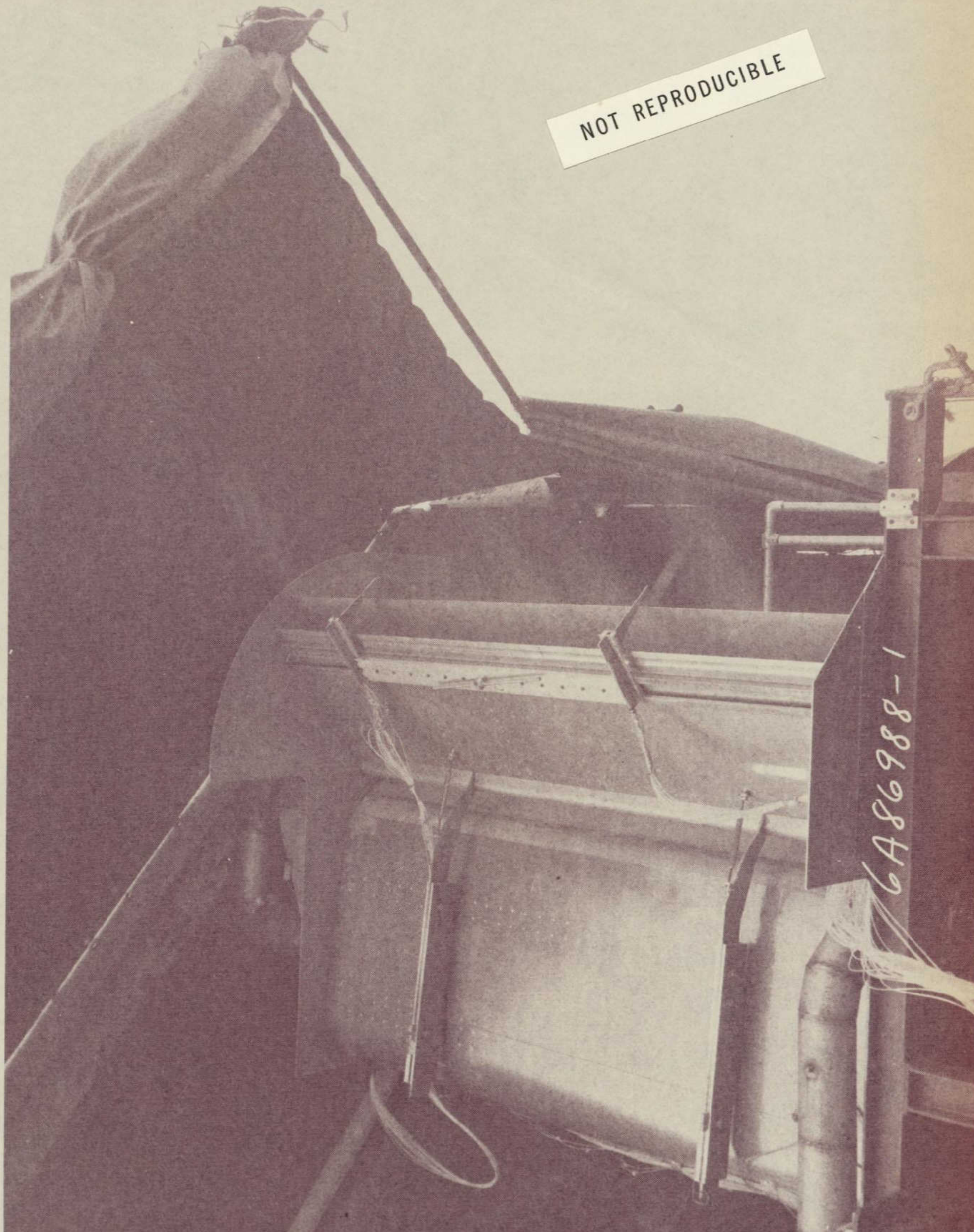

CALC			REVISED	DATE
CHECK				
APPD				
APPD				

MODEL WITH FLAP P_T EXIT RAKES INSTALLED

FIG. 27

D6-24850

THE BOEING COMPANY

AD 973 D-R3

6 7000

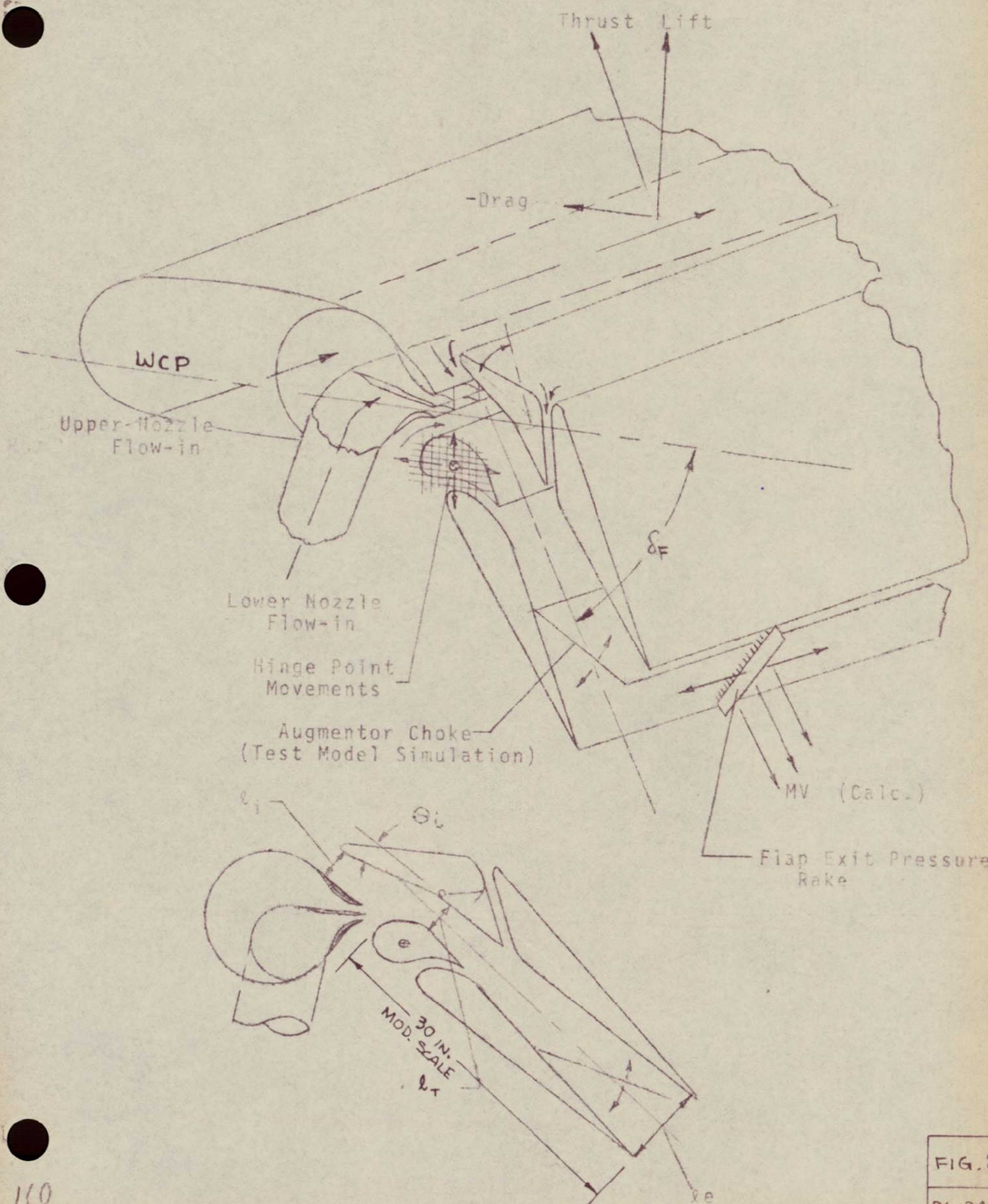
Thrust
Lift
-Drag
WCP
Upper-Nozzle
Flow-in
δ_F
Lower Nozzle
Flow-in
Hinge Point
Movements
Augmentor Choke
(Test Model Simulation)
MV (Calc.)
Flap Exit Pressure
Rake
ℓ_i
Θ_i
e
30 IN.
MOD. SCALE
ℓ_T
ℓe

FIG. 28

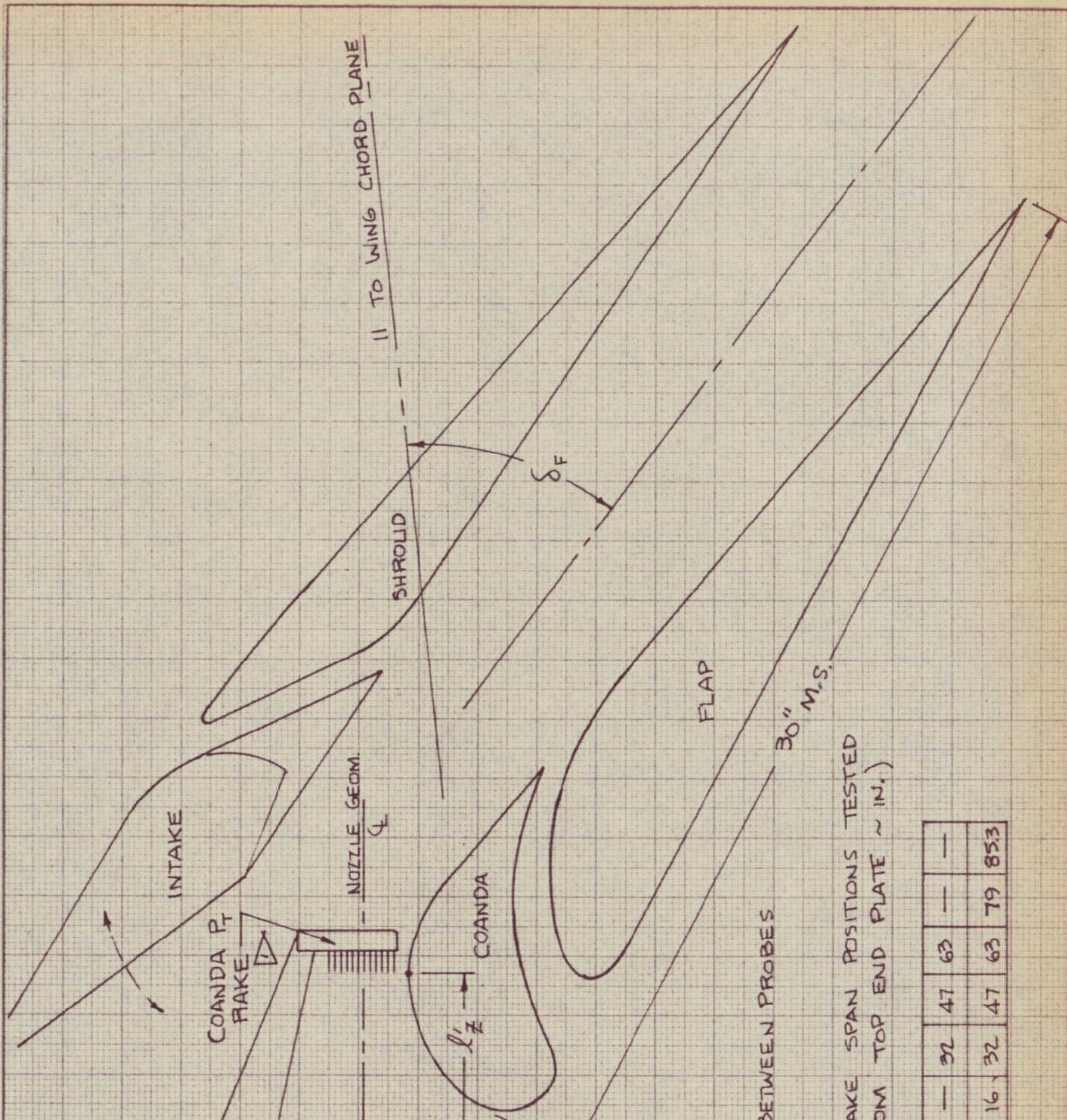

OUTBOARD	—	—	32	47	63	—	—
INBOARD	8	16	32	47	63	79	85.3

CALC		REVISED	DATE	COANDA P_T RAKE INSTALLATION	FIG. 29
CHECK					
APR					D6-24850
APR				THE BOEING COMPANY	PAGE 111

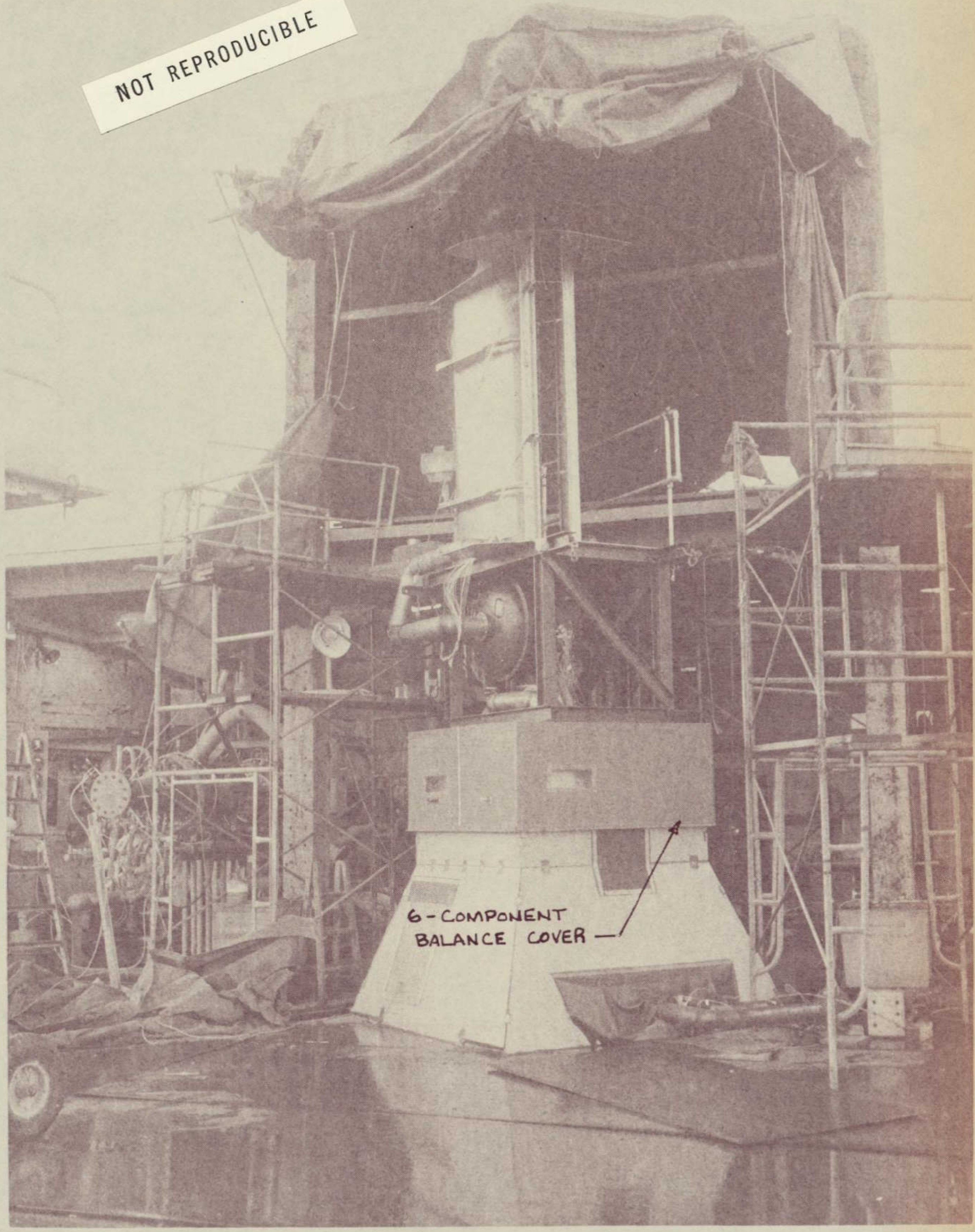

CALC			REVISED	DATE	AUGMENTOR FLAP MODEL INSTALLATION	FIG. 30
CHECK						D6-24850
APPD						
APPD					THE BOEING COMPANY	PAGE 112

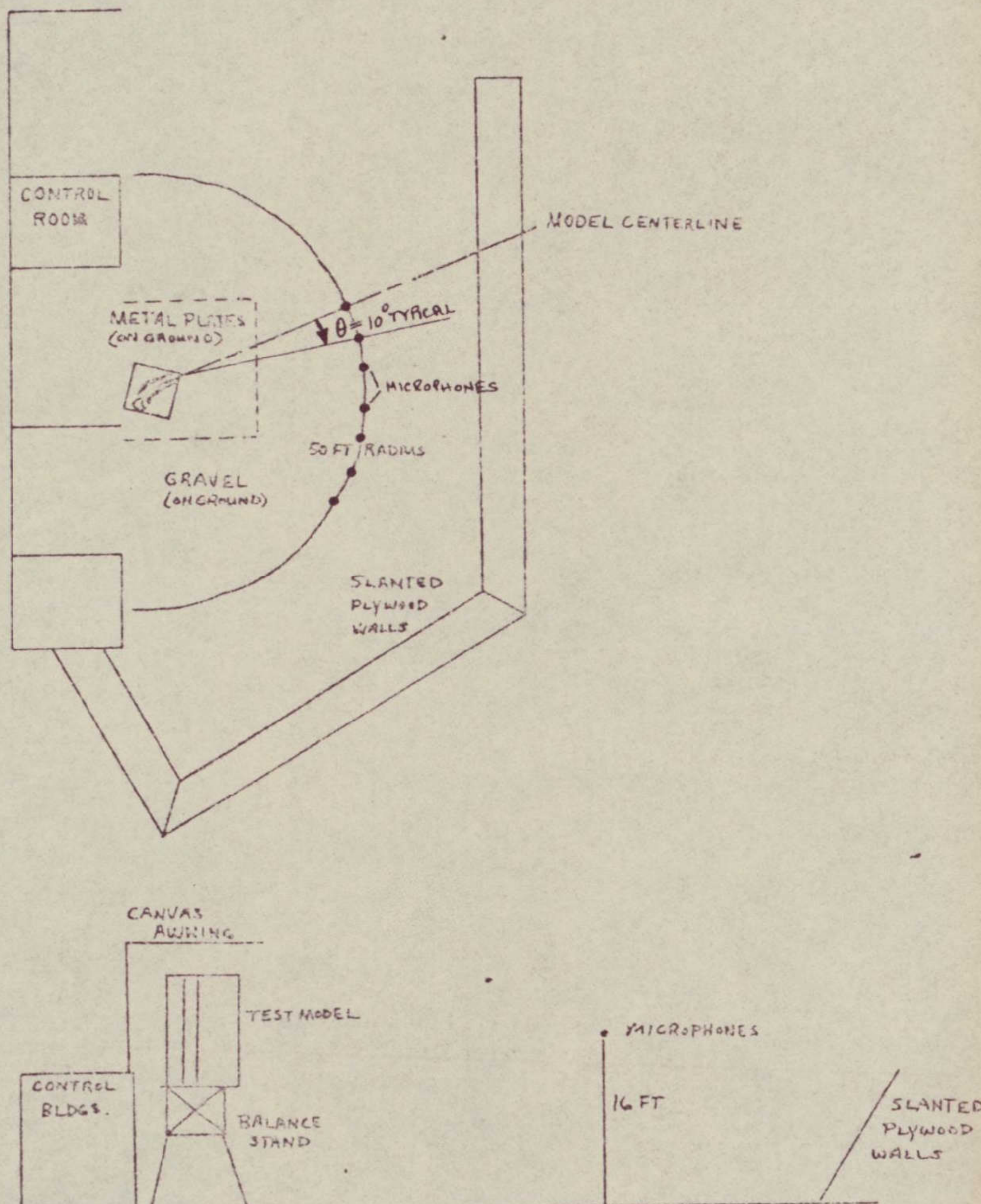

FIG. 31

TEST MODEL AND MICROPHONE POSITIONS

JET-AUGMENTOR WING TEST

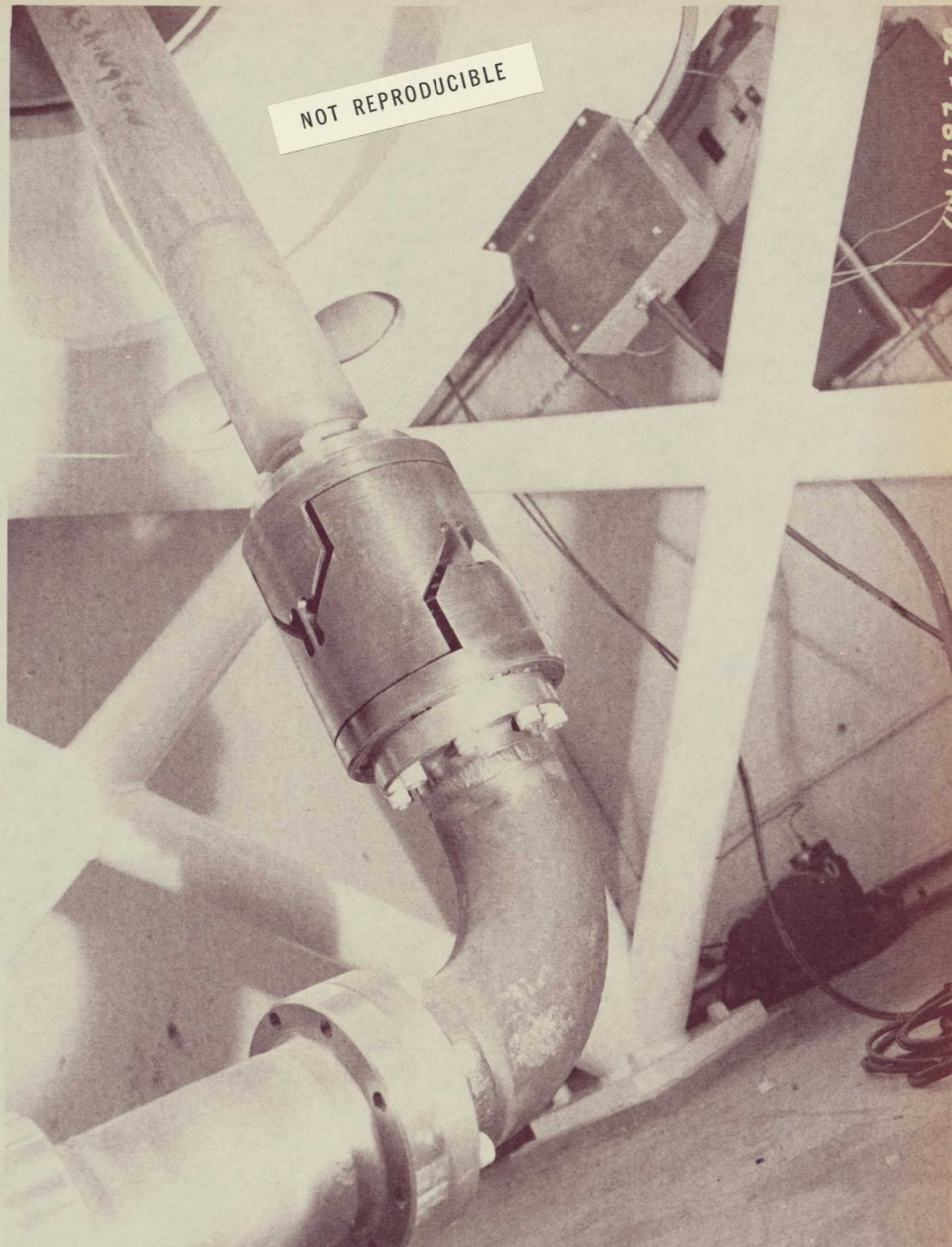

CALC			REVISED	DATE	SIX - COMPONENT BALANCE	FIG. 32
CHECK					BELLOWS - FLEXURE SYSTEM	D6-24850
APPD						
APPD					THE BOEING COMPANY	PAGE 114

114
109

AD 973 D-R3

6 7000

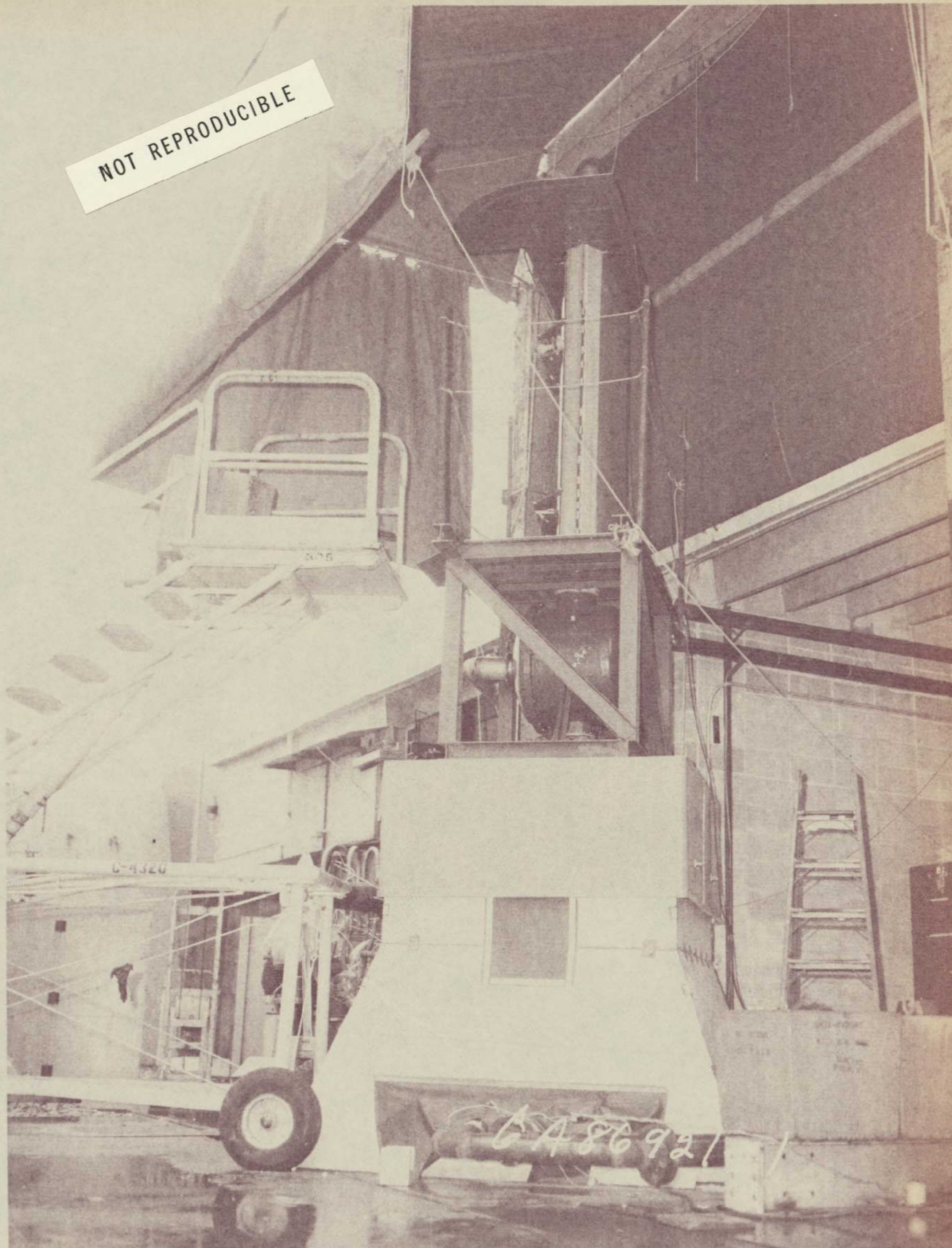

CALC			REVISED	DATE	0.7 SCALE MODEL WITHOUT FLAPS INSTALLED	FIG. 33
CHECK						D6-24850
APPD						
APPD					THE BOEING COMPANY	PAGE 115

115
~~114~~

AD 973 D-R3

6 7000

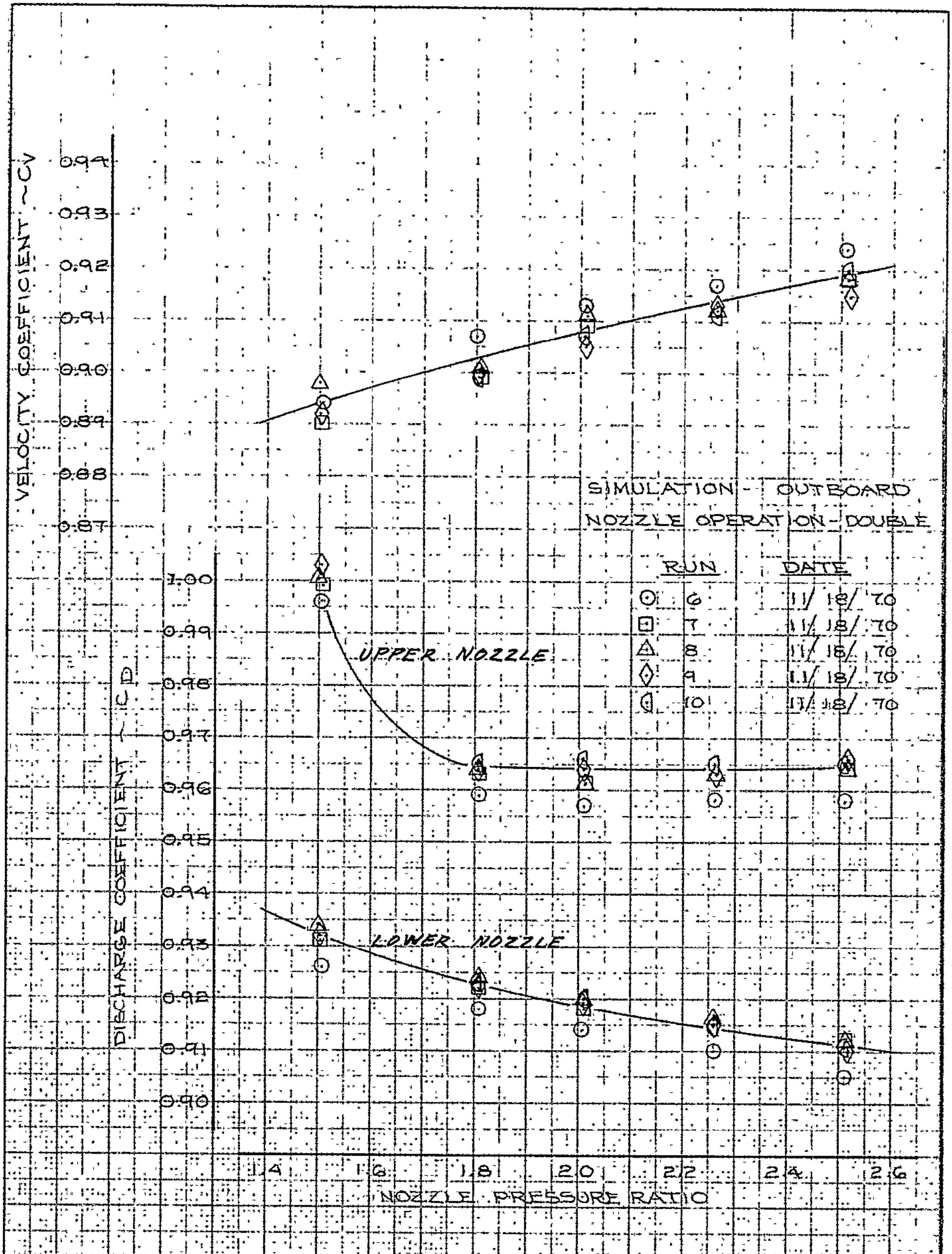

CALC			REVISED	DATE	NOZZLE PERFORMANCE VS PRESSURE RATIO - DOUBLE NOZZLE - OUTBOARD FLAPS OFF	FIG. 34
CHECK						
APR	D. Haakonen	3/30/71				D6-24850
APR					THE BOEING COMPANY	PAGE 116
	[signature]	2/16/71				

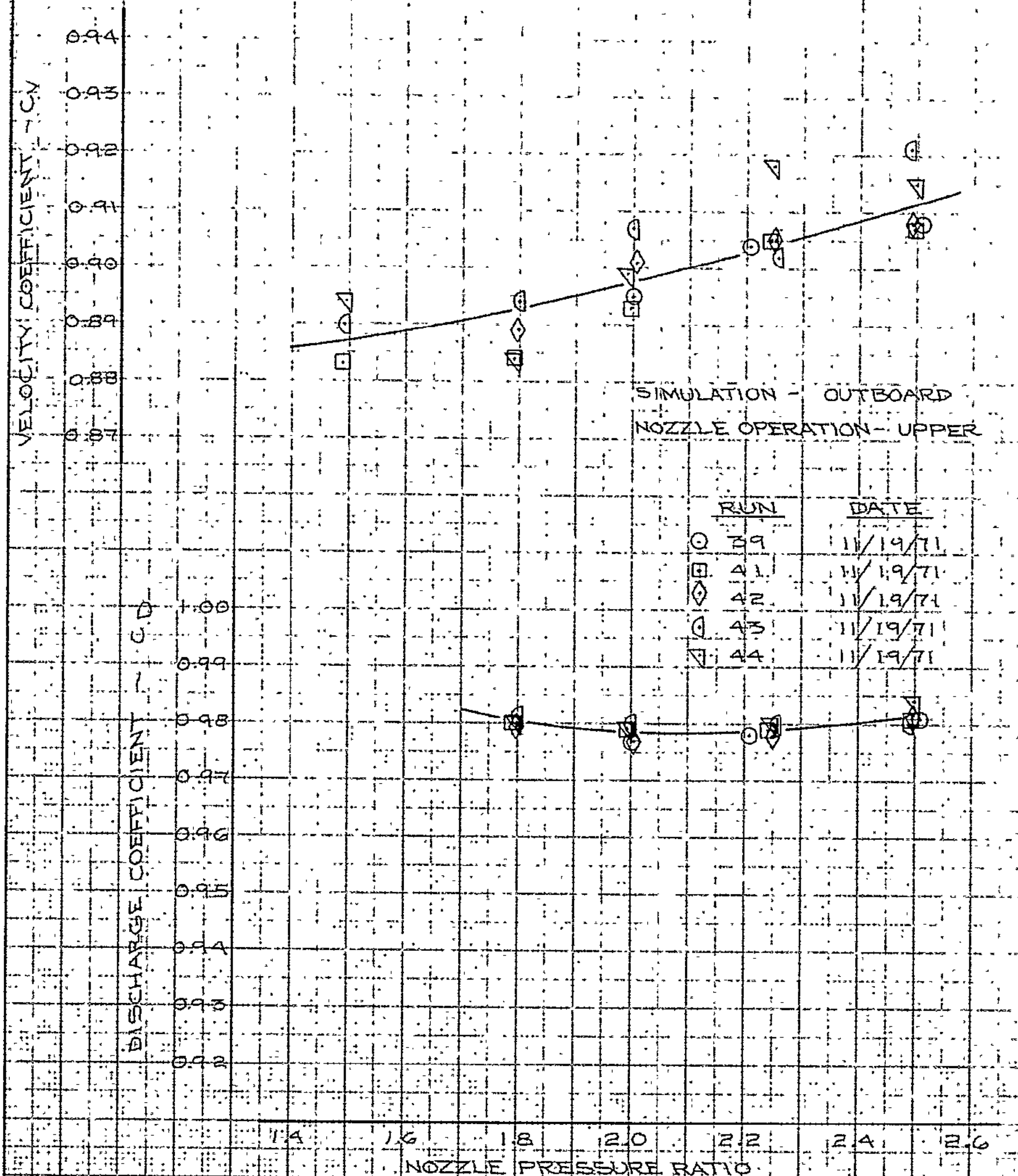

CALC			REVISED	DATE	NOZZLE PERFORMANCE VS PRESSURE RATIO - UPPER NOZZLE - OUTBOARD FLAPS OFF	FIG. 35
CHECK						
APR	D. Waskonn	3/30/71				D6-24850
APR					THE BOEING COMPANY	PAGE 117
	J. Kraft	21/71				

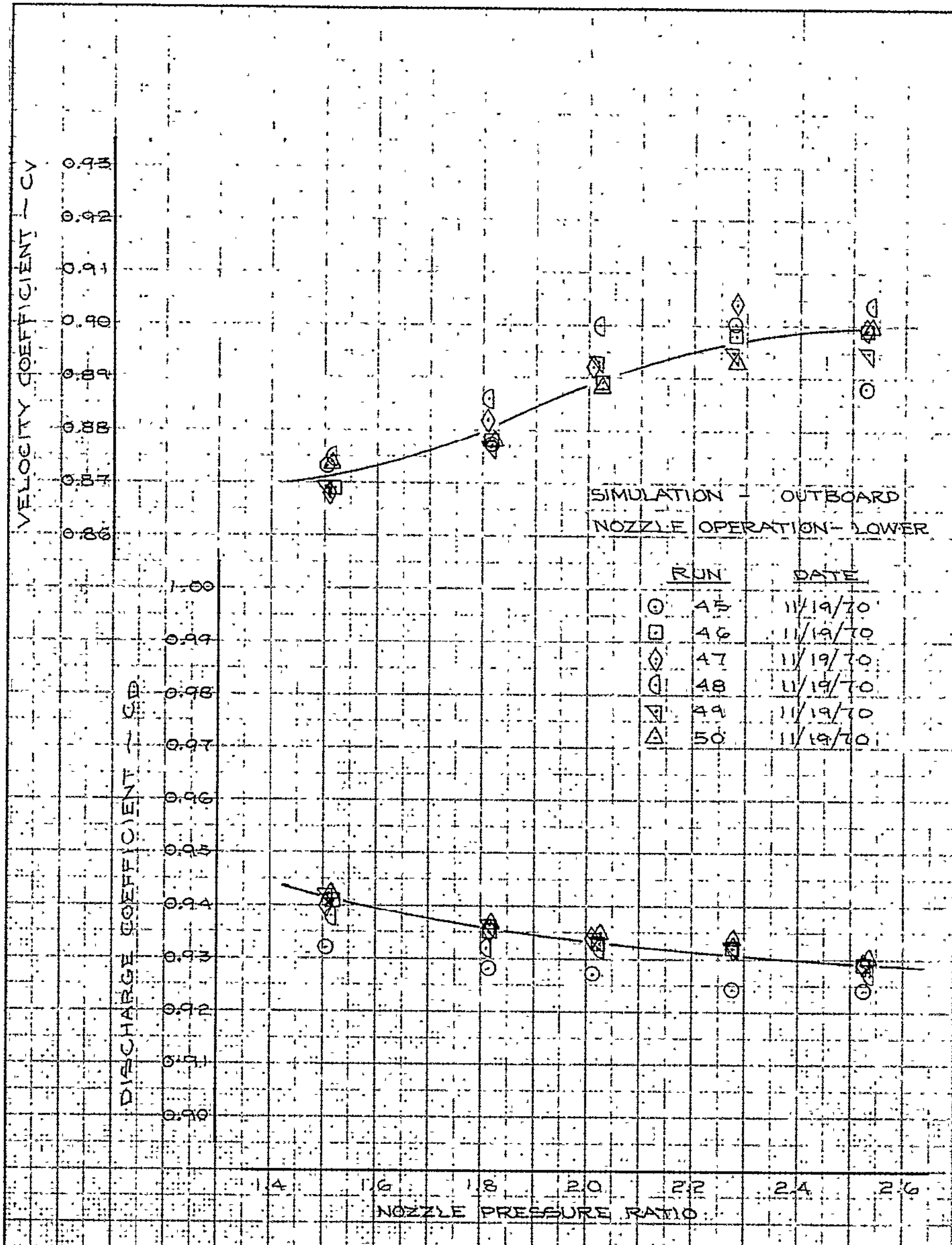

CALC			REVISED	DATE	NOZZLE PERFORMANCE VS PRESSURE RATIO — LOWER NOZZLE — OUTBOARD FLAPS OFF	FIG. 36
CHECK						D6-24850
APR	D. Hashanen	3/30/71				
APR					THE BOEING COMPANY	PAGE 118
	J. Lloyd	2/17/71				

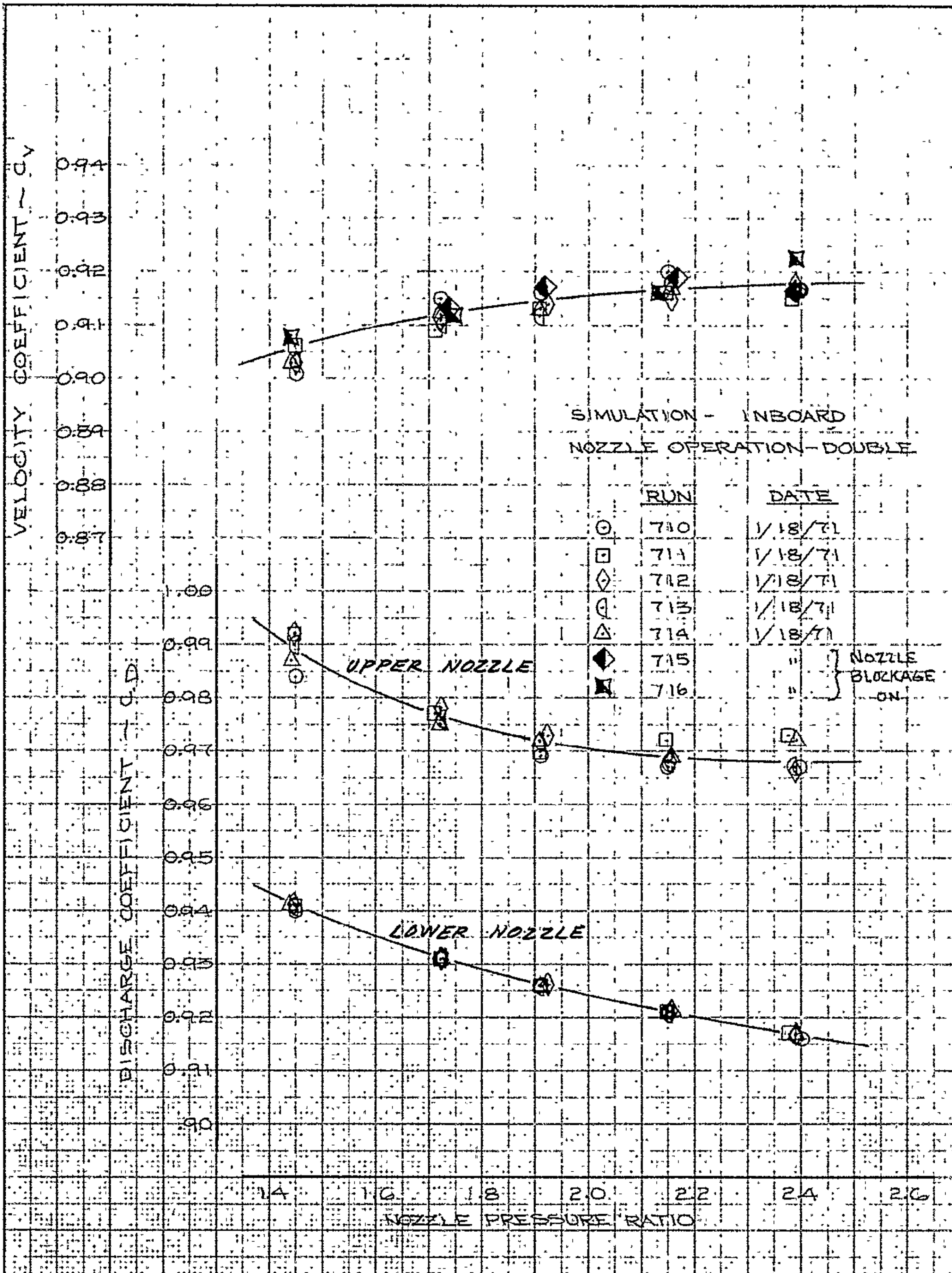

			REVISED	DATE	
CALC					NOZZLE PERFORMANCE VS PRESSURE RATIO - DOUBLE NOZZLE - INBOARD FLAPS OFF
CHECK					
APR	D. Hickman	3/30/71			
APR					THE BOEING COMPANY
	J. Lloyd	2/17/71			

FIG. 37

D6-24850

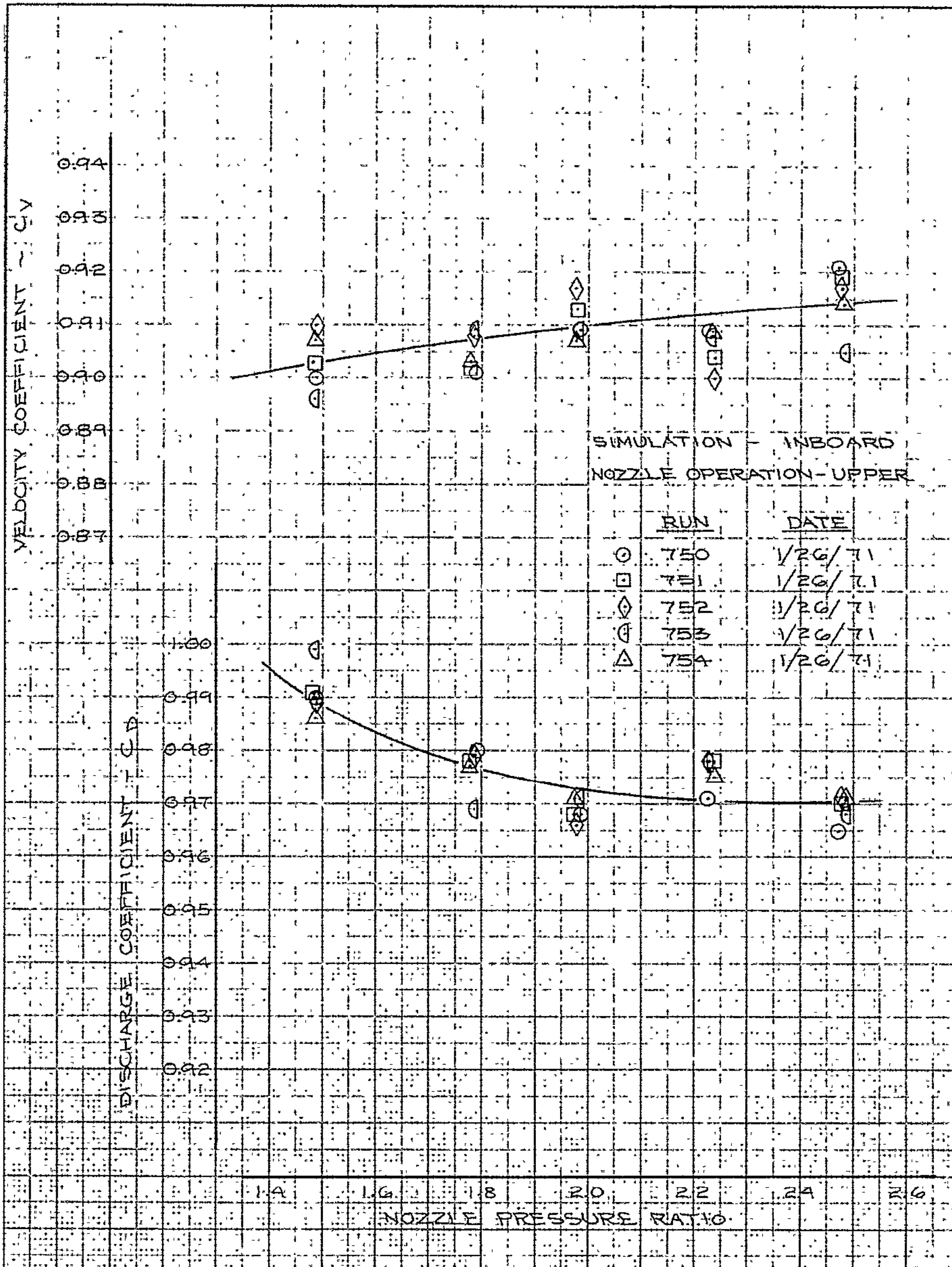

CALC			REVISED	DATE	NOZZLE PERFORMANCE VS PRESSURE RATIO - UPPER NOZZLE - INBOARD FLAPS OFF	FIG. 38
CHECK						D6-24850
APR	D. Harkonen	3/30/71			THE BOEING COMPANY	PAGE 120
APR						
	[illegible]	4/71				

K+E ALBANENE

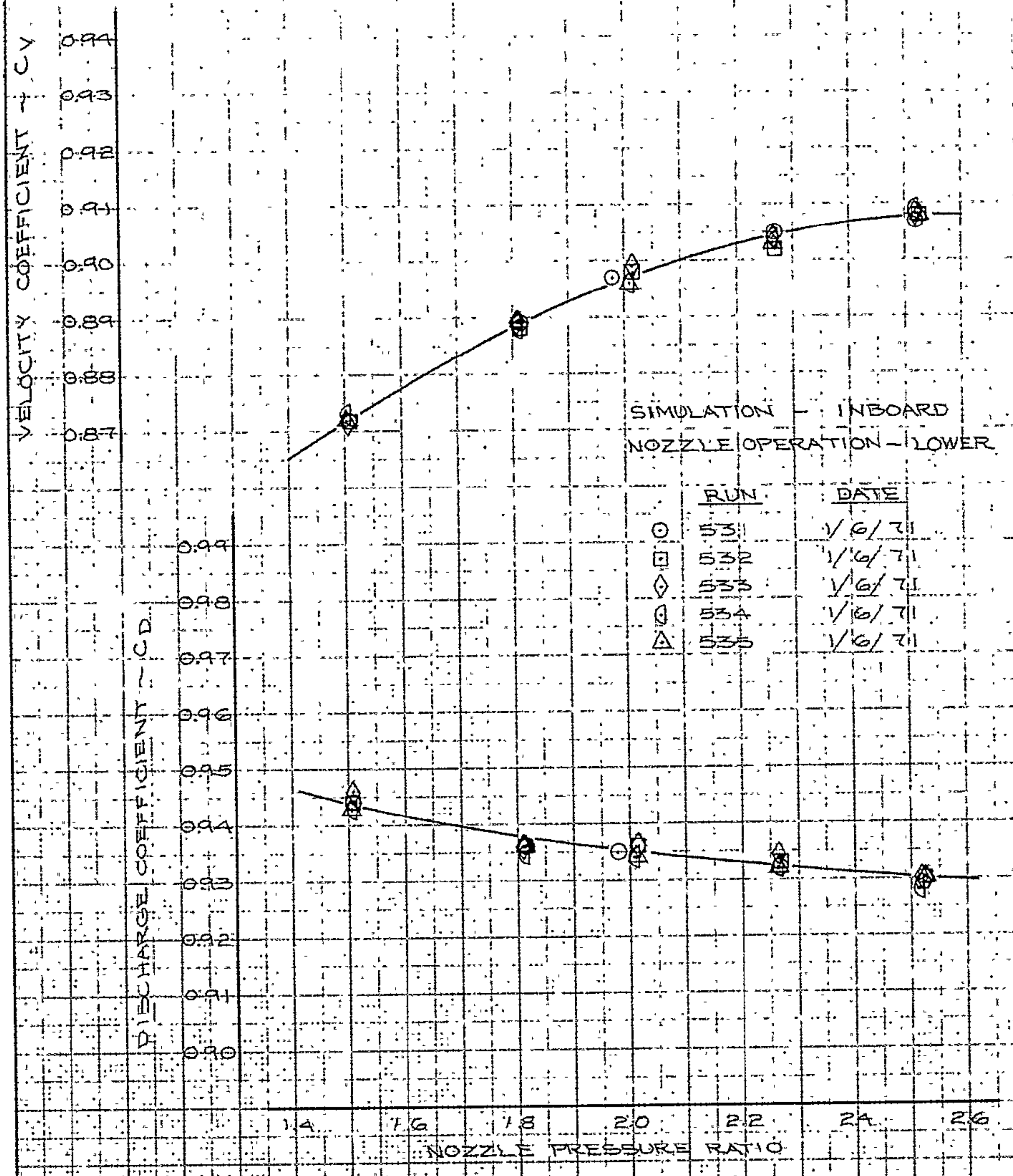

CALC			REVISED	DATE	NOZZLE PERFORMANCE VS PRESSURE RATIO - LOWER NOZZLE - INBOARD FLAPS OFF	FIG. 39
CHECK						D6-24850
APR	D. I. Ja[illegible]	3/30/71				
APR					THE BOEING COMPANY	PAGE 121
	[illegible]	2/17/71				

K+E ALBANENE

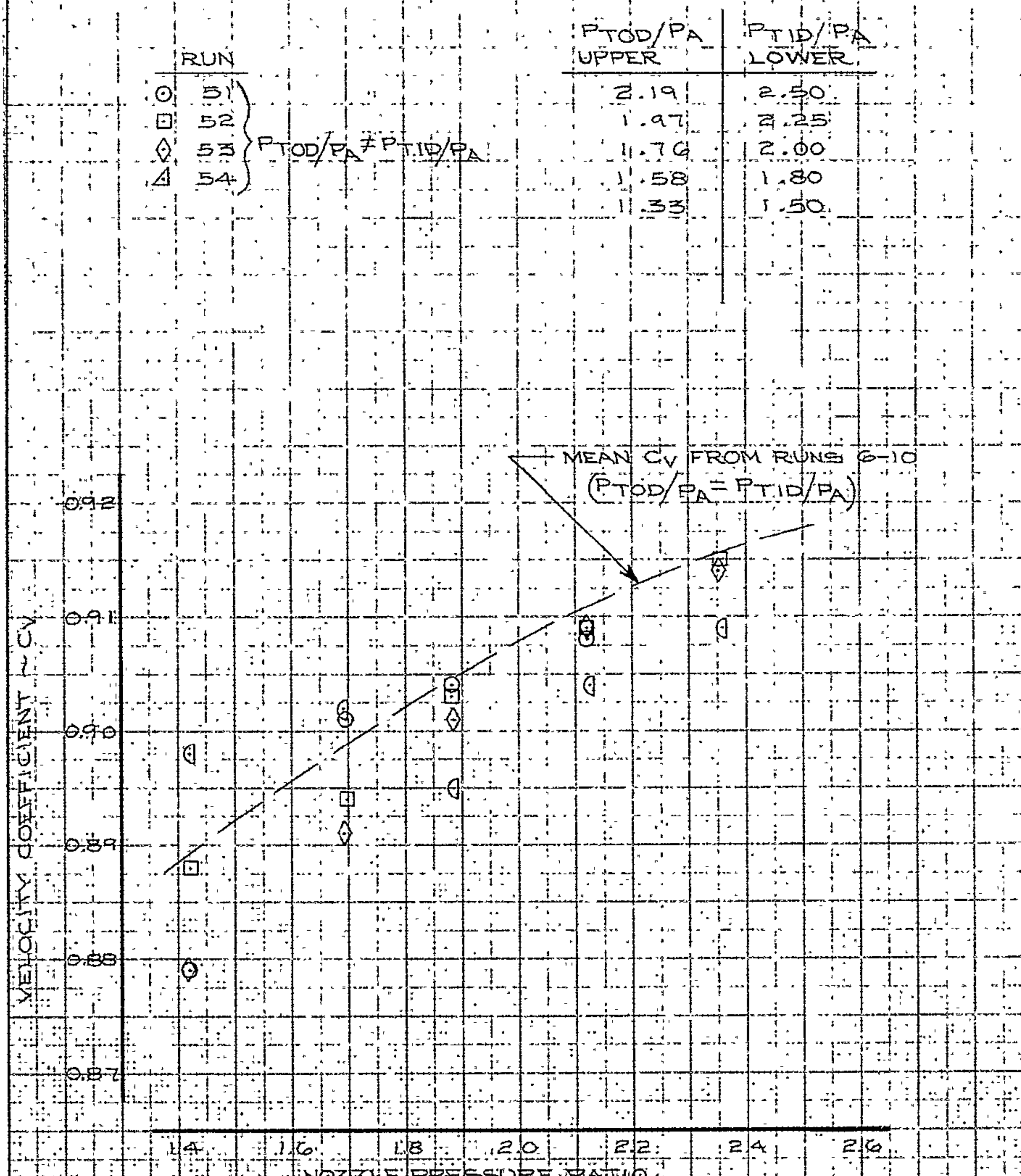

			REVISED	DATE		
CALC					NOZZLE PERFORMANCE AT UNEQUAL NOZZLE PRESSURE RATIOS DOUBLE NOZZLE	FIG. 40
CHECK						D6-24850
APR	D. Haskonen	3/30/71				
APR					THE BOEING COMPANY	PAGE 122
	Lloyt	2/25/71				

K+E ALBANENE

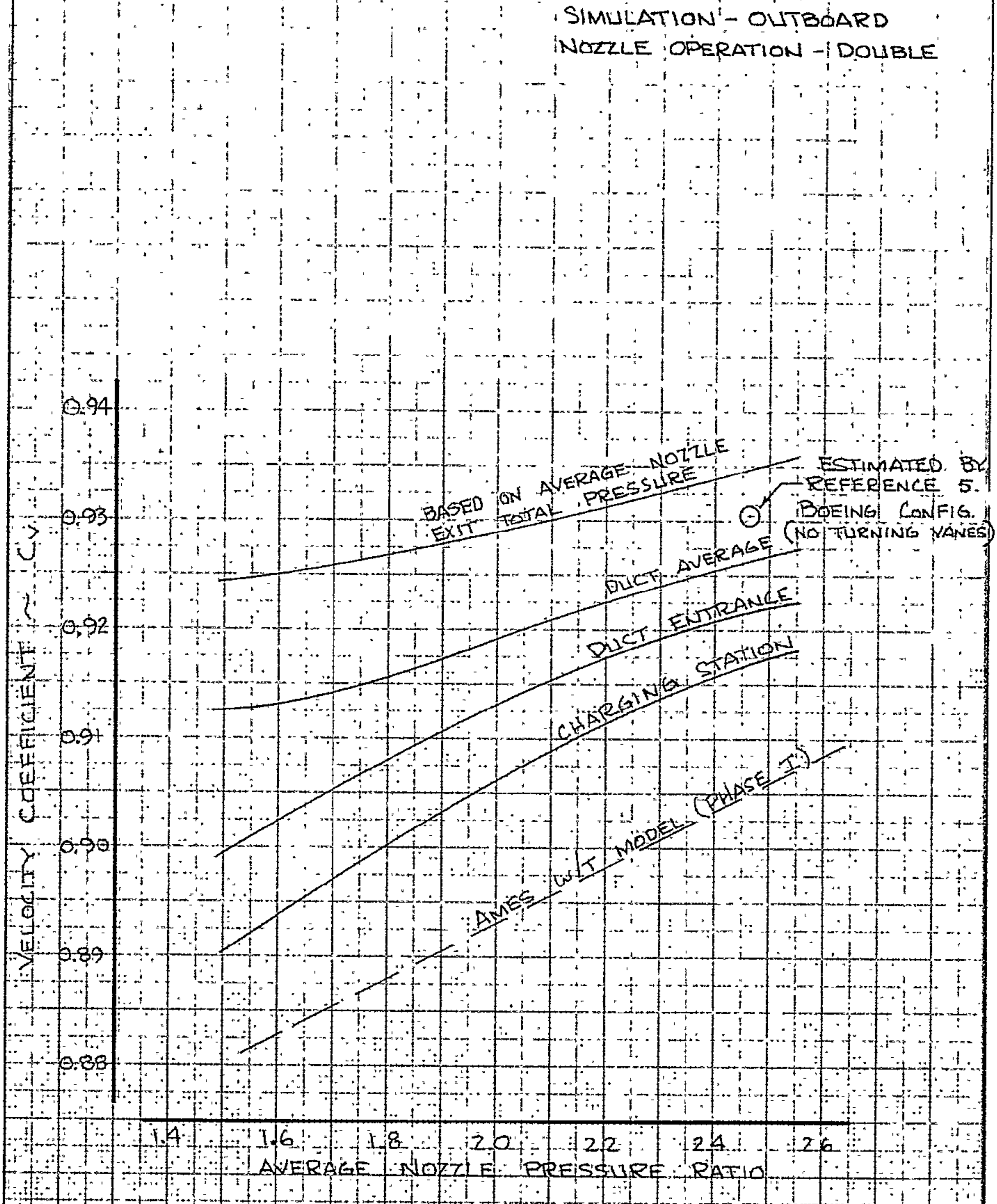

CALC			REVISED	DATE	INFLUENCE OF MODEL CHARGING STATION ON NOZZLE PERFORMANCE LEVELS - DOUBLE NOZZLE	FIG. 41
CHECK						
APR	D. Hachmann	3/30/71				D6-24850
APR					THE BOEING COMPANY	PAGE 123

K+E ALBANENE

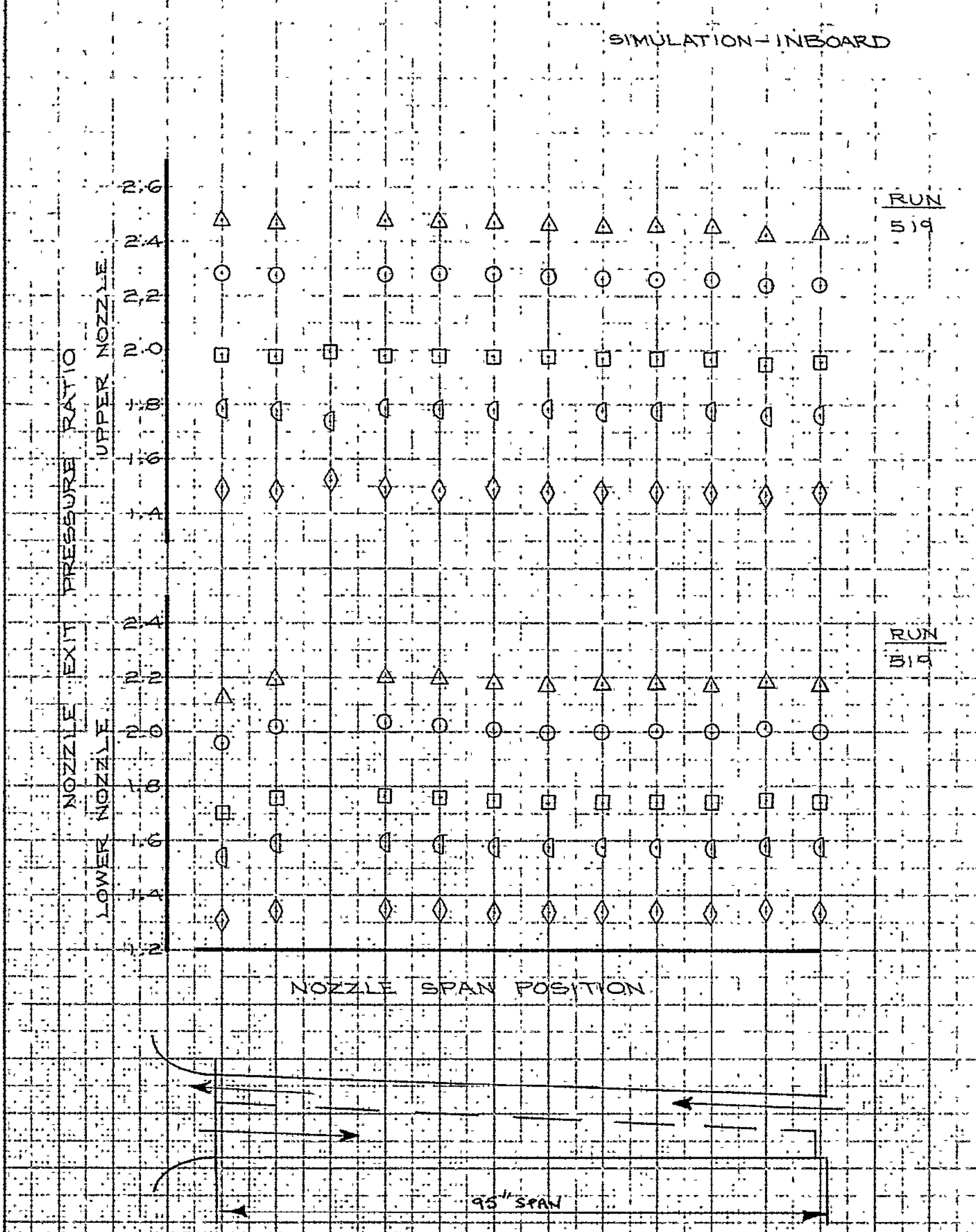

CALC			REVISED	DATE	NOZZLE SPANWISE EXIT TOTAL PRESSURE PROFILES INBOARD SIMULATION	FIG. 42
CHECK						
APR	D. Idechoven	3/30/71				D6-24850
APR					THE BOEING COMPANY	PAGE 124
	Lloyd	2/18/71				

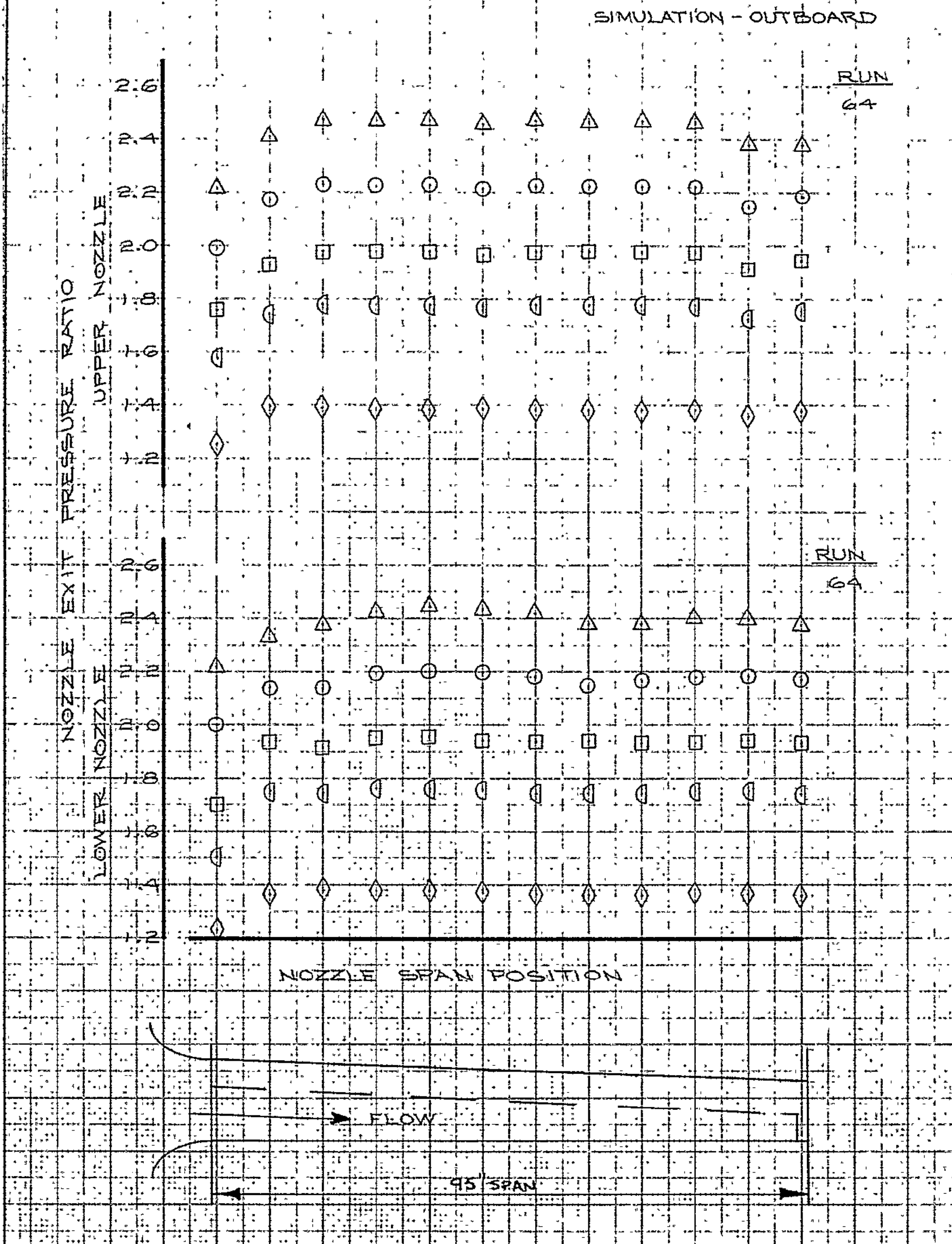

CALC			REVISED	DATE	NOZZLE SPANWISE EXIT TOTAL PRESSURE PROFILES - OUTBOARD SIMULATION	FIG. 43
CHECK						D6-24850
APR	D. I. Sirkonen	3/30/71			THE BOEING COMPANY	PAGE 125
APR						
	J. Hoyt	2/18/71				

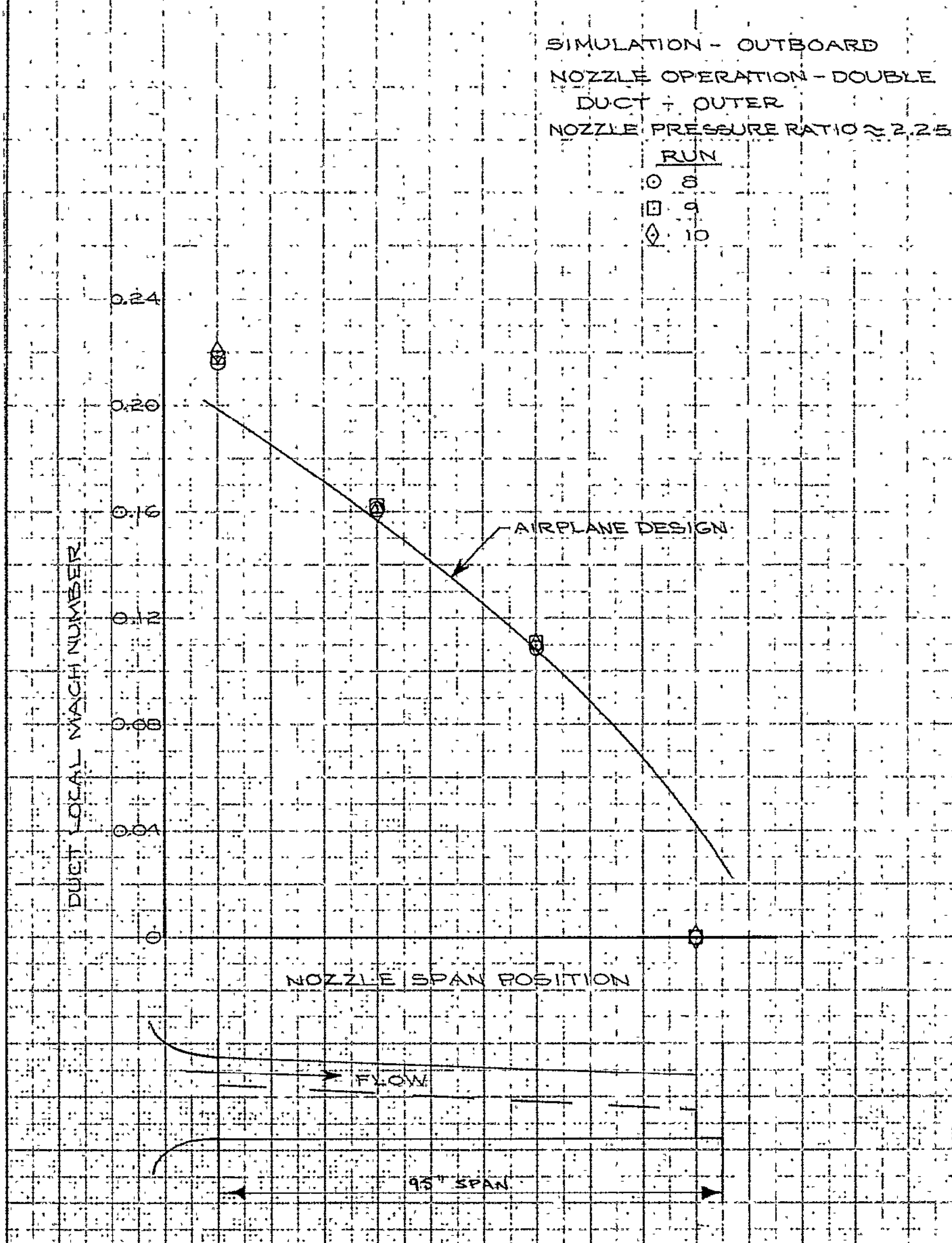

CALC			REVISED	DATE
CHECK				
APR	D. I. Taskonen	3/30/71		
APR				
	J. Hoyt	2/18/71		

OUTER DUCT LOCAL MACH NUMBER
OUTBOARD SIMULATION

FIG. 44

D6-24850

THE BOEING COMPANY

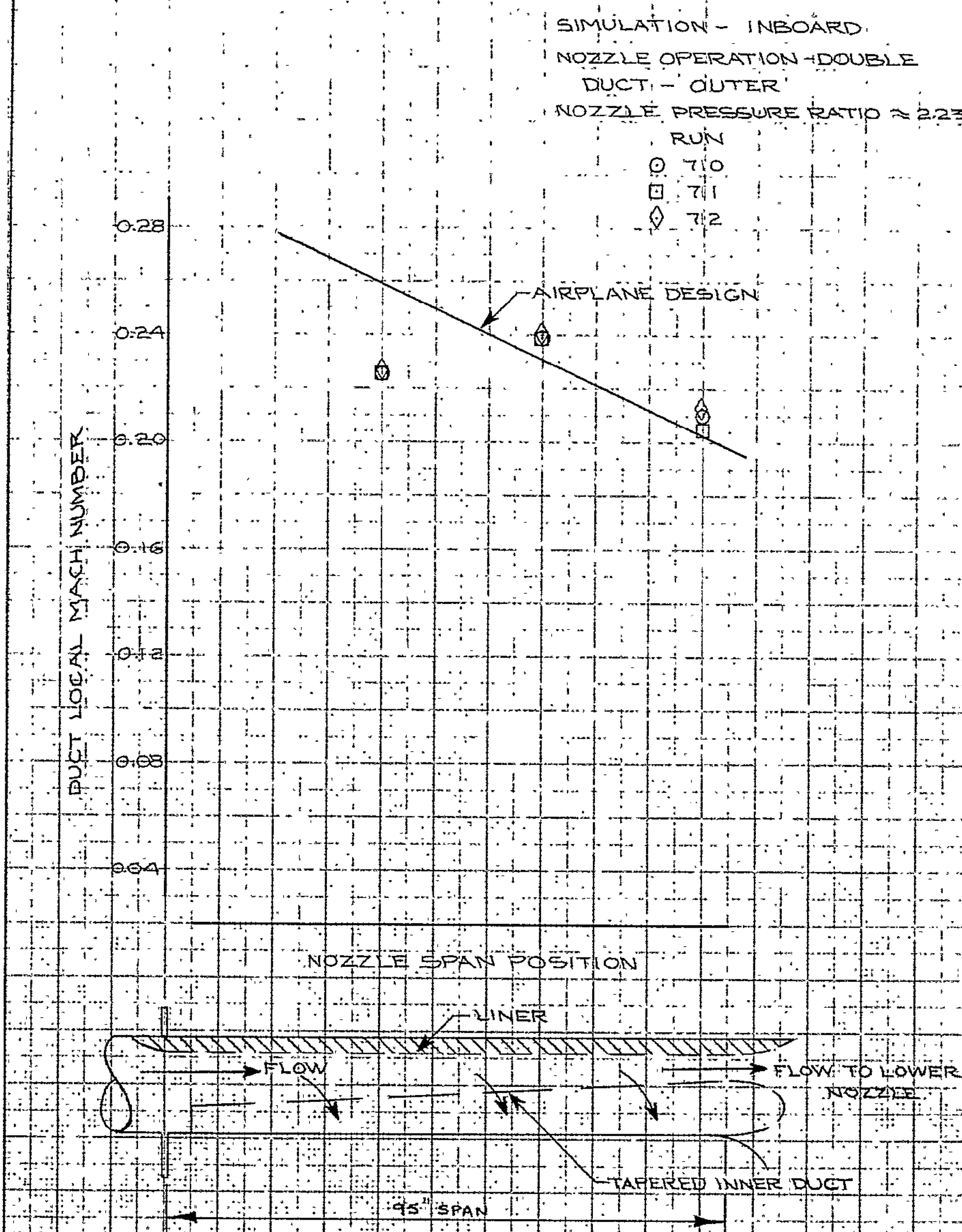

			REVISED	DATE		
CALC					OUTER DUCT LOCAL MACH NUMBER INBOARD SIMULATION	FIG. 45
CHECK						D6-24850
APR	D. Hackman	3/30/71			THE BOEING COMPANY	PAGE 127
APR						
	[illegible]	3/30/71				

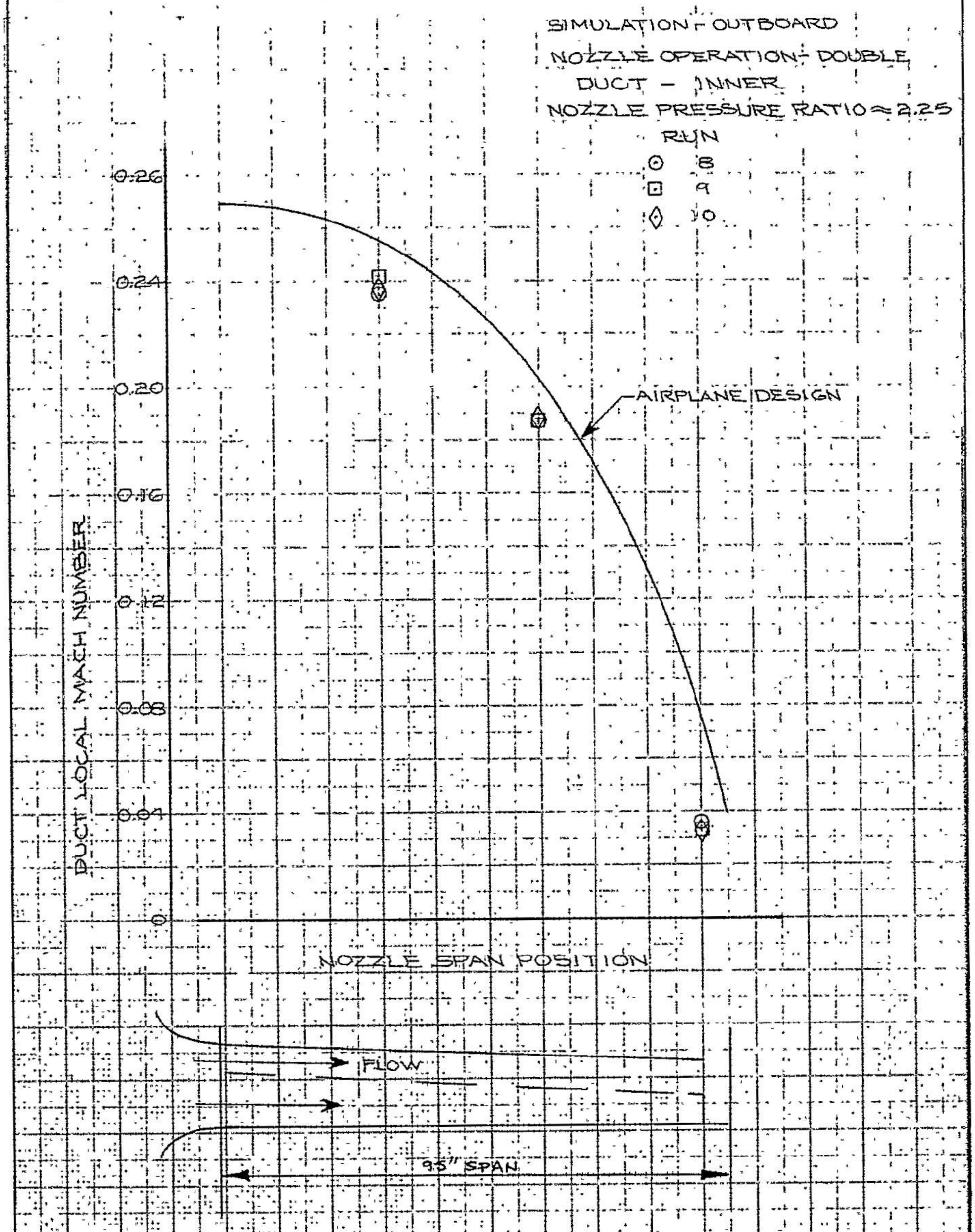

CALC			REVISED	DATE	INNER DUCT LOCAL MACH NUMBER OUTBOARD SIMULATION	FIG. 46
CHECK						D6-24850
APR	D. I. Harhouen	3/30/71				
APR					THE BOEING COMPANY	PAGE 128

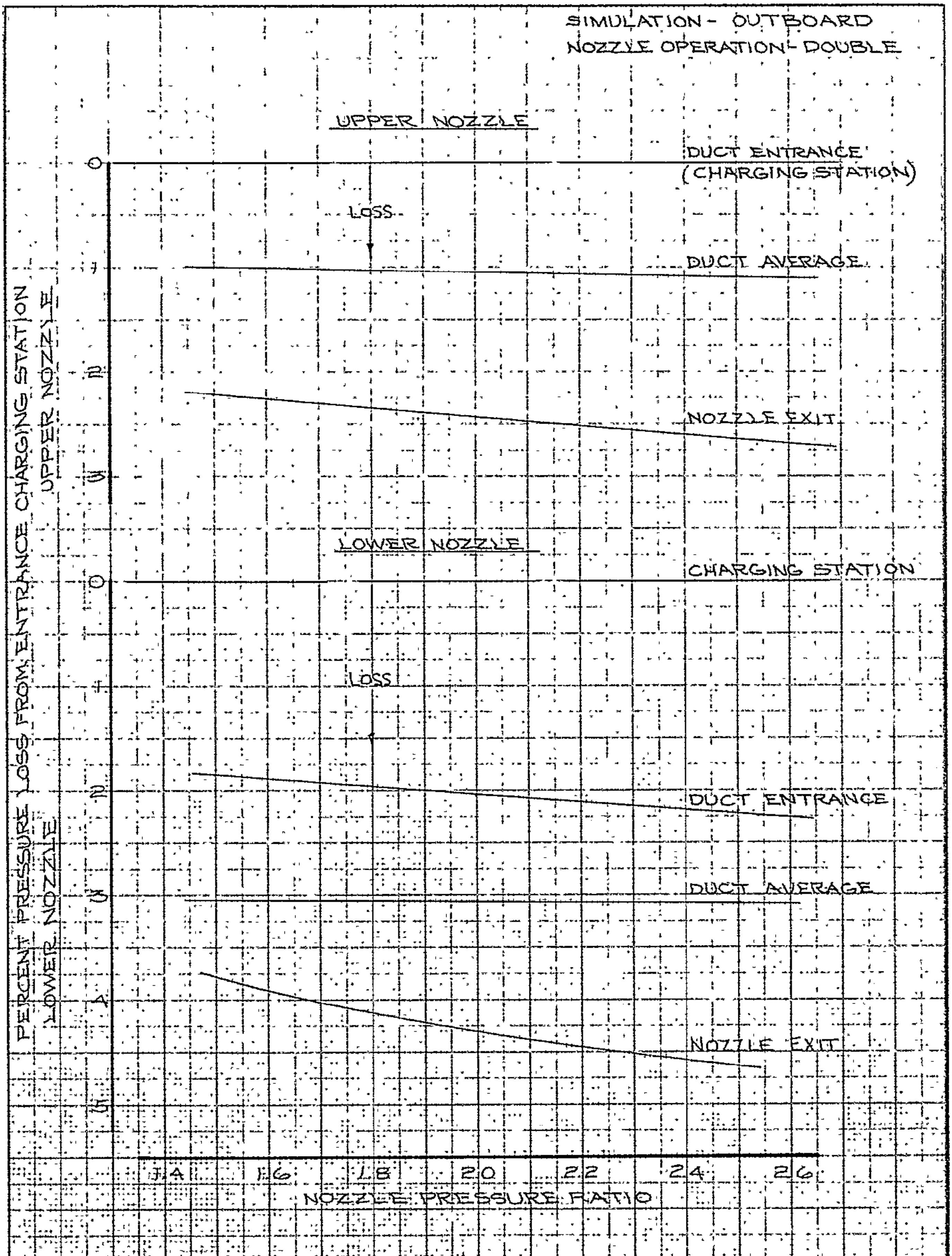

CALC			REVISED	DATE	DUCT - NOZZLE PRESSURE LOSSES OUTBOARD SIMULATION	FIG. 47
CHECK						
APR	J. Haikonen	3/30/71				D6-24850
APR	J. Hoyt	2/23/71			THE BOEING COMPANY	PAGE 129

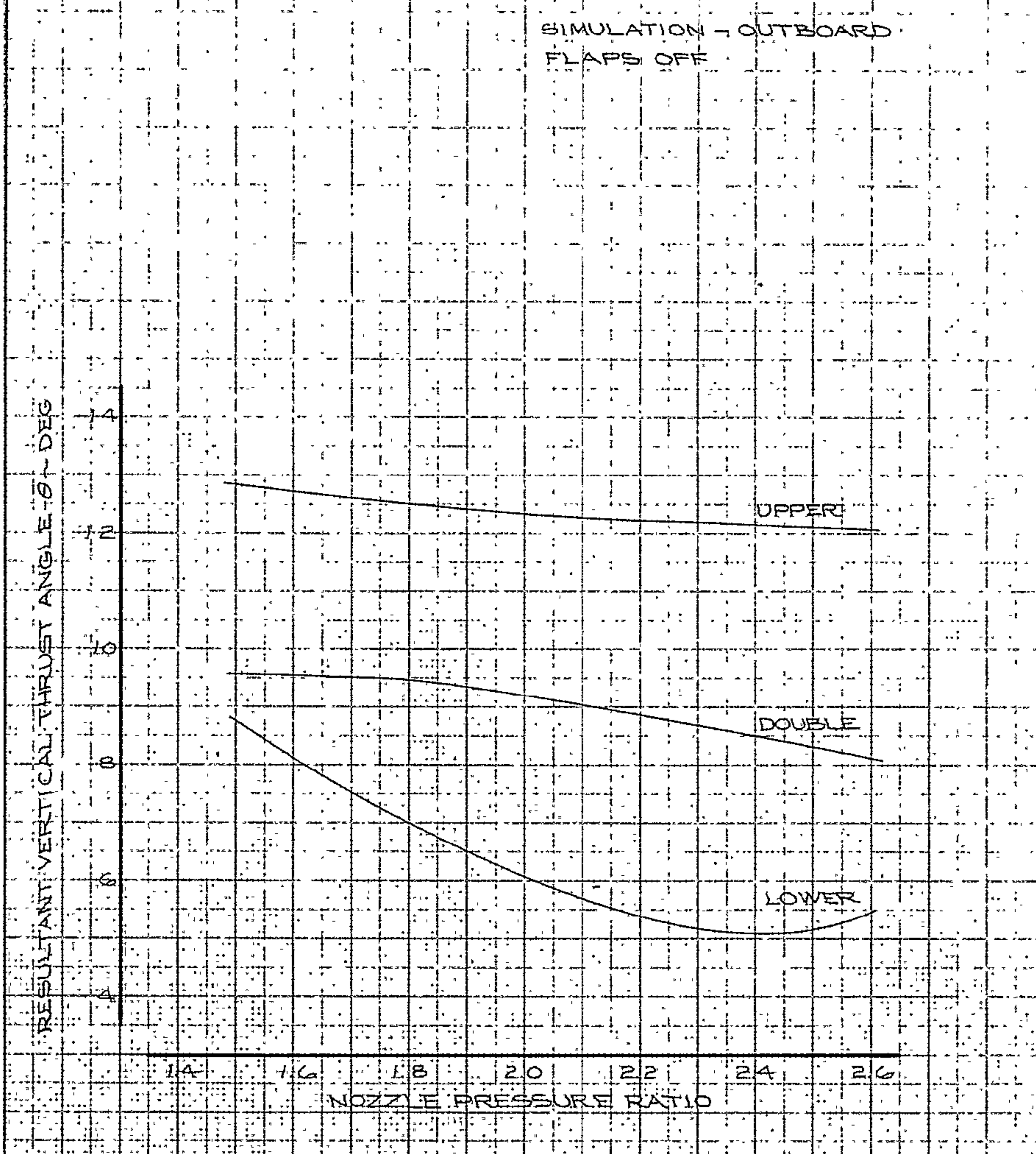

CALC			REVISED	DATE	RESULTANT VERTICAL THRUST ANGLE - ALL NOZZLE OPERATION MODES - OUTBOARD	FIG. 48
CHECK						
APR	D. Hashorum	3/30/71				D6-24850
APR					THE BOEING COMPANY	PAGE 130
	J. Lloyd	7/23/71				

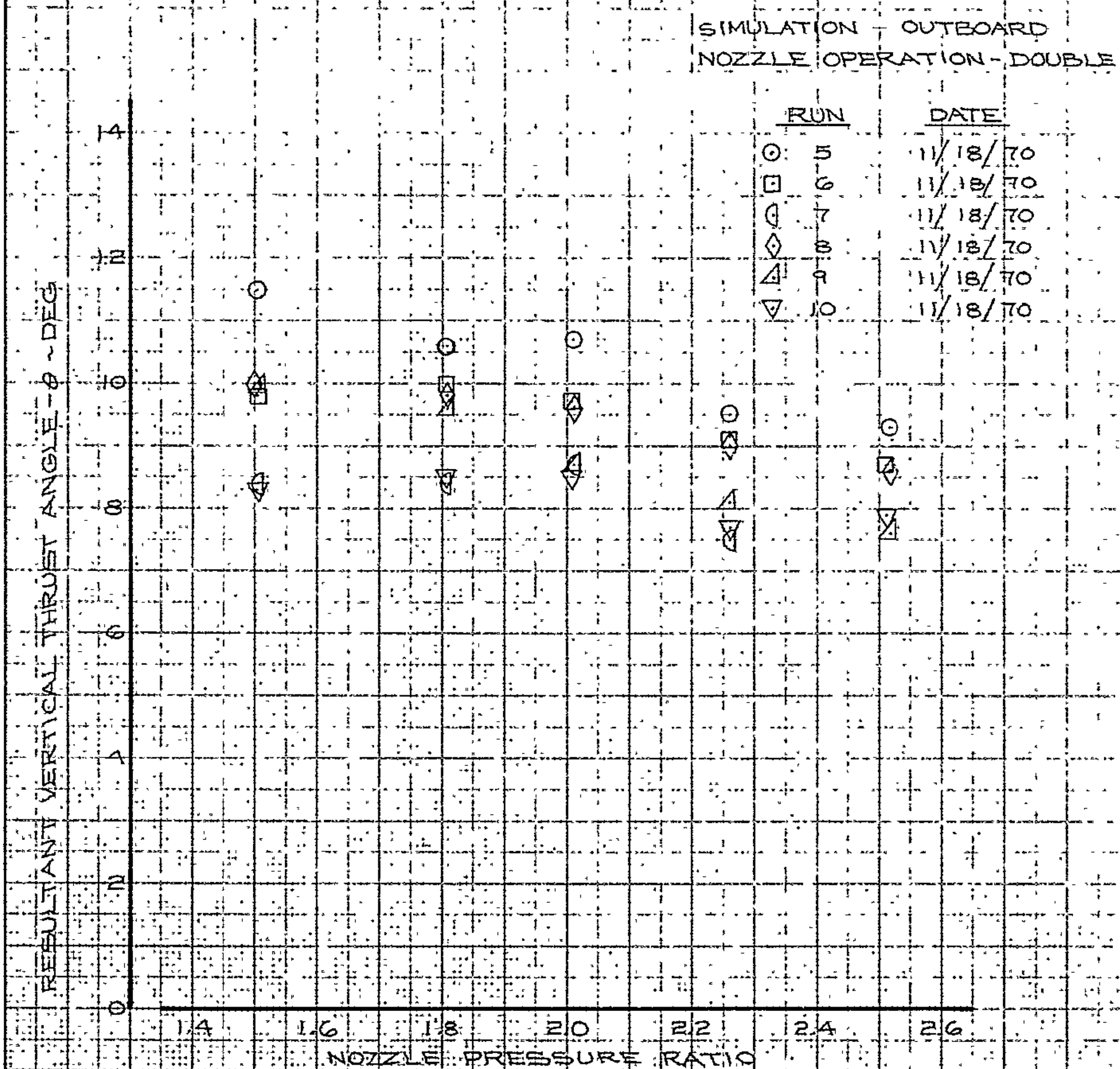

CALC			REVISED	DATE	RESULTANT VERTICAL THRUST ANGLE	FIG. 49
CHECK					UPPER NOZZLE OUTBOARD	D6-24850
APR	D. Hashimoto	3/30/71				
APR					THE BOEING COMPANY	PAGE 131
	J.Hoyt	3/18/71				

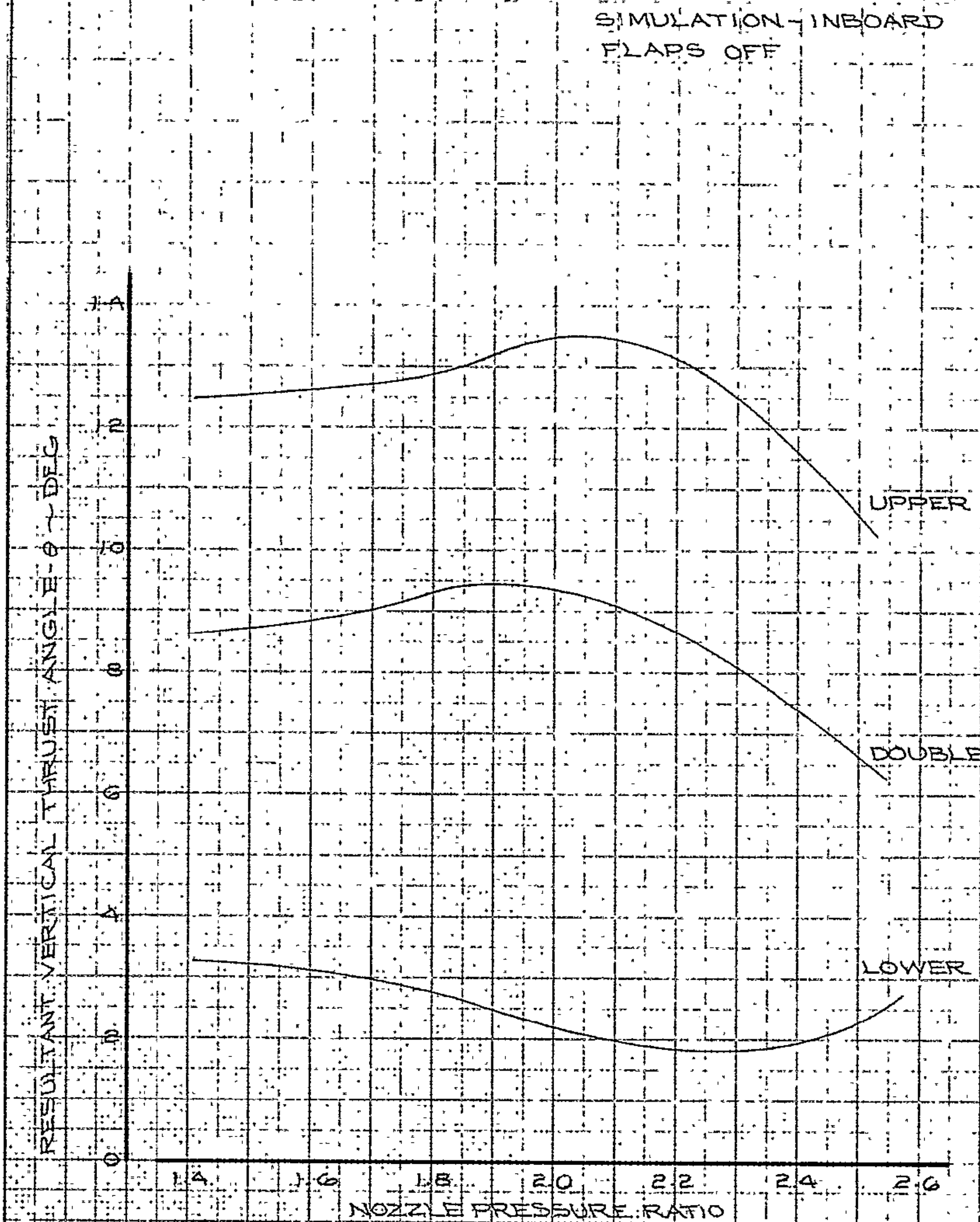

			REVISED	DATE
CALC				
CHECK				
APR	D. I. Jackson	3/30/71		
APR				
	J. Hoyt	2/23/71		

RESULTANT VERTICAL THRUST ANGLE - ALL NOZZLE OPERATION MODES INBOARD

FIG. 50

D6-24850

THE BOEING COMPANY

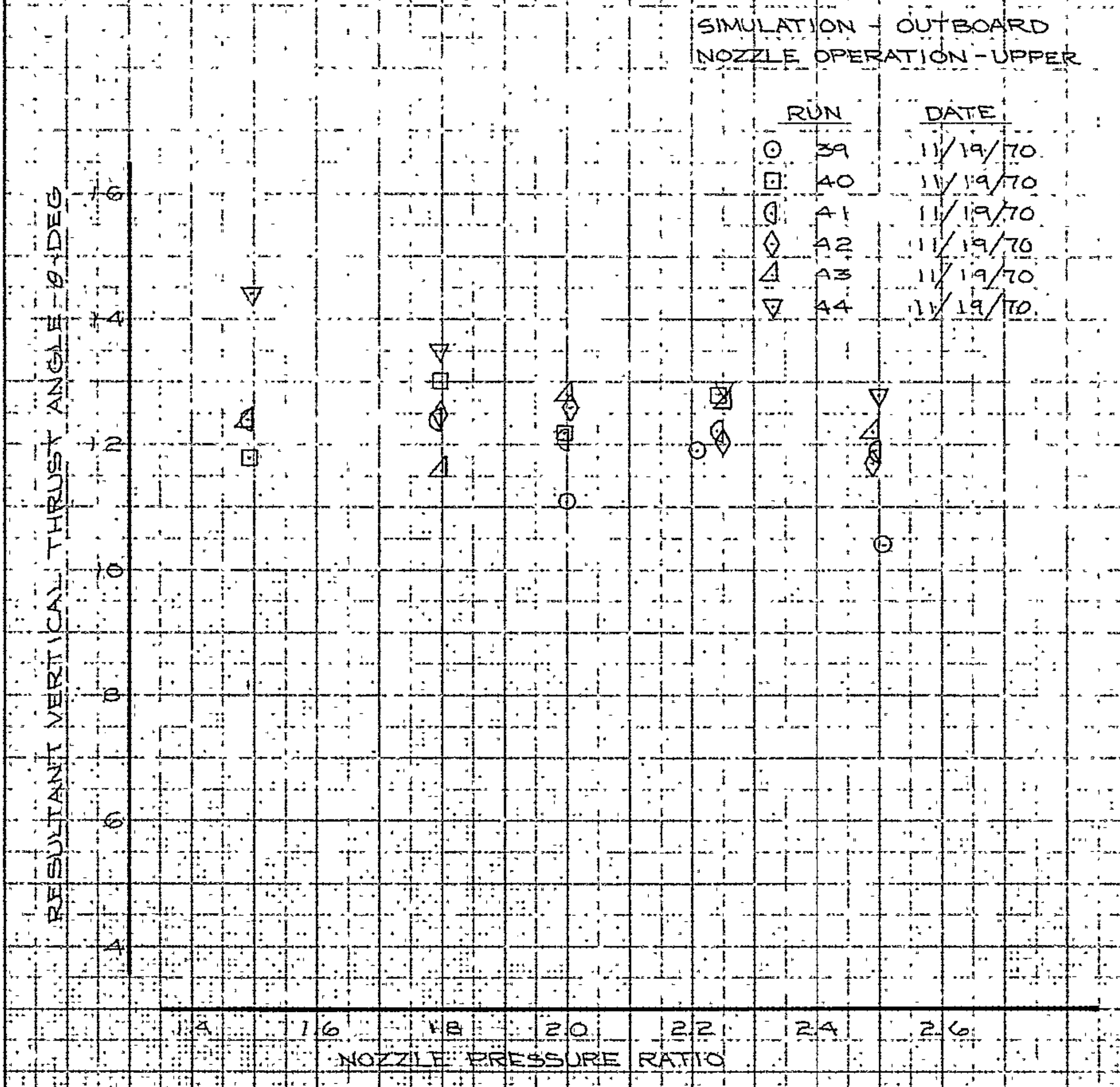

CALC			REVISED	DATE	RESULTANT VERTICAL THRUST ANGLE	FIG. 51
CHECK						
APR	D. Idashonen	3/30/71			UPPER NOZZLE OUTBOARD	D6-24850
APR					THE BOEING COMPANY	PAGE 133

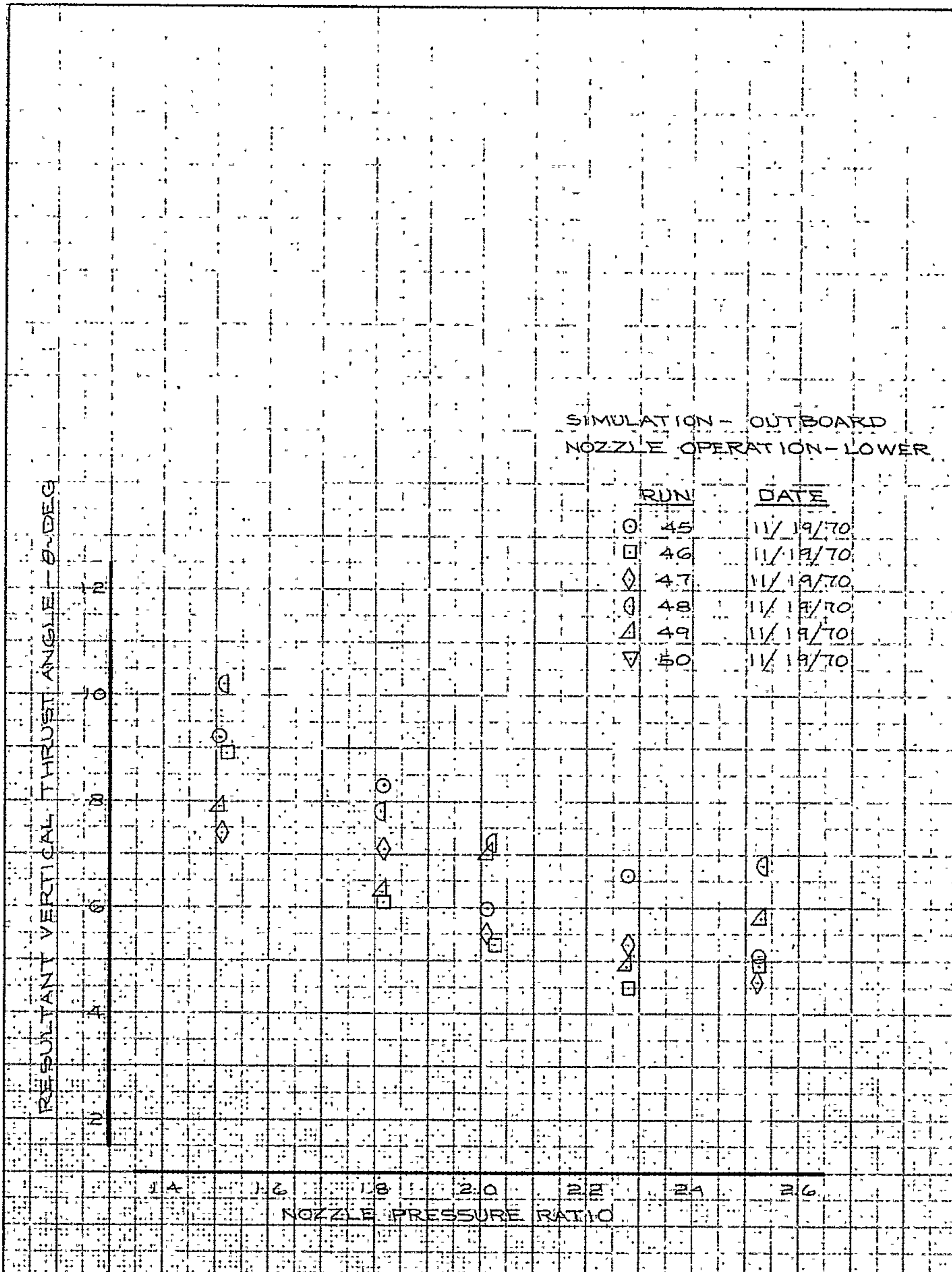

			REVISED	DATE		
CALC					RESULTANT VERTICAL THRUST ANGLE	FIG. 52
CHECK						
APR	D. L. Laskonen	3/30/71			LOWER NOZZLE OUTBOARD	D6-24850
APR						
	j. hoyt	2/18/71			THE BOEING COMPANY	PAGE 134

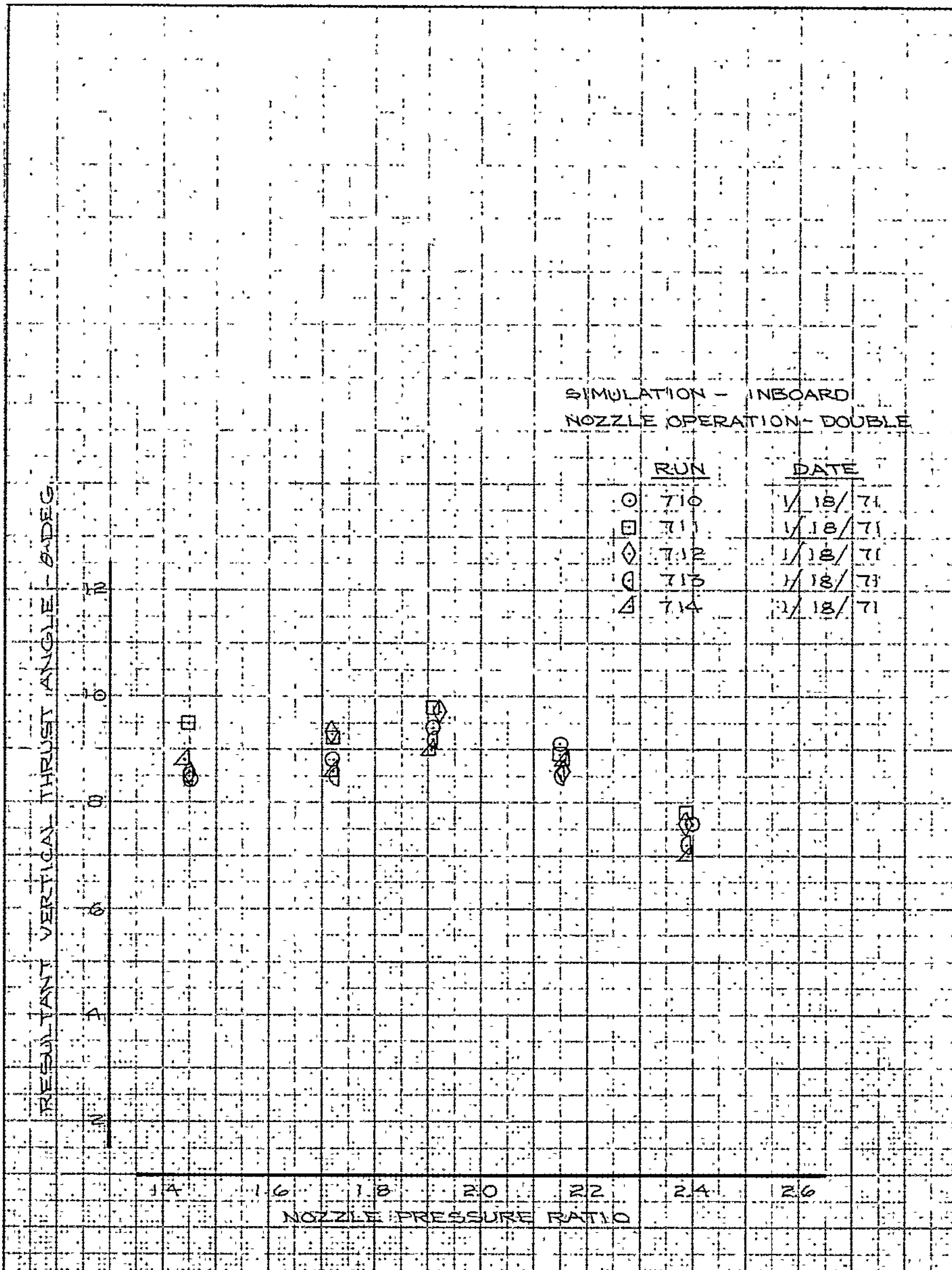

			REVISED	DATE		
CALC					RESULTANT VERTICAL THRUST ANGLE	FIG. 53
CHECK					DOUBLE NOZZLE INBOARD	D6-24850
APR	D. Harhonen	3/30/71			THE BOEING COMPANY	PAGE 135
APR		3/1/71				

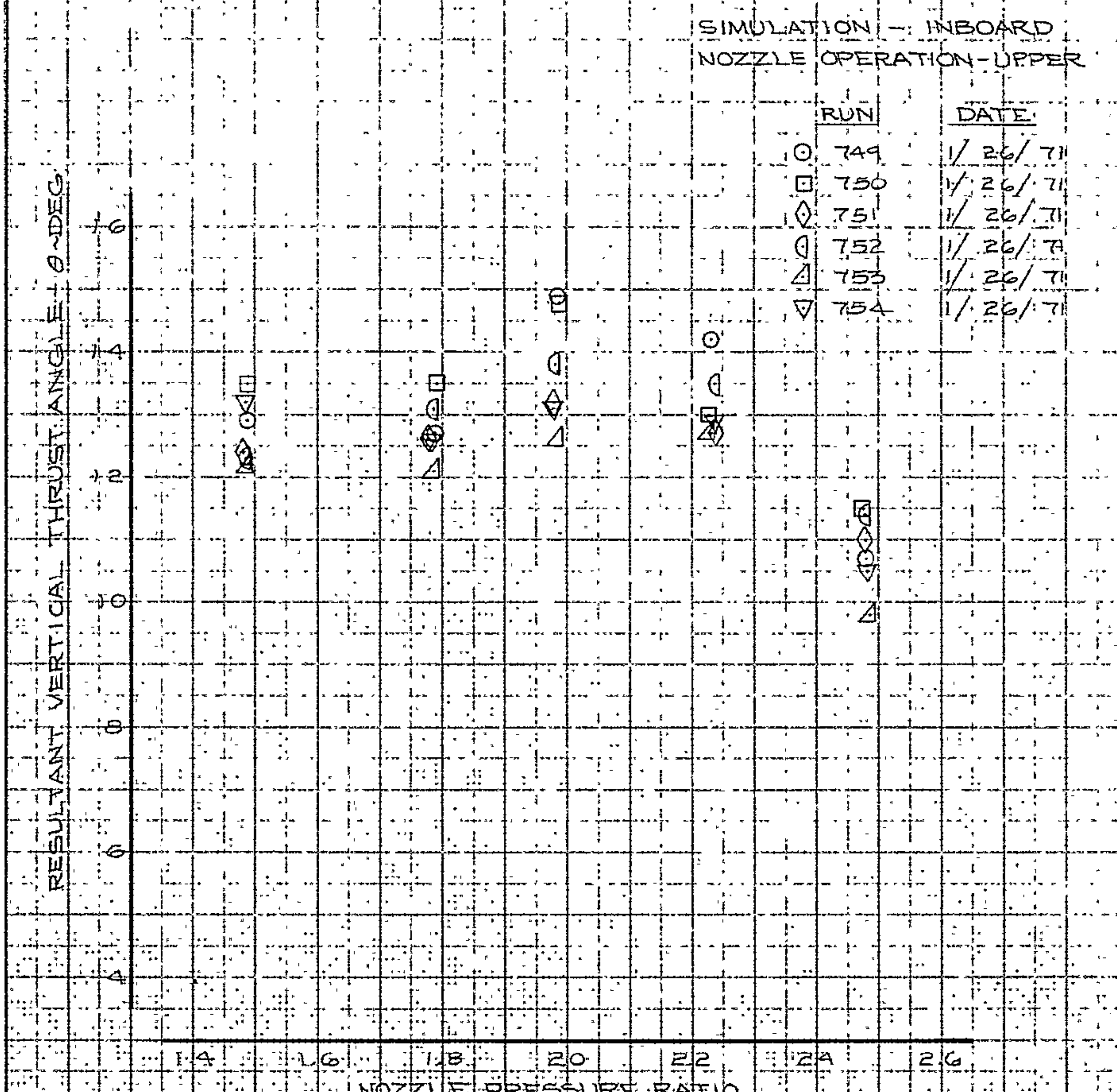

CALC			REVISED	DATE	RESULTANT VERTICAL THRUST ANGLE	FIG. 54
CHECK						
APR	D. Hackmann	3/30/71			UPPER NOZZLE INBOARD	D6-24850
APR					THE BOEING COMPANY	PAGE 136
	J. Kayto	2/18/71				

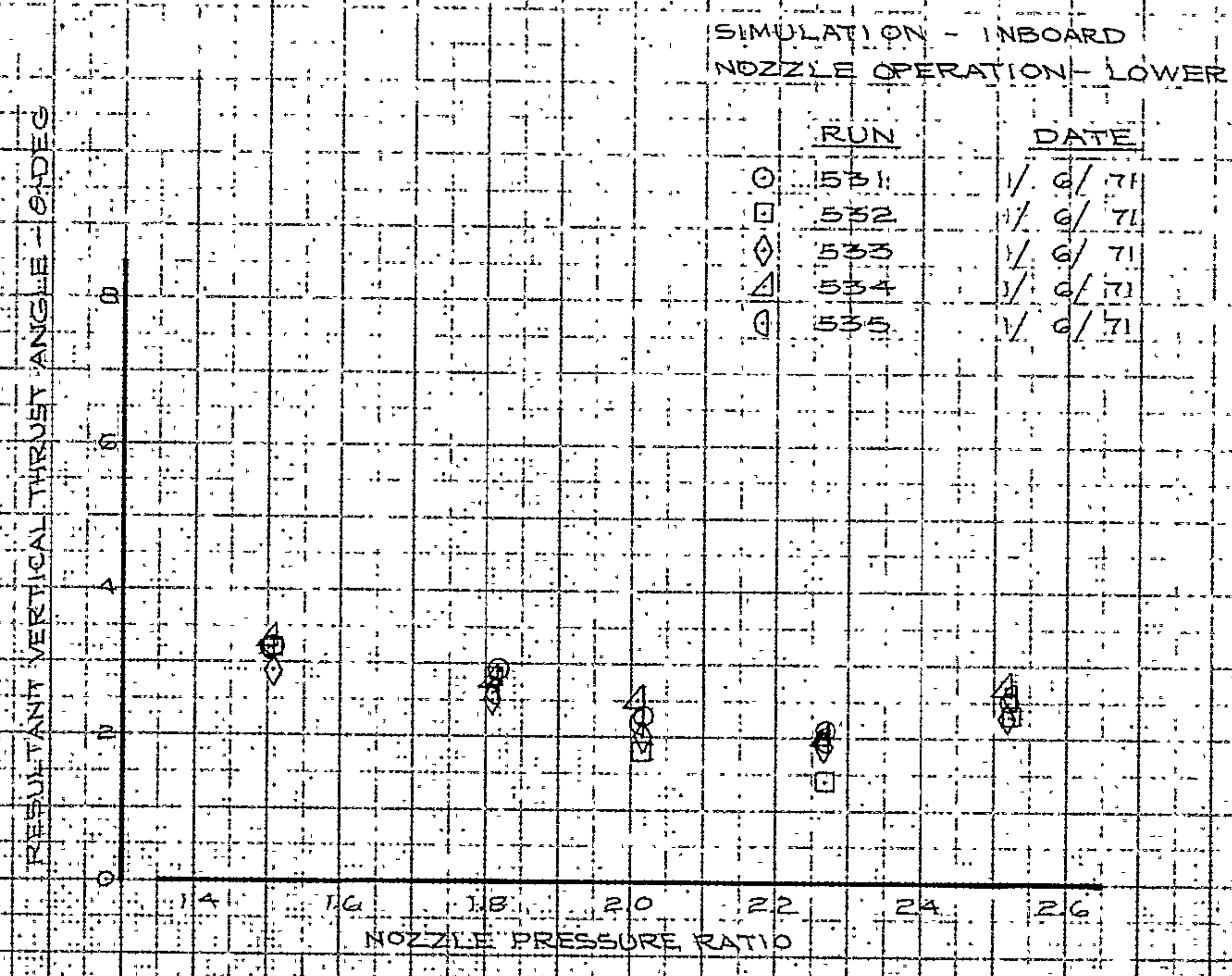

CALC			REVISED	DATE	RESULTANT VERTICAL THRUST ANGLE	FIG. 55
CHECK						
APR	A. J. Jackson	3/30/71			LOWER NOZZLE INBOARD	D6-24850
APR	J. Lloyd	7/18/71			THE BOEING COMPANY	PAGE 137

K+E ALBANENE

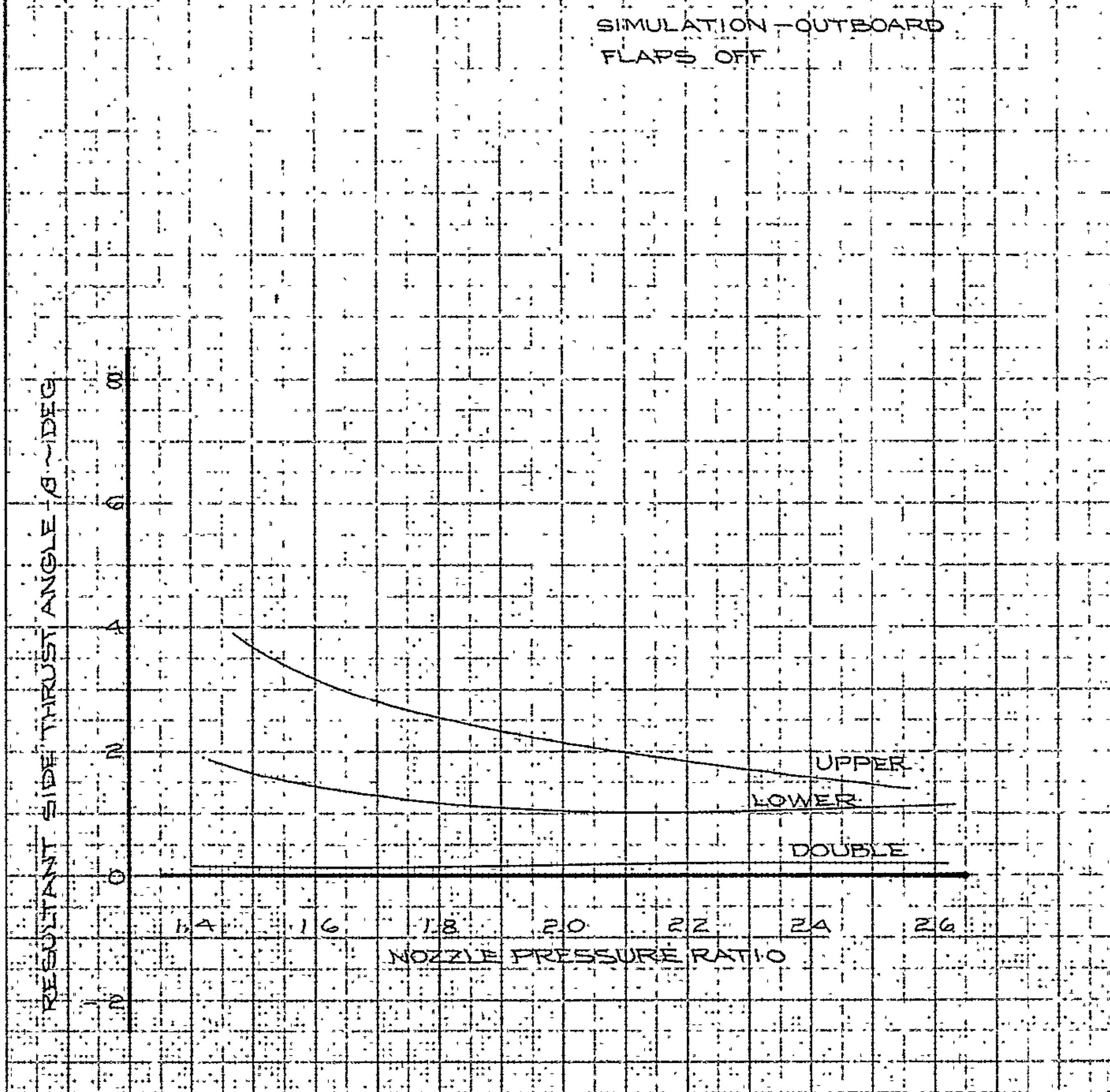

CALC			REVISED	DATE
CHECK				
APR	D. Vachonn	3/30/71		
APR				
	J. Lloyd	2/23/71		

RESULTANT SIDE THRUST ANGLE — ALL NOZZLE OPERATION MODES — OUTBOARD

Fig. 56

D6-24850

THE BOEING COMPANY

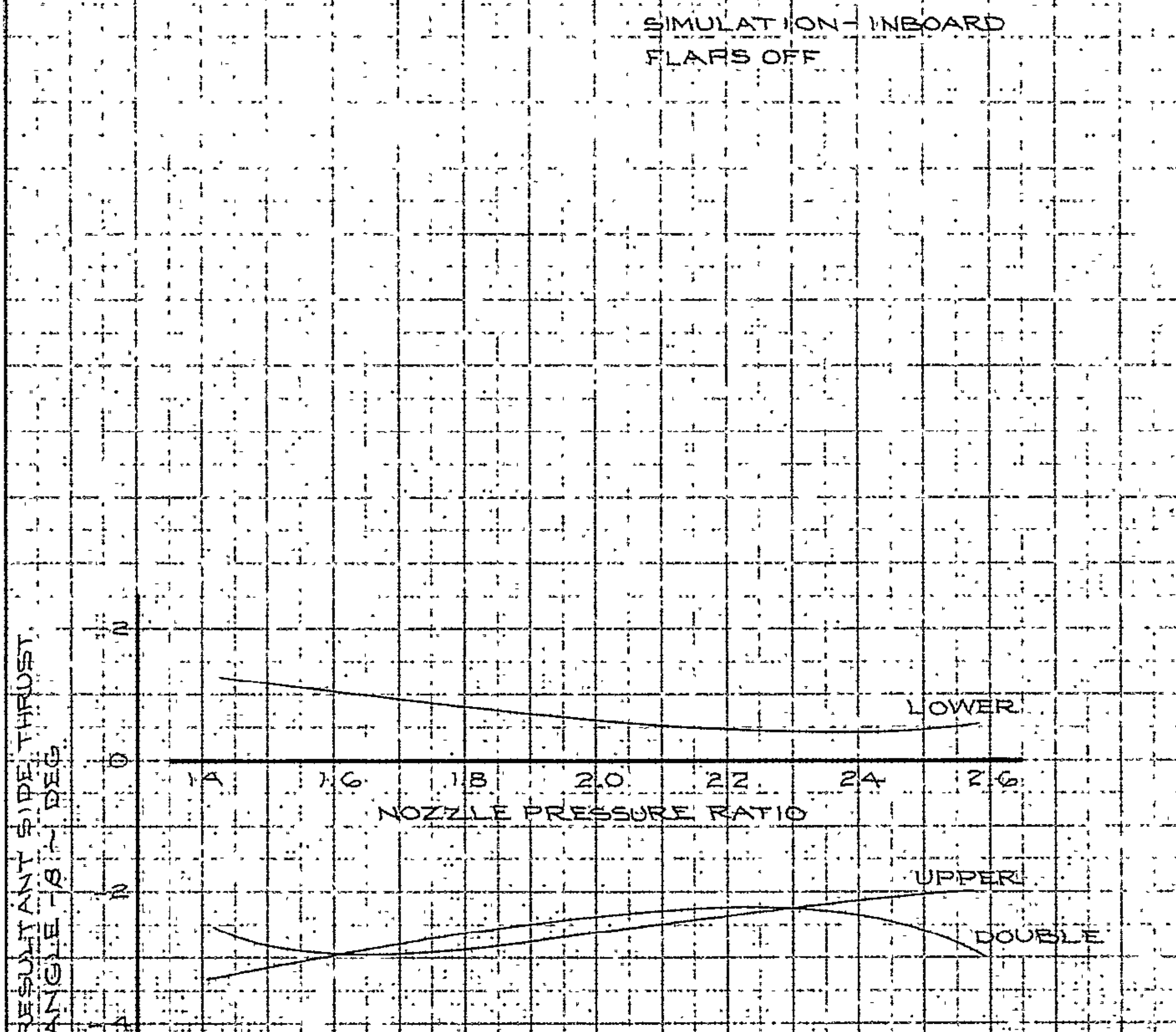

CALC			REVISED	DATE	RESULTANT SIDE THRUST ANGLE - ALL NOZZLE OPERATION MODES INBOARD	FIG. 57
CHECK						
APR	J. Hackaman	3/30/71				D6-24850
APR					THE BOEING COMPANY	PAGE 139
	J. Kloget	2/23/71				

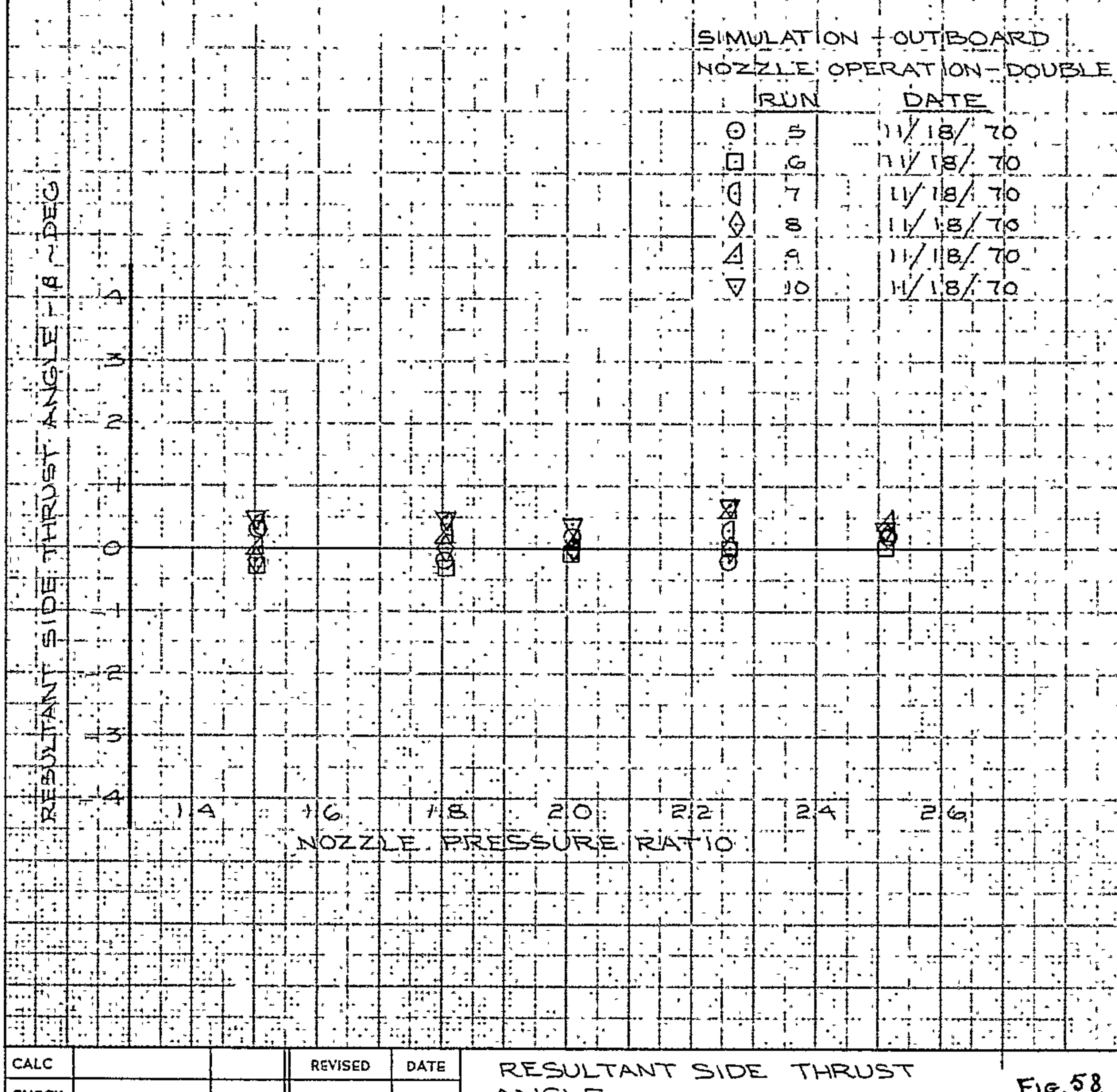

			REVISED	DATE		
CALC					RESULTANT SIDE THRUST ANGLE	FIG. 58
CHECK						
APR	D. Idehonen	3/30/71			DOUBLE NOZZLE - OUTBOARD	D6-24850
APR						
	J. C. Hoyt	21/9/71			THE BOEING COMPANY	PAGE 140

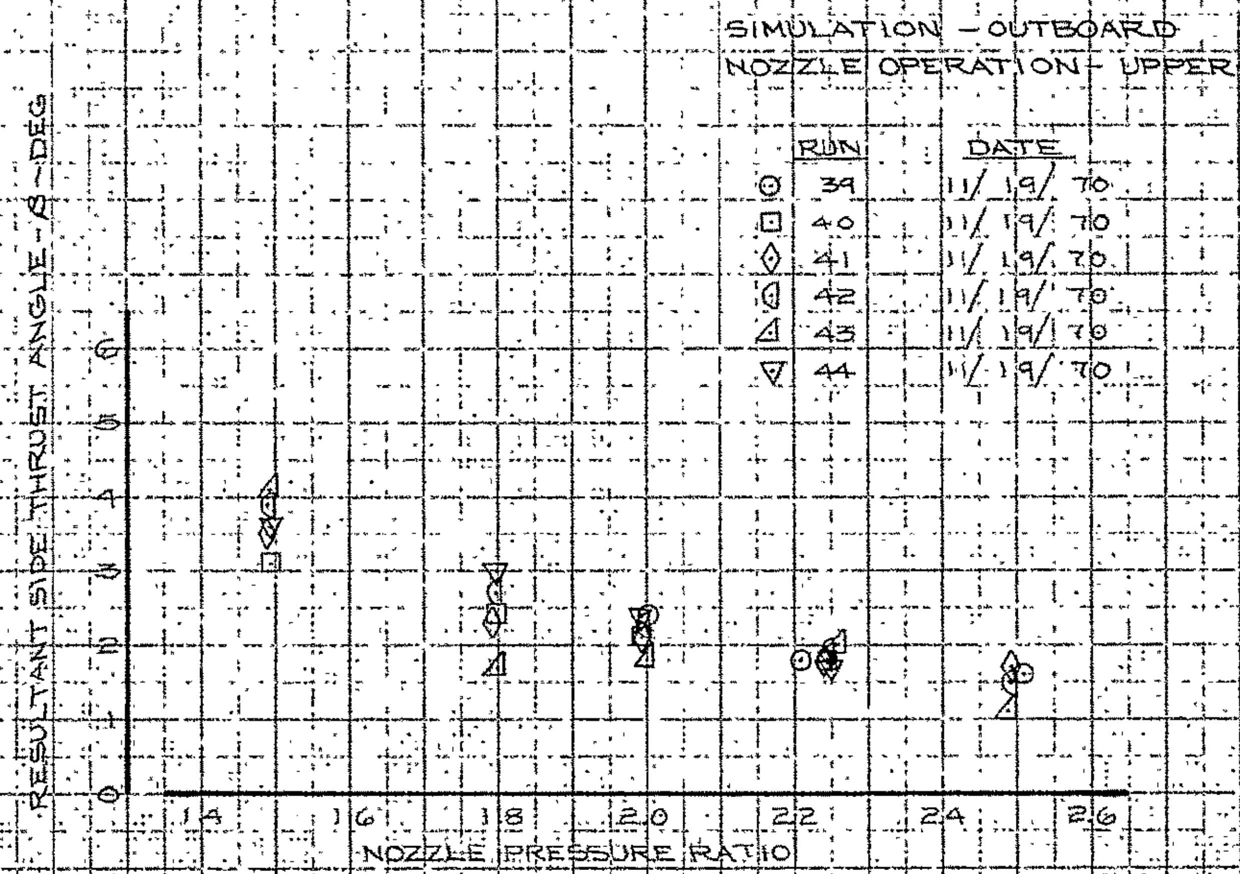

			REVISED	DATE	
CALC					RESULTANT SIDE THRUST ANGLE
CHECK					UPPER NOZZLE OUTBOARD
APR	[illegible]	3/30/71			
APR	[illegible]	2/9/71			THE BOEING COMPANY

FIG. 59

D6-24850

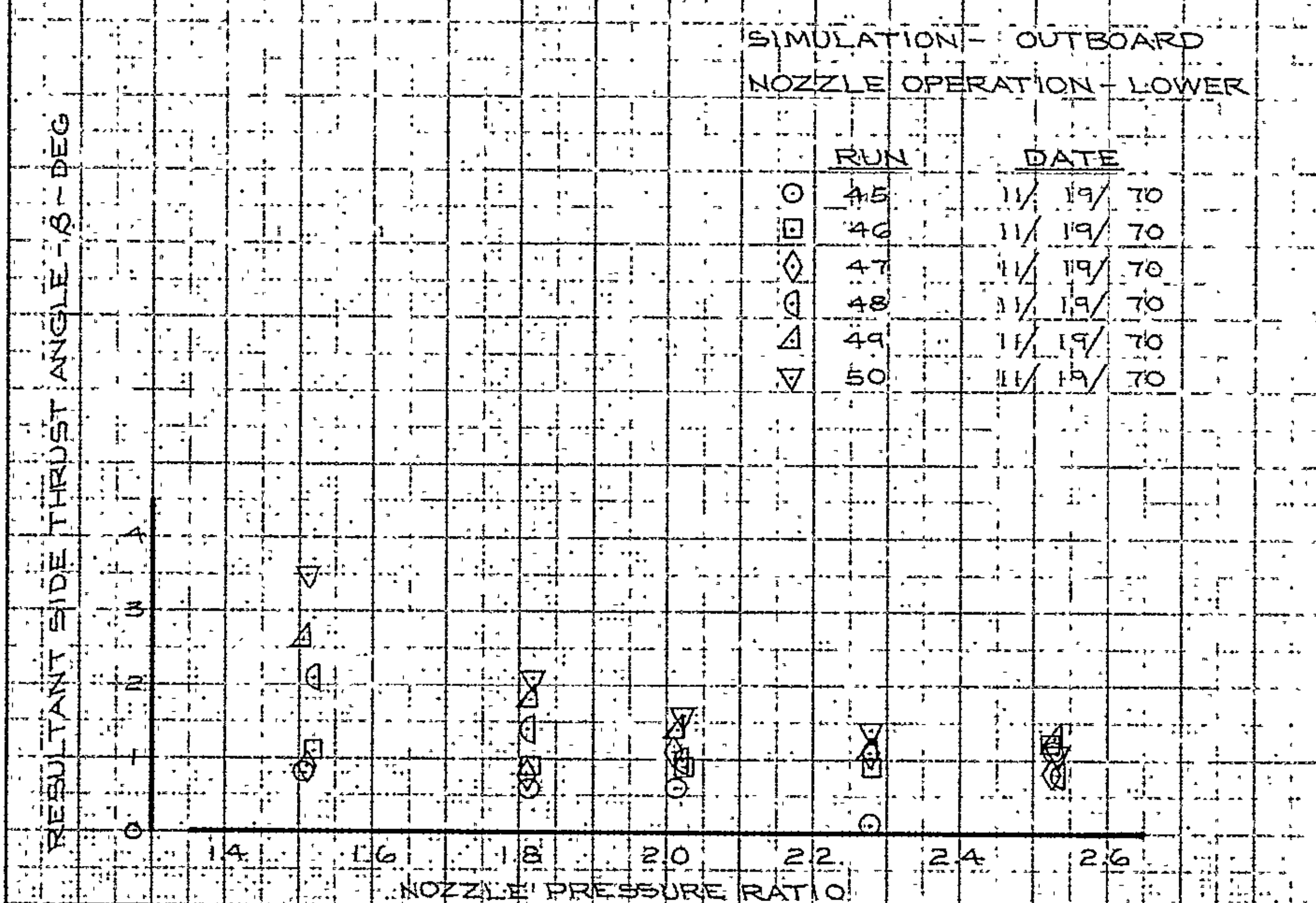

CALC			REVISED	DATE	RESULTANT SIDE THRUST ANGLE	FIG. 60
CHECK						
APR	R. Hashimoto	3/30/71			LOWER NOZZLE - OUTBOARD	D6-24850
APR						
	J. Hoyt	4/19/71			THE BOEING COMPANY	PAGE 142

K+E ALBANENE

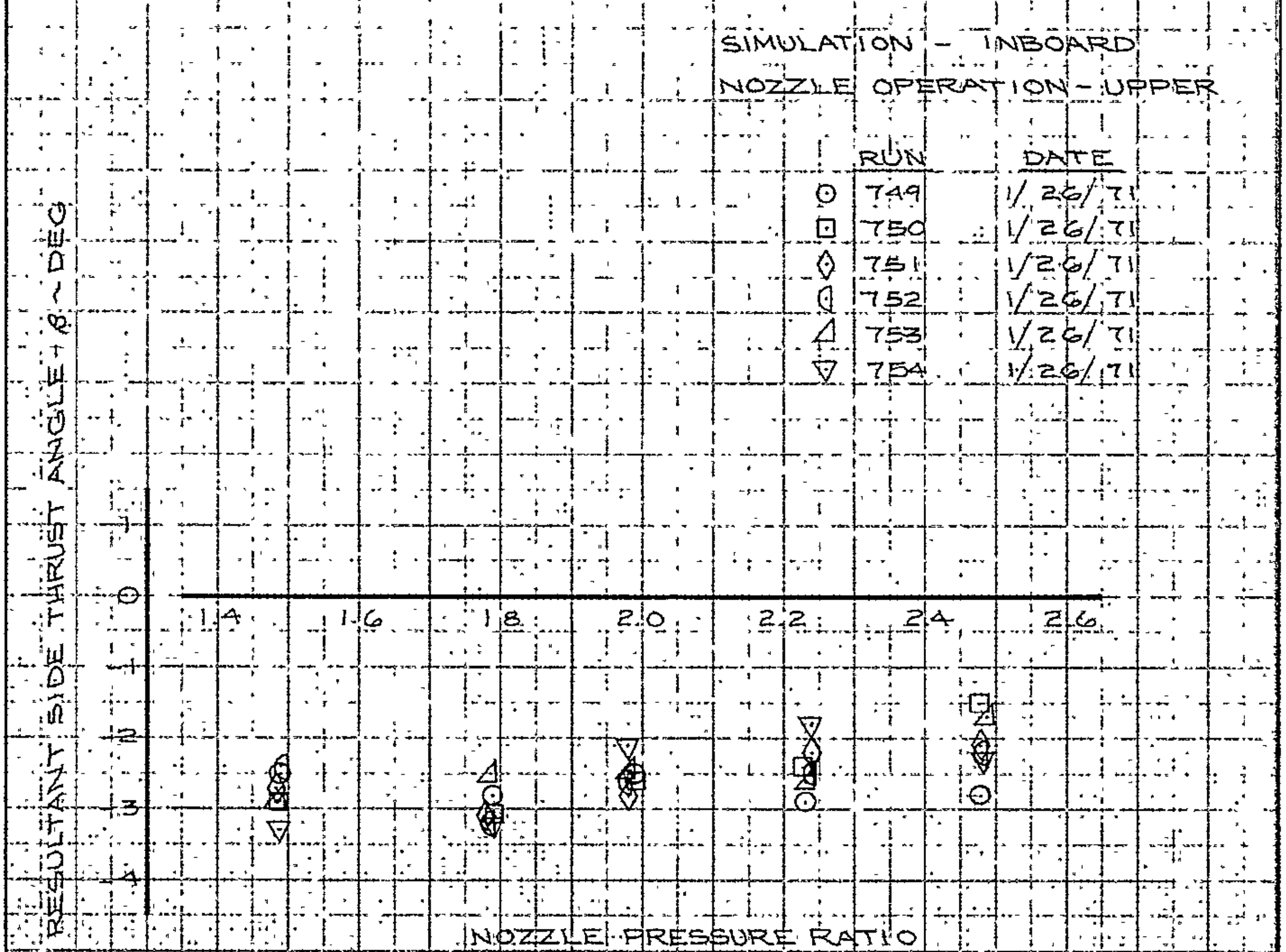

			REVISED	DATE		
CALC					RESULTANT SIDE THRUST ANGLE	FIG. 61
CHECK						
APR	D. Harkonen	3/30/71			UPPER NOZZE INBOARD	D6-24850
APR					THE BOEING COMPANY	PAGE 143
	jiloyt	7/19/71				

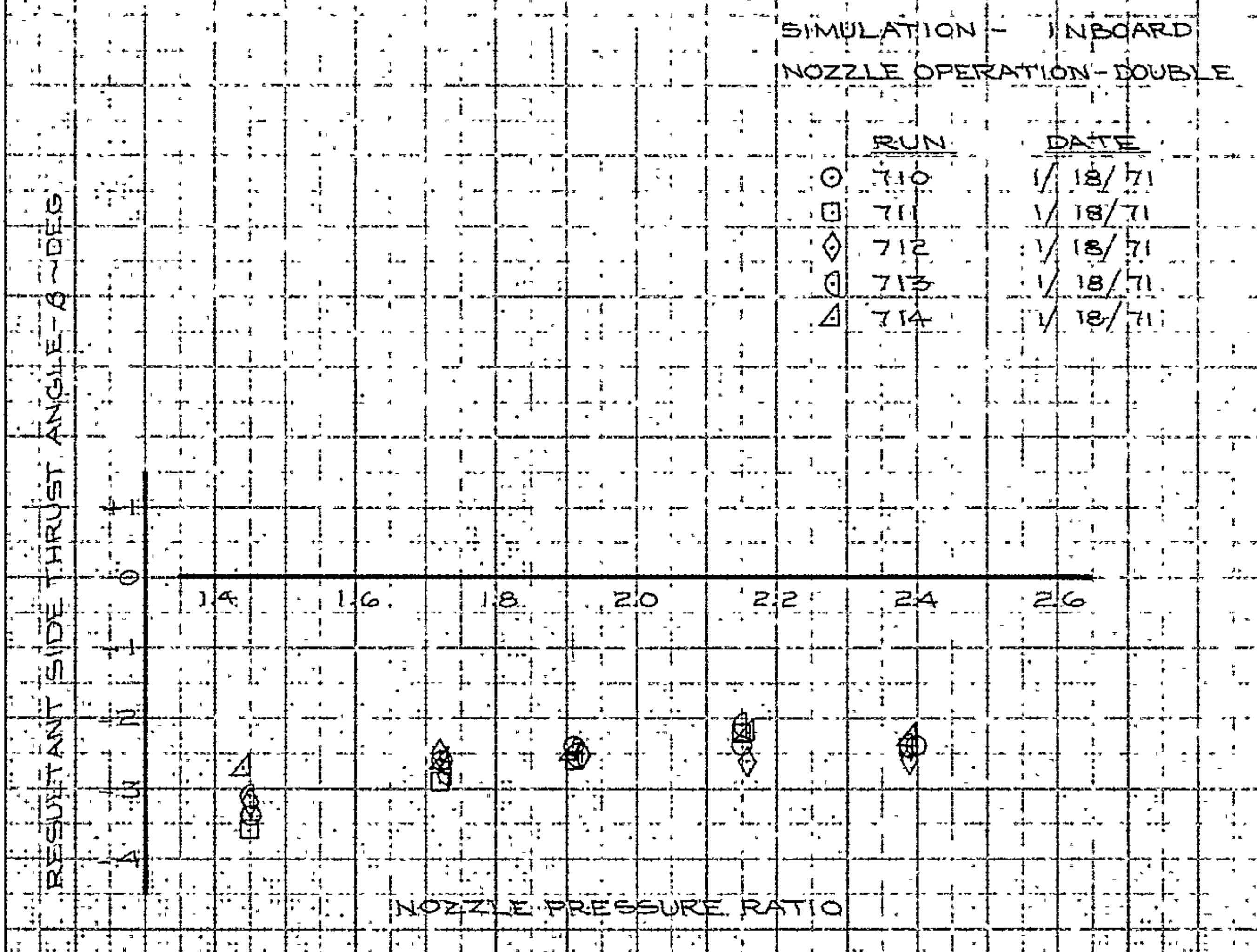

CALC			REVISED	DATE	RESULTANT SIDE THRUST ANGLE	FIG. 62
CHECK						
APR	D. Harkonen	3/30/71			DOUBLE NOZZLE INBOARD	D6-24850
APR						
	J. Kogt	2/19/71			THE BOEING COMPANY	PAGE 144

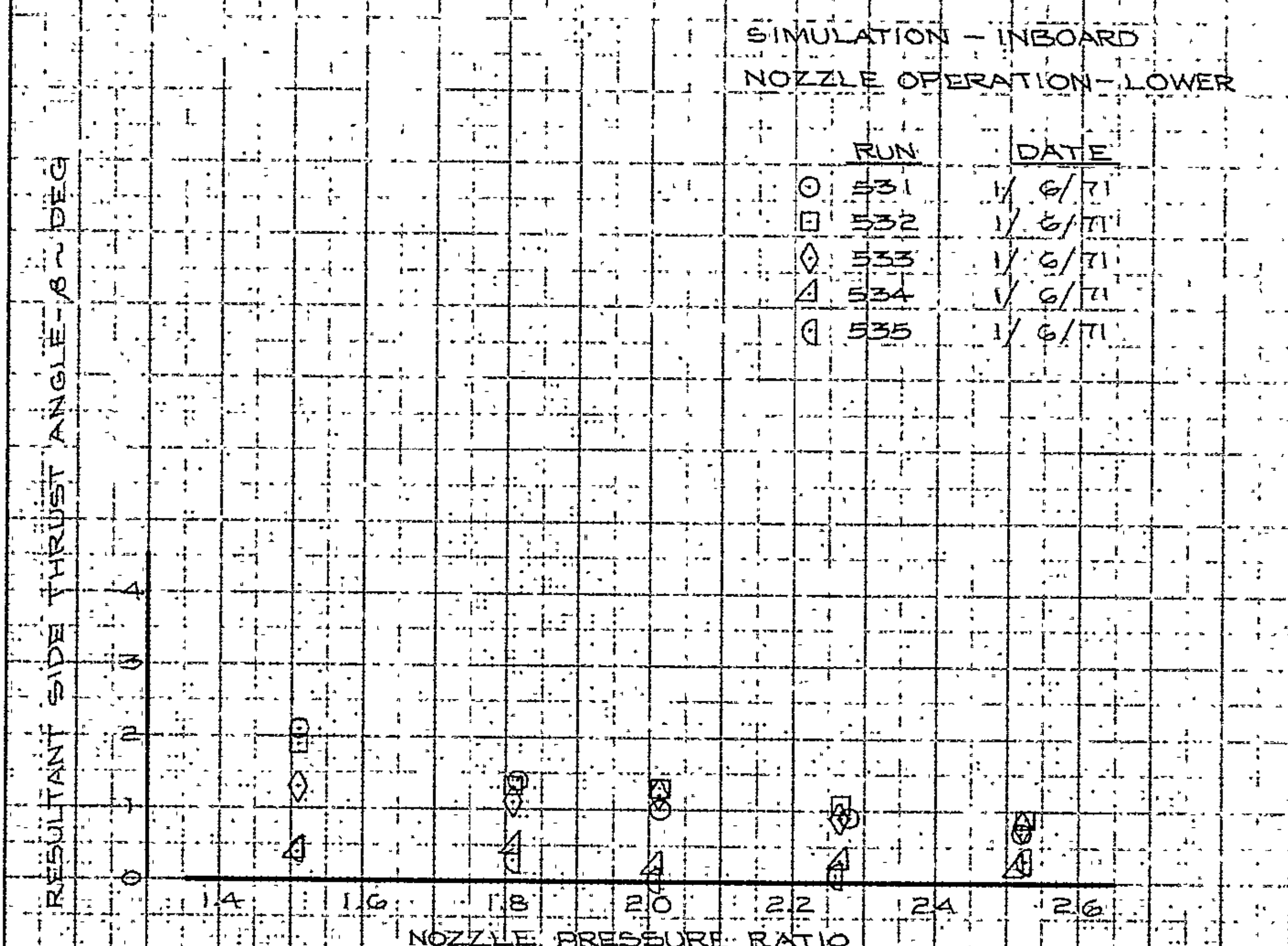

CALC			REVISED	DATE	RESULTANT SIDE THRUST ANGLE
CHECK					FIG. 63
APR	D. Heckman	3/30/71			LOWER NOZZLE INBOARD
APR					D6-24850
	J.R. Hoyt	4/19/71			THE BOEING COMPANY
					PAGE 145

K+E ALBANENE

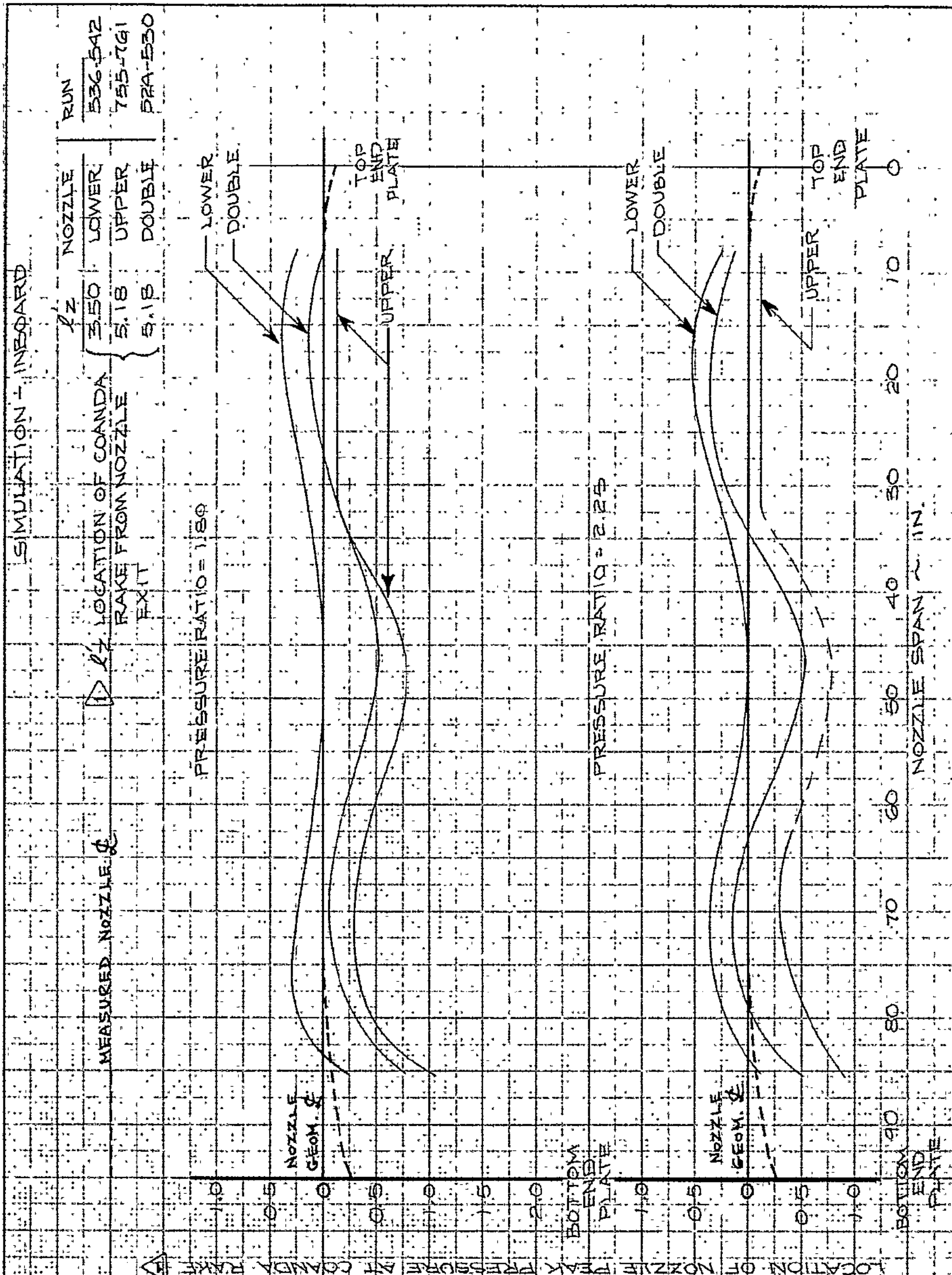

CALC			REVISED	DATE	LOCATION OF NOZZLE EXIT PEAK PRESSURE VS NOZZLE SPAN	FIG. 64
CHECK						
APR	D. Harhanen	3/30/71			INBOARD SIMULATION FLAPS OFF	D6-24850
APR					THE BOEING COMPANY	PAGE 146
	J. Hoyt	3/9/71				

K+E ALBANENE 1956 TRACING PAPER

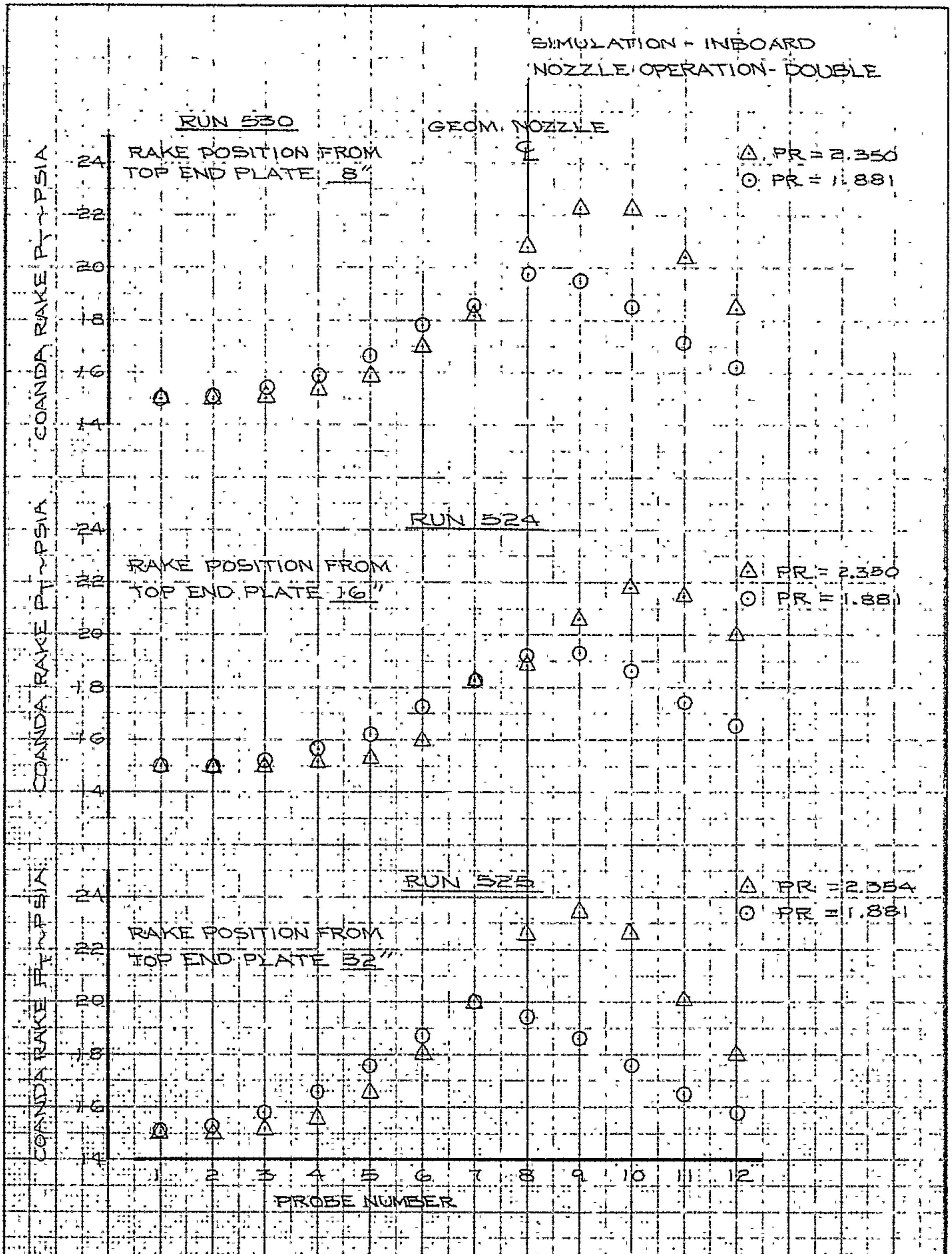

CALC			REVISED	DATE	COANDA RAKE TOTAL PRESSURE PROFILES	FIG. 65
CHECK						
APR	D. Heshmer	3/30/71			DOUBLE NOZZLE INBOARD	D6-24850
APR						
	J. Lloyd	7/22/71			THE BOEING COMPANY	PAGE 147

K+E ALBANENE TRACING PAPER

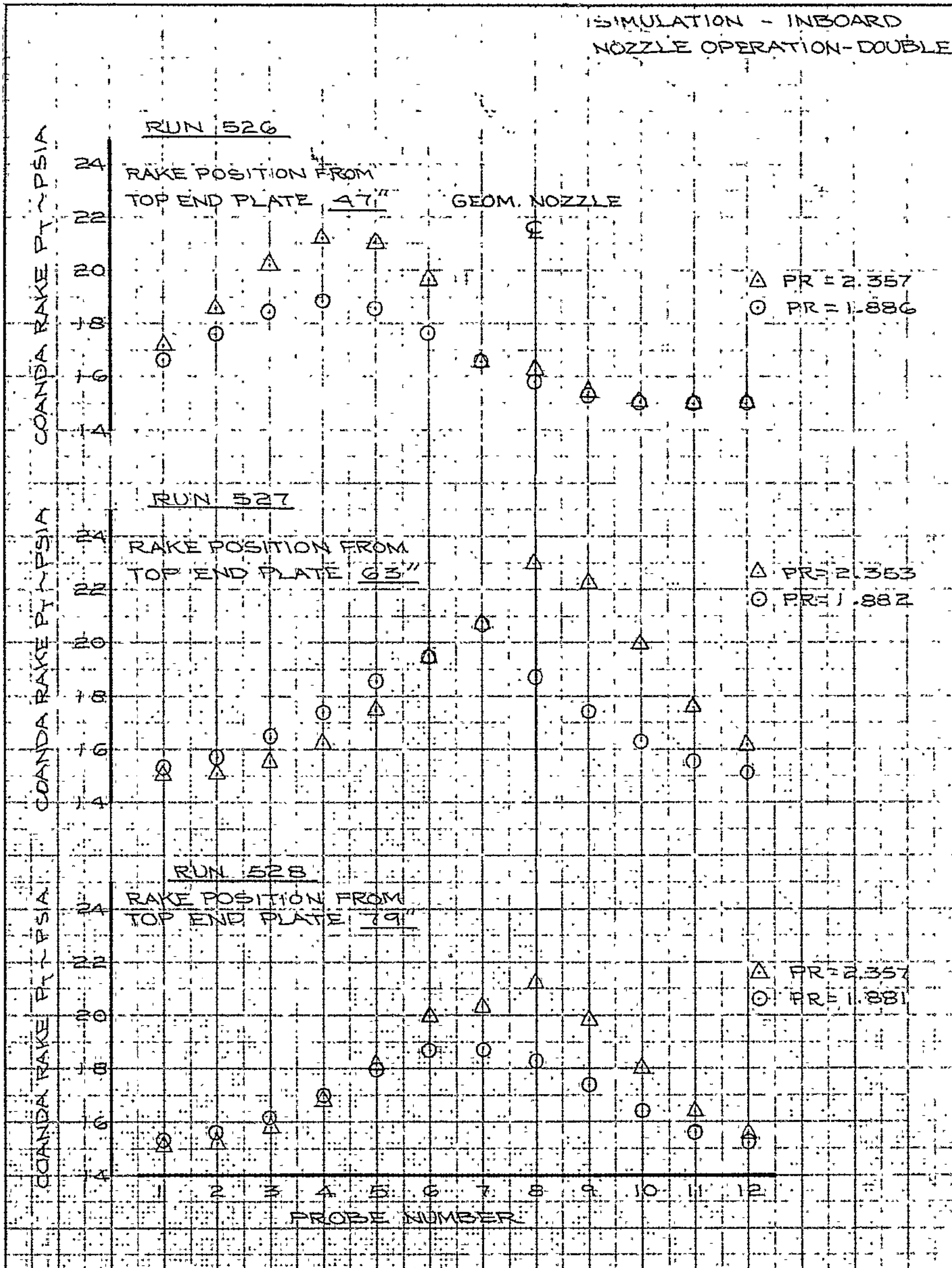

CALC			REVISED	DATE	COANDA RAKE TOTAL PRESSURE PROFILE	FIG. 66
CHECK						
APR	D. L. Hoshaw	3/30/71			DOUBLE NOZZLE INBOARD	D6-24850
APR	S. Hoyt	3/22/71			THE BOEING COMPANY	PAGE 148

K•E ALBANENE

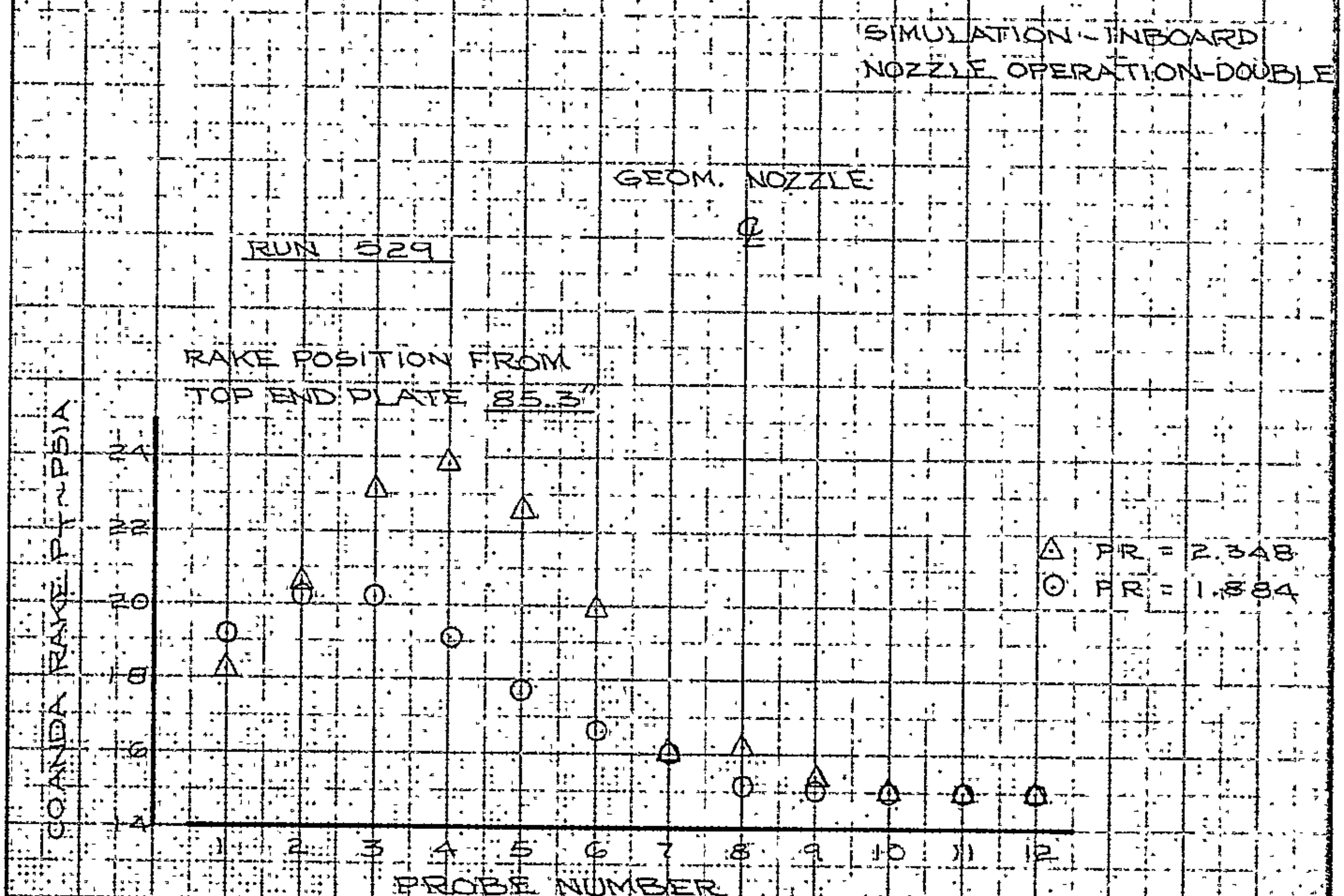

			REVISED	DATE		
CALC					COANDA RAKE TOTAL PRESSURE PROFILES	FIG. 67
CHECK						
APR	D. Harhonen	3/30/71			DOUBLE NOZZLE INBOARD	D6-24850
APR						
	J. Kogl	7/22/71			THE BOEING COMPANY	PAGE 149

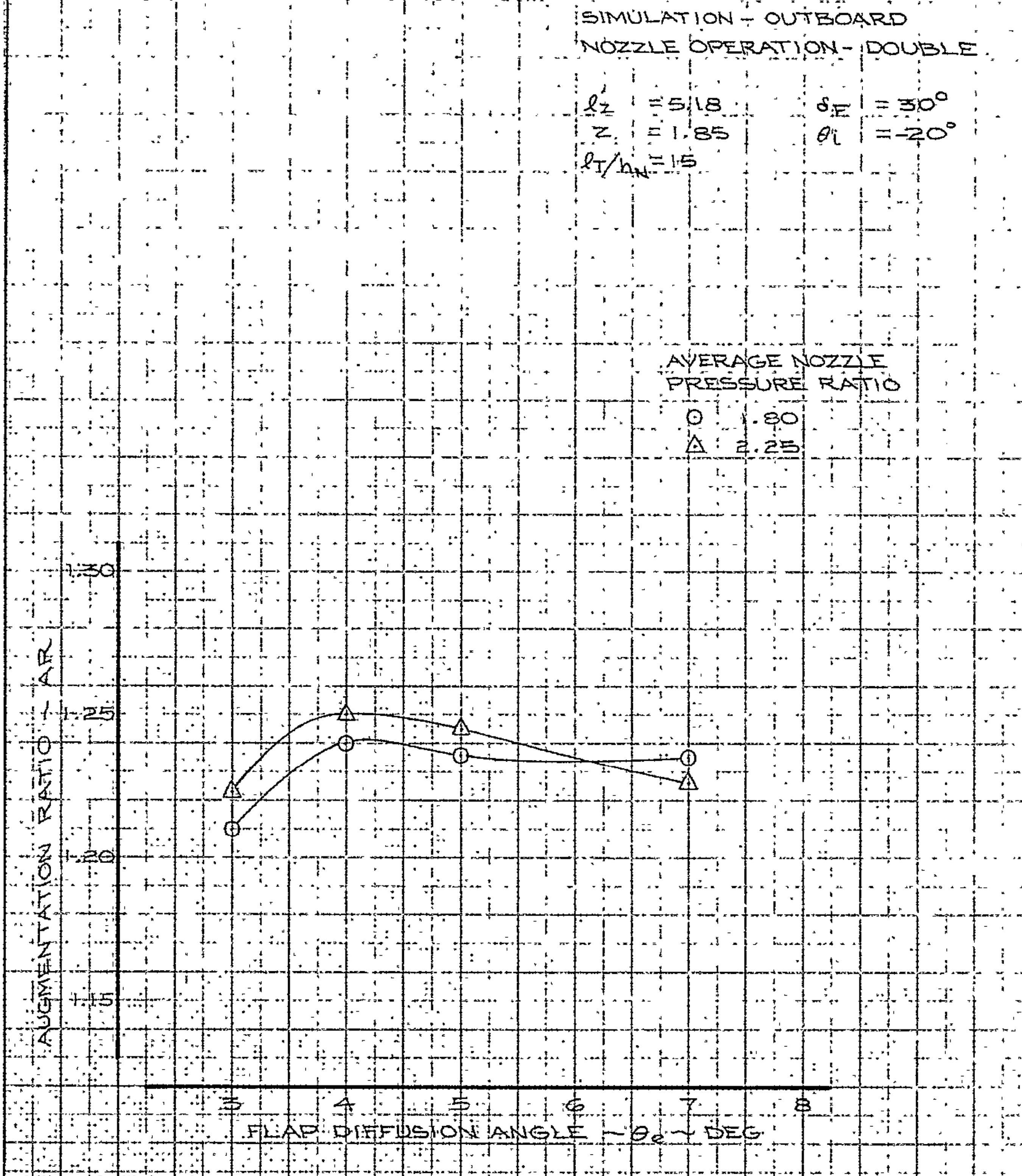

CALC			REVISED	DATE
CHECK				
APR	[signature]	3/30/71		
APR				
	[signature]	2/25/71		

EFFECT OF FLAP DIFFUSION ANGLE ON STATIC PERFORMANCE - $\delta_F = 30°$

FIG. 68

D6-24850

THE BOEING COMPANY

K+E ALBANENE

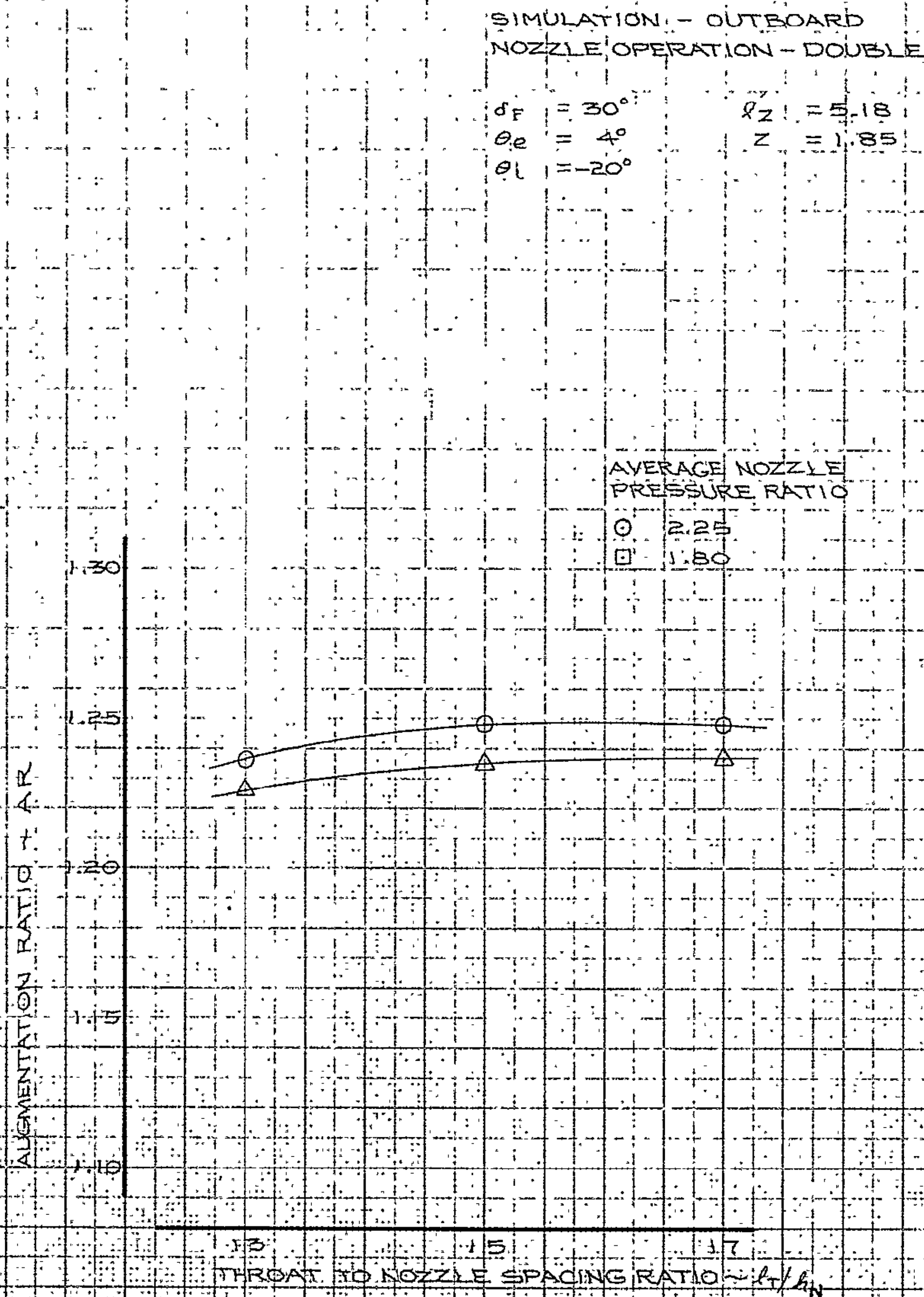

			REVISED	DATE		
CALC					EFFECT OF THROAT TO NOZZLE SPACING RATIO ~ l_T/h_N $\delta_F = 30°$	FIG. 69
CHECK						D6-24850
APR	D. Hashimoto	3/30/71				
APR					THE BOEING COMPANY	PAGE 151
	jeloyt	2/25/71				

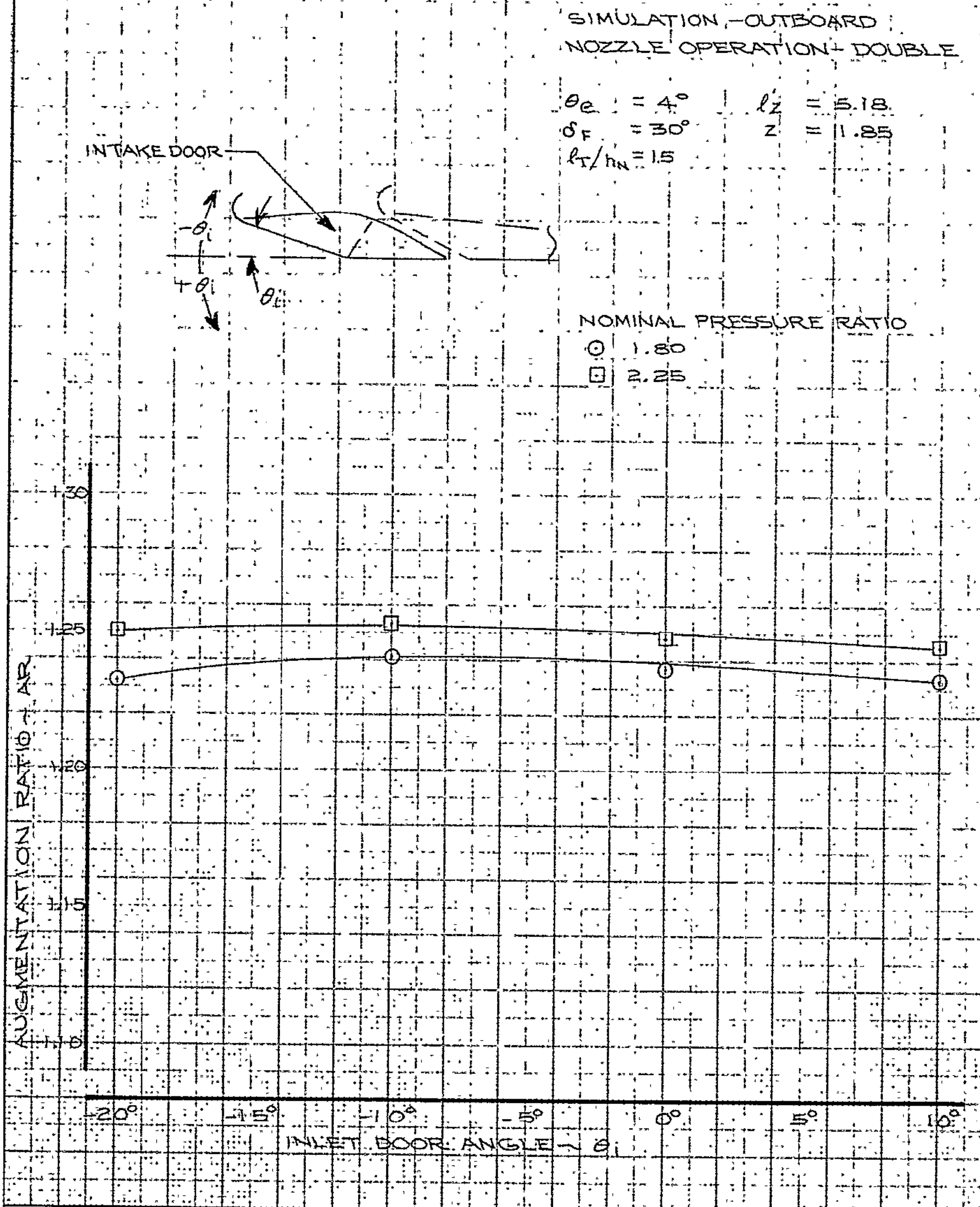

CALC			REVISED	DATE	EFFECT OF INTAKE DOOR OPENING ON STATIC PERFORMANCE $\delta_F = 30°$	FIG. 70
CHECK						D6-24850
APR	D. Holhouen	3/30/71			THE BOEING COMPANY	PAGE 152
APR	jihoyil	2/25/71				

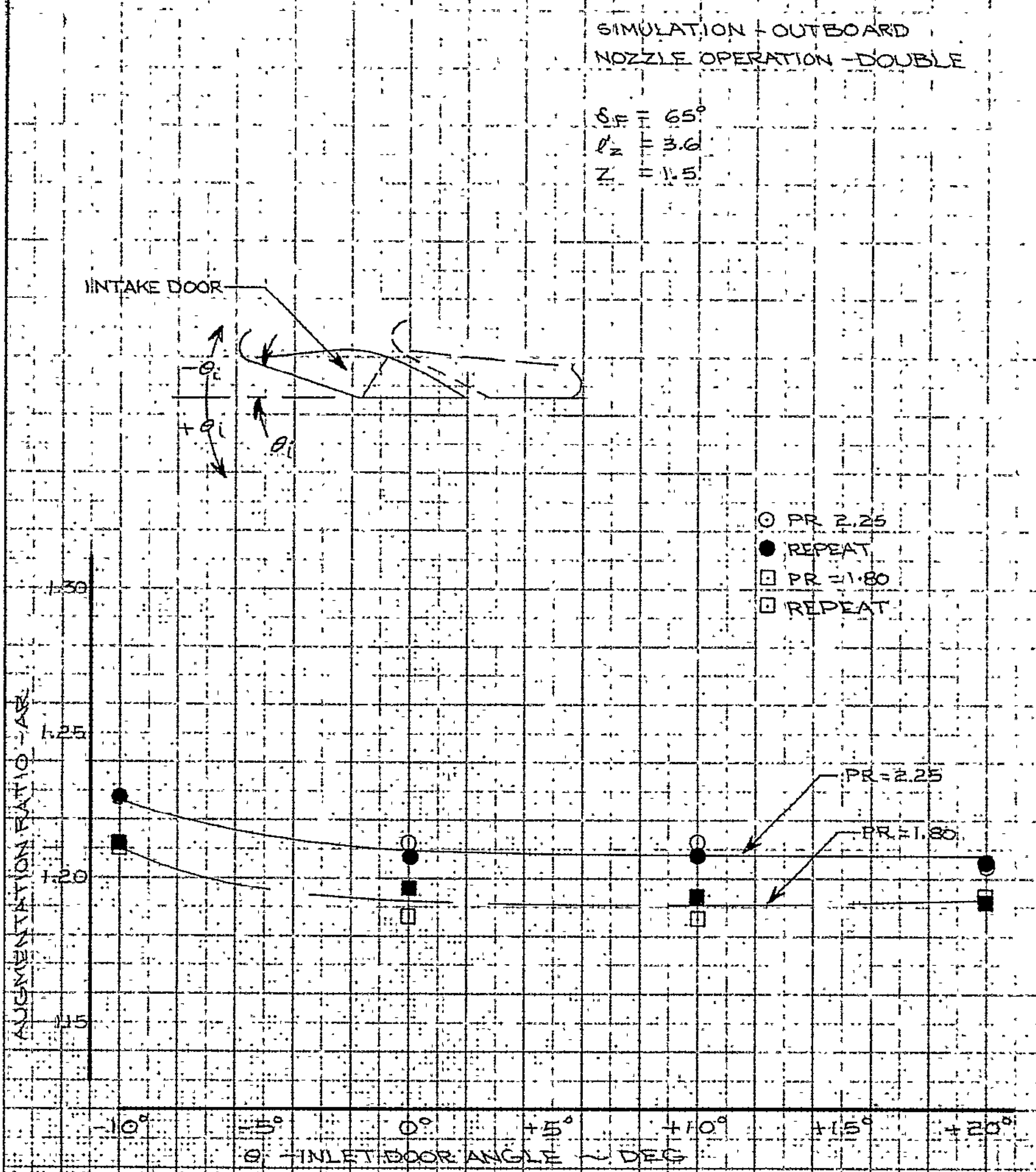

CALC			REVISED	DATE	EFFECT OF INTAKE DOOR OPENING ON STATIC PERFORMANCE $\delta_F = 65°$	FIG. 71
CHECK						
APR	D. Washman	3/30/71				D6-24850
APR					THE BOEING COMPANY	PAGE 153
	J. Hoyt	3/3/71				

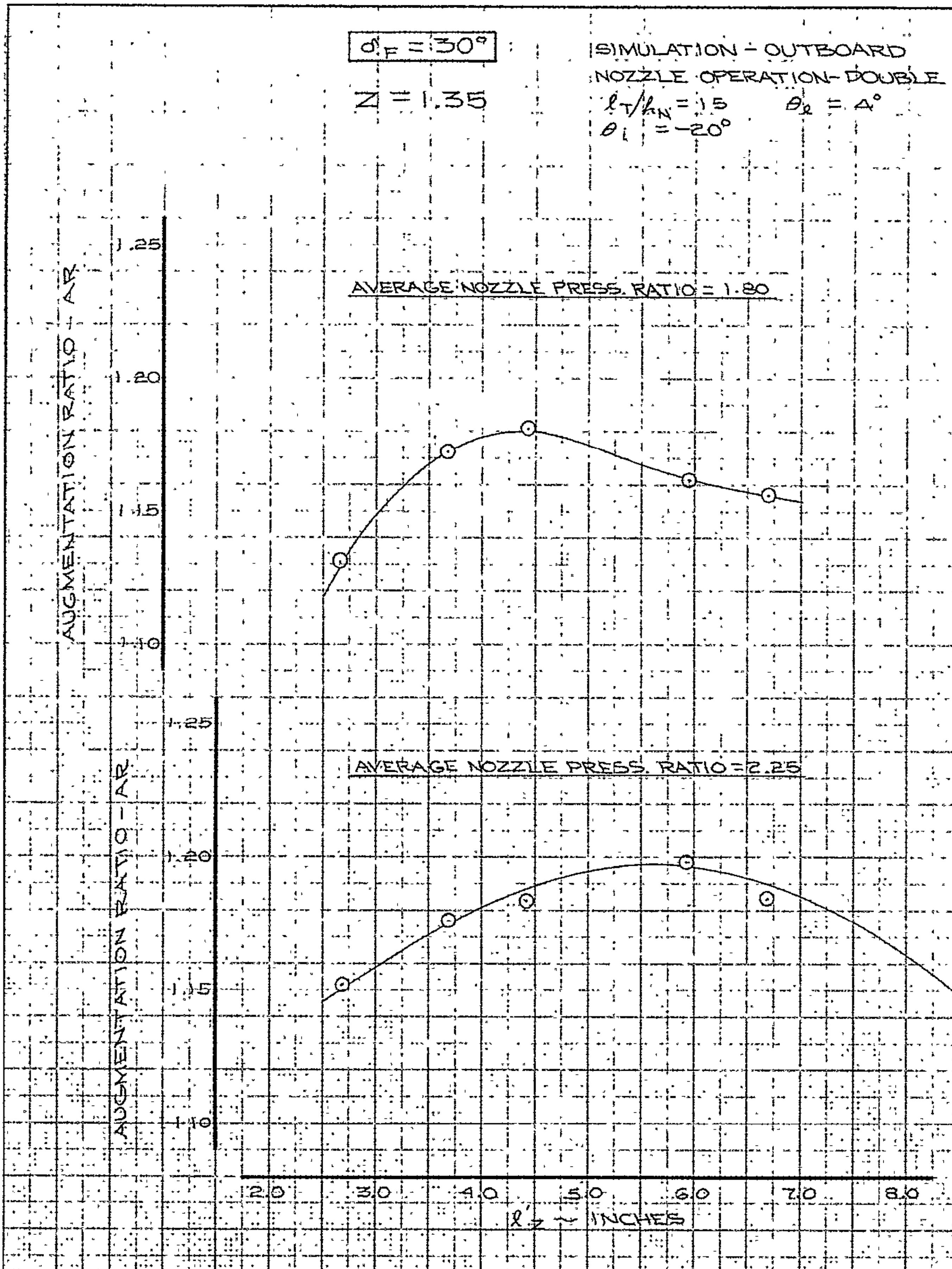

CALC			REVISED	DATE	ℓ'_Z OPTIMIZATION @	FIG. 72
CHECK					$\delta_F = 30°$ $Z = 1.35''$	D6-24850
APR	D. Kashiwa	3/30/71				
APR					THE BOEING COMPANY	PAGE 154
	J. Hoyt	3/26/71				

K+E ALBANENE

$\delta_F \doteq 30°$

$Z \doteq 1.60''$

SIMULATION – OUTBOARD NOZZLE OPERATION – DOUBLE

$\ell_T / h_N = 15$ $\theta_\ell \doteq 4°$

$\theta_i = -20°$

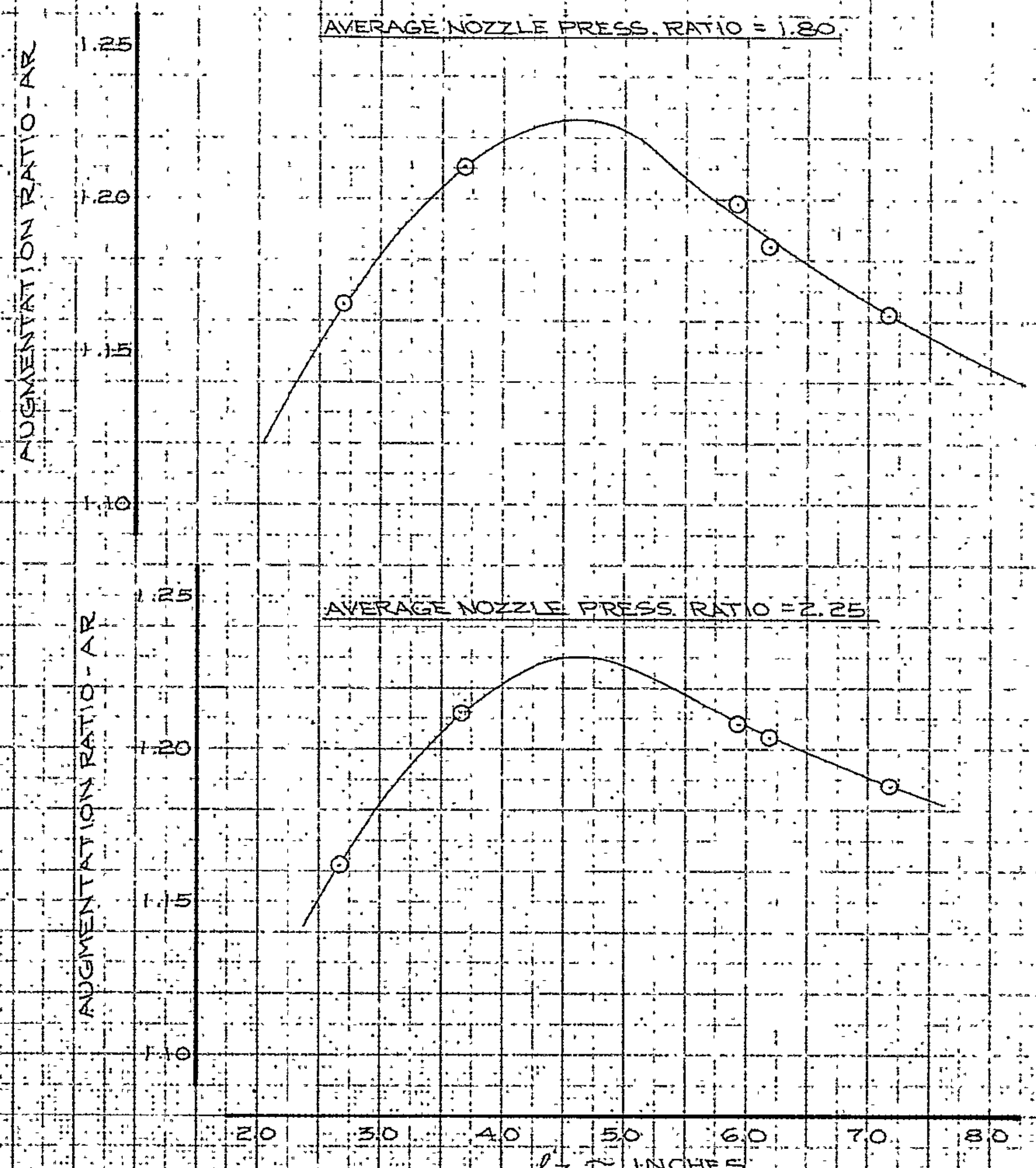

			REVISED	DATE		
CALC					ℓ'_Z OPTIMIZATION @	FIG. 73
CHECK						
APR	D. Hashmen	3/30/71			$\delta_F = 30°$ $Z = 1.60''$	D6-24850
APR						
	J. Hoyt	4/26/71			THE BOEING COMPANY	PAGE 155

K+E ALBANENE

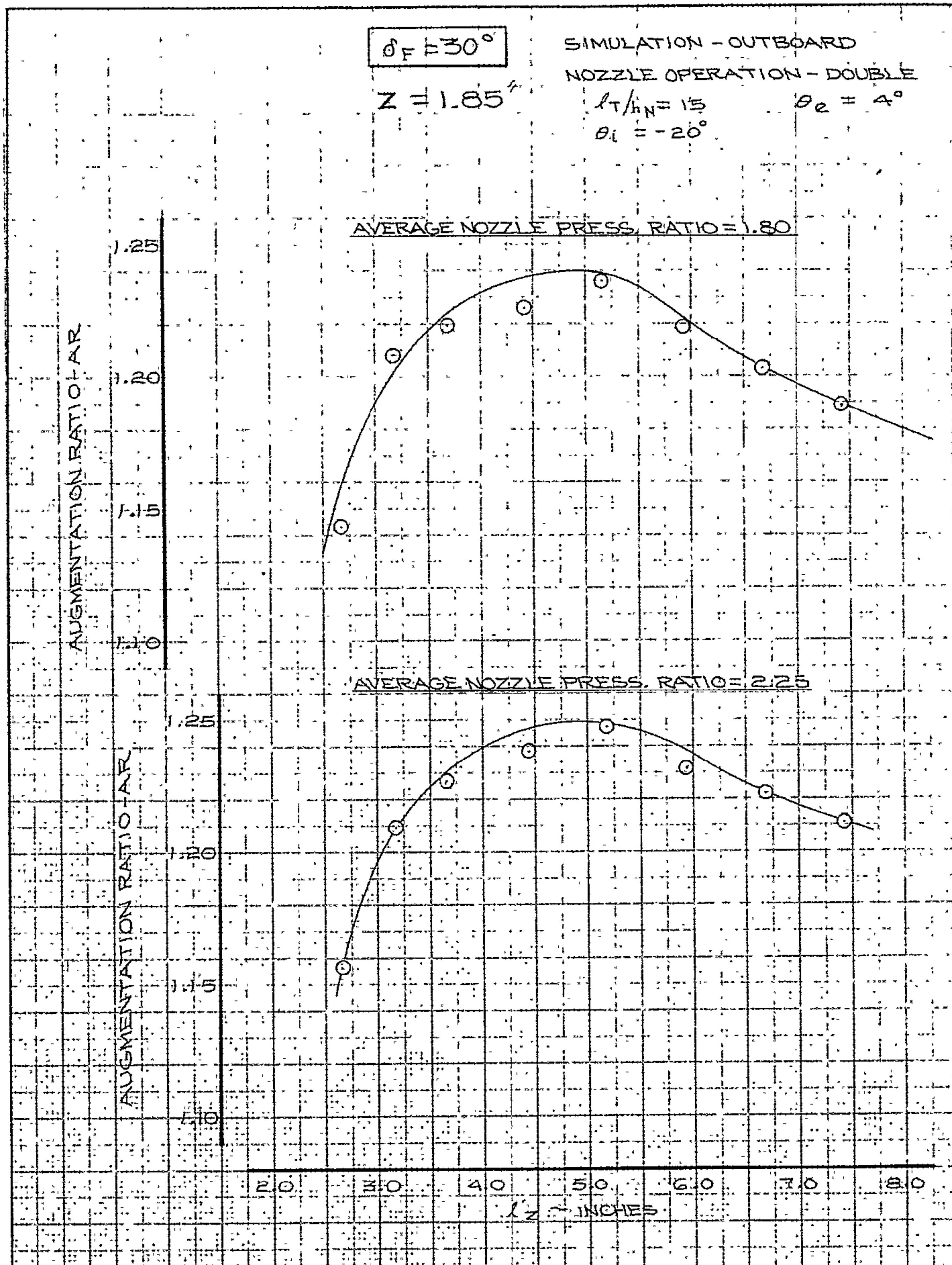

CALC			REVISED	DATE	ℓ'_Z OPTIMIZATION @	FIG. 74
CHECK					$\delta_F = 30°$ $Z = 1.85''$	D6-24850
APR	D. Hardiman	3/30/71				
APR					THE BOEING COMPANY	PAGE 156
	J. Lloyd	2/26/71				

K+E ALBANENE

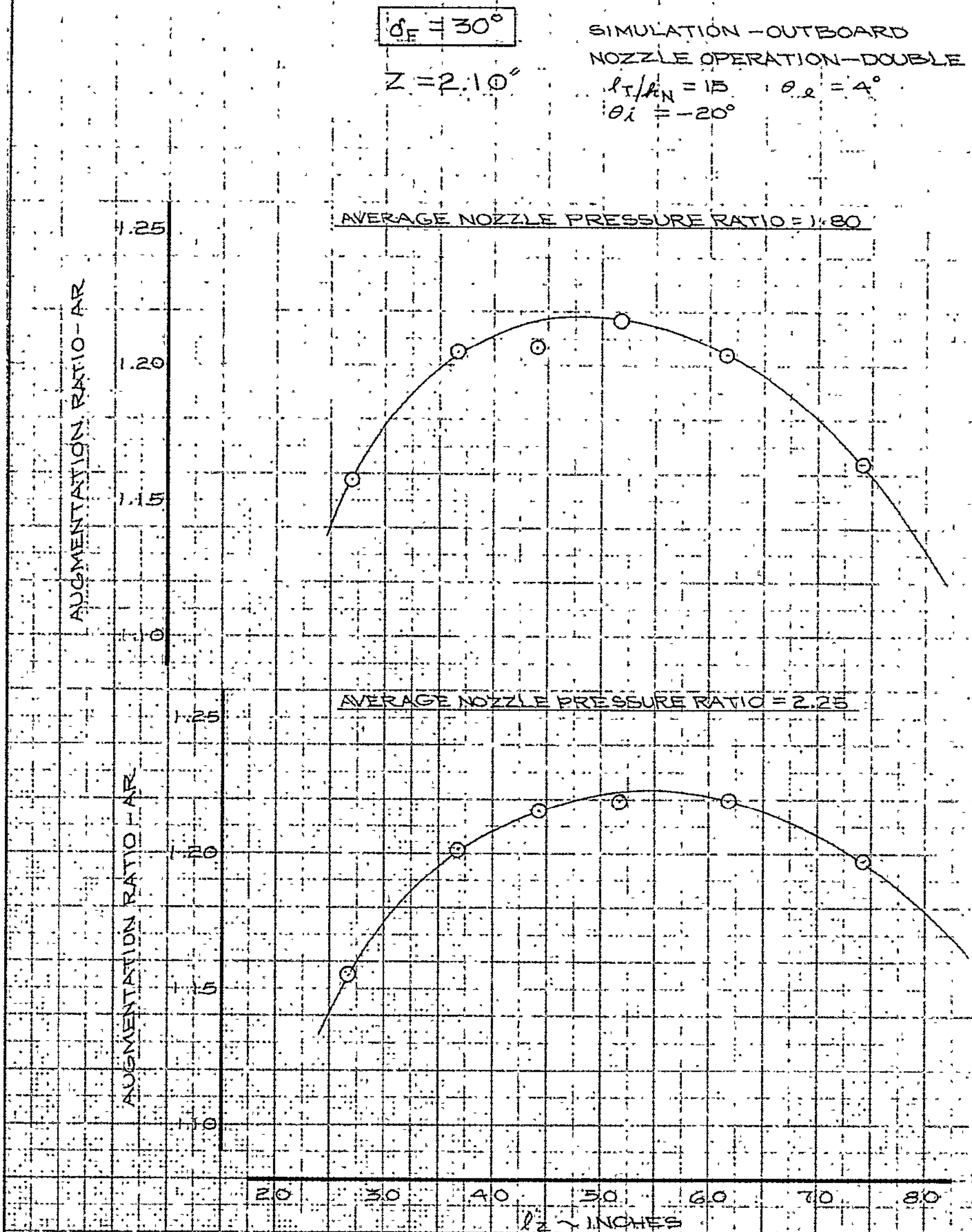

CALC			REVISED	DATE	l'_Z OPTIMIZATION @	FIG. 75
CHECK					$\delta_F = 30°$ $Z = 2.10''$	D6-24850
APR	A. Kashonen	3/30/71				
APR					THE BOEING COMPANY	PAGE 157
	J. Hoyt	2/26/71				

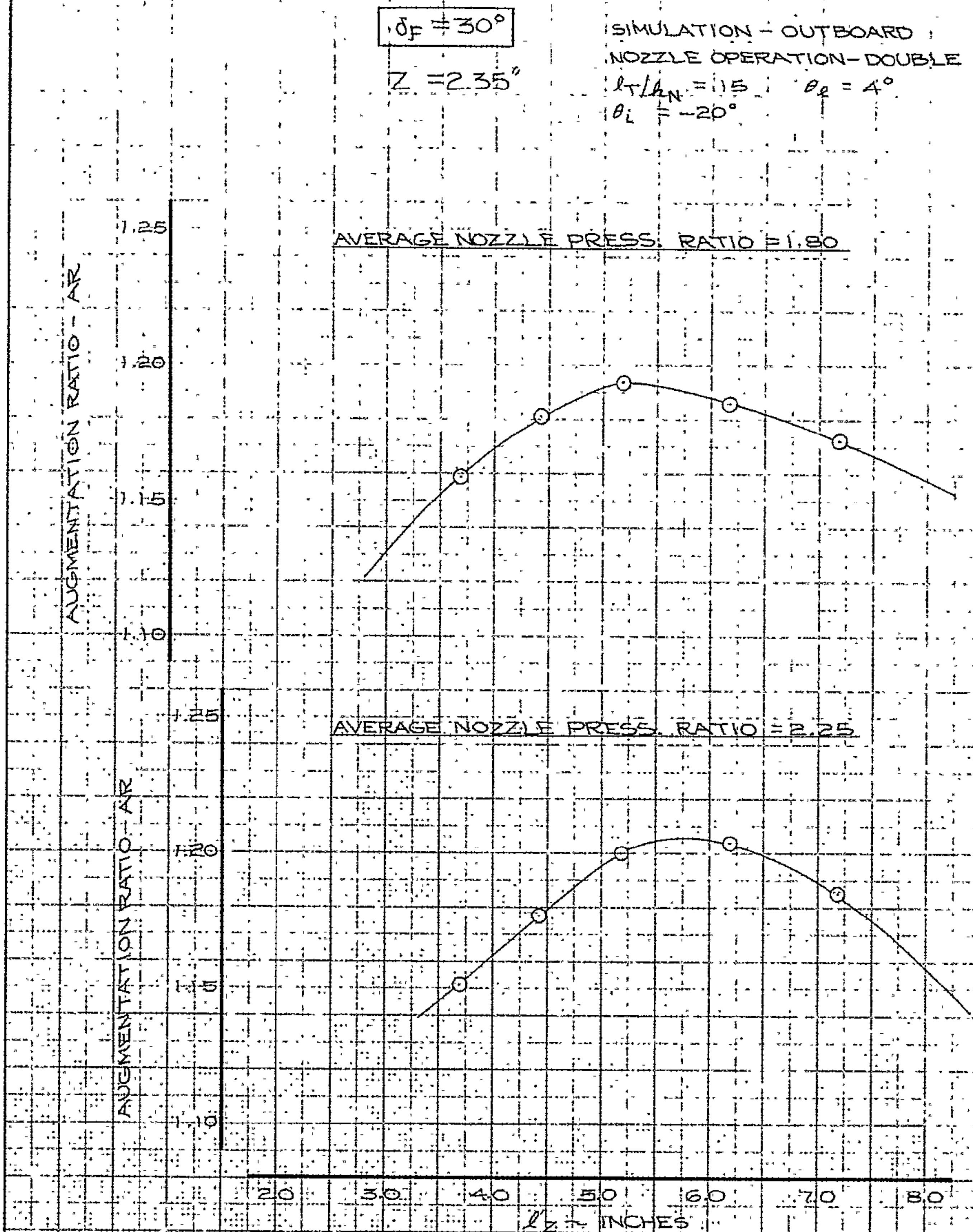

CALC			REVISED	DATE	l'_Z OPTIMIZATION @	FIG. 76
CHECK						
APR	D. Vashonen	3/30/71			$\delta_F = 30°$ $Z = 2.35''$	D6-24850
APR					THE BOEING COMPANY	PAGE 158
	[illegible]	3/26/71				

K+E ALBANENE 105C

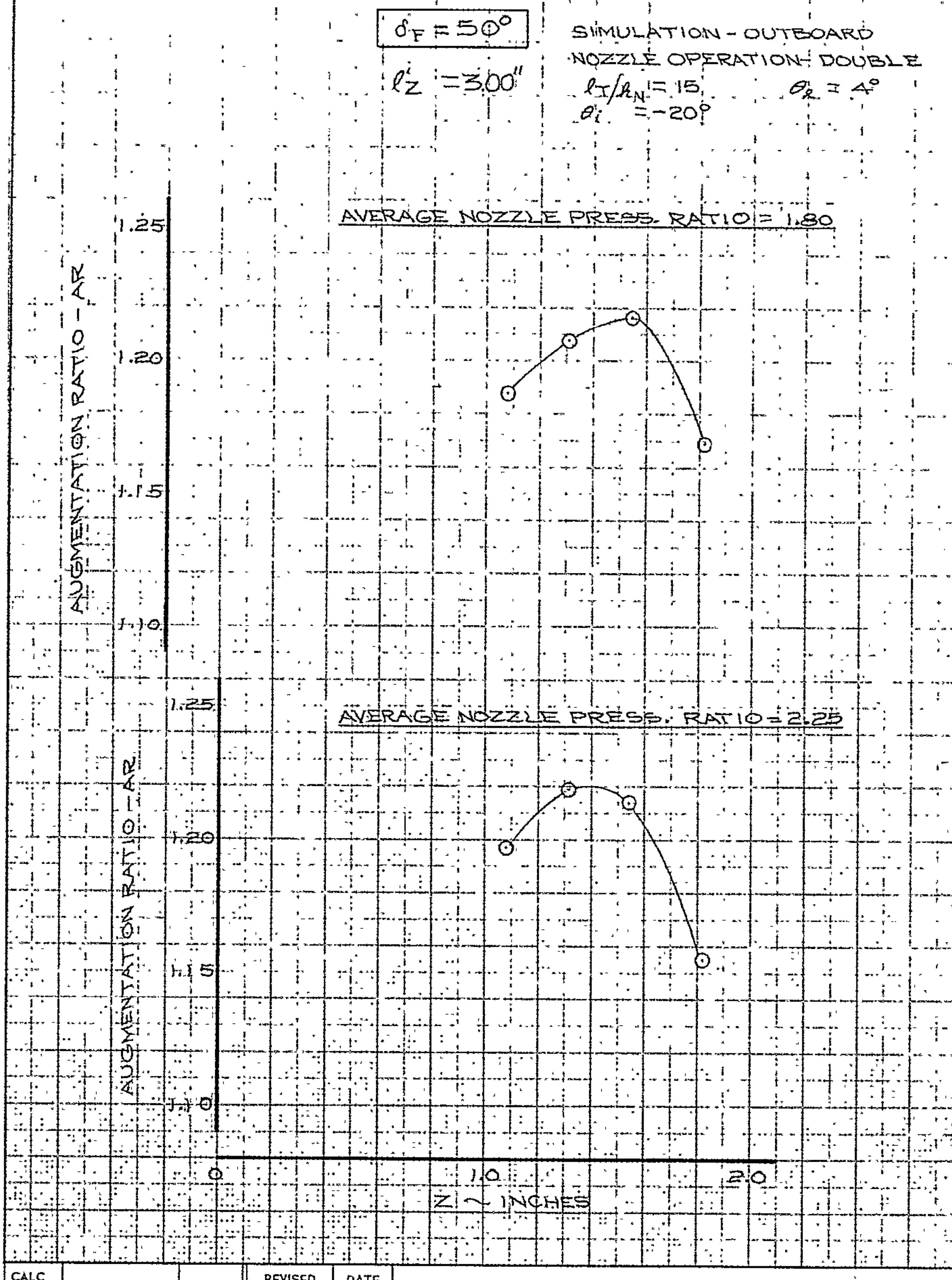

CALC			REVISED	DATE	Z OPTIMIZATION @ $\delta_F = 50°$ $l'_Z = 3.00''$	FIG. 77
CHECK						D6-24850
APR	D. Hachonen	3/30/71			THE BOEING COMPANY	PAGE 159
APR	J. Lloyd	3/1/71				

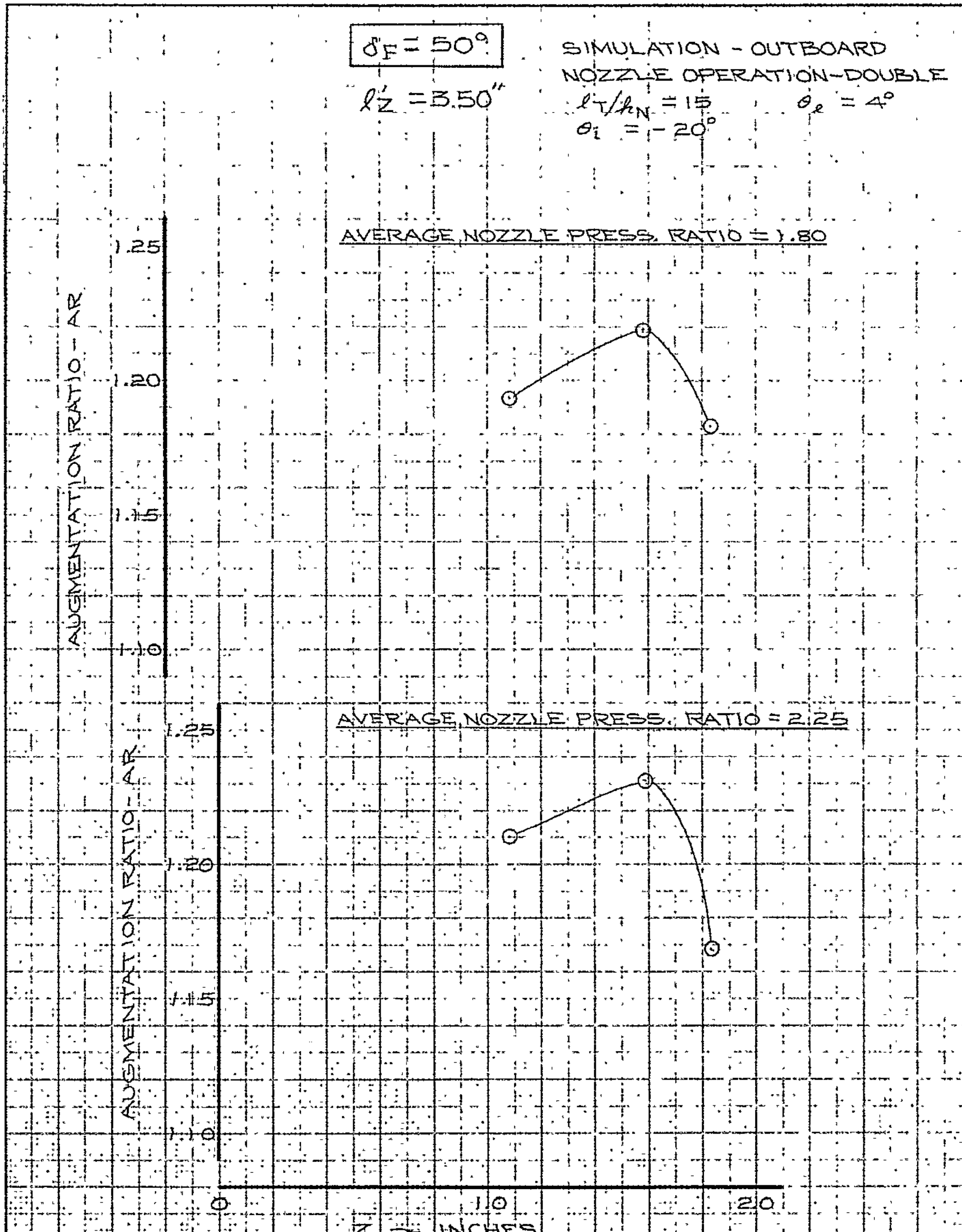

CALC			REVISED	DATE	Z OPTIMIZATION @ δ_F = 50° ℓ'_Z = 3.50"	FIG. 78
CHECK						D6-24850
APR	D. Harhoun	3/30/71				
APR					THE BOEING COMPANY	PAGE 160
	[illegible]	3/1/71				

$\delta_E = 50°$

$l'_Z = 4.06''$

SIMULATION - OUTBOARD NOZZLE OPERATION - DOUBLE

$l_I/h_N = 15$ $\theta_e = 4°$

$\theta_I = -20°$

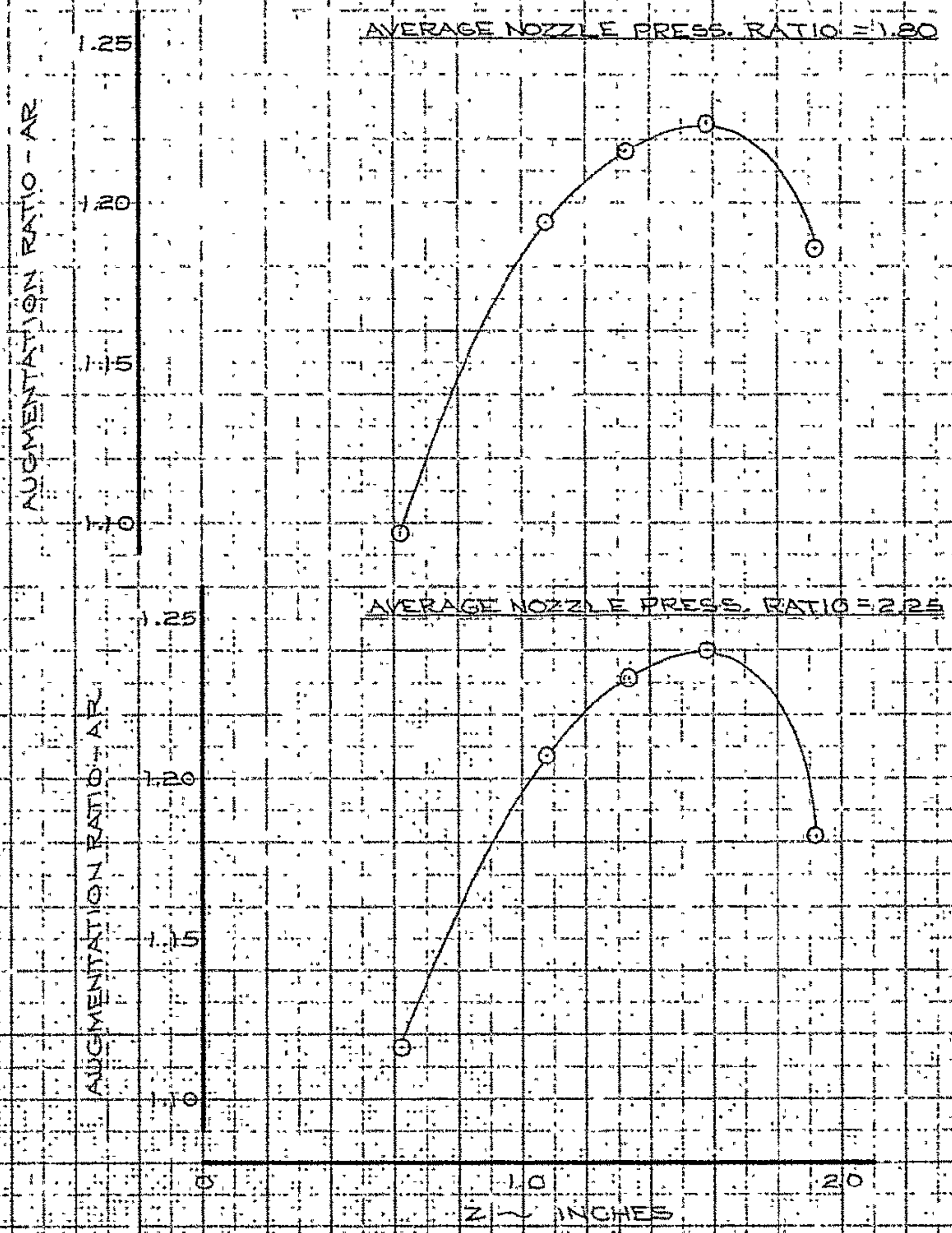

CALC			REVISED	DATE	Z OPTIMIZATION @	FIG. 79
CHECK						
APR	D. Haskonen	3/30/71			$\delta_F = 50°$ $l'_Z = 4.06''$	D6-24850
APR						
	J. Hoyt	3/1/71			THE BOEING COMPANY	PAGE 161

K·E ALBANENE

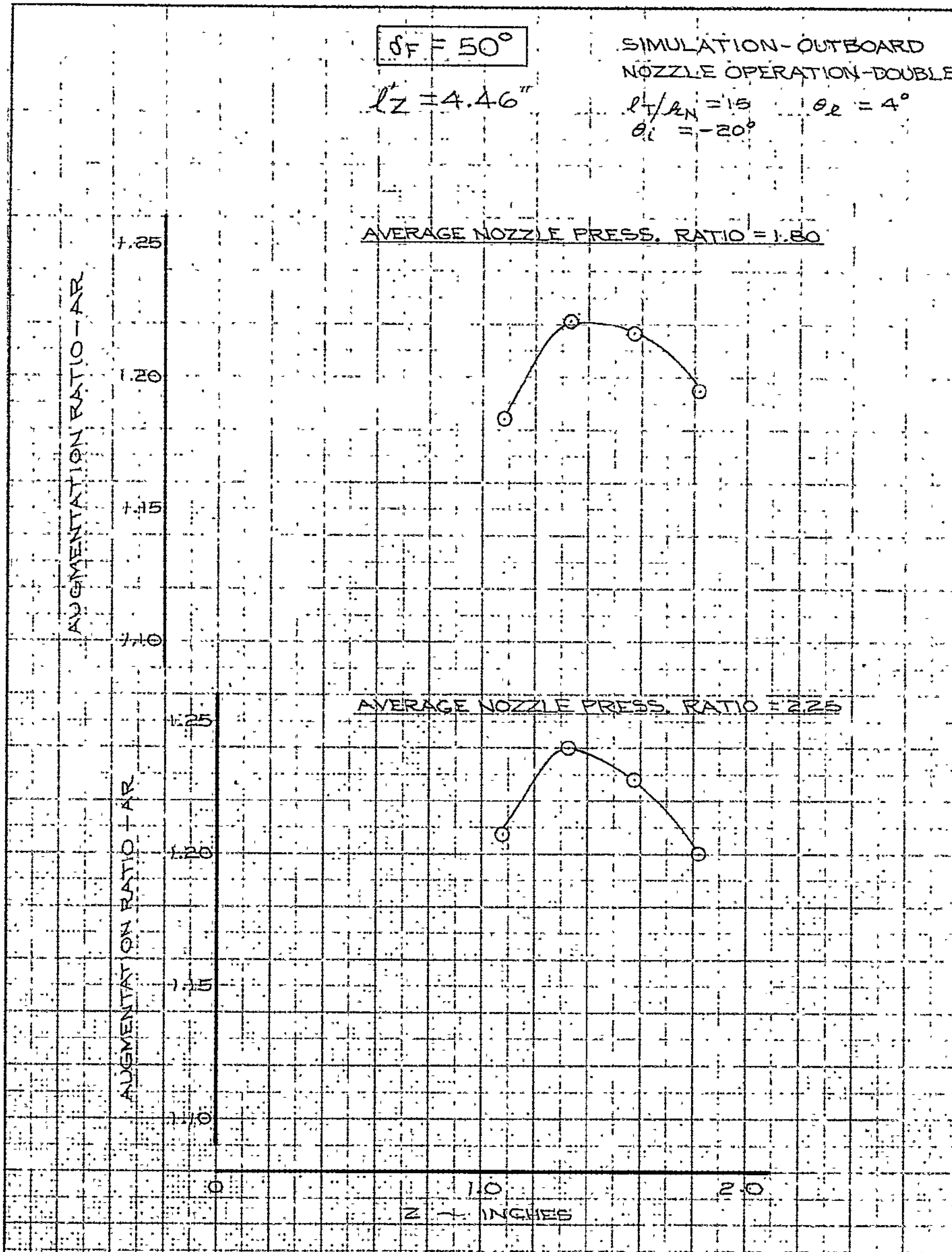

CALC			REVISED	DATE	Z OPTIMIZATION @	FIG. 80
CHECK					$\delta_F = 50°$ l'_Z 4.46"	D6-24850
APR	D. Harkonen	3/30/71				
APR						
	J. Hoyt	3/1/71			THE BOEING COMPANY	PAGE 162

$\delta_F = 50°$

SIMULATION - OUTBOARD NOZZLE OPERATION - DOUBLE

$\ell'_Z = 5.00''$ $\ell_T/h_N = .15$ $\theta_e = 4°$ $\theta_i = -20°$

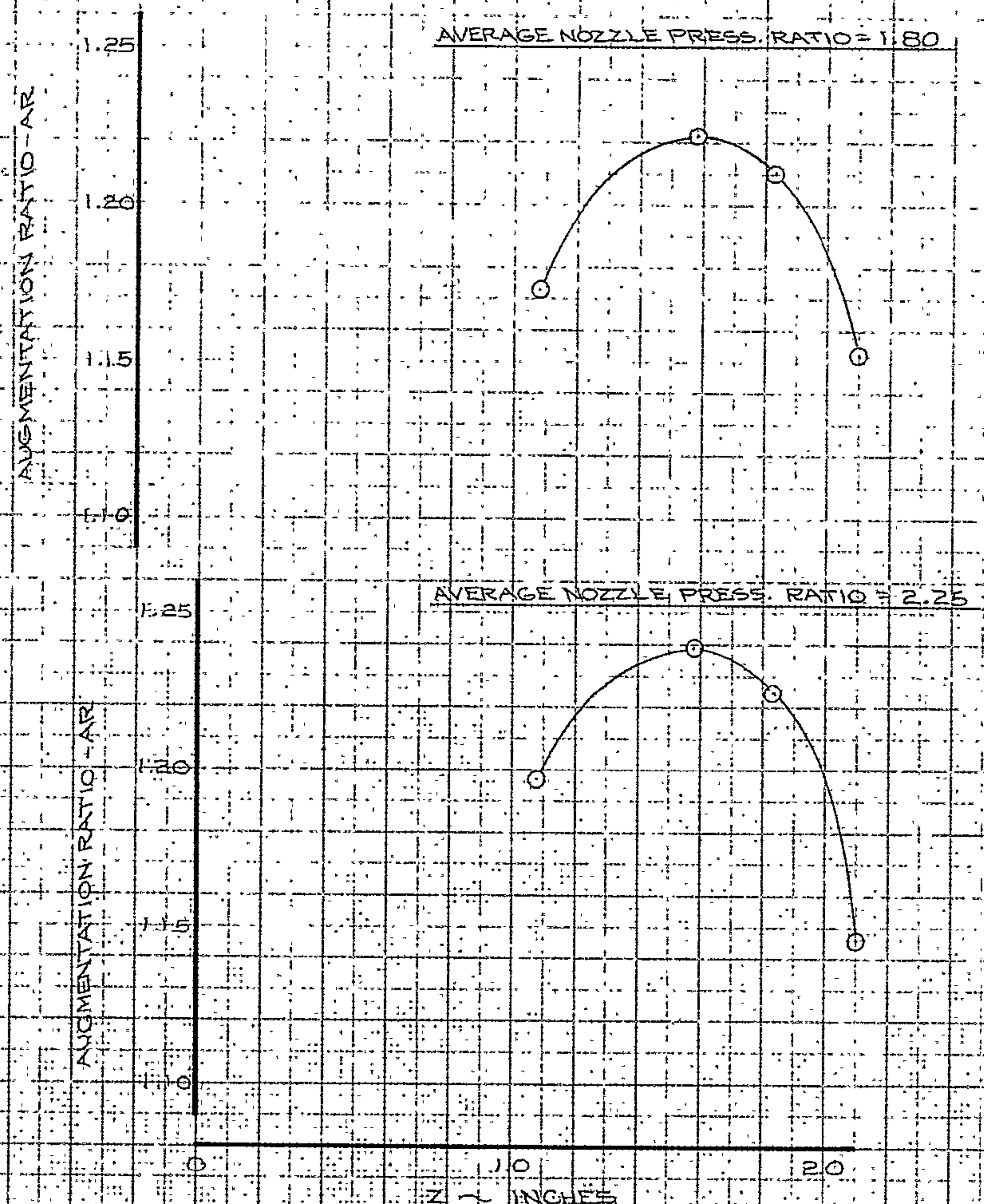

CALC			REVISED	DATE	Z OPTIMIZATION @	FIG. 81
CHECK					$\delta_F = 50°$ $\ell'_Z = 5.00''$	D6-24850
APR	D. Haskonen	3/30/71				
APR					THE BOEING COMPANY	PAGE 163
	[illegible]	2/26/71				

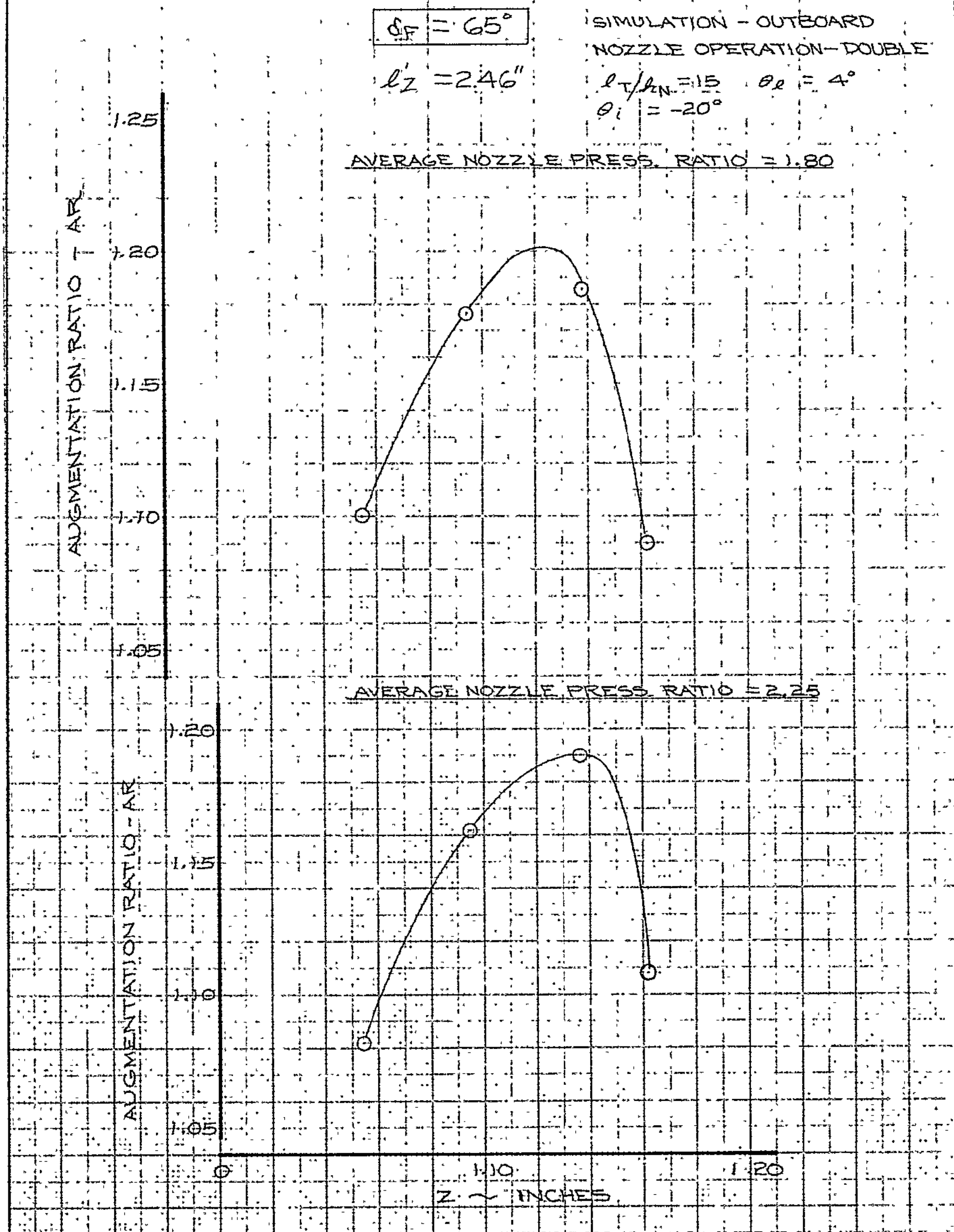

CALC			REVISED	DATE	Z OPTIMIZATION @ $\delta_F = 65°$ $\ell'_Z = 2.46''$
CHECK					FIG. 82
APR	D. Harkness	3/30/71			D6-24850
APR	[signature]	3/1/71			THE BOEING COMPANY
					PAGE 164

K+E ALBANENE

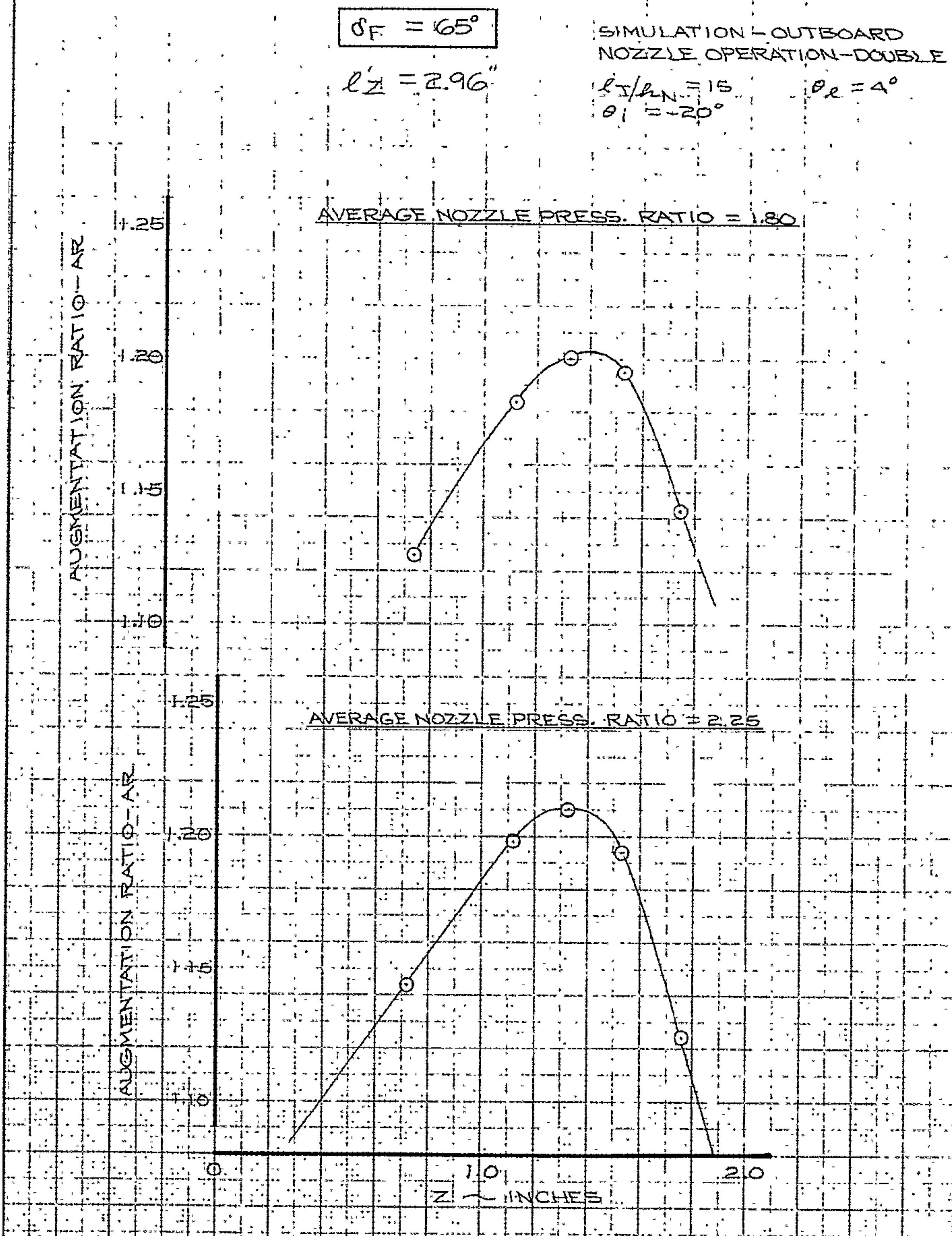

CALC			REVISED	DATE
CHECK				
APR	D. Hashorn	3/30/71		
APR				
	J. Floyd	3/1/71		

Z OPTIMIZATION @ $\delta_F = 65°$ $l'_Z = 2.96''$

FIG. 83

D6-24850

THE BOEING COMPANY

PAGE 165

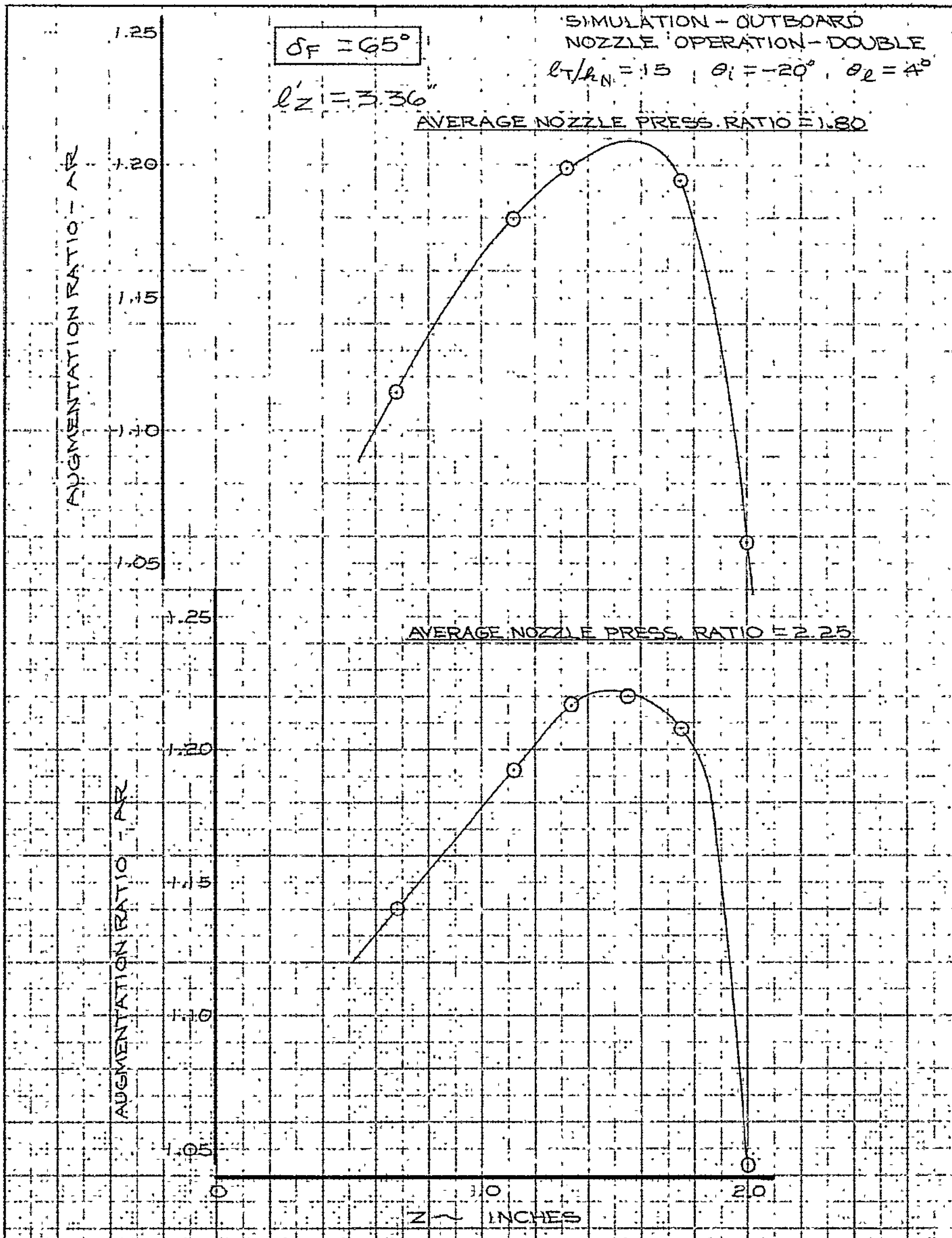

CALC			REVISED	DATE	Z OPTIMIZATION @ $\delta_F = 65°$ $\ell'_Z = 3.36''$	FIG. 84
CHECK						D6-24850
APR	D. Harkonen	3/30/71			THE BOEING COMPANY	PAGE 166
APR	J. Hoyt	3/1/71				

K+E ALBANENE

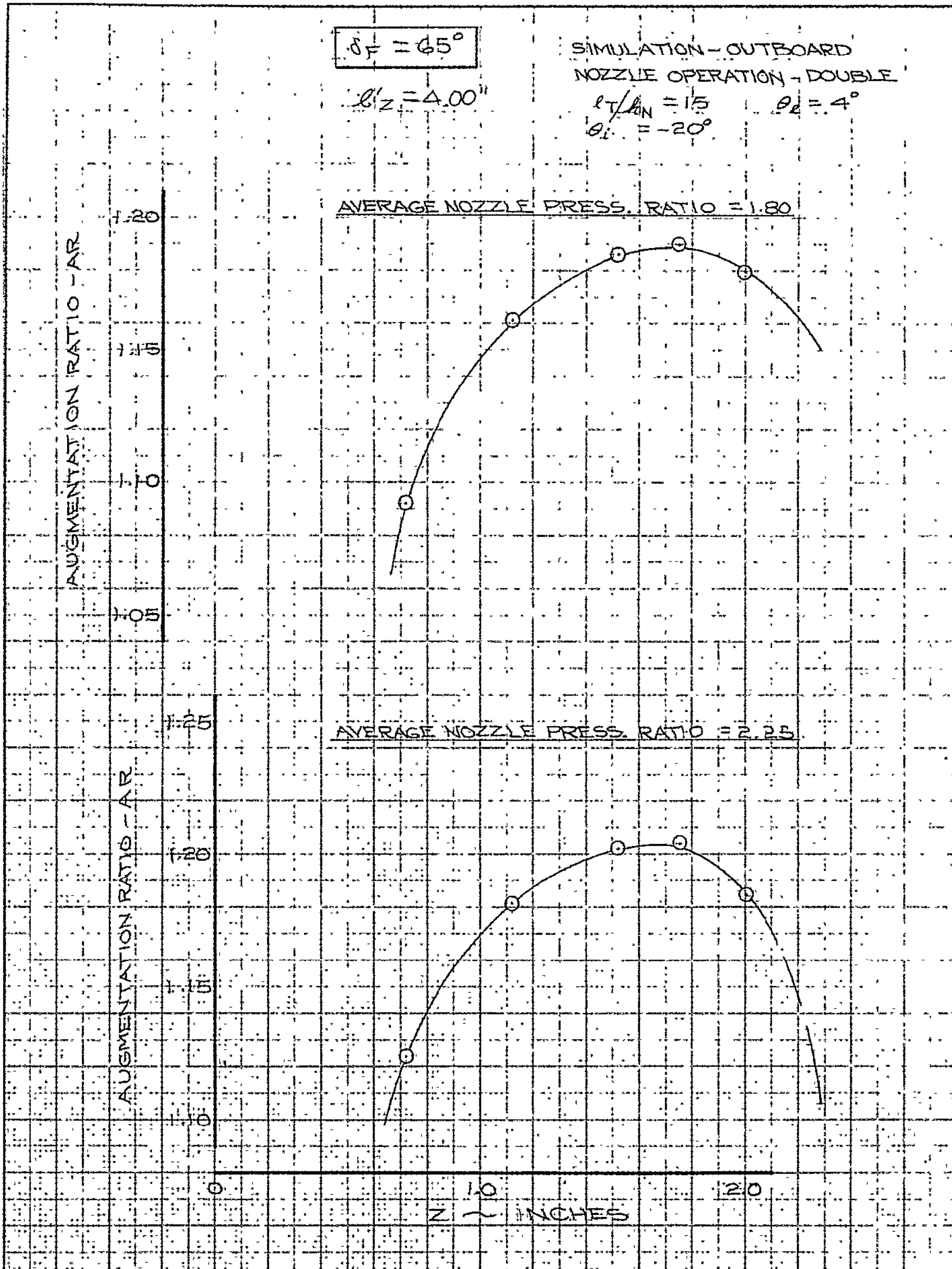

CALC			REVISED	DATE
CHECK				
APR	[signature]	3/30/71		
APR				

Z OPTIMIZATION @ $\delta_F = 65°$ $\ell'_Z = 4.00''$

FIG. 85

THE BOEING COMPANY

D6-24850

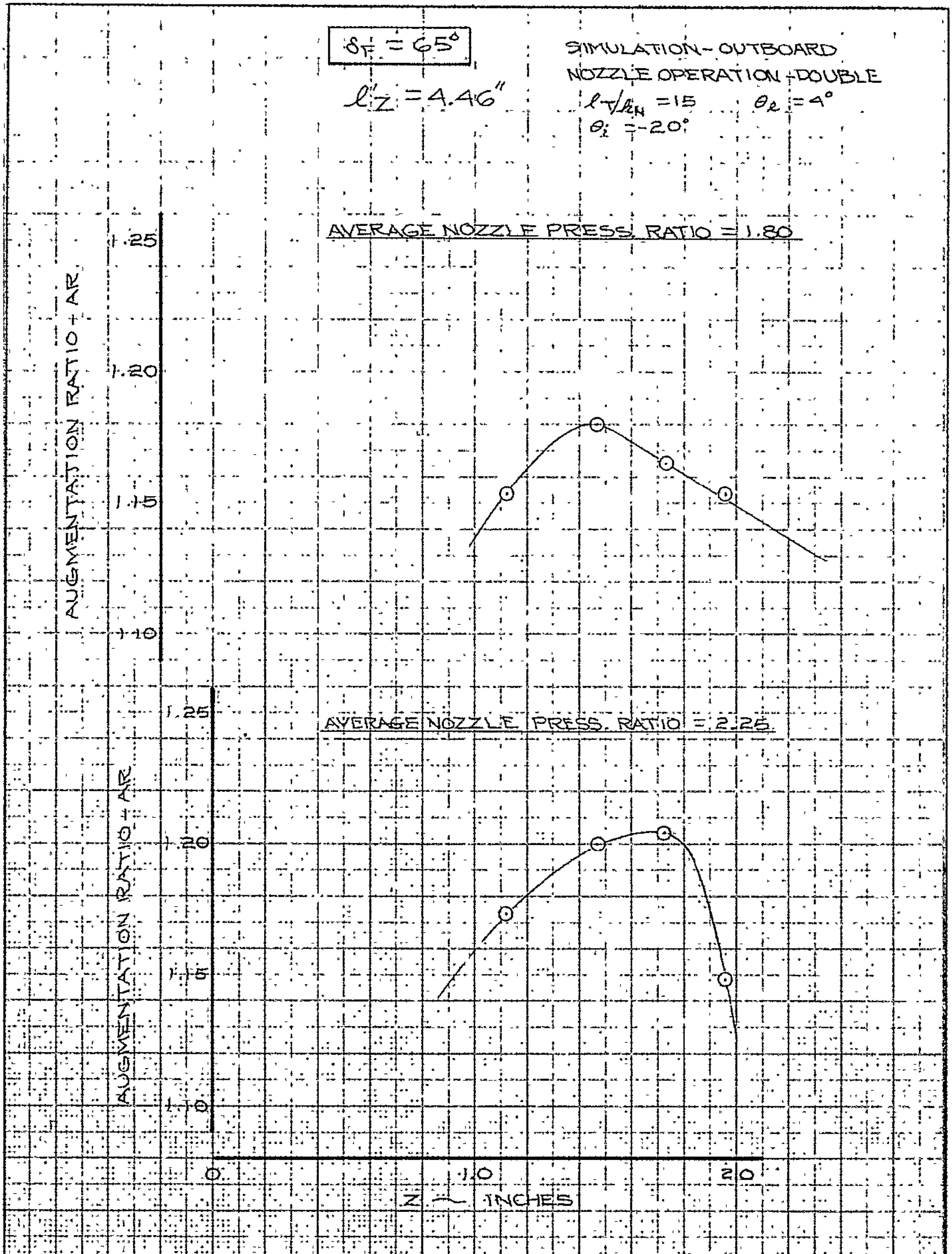

			REVISED	DATE
CALC				
CHECK				
APR	[signature]	3/30/71		
APR				
	[signature]	3/1/71		

Z OPTIMIZATION @ $\delta_F = 65°$ $\ell'_Z = 4.46''$

FIG. 86

D6-24850

THE BOEING COMPANY

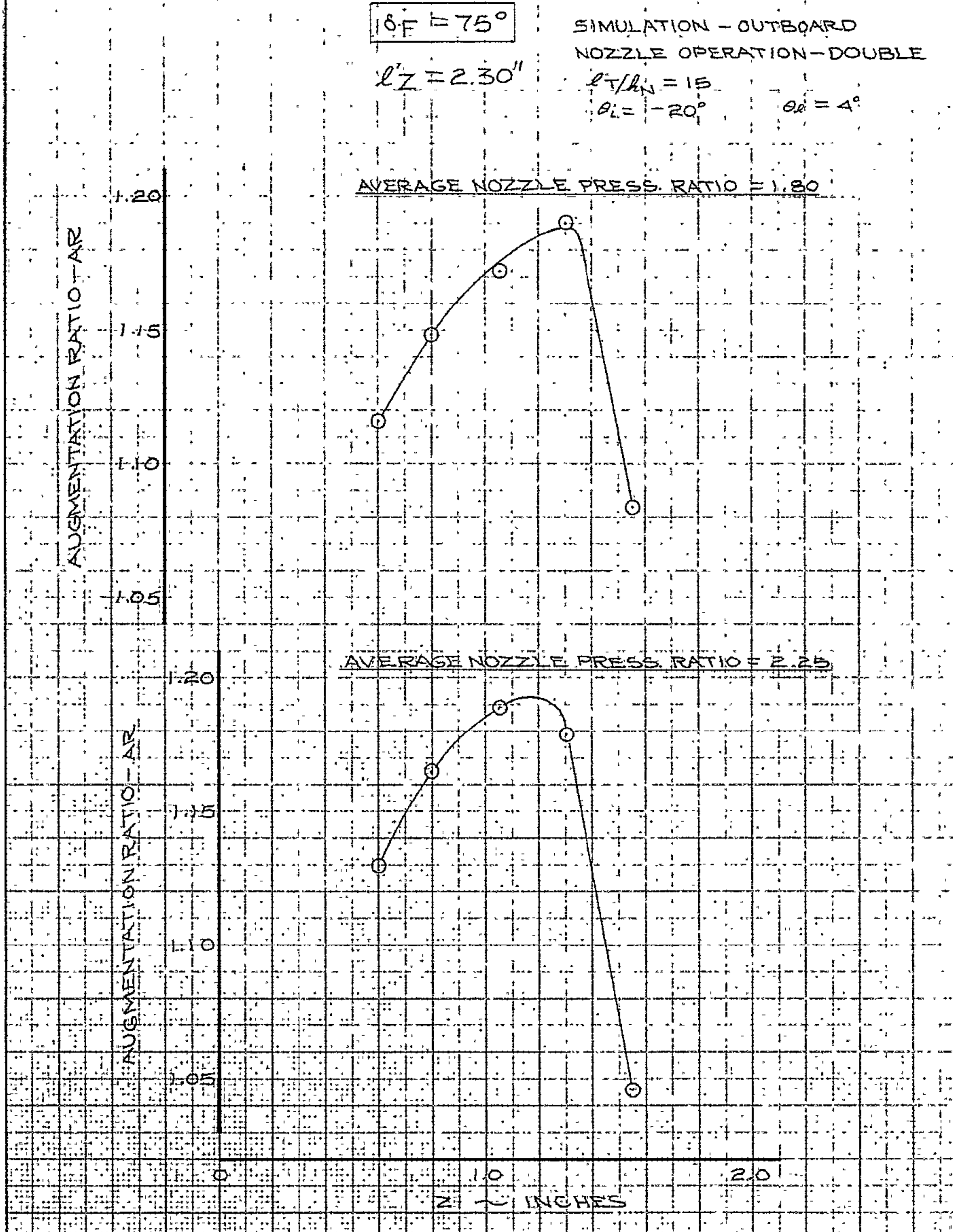

CALC			REVISED	DATE	Z OPTIMIZATION @ $\delta_F = 75°$ $l'_Z = 2.30''$	FIG. 87
CHECK						D6-24850
APR	D. Harhouen	3/30/71				
APR					THE BOEING COMPANY	PAGE 169
	J. Wright	3/2/71				

K•E ALBANENE TUSL

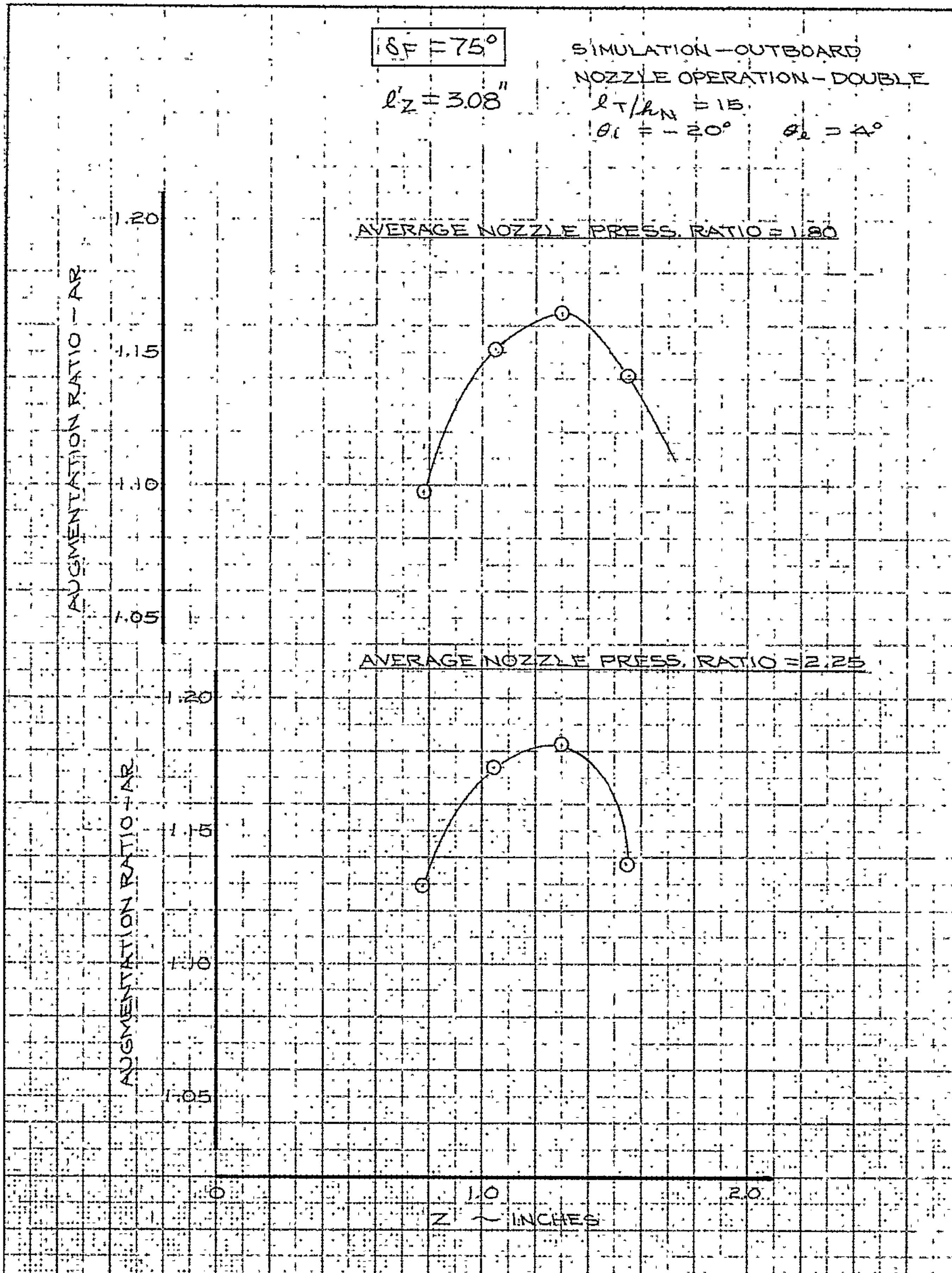

CALC			REVISED	DATE	Z OPTIMIZATION @	FIG. 88
CHECK						
APR	D. Harkonen	3/30/71			$\delta_F = 75°$ $l'_Z = 3.08''$	D6-24850
APR						
	J.C. Hoyt	3/2/71			THE BOEING COMPANY	PAGE 170

K+E ALBANENE

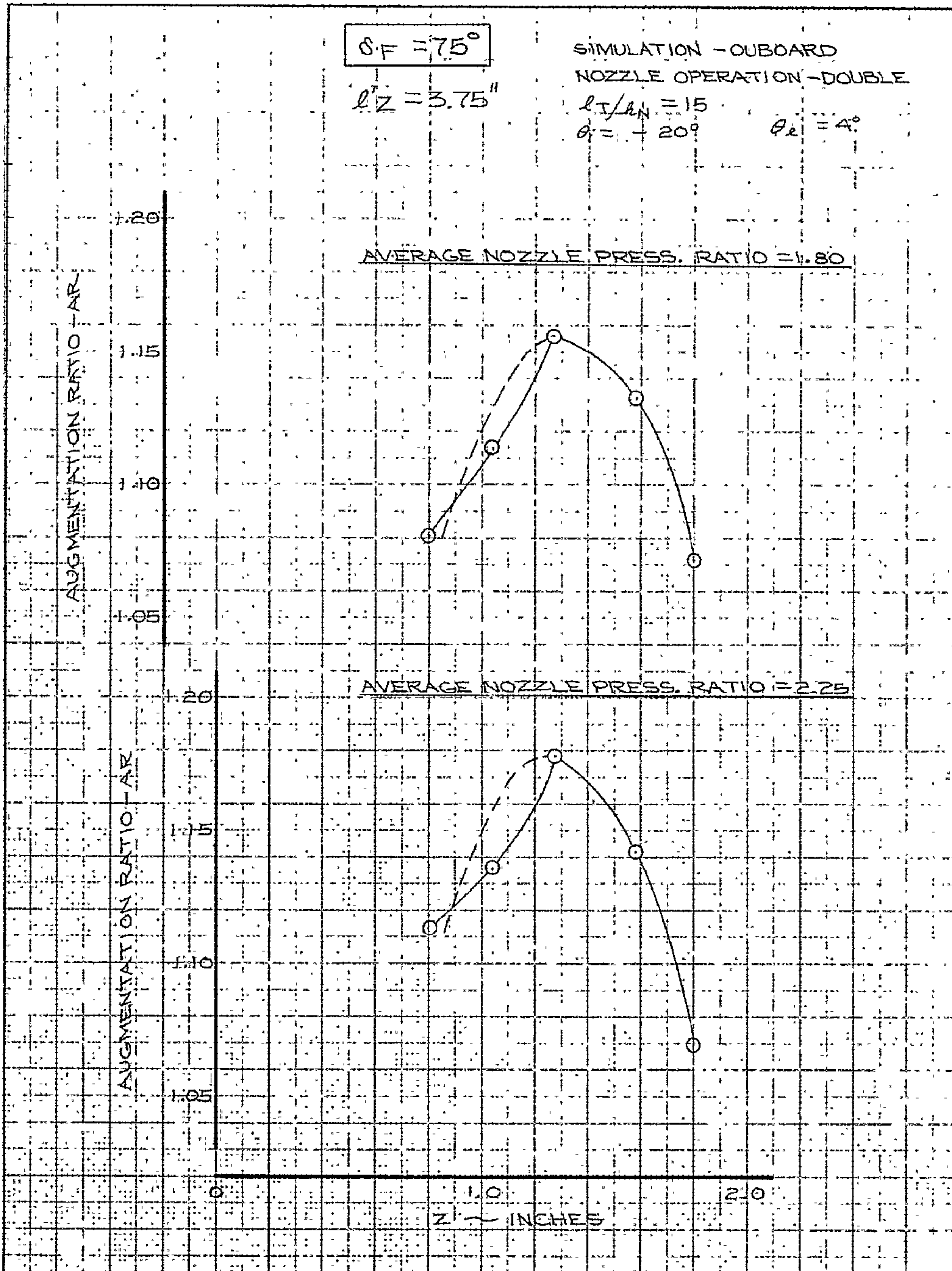

CALC			REVISED	DATE
CHECK				
APR	[signature]	3/30/71		
APR				
	[signature]	3/2/71		

Z OPTIMIZATION @ $\delta_F = 75°$ $l'_Z = 3.75''$

FIG. 89

D6-24850

THE BOEING COMPANY

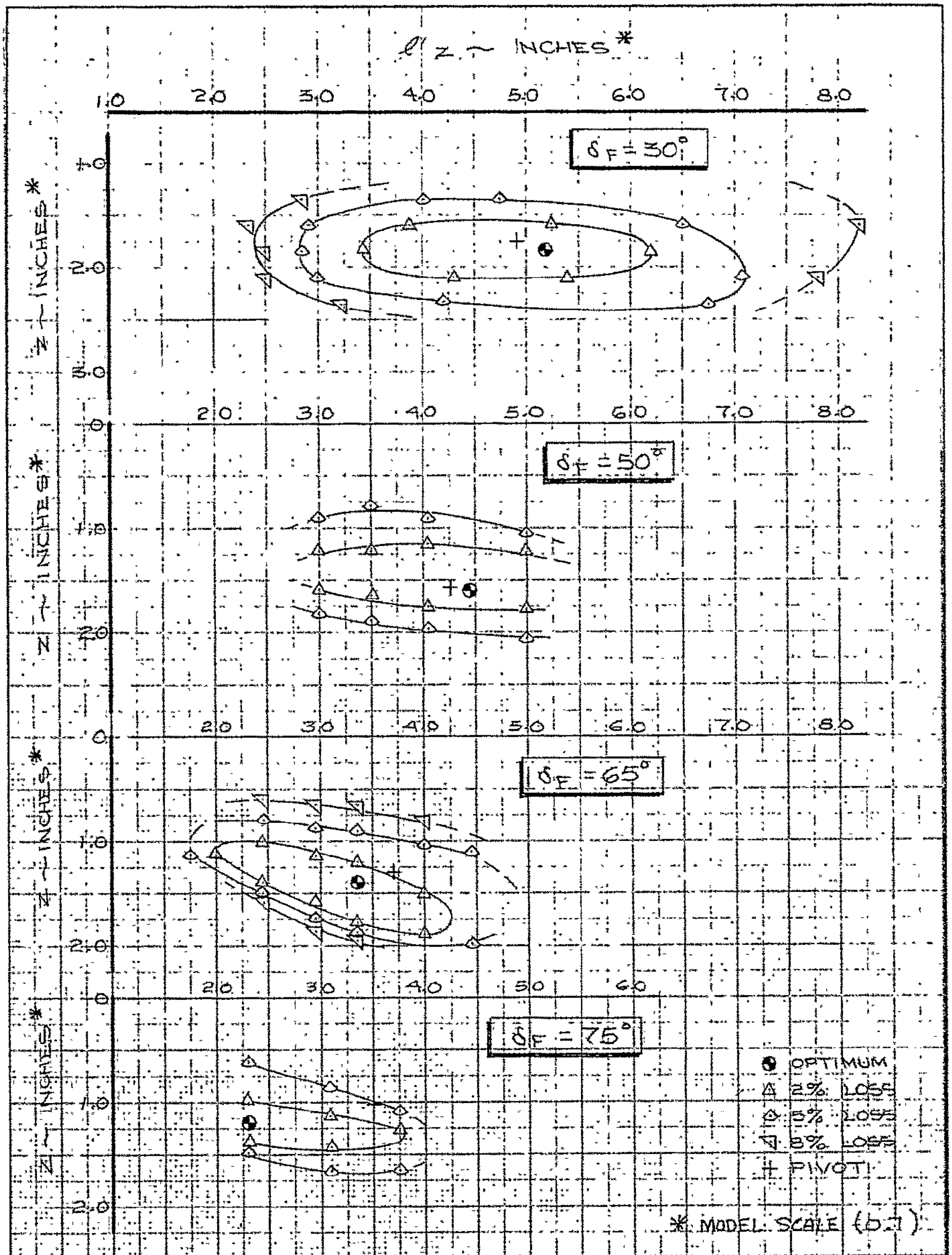

CALC			REVISED	DATE	PERCENT LOSS CONTOURS OUTBOARD SIMULATION DOUBLE NOZZLE - $P_T/P_A = 1.80$	FIG. 90
CHECK						
APR	V. Voskhousen	3/30/71				D6-24850
APR					THE BOEING COMPANY	PAGE 172
	J. Hoyt	3/1/71				

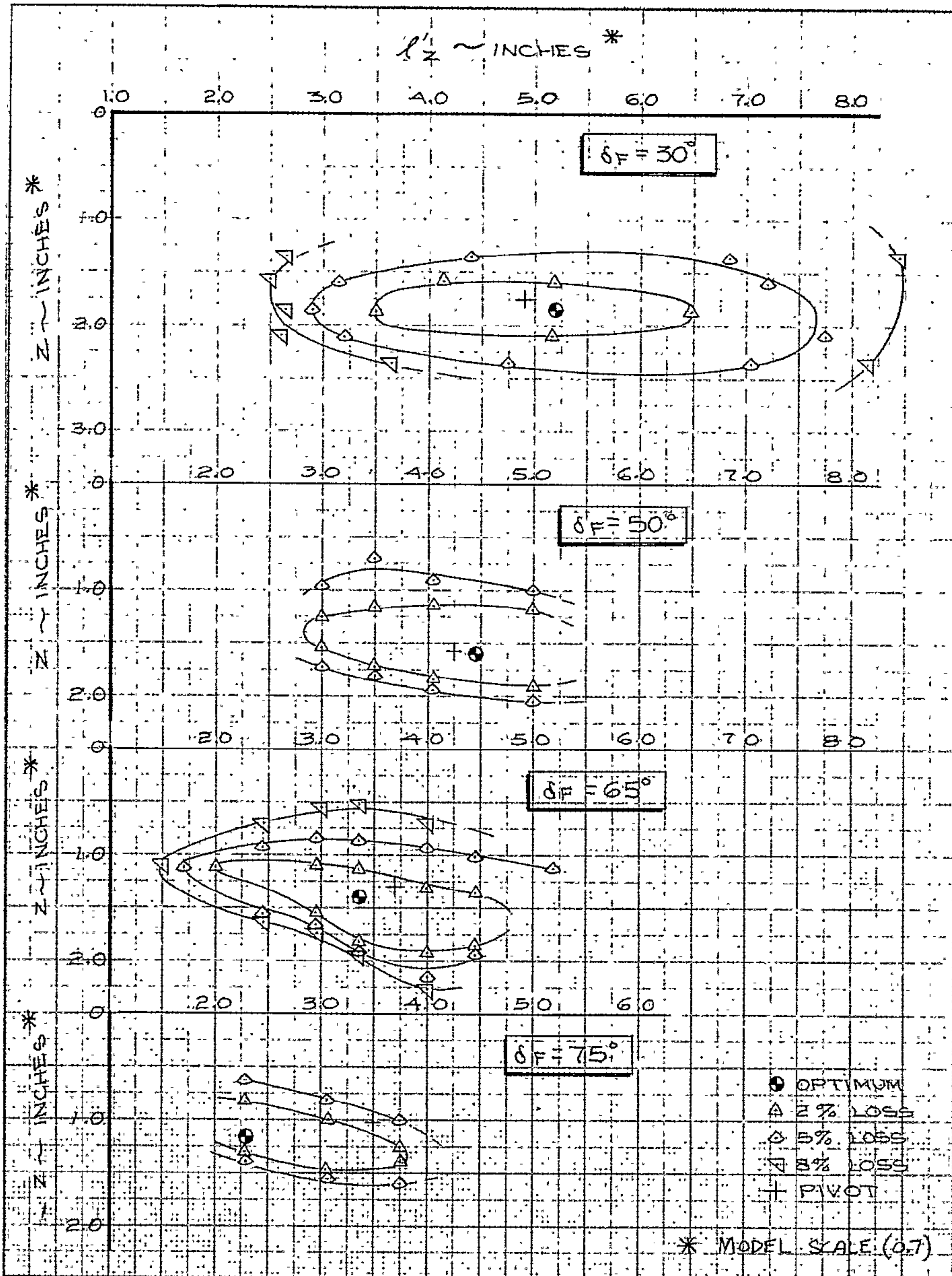

			REVISED	DATE		
CALC					PERCENT LOSS CONTOURS OUTBOARD SIMULATION DOUBLE NOZZLE - $P_T/P_A = 2.25$	FIG. 91
CHECK						
APR	[signature]	3/30/71				D6-24850
APR						
	[signature]	3/15/71			THE BOEING COMPANY	PAGE 173

K+E ALBANENE

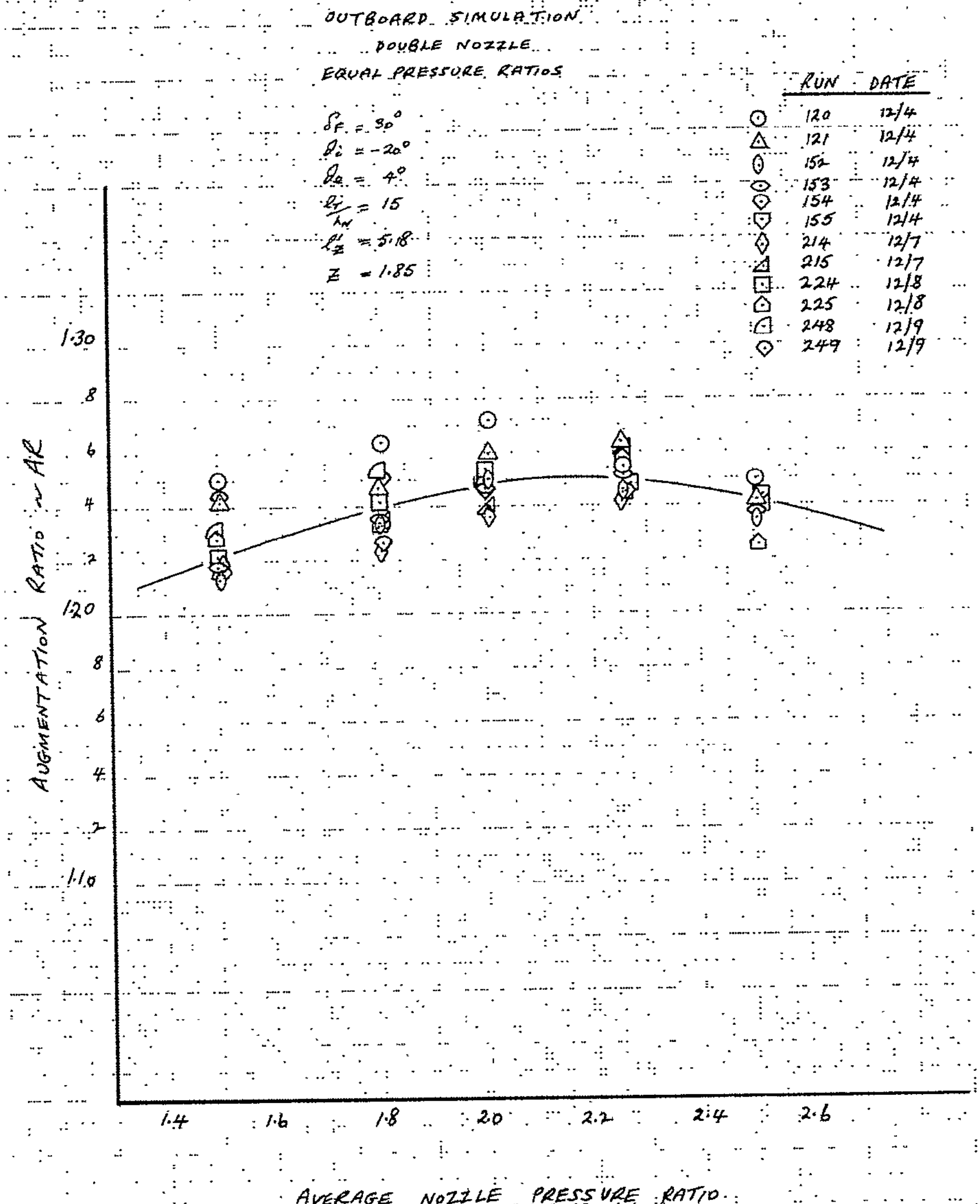

CALC	R.H.T.	DEC. '70	REVISED	DATE	DATA SCATTER AT $\delta_F = 30^\circ$	FIG. 92
CHECK					OPTIMUM CONFIGURATION	D6-24850
APR	D. [illegible]	3/30/71				
APR					THE BOEING COMPANY	PAGE 174

12 IN. FLAP EXTENSIONS INSTALLED

$\delta_F = 50°$

$l'_Z = 4.46''$

SIMULATION – OUTBOARD NOZZLE OPERATION – DOUBLE

$l_T/h_N = 12.4$

$\theta_i = -10°$ $\theta_e = 4.5°$

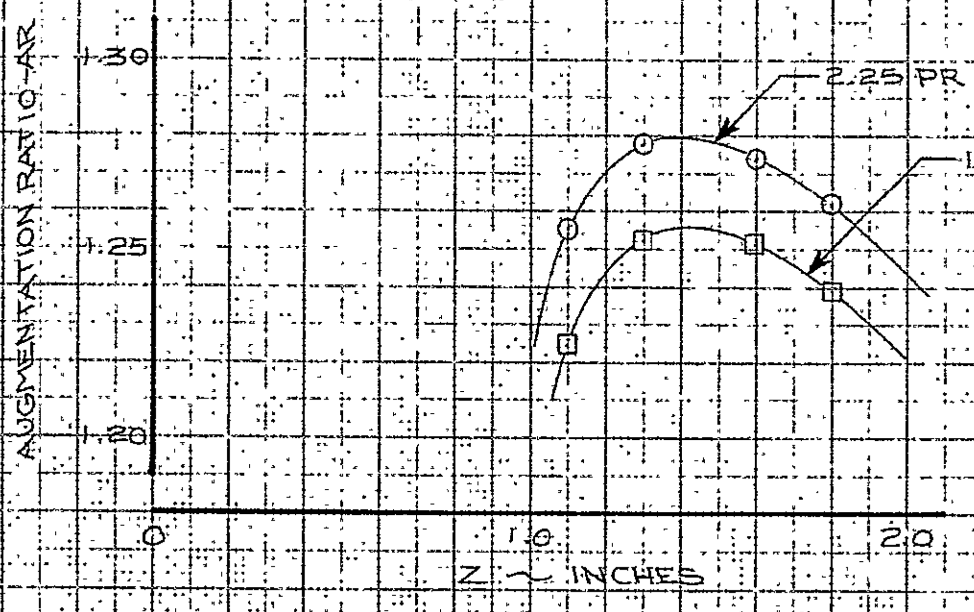

			REVISED	DATE	
CALC					AUGMENTOR PERFORMANCE WITH 12 INCH FLAP EXTENSIONS $\delta_F = 50°$, $l_T/h_N = 12.4$, $\theta_e = 4.5°$
CHECK					
APR	D. Hackmann	3/30/71			FIG. 93
APR					D6-24850
	J.J. Hoyt	3/3/71			THE BOEING COMPANY

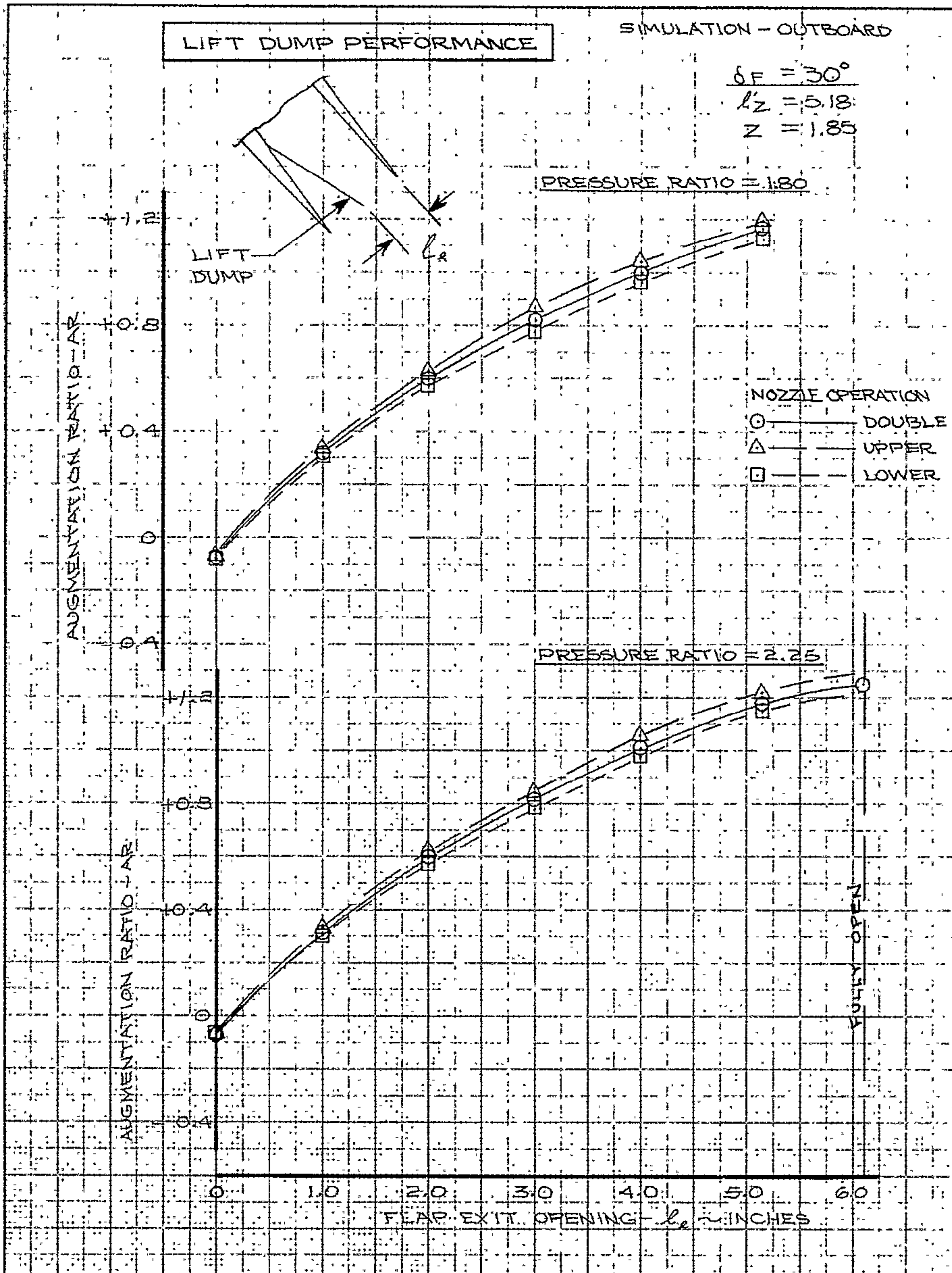

CALC			REVISED	DATE	LIFT DUMP PERFORMANCE	FIG. 94
CHECK					$\delta_F = 30°$	D6-24850
APR	R. Hashimoto	3/30/71				
APR					THE BOEING COMPANY	PAGE 176

K+E ALBANENE

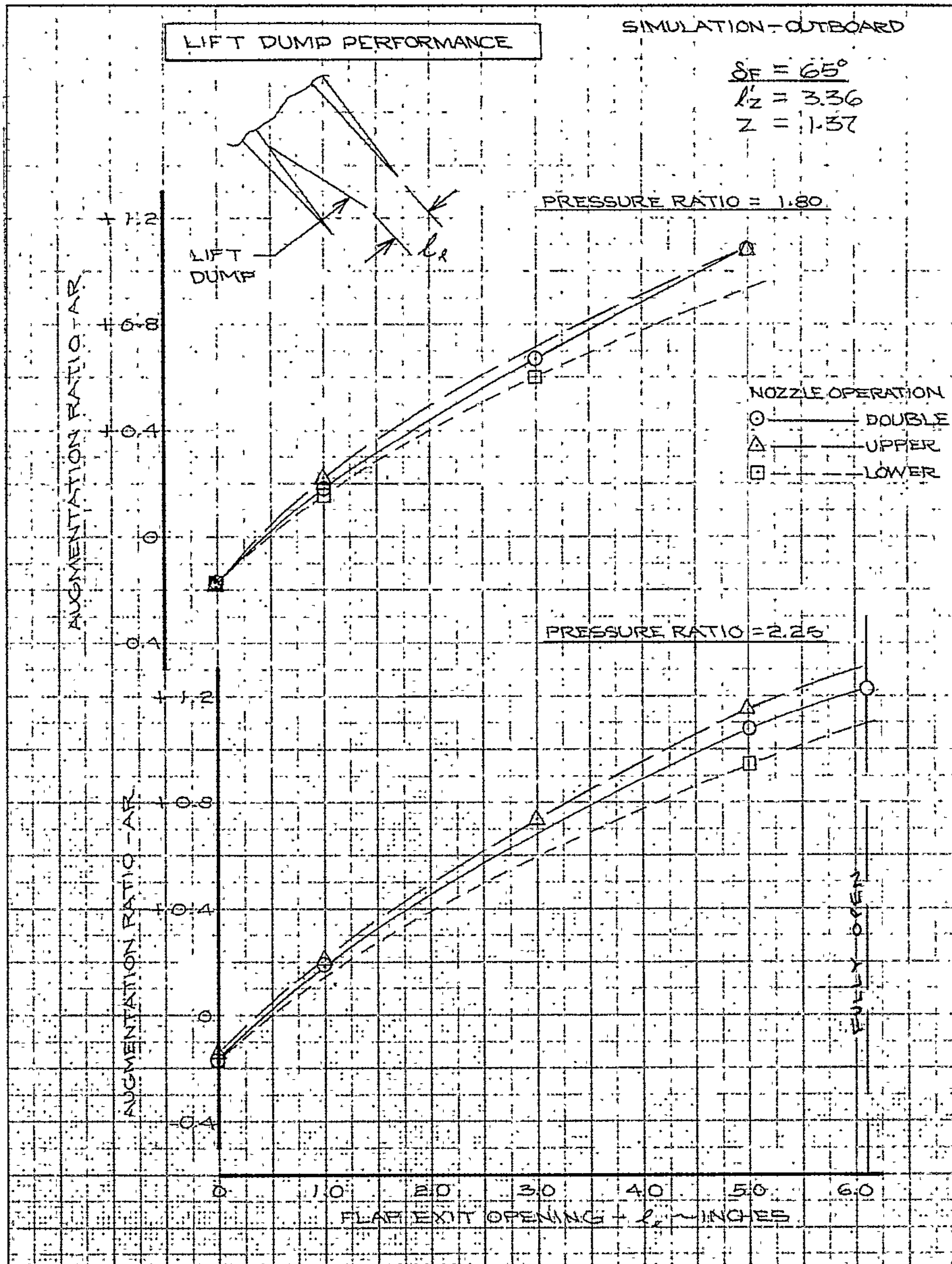

			REVISED	DATE	
CALC					LIFT DUMP PERFORMANCE
CHECK					$\delta_F = 65°$
APR	D. Hardiman	3/30/71			
APR					THE BOEING COMPANY
	J.K. Hoyt	3/5/71			

Fig. 95

D6-24850

K+E ALBANENE

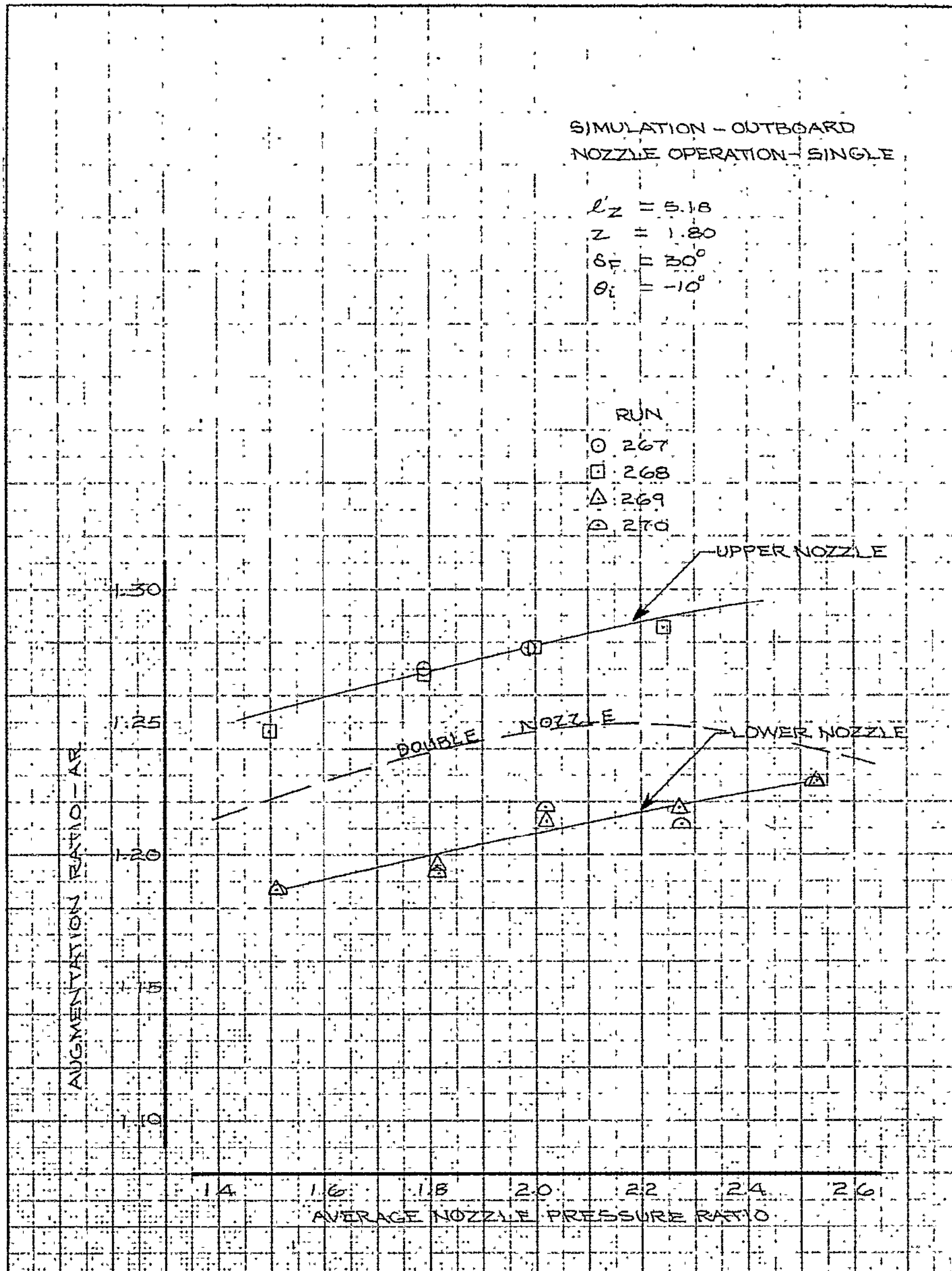

CALC			REVISED	DATE	SINGLE NOZZLE AUGMENTOR PERFORMANCE - NOT OPTIMIZED $\delta F = 30^\circ$	FIG. 96
CHECK						
APR	D. Hochmann	3/30/71				D6-24850
APR					THE BOEING COMPANY	PAGE 178
	[illegible]	3/3/71				

K+E ALBANENE

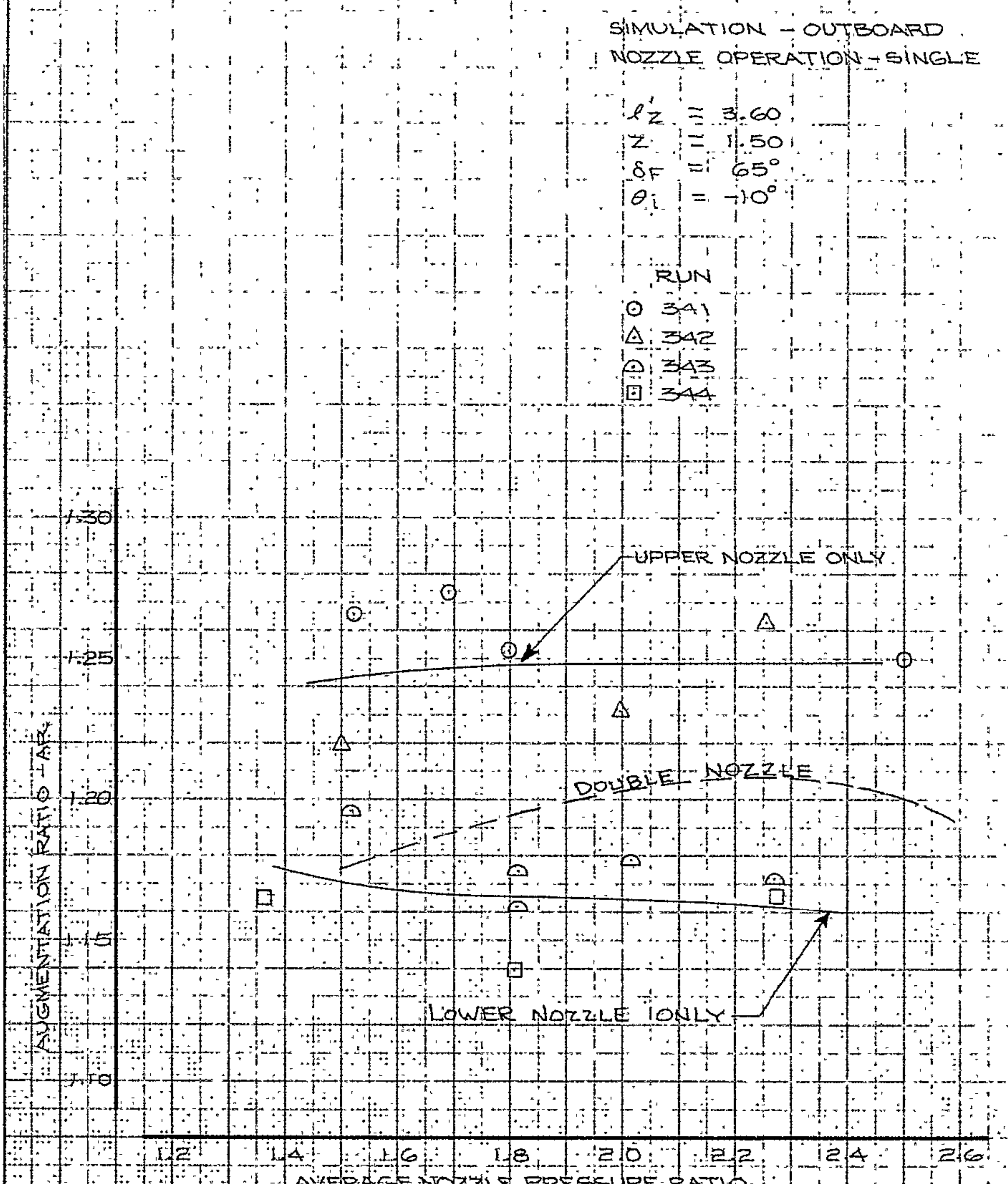

CALC			REVISED	DATE	SINGLE NOZZLE AUGMENTOR PERFORMANCE - NOT OPTIMIZED $\delta_F = 65°$	FIG. 97
CHECK						
APR	D. Harkonen	3/30/71				D6-24850
APR					THE BOEING COMPANY	
	[illegible]	3/3/71				PAGE 179

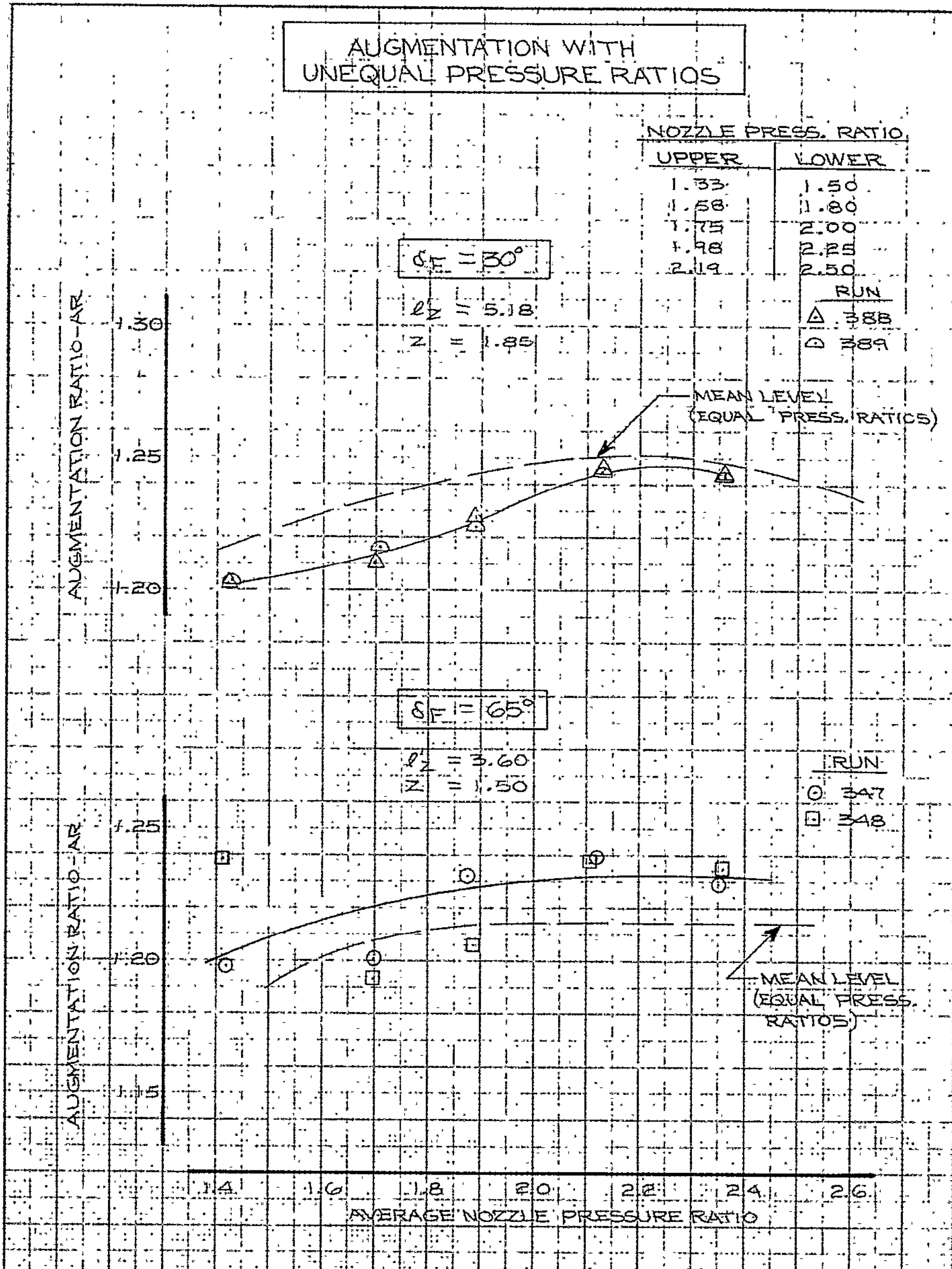

CALC			REVISED	DATE	EFFECT OF UNEQUAL PRESSURE RATIOS ON AUGMENTATION $\delta_F = 30°, 65°$	FIG. 98
CHECK						
APR	D. Harhonen	3/30/71				D6-24850
APR					THE BOEING COMPANY	PAGE 180
	[illegible signature]					

K·E ALBANENE

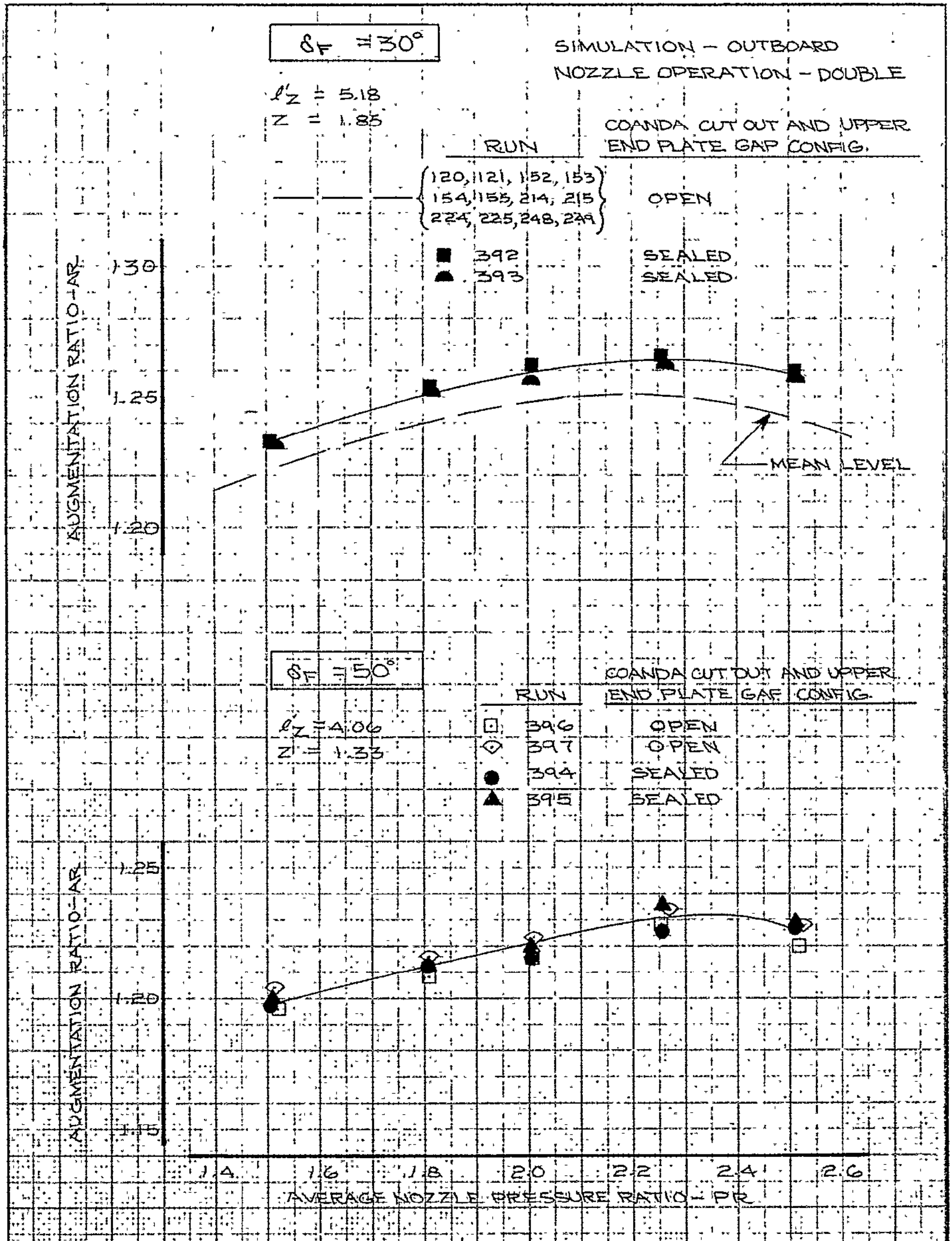

CALC			REVISED	DATE	EFFECT OF SEALING UPPER END PLATE GAPS AND COANDA FLAP BRACKET CUTOUTS	FIG. 99
CHECK						
APR	D. Harkonen	3/30/71				D6-24850
APR					THE BOEING COMPANY	PAGE 181
	J. Hoyt					

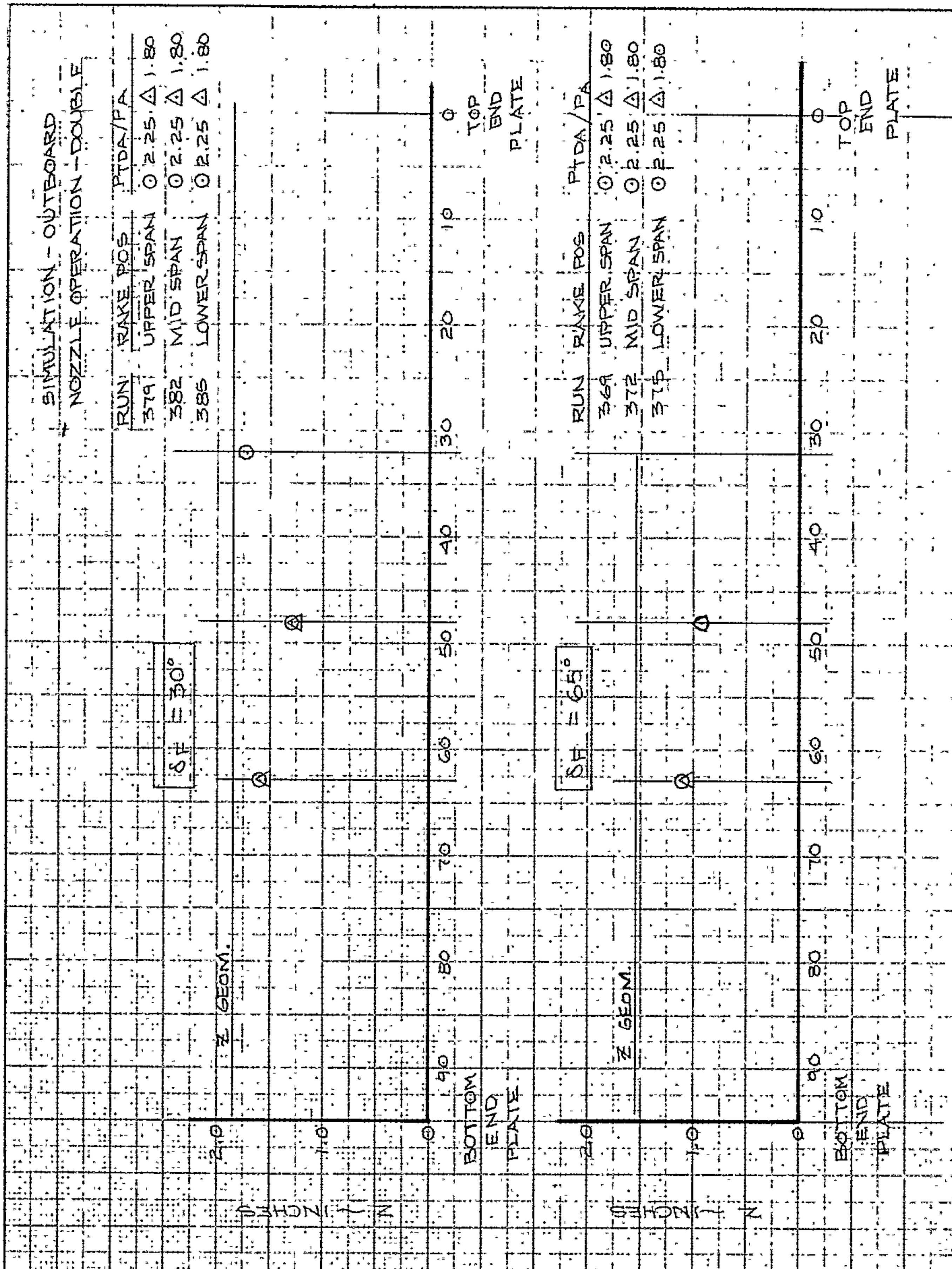

			REVISED	DATE		
CALC					PEAK NOZZLE PRESSURE VERSUS MODEL SPAN - OUTBOARD SIMULATION - DOUBLE NOZZLE	FIG. 100
CHECK						
APR	D. Jsohnen	3/30/71				D6-24850
APR	J. Hoyt	3/31/71			THE BOEING COMPANY	PAGE 182

182

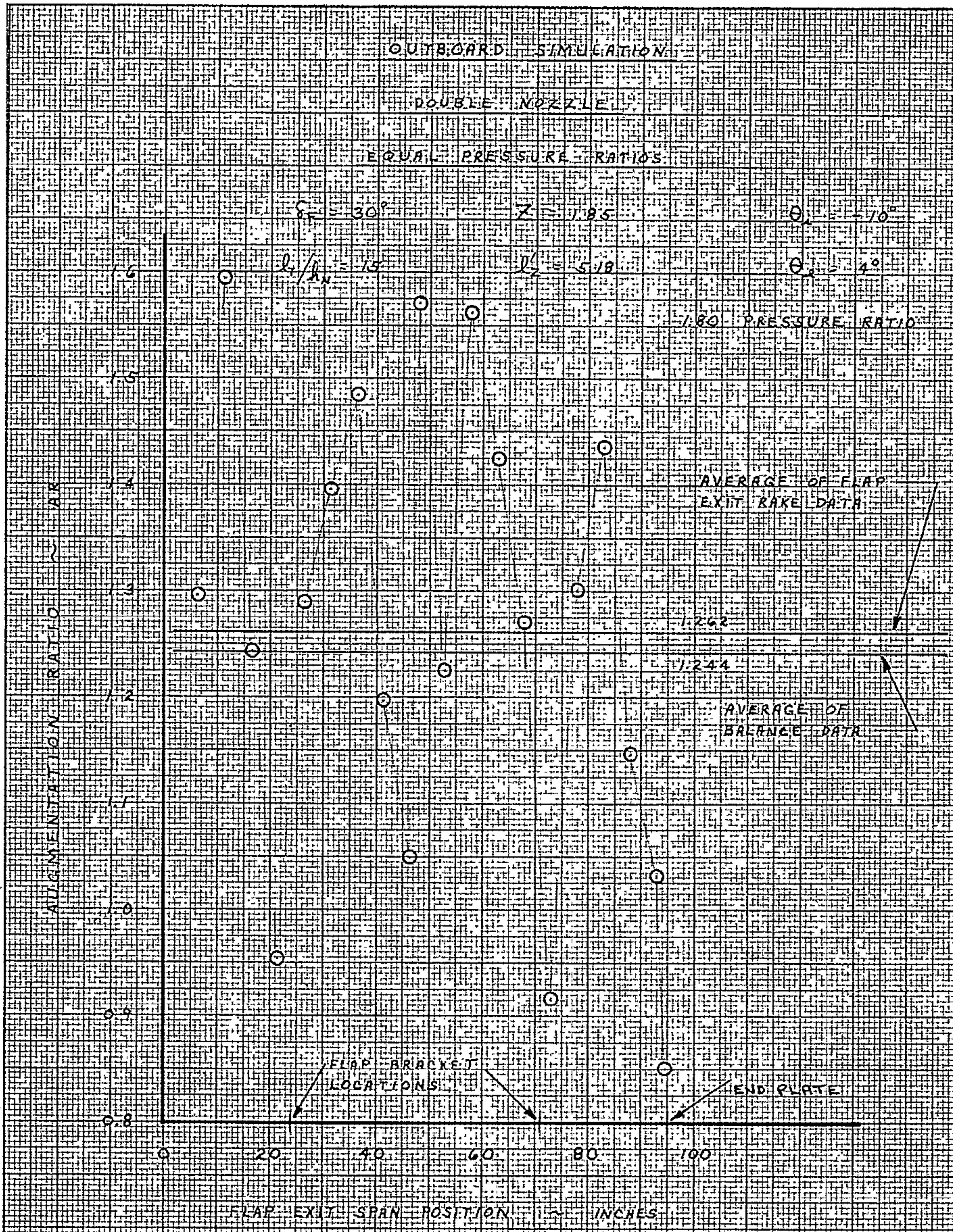

CALC	P. J. R.	12-14-70	REVISED	DATE
CHECK				
APR	D. Hoshorne	3/30/71		
APR				

VARIATION OF AUGMENTATION RATIO WITH SPAN LOCATION

THE BOEING COMPANY

Fig. 101

D6-24850

AD 461 C-R4

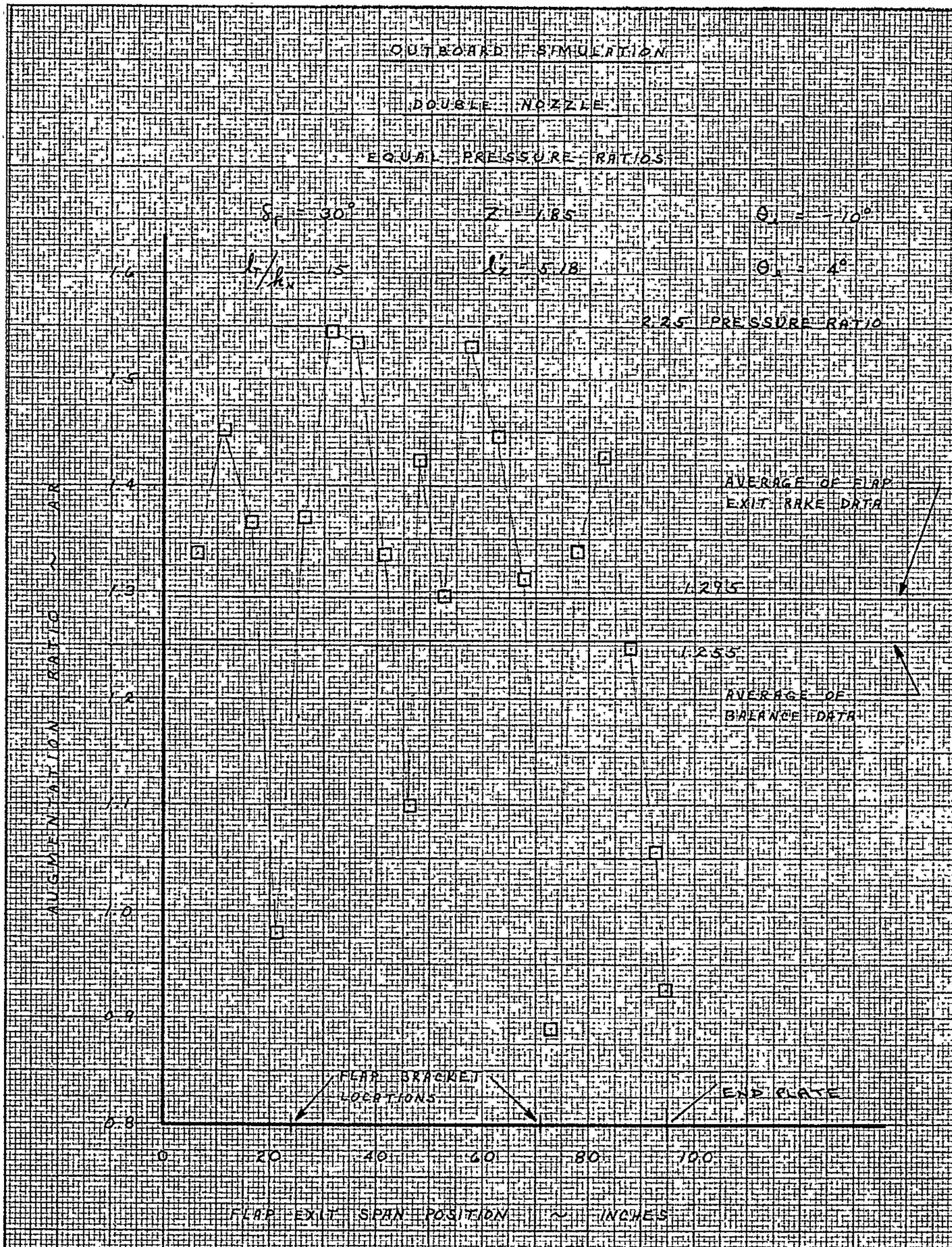

CALC	P. J. R.	12-14-70	REVISED	DATE	VARIATION OF AUGMENTATION RATIO WITH SPAN LOCATION	Fig. 102
CHECK						D6-24850
APR	D. Wadsworth	3/30/71				
APR					THE BOEING COMPANY	PAGE 184

AD 461 C-R4.

K+E ALBANENE 195L TRACING PAPER

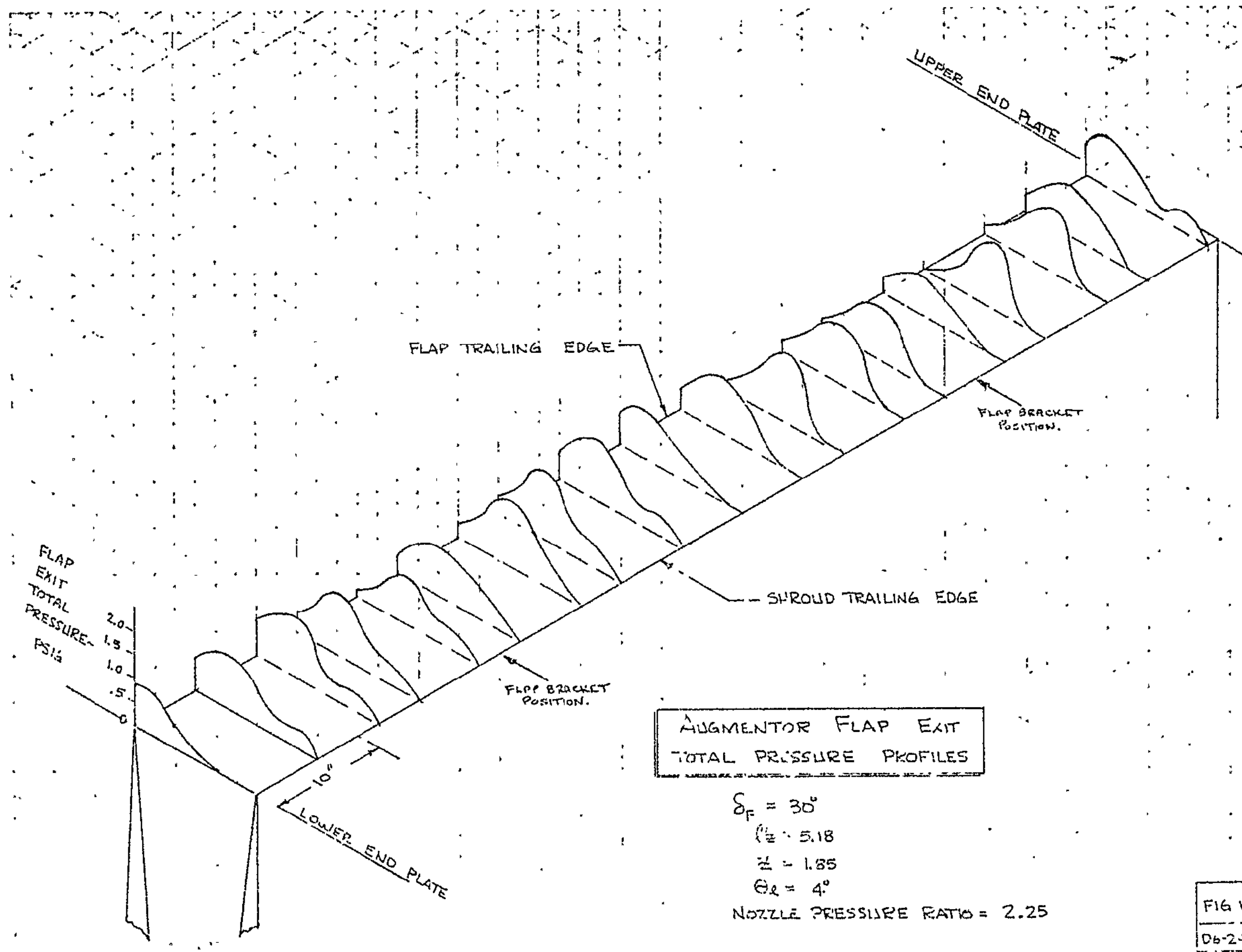

AUGMENTOR FLAP EXIT TOTAL PRESSURE PROFILES

$\delta_F = 30°$

$\ell/z \approx 5.18$

$z/t = 1.85$

$\theta_\ell = 4°$

NOZZLE PRESSURE RATIO = 2.25

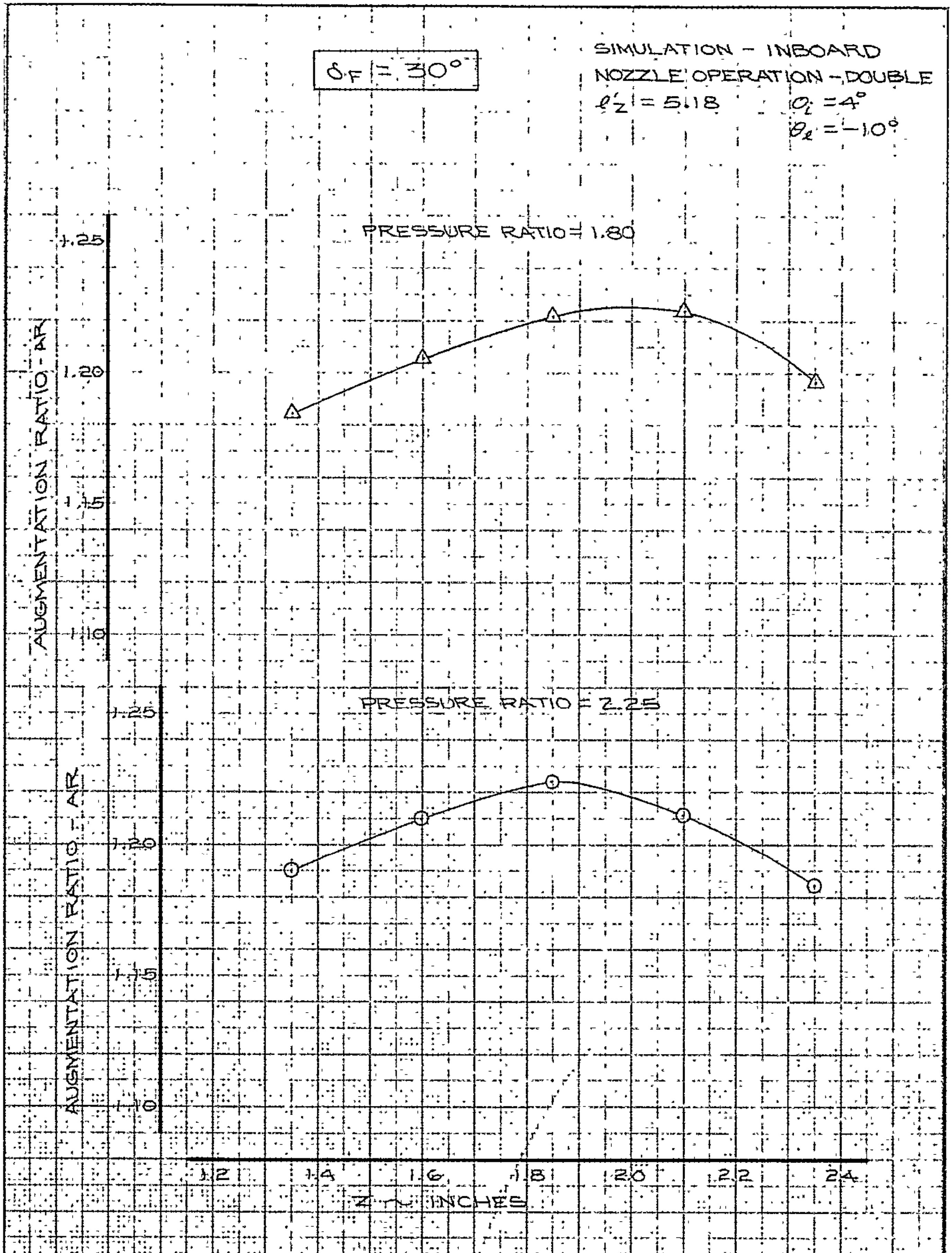

CALC			REVISED	DATE
CHECK				
APR	D. Harkonen	3/30/71		
APR				
	[illegible]	3/10/71		

AUGMENTATION RATIO VS Z

FIG. 104

$\ell'_Z = 5.18$ $\delta_F = 30°$

D6-24850

THE BOEING COMPANY

K+E ALBANENE

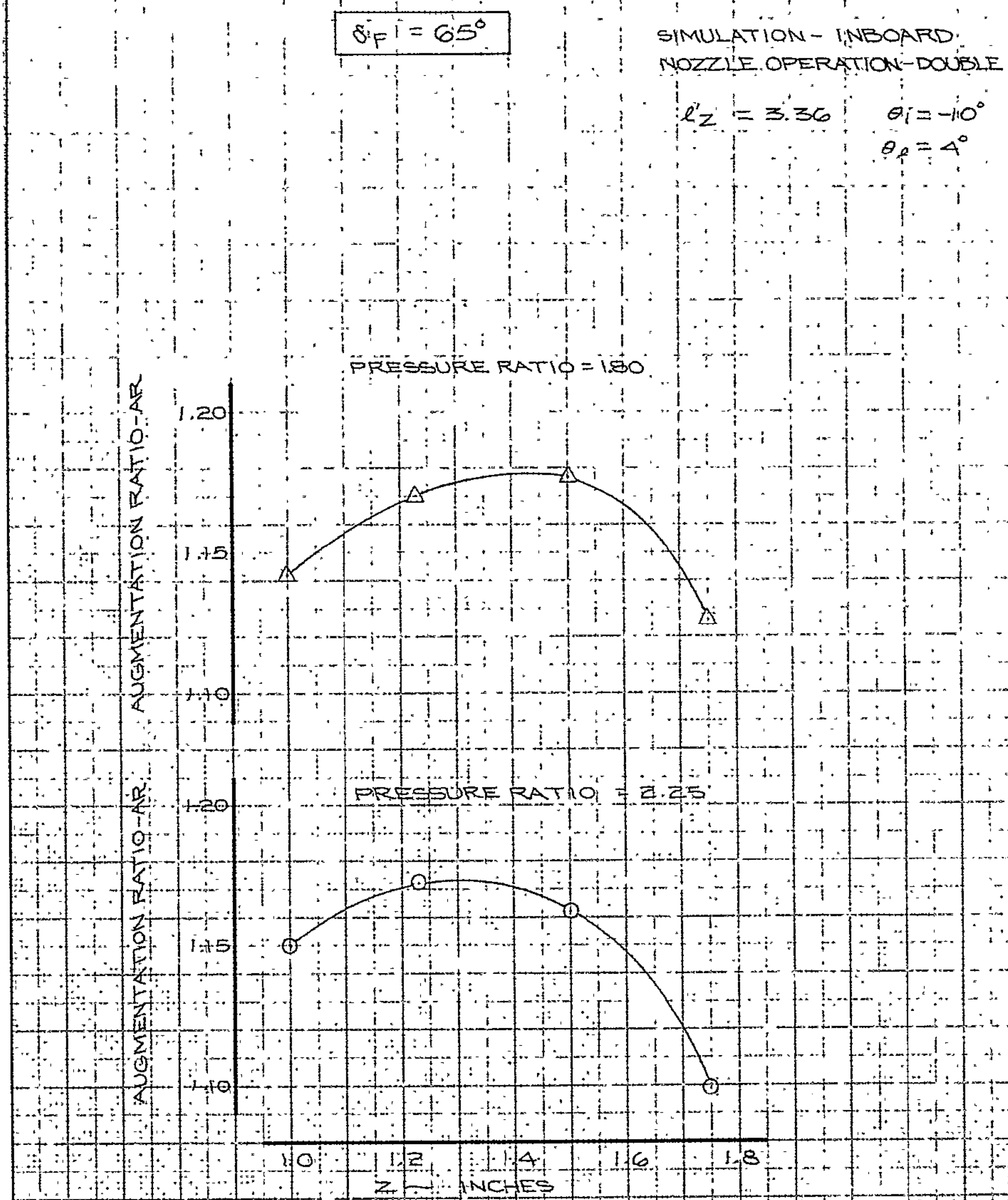

CALC			REVISED	DATE
CHECK				
APR	D. Hackmer	3/30/71		
APR				
	J. Hoyt	3/10/71		

AUGMENTATION RATIO VS Z

FIG. 105

$l'_Z = 3.36$ $\delta_F = 65°$

D6-24850

THE BOEING COMPANY

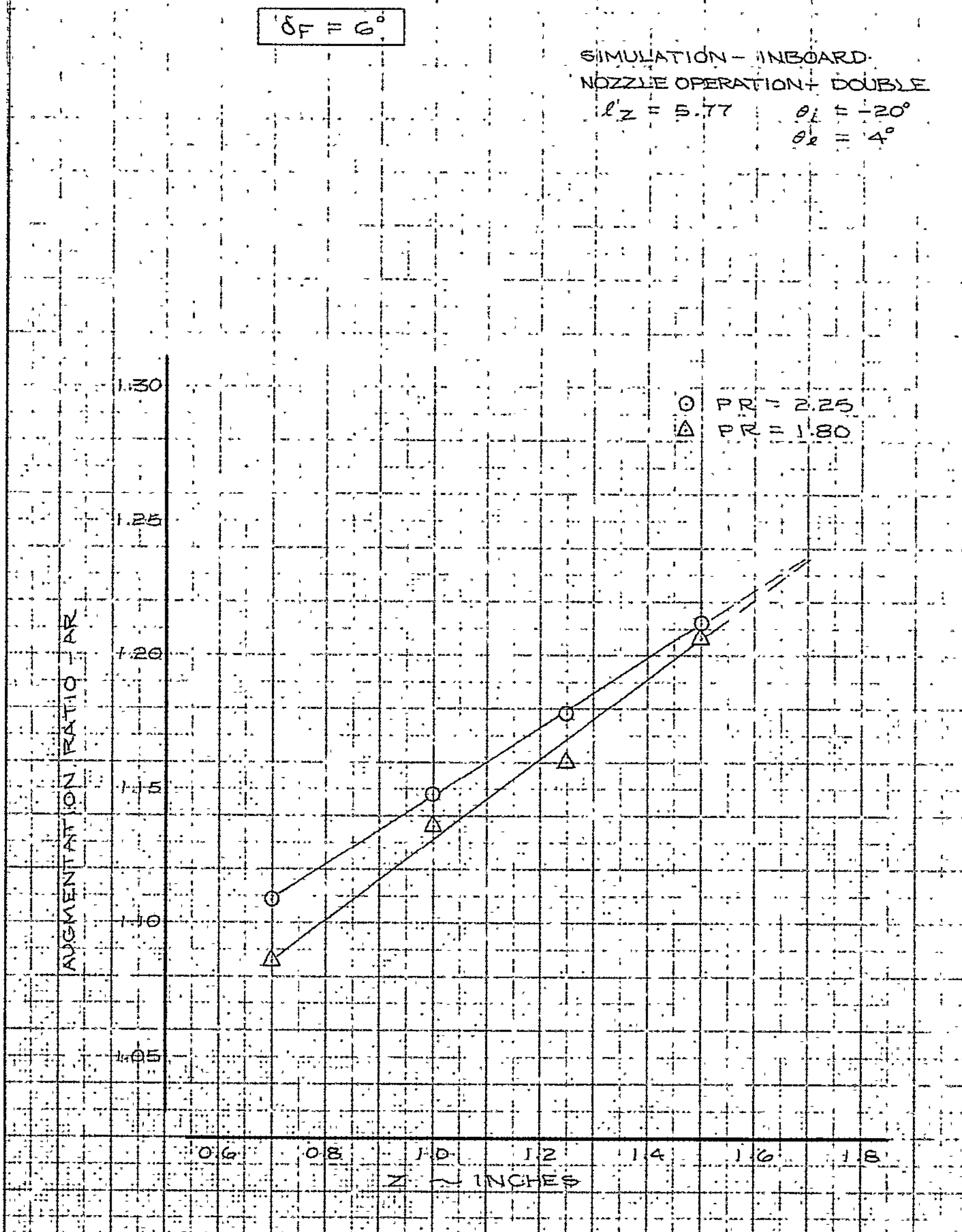

CALC			REVISED	DATE	AUGMENTATION RATIO VS Z	FIG. 106
CHECK						
APR	D. Haskorn	3/30/71			$\ell'_Z = 5.77$ $\delta_F = 6°$	D6-24850
APR						
	[illegible]	3/5/71			THE BOEING COMPANY	PAGE 188

K+E ALBANENE

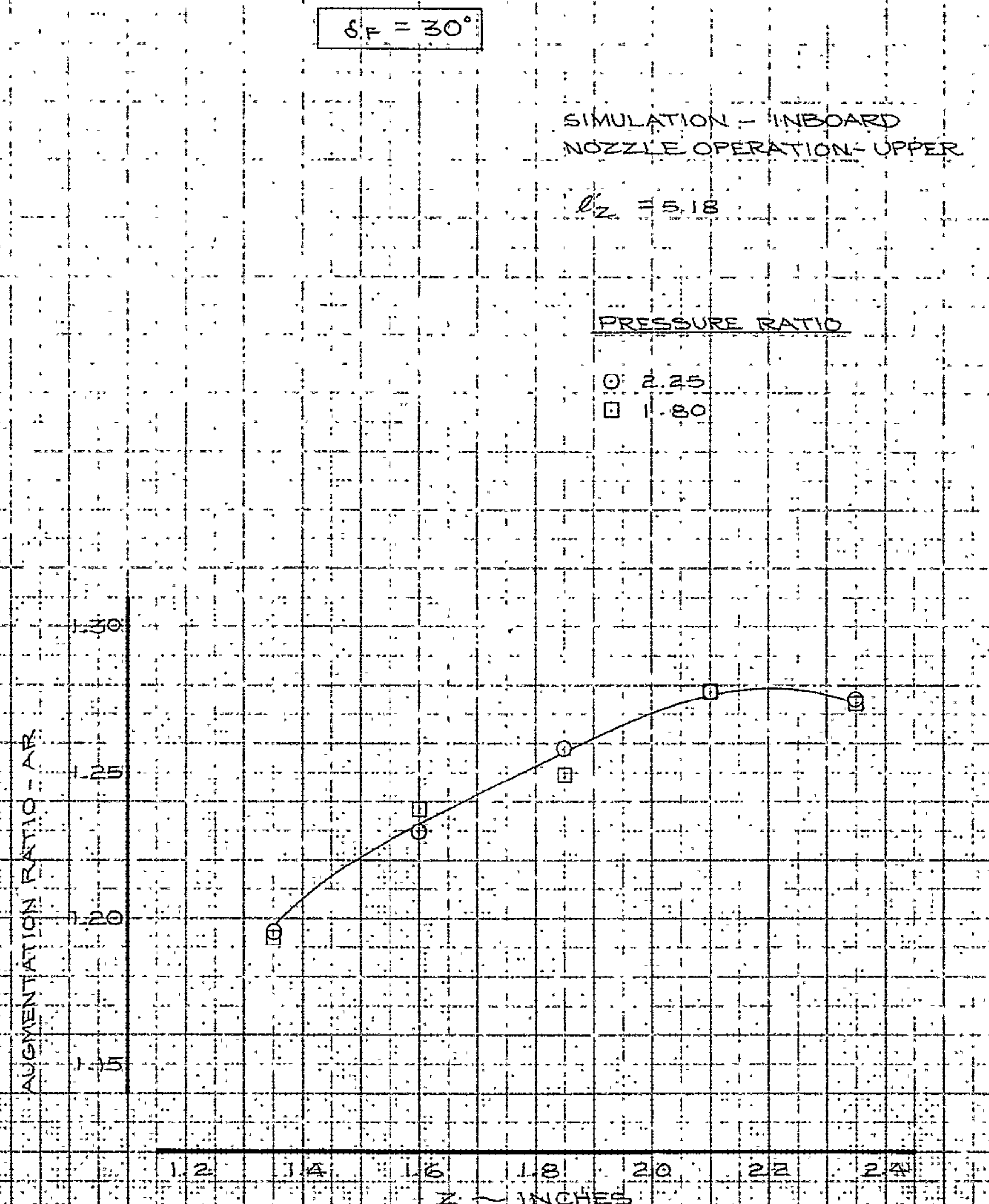

			REVISED	DATE		
CALC					EFFECT OF Z VARIATION	FIG. 107
CHECK					UPPER NOZZLE	
APR	D. Washburn	3/30/71			$\delta_F = 30°$	D6-24850
APR					THE BOEING COMPANY	PAGE 189

$\delta_F = 65°$

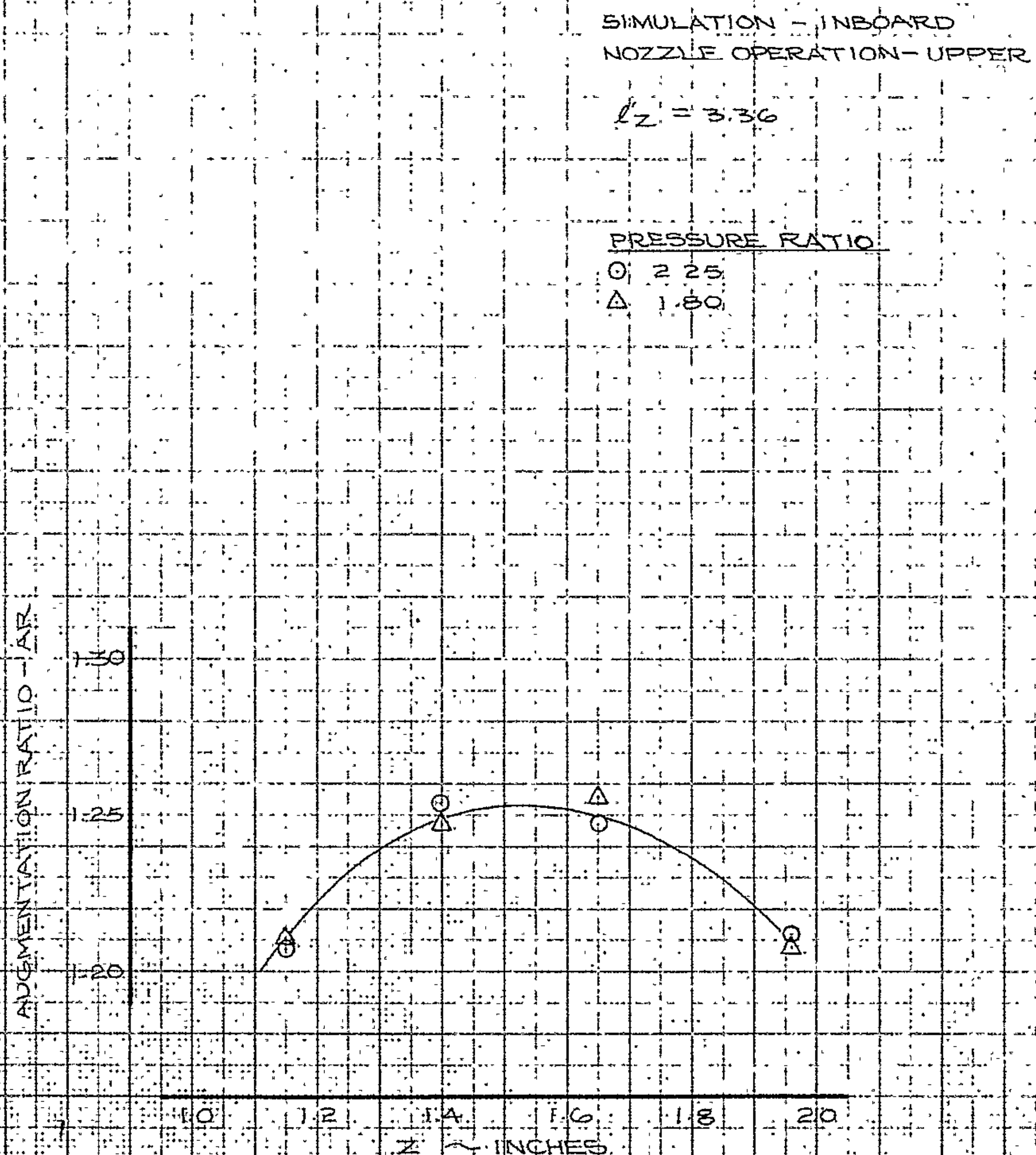

			REVISED	DATE		
CALC					EFFECT OF Z VARIATION	FIG. 108
CHECK					UPPER NOZZE	
APR	D. Harkonen	3/30/71			$\delta_F = 65°$	D6-24850
APR						
	J. Lloyd	3/12/71			THE BOEING COMPANY	PAGE 190

$\delta_F = 30°$

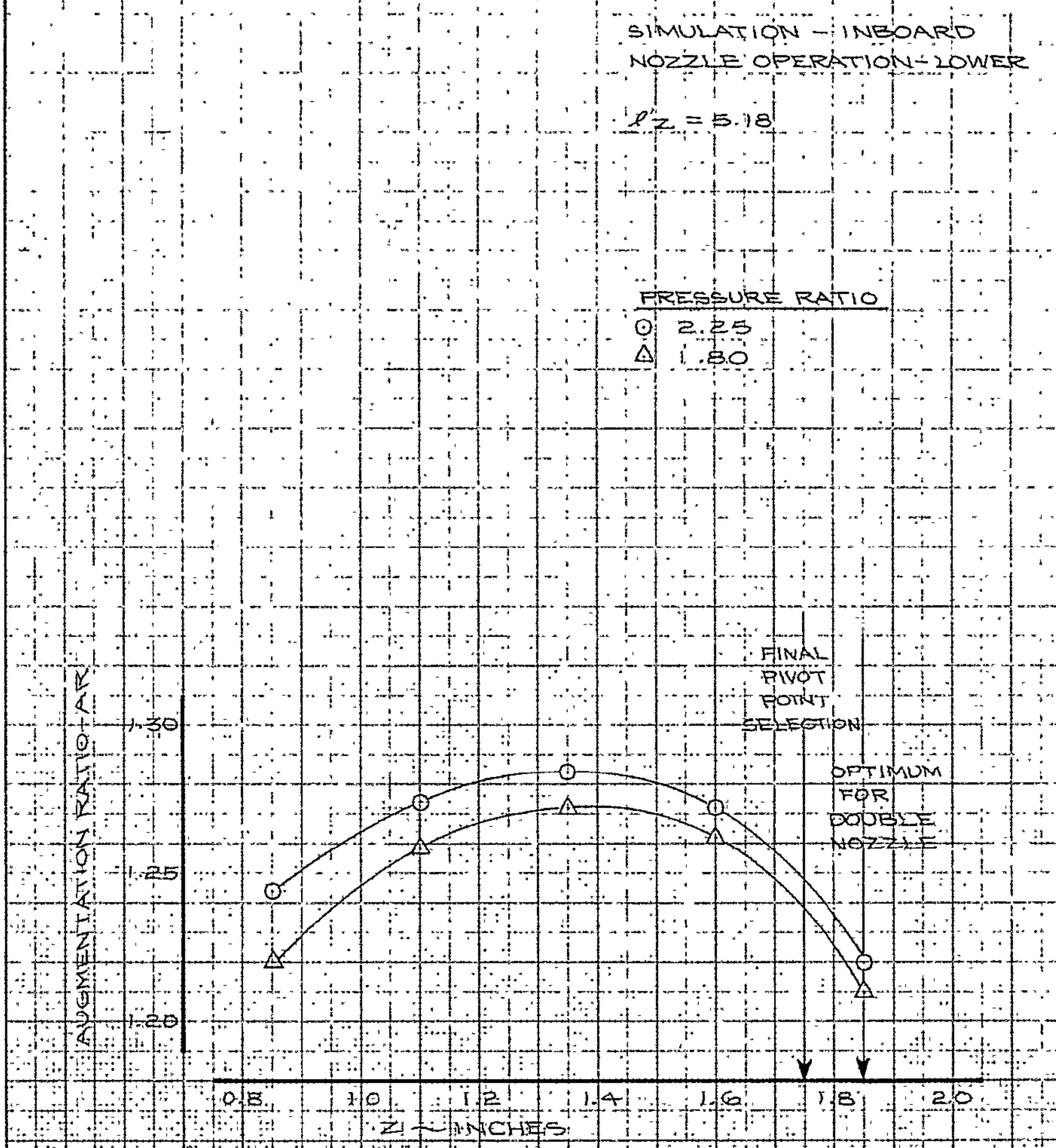

CALC			REVISED	DATE	EFFECT OF Z LOWER NOZZLE ONLY	FIG. 109
CHECK					$\delta_F = 30°$	D6-24850
APR	D. Sonkonen	3/30/71				
APR					THE BOEING COMPANY	PAGE 191
	J. Hoyt	3/12/71				

K+E ALBANENE

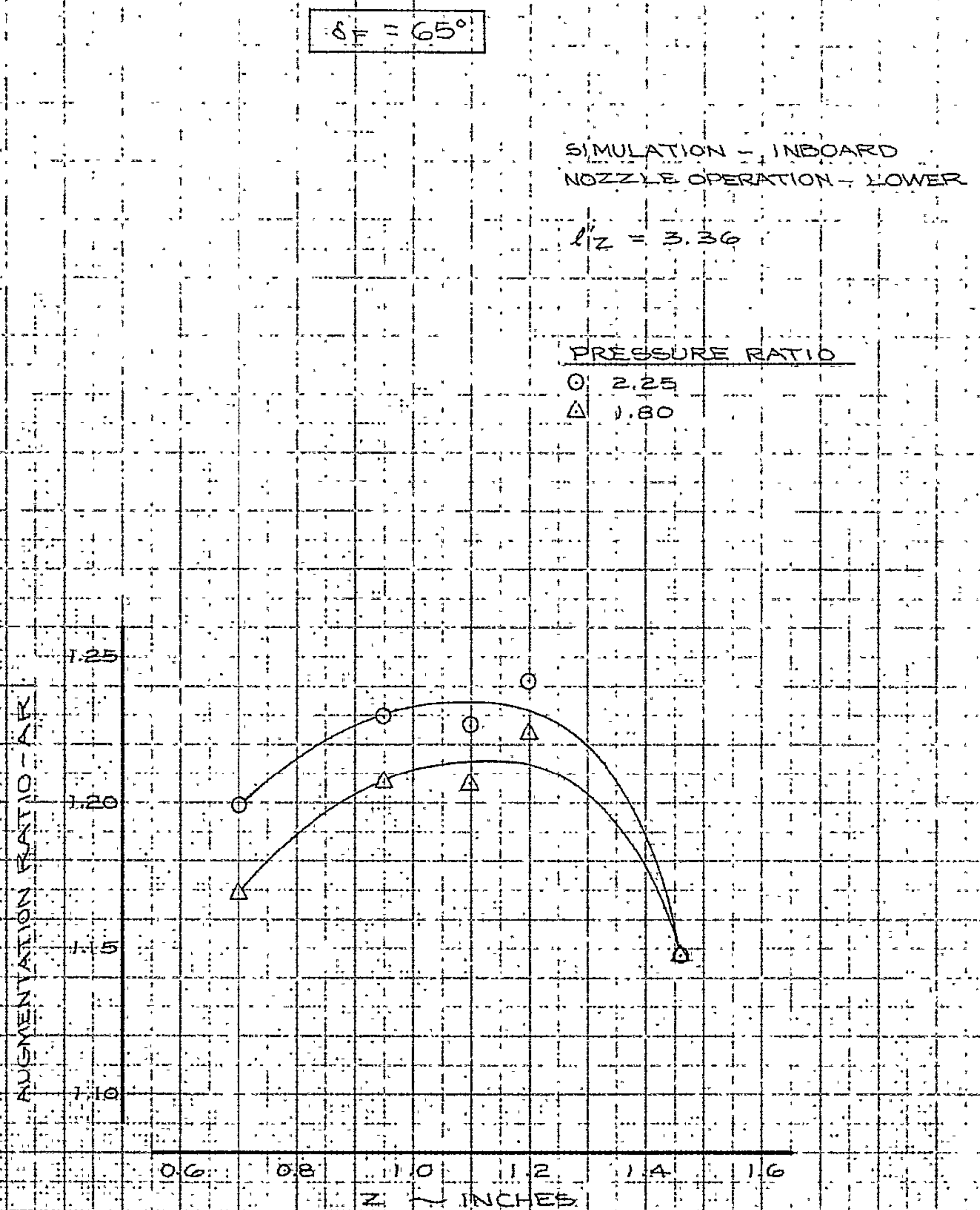

CALC			REVISED	DATE	EFFECT OF Z - LOWER NOZZLE ONLY $\delta_F = 65°$	FIG. 110
CHECK						D6-24850
APR	[signature]	3/30/71			THE BOEING COMPANY	PAGE 192
APR	[signature]	3/12/71				

$\delta_F = 6°$

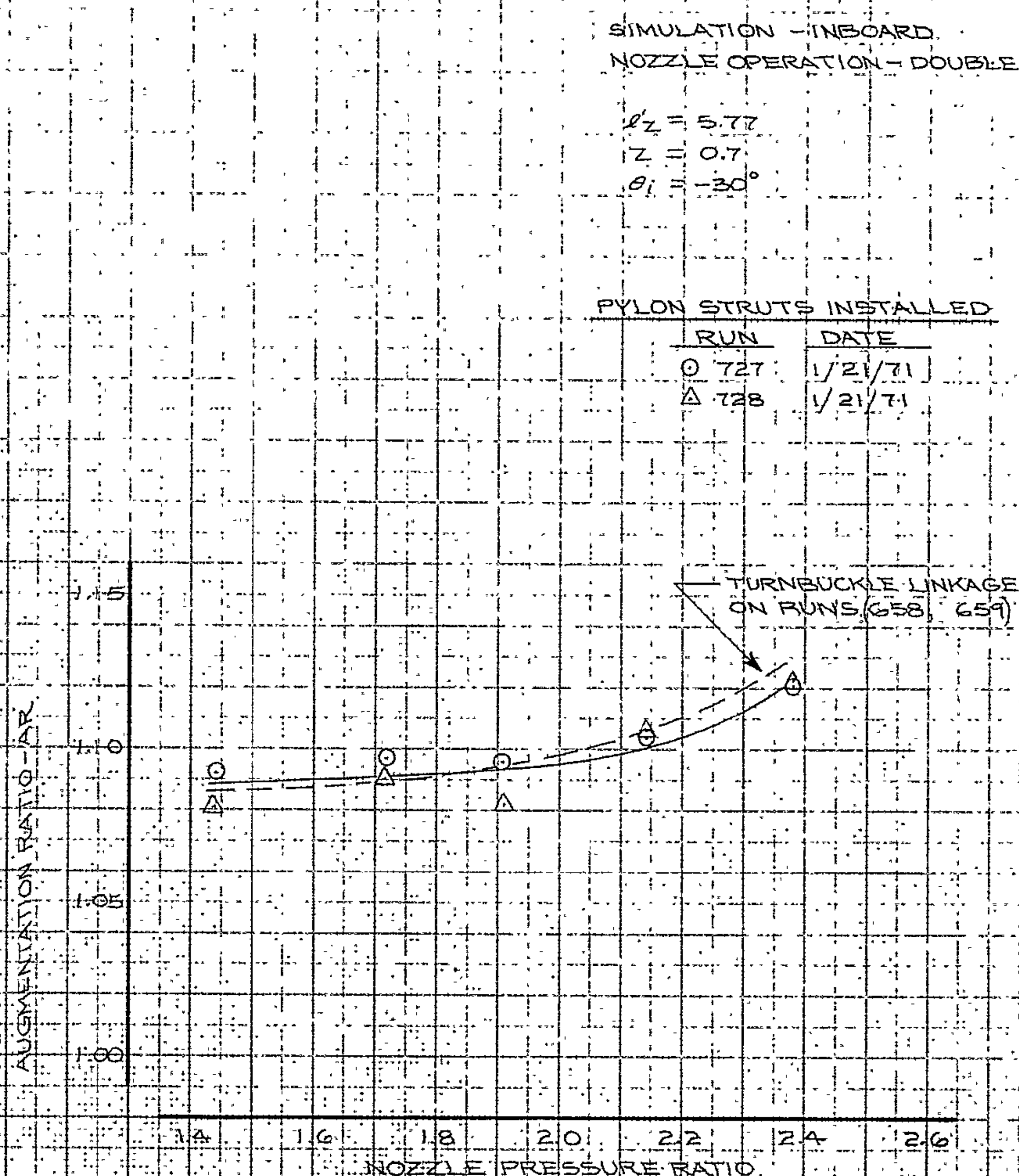

CALC			REVISED	DATE	COMPARISON OF PERFORMANCE BETWEEN PYLON FLAP STRUT AND TURNBUCKLE LINKAGE INSTALLATION - $\delta_F = 6°$
CHECK					
APR	D. Hachmer	3/30/71			
APR	J. Vogt	3/10/71			THE BOEING COMPANY

FIG. 111

D6-24850

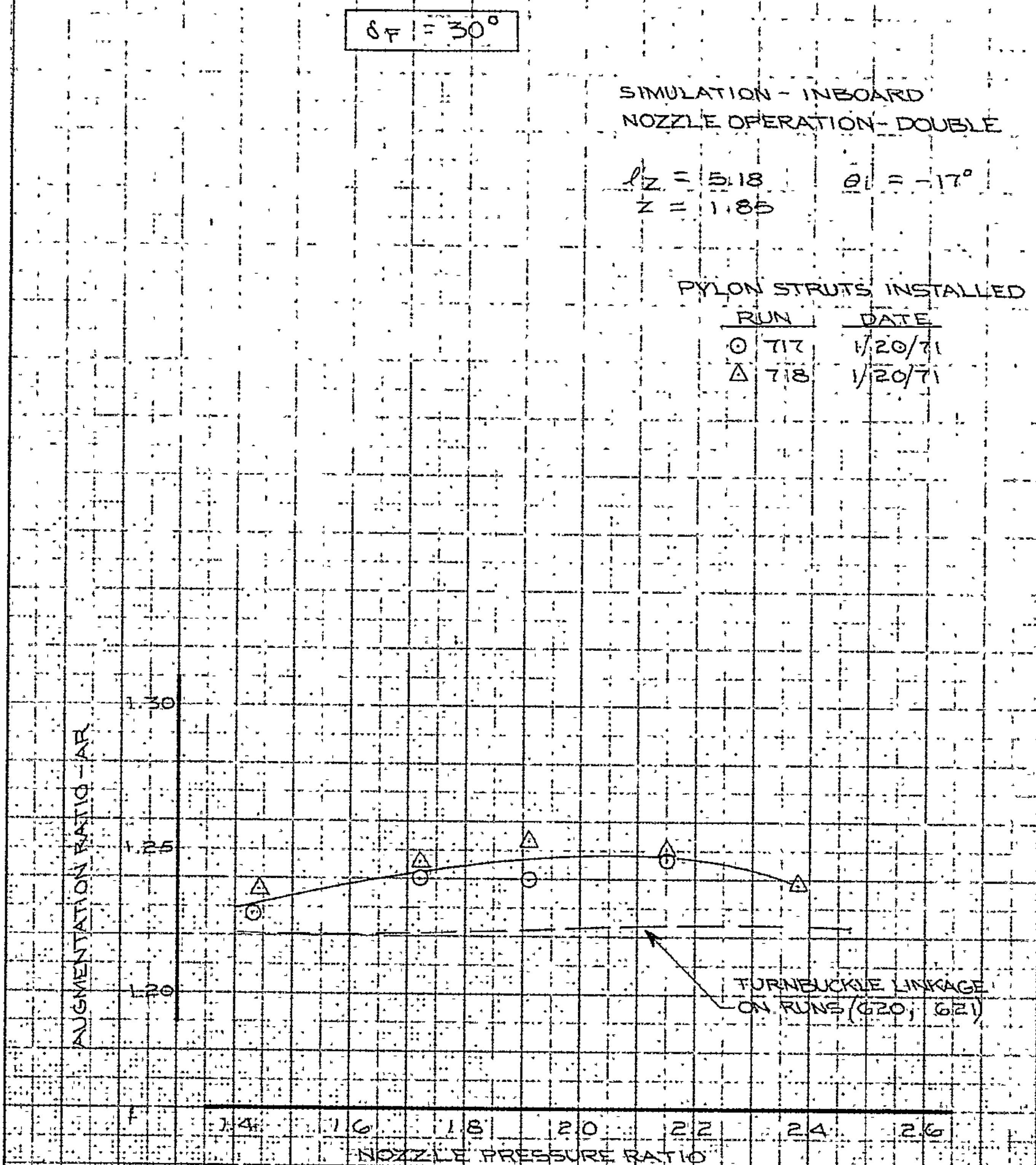

CALC			REVISED	DATE	COMPARISON OF PERFORMANCE BETWEEN PYLON FLAP STRUT AND TURNBUCKLE LINKAGE INSTALLATION - $\delta_F = 30°$	FIG. 112
CHECK						
APR	R. Hashimoto	3/30/71				D6-24850
APR					THE BOEING COMPANY	PAGE 194
	J. Hoyt	3/10/71				

K+E ALBANENE 10FL

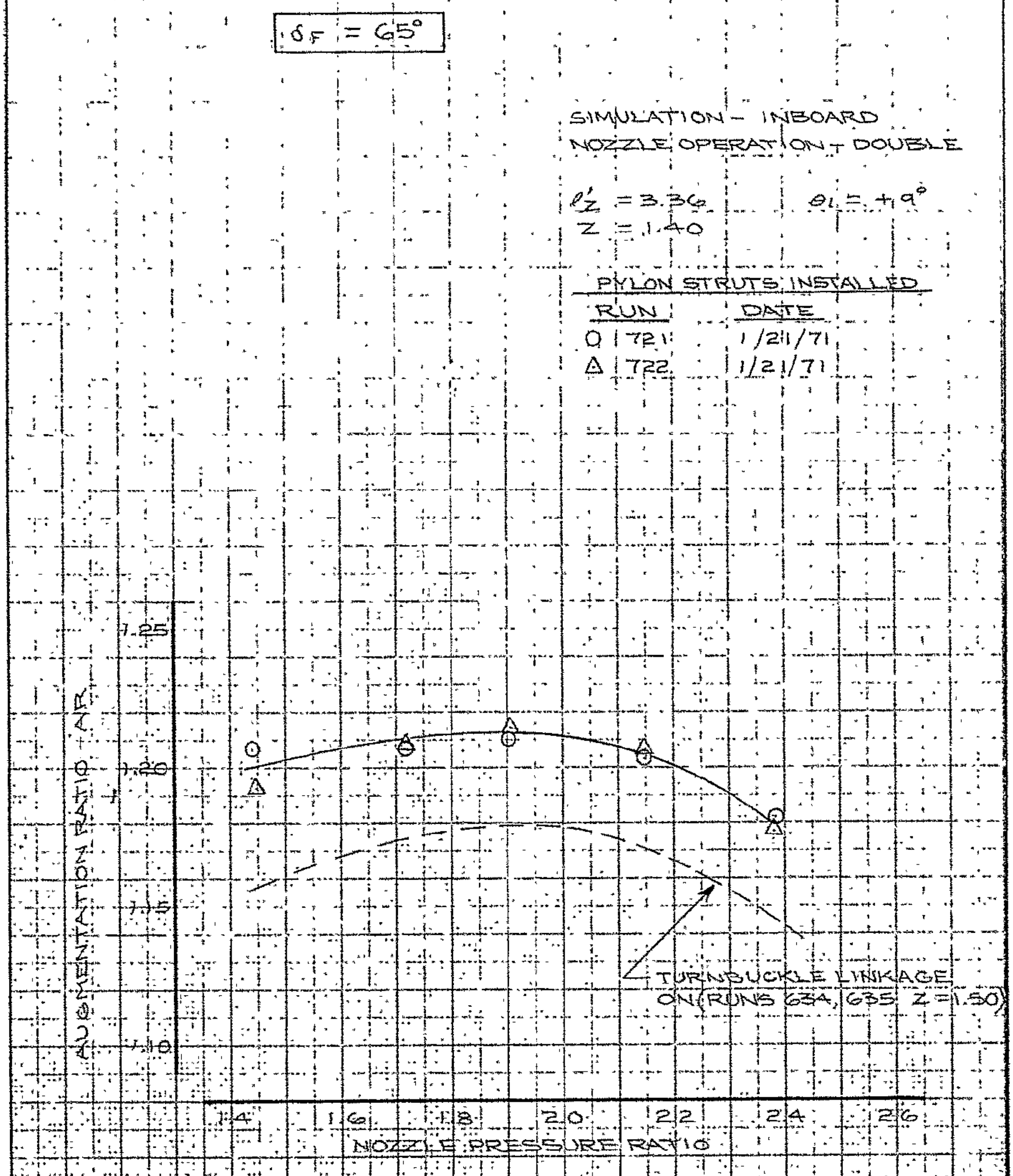

			REVISED	DATE	
CALC					COMPARISON OF PERFORMANCE BETWEEN PYLON FLAP STRUT AND TURNBUCKLE LINKAGE INSTALLATION $\delta_F = 65°$
CHECK					
APR	D. Harkonen	3/30/71			
APR					
	[illegible]	3/11/71			THE BOEING COMPANY

FIG. 113

D6-24850

K·E ALBANENE

$\delta_F = 6°$

FLAPS UP

SIMULATION – INBOARD NOZZLE OPERATION – DOUBLE

$l'_Z = 5.77$
$Z = 0.70$

RUN	CONFIGURATION
■ 725	FLAP BRACKETS, NOZZLE
◗ 726	BLOCKAGE, BENT INTAKE ARM, COANDA "BUMPS"
⊙ 727	PYLON STRUTS ONLY
△ 728	

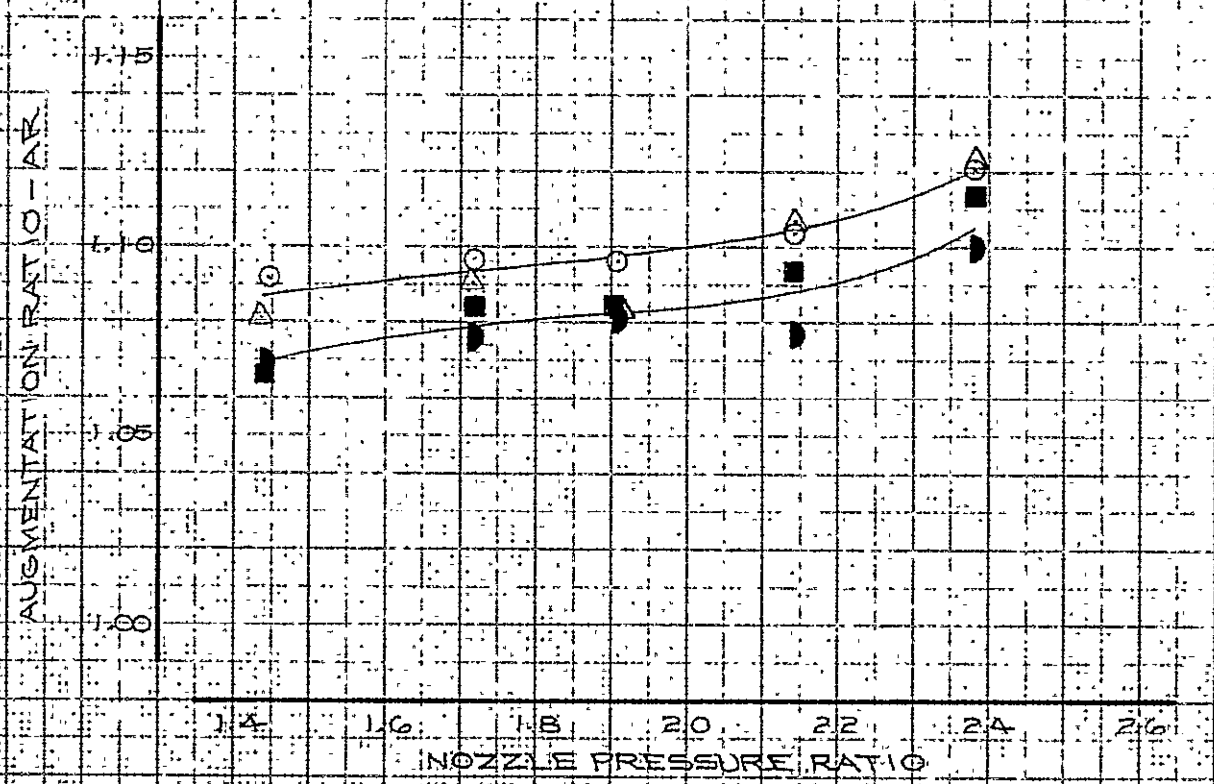

			REVISED	DATE		
CALC					COMPARISON OF PERFORMANCE BETWEEN "CLEAN" FLAP BRACKETRY AND SIMULATED A/P BRACKETS – $\delta_F = 6°$	FIG. 114
CHECK						
APR	D. Vachonun	3/30/71				D6-24850
APR						
	J. Ferayt	3/1/71			THE BOEING COMPANY	PAGE 196

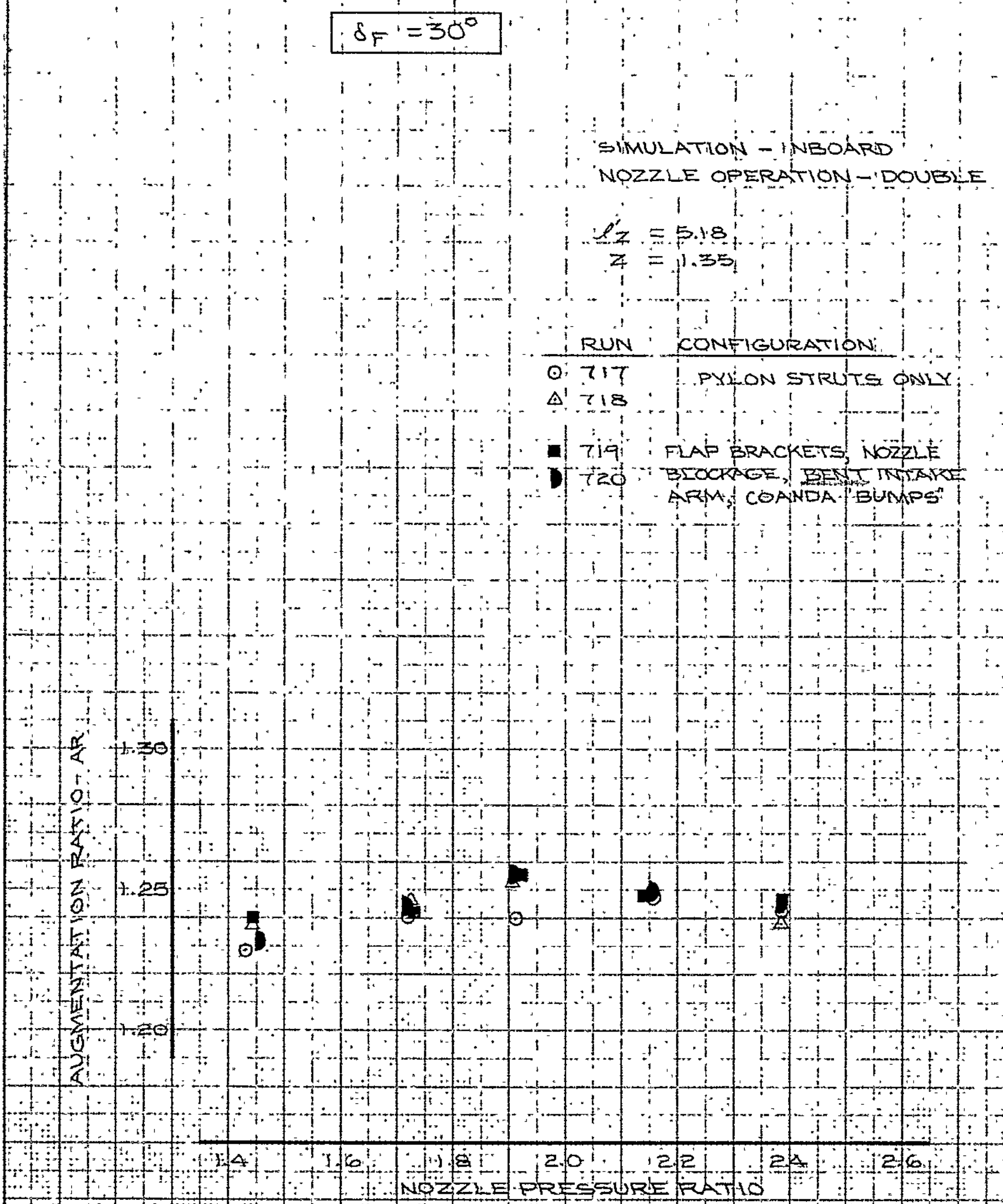

CALC			REVISED	DATE	COMPARISON OF PERFORMANCE BETWEEN "CLEAN" FLAP BRACKETRY AND SIMULATED A/P BRACKETS $\delta_F = 30°$
CHECK					FIG. 115
APR	D. Harkonen	3/30/71			D6-24850
APR					THE BOEING COMPANY
	Jiloyd	3/1/71			PAGE 197

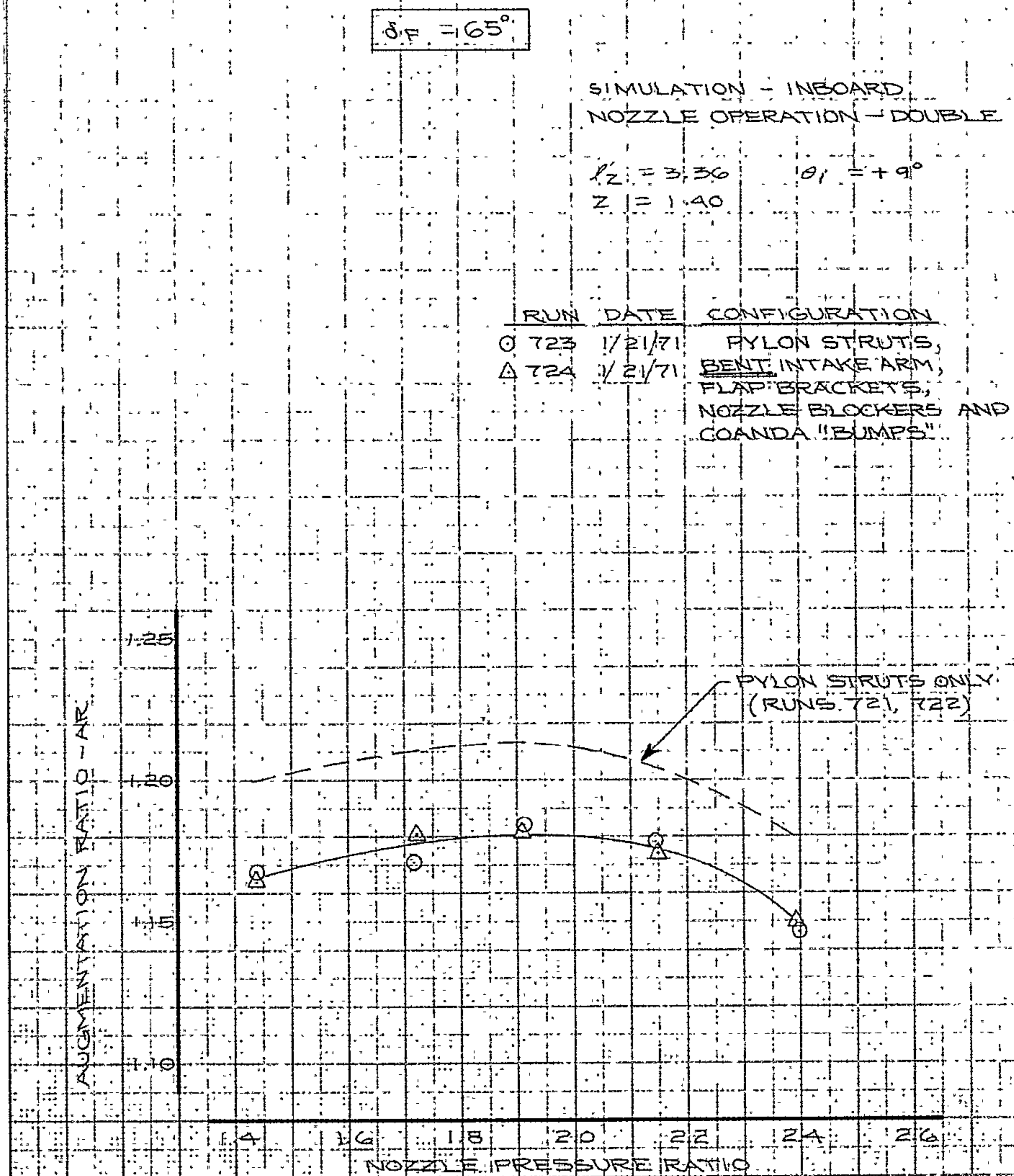

CALC			REVISED	DATE	COMPARISON OF PERFORMANCE BETWEEN "CLEAN" FLAP BRACKETRY AND SIMULATED A/P BRACKETS - $\delta_F = 65°$	FIG. 116
CHECK						D6-24850
APR	D. Hachmann	3/30/71				
APR	j. Hoyt	3/1/71			THE BOEING COMPANY	PAGE 198

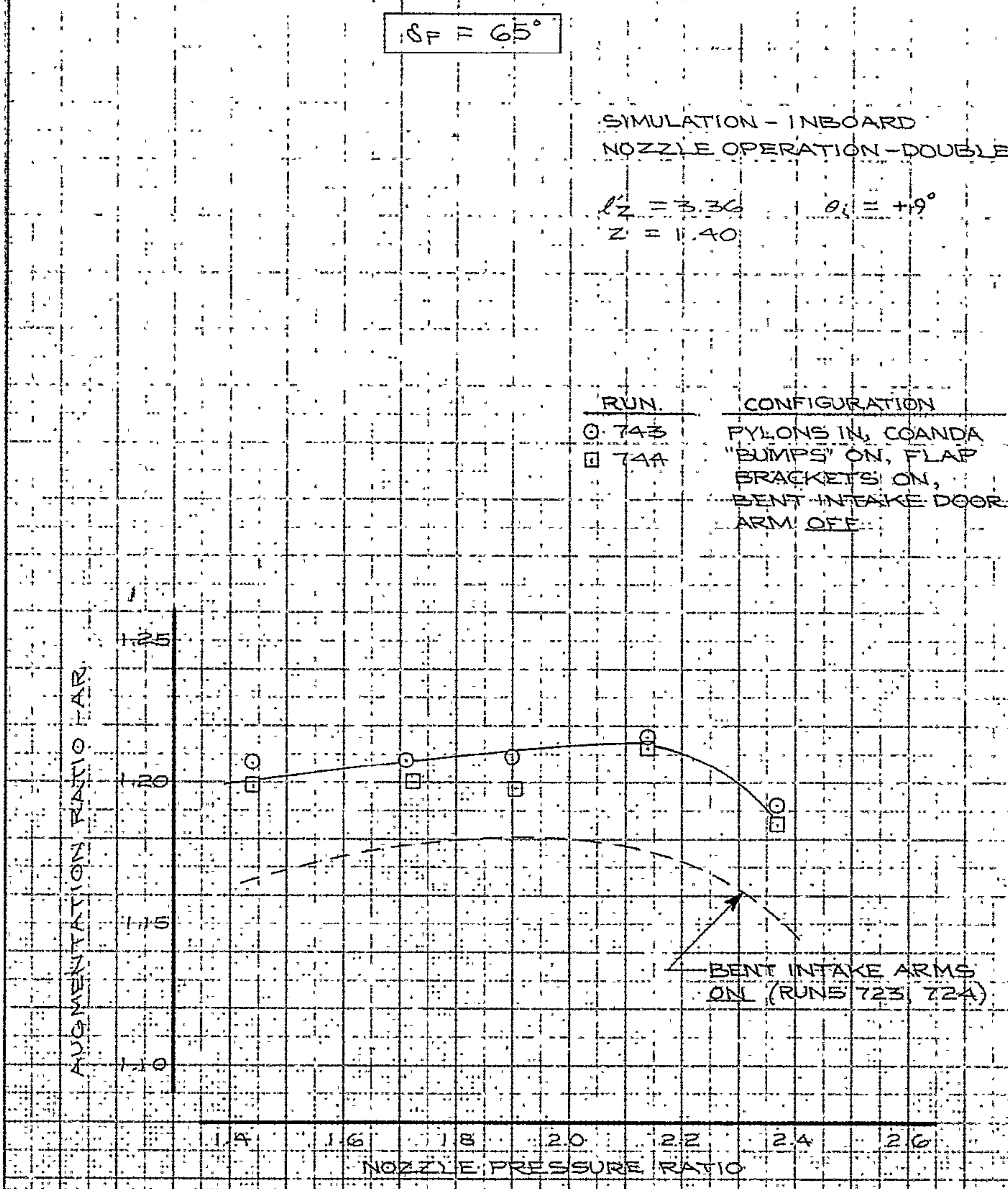

CALC			REVISED	DATE	EFFECTS OF BENT INTAKE DOOR ARM $\delta_F = 65°$	FIG. 117
CHECK						D6-24850
APR	D. Harkonen	3/30/71				
APR					THE BOEING COMPANY	PAGE 199
	J. Hoyt	3/12/71				

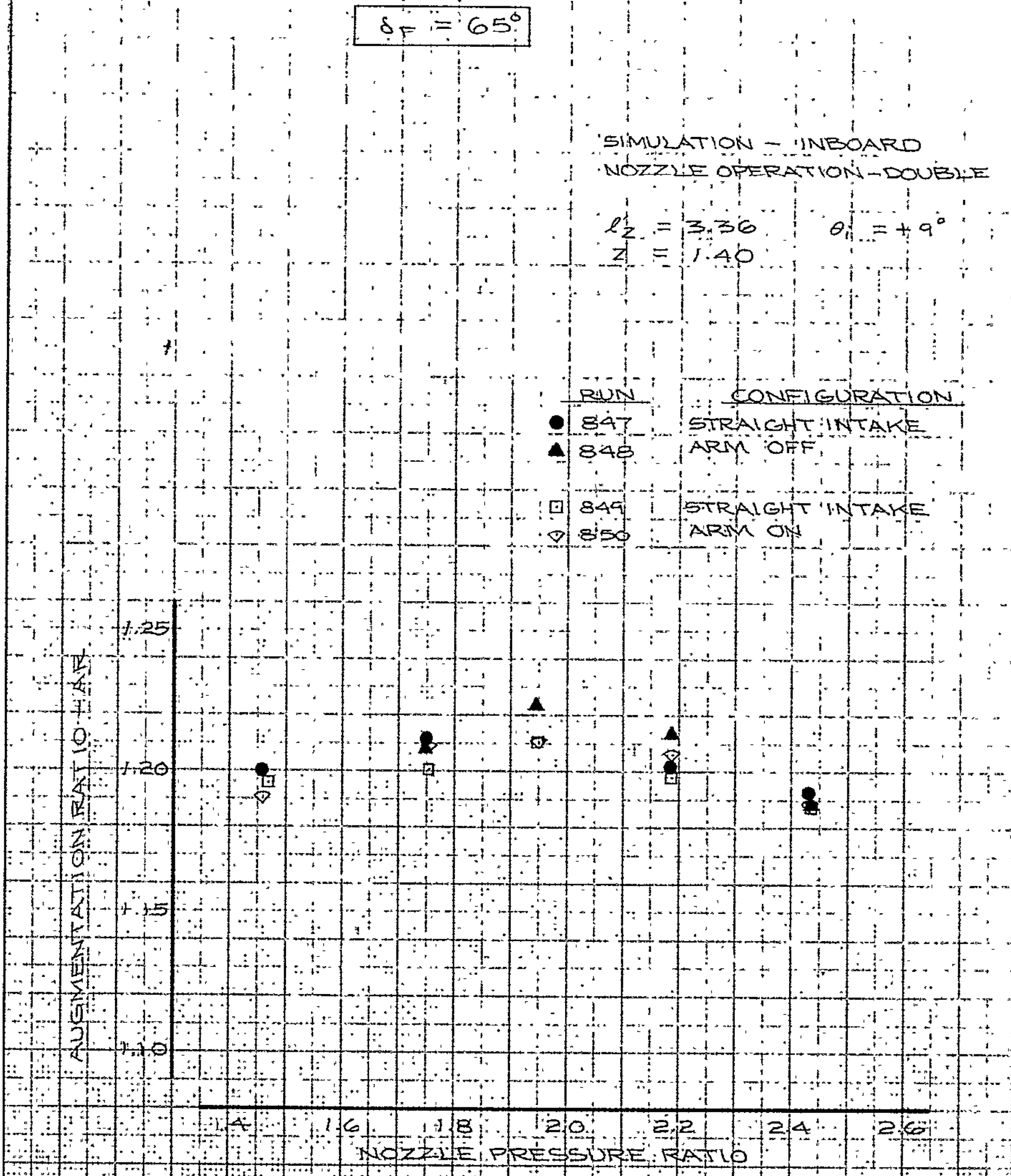

CALC			REVISED	DATE	EFFECTS OF STRAIGHT INTAKE DOOR ARM $\delta_F = 65°$	FIG. 118
CHECK						D6-24850
APR	D. Harkonen	3/30/71			THE BOEING COMPANY	PAGE 200
APR	J. Lloyd	3/12/71				

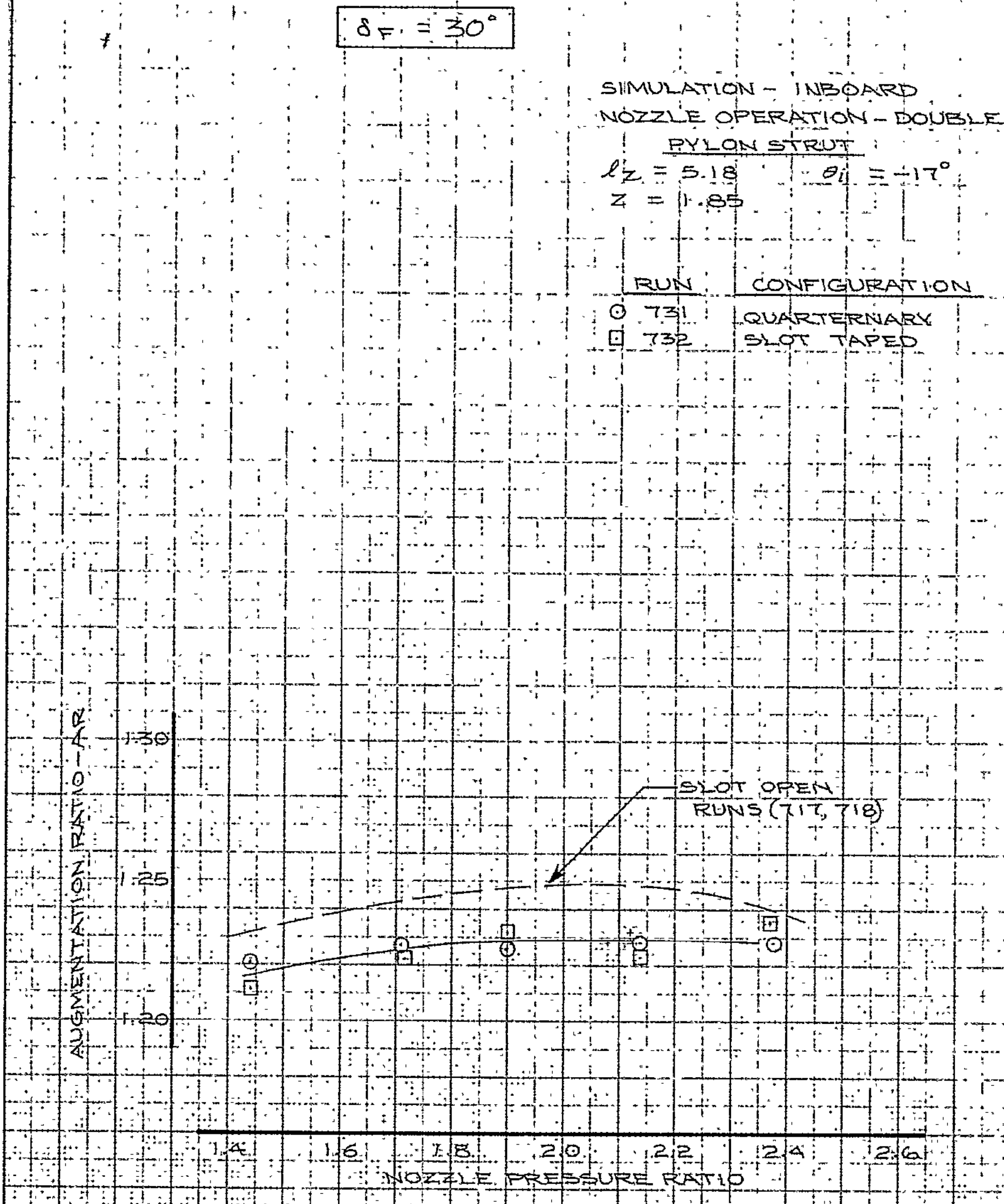

CALC			REVISED	DATE	EFFECT OF BLOCKING OFF QUARTERNARY SLOT $\delta_F = 30°$	FIG. 119
CHECK						D6-24850
APR	D. Hachmen	3/30/71			THE BOEING COMPANY	PAGE 201
APR	J. Hoyt	3/1/71				

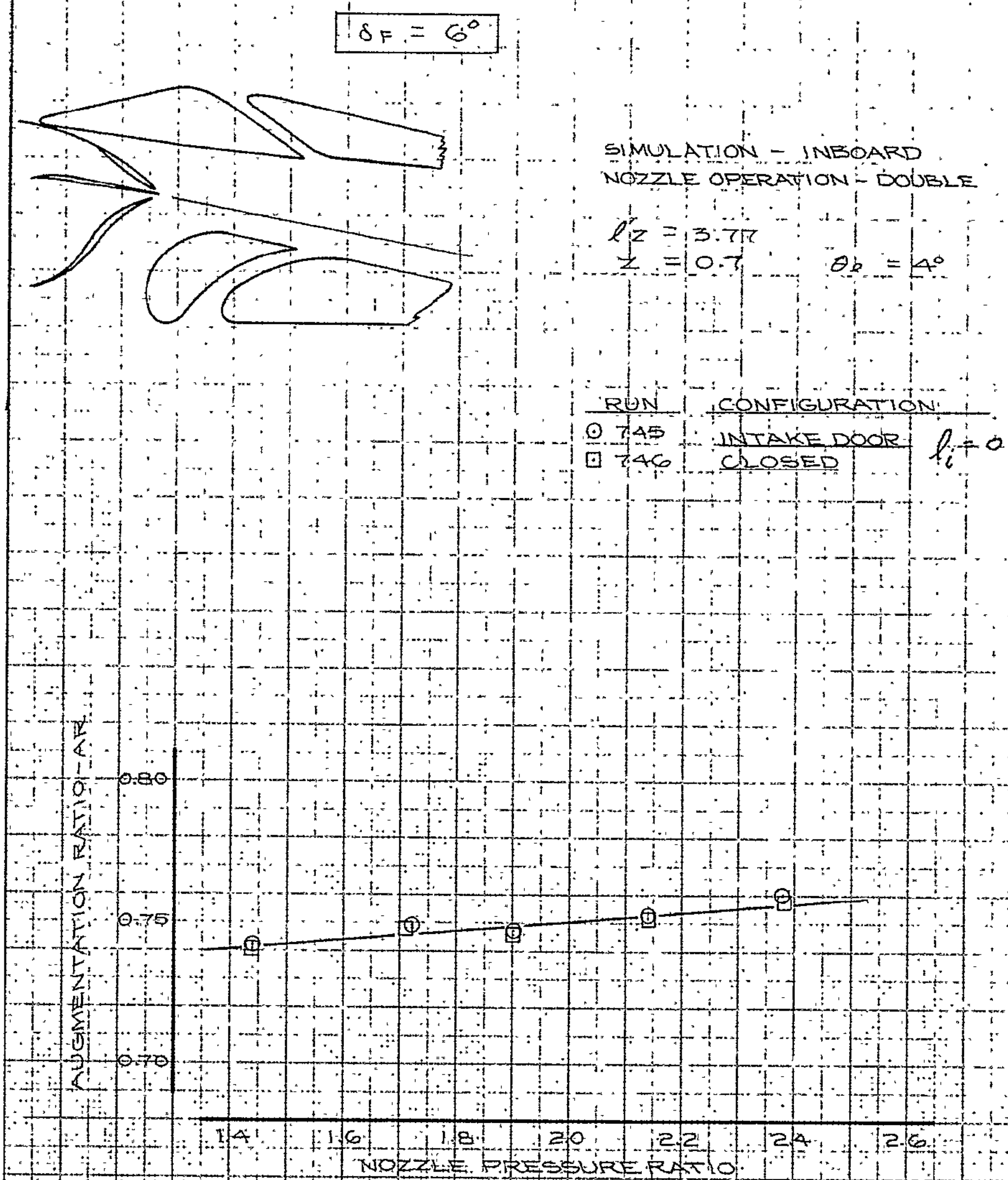

			REVISED	DATE		
CALC					AUGMENTATION RATIO VS NOZZLE PRESSURE RATIO INTAKE DOOR CLOSED δF = 6°	FIG. 120
CHECK						D6-24850
APR	R. Hardman	3/30/71				
APR					THE BOEING COMPANY	PAGE 202
	J. Hoyt	3/12/71				

K+E ALBANENE

$\delta_F = 30°$

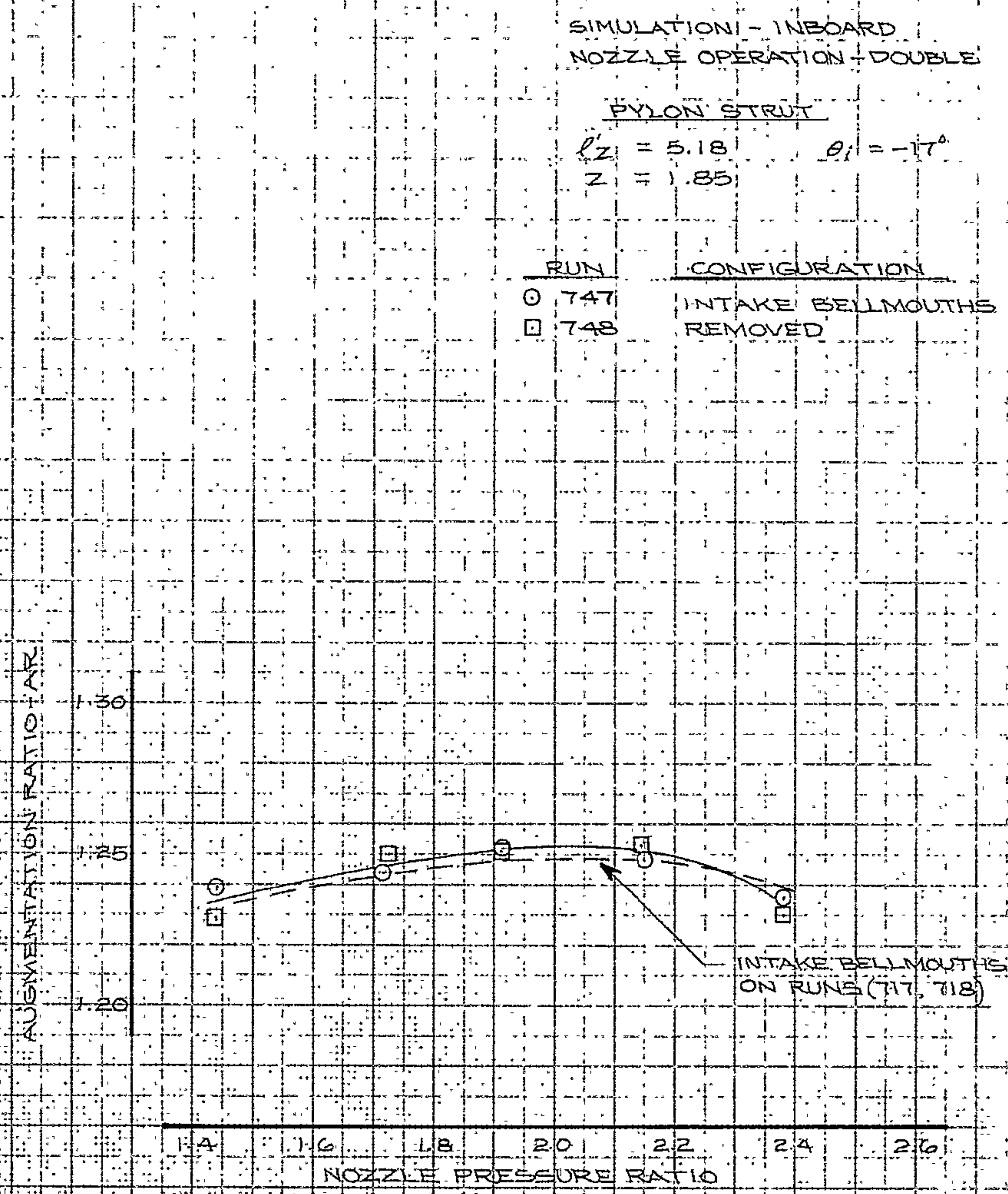

CALC			REVISED	DATE	EFFECT OF INTAKE BELLMOUTHS $\delta_F = 30°$	FIG. 121
CHECK						D6-24850
APR	[signature]	3/30/71				
APR					THE BOEING COMPANY	PAGE 203

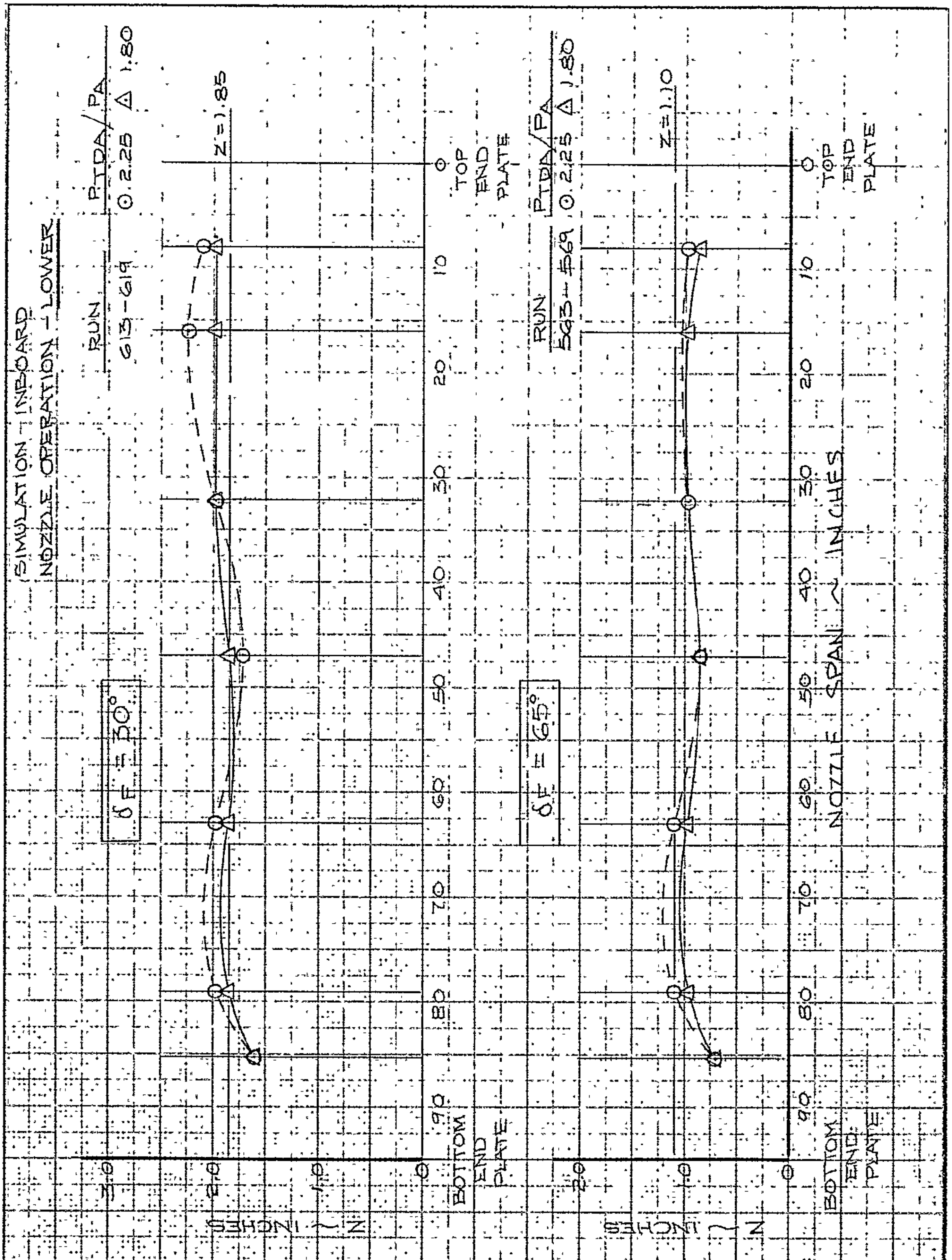

			REVISED	DATE	
CALC					PEAK NOZZLE PRESSURE VS MODEL SPAN - INBOARD SIMULATION LOWER NOZZLE $\delta_F = 30°$ & $65°$
CHECK					
APR	D. Hashmer				
APR					
	jehoyt	3/9/71			THE BOEING COMPANY

FIG. 122

D6-24850

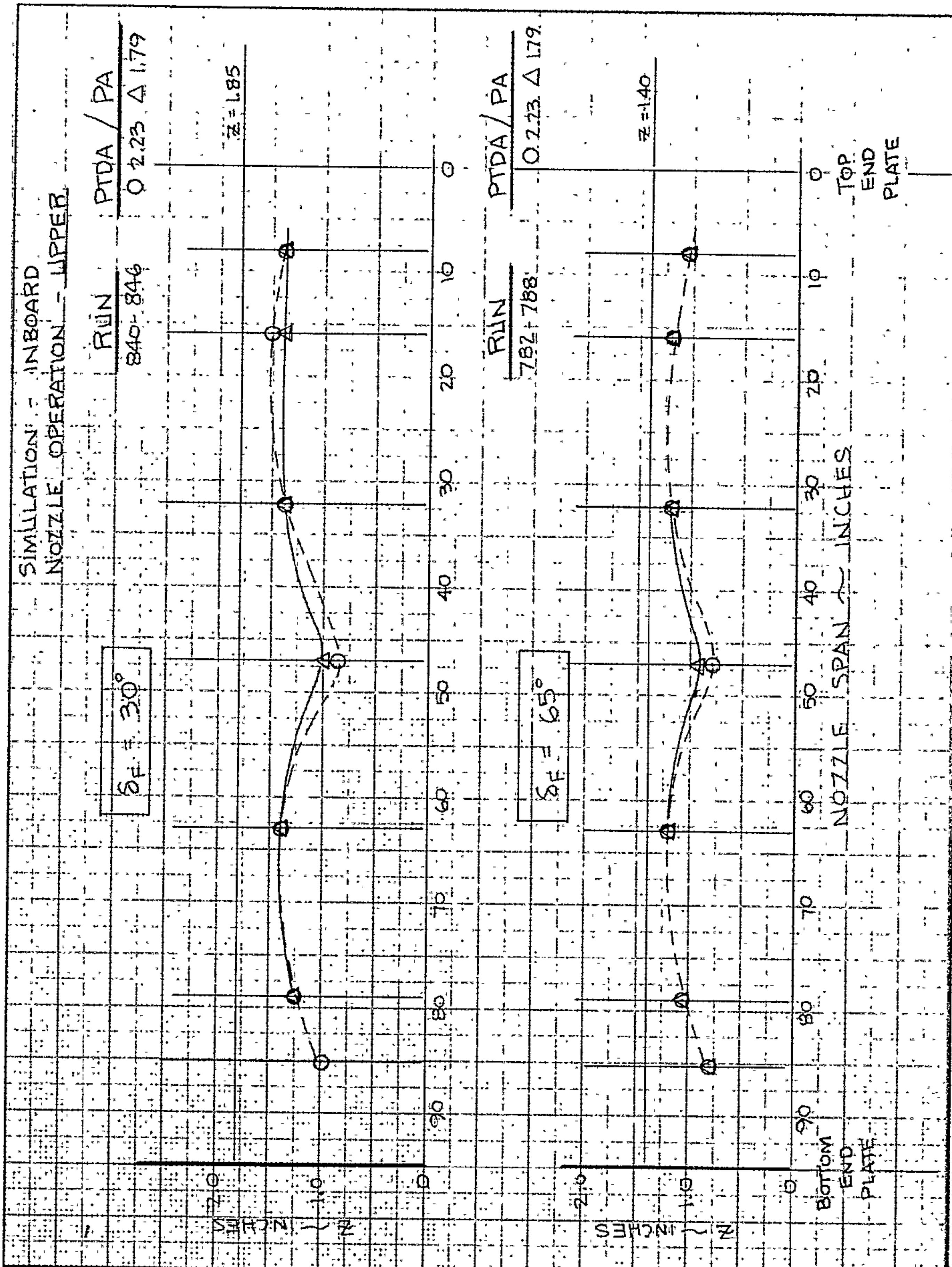

			REVISED	DATE
CALC				
CHECK				
APR	D. Hochonen	3/30/71		
APR				

PEAK NOZZLE PRESSURE
VS MODEL SPAN - INBOARD
SIMULATION
UPPER NOZZLE $\delta_F = 30^\circ$ & 65°

FIG. 123

D6-24850

THE BOEING COMPANY

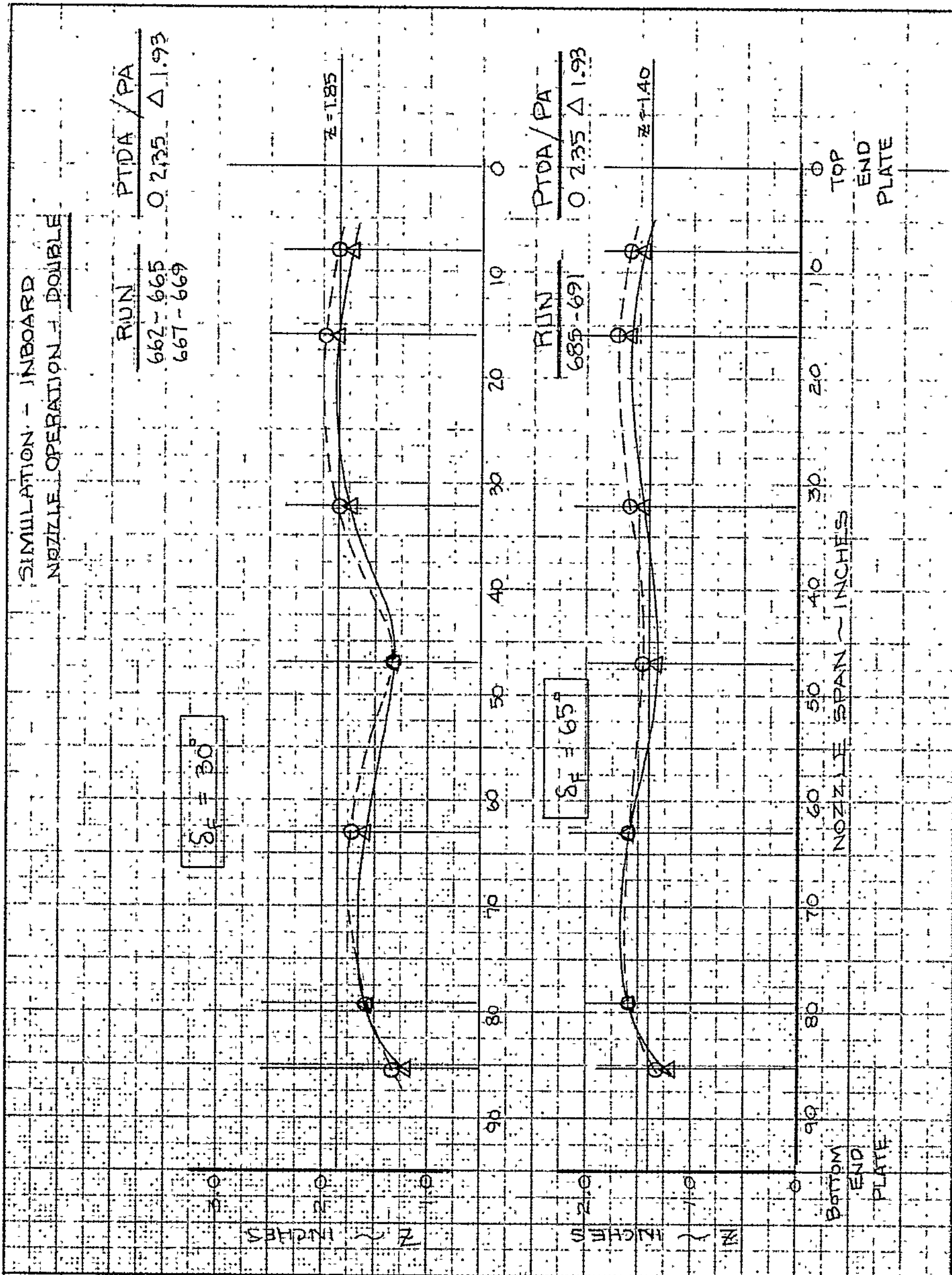

CALC			REVISED	DATE	PEAK NOZZLE PRESSURE VS MODEL SPAN - INBOARD SIMULATION DOUBLE NOZZLE $\delta_F = 30° \,\&\, 65°$	FIG. 124
CHECK						
APR	D. Hardman	3/30/71				D6-24850
APR					THE BOEING COMPANY	PAGE 206

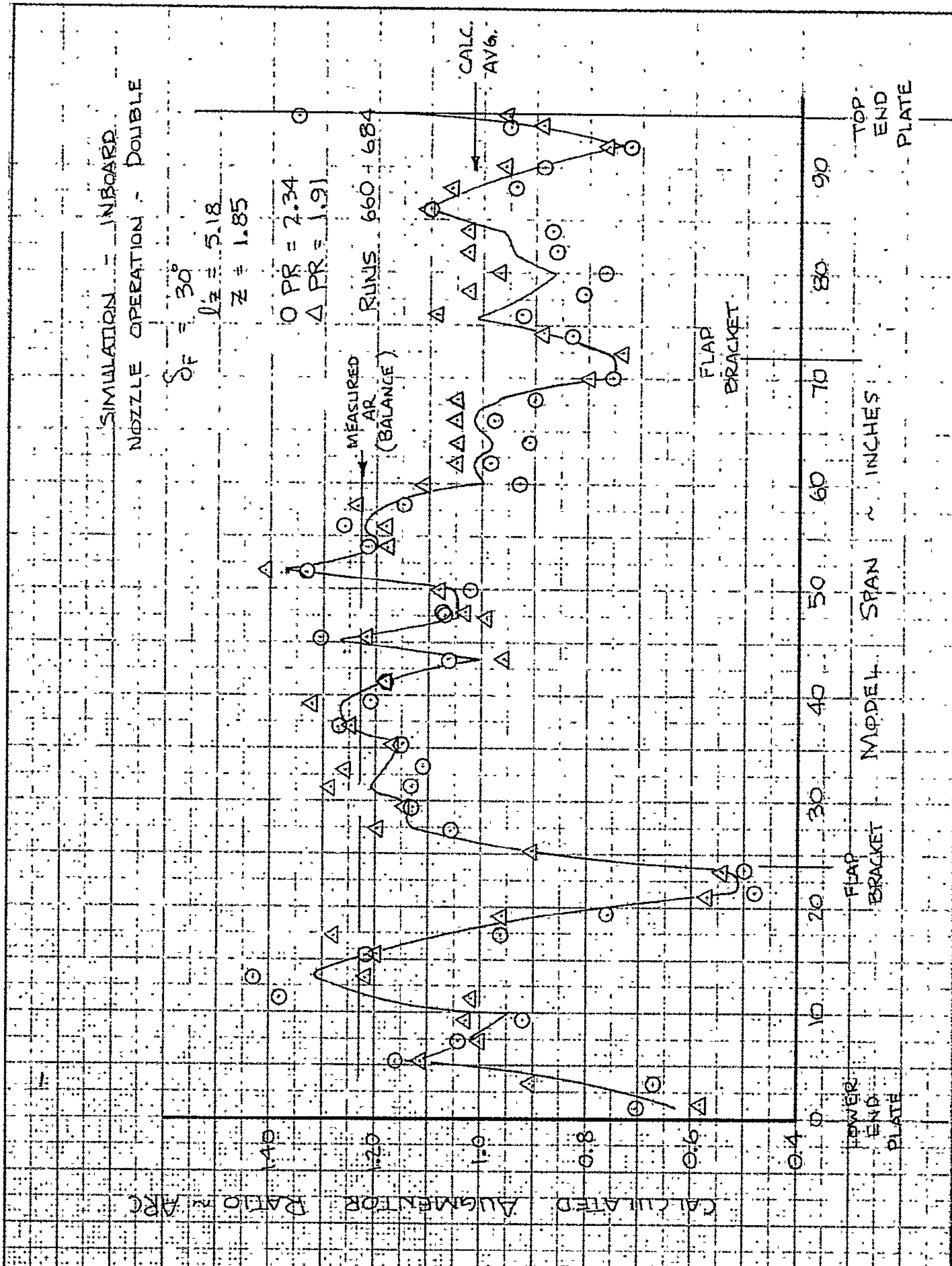

CALC		REVISED	DATE	FLAP EXIT MOMENTUM	FIG. 125
CHECK				SURVEY- INBOARD SIMULATION	D6-24850
APR	D. Kerhonen 3/30/71				
APR				THE BOEING COMPANY	PAGE 207

$\delta_F = 20°$

$\ell'/Z = 5.30$
$Z = 1.03$

SIMULATION – INBOARD NOZZLE OPERATION – DOUBLE

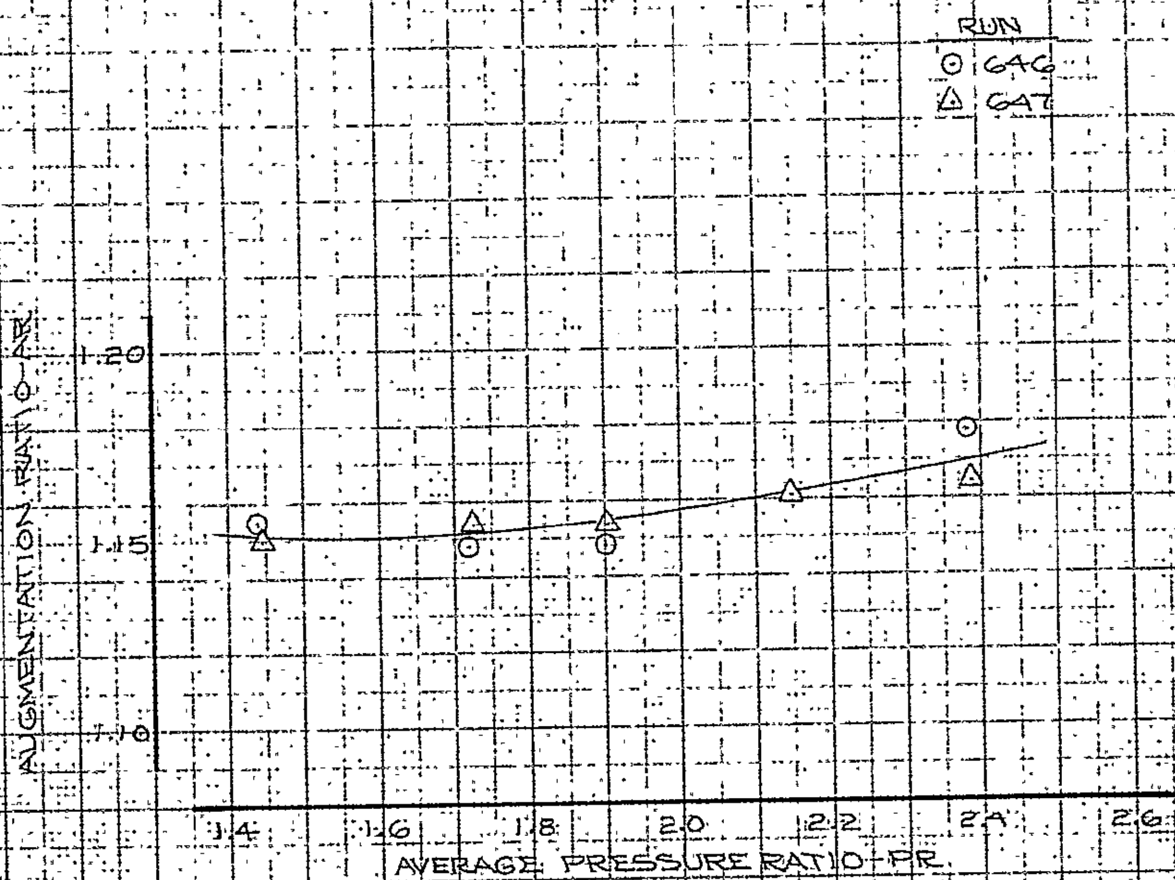

CALC			REVISED	DATE	AUGMENTATION RATIO VS NOZZLE PRESSURE RATIO $\delta_F = 20°$	FIG. 126
CHECK						D6-24850
APR	D. Hashimoto	3/30/71			THE BOEING COMPANY	PAGE 208
APR	J. Lloyd	3/5/71				

K·E ALBANENE

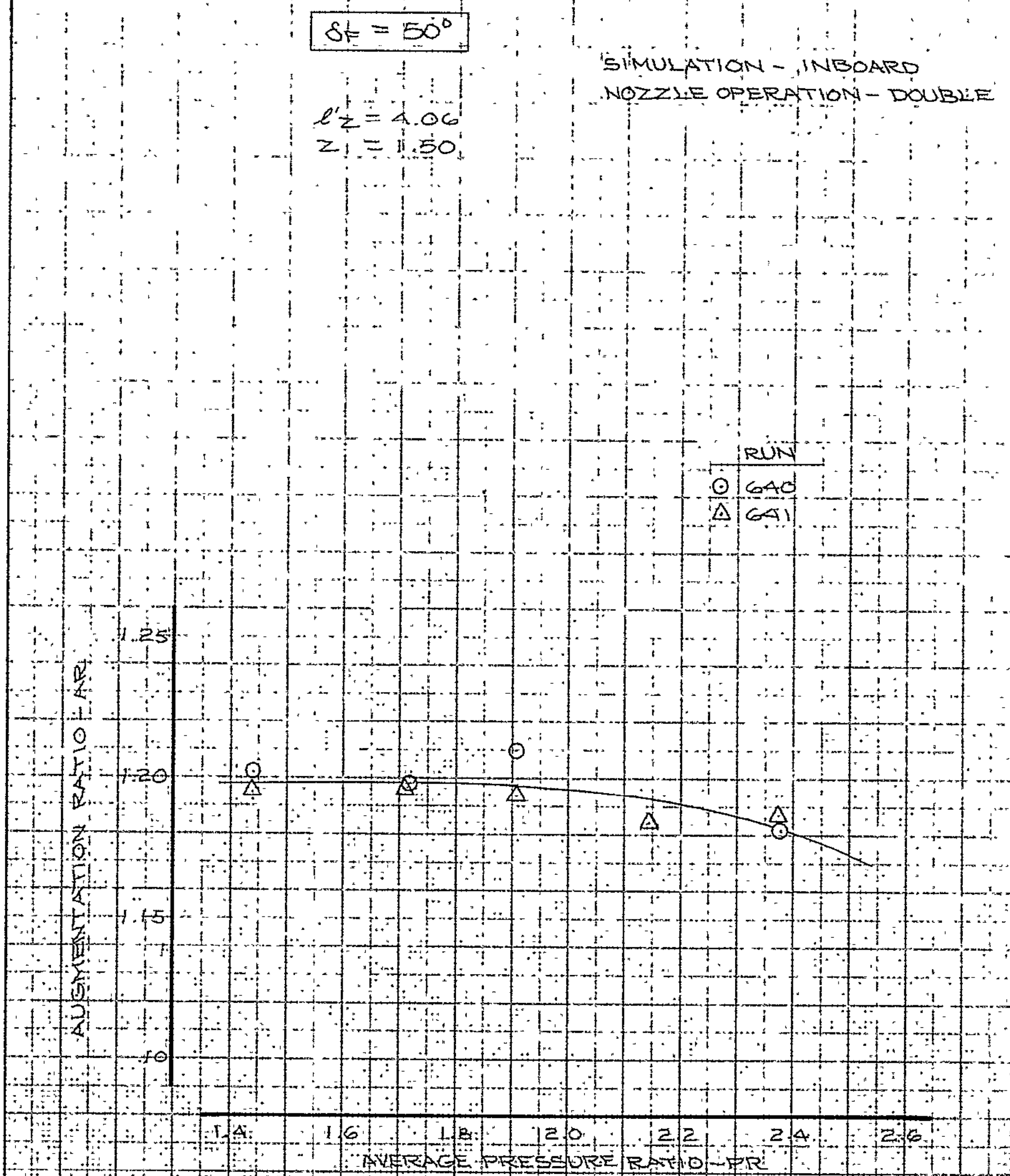

			REVISED	DATE		
CALC					AUGMENTATION RATIO VS NOZZLE PRESSURE RATIO $\delta_F = 50°$	FIG. 127
CHECK						
APR	D. Hashimoto	3/30/71				D6-24850
APR						
	J. Royl				THE BOEING COMPANY	PAGE 209

K+E ALBANENE 10X10 TRACING PAPER

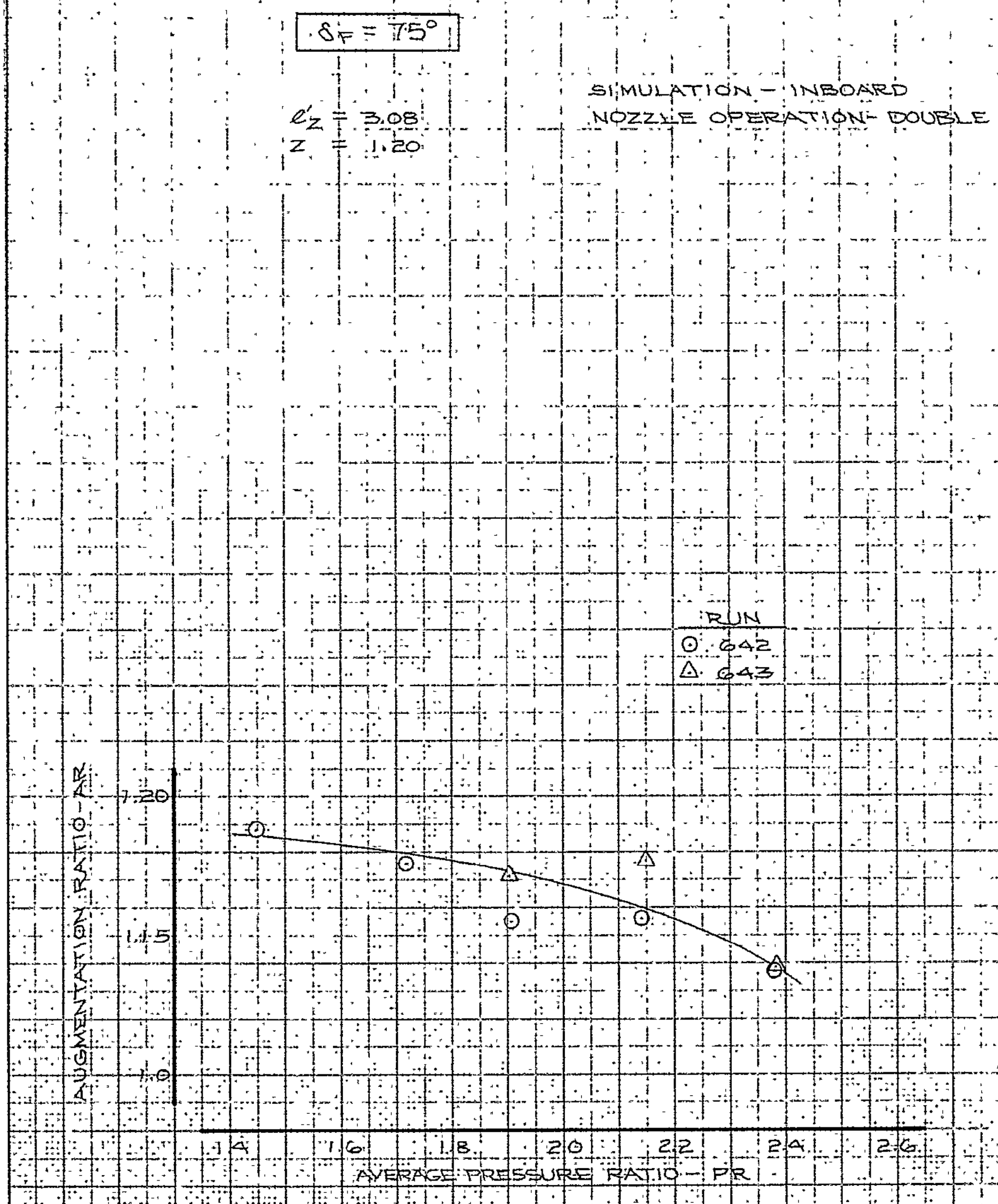

CALC			REVISED	DATE	AUGMENTATION RATIO VS NOZZLE PRESSURE RATIO	FIG. 128
CHECK						
APR	D. Harkonen	3/30/71			$\ell'_Z = 3.08$ $\delta_F = 75°$	D6-24850
APR					THE BOEING COMPANY	PAGE 210
	Lloyd	3/5/71				

216

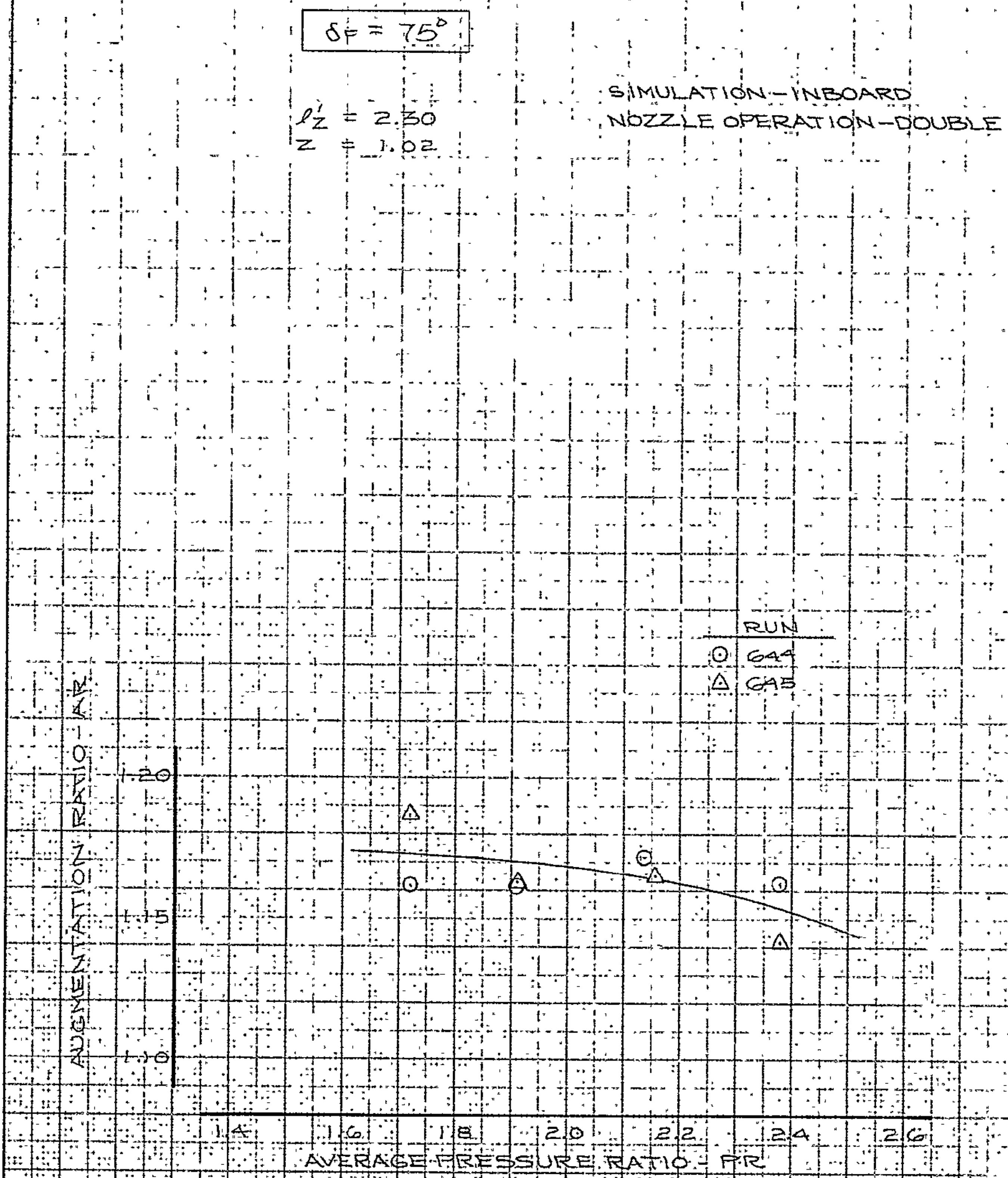

CALC			REVISED	DATE	AUGMENTATION RATIO VS NOZZLE PRESSURE RATIO	FIG. 129
CHECK						
APR	D. Harkonen	3/30/71			$l'_Z = 2.30$, $\delta_F = 75°$	D6-24850
APR					THE BOEING COMPANY	PAGE 211
	J. Rogl	3/5/71				

K+E ALBANENE TRACING PAPER

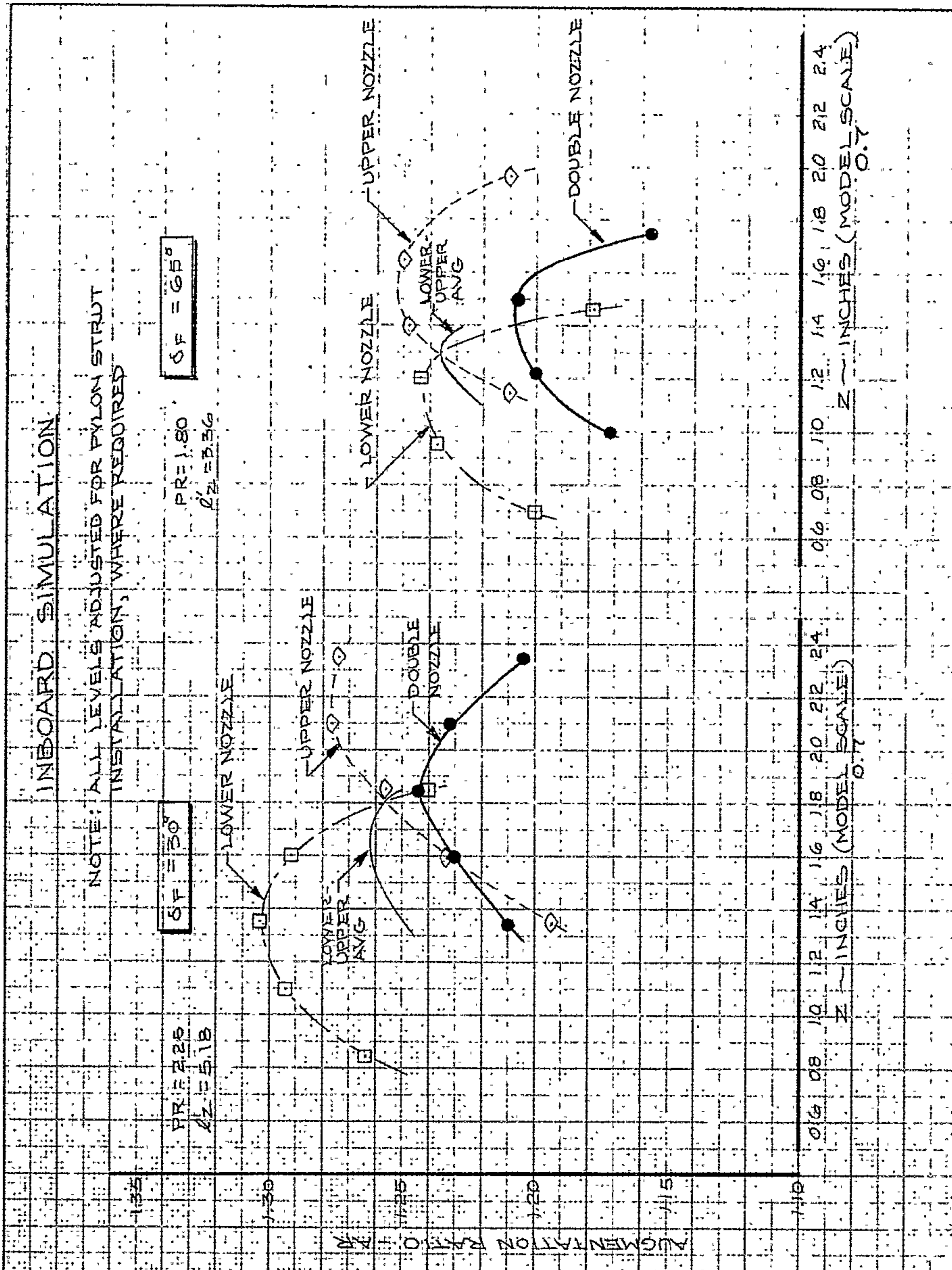

			REVISED	DATE		
CALC					AUGMENTATION RATIO VS Z FOR ALL NOZZLE COMBINATIONS	FIG. 130
CHECK					INBOARD SIMULATION	D6-24850
APR	D. Washmann	3/30/71				
APR					THE BOEING COMPANY	PAGE 212
	jilbyt	3/2/71				

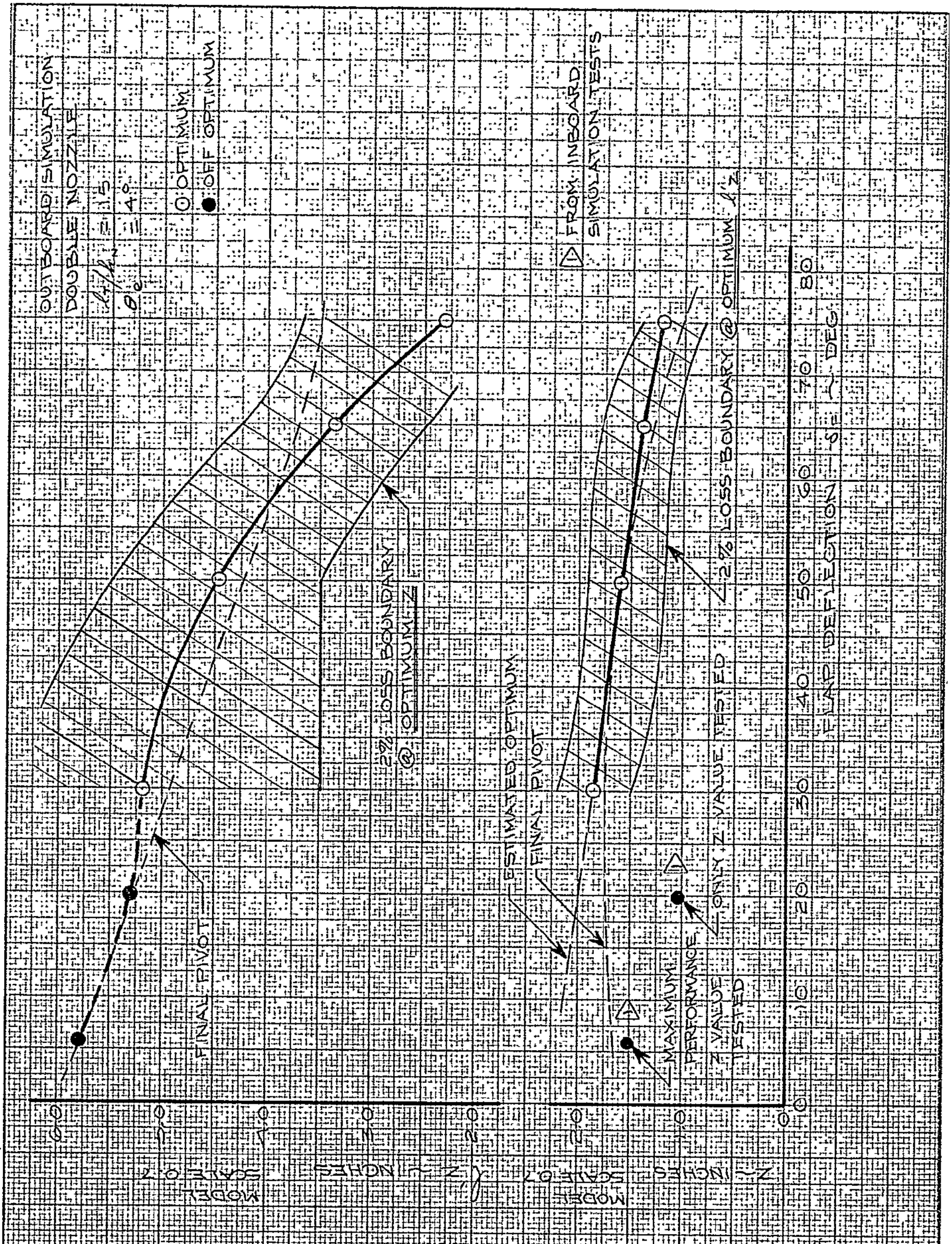

CALC			REVISED	DATE	OPTIMUM Z & l'_Z AND COANDA FLAP PIVOT VS FLAP DEFLECTION ~ δ_F	FIG. 131
CHECK						
APR	D. Hashimoto	3/30/71				D6-24850
APR						
	[illegible]	3/10/71			THE BOEING COMPANY	PAGE 213

AD 401 C R6

K+E ALBANENE 195L TRACING PAPER

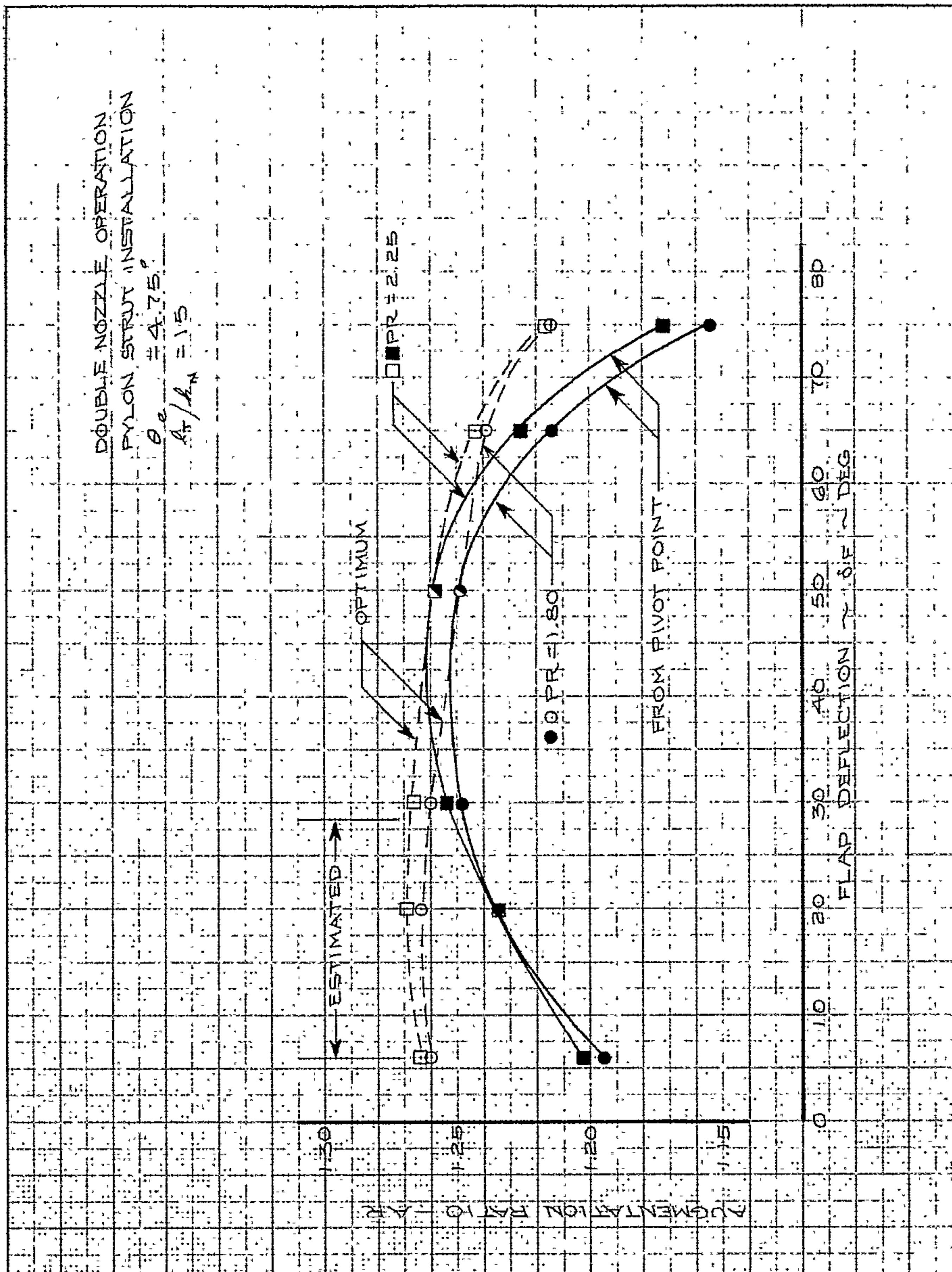

CALC				REVISED	DATE
CHECK					
APR					
APR					
	jchyt	3/15/71			

ESTIMATED AIRPLANE AUGMENTOR STATIC PERFORMANCE VS FLAP DEFLECTION - δ_F

FIG. 132

D6-24850

THE BOEING COMPANY

14

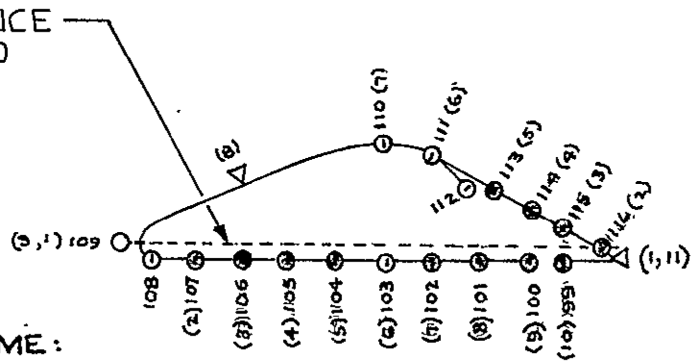

CODE NAME:
INTAKE-C

REF. CHORD:
15.36" (M.S.)
22.00" (F.S.)

D NO.	TAP NO. (PSF NO.)	X/C	Zp/C	SURFACE	PRESSURE DATA QUALITY	COMMENTS
1		1.0	-.0228	T.E.	INSERTED	EXTRAPOLATE & AVG
2	116	.98	-.0098	UPPER SURFACE	OK	
3	115	.90	.0325		OK	
4	114	.821	.08		OK	
5	113	.743	.126		OK	
	112	.685	.145		BAD	OMIT
6	111	.611	.197		BAD	INTERPOLATE
7	110	.525	.216		BAD	ASSUME ΔP=0
8		.153	.079		INSERTED	ASSUME ΔP=0
9	109	0.	0.	L.E.	BAD	EXTRAPOLATE & AVG
1	109	0.	0.	L.E.	BAD	EXTRAPOLATE & AVG
	108	.0163	-.0228	LOWER SURFACE	BAD	OMIT
2	107	.0846	-.0228		OK	
3	106	.153	-.0228		OK	
4	105	.244	-.0228		OK	
5	104	.358	-.0228		OK	
6	103	.471	-.0228		BAD	INTERPOLATE
7	102	.595	-.0228		OK	
8	101	.708	-.0228		OK	
9	100	.822	-.0228		OK	
10	99	.936	-.0228		OK	
11		1.0	-.0228	T.E.	INSERTED	EXTRAPOLATE & AVG

ENGR.	D. H. P.	3-23-71	REVISED	DATE	INTAKE CENTER CHORD	MODIFIED C-8A
CHECK						FIG. 133
APR					THE BOEING COMPANY RENTON, WASHINGTON	D6-24850
APR						

215
~~230~~

AD 1017-R6

6-7000

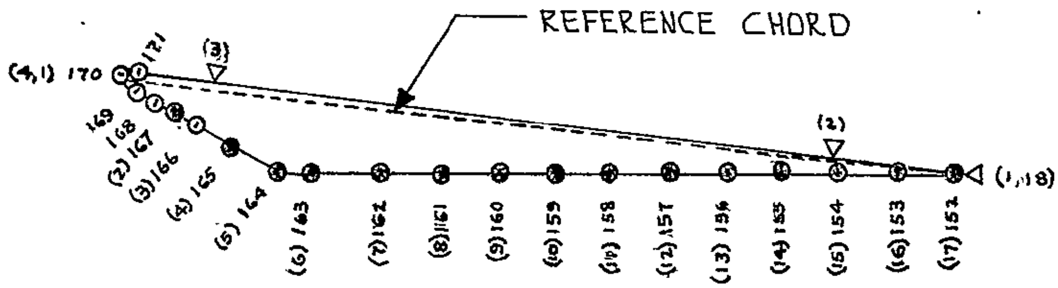

CODE NAME:
SHROUD-C

REF CHORD
26.38" (M.S.)
37.3" (F.S.)

D NO.	TAP NO. (PSF NO.)	X/c	Zp/c	SURFACE	PRESSURE DATA QUALITY	COMMENTS
1		1.0	0.	T.E.	INSERTED	EXTRAPOLATE & AVG
2		.855	.0019	UPPER SURFACE	INSERTED	ASSUME ΔP=0
3		.0975	.0102		INSERTED	ASSUME ΔP=0
	171	.0072	.0066		BAD	OMIT
4	170	0.	0.	L.E.	BAD	EXTRAPOLATE & AVG
1	170	0.	0.	L.E.	BAD	EXTRAPOLATE & AVG
	169	.0076	-.0114		BAD	OMIT
	168	.0372	-.0205		BAD	OMIT
2	167	.0607	-.0307		OK	
3	166	.0975	-.047		BAD	INTERPOLATE
4	165	.146	-.0686	LOWER SURFACE	OK	
5	164	.195	-.0884		OK	
6	163	.214	-.0906		OK	
7	162	.301	-.0812		OK	
8	161	.354	-.0755		OK	
9	160	.416	-.0686		OK	
10	159	.458	-.0626		OK	
11	158	.538	-.0535		OK	
12	157	.618	-.044		OK	
13	156	.697	-.035		OK	
14	155	.776	-.025		OK	
15	154	.855	-.0163		OK	
16	153	.92	-.0083		OK	
17	152	.99	-.00076		OK	
18		1.0	0.	T.E.	INSERTED	EXTRAPOLATE & AVG

ENGR.	D.H.P.	3-23-71	REVISED	DATE
CHECK				
APR				
APR				

SHROUD
CENTER CHORD

THE BOEING COMPANY
RENTON, WASHINGTON

MODIFIED C-8A
FIG. 134
D6-24850

216
~~231~~

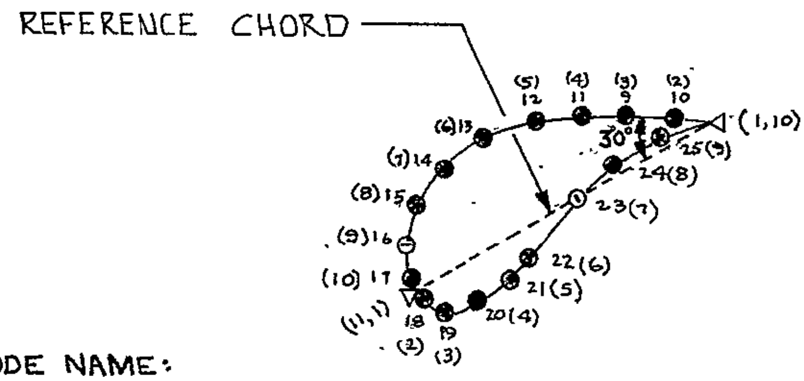

CODE NAME:
COANDA-C

REF CHORD
9.89" (M.S.)
13.6" (F.S.)

D NO.	TAP NO. (PSF NO.)	X/C	Z_P/C	SURFACE	PRESSURE DATA QUALITY	COMMENTS
1		1.0	0.	T. E.	INSERTED	EXTRAPOLATE & AVG
2	10	.917	.0486	UPPER SURFACE	OK	
3	9	.794	.118		OK	
4	11	.670	.190		OK	
5	12	.548	.256		OK	
6	13	.409	.284		OK	
7	14	.271	.266		OK	
8	15	.146	.205		OK	
9	16	.0455	.106		BAD	INTERPOLATE
10	17	.00101	.0111		OK	
11		0.	0.	L. E.	INSERTED	EXTRAPOLATE & AVG
1		0.	0.	L. E.	INSERTED	EXTRAPOLATE & AVG
2	18	.0243	-.094	LOWER SURFACE	OK	
3	19	.0758	-.143		OK	
4	20	.141	-.168		OK	
5	21	.232	-.130		OK	
6	22	.316	-.0747		OK	
7	23	.510	.0091		BAD	INTERPOLATE
8	24	.719	.0415		OK	
9	25	.930	.0202		OK	
10		1.0	0.	T. E.	INSERTED	EXTRAPOLATE & AVG

ENGR.	D. H. P.	3-23-71	REVISED	DATE	COANDA CENTER CHORD	MODIFIED C-8A
CHECK						FIG. 135
APR					THE BOEING COMPANY RENTON, WASHINGTON	D6-24850
APR						

217
~~232~~

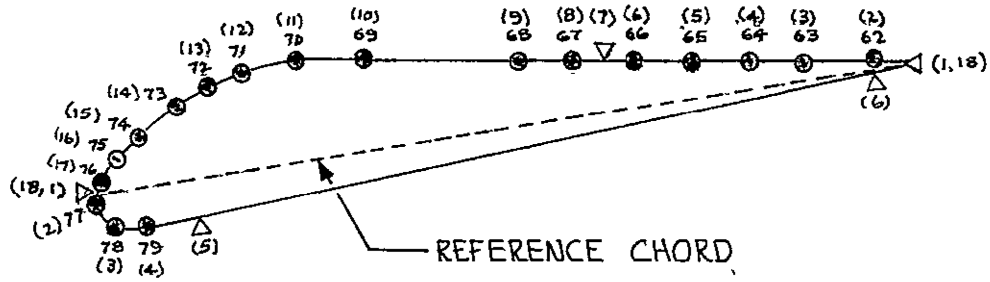

CODE NAME:
FLAP---C
& FLAP C-C

REF CHORD:
25.38" (M.S.)
36.15" (F.S.)

D NO.	TAP NO. (PSF NO.)	X/c	Zp/c	SURFACE	PRESSURE DATA QUALITY	COMMENTS
1		1.0	0.	T.E.	INSERTED	EXTRAPOLATE & AVG
2	62	.985	.00276		OK	
3	63	.914	.0158		OK	
4	64	.807	.0363		OK	
5	65	.700	.0565		OK	
6	66	.593	.0766		OK	
7		.512	.0914		INSERTED	EXTRAPOLATE
8	67	.510	.0924		OK	
9	68	.428	.107		OK	
10	69	.314	.128	UPPER SURFACE	OK	
11	70	.258	.132		OK	
12	71	.202	.127		OK	
13	72	.148	.113		OK	
14	73	.096	.0905		OK	
15	74	.050	.0596		OK	
16	75	.0138	.0316		BAD	INTERPOLATE
17	76	.00119	.0099		OK	
18		0.	0.	L.E.	INSERTED	EXTRAPOLATE & AVG
1		0.	0.	L.E.	INSERTED	EXTRAPOLATE & AVG
2	77	.0047	-.013		OK	
3	78	.0205	-.0241		OK	
4	79	.0418	-.0244	LOWER SURFACE	OK	
5		.096	-.0232		INSERTED	ASSUME ΔP=0
6		.985	-.0004		INSERTED	ASSUME ΔP=0
7		1.0	0.	T.E.	INSERTED	EXTRAPOLATE & AVG

ENGR.	D.H.P.	3-23-71	REVISED	DATE	FLAP	MODIFIED C-8A
CHECK					CENTER CHORD	FIG. 136
APR					THE BOEING COMPANY RENTON, WASHINGTON	D6-24850
APR						

218
233

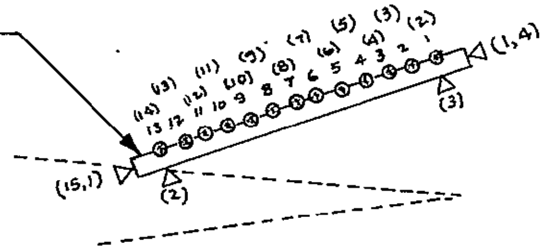

CODE NAME:
CHOKE --C

REF CHORD:
13.03" (M.S.)
18.47" (F.S.)

D NO.	TAP NO. (PSLD NO.)	X/C	ZP/C	SURFACE	PRESSURE DATA QUALITY	COMMENTS
1		1.0	0.	T.E.	INSERTED	EXTRAPOLATE & AVG
2	1	.985	↑	UPPER SURFACE	OK	
3	2	.914			OK	
4	3	.843			OK	
5	4	.774			OK	
6	5	.702			OK	
7	6	.632			OK	
8	7	.561			OK	
9	8	.491			OK	
10	9	.42			OK	
11	10	.350			OK	
12	11	.284			OK	
13	12	.204			OK	
14	13	.126	↓		DELETED	
15		0.	0.	L.E.	INSERTED	EXTRAPOLATE
1		0.		L.E.	INSERTED	EXTRAPOLATE
2		.204		LOWER SURFACE	INSERTED	ASSUME ΔP OF PSF 66
3		.985			INSERTED	ASSUME ΔP OF PSF 62
4		1.0		T.E.	INSERTED	EXTRAPOLATE & AVG

ENGR.	D.H.P.	3-23-71	REVISED	DATE	AUGMENTOR CHOKE	MODIFIED C-8A
CHECK					CENTER CHORD	FIG. 137
APR					THE BOEING COMPANY RENTON, WASHINGTON	D6-24850
APR						

219
~~234~~

AD 1017-R6

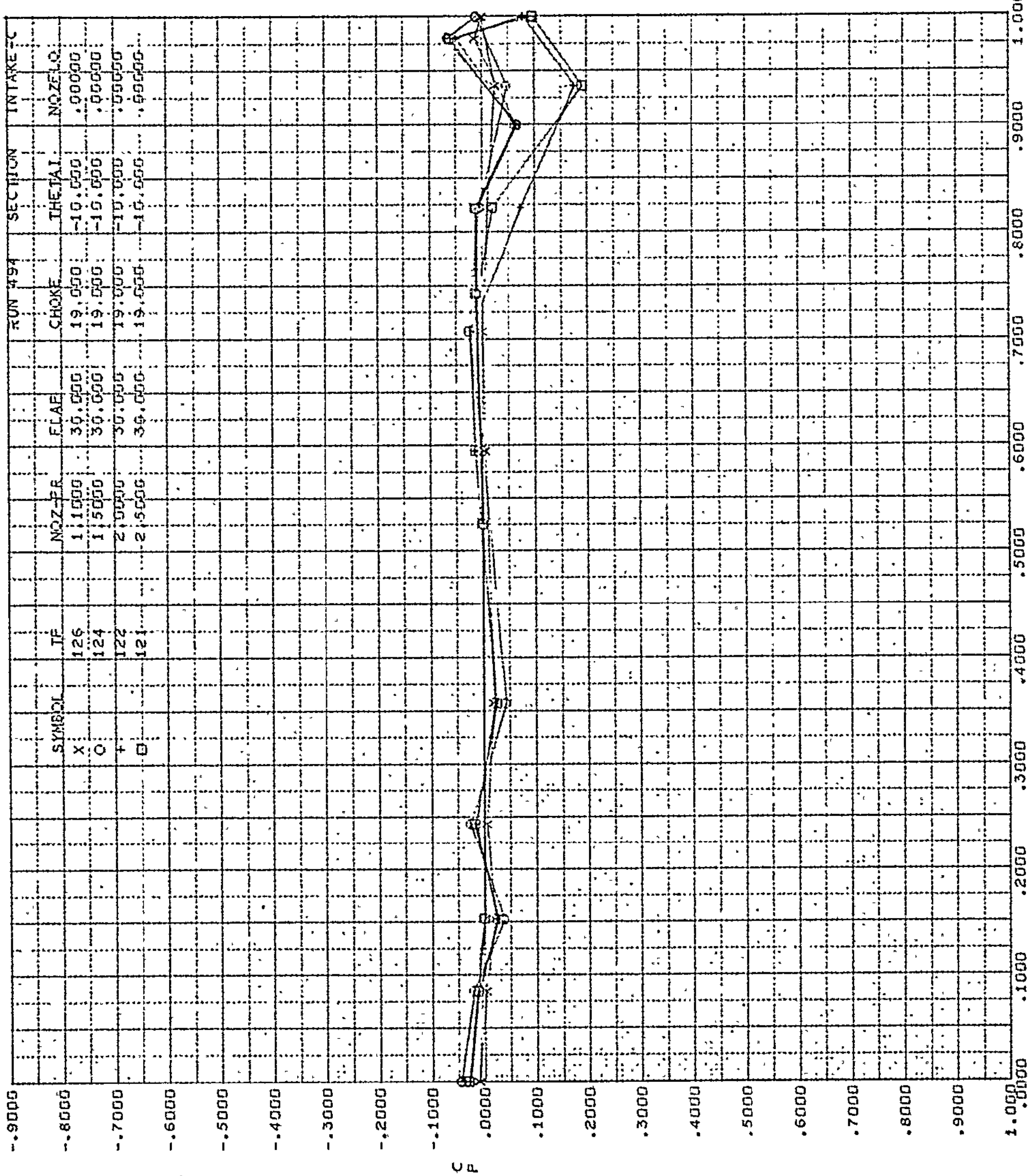

FIG. 138

BUFFALO - STATIC

MODIF. C8A MODEL - OUTBD NOZ.,NOZFLO =0(DUAL),1(UPR),2(LWR)

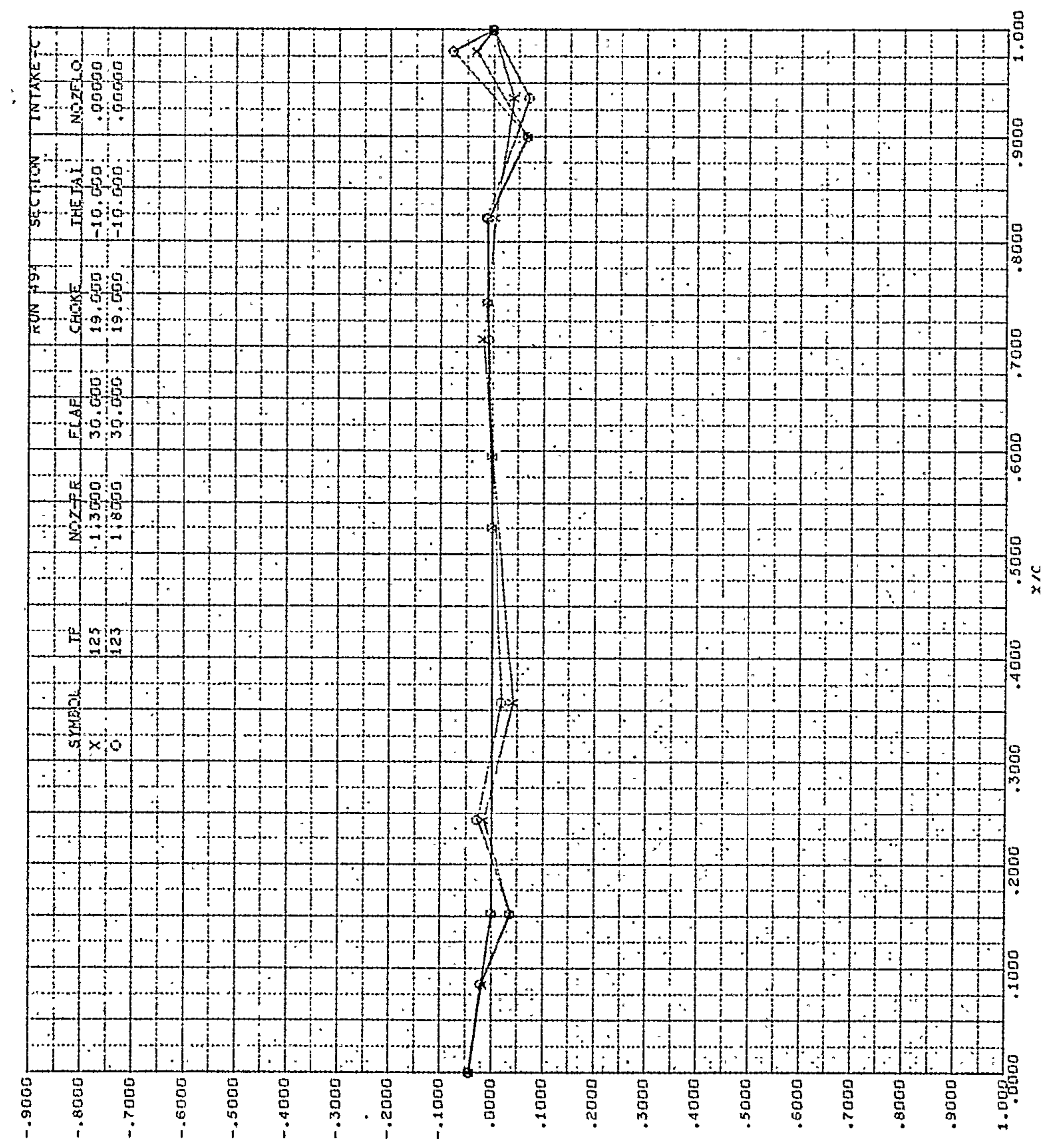

BUFFALO - STATIC

FIG. 139

MODIF. C8A MODEL - OUTBD NOZ.,NOZFLO =0(DUAL),1(UPR),2(LWR)

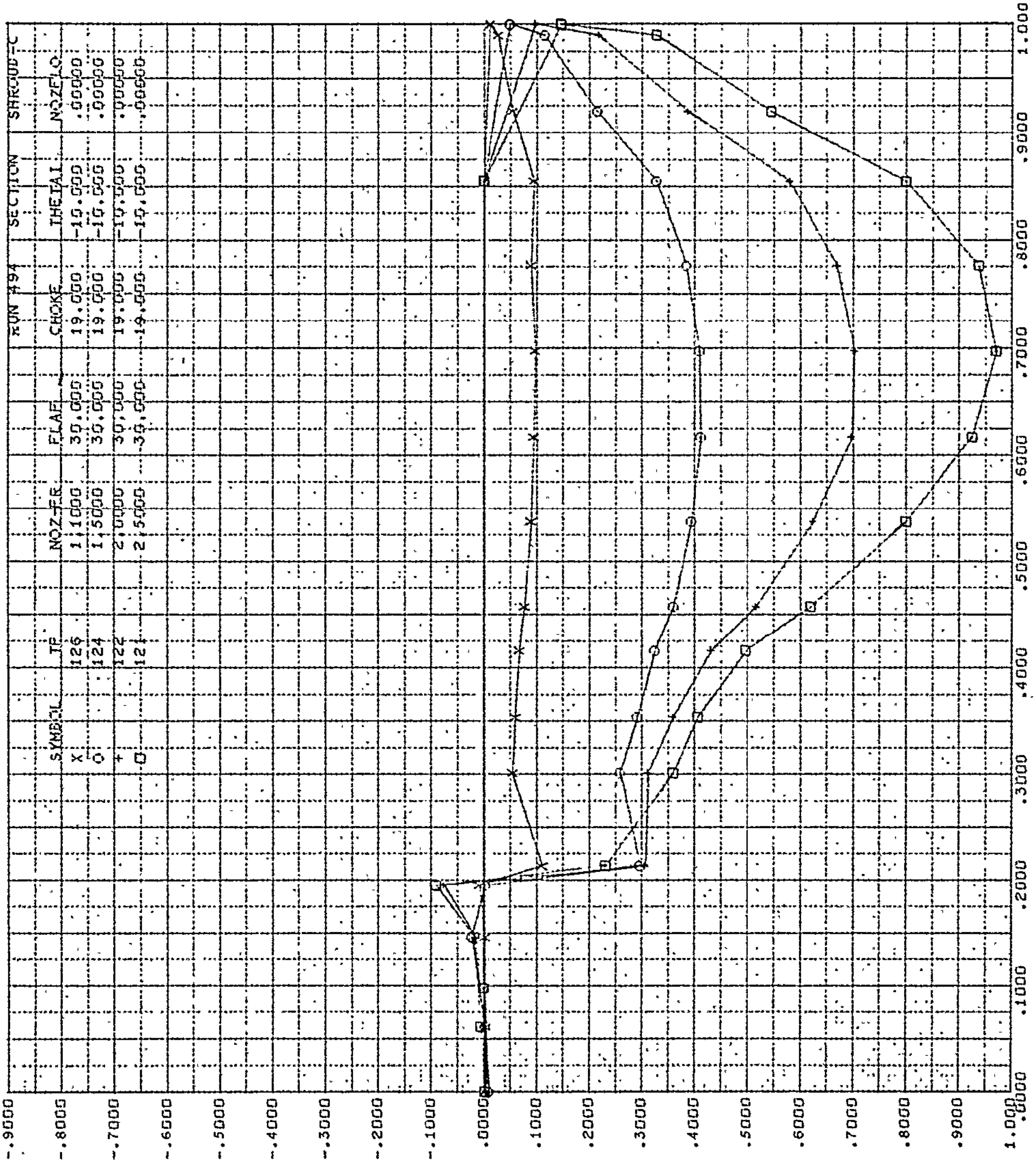

FIG. 140

BUFFALO - STATIC

MODIF. C8A MODEL - OUTBD NOZ.,NOZFLO =0(DUAL),1(UPR),2(LWR)

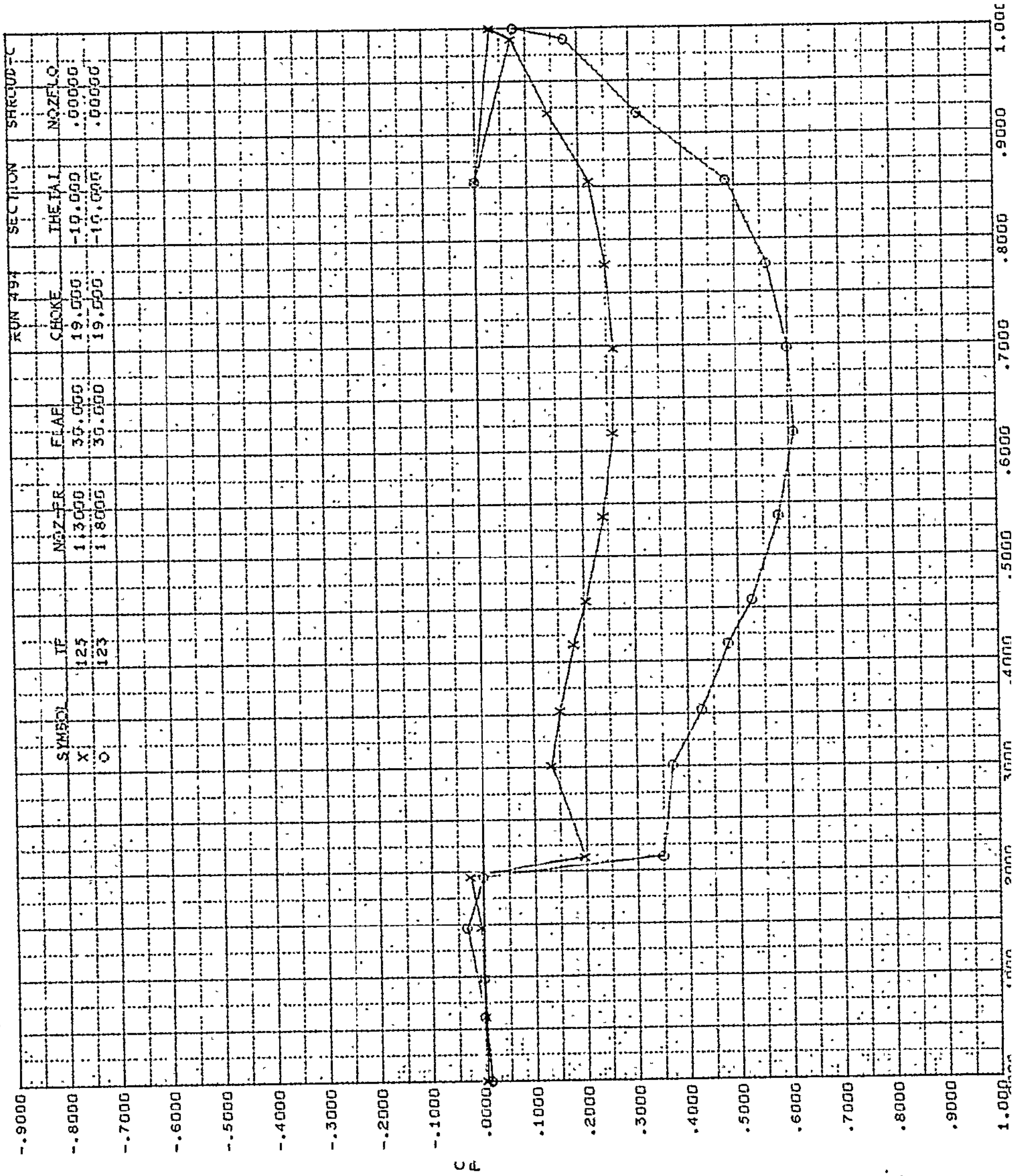

FIG. 141

BUFFALO - STATIC

MODIF. C8A MODEL - OUTBD NOZ.,NOZFLO
=0(DUAL),1(UPR),2(LWR)

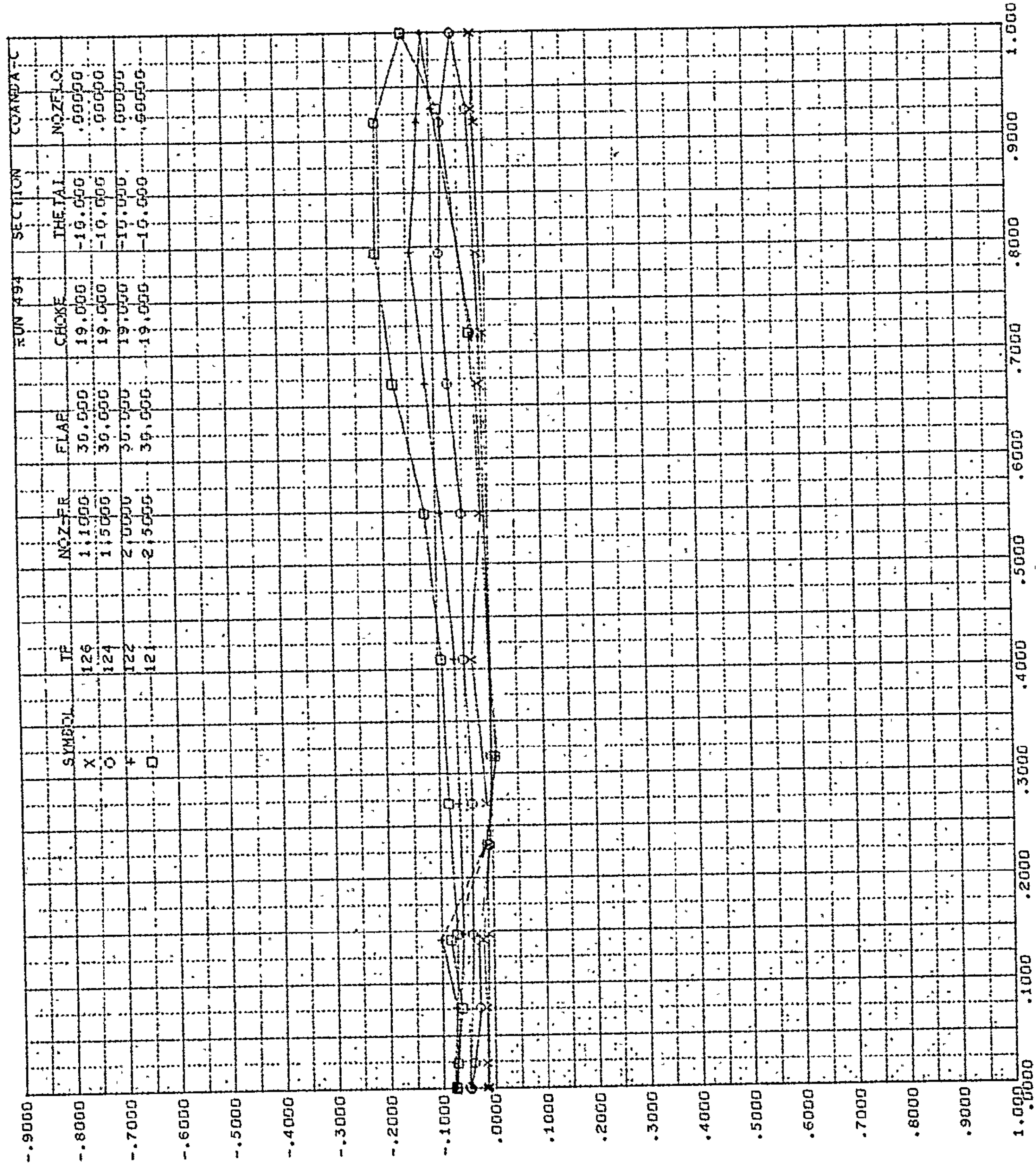

FIG. 142

BUFFALO - STATIC

MODIF. C8A MODEL - OUTBD NOZ.,NOZFLO
=0(DUAL),1(UPR),2(LWR)

D6-24850

PAGE 224

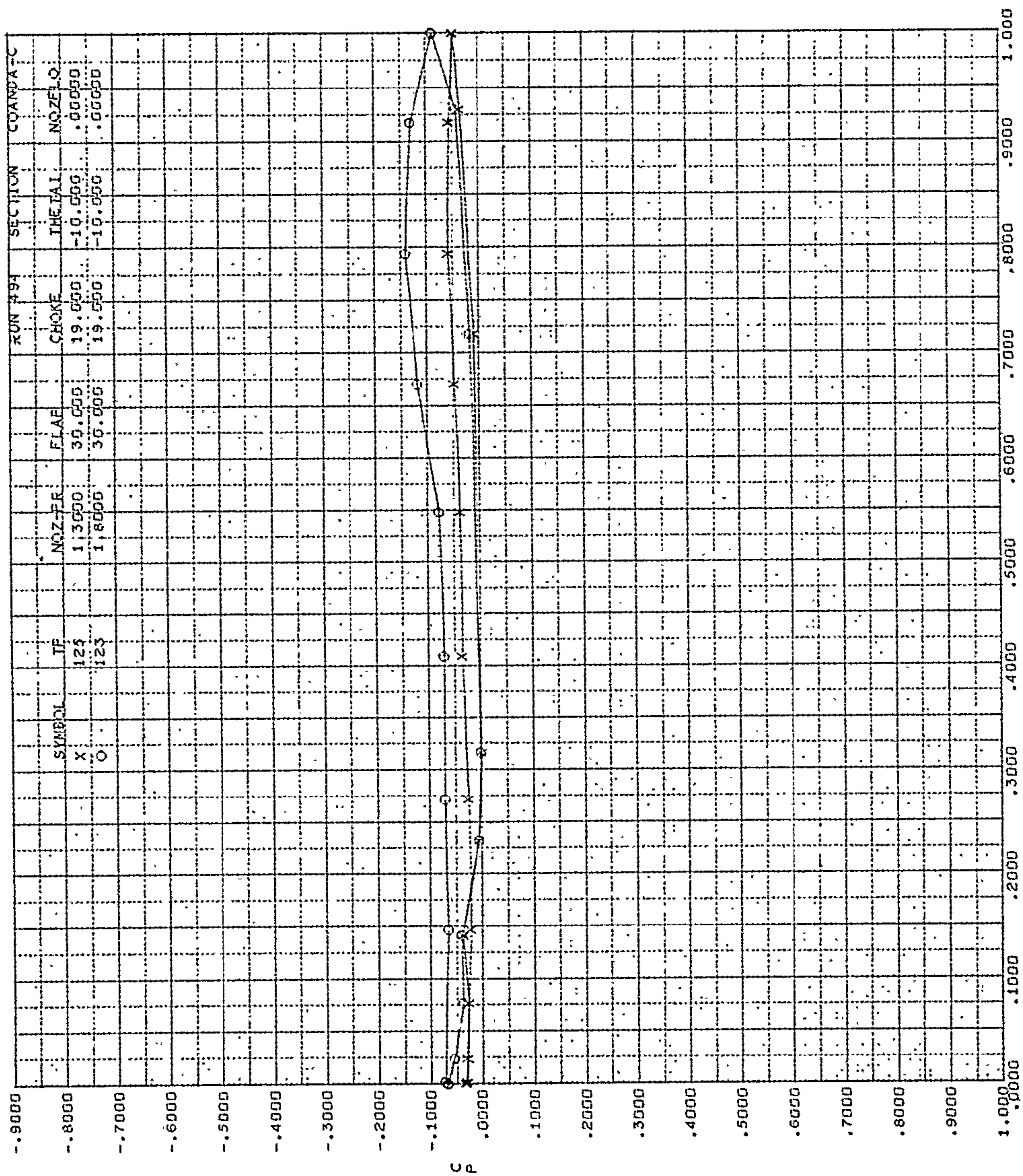

FIG. 143

BUFFALO - STATIC

MODIF. C8A MODEL - OUTBD NOZ.,NOZFLO =0(DUAL),1(UPR),2(LWR)

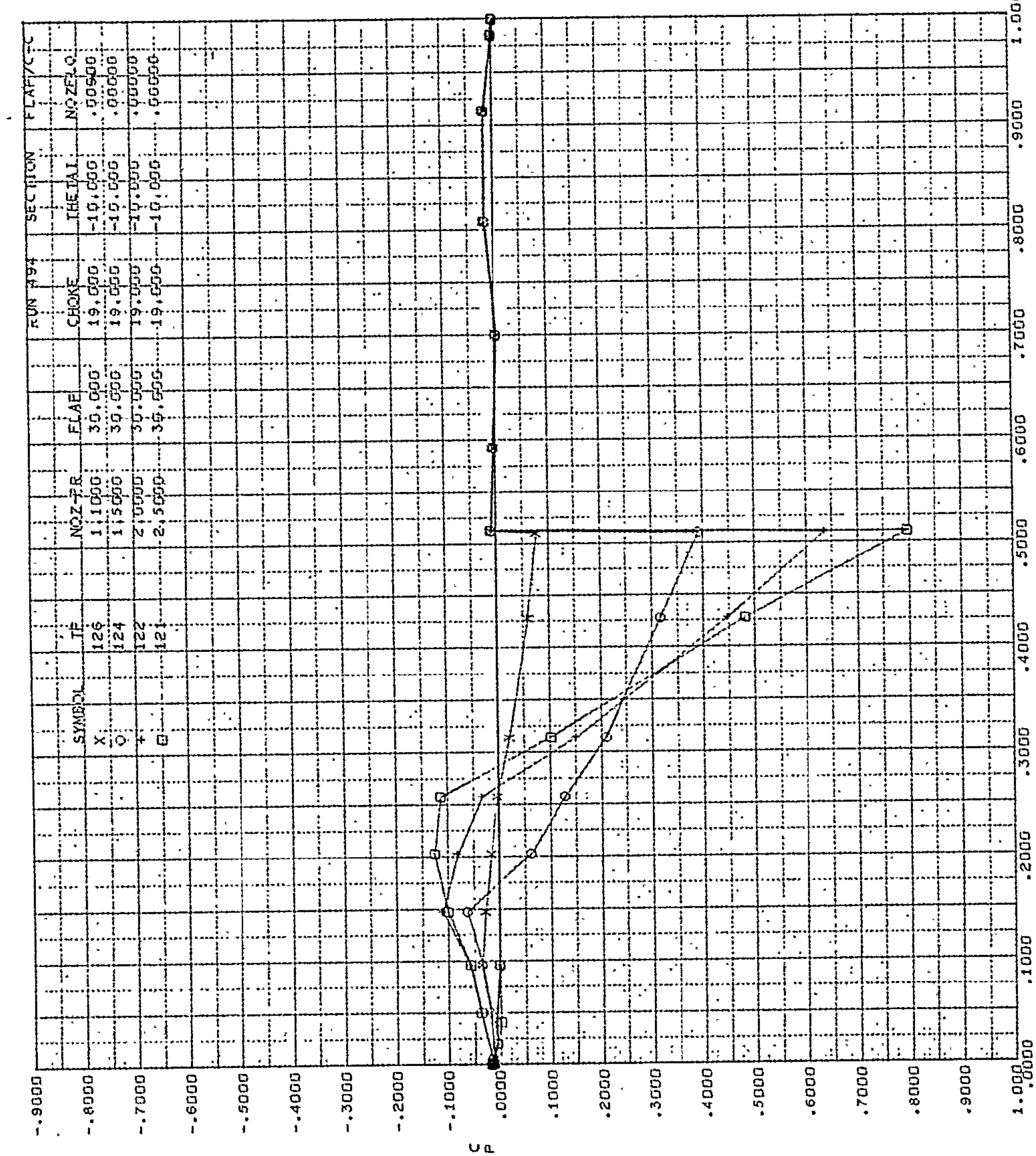

FIG. 144

BUFFALO - STATIC

MODIF. C8A MODEL - OUTBD NOZ.,NOZFLO =0(DUAL),1(UPR),2(LWR)

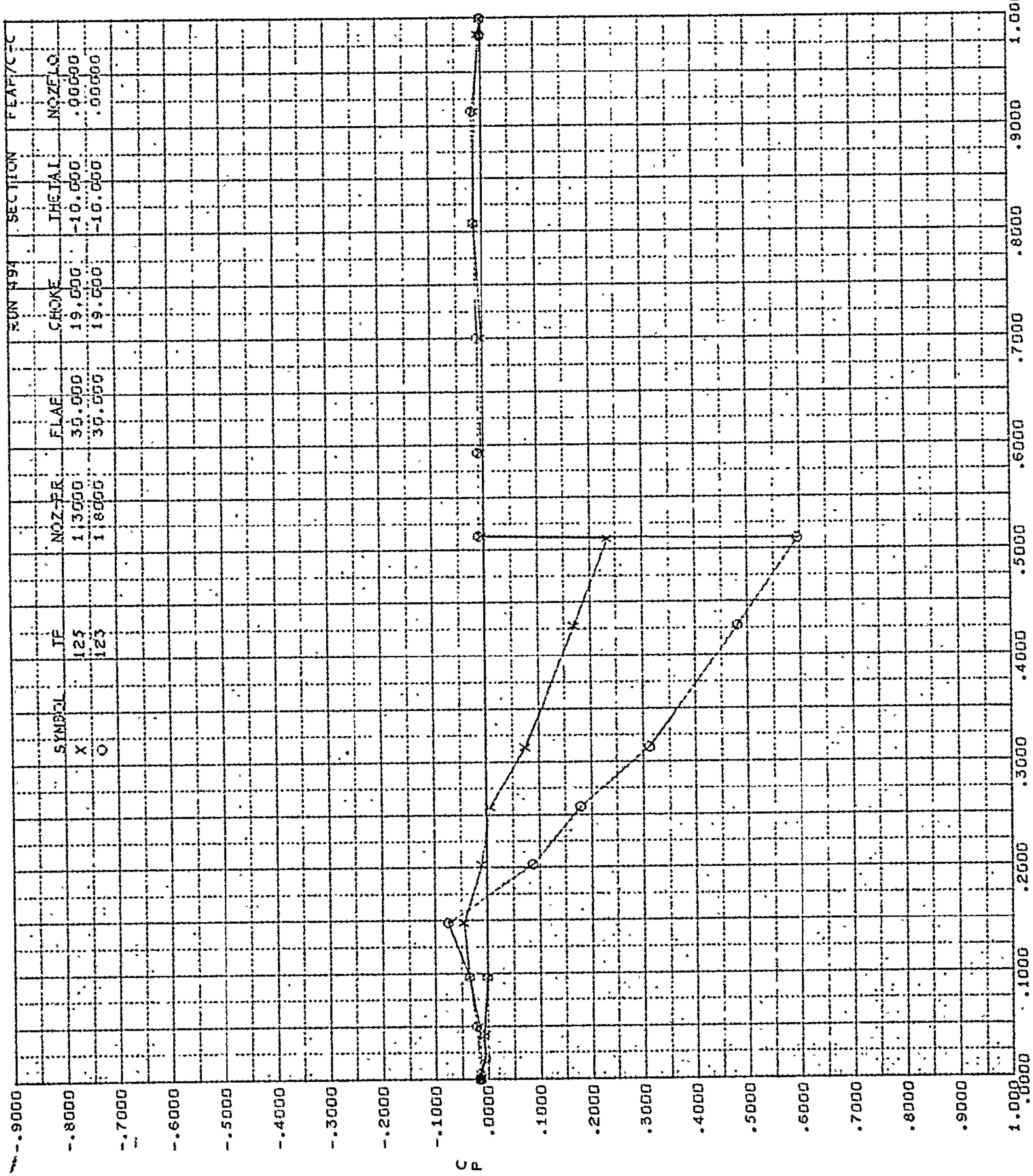

FIG. 145

BUFFALO - STATIC

MODIF. C8A MODEL - OUTBD NOZ.,NOZFLO
=0(DUAL),1(UPR),2(LWR)

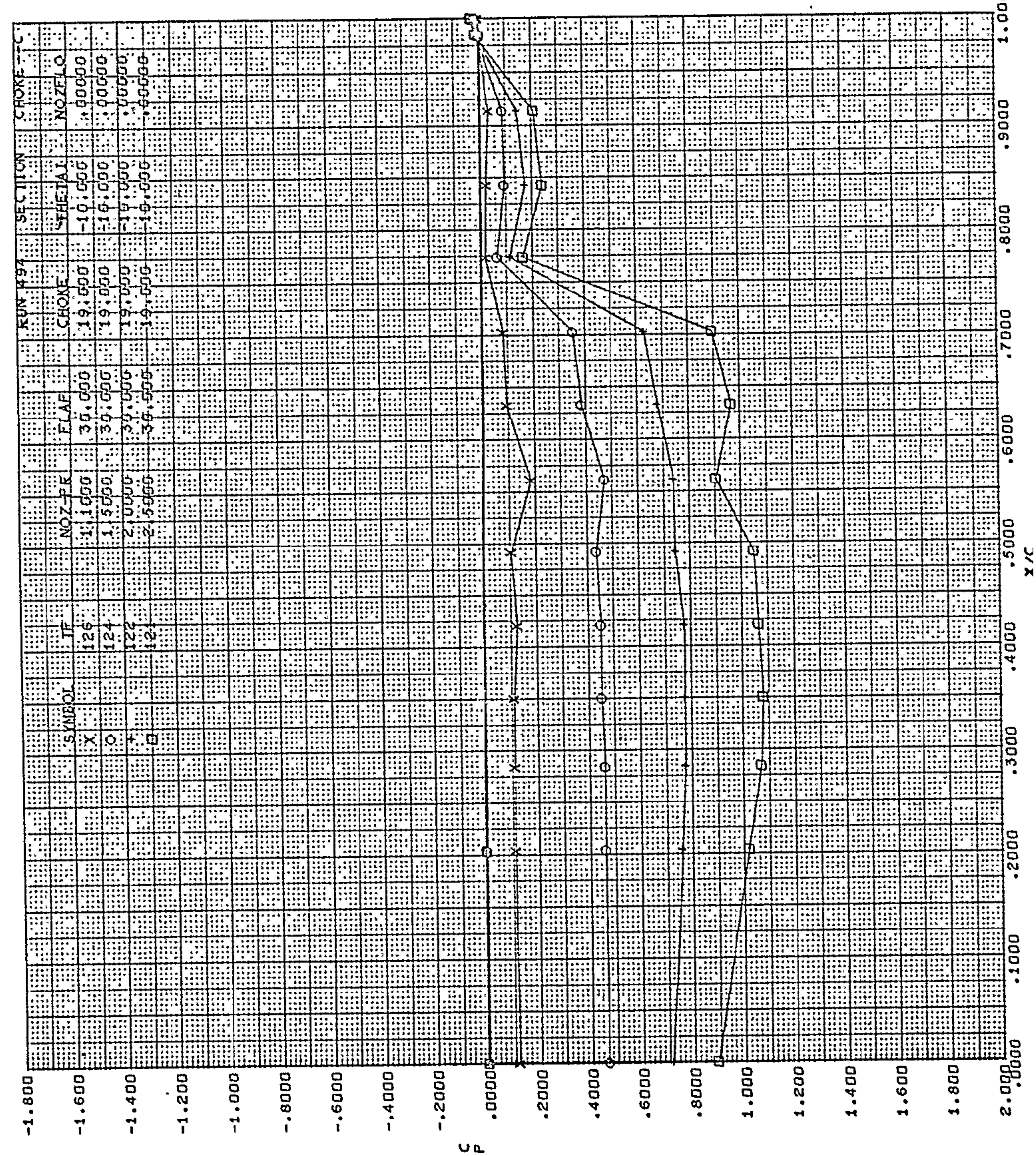

BUFFALO - STATIC

FIG. 146

MODIF. C8A MODEL - OUTBD NOZ.,NOZFLO
=0(DUAL),1(UPR),2(LWR)

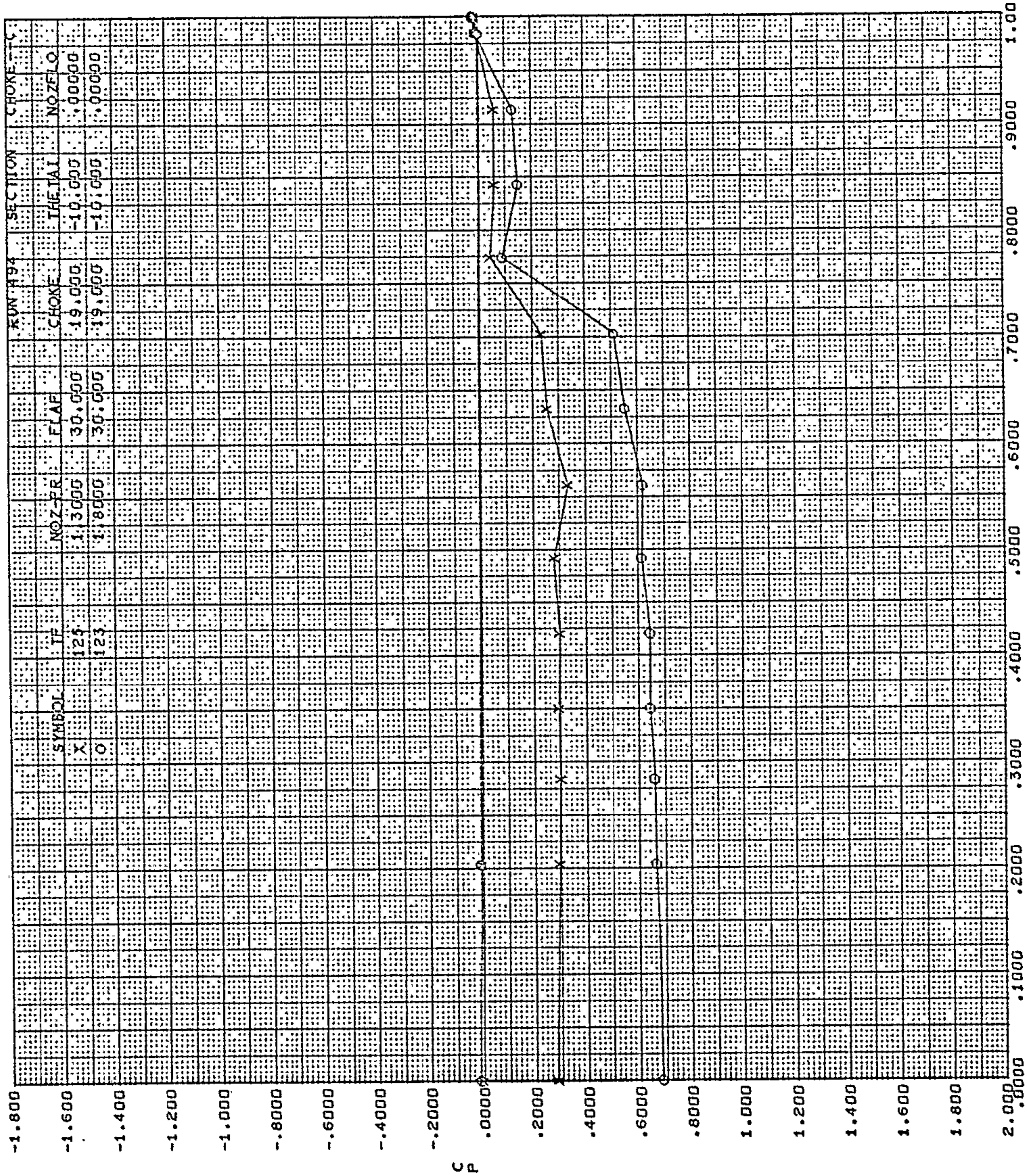

BUFFALO - STATIC FIG. 147

MODIF. C8A MODEL - OUTBD NOZ.,NOZFLO
=0(DUAL),1(UPR),2(LWR)

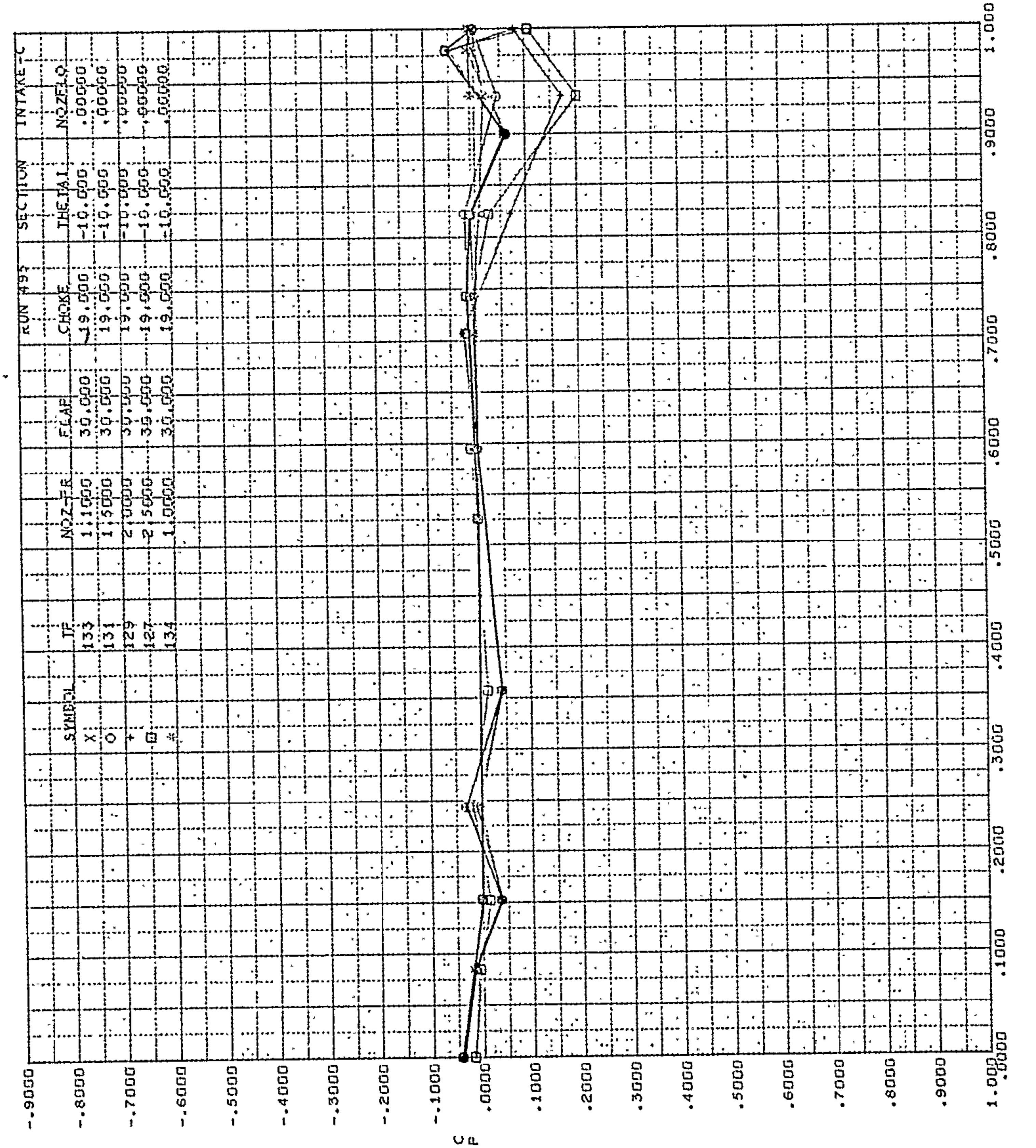

FIG. 148

BUFFALO - STATIC

MODIF. C8A MODEL - OUTBD NOZ.,NOZFLO =0(DUAL),1(UPR),2(LWR)

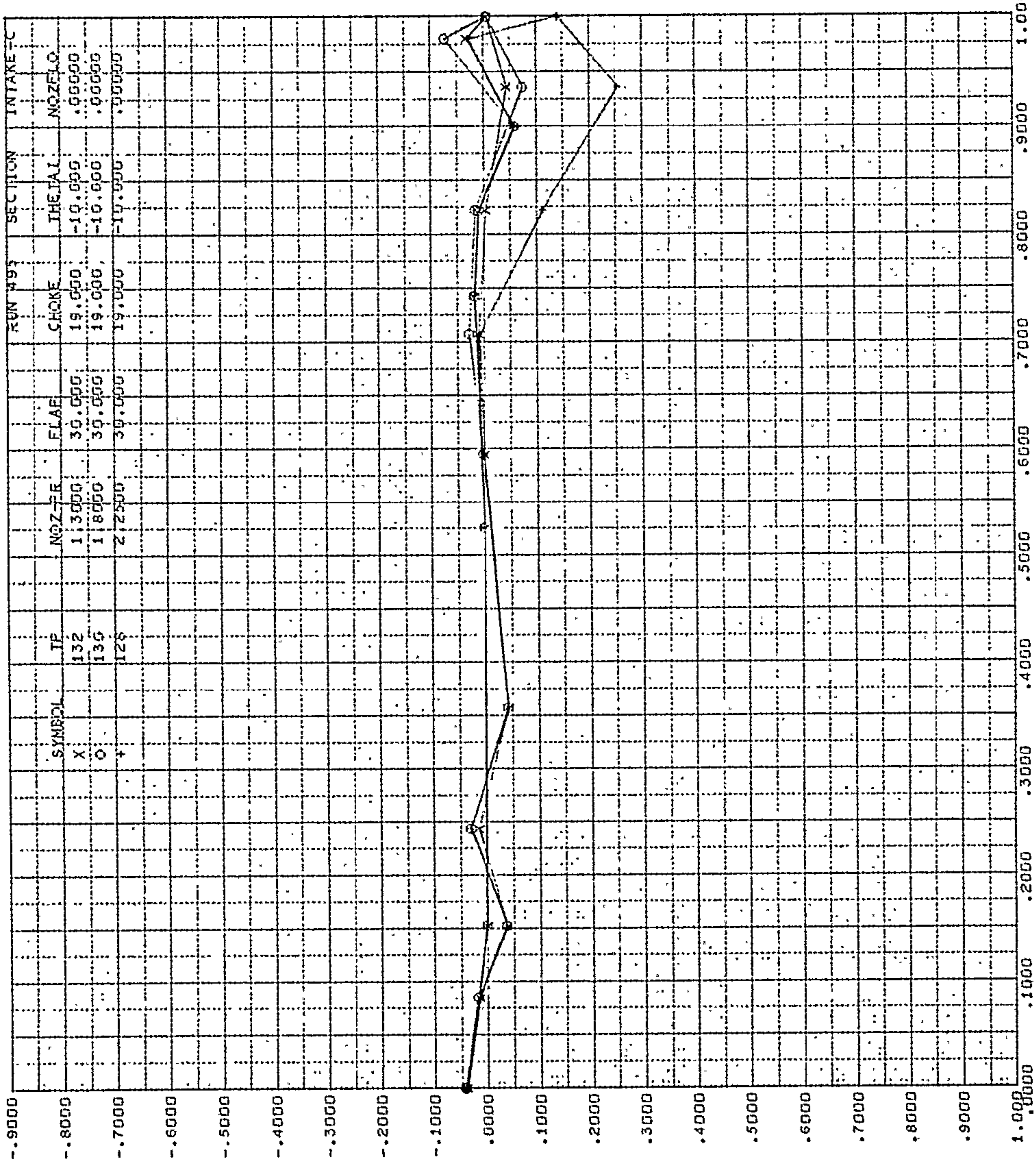

FIG. 149

BUFFALO - STATIC

MODIF. C8A MODEL - OUTBD·NOZ.,NOZFLO
=0(DUAL),1(UPR),2(LWR)

D6-24850
PAGE 231

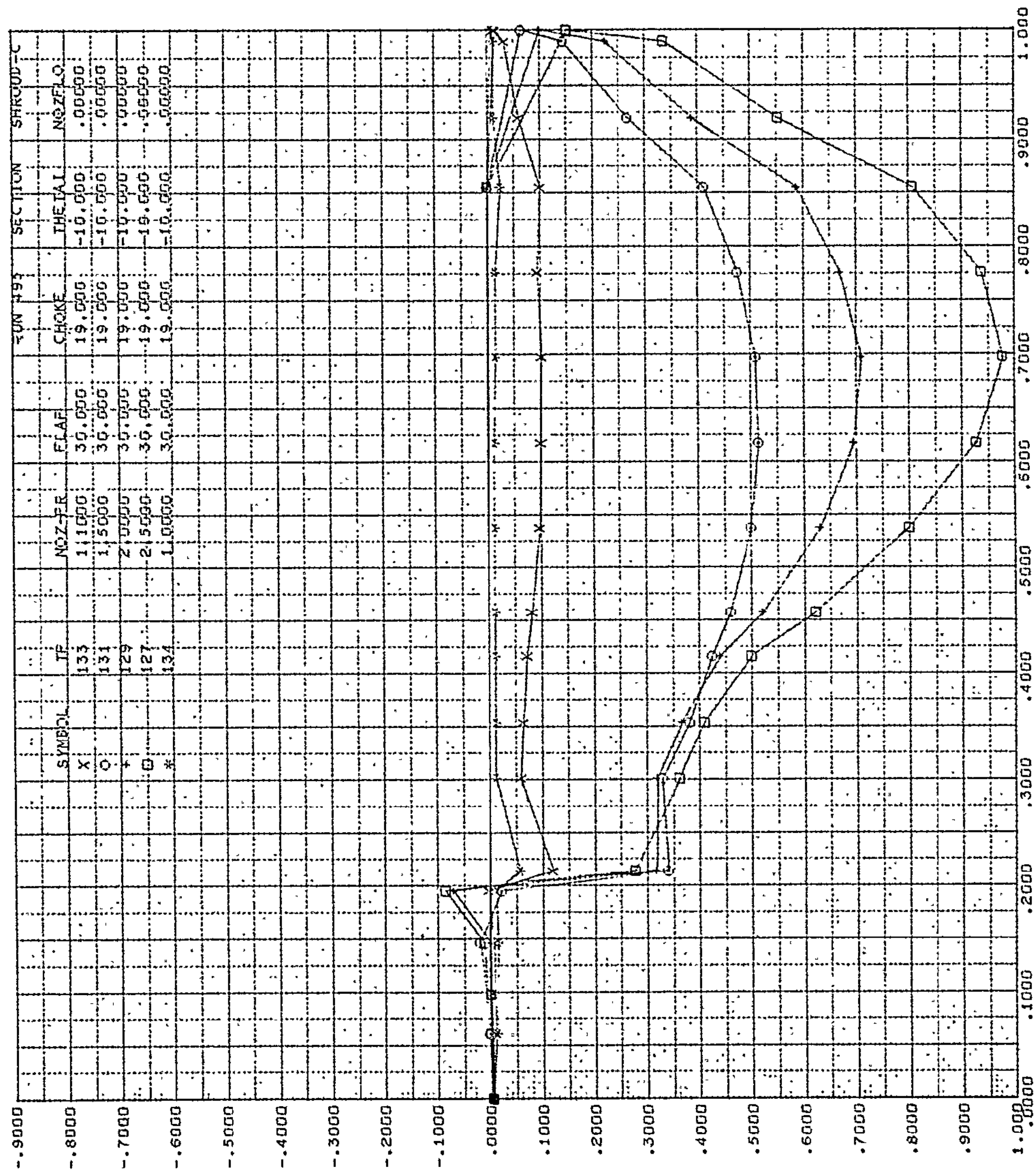

FIG. 150

BUFFALO - STATIC

MODIF. C8A MODEL - OUTBD NOZ.,NOZFLO
=0(DUAL),1(UPR),2(LWR)

D6-24850
PAGE 232

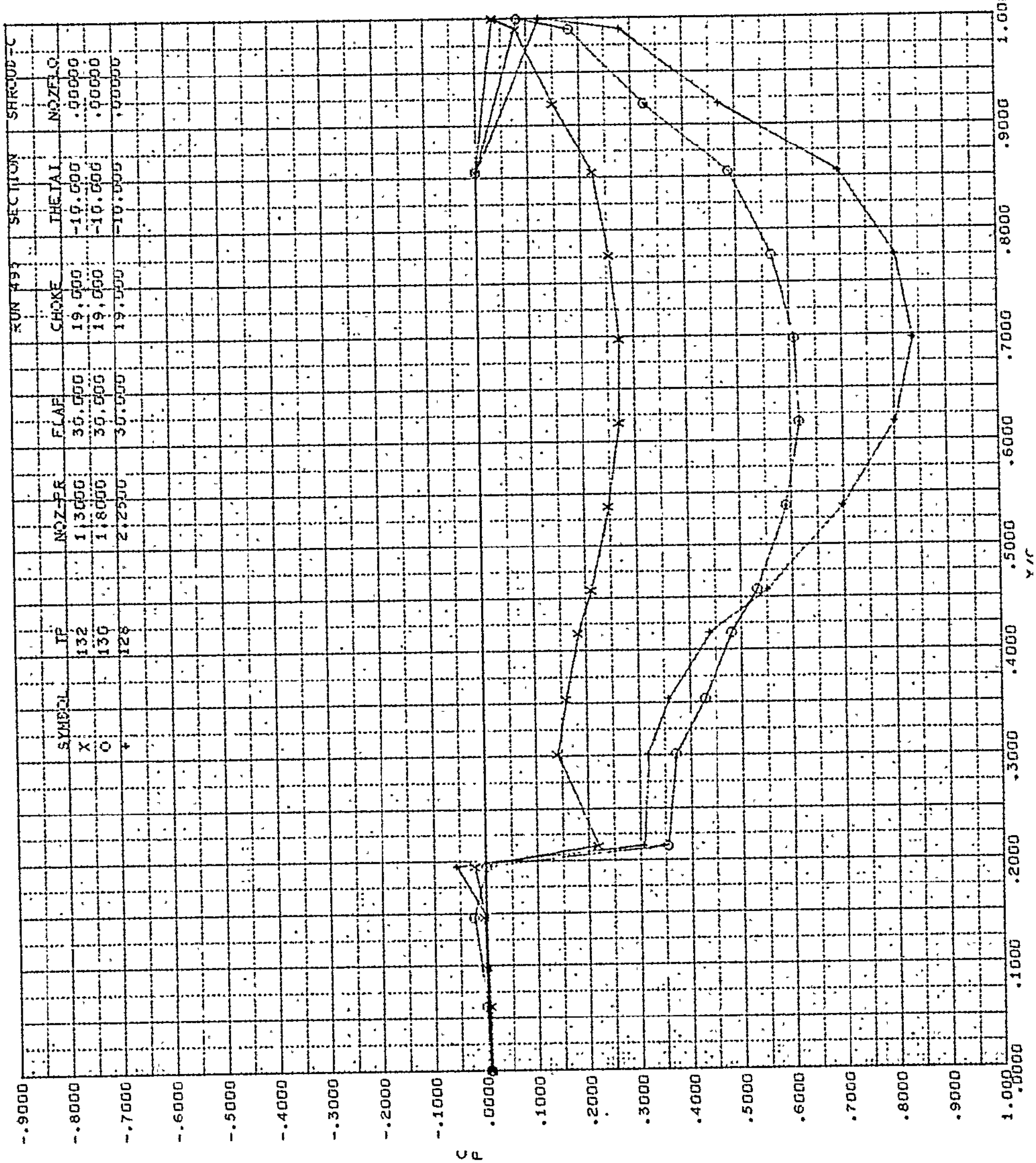

FIG. 151

BUFFALO - STATIC

MODIF. C8A MODEL - OUTBD NOZ.,NOZFLO
=0(DUAL),1(UPR),2(LWR)

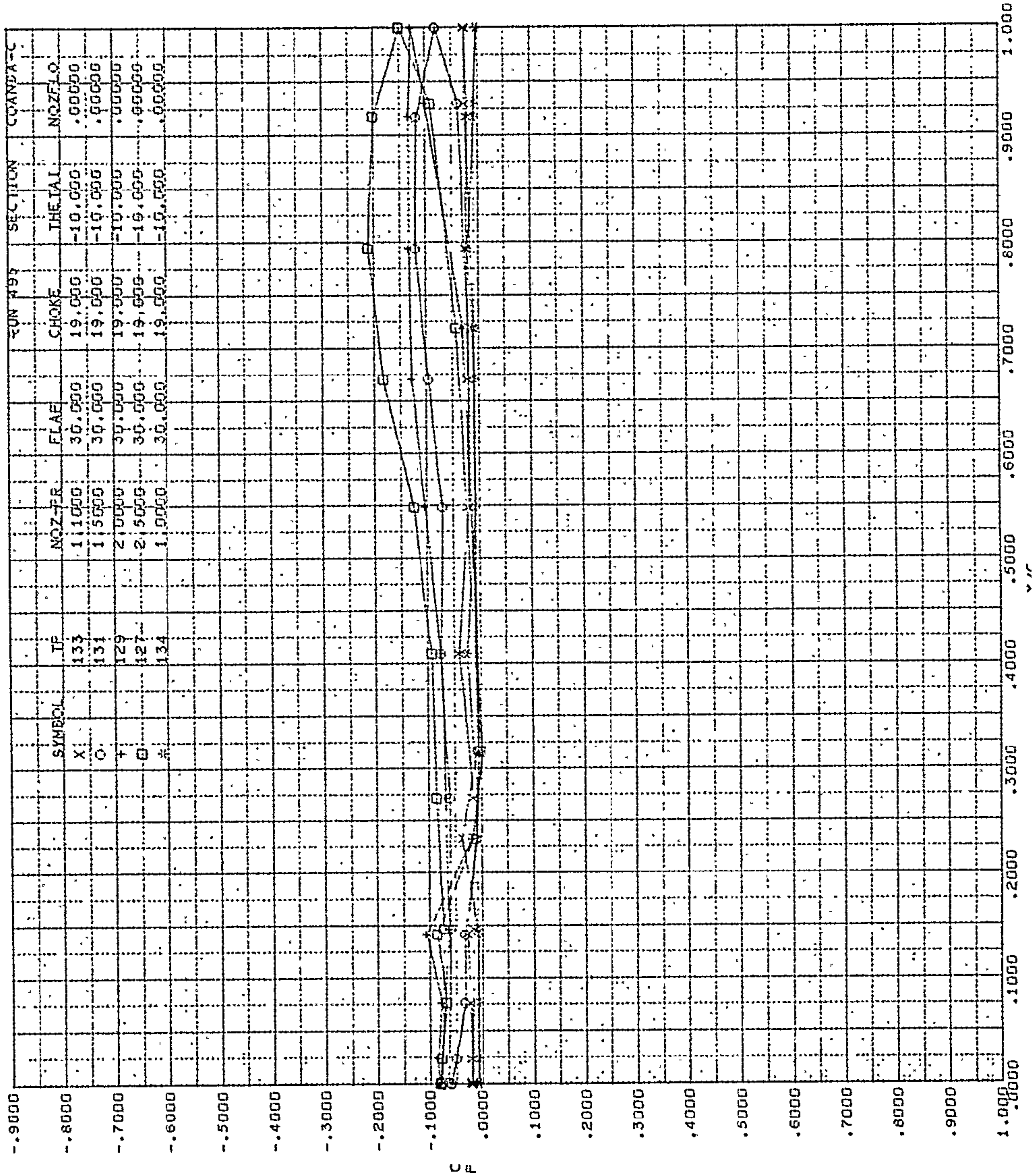

FIG. 152

BUFFALO - STATIC

MODIF. C8A MODEL - OUTBD NOZ.,NOZFLO =0(DUAL),1(UPR),2(LWR)

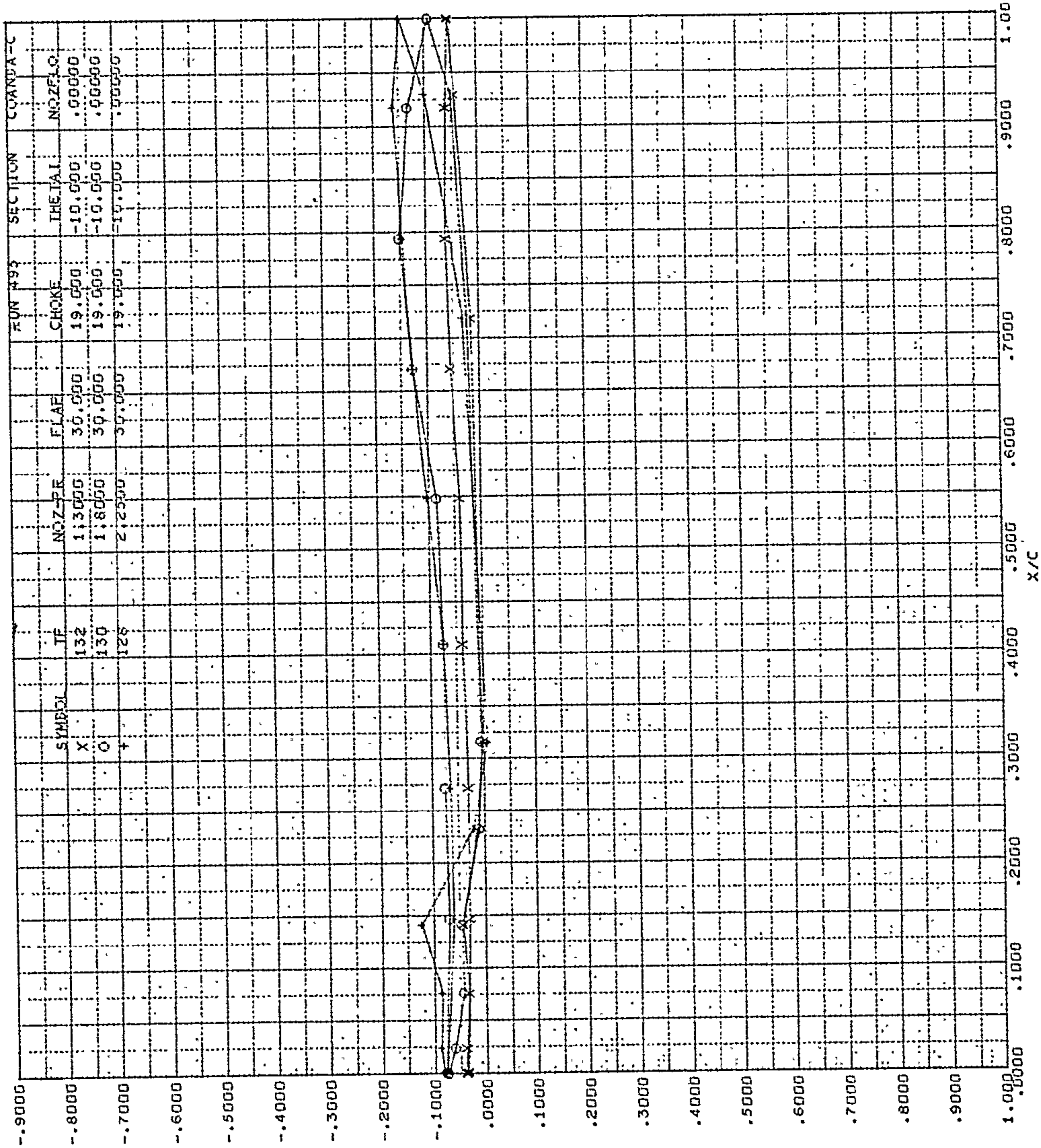

FIG. 153

BUFFALO - STATIC

MODIF. C8A MODEL - OUTBD NOZ.,NOZFLO =0(DUAL),1(UPR),2(LWR)

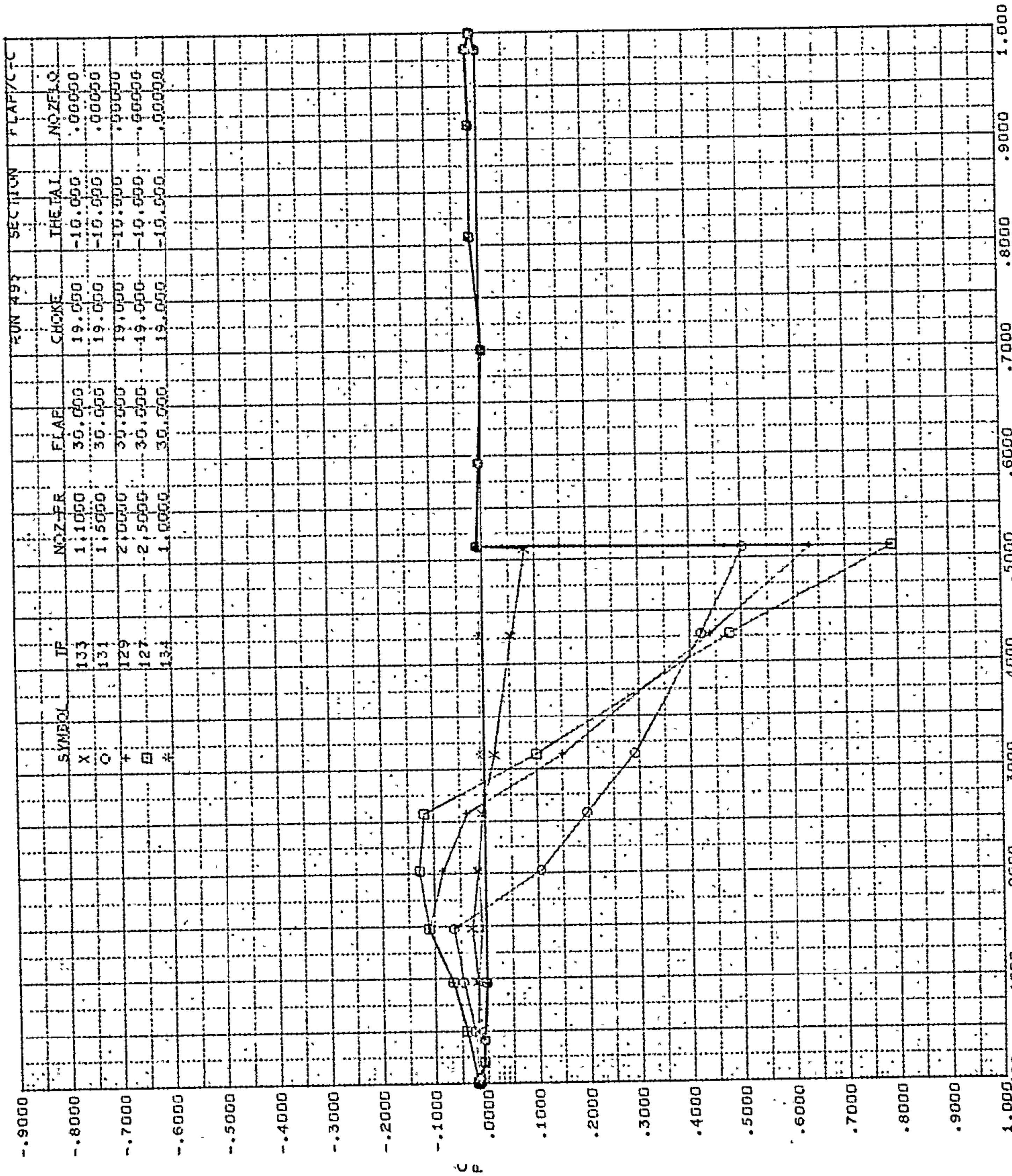

FIG. 154

BUFFALO - STATIC

MODIF. C8A MODEL - OUTBD NOZ.,NOZFLO
=0(DUAL),1(UPR),2(LWR)

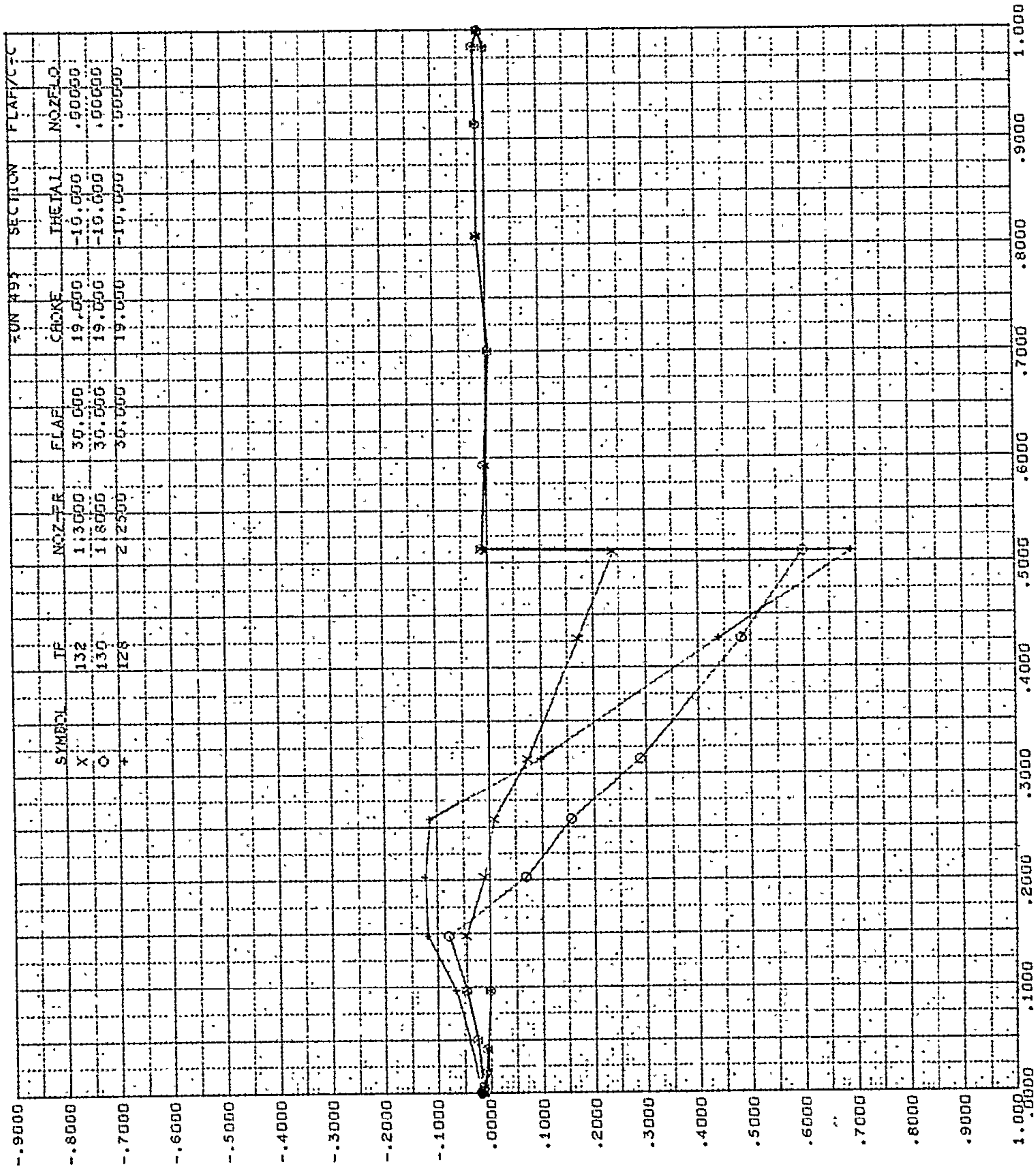

FIG. 155

BUFFALO - STATIC

MODIF. C8A MODEL - OUTBD NOZ.,NOZFLO
=0(DUAL),1(UPR),2(LWR)

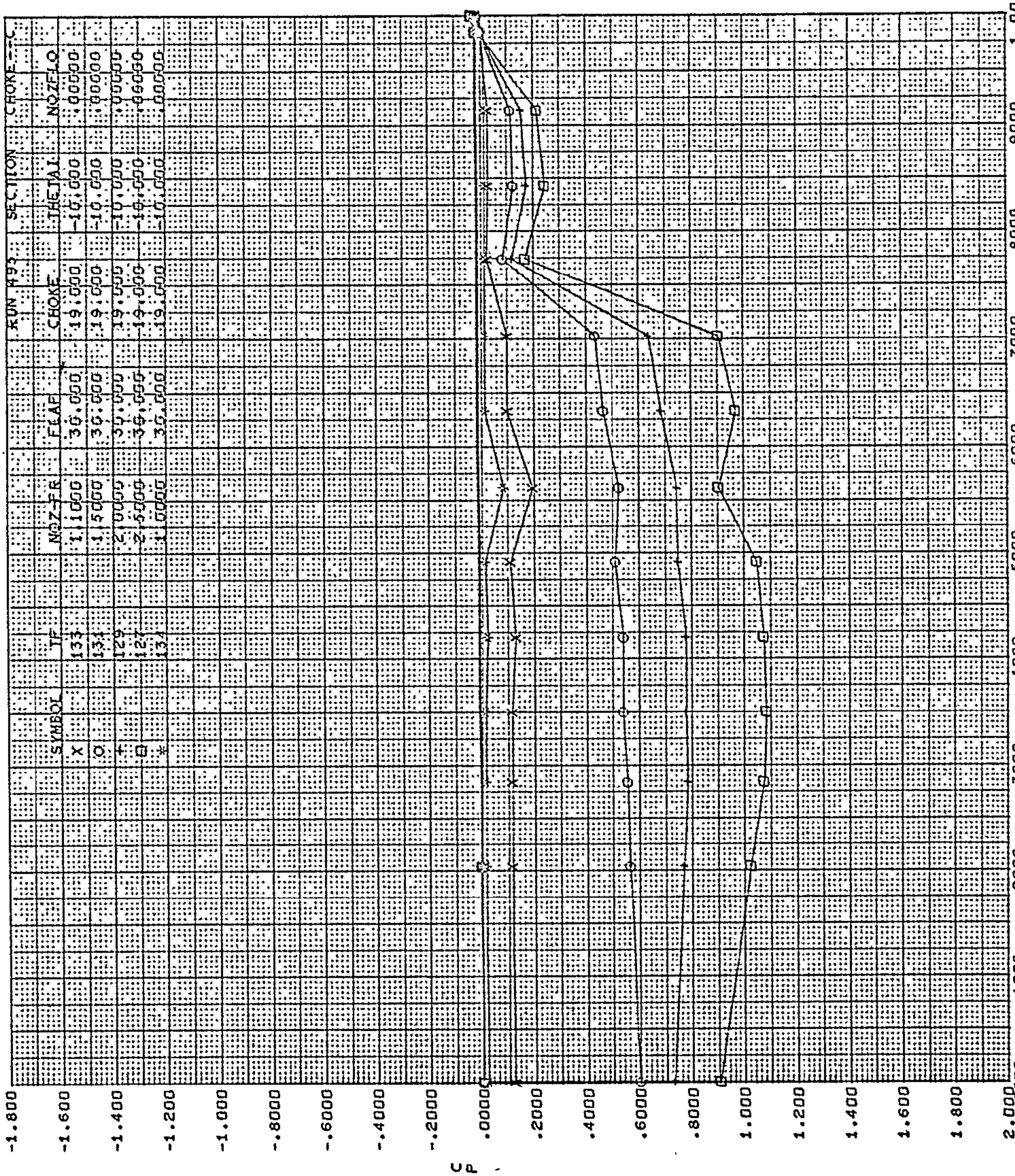

BUFFALO - STATIC

FIG. 156

MODIF. C8A MODEL - OUTBD NOZ.,NOZFLO
=0(DUAL),1(UPR),2(LWR)

D6-24850

PAGE 238

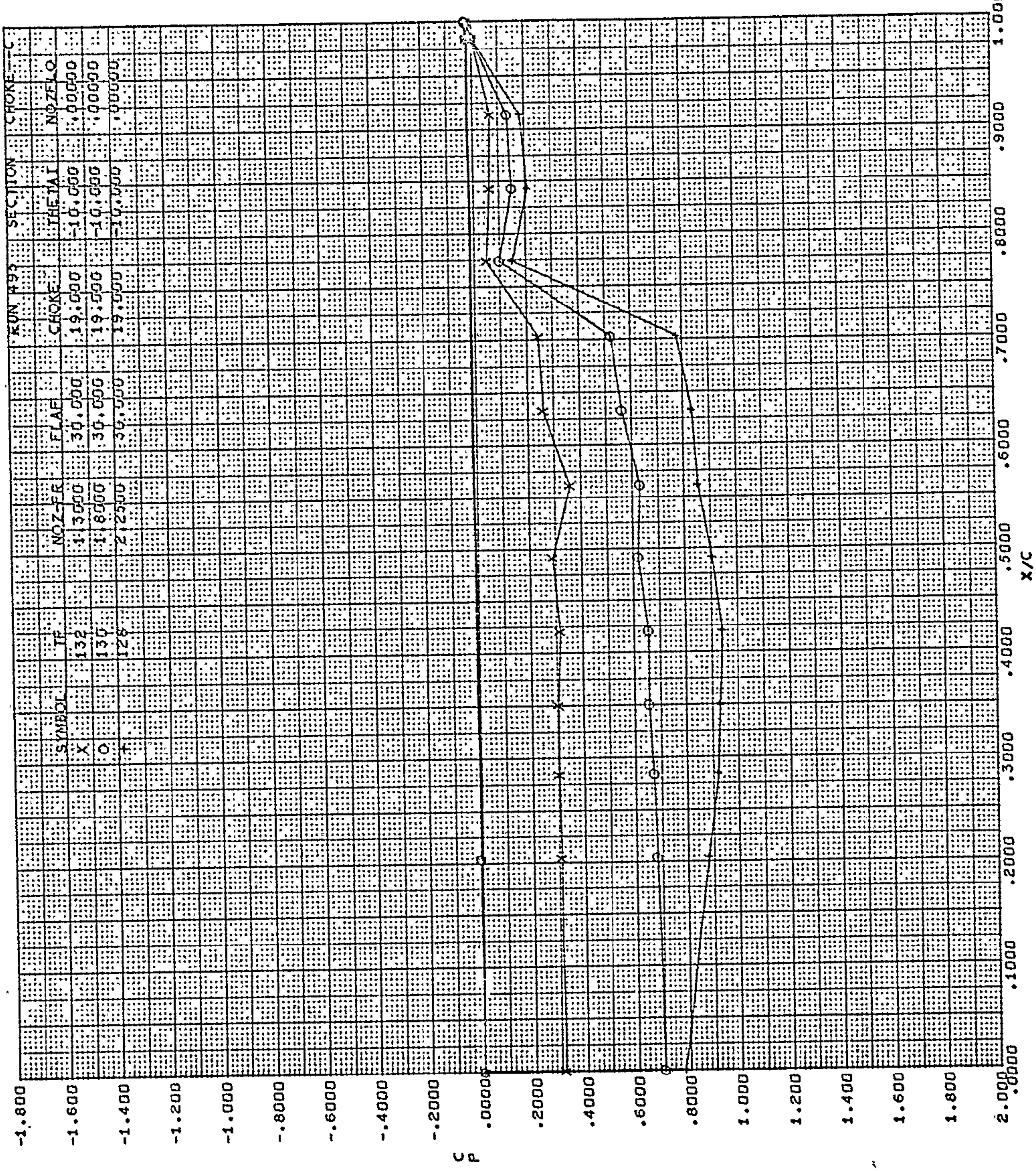

BUFFALO - STATIC FIG. 157

MODIF. C8A MODEL - OUTBD NOZ., NOZFLO =0(DUAL), 1(UPR), 2(LWR)

9
4

D6-24850

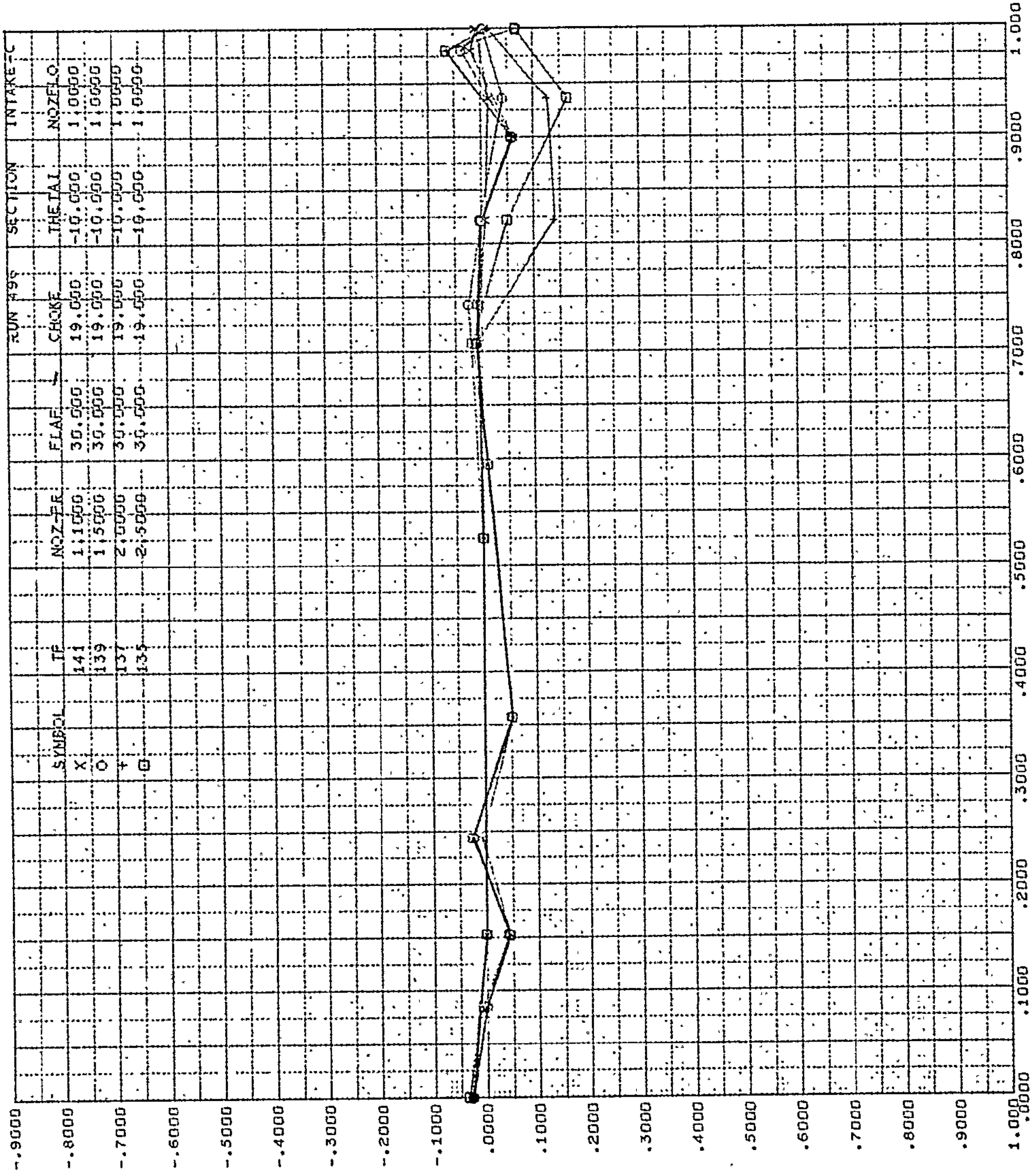

FIG. 158

BUFFALO - STATIC

MODIF. C8A MODEL - OUTBD NOZ.,NOZFLO
=0(DUAL),1(UPR),2(LWR)

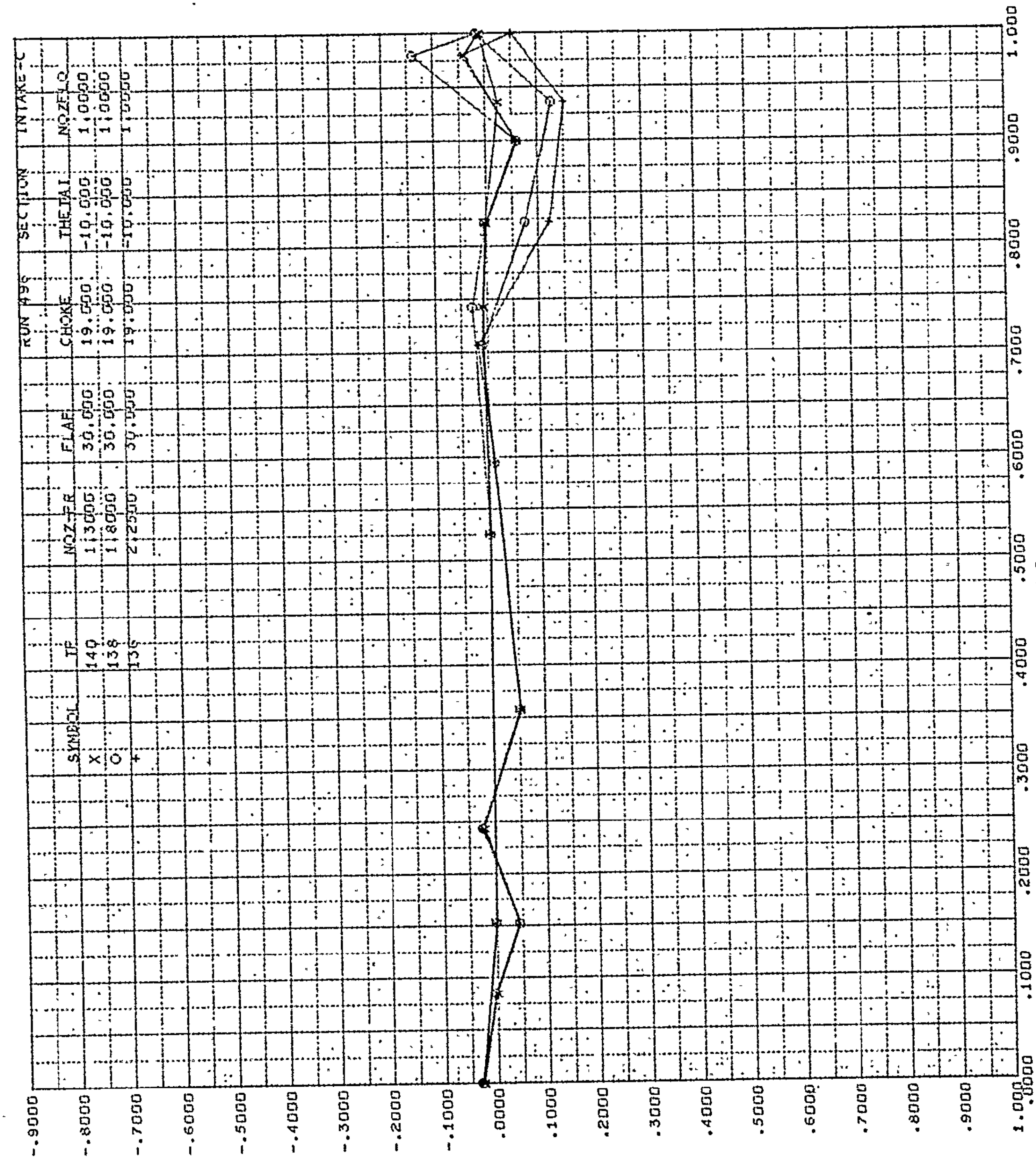

FIG. 159

BUFFALO - STATIC

MODIF. C8A MODEL - OUTBD NOZ.,NOZFLO =0(DUAL),1(UPR),2(LWR)

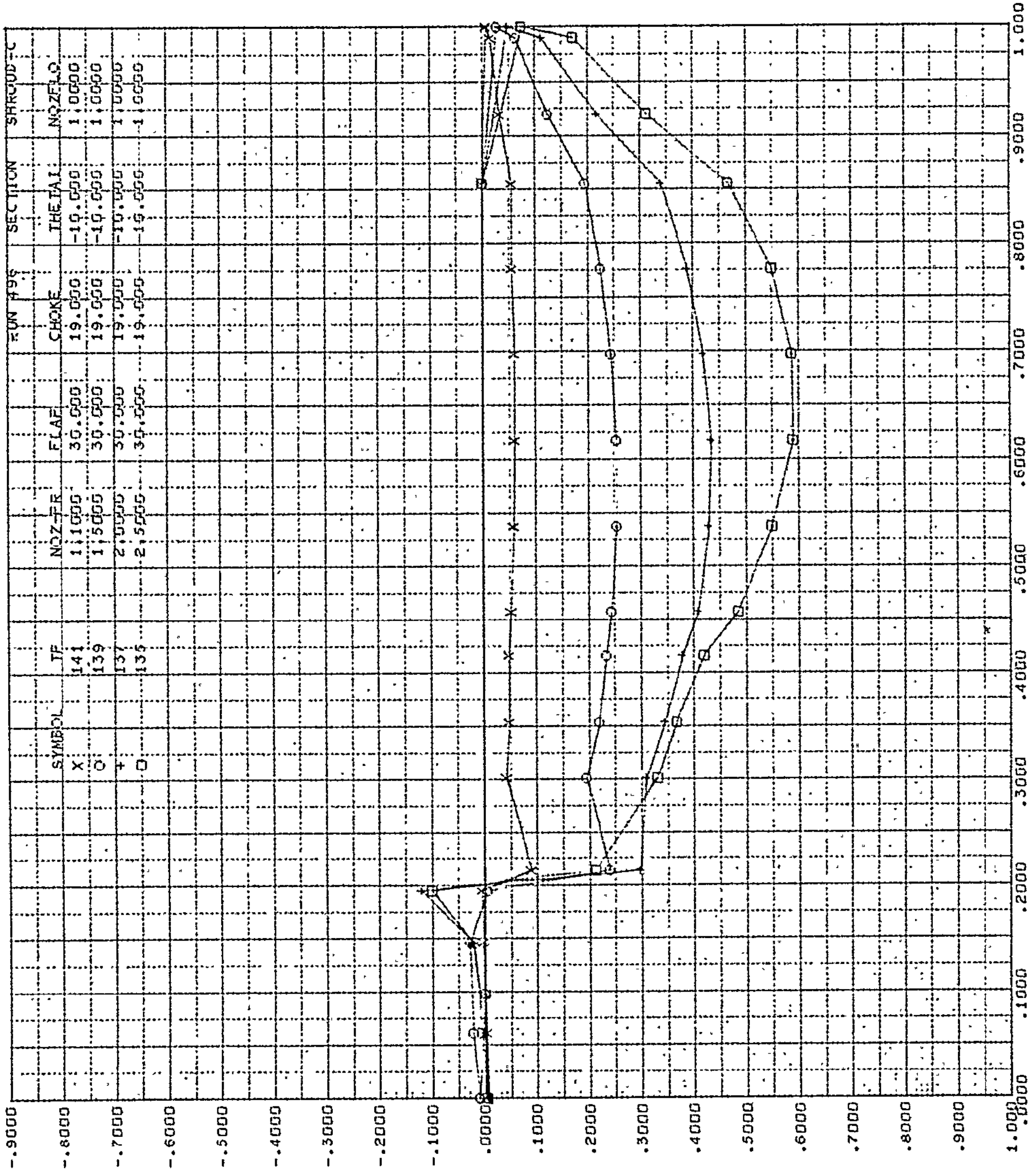

FIG. 160

BUFFALO - STATIC

MODIF. C8A MODEL - OUTBD NOZ.,NOZFLO =0(DUAL),1(UPR),2(LWR)

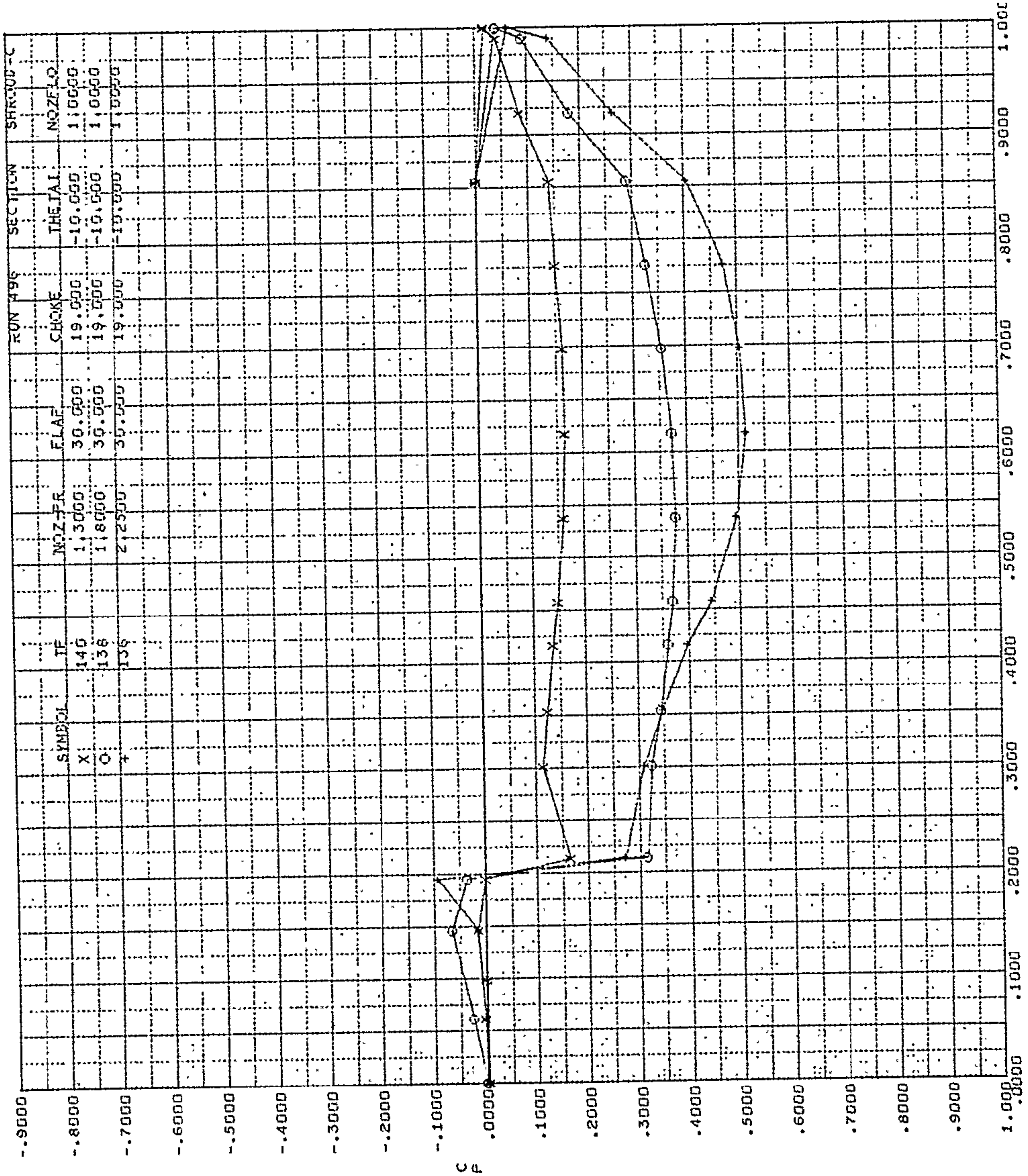

FIG. 161

BUFFALO - STATIC

MODIF. C8A MODEL - OUTBD NOZ.,NOZFLO
=0(DUAL),1(UPR),2(LWR)

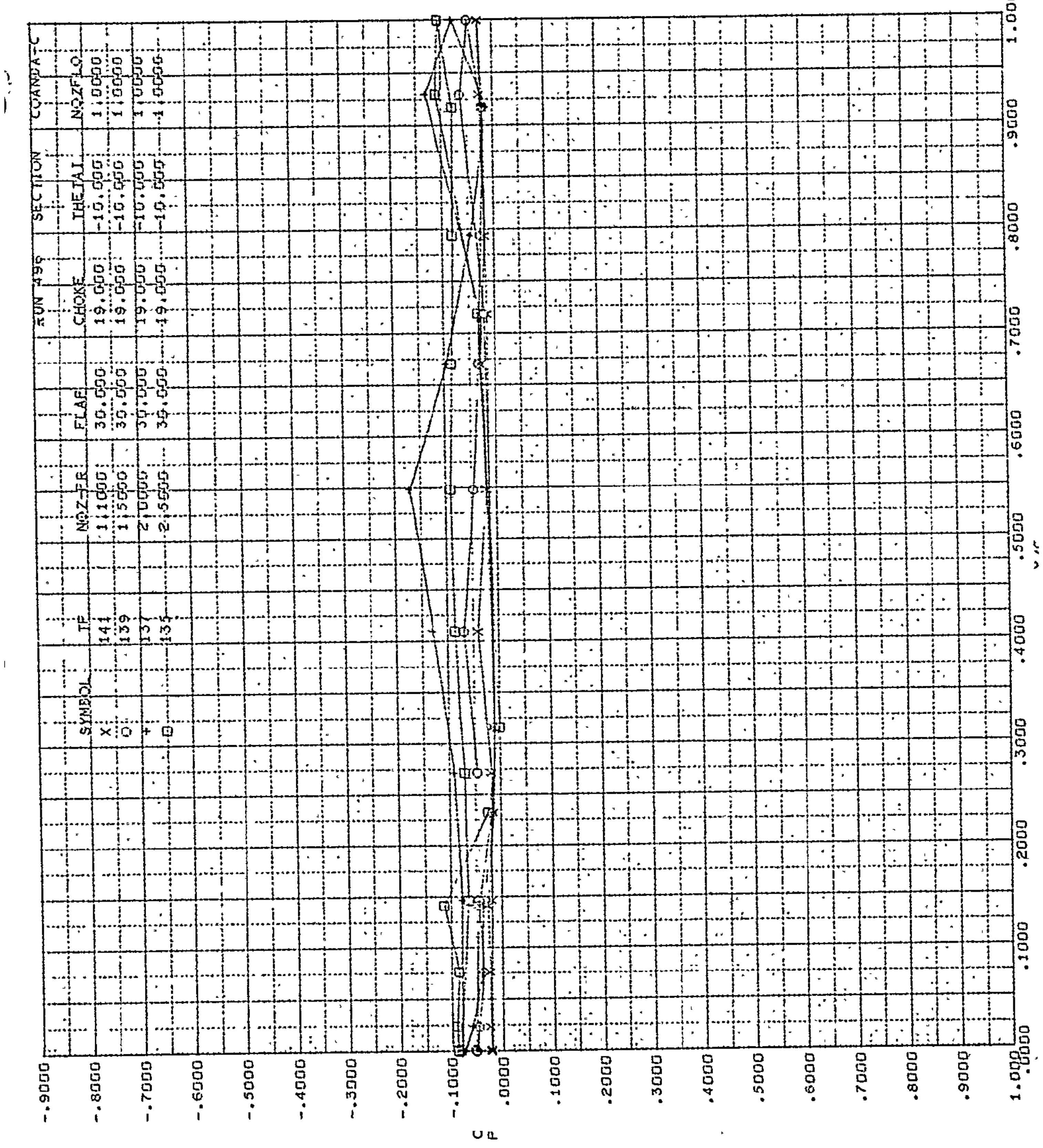

FIG. 162.

BUFFALO - STATIC

MODIF. C8A MODEL - OUTBD NOZ., NOZFLO
=0(DUAL), 1(UPR), 2(LWR)

D6-24850

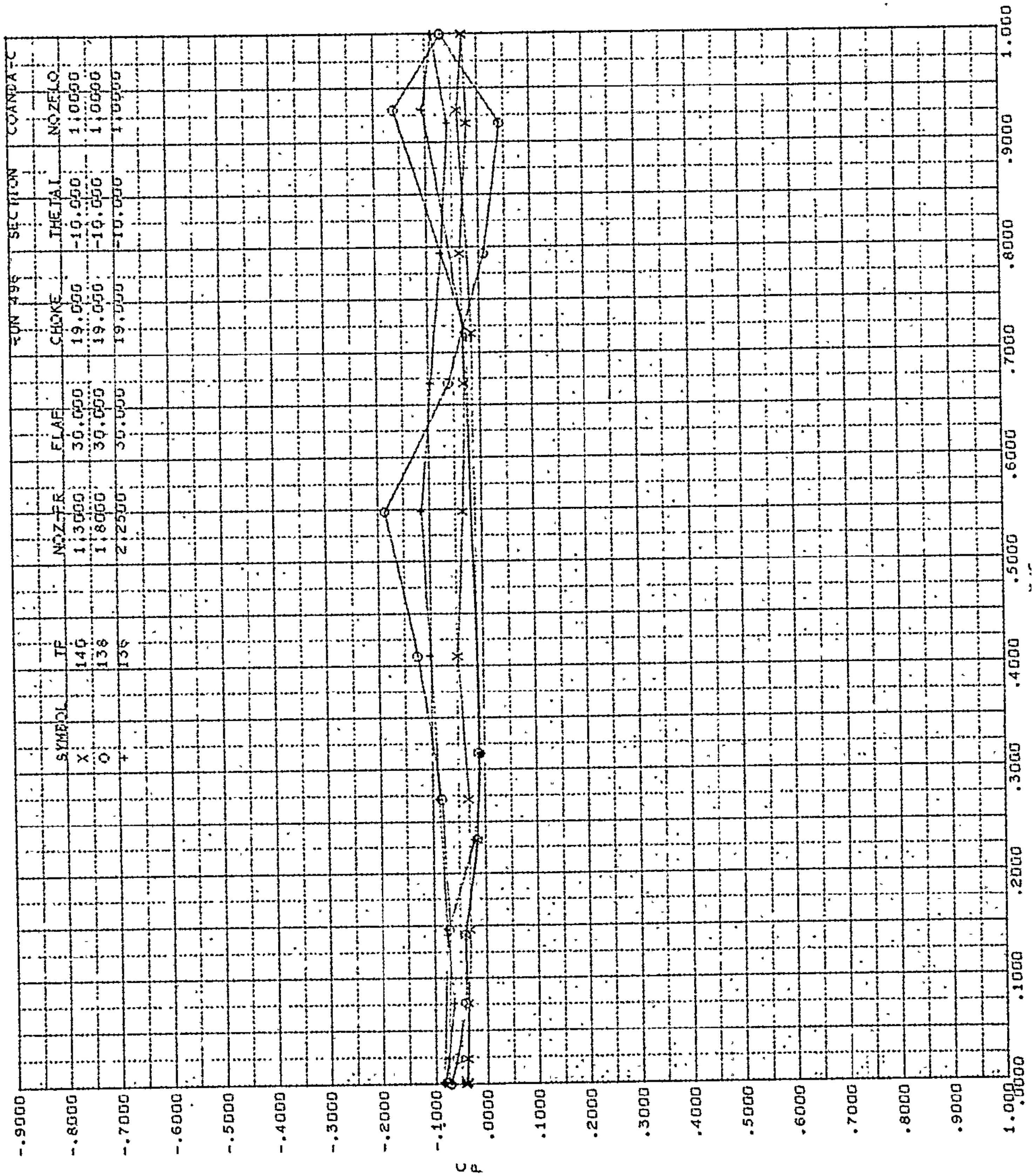

FIG. 163

BUFFALO - STATIC

MODIF. C8A MODEL - OUTBD NOZ.,NOZFLO
=0(DUAL),1(UPR),2(LWR)

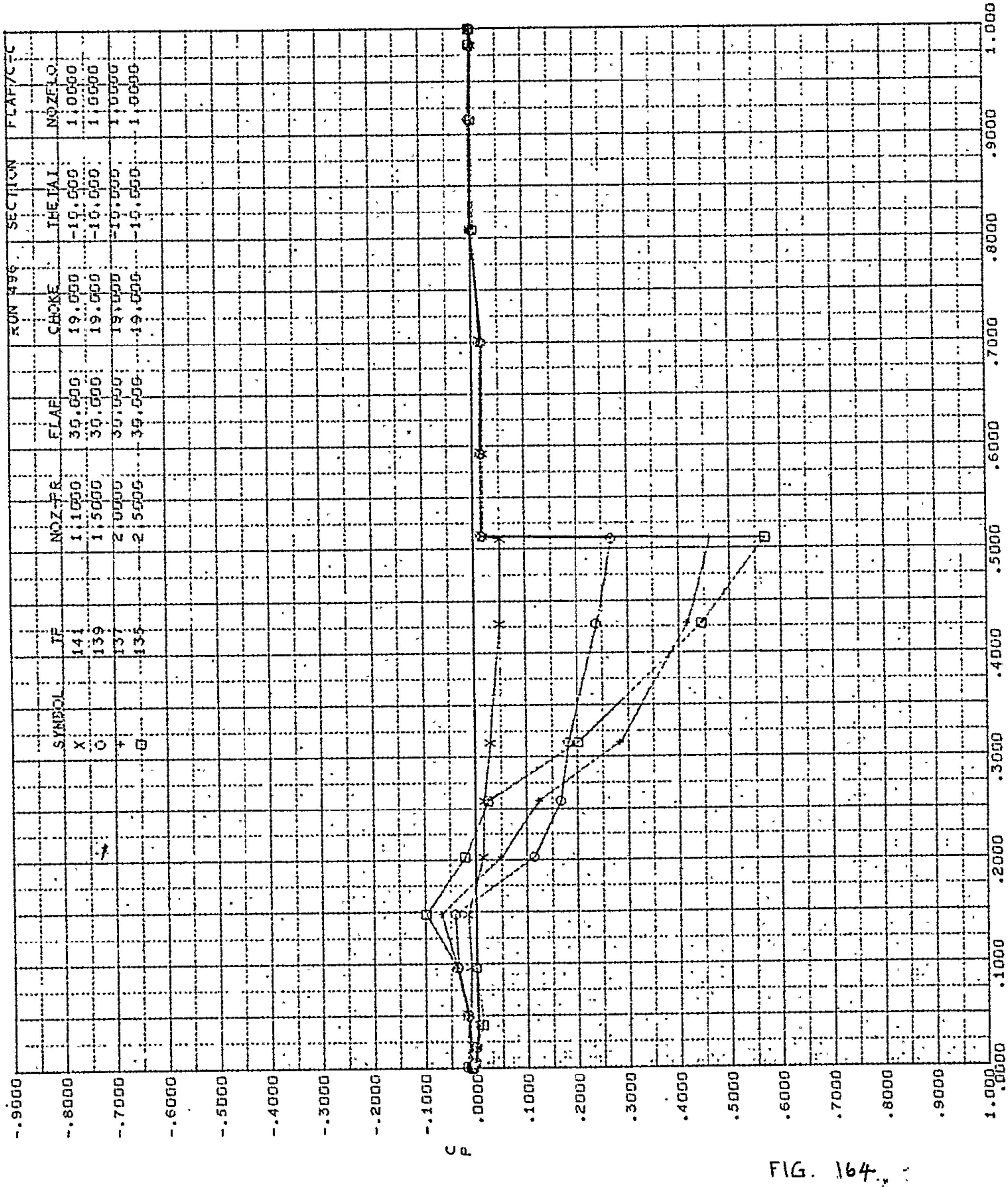

FIG. 164.

BUFFALO - STATIC

MODIF. C8A MODEL - OUTBD NOZ., NOZFLO =0(DUAL), 1(UPR), 2(LWR)

D6-24850

PAGE 246

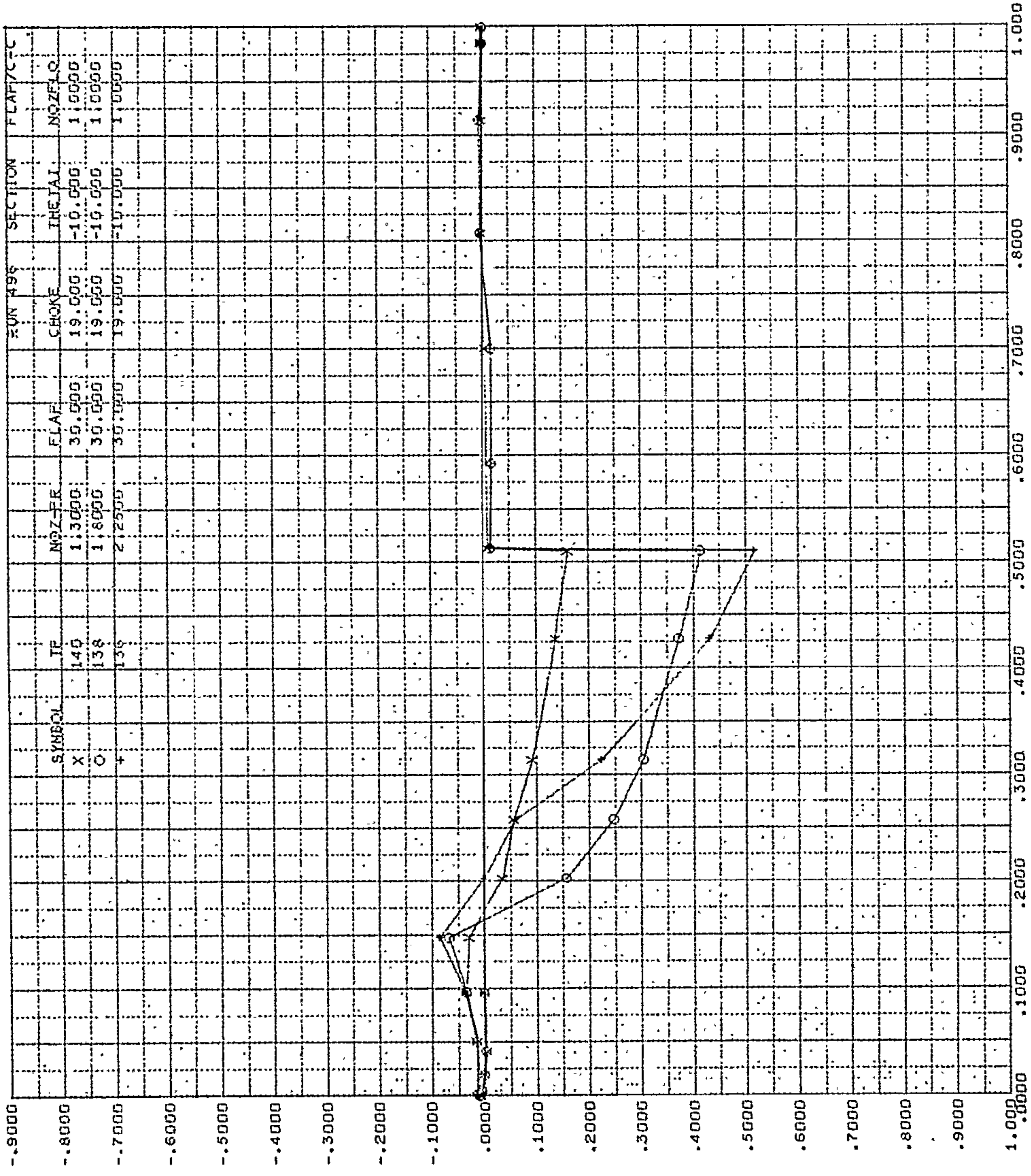

BUFFALO - STATIC

FIG. 165

MODIF. C8A MODEL - OUTBD NOZ.,NOZFLO =0(DUAL),1(UPR),2(LWR)

D6-24850

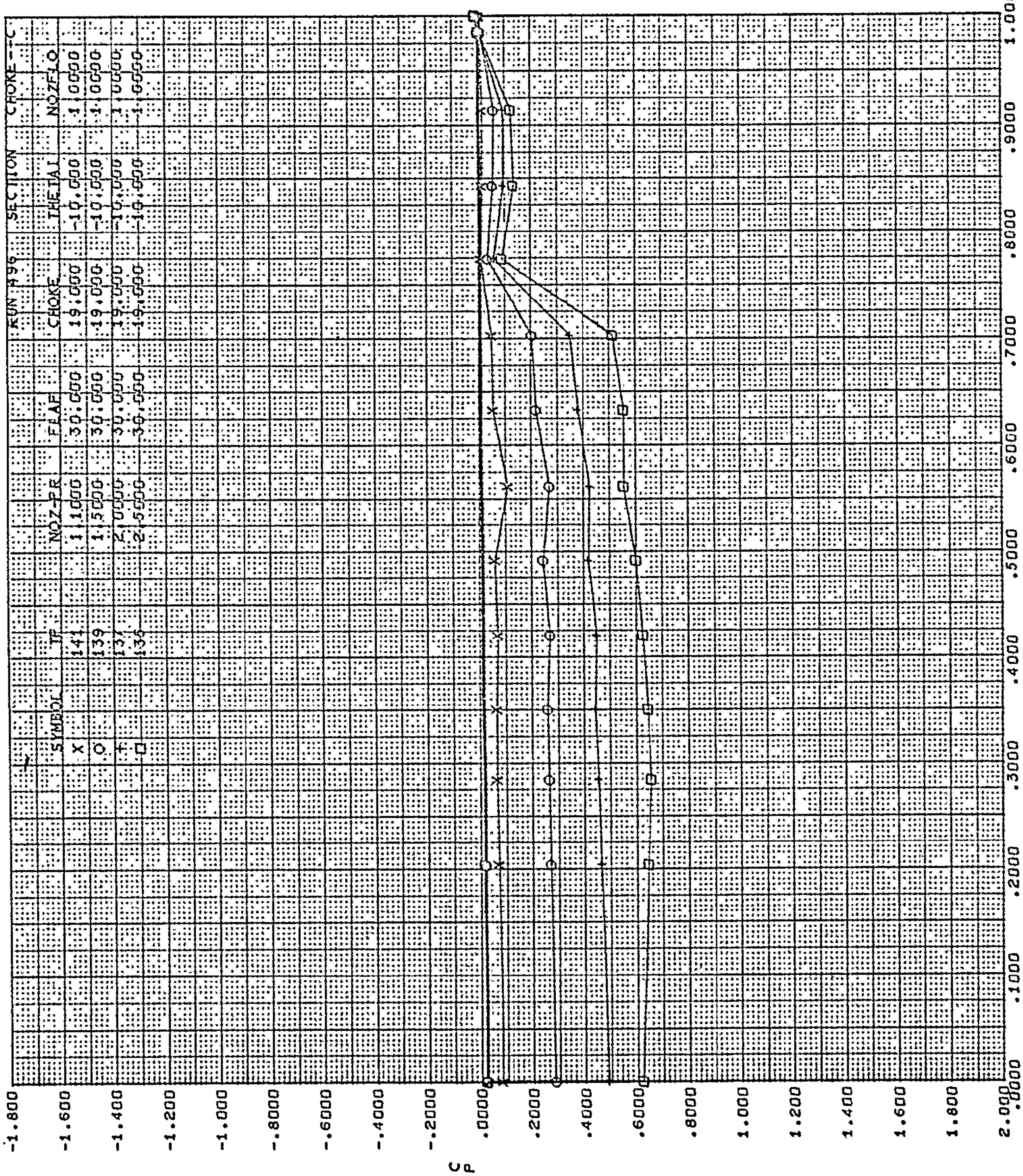

BUFFALO - STATIC

FIG. 166

MODIF. C8A MODEL - OUTBD NOZ.,NOZFLO =0(DUAL),1(UPR),2(LWR)

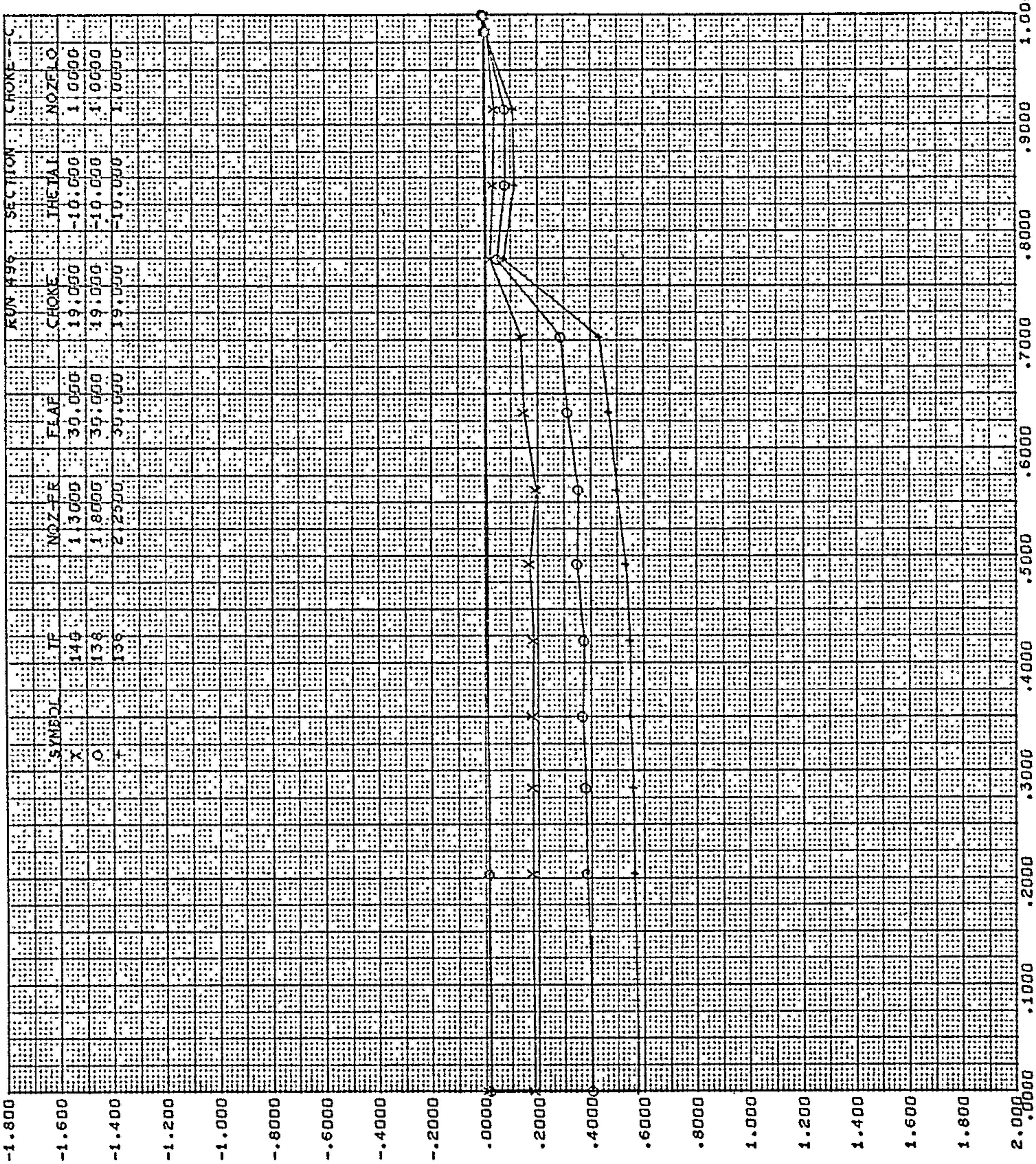

BUFFALO - STATIC

FIG. 167

MODIF. C8A MODEL - OUTBD NOZ.,NOZFLO
=0(DUAL),1(UPR),2(LWR)

7-249

11^

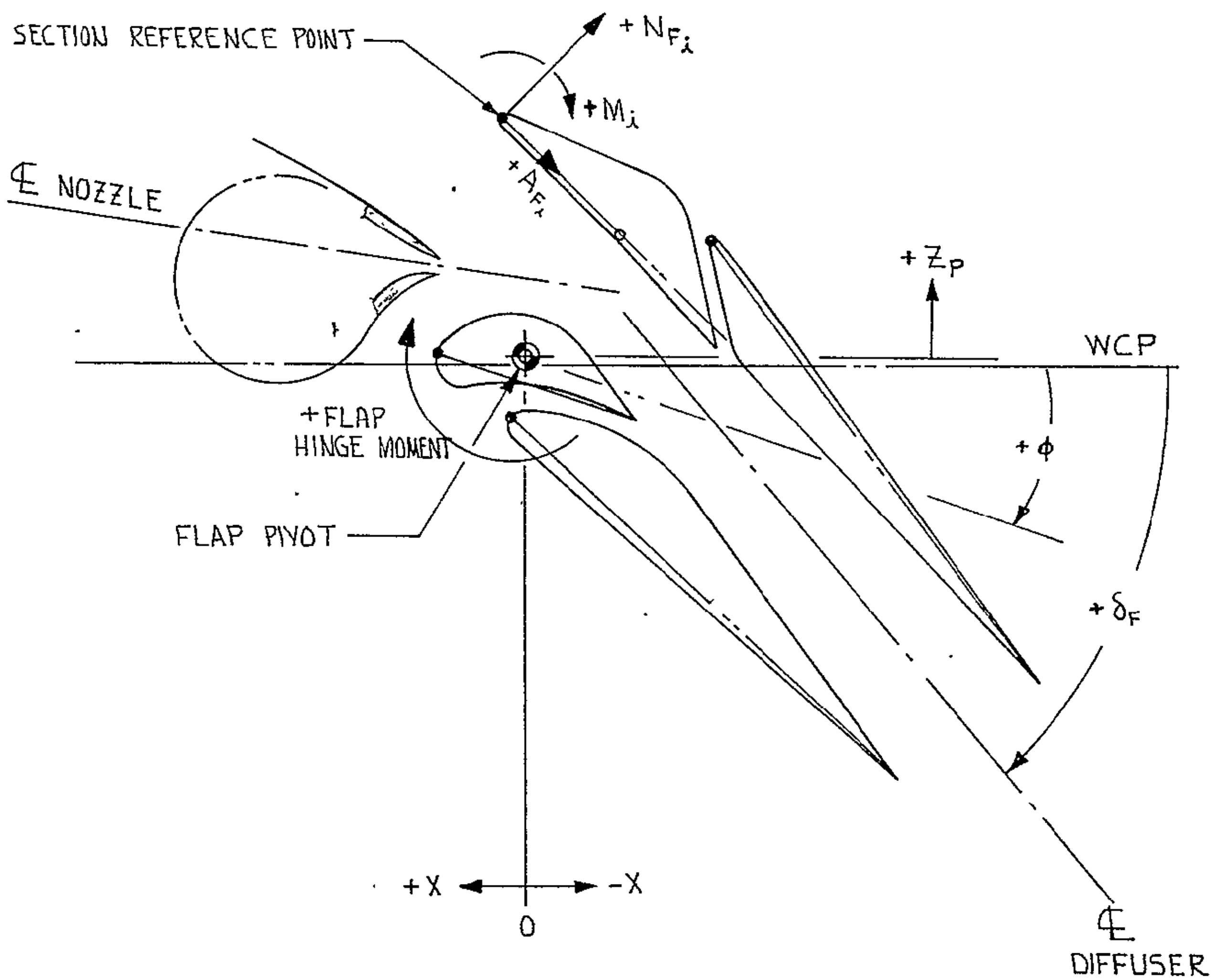

NOTE:

THE REFERENCE POINT OF EACH SECTION MUST BE LOCATED IN RELATION TO THE FLAP PIVOT BY X, Z_p AND ϕ.

FIG. 168

			REVISED	DATE		
CALC	F WRIGHT	3-23-71			SIGN CONVENTIONS FOR FLAP HINGE MOMENT DETERMINATION	MODIFIED C-8A
CHECK						D6-24850
APPD					THE BOEING COMPANY	PAGE 250
APPD						

FIGURE 169

DOUBLE NOZZLE

DOUBLE NOZZLE REPEAT

UPPER NOZZLE

FLAP STATIC HINGE MOMENTS

- ONE FLAP SEGMENT
- DOUBLE NOZZLE OPERATION
- FULL SCALE MODIFIED C-8A GEOMETRY

LEGEND	δ_F
————	6°
- - - - - -	20°
— - — -	30°
— — —	50°
— - - —	65°
—— - ——	75°

FLAPS 6°, 20°, 30°, 50°, 65° & 75°

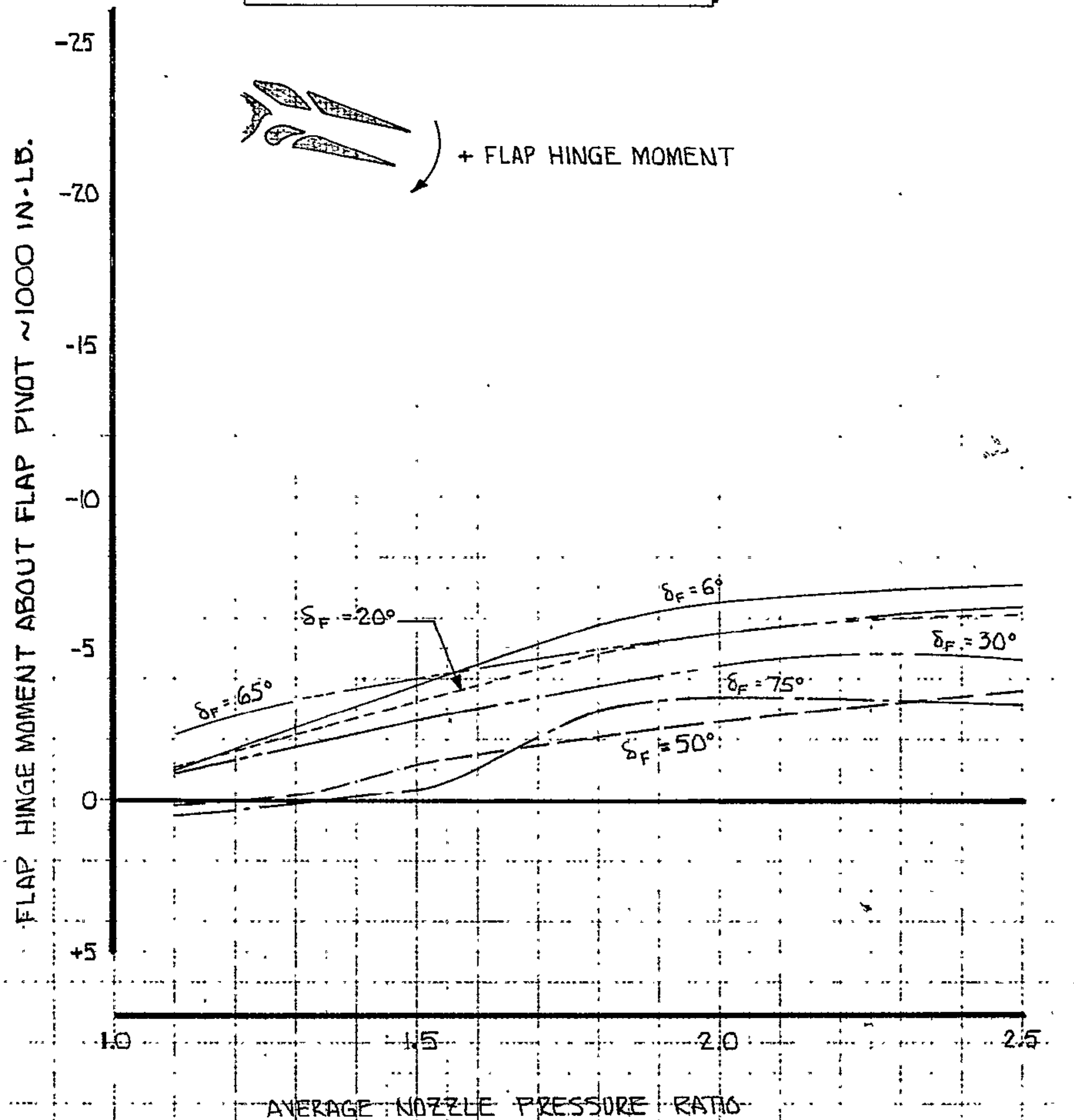

FIG. 170

CALC	F. WRIGHT	3-10-71	REVISED	DATE	AUGMENTOR FLAP STATIC TEST HINGE MOMENTS WITH CHOKE IN FAIRED POSITION	MODIFIED C-8A
CHECK						
APR						D6-24850
APR					THE BOEING COMPANY	PAGE 252

252

~~307~~

FLAP STATIC HINGE MOMENTS
- ONE FLAP SEGMENT
- DOUBLE NOZZLE OPERATION
- FULL SCALE MODIFIED C-8A GEOMETRY
- FLAPS 30°

FLAPS 30°

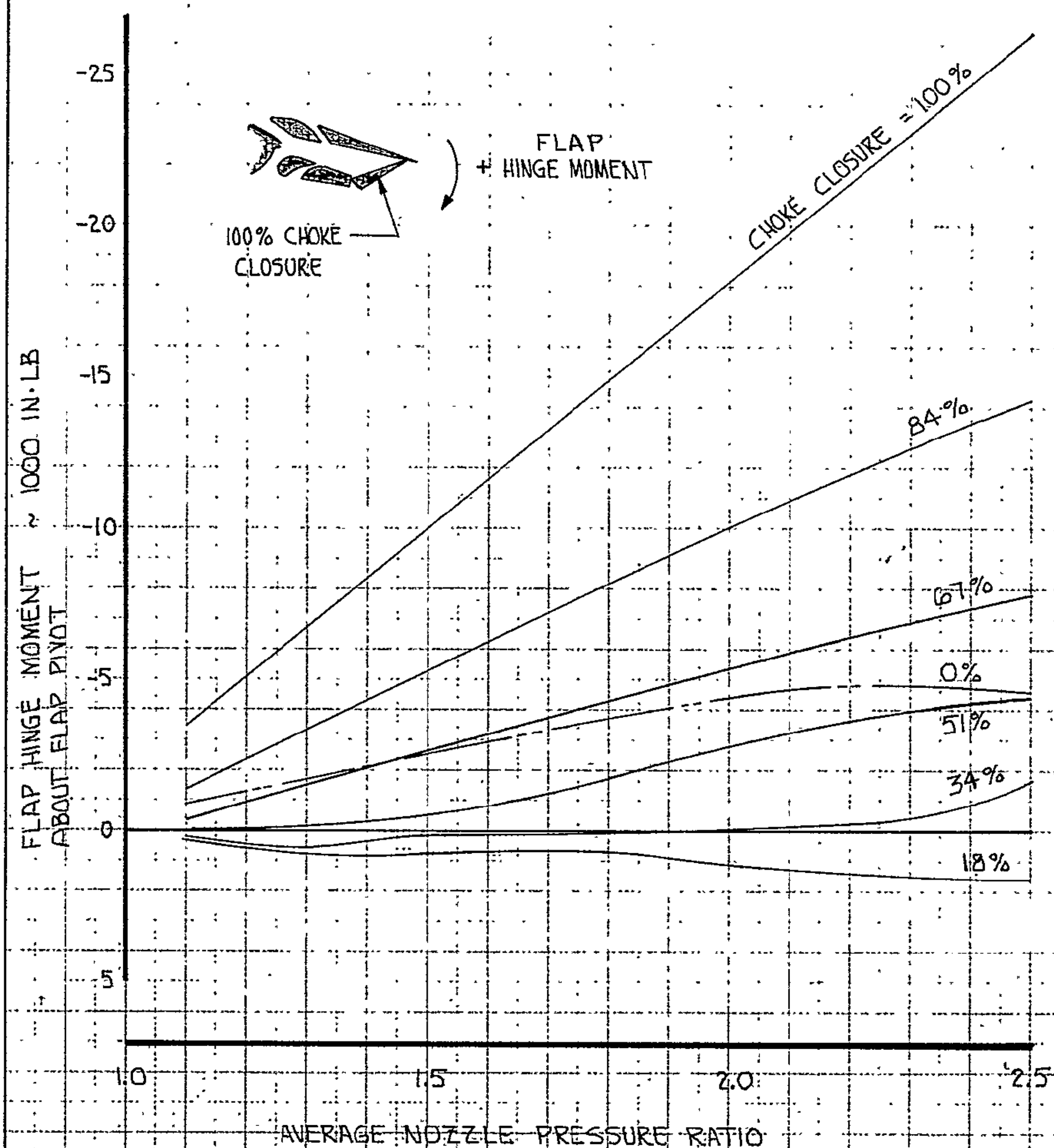

FIG. 171

CALC	F.WRIGHT	3·10·71	REVISED	DATE	EFFECT OF AUGMENTOR CHOKE ON STATIC TEST FLAP HINGE MOMENTS, FLAPS 30°	MODIFIED C-8A
CHECK						D6-24850
APR					THE BOEING COMPANY	PAGE 253
APR						

253

308

AD 461 C R6

K+E ALBANENE 195L 6 5 G-6000 TRACING PAPER

FLAPS 65°

FLAP STATIC HINGE MOMENTS
- ONE FLAP SEGMENT
- DOUBLE NOZZLE OPERATION
- FULL SCALE MODIFIED C-8A GEOMETRY
- FLAPS 65°

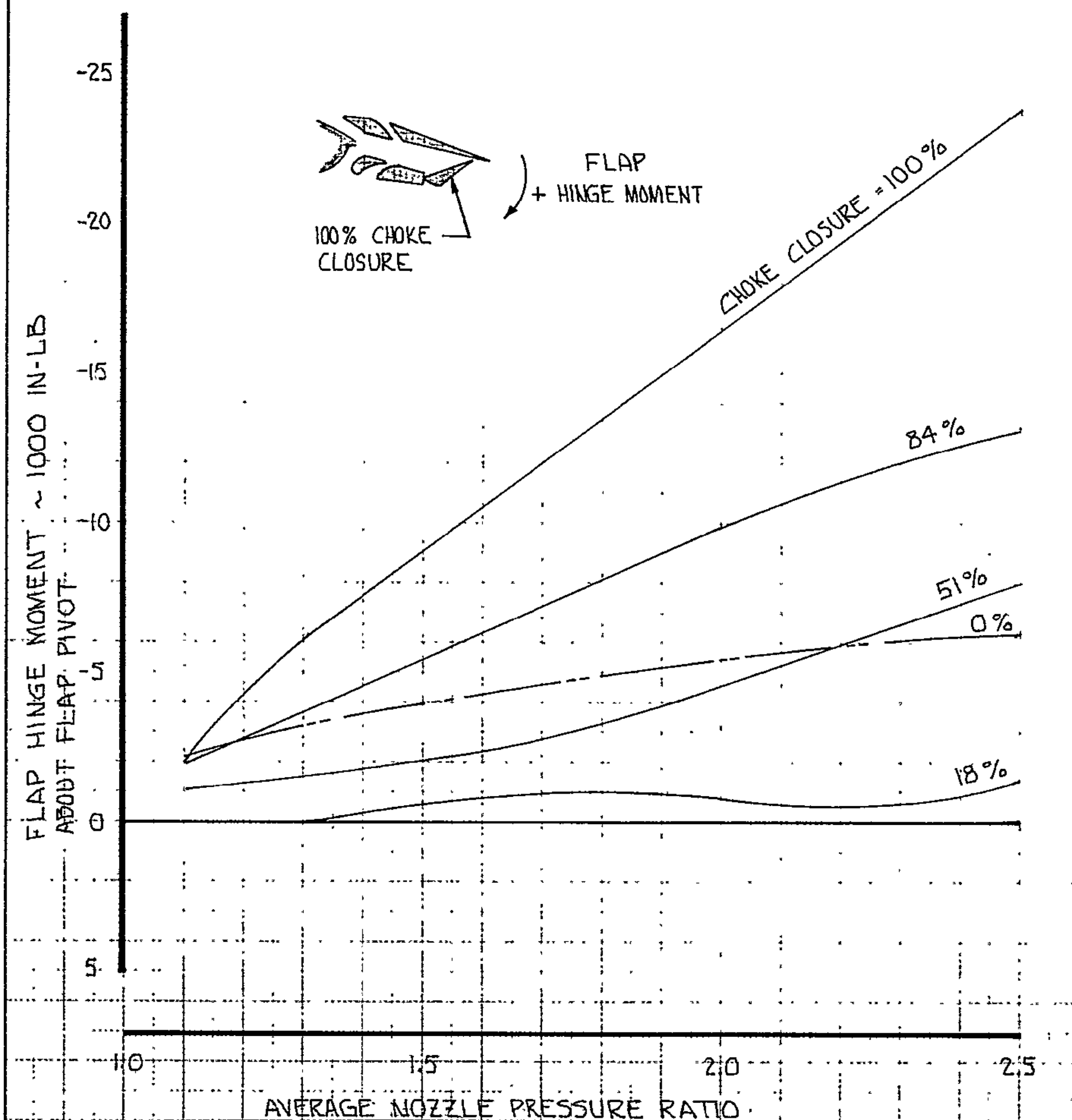

FIG. 172

CALC	F.WRIGHT	3-10-71	REVISED	DATE	EFFECT OF AUGMENTOR CHOKE ON STATIC TEST FLAP HINGE MOMENTS, FLAPS 65°	MODIFIED C-8A
CHECK						D6-24850
APR					THE BOEING COMPANY	PAGE 254
APR						

254

309

AD 461 C R6

K+E ALBANENE

0.7 SCALE STATIC TEST MODEL

- DIFFUSER ANGLE = 4°
- CHOKE CHORD = 13.03 IN. (MODEL SCALE)

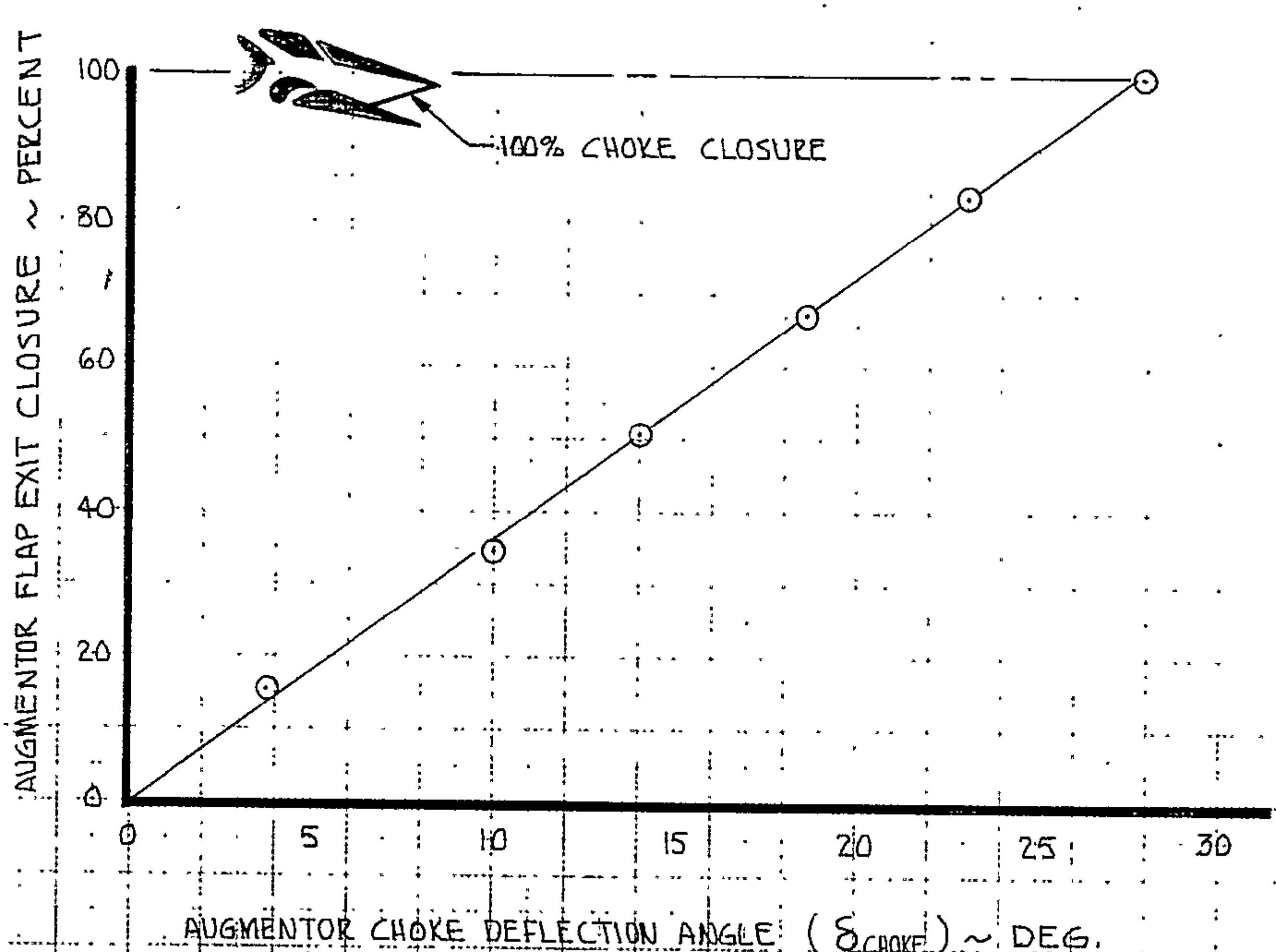

FIG. 173

CALC	F. WRIGHT	3-22-71	REVISED	DATE	RELATIONSHIP BETWEEN CHOKE DEFLECTION ANGLE AND PERCENT FLAP EXIT CLOSURE
CHECK					MODIFIED C-8A
APR					D6-24850
APR					THE BOEING COMPANY
					PAGE 255

255

310

AG 461 - R6

K+E ALBANENE 1956 5 - G-5000

CHOKE STATIC HINGE MOMENTS

- ONE CHOKE SEGMENT
- HINGE MOMENT ABOUT CHOKE L.E.
- DOUBLE NOZZLE OPERATION
- FULL SCALE MODIFIED C-8A GEOMETRY
- FLAPS 30°

FLAPS 30°

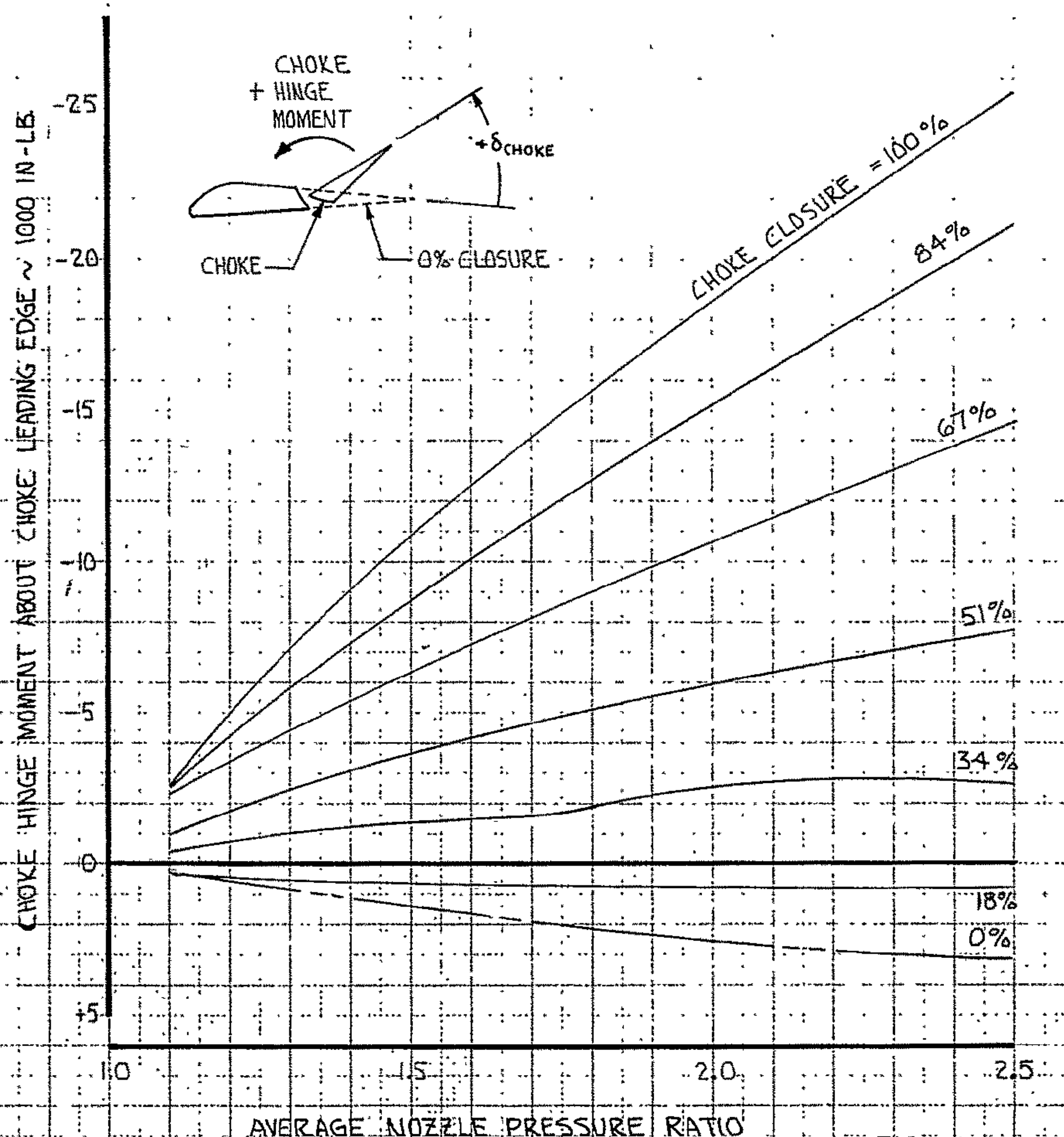

FIG. 174

CALC	F. WRIGHT	3-10-71	REVISED	DATE	STATIC TEST CHOKE HINGE MOMENTS ABOUT CHOKE LEADING EDGE, FLAPS 30°	MODIFIED C-8A
CHECK						
APR						D6-24850
APR					THE BOEING COMPANY	PAGE 256

256

344

AD 461 C-R6

K+E ALBANENE 1956 8 5 G-8000

CHOKE STATIC HINGE MOMENTS

FLAPS 65°

- ONE CHOKE SEGMENT
- HINGE MOMENT ABOUT CHOKE L.E.
- DOUBLE NOZZLE OPERATION
- FULL SCALE MODIFIED C-8A GEOMETRY
- FLAPS 65°

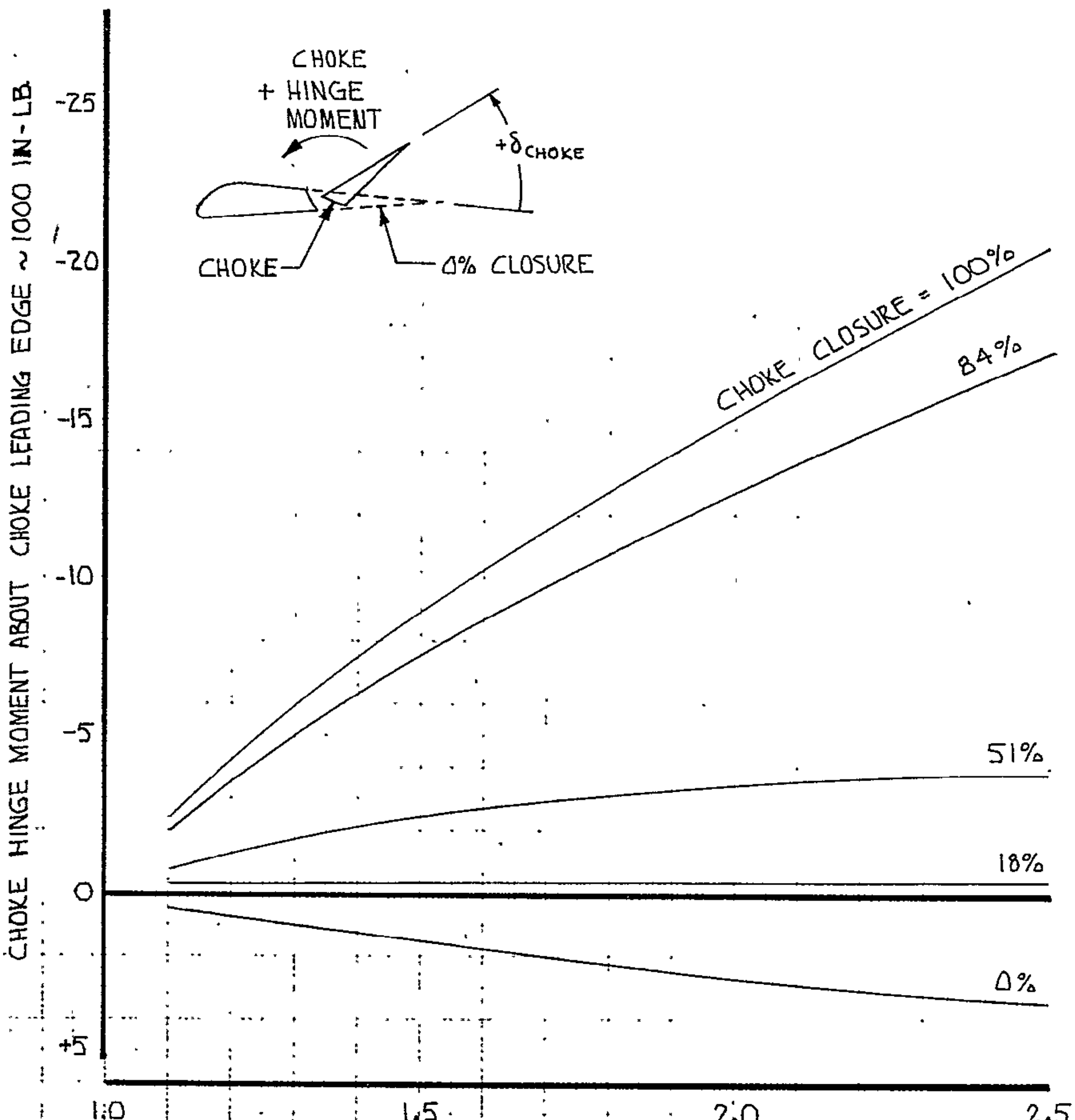

FIG. 175

CALC	F. WRIGHT	3-10-71	REVISED	DATE	STATIC TEST CHOKE HINGE MOMENTS ABOUT CHOKE LEADING EDGE, FLAPS 65°	MODIFIED C-8A
CHECK						D6-24850
APR						
APR					THE BOEING COMPANY	PAGE 257

257
~~312~~

K+E ALBANENE

CHOKE STATIC HINGE MOMENTS

- ONE CHOKE SEGMENT
- HINGE MOMENT ABOUT 26.2% CHOKE CHORD
- DOUBLE NOZZLE OPERATION
- FULL SCALE MODIFIED C-8A GEOMETRY
- FLAPS 30°

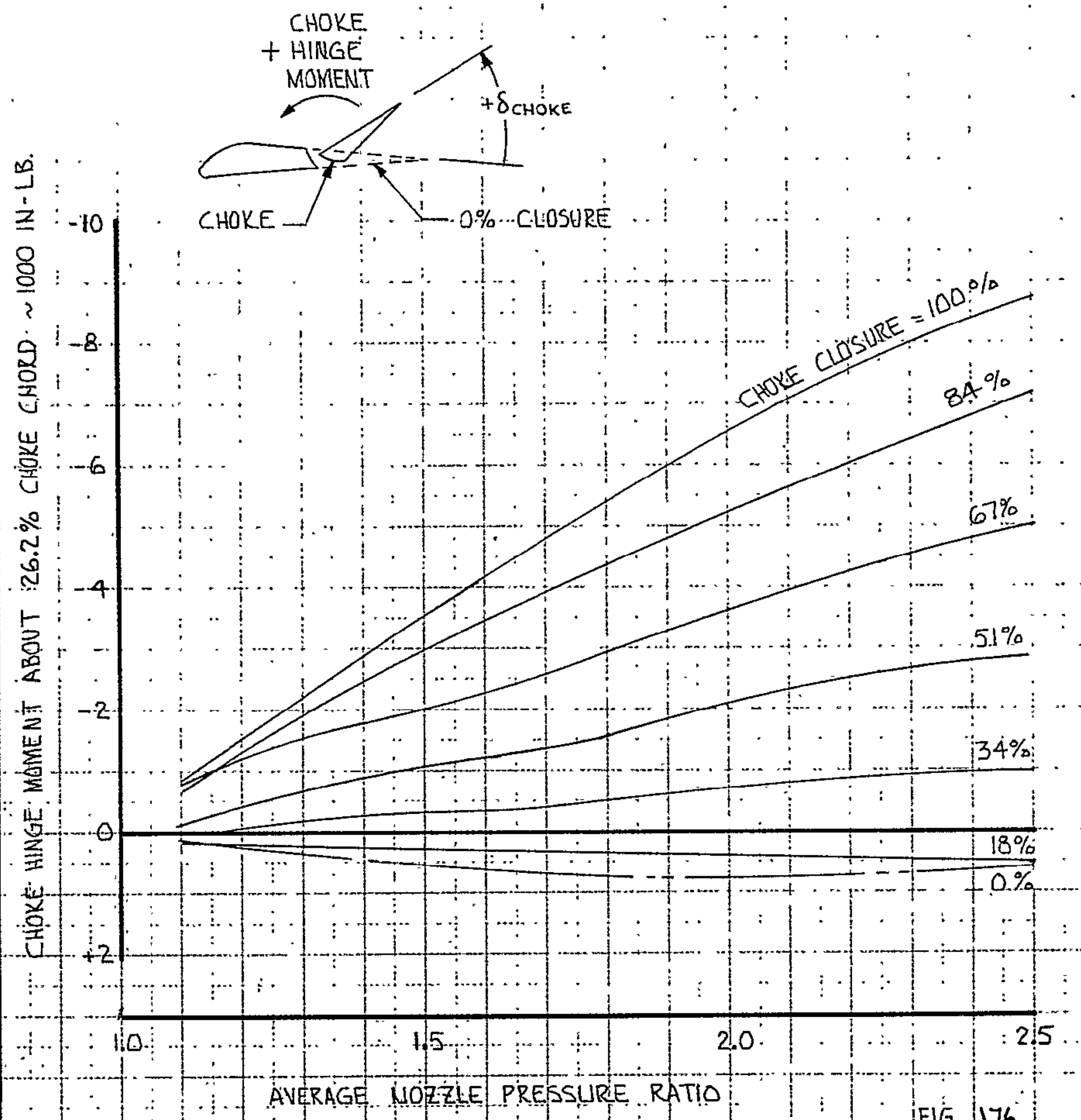

FIG. 176

CALC	F. WRIGHT	3-10-71	REVISED	DATE	STATIC TEST CHOKE HINGE MOMENTS ABOUT 26.2% CHOKE CHORD LINE, FLAPS 30°	MODIFIED C-8A
CHECK						
APR						D6-24850
APR					THE BOEING COMPANY	PAGE 258

258.
~~33~~

CHOKE STATIC HINGE MOMENTS

- ONE CHOKE SEGMENT
- HINGE MOMENT ABOUT 26.2% CHOKE CHORD
- DOUBLE NOZZLE OPERATION
- FULL SCALE MODIFIED C-8A GEOMETRY
- FLAPS 65°

FLAPS 65°

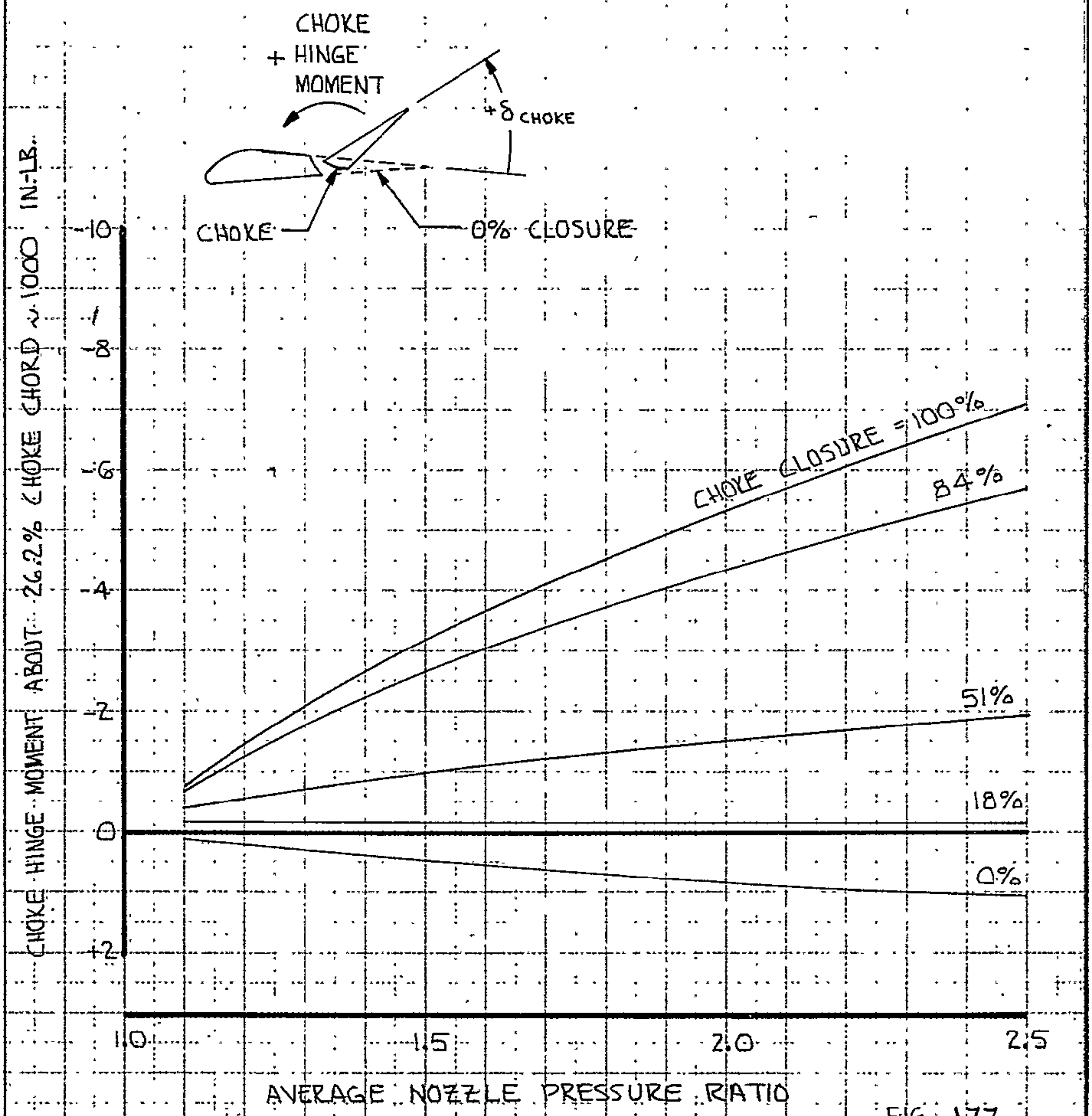

FIG. 177

CALC	F.WRIGHT	3.10.71	REVISED	DATE	STATIC TEST CHOKE HINGE MOMENTS ABOUT 26.2% CHOKE CHORD LINE, FLAPS 65°	MODIFIED C-8A
CHECK						D6-24850
APR					THE BOEING COMPANY	PAGE 259
APR						

259
~~310~~

AD 461 C-R6

K•E ALBANENE 195L 5 5 G-8000 TRACING PAPER

- BOEING 0.7 SCALE STATIC TEST
- DOUBLE NOZZLE OPERATION
- $S_{REF} = 424 \text{ FT}^2$
- EQUIVALENT DYNAMIC PRESSURE = 5.9 PSF
- C_{J_I} BASED ON ISENTROPIC THRUST OF 4 FLAP SEGMENTS

$$C_{J_I} = \frac{4\,(T_I)_{\text{ONE FLAP SEGMENT}}}{q \cdot S_{REF}}$$

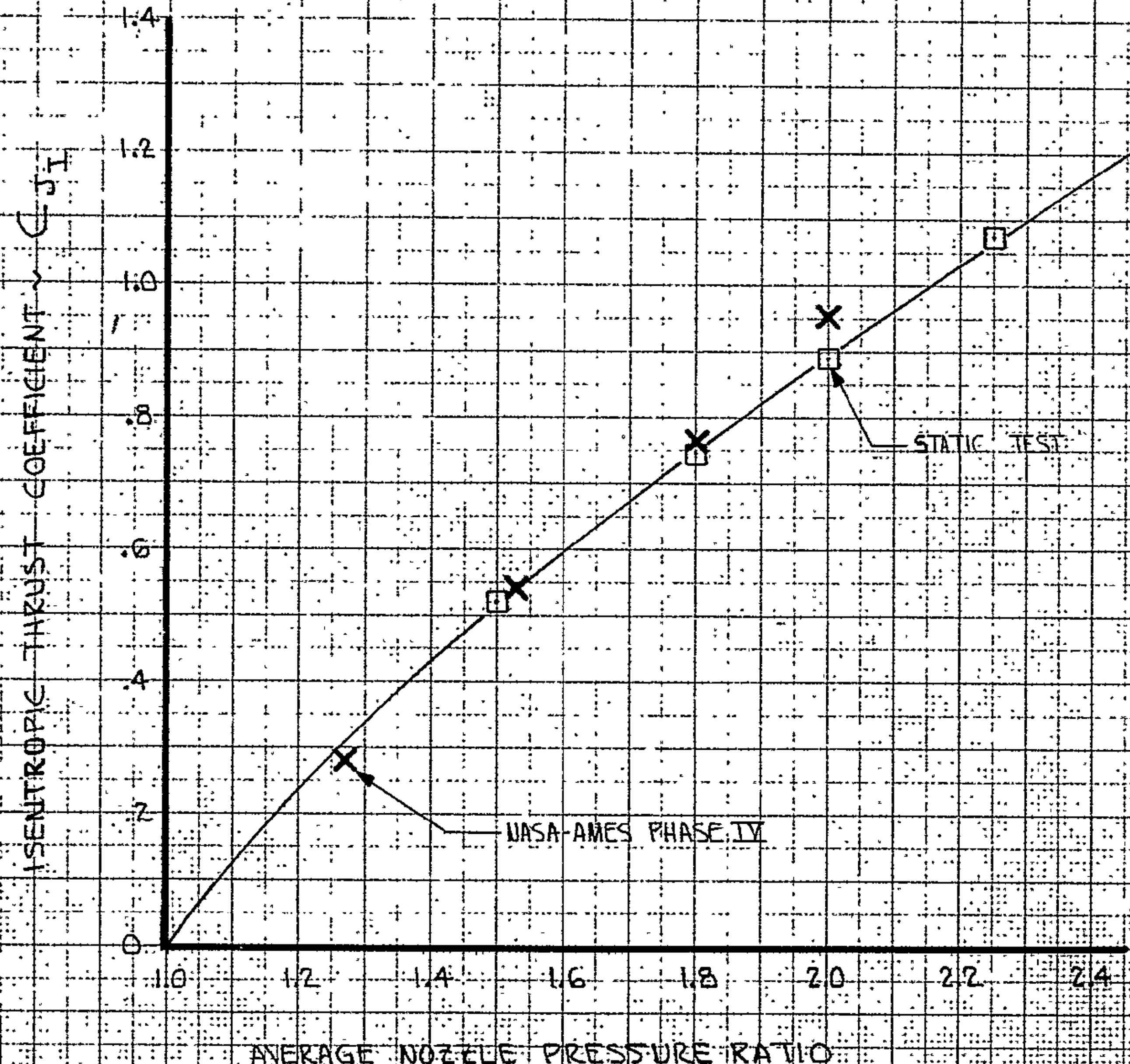

FIG. 178

CALC	F. WRIGHT	3·16·71	REVISED	DATE	VARIATION OF C_{J_I} WITH NOZZLE PRESSURE RATIO, STATIC TEST MODEL, EQUIVALENT DYNAMIC PRESSURE = 5.9 PSF	MODIFIED C-8A
CHECK						D6-24850
APR					THE BOEING COMPANY	PAGE 260
APR						

260
3.5

TD 461 C-R4

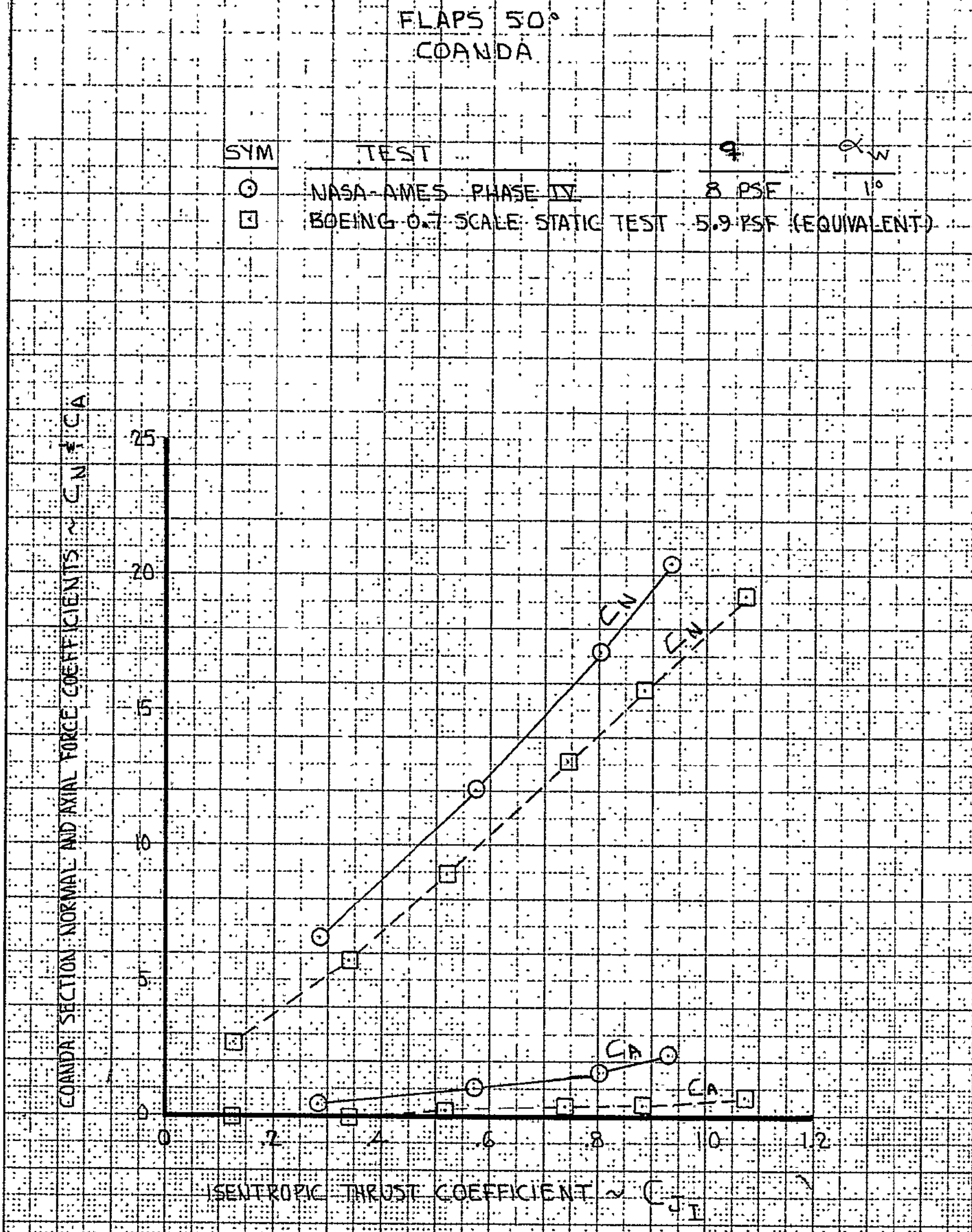

FIG. 179

CALC	F. WRIGHT	3-16-71	REVISED	DATE	COANDA SECTION C_N AND C_A VERSUS C_{J_I}, FLAPS 50°	MODIFIED C-8A
CHECK						D6-24850
APR					THE BOEING COMPANY	PAGE 261
APR						

261
~~315~~

AD 461 C-R6

K+E ALBANENE 195L 8.5 G-8000

FLAPS 50°
COANDA

SYM	TEST	q	α_W
○	NASA-AMES PHASE IV	8 PSF	1°
⊡	~~BOEING 0.7 SCALE STATIC TEST~~	~~5.9 PSF (EQUIVALENT)~~	

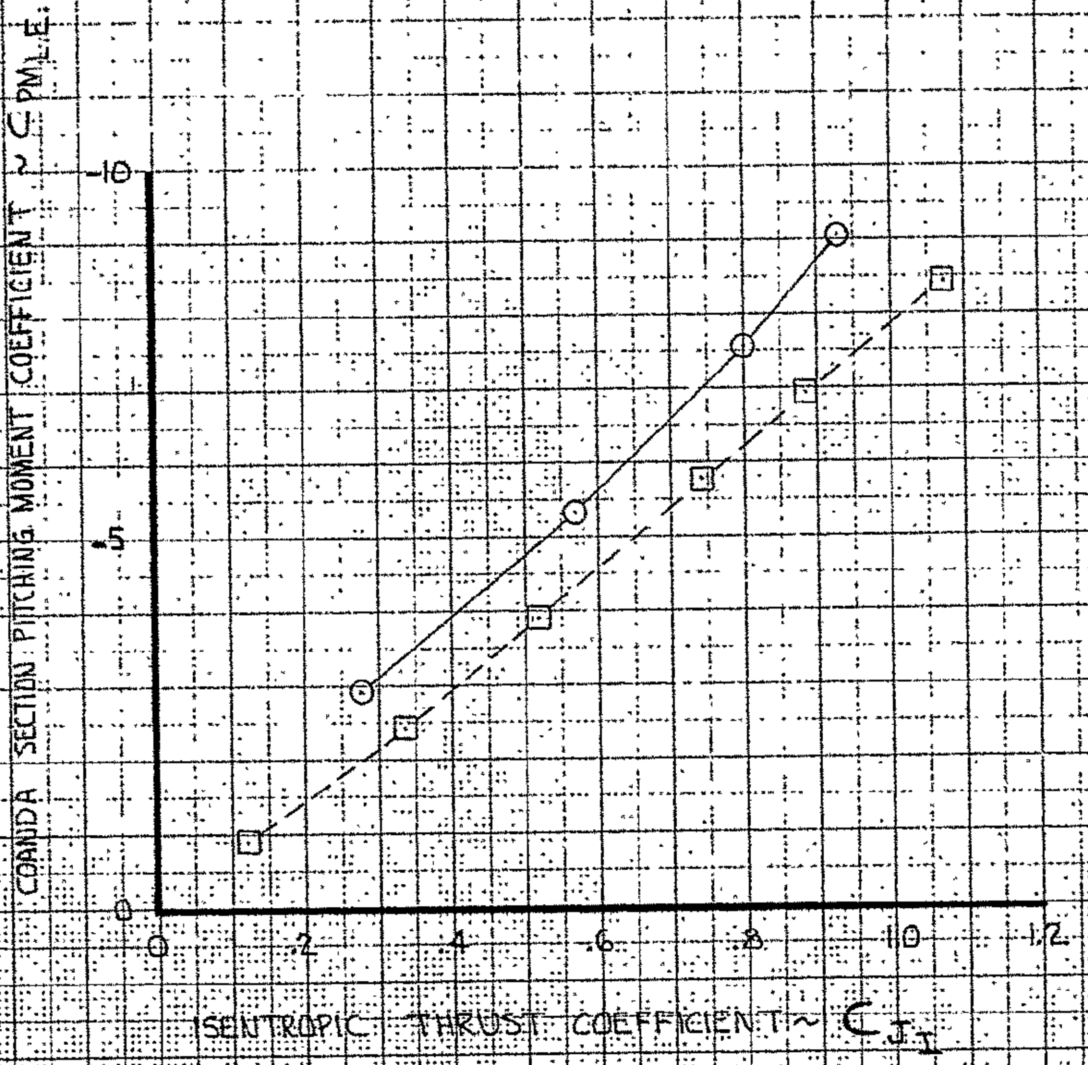

FIG. 180

CALC	F. WRIGHT	3-16-71	REVISED	DATE
CHECK				
APR				
APR				

COANDA SECTION $C_{PM_{L.E.}}$ VERSUS C_{J_I}, FLAPS 50°

MODIFIED C-8A

D6-24850

THE BOEING COMPANY

262
~~317~~

AD 461 C-R6

K·E ALBANENE 195L 8.5 G-8000 TRACING PAPER

FLAPS 50°
FLAP SEGMENT

SYM	TEST	q	α_W
⊙	NASA-AMES PHASE IV	8 PSF	1°
⊡	BOEING 0.7 SCALE STATIC TEST	5.9 PSF (EQUIVALENT)	

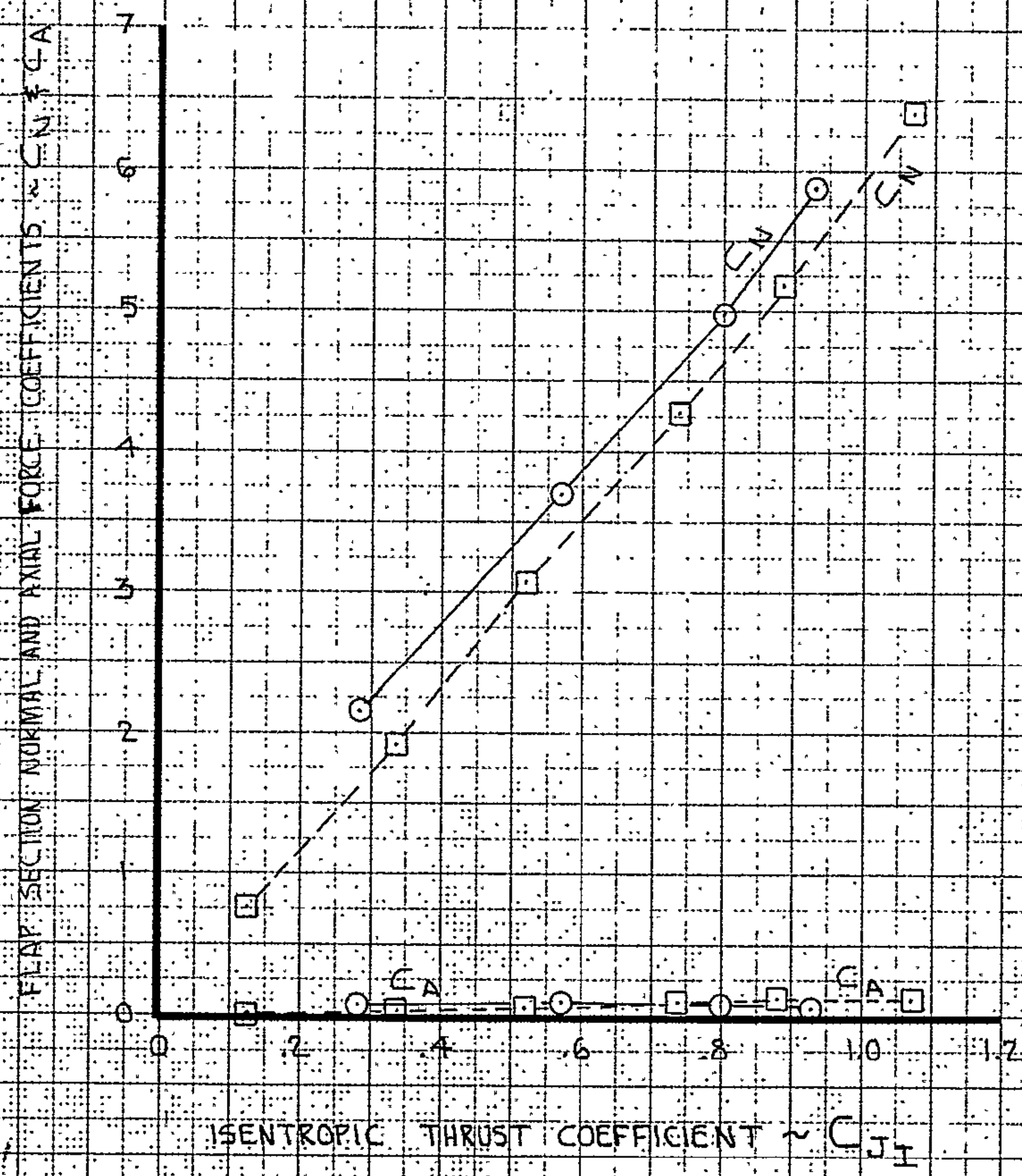

FIG. 181

CALC	F. WRIGHT	3-16-71	REVISED	DATE	FLAP SEGMENT SECTION C_N AND C_A VERSUS C_{J_I}, FLAPS 50°
CHECK					
APR					THE BOEING COMPANY
APR					

MODIFIED C-8A

D6-24850

263

3

FLAPS 50°

FLAP SEGMENT

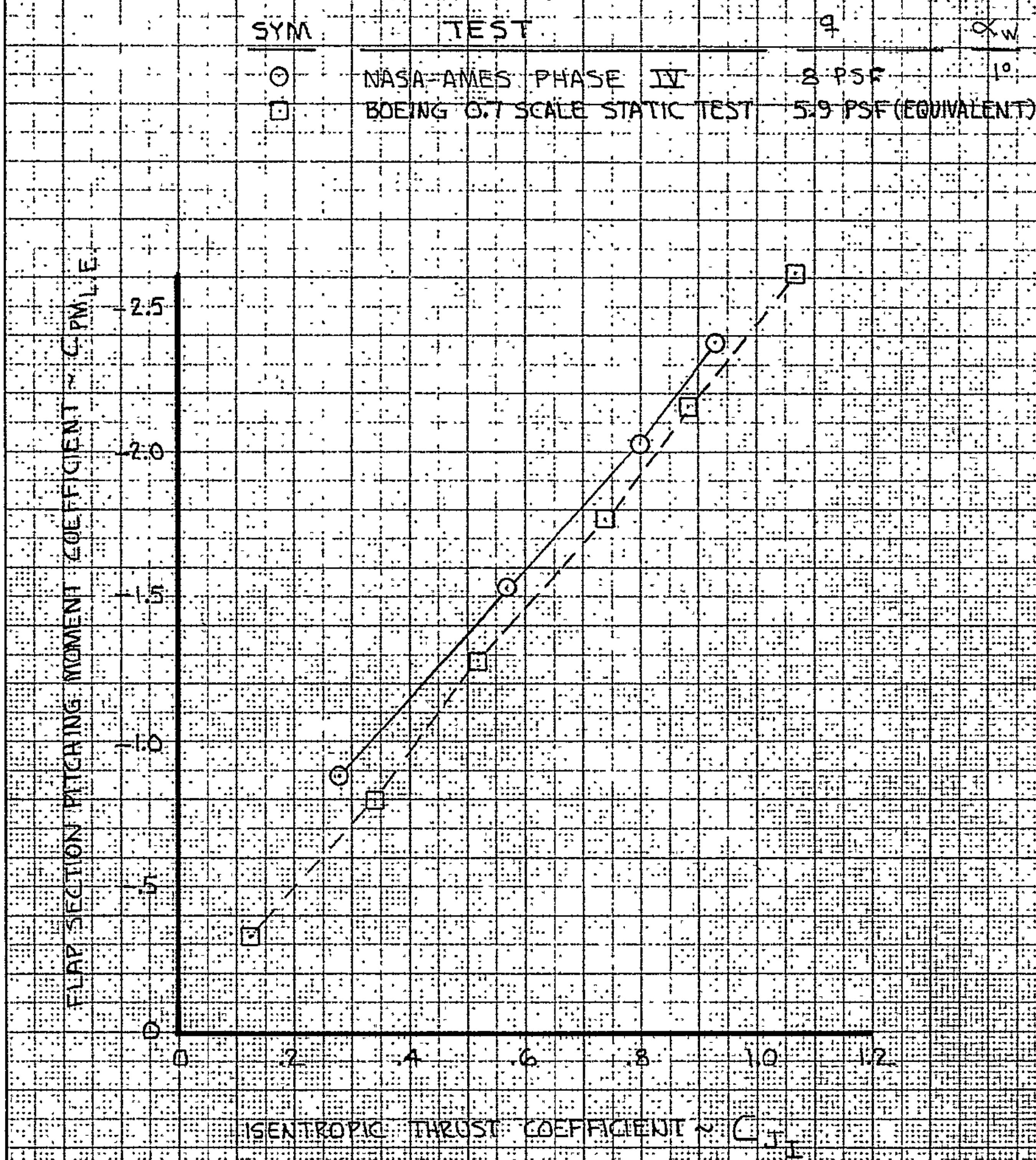

FIG. 182

CALC	F. WRIGHT	3-16-71	REVISED	DATE	FLAP SEGMENT SECTION $C_{PM_{L.E.}}$ VERSUS C_{J_I}, FLAPS 50°	MODIFIED C-8A
CHECK						D6-24850
APR					THE BOEING COMPANY	PAGE 264
APR						

264

~~319~~

TD 461 C-R4

K·E ALBANENE 195L TRACING PAPER

FLAPS 50°
SHROUD

SYM	TEST	q	α_W
⊙	NASA AMES PHASE IV	8 PSF	1°
⊡	BOEING 0.7 SCALE STATIC TEST	5.9 PSF (EQUIVALENT)	

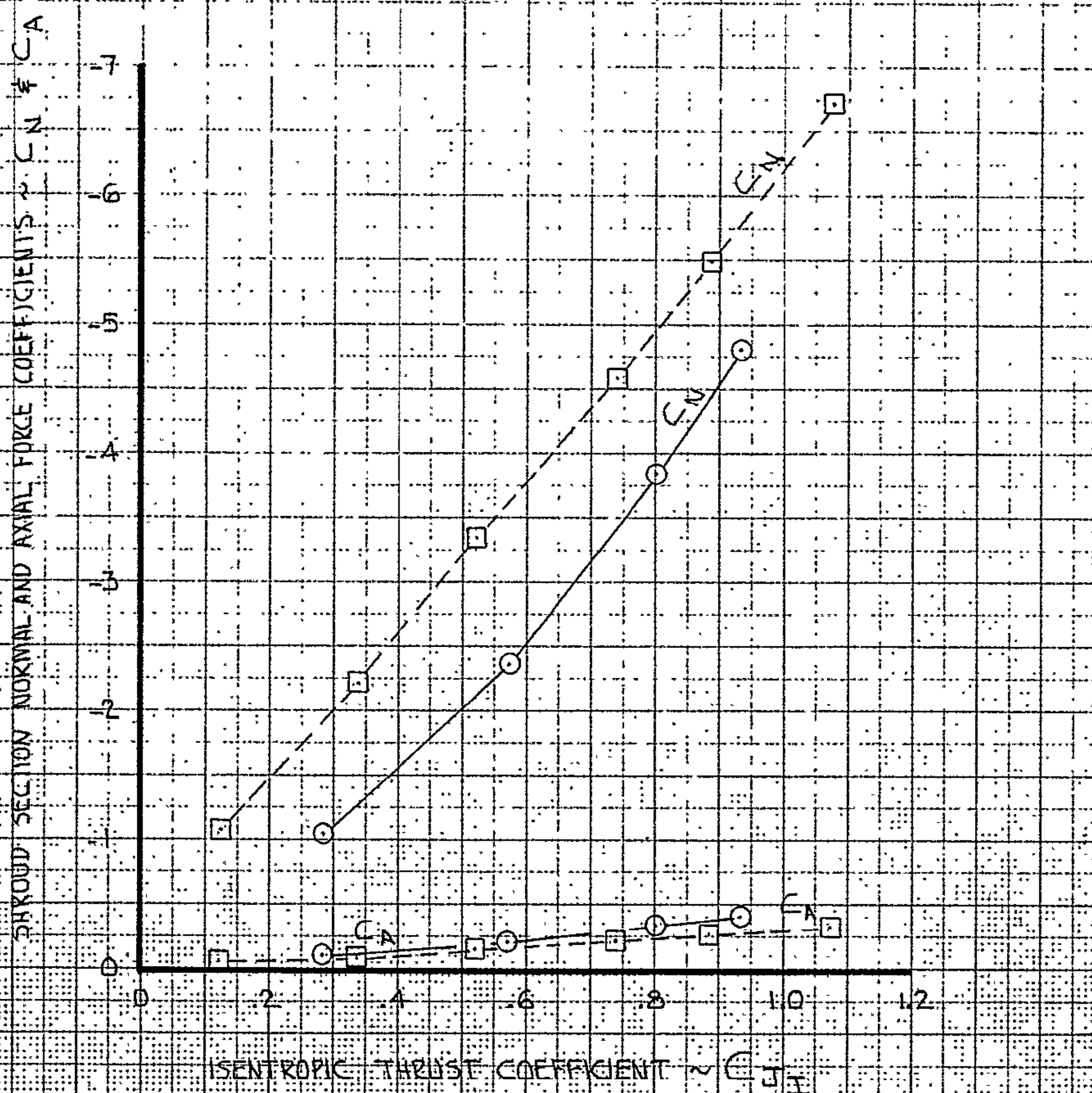

FIG. 183

CALC	F. WRIGHT	3-16-71	REVISED	DATE	SHROUD SECTION C_N AND C_A VERSUS C_{J_I}, FLAPS 50°	MODIFIED C-8A
CHECK						D6-24850
APR					THE BOEING COMPANY	PAGE 265
APR						

265

300

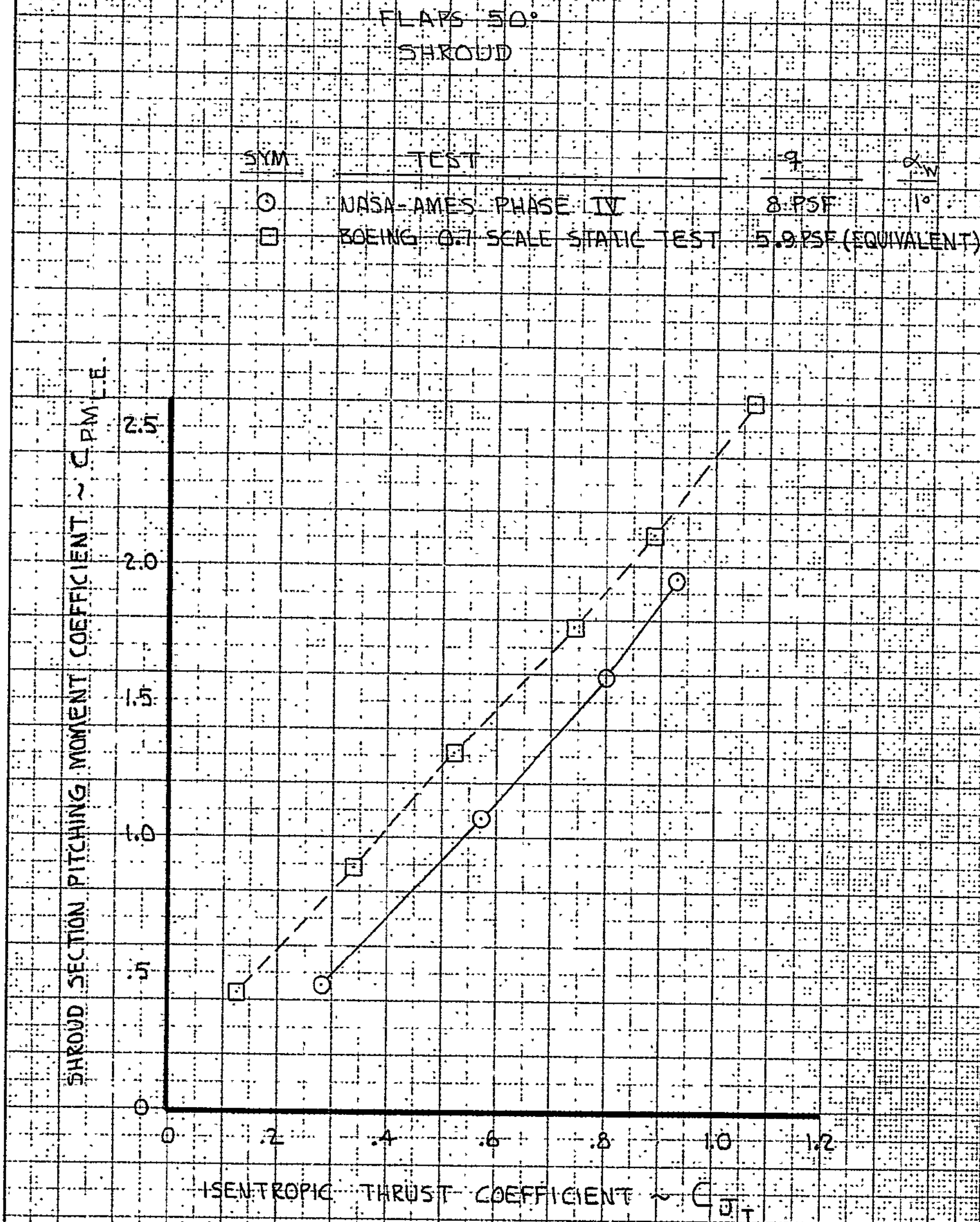

FIG. 184

CALC	F. WRIGHT	3-16-71	REVISED	DATE	SHROUD SECTION $C_{PM_{L.E.}}$ VERSUS C_{J_I} FLAPS 50°	MODIFIED C-8A
CHECK						D6-24850
APR					THE BOEING COMPANY	PAGE 266
APR						

266

321

TD 461 C-R4

K+E ALBANENE 195L TRACING PAPER

FLAPS 75°
SHROUD

SYM	TEST	q	α_W
⊙	NASA-AMES PHASE IV	8 PSF	1°
⊡	BOEING 0.7 SCALE STATIC TEST	5.9 PSF (EQUIVALENT)	

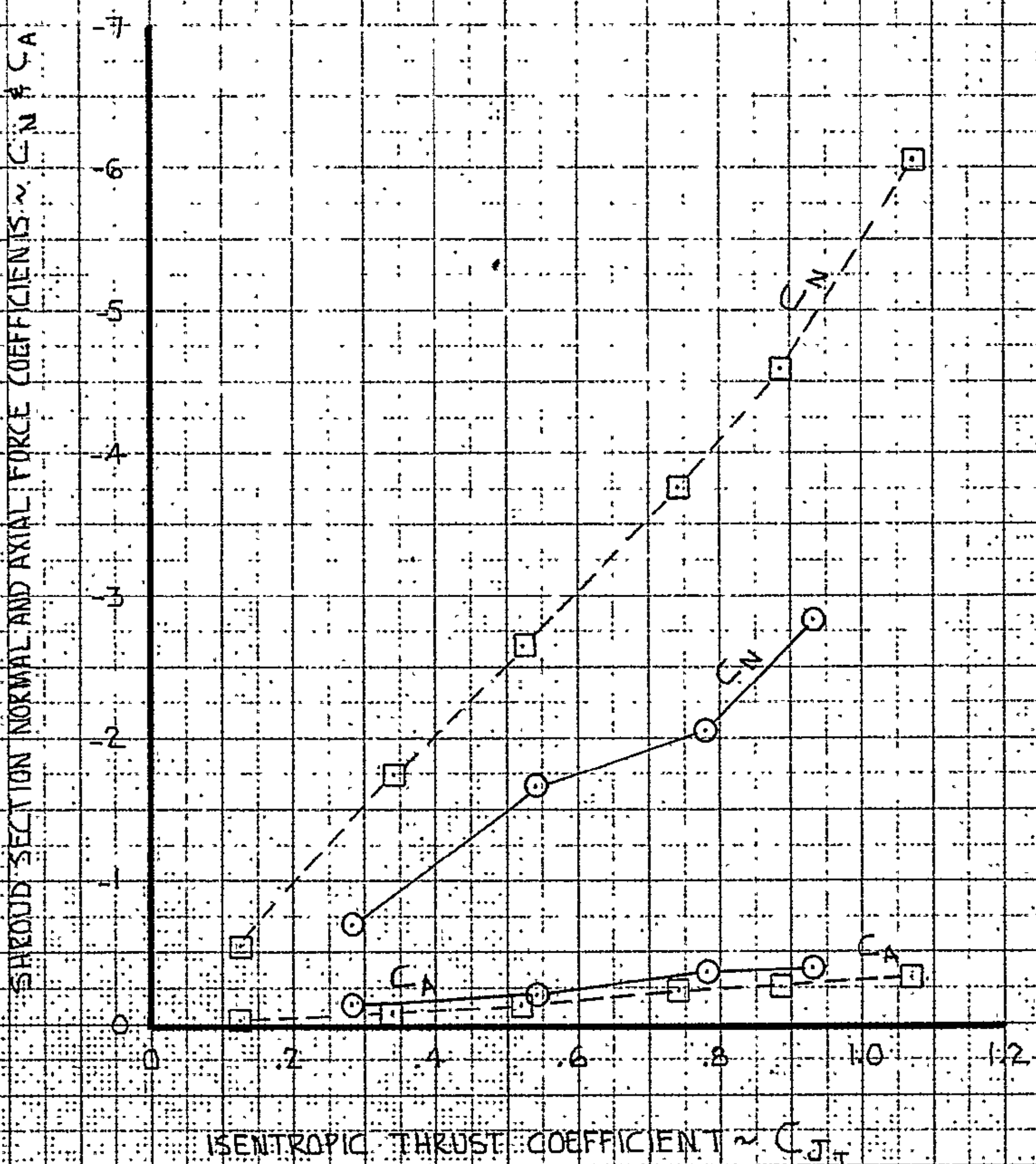

FIG. 185

CALC	F. WRIGHT	3-16-71	REVISED	DATE	SHROUD SECTION C_N AND C_A VERSUS C_{J_I}, FLAPS 75°	MODIFIED C-8A
CHECK						D6-24850
APR						
APR					THE BOEING COMPANY	PAGE 267

267
~~333~~

FLAPS 75°
SHROUD

SYM	TEST	q	α_W
⊙	NASA-AMES PHASE IV	8 PSF	1°
⊡	BOEING 0.7 SCALE STATIC TEST	5.9 PSF (EQUIVALENT)	

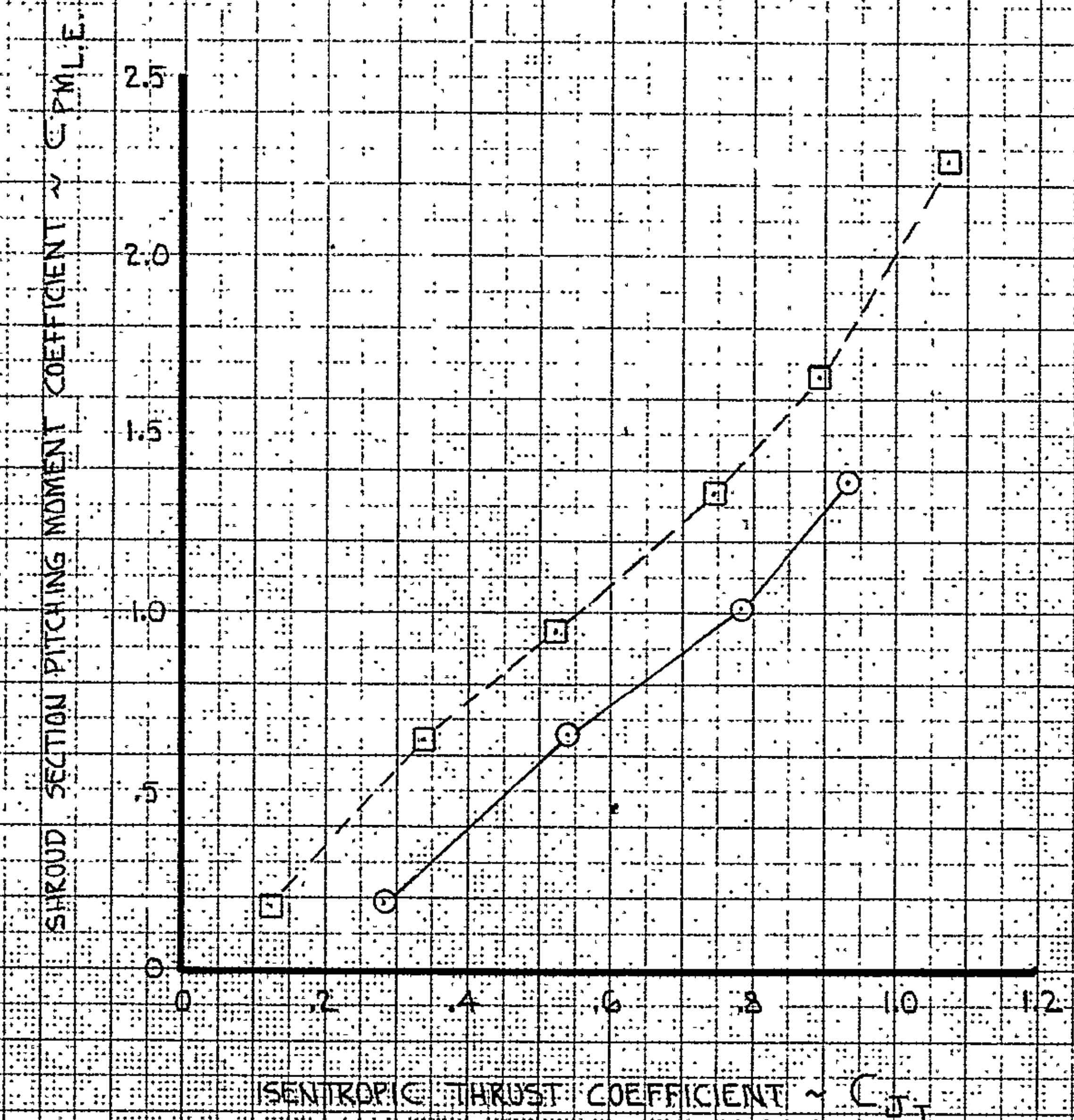

FIG. 186

CALC	F. WRIGHT	3-16-71	REVISED	DATE	SHROUD SECTION $C_{PM_{L.E.}}$ VERSUS C_{J_I}, FLAPS 75°	MODIFIED C-8A
CHECK						D6-24850
APR					THE BOEING COMPANY	PAGE 268
APR						

AD 461 C R6

268
323

K+E ALBANENE 1956 85 G-8000

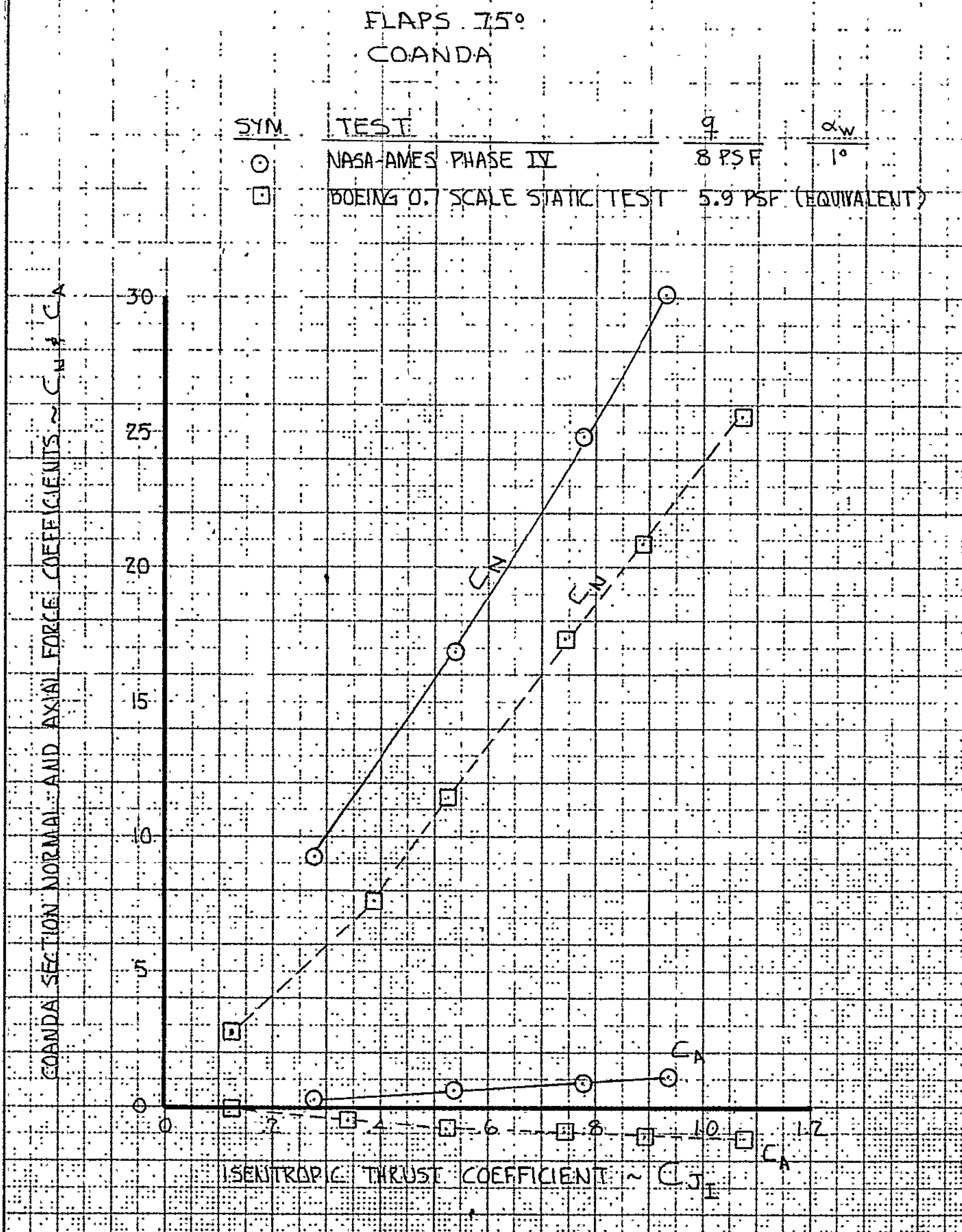

FIG. 187

CALC	F. WRIGHT	3-16-71	REVISED	DATE	COANDA SECTION C_N AND C_A VERSUS C_{J_I}, FLAPS 75°
CHECK					MODIFIED C-8A
APR					D6-24850
APR					THE BOEING COMPANY
					PAGE 269

269
32~~4~~

AD 461 C-R6

K•E ALBANENE 195L 8 5 G-8000 TRACING PAPER

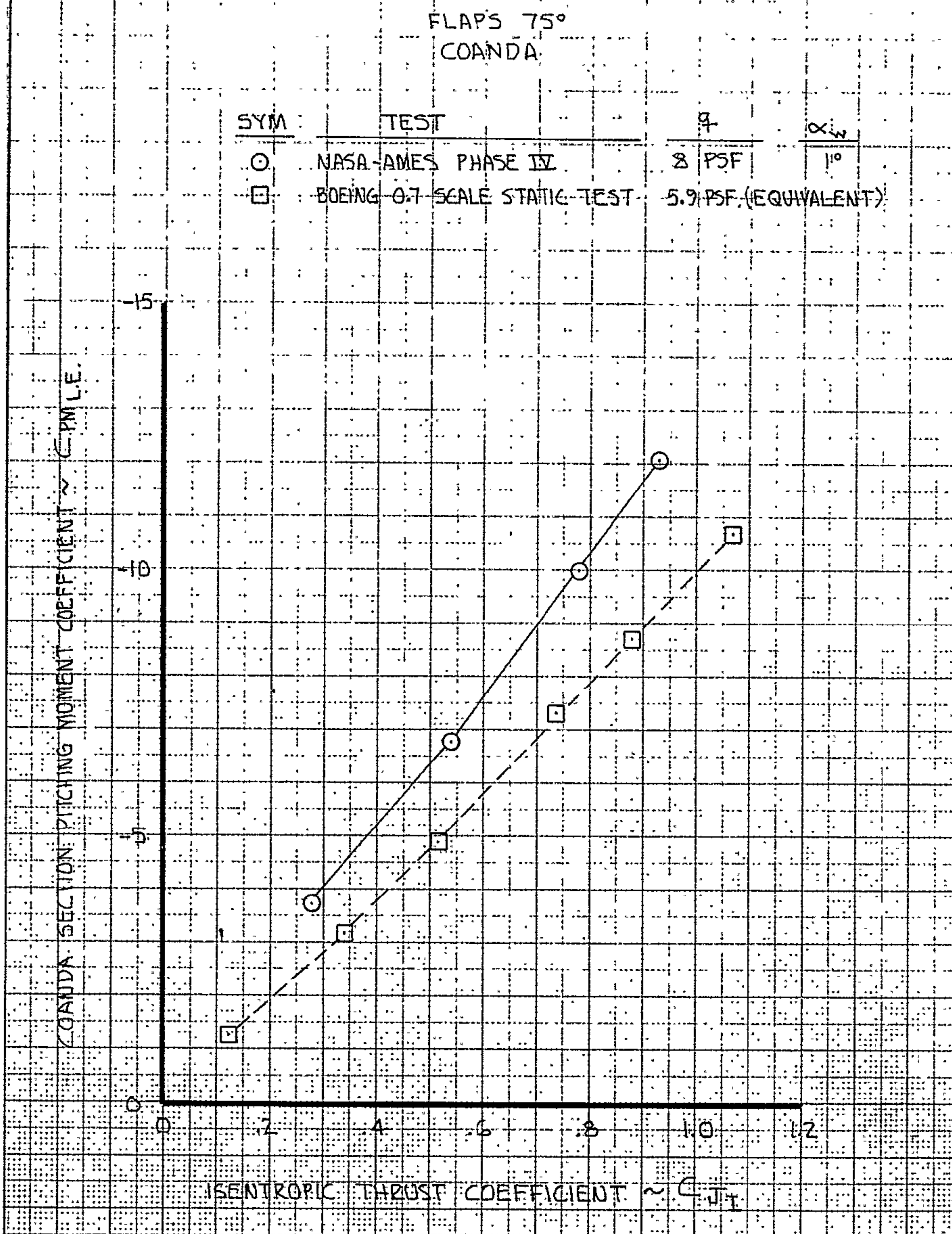

FIG. 188

CALC	F. WRIGHT	3-16-71	REVISED	DATE	COANDA SECTION $C_{PM_{L.E.}}$ VERSUS C_{J_I}, FLAPS 75°	MODIFIED C-8A
CHECK						D6-24850
APR					THE BOEING COMPANY	PAGE 270
APR						

270

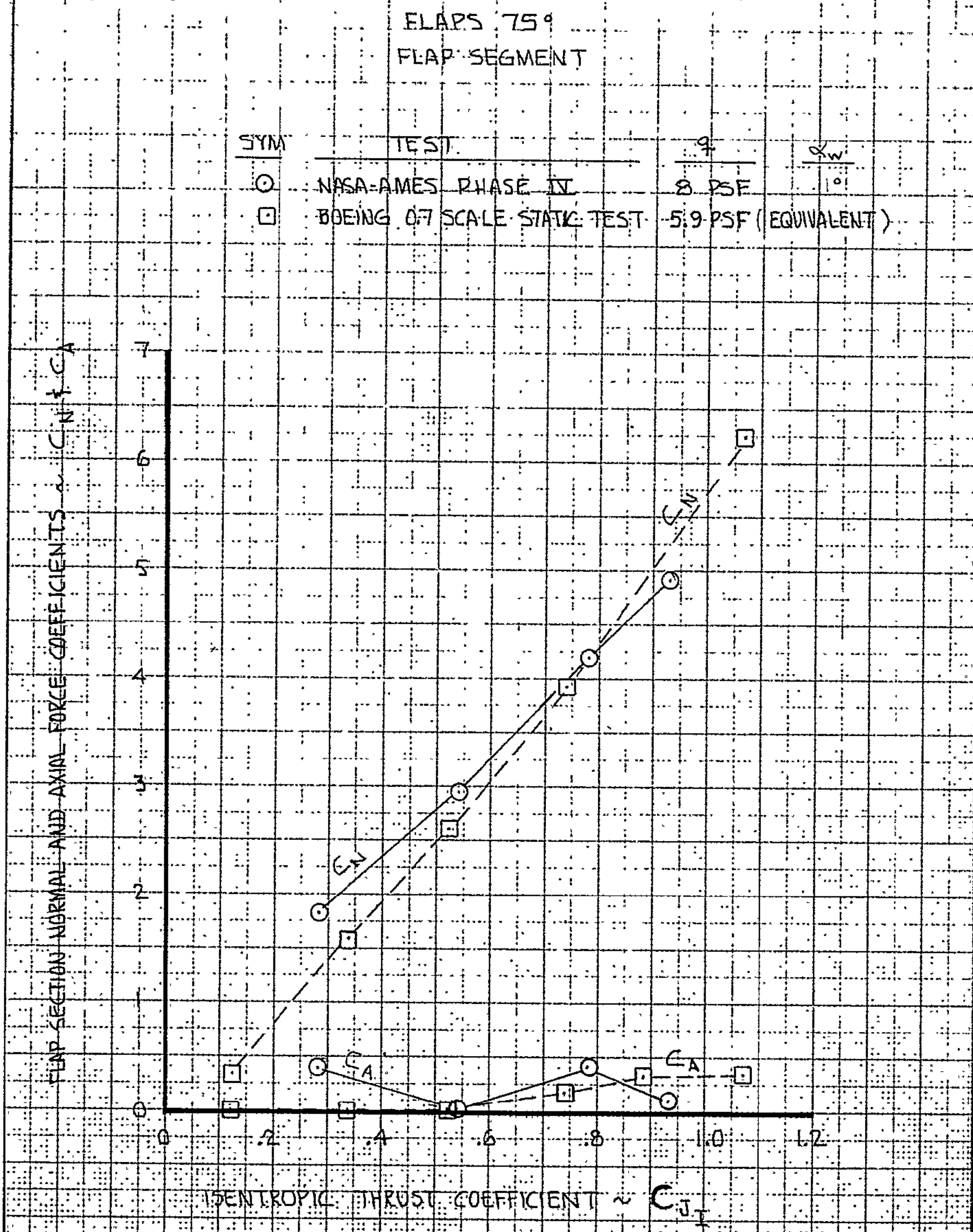

FIG. 189

CALC	F. WRIGHT	3-16-71	REVISED	DATE	FLAP SEGMENT SECTION C_N AND C_A VERSUS C_{J_I}, FLAPS 75°	MODIFIED C-8A
CHECK						D6-24850
APR					THE BOEING COMPANY	PAGE 271
APR						

274.
~~326~~

AD 461 C-R6

K+E ALBANENE 195L 8 5 G-8000

FLAPS 75°
FLAP SEGMENT

SYM	TEST	q	α_W
⊙	NASA-AMES PHASE IV	8 PSF	1°
⊡	BOEING 0.7 SCALE STATIC TEST	5.9 PSF (EQUIVALENT)	

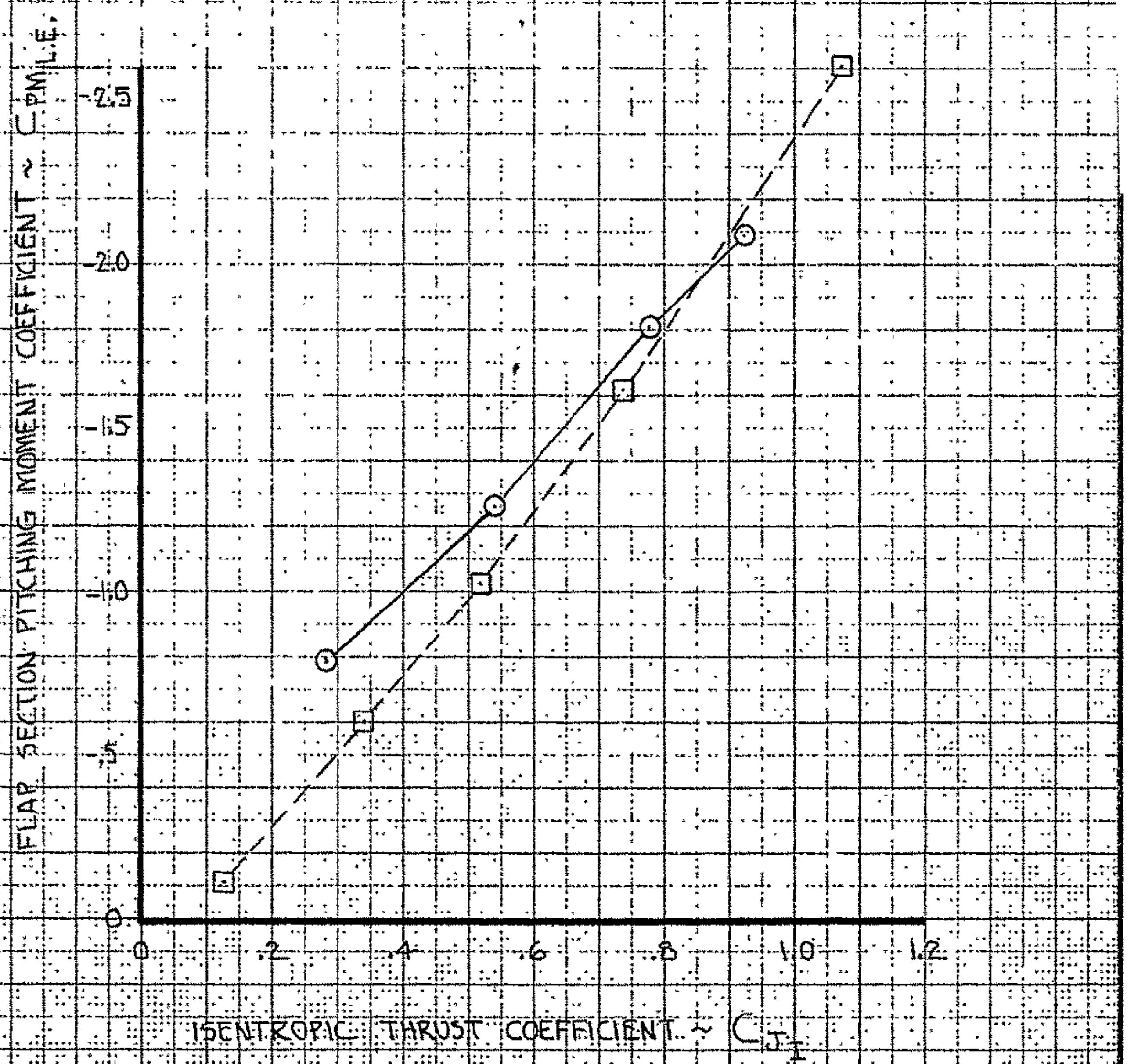

FIG. 190

			REVISED	DATE		
CALC	F. WRIGHT	3-16-71			FLAP SEGMENT SECTION $C_{PM_{L.E.}}$ VERSUS C_{J_I}, FLAPS 75°	MODIFIED C-8A
CHECK						D6-24850
APR					THE BOEING COMPANY	PAGE 272
APR						

AD 461 C-R6

K+E ALBANENE 195L TRACING PAPER 8.5 G-8000

Position Parameters for Jet-Augmentor Flap

Flap Angle	Run No.	θ_i	δ_{FD}	l_e	l_t	l_i	l_z	z
30°	106	20°	7°	8.41 IN.	5.19 IN.	6.58 IN.	5.18 IN.	1.85 IN
	148 149	20	7	6.90	3.56	4.97	5.18	1.60
	379	10	4	6.10	5.09	5.09	5.18	1.85
	476	10	4/3.75 (1)	5.15	4.10	5.10	5.18	1.58
50	218 219	20	4	6.13	4.10	7.78	4.46	1.58
	271 272	10	4.5 (2)	6.24	3.40	6.72	4.46	1.33
	411	10	4	6.10	4.10	6.42	3.00	1.31
	412	10	4	6.10	4.10	6.43	3.00	1.08
	464	10	4	6.10	4.10	7.01	4.06	1.52
65	378	10	4	6.10	4.10	8.27	3.36	1.45
75	436 437	10	4	6.10	4.10	9.87	3.75	1.27

(1) LIFT DUMP INSTALLED
(2) INCLUDES 12" FLAP EXTENTIONS

FIG. 191

AUDIO FREQUENCY

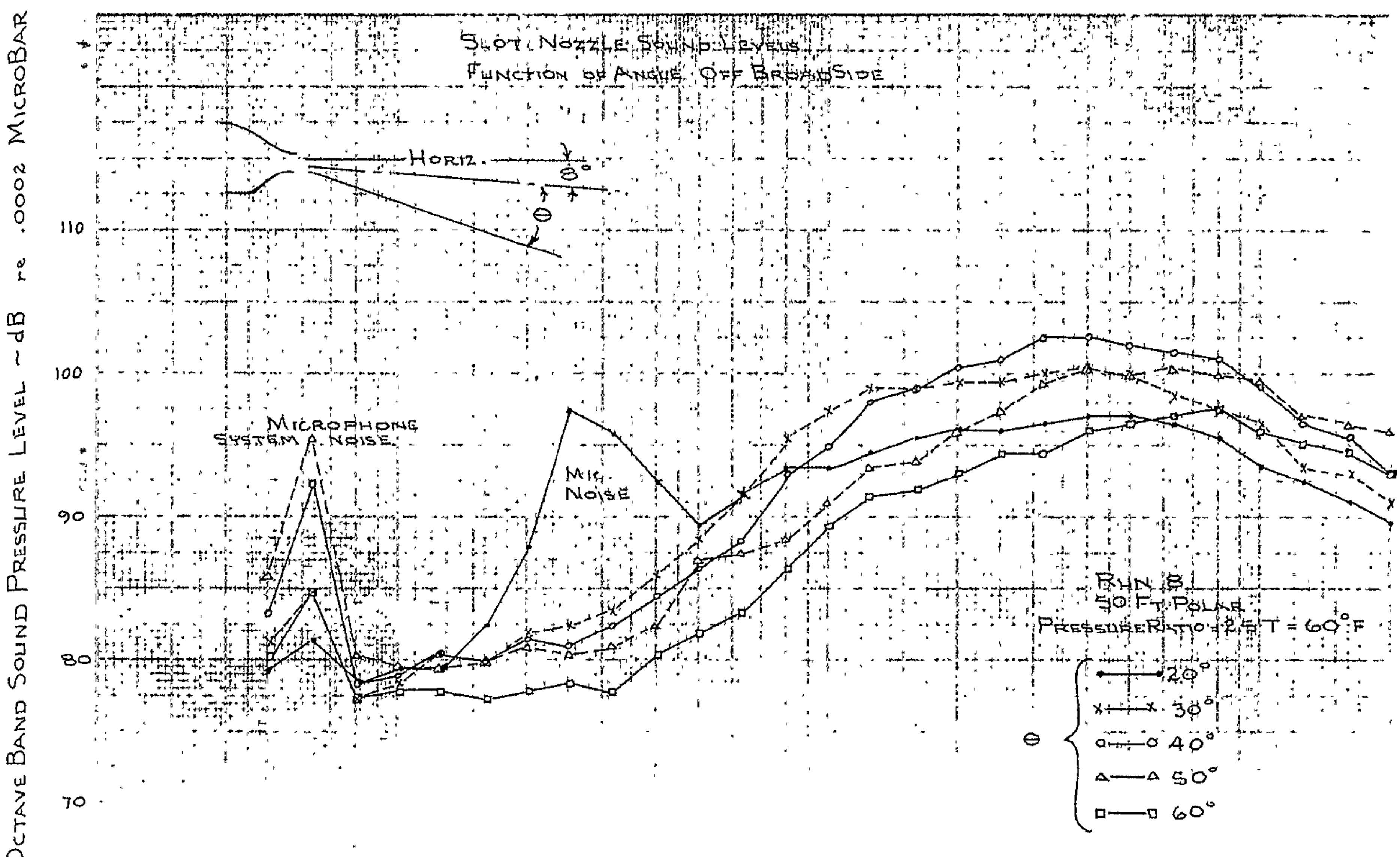

FIG. 192

D6-24850

274

276

AUDIO FREQUENCY

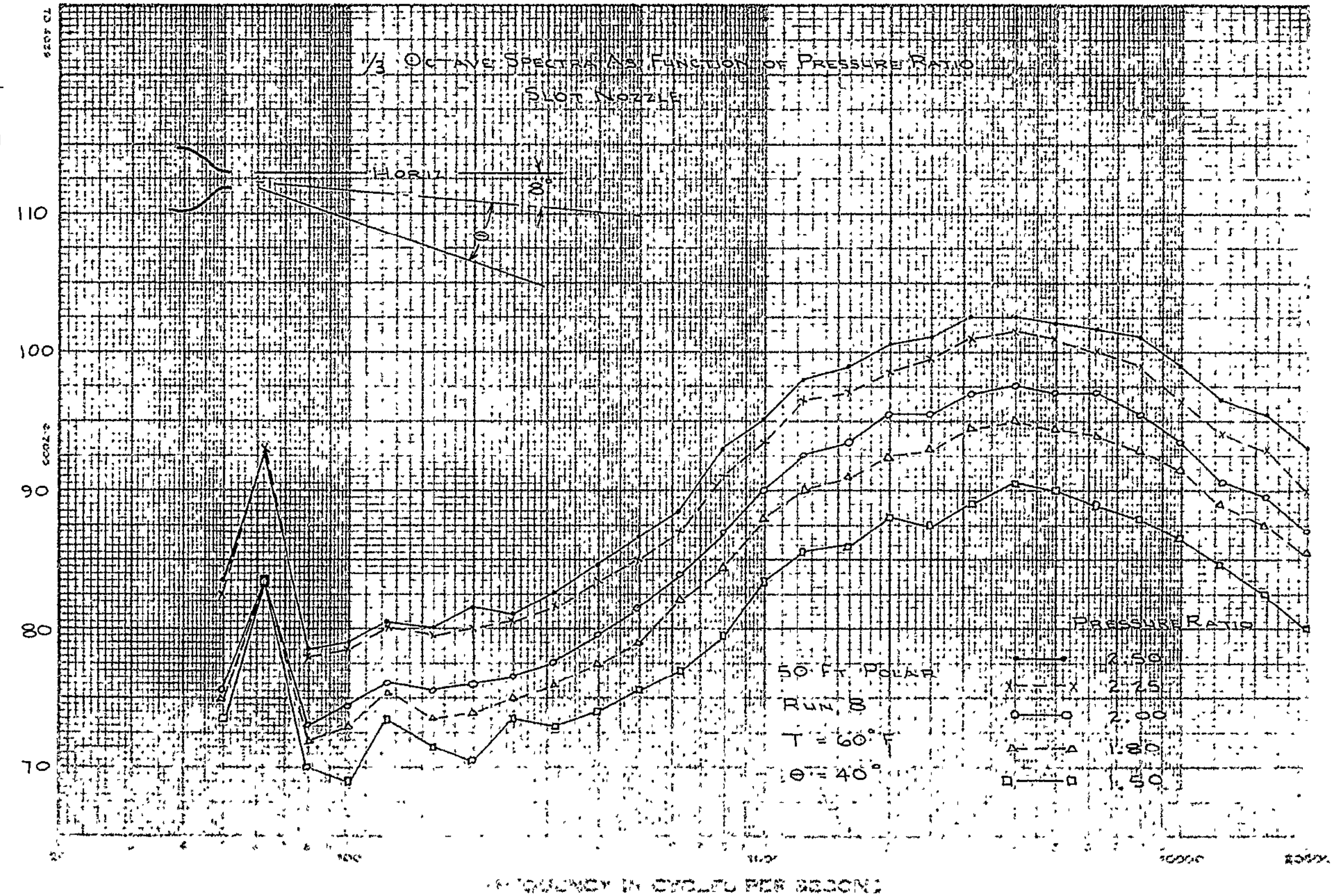

Fig. 193

D6-24850

275

BOEING

AUDIO FREQUENCY

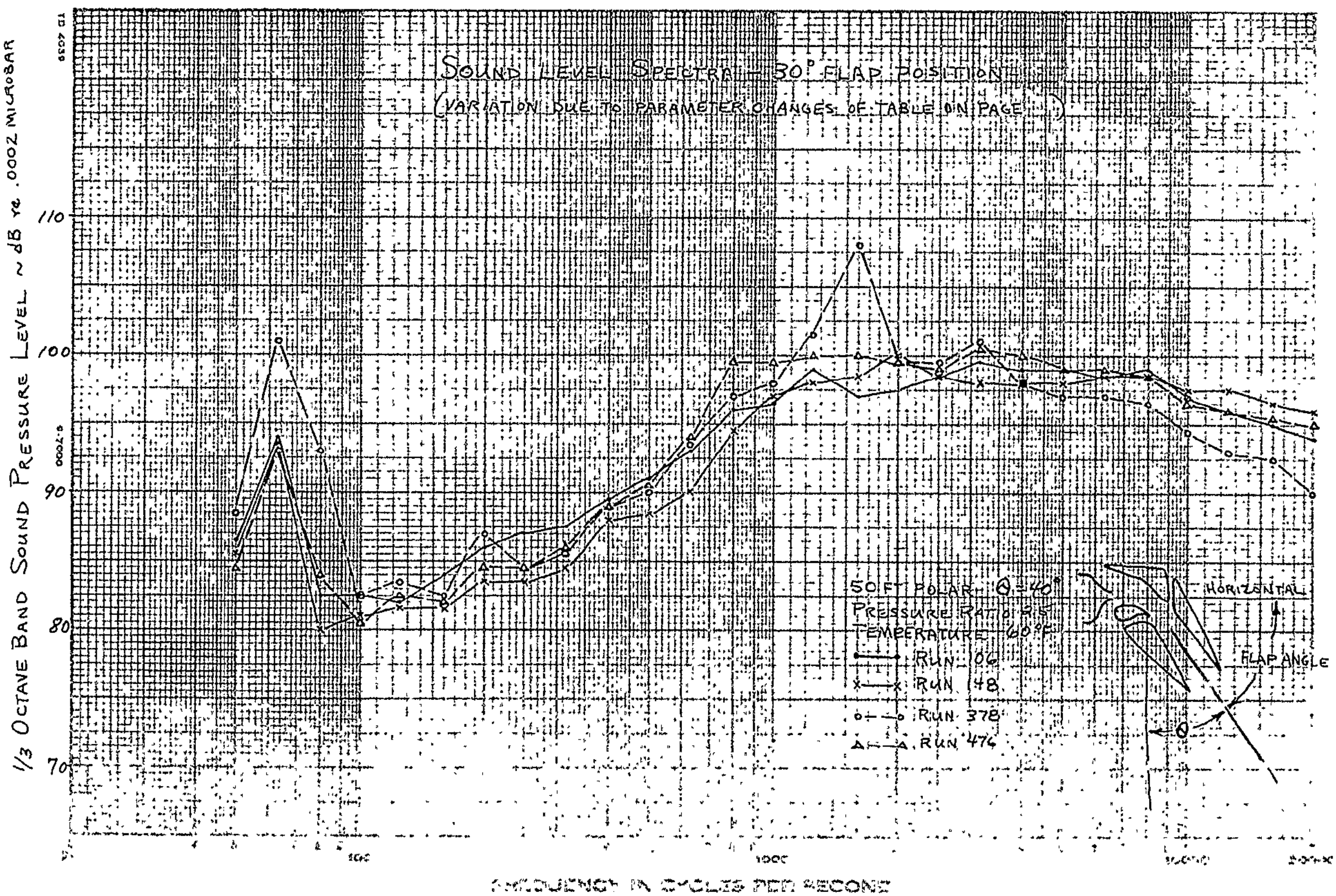

FIG. 194

D6-24850

276

BOEING

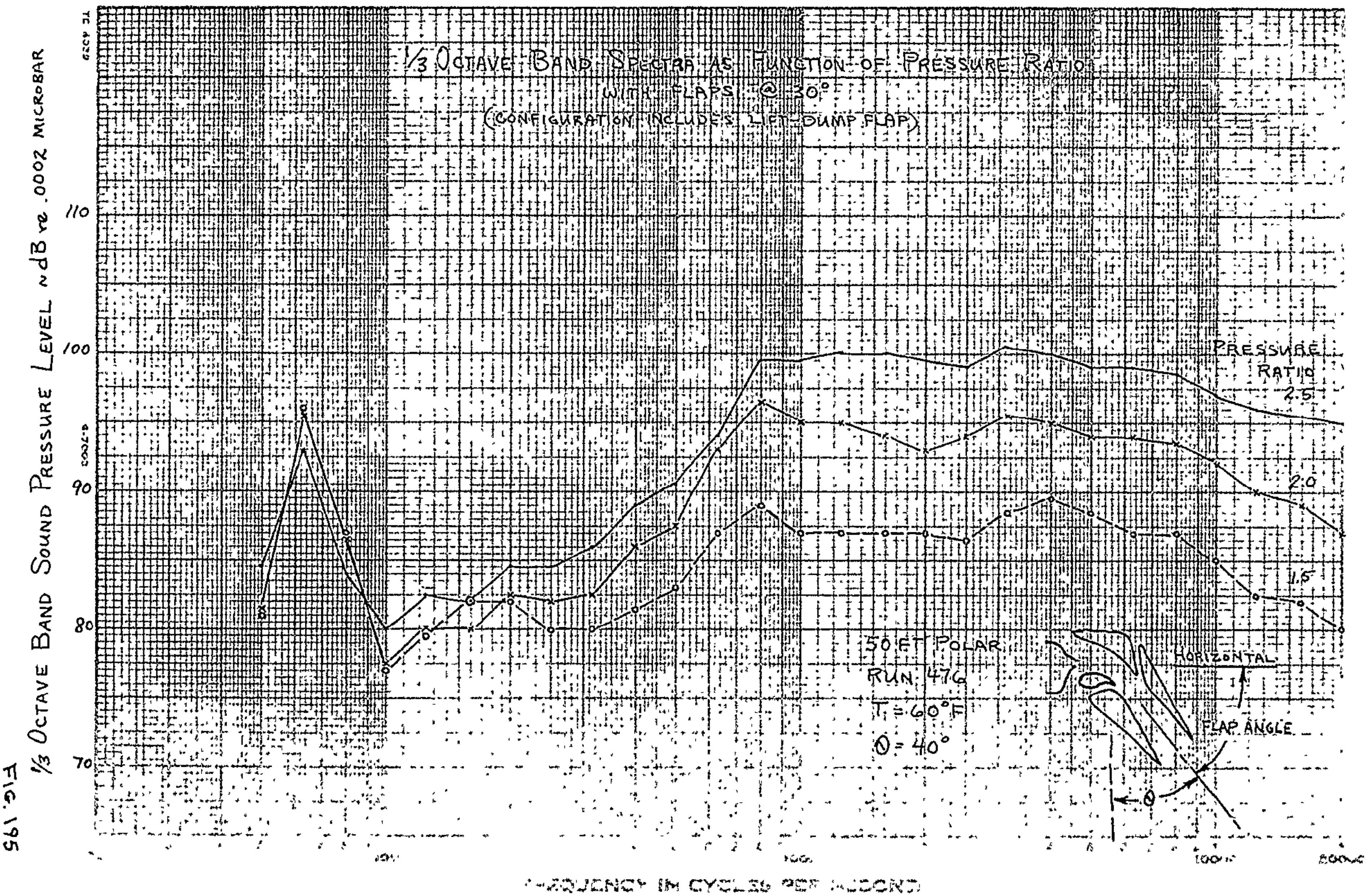

Fig. 195

D6-24850

277

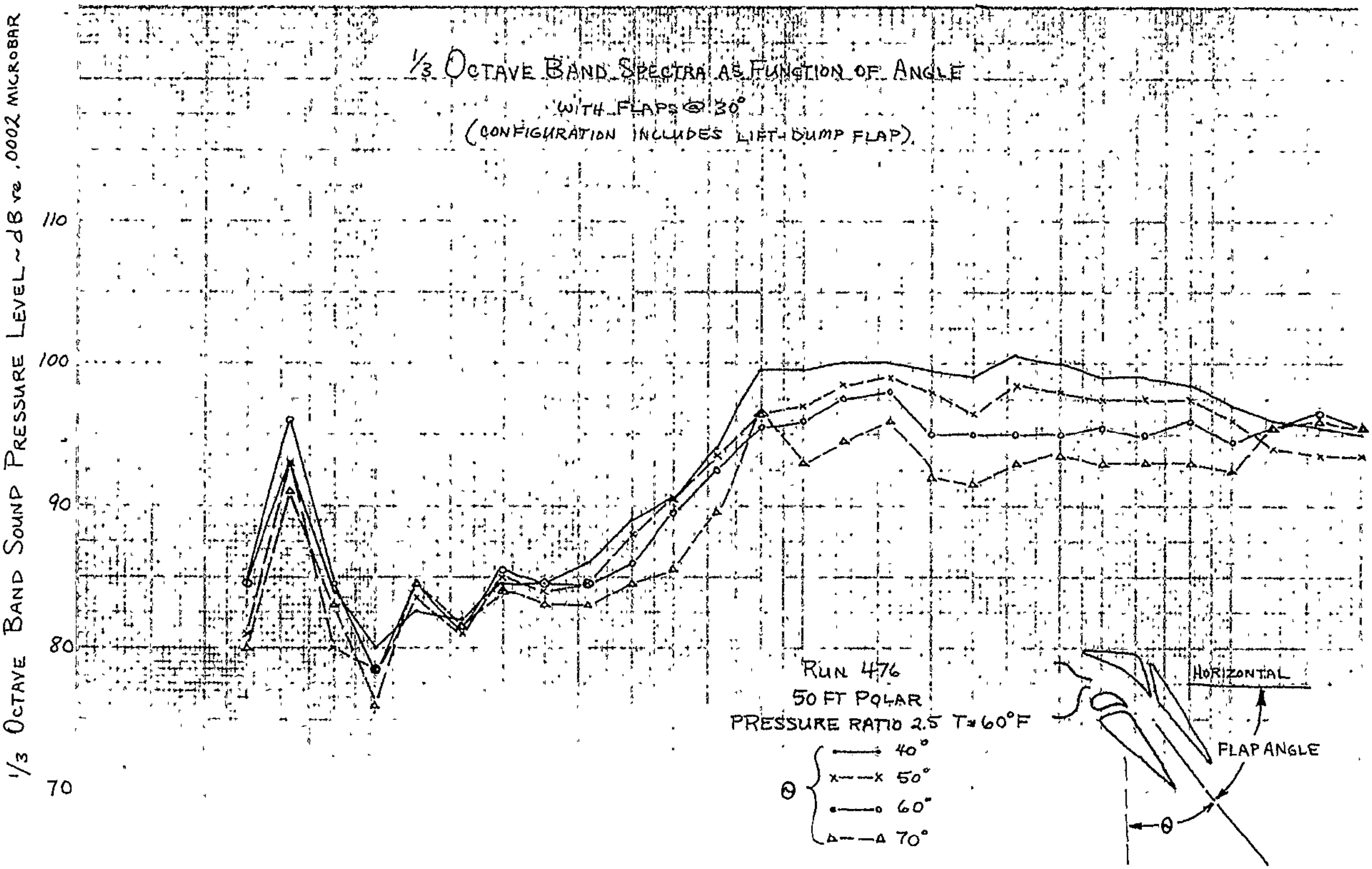

FIG. 196

D6-24850

278

AUDIO FREQUENCY

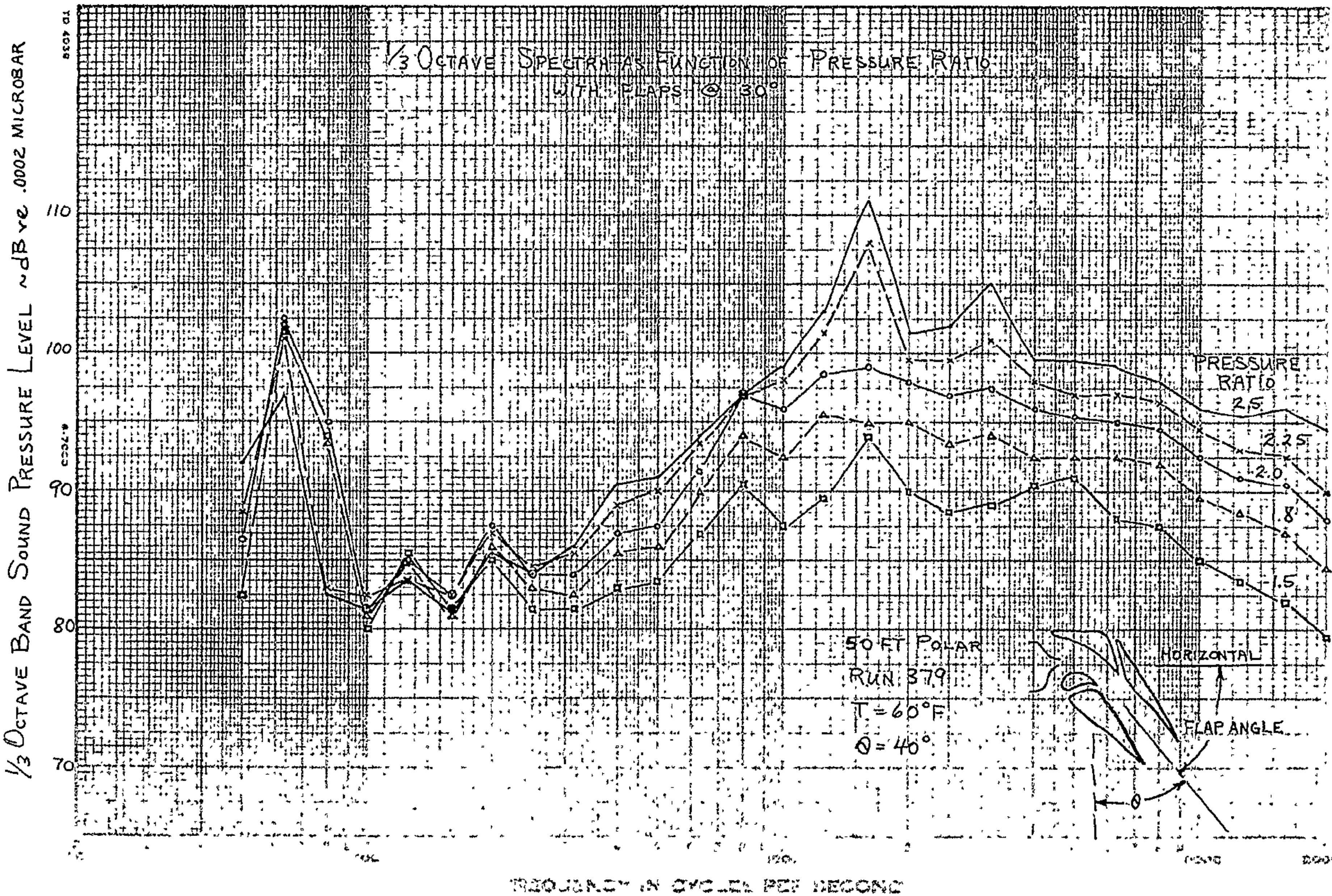

Fig. 197

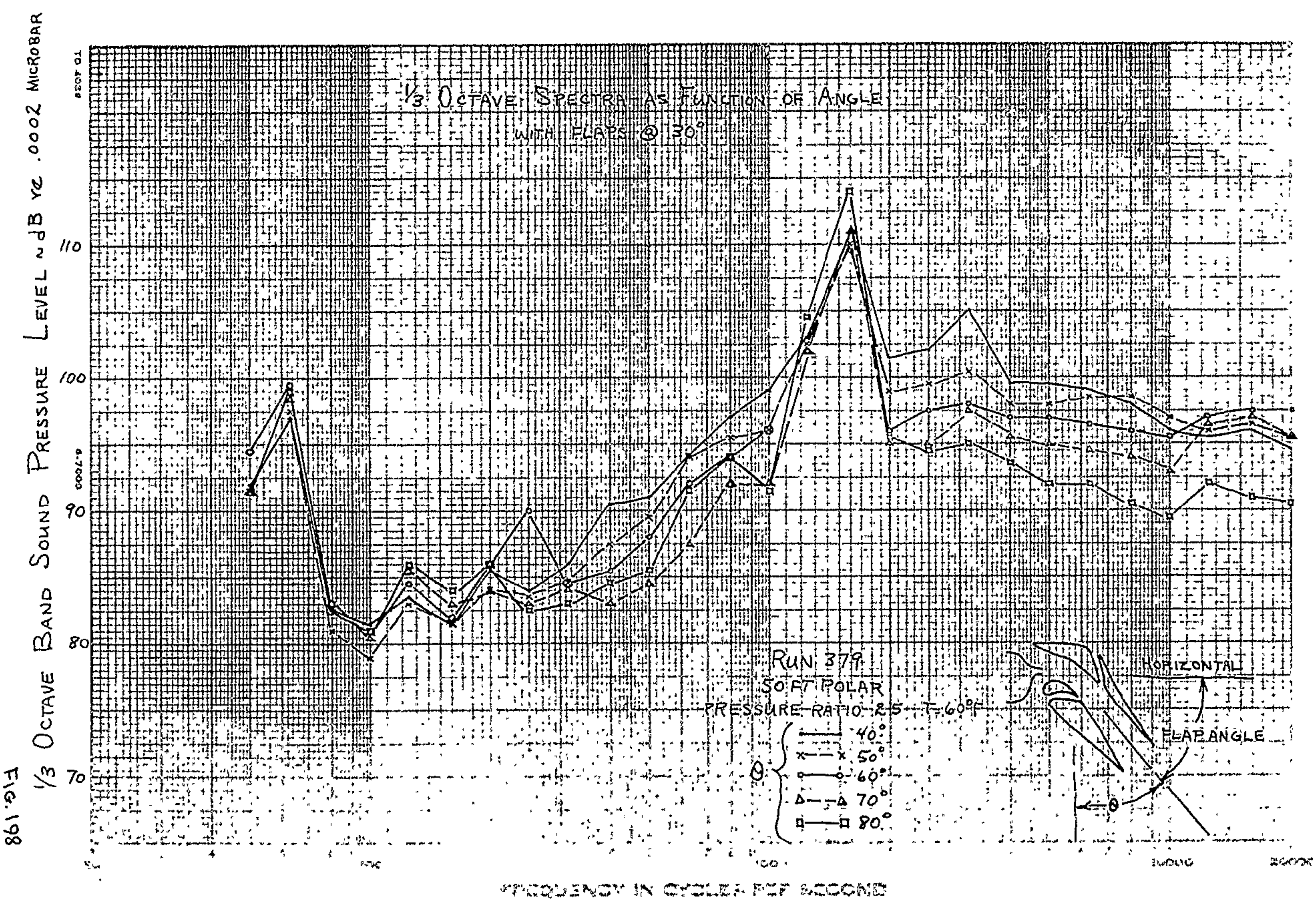

Fig. 198

D6-24850

280

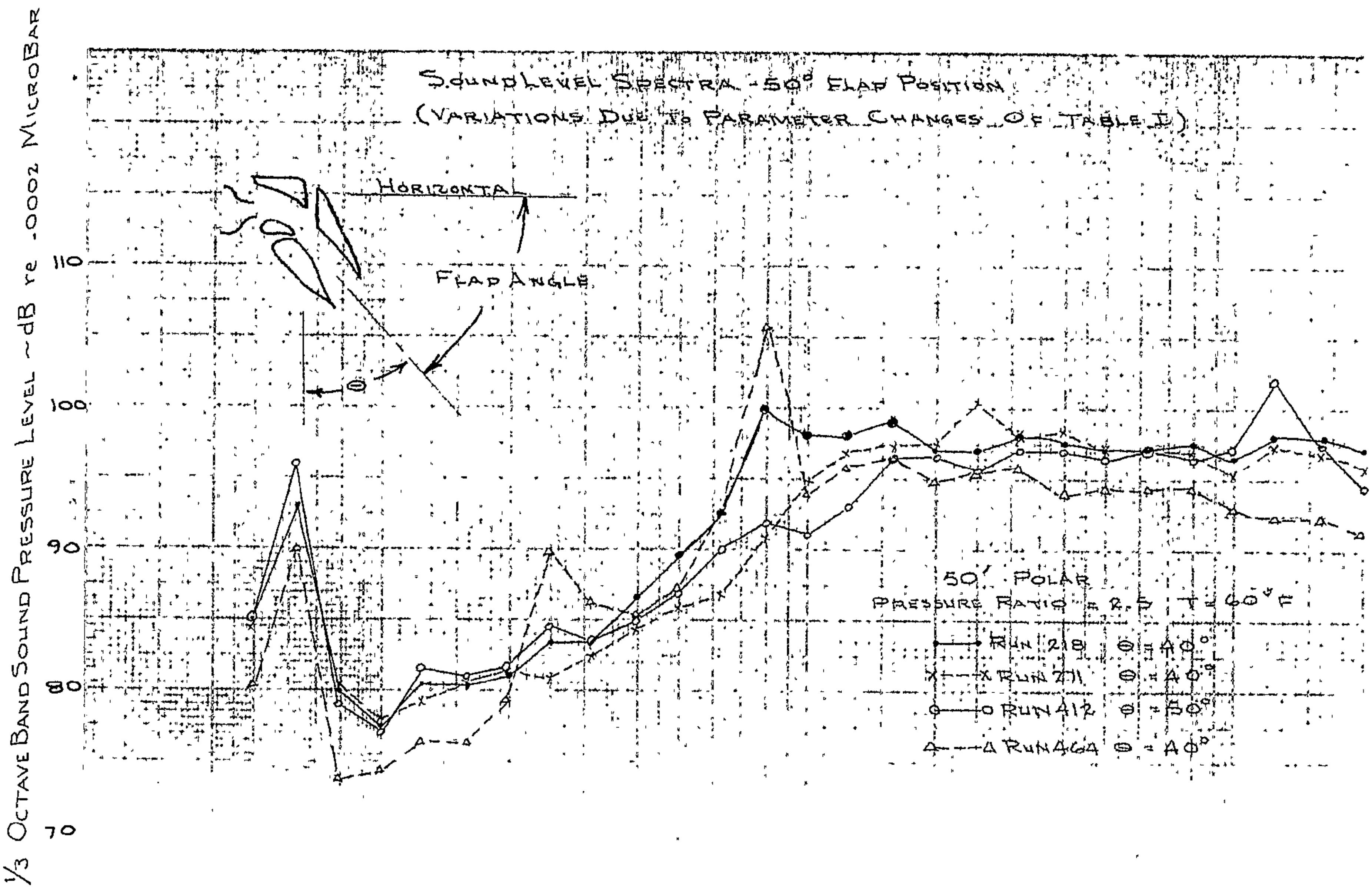

SOUND LEVEL SPECTRA - 50° FLAP POSITION
(VARIATIONS DUE TO PARAMETER CHANGES OF TABLE I)
HORIZONTAL
FLAP ANGLE
θ
50' POLAR
PRESSURE RATIO = 2.5 T = 60°F
RUN 28 θ = 40°
RUN 271 θ = 40°
RUN 412 θ = 30°
RUN 464 θ = 40°
1/3 OCTAVE BAND SOUND PRESSURE LEVEL ~dB re .0002 MICROBAR
70
80
90
100
110

FIG. 199

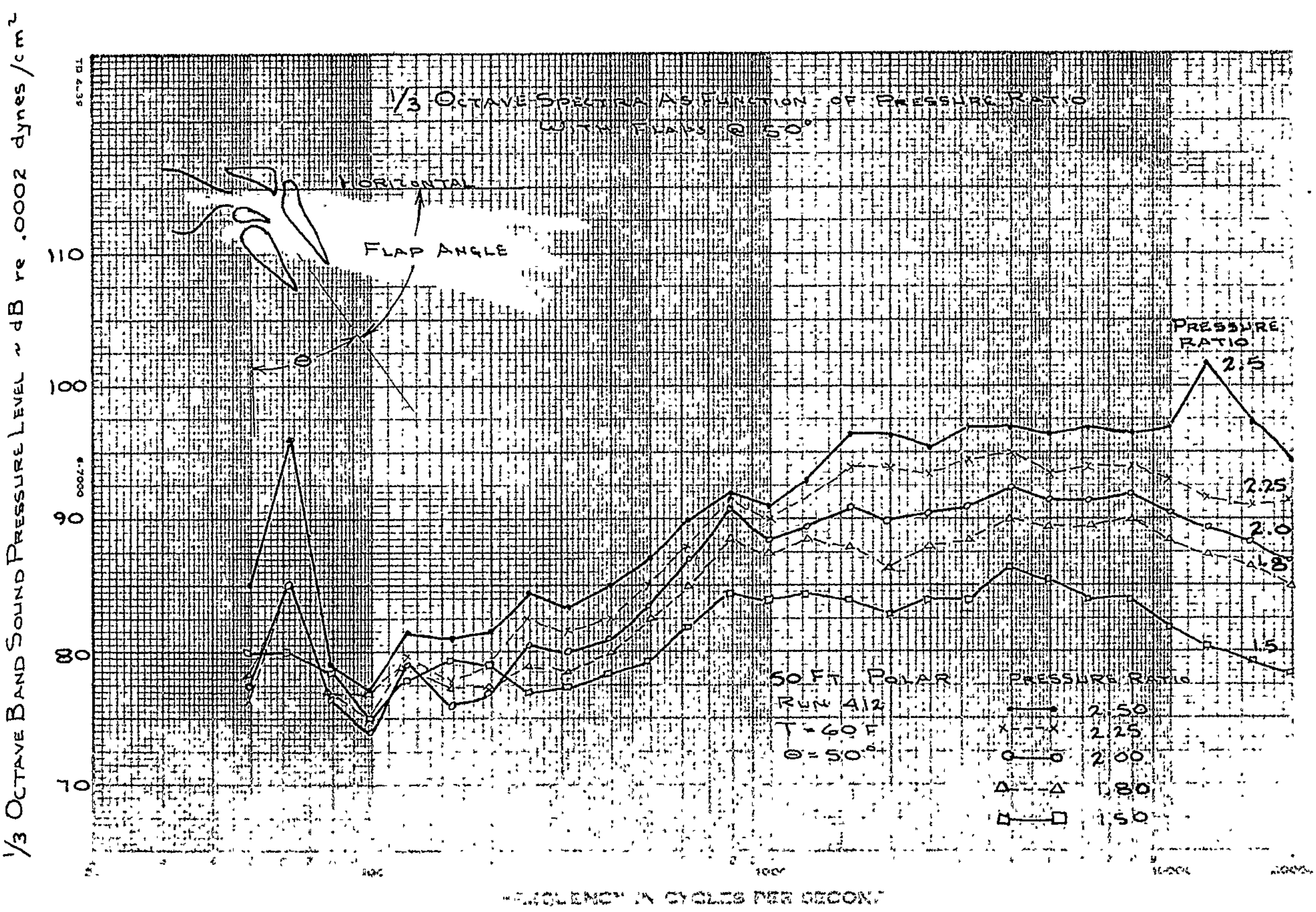

Fig. 200

BOEING
D6-24850
282

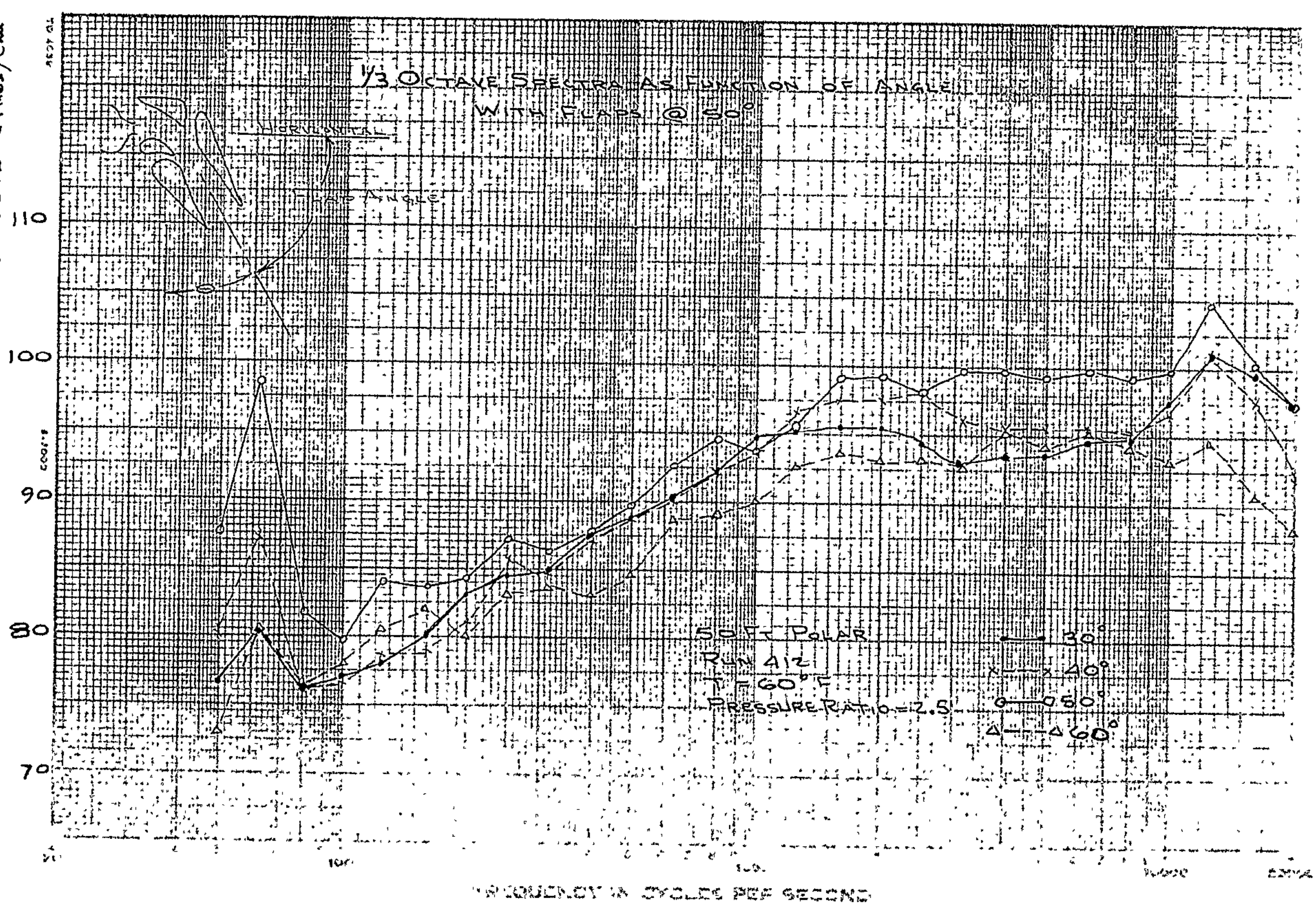

283
DL-24850

FIG. 201

AUDIO FREQUENCY

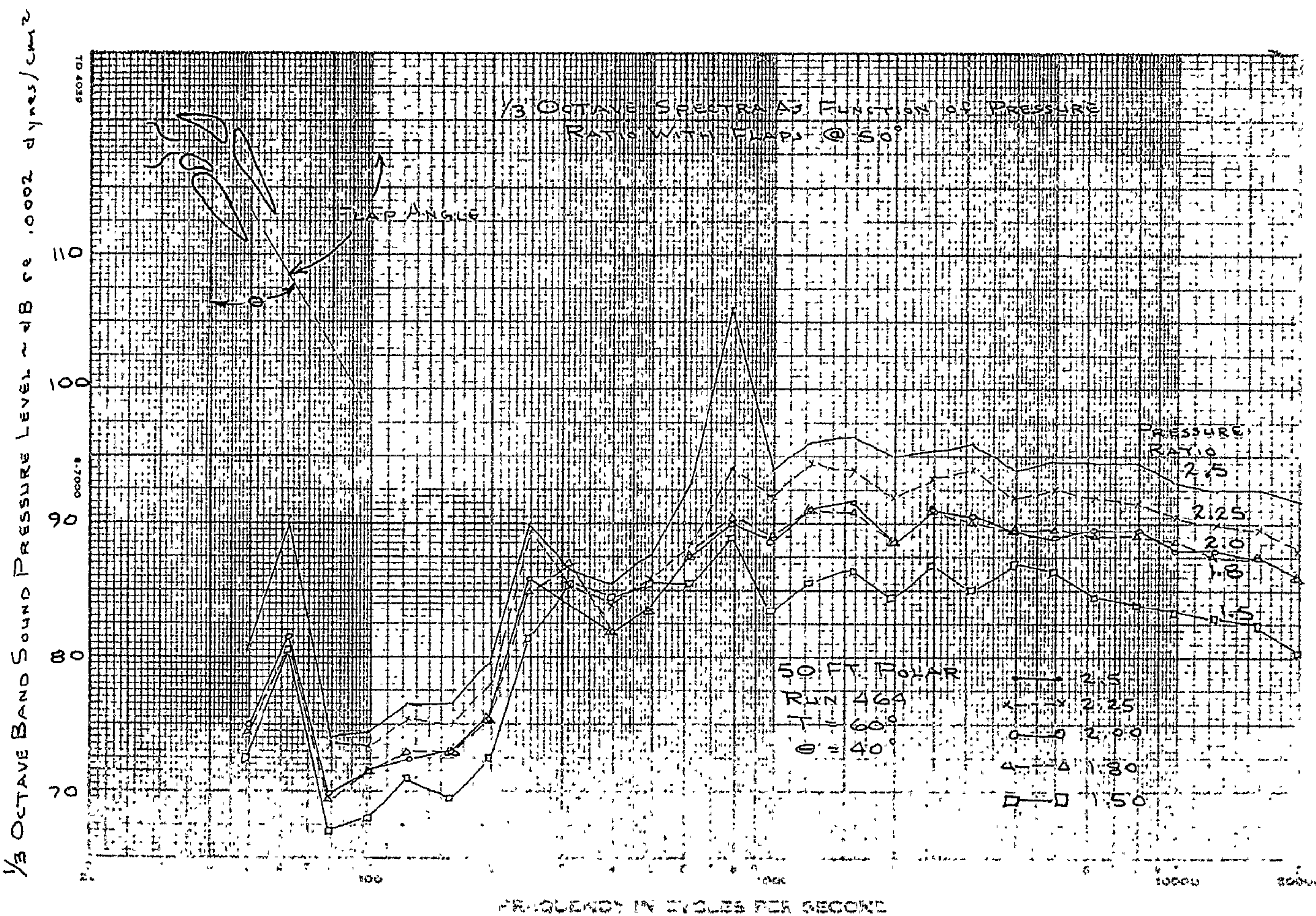

Page 284
No. DL-24850
Fig. 202

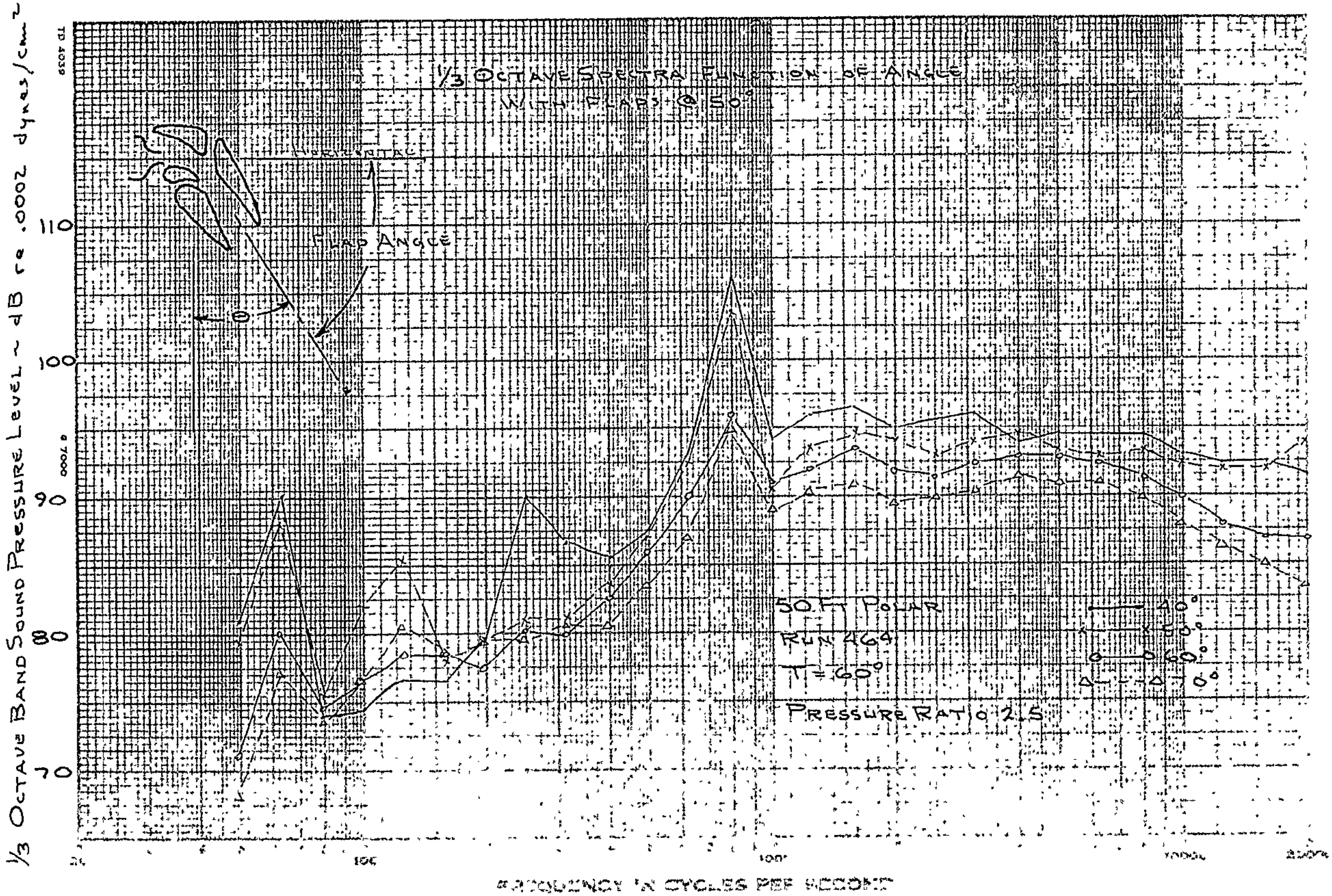

FIG. 203

D6-24850

285

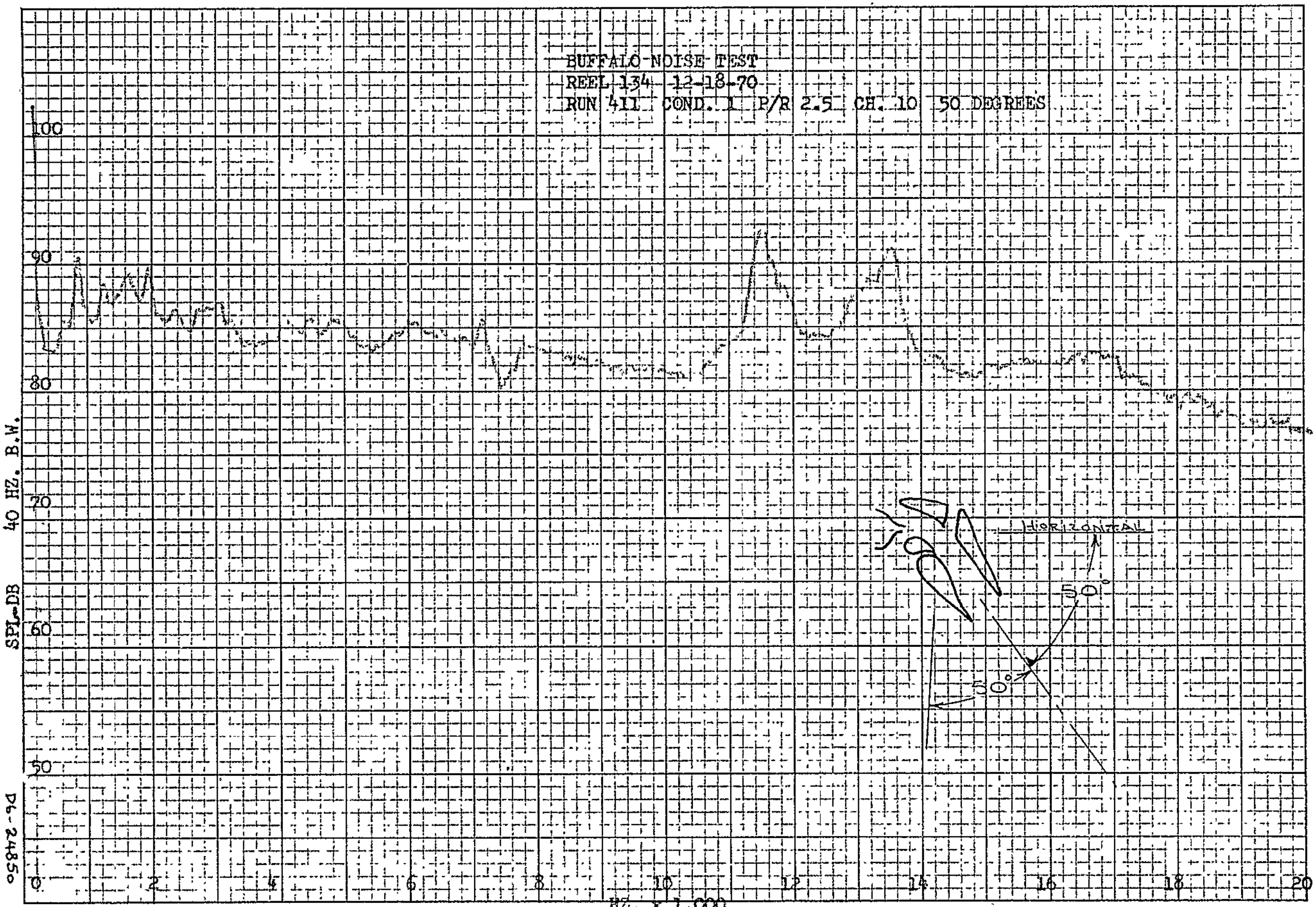

D6-24850
Page 286

FIG. 20

AUDIO FREQUENCY

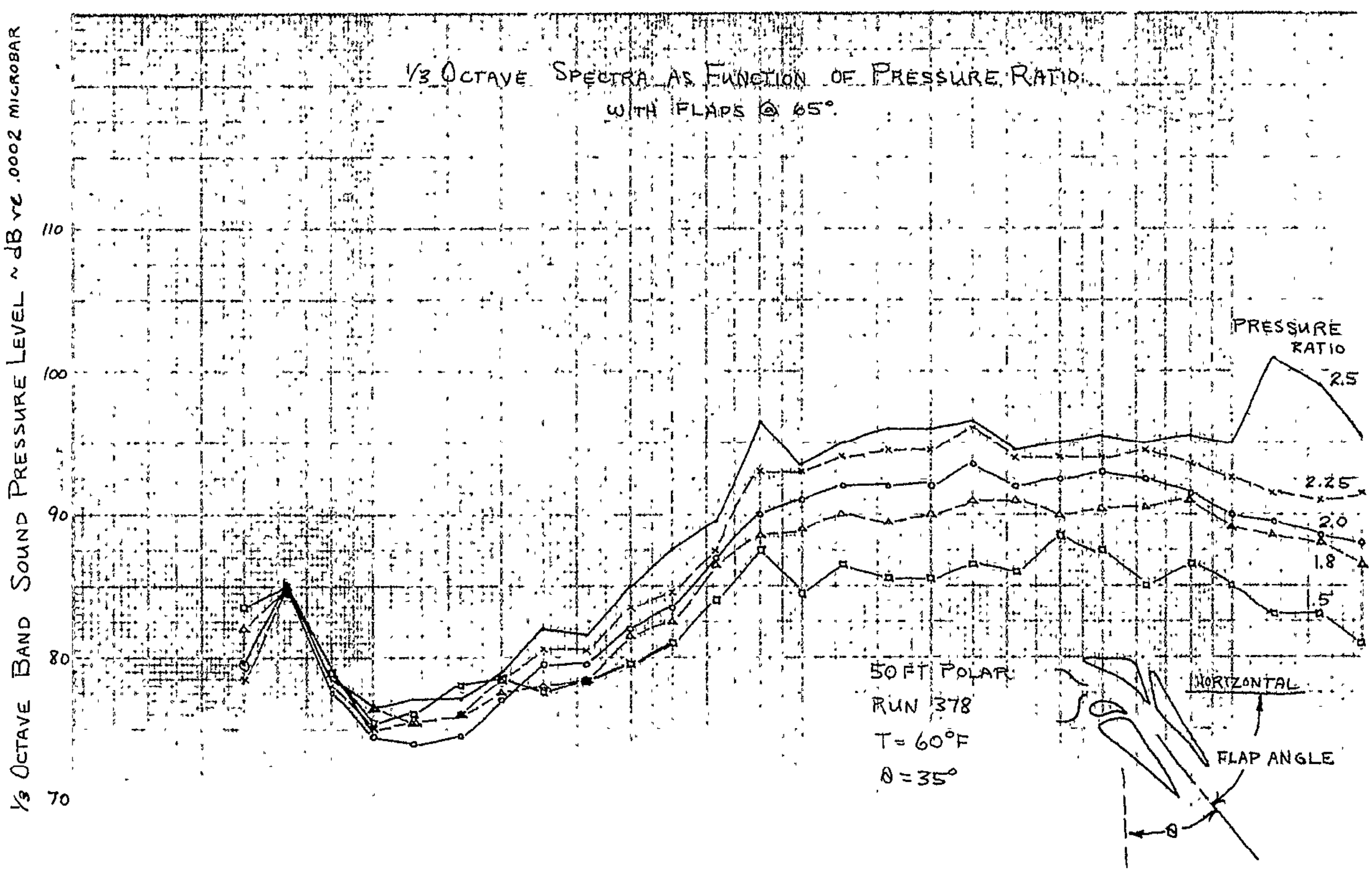

FIG. 205

D6-24850

287

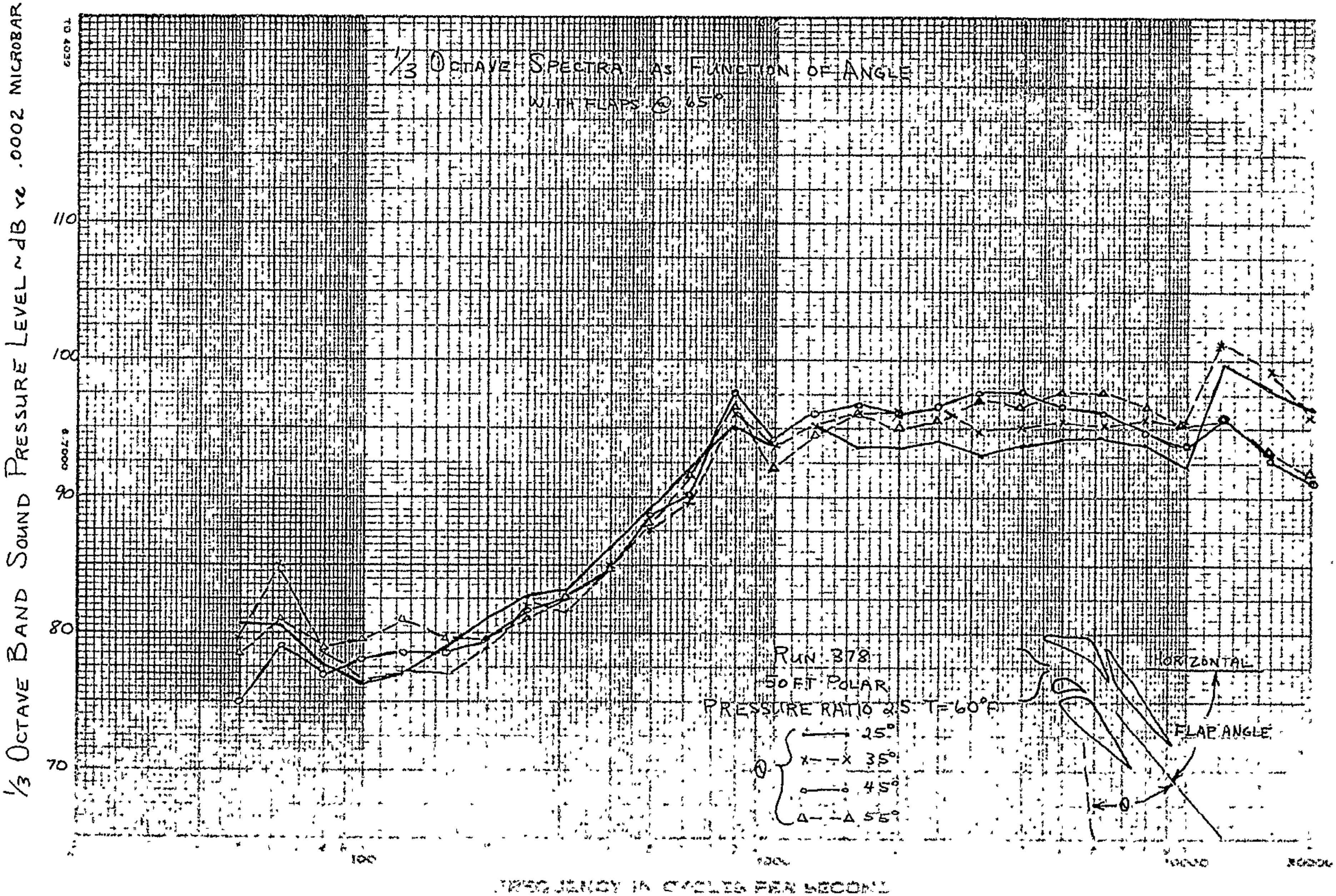

Fig. 206

D6-24850

Page 288

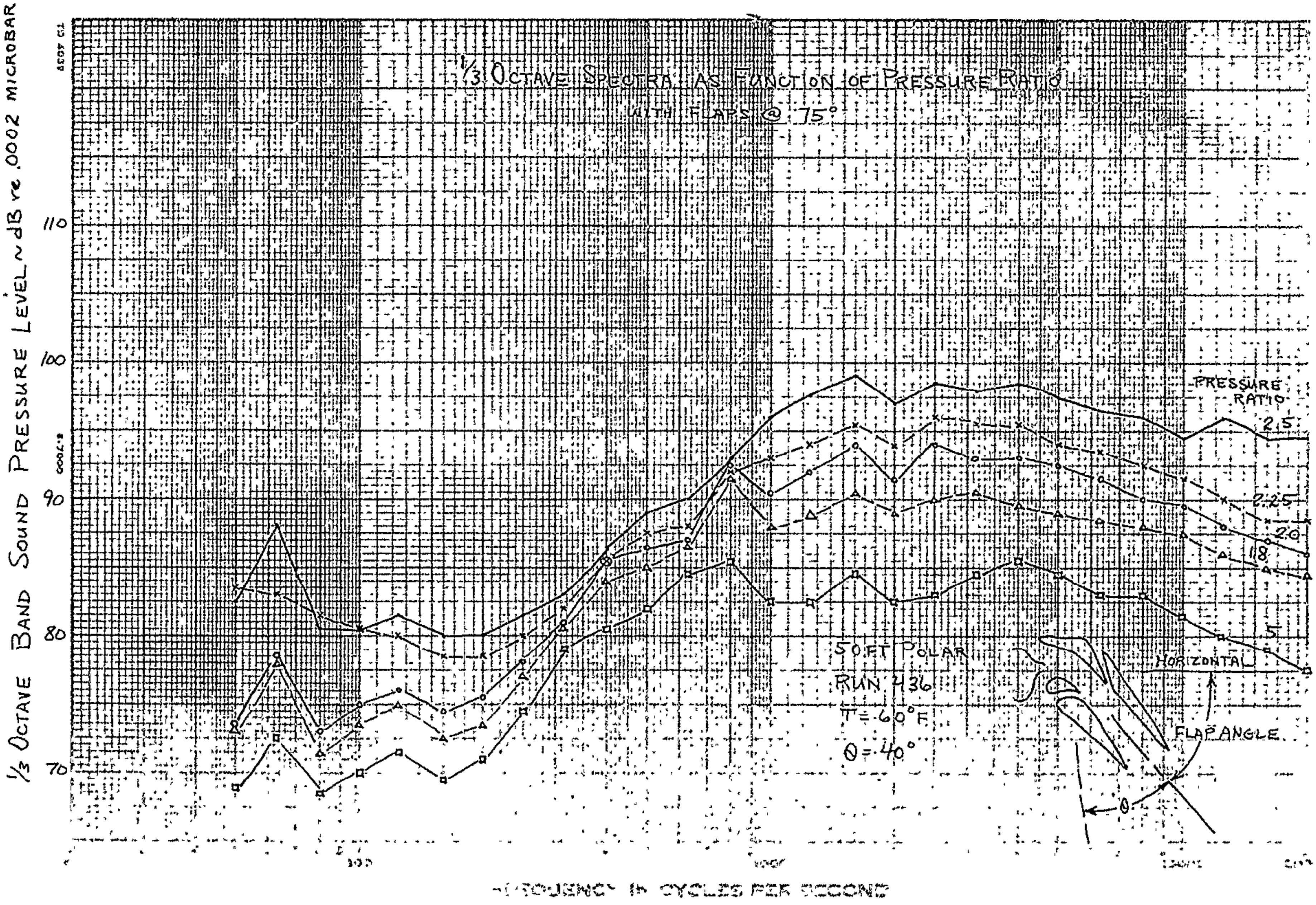

FIG. 207 1/3 OCTAVE

NO. D6-24850

289

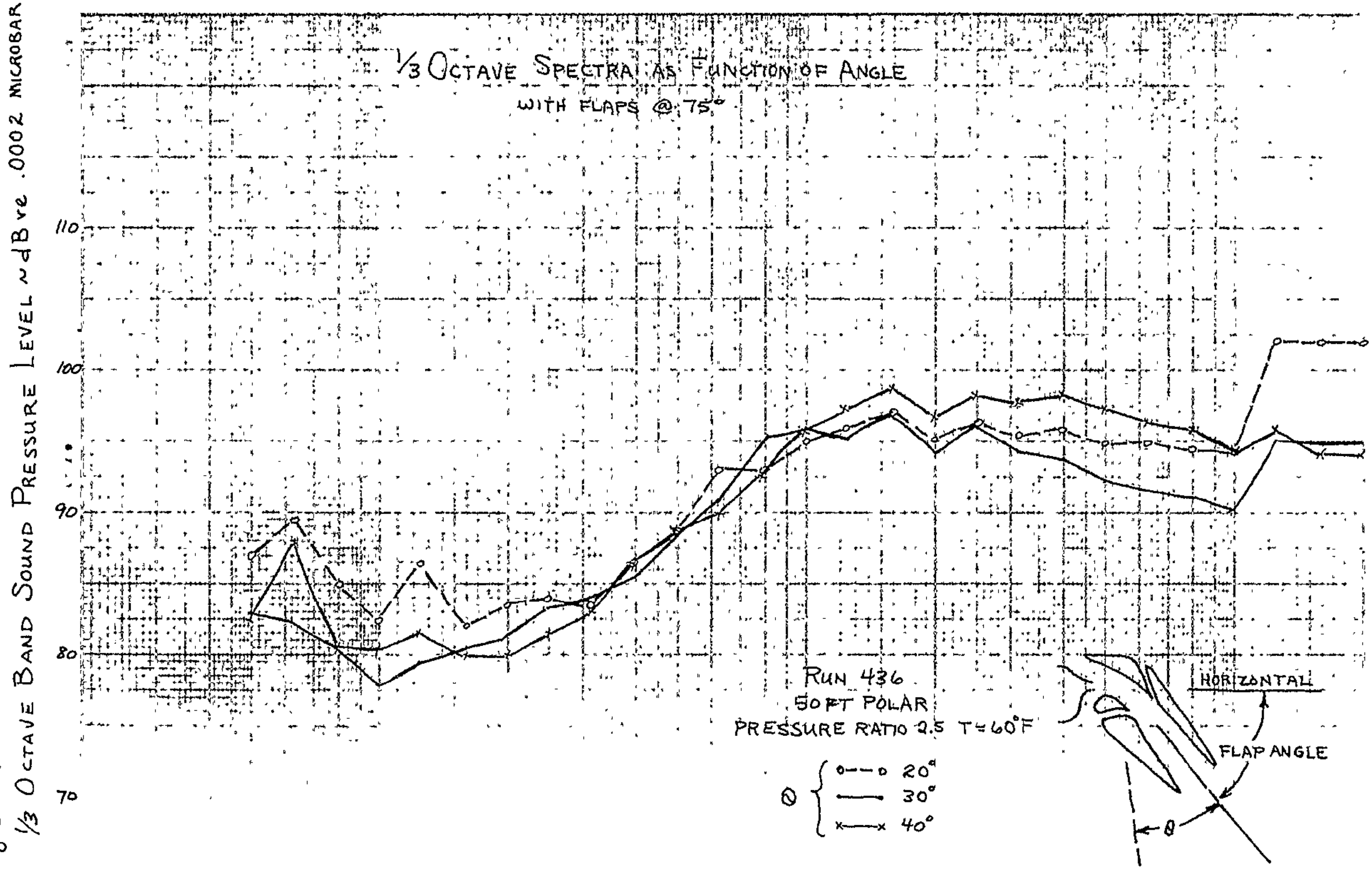

FIG. 208

D6-24850

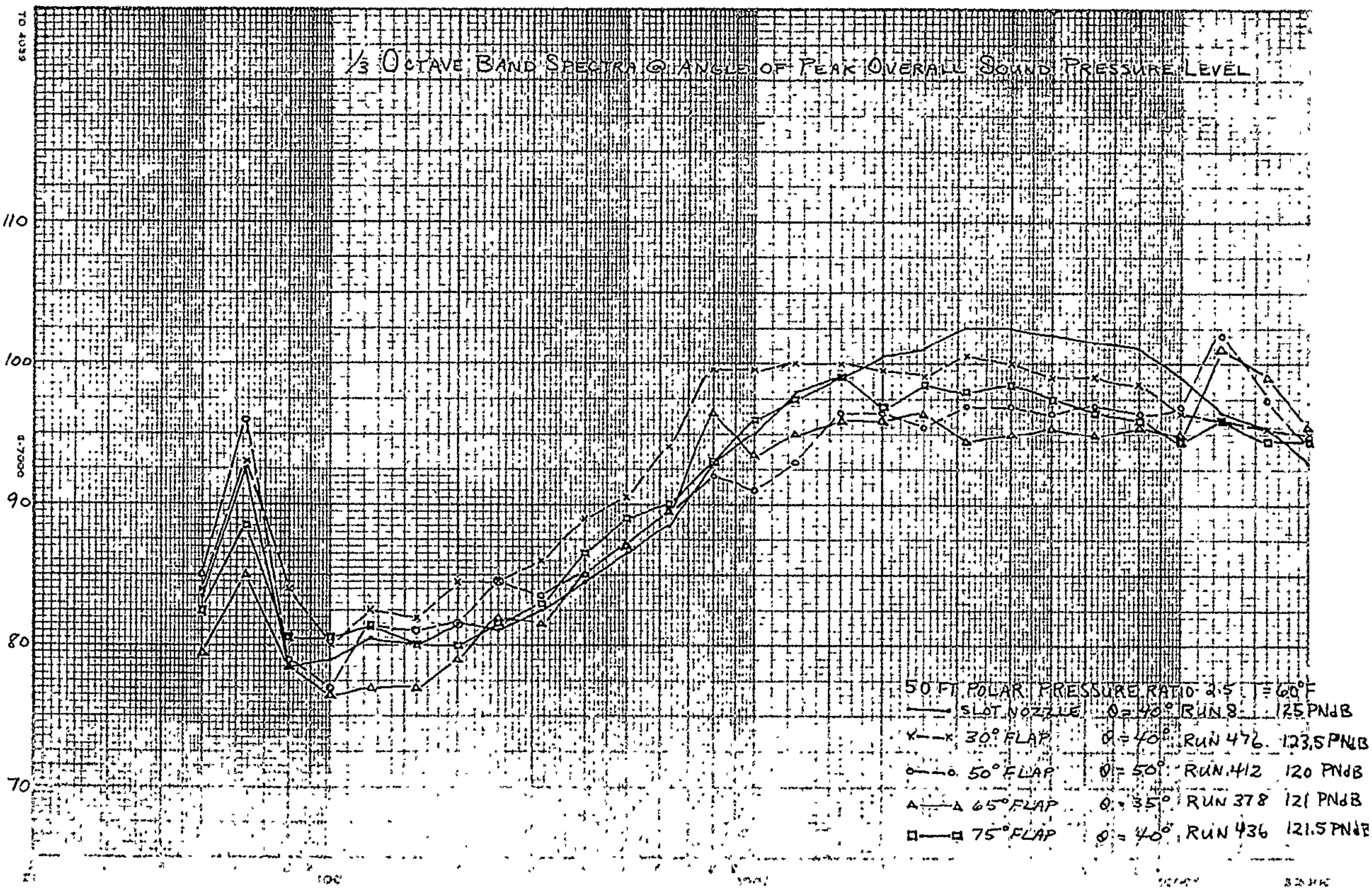

FIG. 209

D6-24850

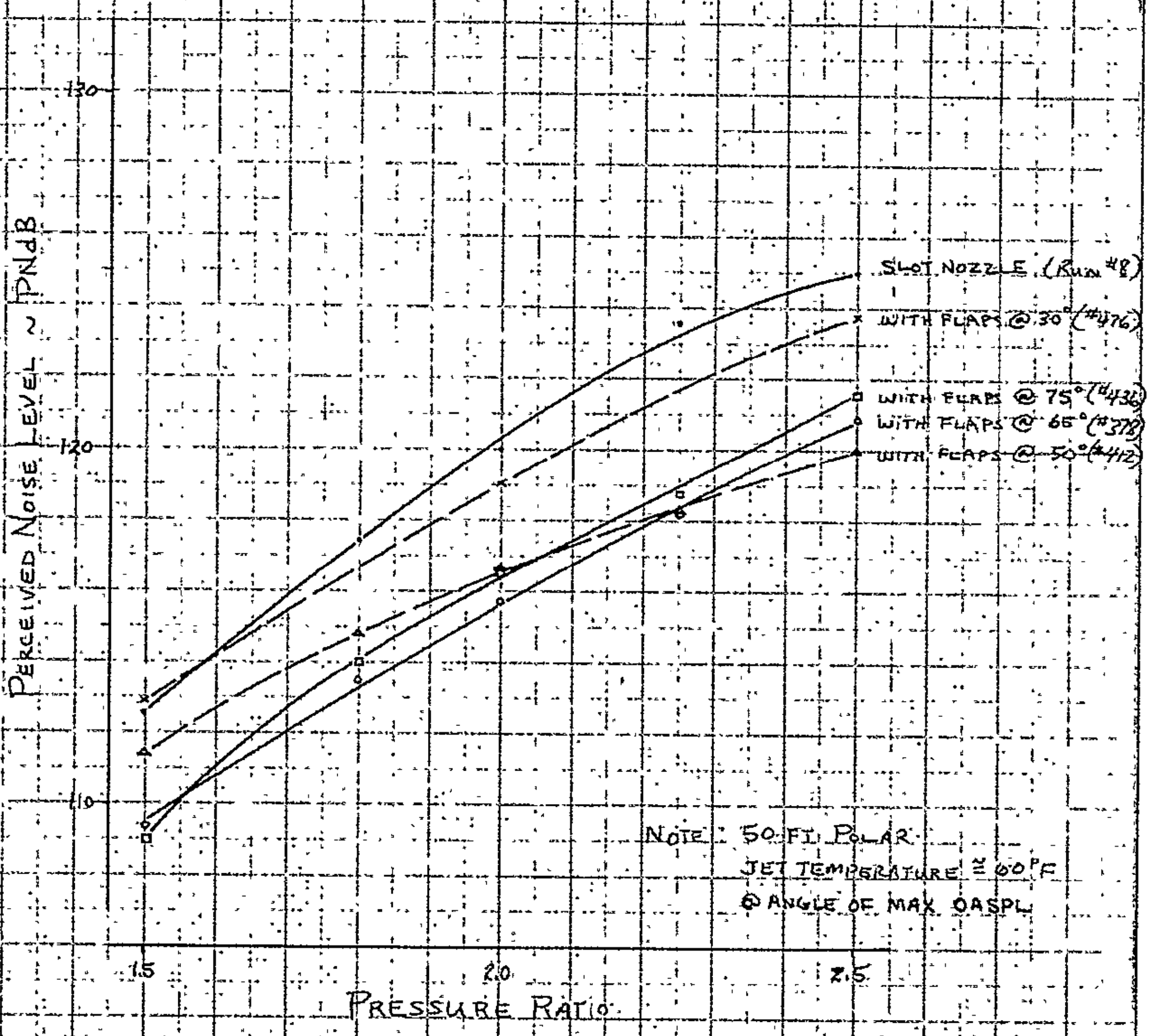

CALC	CFW	4/30/71	REVISED	DATE	NOISE LEVELS OF JET-AUGMENTOR FLAPS AS FUNCTION OF PRESSURE RATIO	FIG. 210
CHECK						
APR						D6-24850
APR					THE BOEING COMPANY	PAGE 292

APPENDIX

BASIC EQUATIONS USED

- Resultant thrust $T - \sqrt{(L)^2 + (-D)^2 + (S)^2}$

- Resultant vertical thrust angle Θ = arc sin L/T

- Resultant side thrust angle β = arc sin S/T

- Nozzle velocity coefficient C_v (flaps off) or augmentation ratio AR (flaps on) = $\dfrac{T}{\dot{M}_M V_I}$ single flow case

or $\dfrac{T}{\dot{M}_{M_{UN}} \cdot V_{I_{UN}} + \dot{M}_{M_{LN}} \cdot V_{I_{LN}}}$ dual flow case

UN - upper nozzle

LN - lower nozzle

where: $\dot{M}_M$ - the measured mass flow rate

V_I - isentropic velocity = $\sqrt{\dfrac{2\gamma g R T_T}{\gamma - 1}\left[1 - \left(\dfrac{P_T}{P_A}\right)^{\frac{1-\gamma}{\gamma}}\right]}$

where γ = 1.40

g = 32.174 ft/sec

PT/PA = pressure ratio at duct entrance charging station

- Nozzle flow ciefficient C_D = $\dfrac{\dot{M}_M}{\dot{M}_I}$

AD 1546 D

where: W_M measured flow rate lb/sec

W_I = isentropic flow rate = $\dfrac{A_{ex} P_T}{\sqrt{T}} \sqrt{\dfrac{\gamma g}{R}} \sqrt{\dfrac{2}{\gamma-1}\left[\left(\dfrac{P_T}{P_A}\right)^{\frac{\gamma-1}{\gamma}}\right]} \sqrt{\left(\dfrac{P_T}{P_A}\right)^{-\frac{\gamma+1}{\gamma}}}$

A_{ex} = Nozzle measured exit area, in^2.

o Duct Mach number from the function $P_{SD}/P_{T_A} = \left(1 + \dfrac{\gamma-1}{2} M^2\right)^{-\frac{\gamma}{\gamma-1}}$

where: P_{SD} = Duct Static pressure

P_{TD} = Duct total pressure

M = Local Mach number

o Calculated flap exit augmentation ratio , ARC = $\dfrac{T_c}{W_M V_I}$

where: T_C = total calculated flap exit rake thrust which equals the sum of the thrust at each P_T probe (T_{CP}).

$$T_{CP} = P_A \gamma A_P M_P^2$$

where: P_A = ambient pressure

γ = 1.40

A_P = $\dfrac{\text{total flap exit area}}{\text{no. of probes}}$

M = local Mach no. at each probe

AD 1546D

REV SYM